Technical Report

TR-03-18

Matrix fluid chemistry experiment

Final report
June 1998 – March 2003

Edited by:

John A T Smellie, Conterra AB, Sweden
H Niklaus Waber, University of Bern, Switzerland
Shaun K Frape, University of Waterloo, Canada

June 2003

Svensk Kärnbränslehantering AB
Swedish Nuclear Fuel
and Waste Management Co
Box 5864
SE-102 40 Stockholm Sweden
Tel 08-459 84 00
+46 8 459 84 00
Fax 08-661 57 19
+46 8 661 57 19

Matrix fluid chemistry experiment

Final report
June 1998 – March 2003

Edited by:

John A T Smellie, Conterra AB, Sweden
H Niklaus Waber, University of Bern, Switzerland
Shaun K Frape, University of Waterloo, Canada

June 2003

The full report including all Appendices is available as a .pdf-file on the enclosed CD-ROM-disc. The printed version contains only the main text and a list of the Appendices.

A pdf version of this document can be downloaded from www.skb.se

Acknowledgements

The Matrix Fluid Chemistry Experiment at the Äspö Hard Rock Laboratory (HRL) was carried out between June 1988 and March 2003 and was funded by the Swedish Nuclear Fuel and Waste Management Company (SKB). In this respect the interest and support from Olle Olsson, Peter Wikberg, Christer Svemark and Ignasi Puigdomènech have been much appreciated. Reliable and efficient site technical help at the Äspö HRL was given by Patrik Hagman and Lars Andersson and laboratory support at the Äspö HRL by Anna Säfvestad, Christina Mattsén, Janette Carnström and Ann-Sofie Svensson. Posiva Oy (Finland) is thanked for funding the contribution of Seppo Gehör (Kivitieto Oy), Nagra (Switzerland) for their support of Nick Waber (University of Bern) and BRGM (France) for the participation of Joél Casanova.

All the participant scientific investigators are thanked for contributing to a very stimulating and rewarding project. The investigators were:

Alexander Blyth	(University of Waterloo, Canada)
Joél Casanova	(BRGM, France)
Shaun Frape	(University of Waterloo, Canada)
Seppo Gehör	(Kivitieto Oy, Finland)
Erik Gustafsson	(Geosigma AB, Sweden)
Douglas Hirst	(University of Waterloo, Canada)
Janette Carnström	(SKB, Sweden)
Marcus Laaksoharju	(GeoPoint AB, Sweden)
Sten Lindblom	(Stockholm University, Sweden)
Christina Mattsén	(SKB, Sweden)
Karsten Pedersen	(Göteborg University, Sweden)
Ann-Sofie Svensson	(SKB, Sweden)
Anna Säfvestad	(SKB, Sweden)
Eva-Lena Tullborg	(Terralogica AB, Sweden)
Niklaus Waber	(University of Bern, Switzerland)
Bill Wallin	(Geokema AB, Sweden)

Ingvar Rhén (VIAK VBB, Sweden) was involved in the initial planning, drilling and borehole completion activities of the programme.

Preface

This report presents in full the results from the Matrix Fluid Chemistry Experiment as most of the documentation is compiled in internal SKB reports which can not be referred to. The majority of the participants have contributed directly to this report and are individually acknowledged in order of importance at the beginning of each chapter. Editing has attempted to ensure clarity and uniformity and the chapters are followed by a brief summary. Together, these summaries provide the basis to the overall conclusion chapter.

Abstract

The Matrix Fluid Chemistry Experiment set out to determine the composition and evolution of matrix pore fluids/waters in low permeable rock located at repository depths in the Äspö Hard Rock Laboratory (HRL). Matrix pore fluids/waters can be highly saline in composition and, if accessible, may influence the near-field groundwater chemistry of a repository system. Characterising pore fluids/waters involved in-situ borehole sampling and analysis integrated with laboratory studies and experiments on rock matrix drillcore material.

Relating the rate of in-situ pore water accumulation during sampling to the measured rock porosity indicated a hydraulic conductivity of 10^{-14}–10^{-13} ms^{-1} for the rock matrix. This was in accordance with earlier estimated predictions. The sampled matrix pore water, brackish in type, mostly represents older palaeogroundwater mixtures preserved in the rock matrix and dating back to at least the last glaciation. A component of matrix pore 'fluid' is also present. One borehole section suggests a younger groundwater component which has accessed the rock matrix during the experiment. There is little evidence that the salinity of the matrix pore waters has been influenced significantly by fluid inclusion populations hosted by quartz. Crush/leach, cation exchange, pore water diffusion and pore water displacement laboratory experiments were carried out to compare extracted/calculated matrix pore fluids/waters with in-situ sampling. Of these the pore water diffusion experiments appear to be the most promising approach and a recommended site characterisation protocol has been formulated.

The main conclusions from the Matrix Fluid Chemistry Experiment are:

- Groundwater movement within the bedrock hosting the experimental site has been enhanced by increased hydraulic gradients generated by the presence of the tunnel, and to a much lesser extent by the borehole itself.
- Over experimental timescales (~ 4 years) solute transport through the rock matrix is mainly by small-scale advection via an interconnected microfracture network and by diffusion.
- Over repository timescales diffusion of pore fluid/water from the rock matrix to the adjacent microfracture groundwaters will become more important depending on the nature of existing chemical gradients.
- At Äspö, permeable bedrock at all scales has facilitated the continuous removal and replacement of the interconnected pore space waters over relatively short periods of geological time, probably hundreds to a few thousands of years.

Executive summary

Background

Much of the pre-HRL (Hard Rock Laboratory) groundwater sampled to explain the hydrochemical character of the Äspö site, mostly to depths of 500–600 m, has been collected from water-conducting fracture zones with high transmissivities ($T > 10^{-9}$ m^2s^{-1}). Consequently, these fracture groundwaters probably attain their chemical character mostly by mixing waters of different origin rather than by chemical water/rock interaction. In contrast, little is known about groundwater compositions from low transmissive parts ($T < 10^{-10}$ m^2s^{-1}) of the bedrock. Under such conditions interaction with circulating groundwater is limited or essentially does not occur at all. Long residence times therefore are characteristic and the composition of the groundwaters is more likely influenced to varying degrees by the rock matrix pore fluid/water chemistry. The accessibility of these fluids/waters, and their ability to move through the rock matrix, depends on whether or not the different pore spaces are connected. Assuming a rock matrix fabric of interconnected pores and microfractures, and bearing in mind that rocks of low transmissivity constitute the major volume of the bedrock mass in any granite body, matrix pore fluids/waters are suspected to contribute significantly to the chemistry of deep fracture groundwaters.

Under undisturbed conditions the matrix pore fluids/waters in crystalline rock environments are suspected to be highly saline in composition. There are several potential sources to this salinity, for example allothtonous sources such as ancient seawaters or basinal brines and evaporites, and younger brackish waters, and authochtonous sources such as residual metamorphic/igneous fluids, hydrolysis of silicate minerals, and dissolution/leaching of interstitial salts present in the rock matrix. An additional source, emphasising crystalline rocks, may derive from the rupture and/or dissolution of fluid inclusions (the enclosed fluid of which may be allochtonous or authochtonous in origin) located in and/or around some of the major rock-forming minerals (mostly quartz). It is generally accepted that no one process or source can account for the observed salinities in basement Shield areas and most reported occurrences seem to represent mixtures of meteoric water with a highly concentrated brine.

The possibility of highly saline matrix pore fluids/waters may have important repercussions on long-term safety surrounding deep geological disposal of high-level radioactive wastes. To model near-field repository processes requires specific knowledge of the near-field input groundwater compositions expected during the lifespan of the repository. Therefore, knowledge of the composition and origin of the matrix pore fluid/water should provide a more realistic hydrochemical input to near-field performance and safety assessment calculations, since deposition of spent fuel will be restricted to rock volumes of low transmissivity. Even though it has been argued that the Swedish engineered barrier system may not be particularly sensitive to high salinity, limits have been set (up to 100 g/L TDS) and the expected near-field salinities need therefore to be quantified.

The term ‘matrix pore fluid’ is used in this report to include the following fluid types: a) the water in the pore space of a rock that is only accessible by diffusion, b) the water residing in dead-end pores, and c) the fluid enclosed in mineral fluid inclusions. The term ‘matrix pore water’ is used when referring to the water in the connected pore space of the rock matrix that is accessible for interaction with groundwaters circulating in nearby microfractures. The Matrix Fluid Chemistry Experiment (MFE) aimed at initially characterising the ‘matrix pore fluid’ using various laboratory methods and approaches. The final goal of the investigations was to characterise the in-situ ‘matrix pore water’.

MFE-borehole: Drilling, completion, sampling and analysis

A suitable rock mass of low hydraulic transmissivity was identified at the Äspö HRL at a depth of approx 420 m depth, corresponding to expected repository depths. The borehole was drilled in June 1998 at an upward inclination of approx 30° to a distance of 11.70 m from the tunnel face; installation of sampling equipment was carried out soon afterwards (Figure 1). To maintain reducing conditions, all borehole activities were carried out under an overpressure of nitrogen. Moreover, the borehole equipment and the borehole were sterilised prior to completion to avoid excessive microbial activity during the experiment.

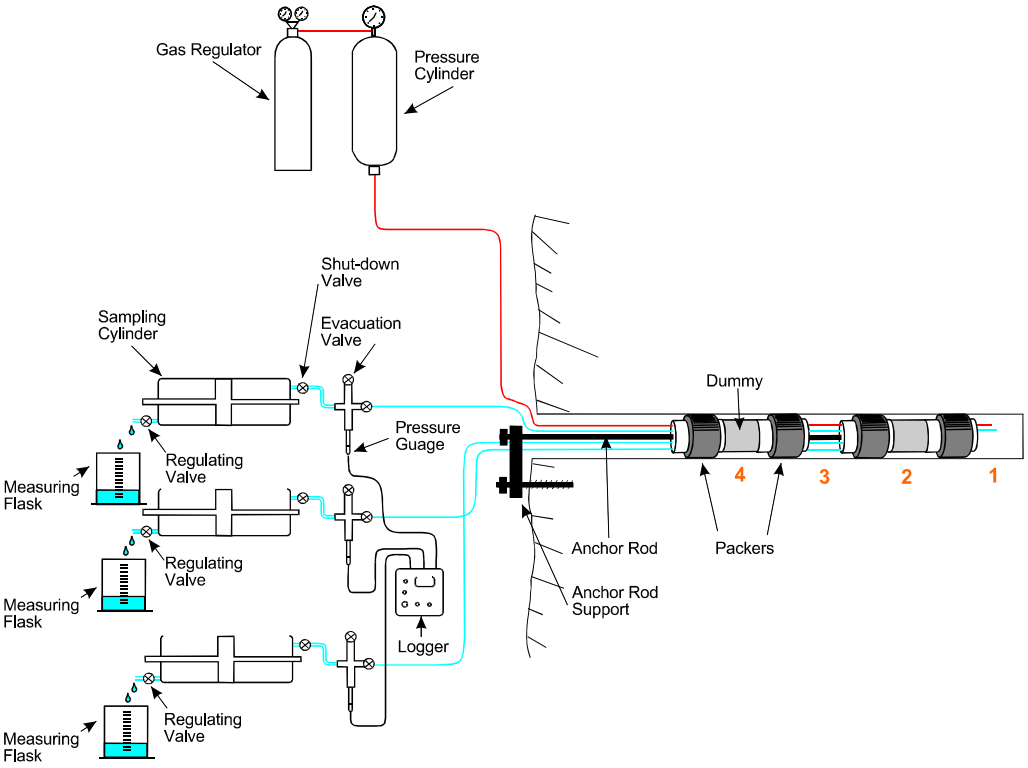

Figure 1. *Matrix Fluid Chemistry Experiment. MFE-borehole sections 2 and 4 were specifically selected to collect matrix pore water; sections 1–4 were continuously monitored for pressure but could also be sampled. The contact between Äspö diorite and Ävrö granite occurs in section 3 at 8.5 m from the tunnel face.*

Continuous monitoring of pressure in the four borehole sections commenced directly after installation of the packer/sampling equipment and continued for the duration of the experiment. Since the pressure in the isolated borehole sections was close to, but still less than the hydrostatic pressure, any increasing in pressure therefore should indicate a build-up of gas and/or matrix pore water diffusing into the isolated borehole sections from the host rock. Figure 2 shows the pressure curves from start to finish of the experiment (June 1998 to March 2003); the break in the curves in December 1999, October 2001 and February 2003 indicates the three sampling campaigns when sections 1 and 4 (first campaign), sections 1 to 4 (second campaign) and sections 1 to 4 (third sampling campaign) were opened for sampling. Because of the generally small and variable volumes of fluid extracted from the borehole sections, a full analysis was not possible and certain priorities had to be set following each campaign. Priorities included pH, alkalinity, major ions and cations, $\delta^{18}O$, δD, $\delta^{13}C$, ^{14}C, $^{86}Sr/^{87}Sr$ and $\pm\ ^{37}Cl$. Gas analysis, when conducted, included H_2, CO, CO_2, CH_4, C_2H_4 and C_2H_6.

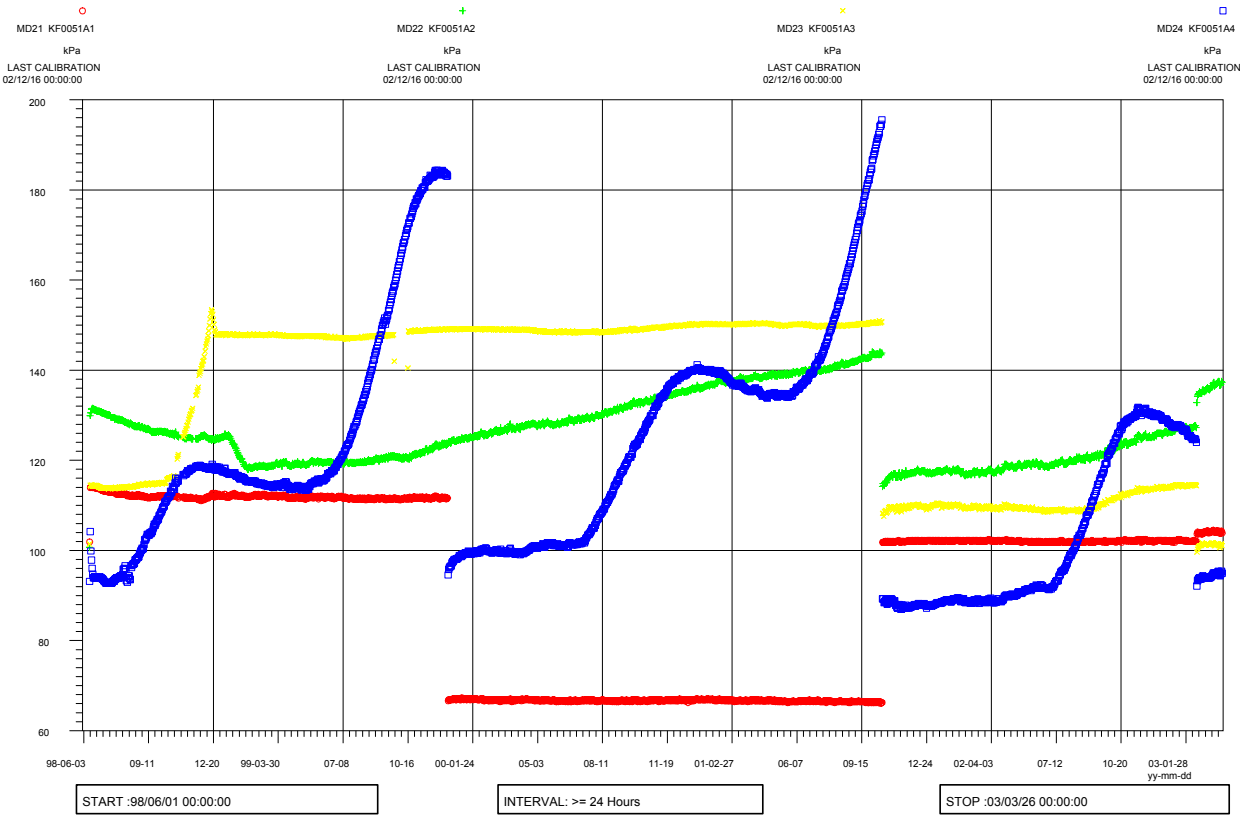

Figure 2. *Pressure monitoring curves for each of the four isolated MFE-borehole sections for the duration of the experiment (up to March 2003). Colours relate to borehole sections 1(red), 2 (green), 3 (yellow) and 4 (blue). Sections 2 and 4 were specifically demarcated for matrix pore water sampling. The break in the curves in December 1999, October 2001 and February 2003 indicates the three sampling campaigns when sections 1 and 4 (first), sections 1 to 4 (second) and sections 1 to 4 (third) were opened for sampling.*

MFE-borehole: Drillcore investigations

Not only is it important to sample and characterise the matrix pore waters, but also to understand their origin and how solute transport occurs through the rock matrix. To this end the MFE-drillcore, in particular those portions representing the borehole sections sampled, underwent a detailed characterisation to distinguish between accessible and inaccessible matrix pore fluids/waters. This involved crush/leach and out-diffusion laboratory studies, fluid inclusion characterisation and porosity measurements together with detailed mineralogy, petrology and geochemistry.

Mineralogy, geochemistry and porosity

Two major rock types are present in the MFE-borehole; Äspö diorite and Ävrö granite. The transition from diorite to granite is observed as a decrease in mafic content and plagioclase countered by an increase in quartz and K-feldspar. The mineralogical composition of these two major rock types serves as an important constraint on the pore water composition, for example the impact of oxidised Fe-oxides and Fe-hydroxides and sulphide minerals on the pore water redox potential and influence of clay phases on cation exchange.

Geochemical variations between diorite and granite are in accordance with mineralogical differences. However, chemical differences are too small to have a significant influence on the matrix pore fluid; the only exception might be certain metallic trace elements which are more abundant in the diorite in minerals susceptible to alteration.

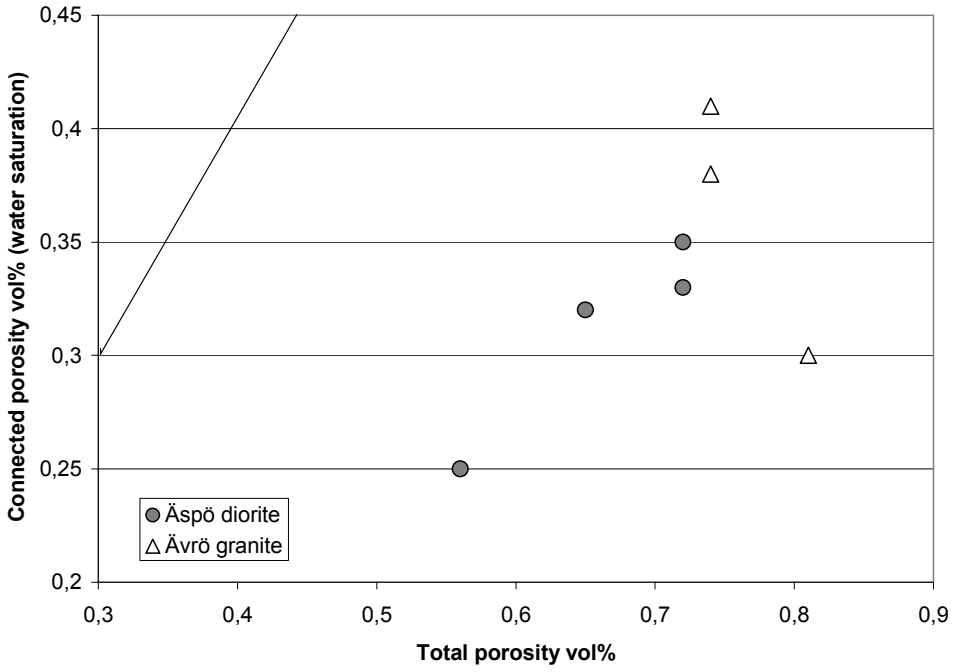

Figure 3. *Total porosity derived from grain and bulk density versus connected porosity derived by water re-saturation techniques. The line represents a ratio of 1 to 1.*

Variations in mineralogy also reflect differences in grain density, in particular the content of mafic minerals, and also appear to influence measurements of the total porosity, as derived from bulk and grain density, which is greater for the Ävrö granite (0.76 ± 0.04 vol%) than for Äspö diorite (0.66 ± 0.08 vol%) (Figure 3). In contrast, the connected porosity, as derived by water loss and water resaturation techniques, is similar for Äspö diorite (0.44 ± 0.07 vol%) and the Ävro granite (0.40 ± 0.02 vol%) within the accuracy of the methodologies used in its determination.

The connected porosity determined by water resaturation was more difficult to achieve in the Äspö diorite than in the Ävrö granite, highlighting the textural differences between these rock types. For example, the layered arrangement of platy mafic minerals in the diorite results in a highly anisotropic flow field and causing a slower resaturation compared to the granite. Generally these data support the hydraulic interpretation of the matrix borehole.

The greater difference in total to connected porosity (i.e. water-content porosity) in the Ävrö granite than in the Äspö diorite corresponds closely to the independently calculated volume of fluid inclusions. This strongly suggests that the measured non-connected (i.e. not accessible for water diffusion) porosity constitutes almost entirely the amount of fluid inclusions present. These findings are in accordance with the greater abundance of quartz and fluid inclusions comprising the Ävrö granite compared to the Äspö diorite.

Fluid inclusions

The matrix pore fluids/waters were expected to be highly saline in character and one potential source of this salinity was the fluid inclusion populations associated dominantly with quartz. The objectives of the fluid inclusion studies were therefore to characterise the fluid inclusion populations, determine the nature (i.e. salinity) of the included fluids, to examine carefully for any evidence of leakage, and to establish the mechanisms of leakage if shown to have occurred.

The study of fluid inclusions focussed mainly on quartz since it contains the large majority of inclusions and its brittle nature makes it vulnerable for inclusion leakage during tectonic stress. Heterogeneities are restricted to open and healed fractures, isolated or clustered fluid inclusions and mineral inclusions. Grain boundaries within quartz aggregates also constitute heterogeneities. The healing/sealing of microfractures and grain boundaries in quartz is an important process giving rise to the formation and trapping of fluid inclusions. There are numerous examples of fluid inclusion planes (FIPs) outlined by inclusion trails traversing different generations of quartz formation. A key issue is at what times during the geological history of the Äspö region where these fractures formed and then sealed.

An additional objective was to derive a common methodology for the description, analysis and interpretation of fluid inclusion populations that could be transferred to a site characterisation protocol. The methods used to characterise the morphology and chemistry of the fluid inclusions comprised Optical Microscopy, Cathodoluminescence, Microthermometry, Laser Raman Microspectroscopy and Laser Ablation ICP-MS.

Basically, four types of fluid inclusion populations have been identified (Types I–IV) and are schematically illustrated in Figure 4. These comprise:

- Primary, intracrystalline magmatic Type I fluid inclusions (400°–500°C; 5–30 eq.wt% NaCl).
- Fluid Inclusion Planes (FIPs) containing magmatic/hydrothermal Type II/III fluid inclusions aligned along healed fractures/fissures (100°–300°C; 1–26 eq.wt% NaCl).
- Type IV intracrystalline boundary grain inclusions (60°–70°C; mostly gas filled; some contain 5–15 eq.wt% NaCl).

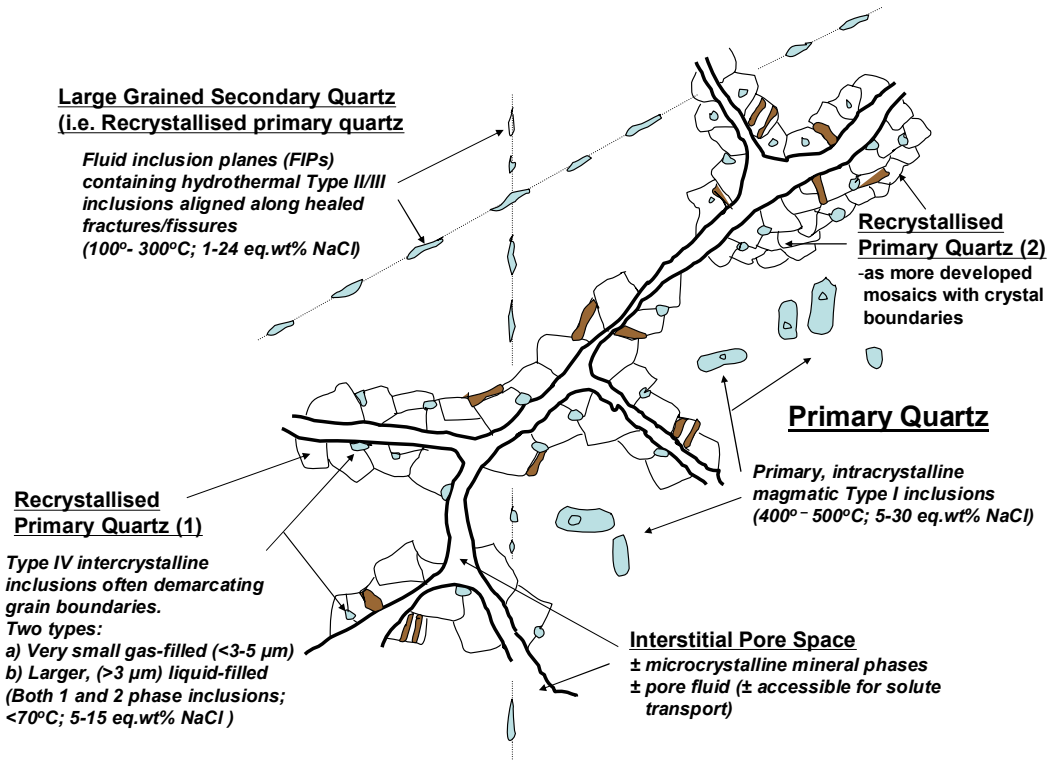

Figure 4. *Schematic representation of the major fluid inclusion types present in the Äspö diorite. Note that the Ävrö granite shows more examples of recrystallised quartz (but not necessarily more developed) than the Äspö diorite. Brown phases represent biotite laths.*

The amount of fluid in the rock matrix contained in the fluid inclusions has been estimated to be around 0.3 vol% for the Äspö diorite and 0.6 vol% for the Ävrö granite. As indicated above, the general range of fluid inclusion salinity is between 0.2 and 30 eq.wt% NaCl; $CaCl_2$ sometimes dominates over NaCl. Most grain boundary inclusions are gas filled with only a few liquid varieties with salinities between 5 and 15 eq.wt% NaCl. Overall, the fluid inclusion populations are characterised by a moderately high salinity which may be accessible through deformation and leakage to the interstitial pore space in the rock matrix.

The question of fluid inclusion leakage into the interstitial pore space and, ultimately influencing the matrix pore fluid/water chemistry, cannot be unequivocally resolved. However, there is evidence from petrofabric studies of an on-going process of tectonic stress-release accompanying isostatic recovery following glacial ice melt which could provide a convenient mechanism for fracturing inclusions hosted by quartz and releasing fluids into the immediately accessible rock matrix.

Evidence of in- and out-diffusion processes

The nature of in- and out-diffusion processes around an identified microfracture in the Äspö diorite was assessed using microscopy, porosity measurements, bulk rock chemistry and U-decay series isotopes. Evidence of chemical and isotopic gradients may help to further understand the evolution of the matrix pore water chemistry.

The results showed no chemical evidence of low temperature alteration or chemical gradients and most chemical variation in the wall rock adjacent to the microfracture can be explained by mineralogical heterogeneity. In contrast there was an increase in porosity adjacent to the microfracture edge corresponding to $^{234}U/^{238}U$ disequilibrium. This isotopic disequilibrium suggests that within the last 1 Ma water/rock interaction has (and probably is) occurring marginal to the microfracture and this has been accompanied by an accumulation of uranium.

It has not been possible to determine microscopically whether the studied microfracture is a presently open, semi-open or mainly sealed in-situ fracture, but the uranium isotopic disequilibrium data suggest it has been open at some stage in the ‘recent’ geological past (< 1 Ma), and therefore it seems realistic to assume that it acts as a present-day ‘more porous pathway’ to pore fluid movement through the rock matrix.

Hydraulic character of the rock matrix

At an early stage in the matrix fluid experiment, estimated times (Figure 5) to accumulate 250 mL matrix pore water (approximating to the respective volumes of Sections 2 and 4 earmarked for sampling; cf Figure 1) were predicted based on a range of hydraulic conductivity values. Both 2-dimensional radial flow and 3-dimensional spherical Darcian flow were considered assuming differential pressures within 10–35 bar and a radius of influence of 5–10 m.

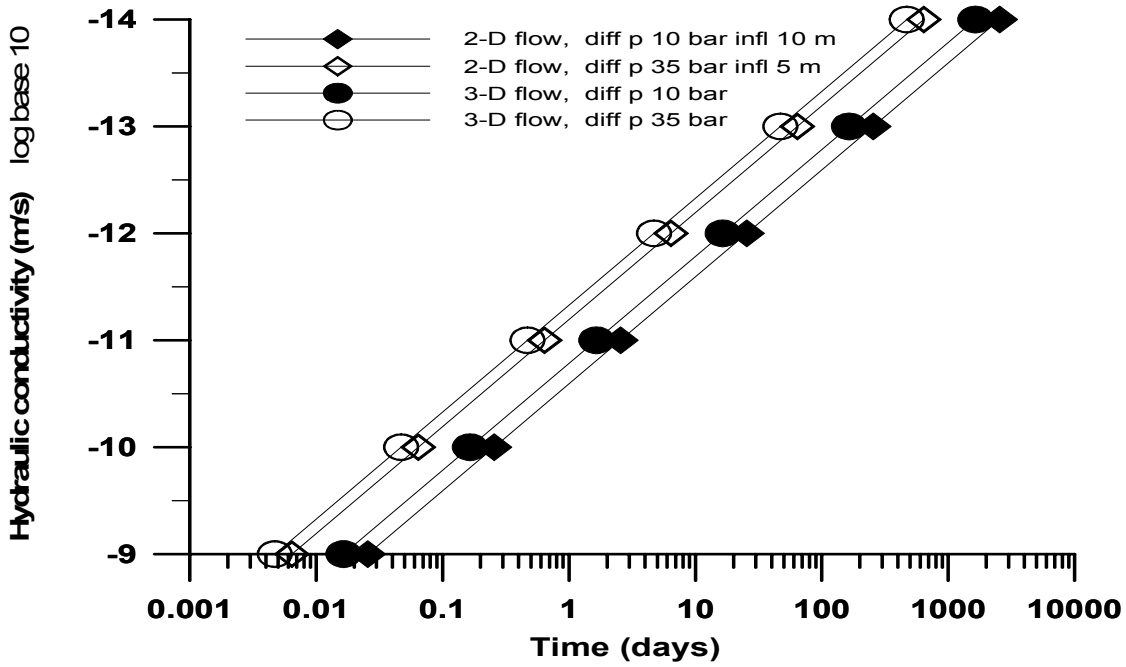

Figure 5. *Predicted times to accumulate 250 mL of matrix pore water, based on a range of hydraulic conductivities, considering both radial and spherical Darcian flow and assumed differential pressure within 10–35 bar and radius of influence 5–10 m.*

At a conductivity of $1 \cdot 10^{-13}$ ms^{-1} an accumulation of 250 mL matrix pore water would require 2–9 months, and at a conductivity of $1 \cdot 10^{-14}$ ms^{-1} it would need from 16 months to 7 years depending on the flow regime. Compared to the monitored boreholes (cf Figure 1), after 15 months of the experiment still no pressure increase was measured in borehole Section 2. In Section 4 the pressure had increased, but not to a level corresponding to the accumulation of 250 mL of matrix pore water. These predicted pore water flow times are in accordance with the estimated rock matrix hydraulic conductivity and the measured porosity and suggest that the hydraulic conductivity in the matrix rock block lies somewhere around 10^{-14}–10^{-13} ms^{-1}.

MFE-borehole: Rock pore water studies

To characterise the matrix pore water accessible for solute transport two approaches have been applied: 1) using indirect laboratory methods based on drillcore material, and 2) using direct long-term in-situ sampling of pore water in isolated borehole intervals. While long-term in-situ sampling is only feasible in an underground laboratory facility, indirect laboratory methods based on the analysis of drillcore material can be very useful for a more speedy evaluation of pore water chemistry.

In this present study indirect laboratory methods for the characterisation of the pore water chemistry involved aqueous leaching, cation exchange, pore water diffusion and pore water displacement. A drawback of such methods is that each one can only provide part of the answer and they have to be applied complementary and in conjunction with geochemical modelling in order to derive the complete chemical composition of the pore water chemistry. It was hoped that the accumulated pore water in the borehole intervals over months to years would be representative for the in-situ pore water and that its composition could act as a constraint for the identification of possible experimental artefacts in the indirect methods applied. The identification of such artefacts is important for the successful transfer of such indirect methods to sites where no long-term experiments can be performed in-situ.

Aqueous leaching

Aqueous leaching was performed on dried and ground (different grain sizes) rock material of Äspö diorite and Ävrö granite**.** During drying of the still intact, fully saturated core material, dissolved constituents in the pore water will precipitate as highly soluble salts following complex evaporation cycles. Crushing and grinding of the rock material will additionally liberate fluid trapped in mineral fluid inclusions. The mineralisation of a leachate solution is thus the sum of: a) the constituents originally dissolved in the pore water, b) the constituents present in the inclusion fluid, and c) water/rock interaction during the leaching process. Following each leaching the leachate was analysed for major and trace elements, $^{87}Sr/^{86}Sr$ isotopic ratios and the ^{37}Cl isotope composition.

Results showed that the impact of inclusion fluids on the leach solutions was significant (Figure 6). This inhibits the derivation of compositional aspects of the pore water residing in the connected porosity, not only for non-conservative but also for conservative compounds such as Cl and Br. Consequently, optical and microthermometric fluid inclusion investigations should be mandatory before any aqueous leaching experiments are performed in order to evaluate the feasibility of leach solutions for the derivations of the pore water composition of crystalline rocks.

Isotope ratios of strontium and chlorine of the leach solutions supported a mixing of fluids from different origins in the leach solutions. The strontium isotopes further indicated a significant influence of Al-silicate alteration during leaching.

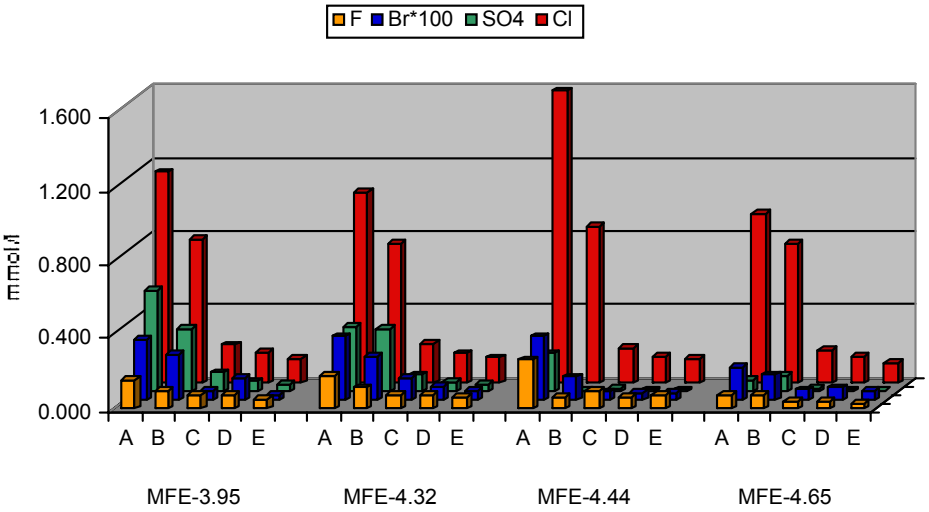

Figure 6. *Äspö diorite: Anion concentrations in leach solutions of different grain-size fractions (A=<63 µm, B=<0.5 mm, C=1–2 mm, D=2–3 mm, E=>3 mm).*

Cation exchange

In the Äspö crystalline rocks, clay minerals are secondary products of hydrothermal or low temperature weathering alterations of the primary, magmatic minerals. Although the clay fraction in these rocks comprises only about 5% of the total rock, cation exchange might have some importance as a control on the pore water chemistry. This is because the clays mainly occur along grain boundaries and hair fissures. In such zones, which are accessible for pore water, the relative abundance of clays is higher than in the whole rock. The cation exchange properties were determined for two samples using the Nickel-Ethylenediamine (Ni-(en)) Method**.**

Unfortunately results showed that methods using a highly selective exchange complex have a limited applicability to crystalline rocks with a low cation exchange capacity and a substantial influence of inclusion fluid on the exchange solutions.

Pore water diffusion

Simple out-diffusion experiments was performed on three core samples to explore the in-situ pore water composition. Given appropriate time, diffusion of the components dissolved in the pore water of the rock matrix into the double deionised water was expected to reach a steady-state. With knowledge of the water content of the rock samples, the concentrations of non-reactive (free) solutes could be calculated to pore water concentrations. For reactive (controlled) solutes, the concentration changes induced by rock/water interactions could be estimated utilising geochemical modelling strategies.

Results showed that steady-state conditions were most probably not attained during the experiment due to time constraints. Furthermore, since the rock samples did not come from the actual matrix borehole and therefore may differ slightly in composition even though from the same matrix block, differences in chemistry between the diffusion experiment waters and in-situ waters sampled from the MFE-borehole may exist. Consequently, no final conclusion could be drawn with respect to the pore water composition of the investigated rock samples. Pore water diffusion experiments in combination with geochemical modelling, however, appear to be most promising to evaluate at least the conservative chemical and isotopic parameters of the pore water residing in the connected porosity of crystalline rocks.

Pore water displacement

In August 1999 a high pressure experiment was initiated which essentially tried to force double distilled (Ultrapure) water through a drillcore portion (100 x 50 mm) in order to extract matrix pore water. The drillcore portion, selected adjacent to borehole Section 4, was mounted in a moisture proof membrane with an applied hydrostatic stress of 11.7 MPa (i.e. equivalent to the lithostatic stress at the MFE-borehole location in Tunnel 'F') and a pore pressure of 6 MPa was applied to the distilled water.

Up until October 1999 no movement was observed and the pore pressure was accordingly increased to 9.5 MPa. Some activity was observed in November 1999 which subsequently slowed down and stopped; since then to the present time (June 2003) no movement of matrix fluid through the core has been observed. However there have been indications of a loss of distilled water from above the core (some mLs) during the experiment. Since the water is not believed to be escaping from the highly pressurised sealed unit, this may suggest the filling of empty pore space in the rock due to partial desaturation of the sample during storage and handling, or, alternatively, evaporation of fluid on the underside of the core.

Pore water displacement experiments under high pressure appear to be of limited applicability for pore water characterisation of such crystalline rocks. The limiting factor here is the combination of low water content and low hydraulic conductivity of the rocks; a very large volume of rock is required in order to obtain a reasonable pore water volume displaced for analysis.

MFE-borehole: In-situ borehole water

The term 'borehole water' describes the measured composition of the water that has seeped into the different packed-off sections in the MFE-borehole over time periods of several months. The composition of such borehole water can deviate substantially from the real in-situ pore water composition, resulting from, for example, microbial activity, redox reactions, corrosion, etc. These possibilities were evaluated during sampling and analyses.

Water samples were obtained on three separate occasions during the four years and three month duration of the experiment. The pressure build-up in Section 1 was constantly very low and no water (only gas) could be sampled; in order of sampled volumes of water, Section 4 yielded most and Section 2 least (cf Figure 1). The sampled borehole waters are generally Na-(Ca)-Cl in type with Cl concentrations around 5000 mg/L in the Äspö diorite and around 2900 mg/L in the Ävrö granite some 2 m away (Figure 7). The borehole waters sampled from the Äspö diorite and the Ävrö granite also differ significantly in their isotope composition of water and strontium (Figure 8). The chlorine isotope composition is identical for the waters from the diorite and granite sampled within a distance of about 3 m in the borehole, but significantly enriched in ^{37}Cl in the diorite water sampled further away.

The accumulation of H_2S gas in all four sampling sections indicated that sulphate reduction (later confirmed) had occurred in spite of the attempt to sterilise the borehole and the equipment prior to installation.

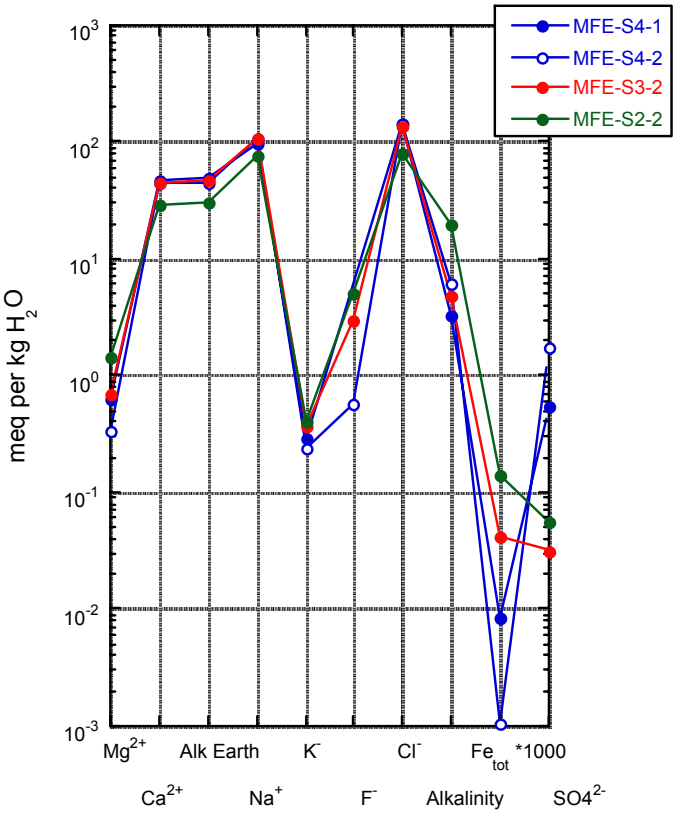

Figure 7. *Schoeller diagram of the borehole waters sampled from Sections 2, 3, and 4 in the MFE-borehole (alkalinity = total alkalinity; Fe_{tot} is expressed as Fe^{2+}).*

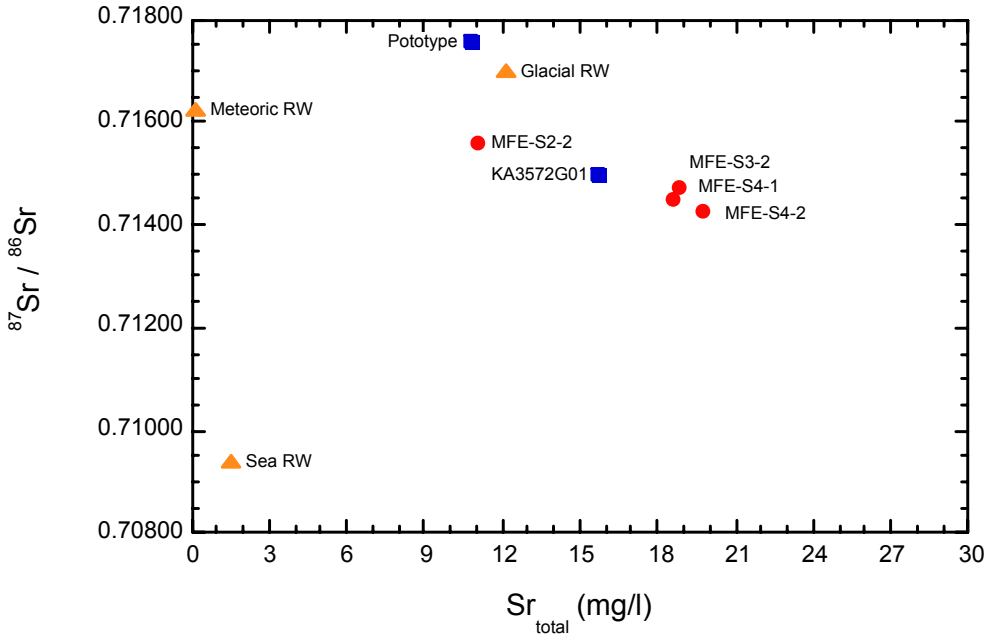

Figure 8. *Sr-isotope ratio vs 1/Sr of MFE-borehole water. Also shown are groundwaters from locations in the vicinity of the MFE-borehole (i.e. Prototype; Borehole KA357201) and reference waters (RW) proposed for the Äspö site.*

If the MFE-borehole rock matrix system was dominated by diffusion, and close to or at steady state conditions, a more homogeneous compositional distribution would be expected. The observed chemical and isotopic heterogeneities therefore indicate that these waters have been significantly perturbed, in particular that of extensive bacterially mediated sulphate- and iron-reduction processes which have altered the in-situ conditions. With the small amount of available borehole water volume, however, not all necessary parameters could be analysed in order to correct for these perturbations. Nevertheless it has to be concluded from this study that the sampled borehole waters do not represent the ancient in-situ pore water end-member that was in equilibrium with the rock matrix and that was hoped to be sampled.

MFE-borehole: The hydrogeology and hydrochemistry of the near-vicinity environment

In the rock matrix it is important to relate the accessible pore water chemistry to the chemistry of the groundwaters present in nearby microfracture zone(s) of low hydraulic transmissivity ($T = 10^{-12}$–10^{-9} m^2s^{-1}). In turn, it is important to relate these microfracture groundwaters to larger scale fracture zone networks of even greater transmissivity ($T = 10^{-10}$–10^{-7} m^2s^{-1}), which is the range normally sampled in hydrogeochemical site characterisation programmes. This is conceptually illustrated in Figure 9. Since the groundwaters that eventually will come in contact with the spent fuel deposition holes in a repository situation (i.e. equivalent to the position of the MFE-borehole in Figure 9) will gain access along such advective pathways of increasingly diminishing transmissivity, the influence of the matrix pore water on the advective microfracture groundwaters in these low transmissive rock masses

(and vice versa) will be of importance as interaction may change the chemistry of the near-field groundwaters.

These fracture systems, however, since they represent variations in transmissivity, orientation and represent different geographical locations, may also be characterised by different hydrochemical signatures. However, when these groundwater variations permeate to the low transmissive rock matrix, longer residence times and increased water/rock interaction plus the potential influence of in- and out-diffusion of pore fluids from the rock matrix into fracture zones, or vice versa, will all contribute to a greater homogenisation of the groundwaters representing the near-field hydrochemical environment.

To address these issues adequately, a reliable hydraulic and hydrochemical database on a site-scale was compiled. This involved available data related to hydraulic parameters and hydrochemistry from the Äspö HRL close to and at equivalent depths to the matrix fluid experiment. Four major sources of data were used: CHEMLAB and Microbe experiments, TRUE Block Scale Experiment, Prototype Repository Experiment and new ^{37}Cl data. It was hoped that the evaluation of these data might provide some link between transmissivity and groundwater chemistry which hitherto has not been addressed quantitatively in the Äspö hydrochemical programme, mainly because of the difficulty in measuring the low ranges of transmissivities (< 10^{-10} m^2s^{-1}) and also the time-consuming nature of sampling from such hydraulic features. Three scales were evaluated: a) Semi-regional Scale (undisturbed, Pre-HRL conditions and disturbed, Post-HRL conditions) , b) Sub site-scale (area of approx 100 m^2) to include the 'J' Niche, Prototype and TRUE Block scale experimental areas, and c) the MFE-borehole itself relating to the scale of a single deposition hole for spent nuclear fuel.

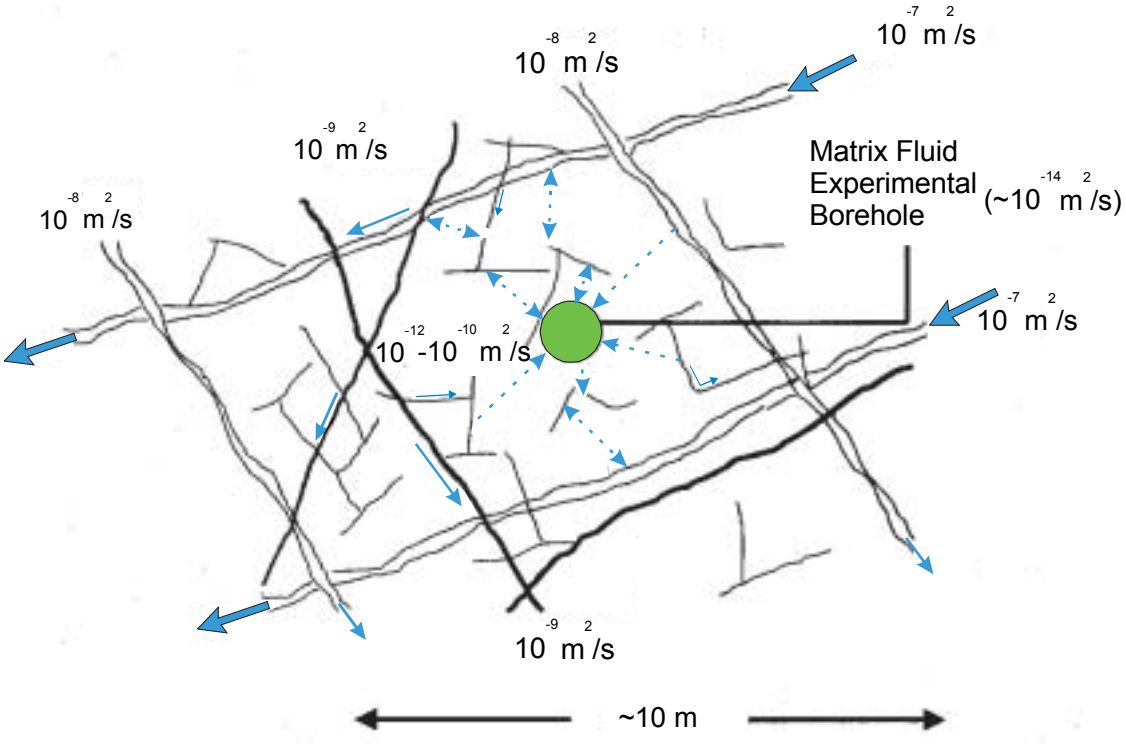

Figure 9. *Conceptual hydraulic model of the matrix rock block showing the location of the MFE-borehole.*

The general conclusions from this study are:

- Large-scale groundwater movement through the bedrock during disturbed conditions occurs within the medium to high hydraulically active fractures. Over the range of transmissivity represented by these sampled fractures ($T = 10^{-10}$–10^{-5} m^2s^{-1}), there is little obvious correlation between hydraulic properties and groundwater chemistry.
- Under disturbed conditions the new hydrochemical and isotopic data support earlier work that indicated the hydraulic drawdown of a modern groundwater component into the Äspö HRL, such as Baltic Sea and meteoric precipitation waters, to the detriment of older saline and glacial melt water components which have been diluted or removed respectively.
- This drawdown has influenced particularly the Prototype samples, despite the generally low transmissive character of the sampling locations ($T = 10^{-10}$–10^{-7} m^2s^{-1}). The 'J' niche and TRUE Block Scale sites are less affected.
- Groundwater compositions from sub-vertical fracture zones bordering the matrix borehole block reflect the upconing of saline groundwaters typical of the deepest (~ 1000 m) samples studied at Äspö.
- Access of groundwaters from highly transmissive fractures to the rock matrix is mainly by advective flow through an interconnected network of microfractures characterised by ever decreasing dimensions and hydraulic conductivities. Within the rock matrix itself solute transport is dominated by diffusion processes.
- The MFE-borehole water samples reflect a generally similar major ion character to nearby fracture compositions (with the exception of SO_4 and Mg).
- Borehole sections 3 and 4 represent older palaeogroundwaters preserved in the low hydraulically transmissive rock matrix. A component of matrix 'pore fluid' is also present.
- Borehole Section 2 suggests a younger groundwater component which has accessed the rock matrix during the experiment.
- Short-term movement of water (i.e. during the timescale of the experiment) through the rock matrix is mainly by small-scale advection via a connecting network of microfractures and by diffusion.
- Over repository timescales (i.e. thousands to hundreds of thousands of years) a greater contribution from diffusion of pore fluid/water from the rock matrix itself will be present since the microfracture groundwaters will have had more time to undergo exchange by in- or out-diffusion mechanisms.
- As a whole, groundwater movement within the bedrock interconnected fracture systems has been greatly enhanced by the increased hydraulic gradients generated by the presence of the tunnel, and to a much lesser extent by the MFE-borehole itself.
- At Äspö, permeable bedrock at all scales has facilitated the continuous removal and replacement of the interconnected pore space waters over relatively short periods of geological time, probably hundreds to a few thousands of years.

Site characterisation implications

One of the objectives of the matrix experiment was to establish methodologies that could be transferred conveniently to site characterisation investigations. Obviously it would be impractical to conduct long-term sampling and analysis of matrix pore waters similar to that described in this study. Emphasis should therefore be on the rock matrix itself, focussing on suitable method(s) to rapidly extract and chemically characterise the accessible matrix pore water. In this respect the laboratory pore water diffusion studies conducted have resulted in a methodology to accomplish this objective and a recommended site characterisation protocol has been formulated.

Main conclusions

- Groundwater movement within the bedrock hosting the experimental site has been enhanced by increased hydraulic gradients generated by the presence of the tunnel, and to a much lesser extent by the borehole itself.
- Over experimental timescales (~ 4 years) solute transport through the rock matrix is mainly by small-scale advection via an interconnected microfracture network and by diffusion.
- Over repository timescales diffusion of pore fluid/water from the rock matrix to the adjacent microfracture groundwaters will become more important depending on the nature of existing chemical gradients.
- At Äspö, permeable bedrock at all scales has facilitated the continuous removal and replacement of the interconnected pore space waters over relatively short periods of geological time, probably hundreds to a few thousands of years.

Contents

List of Appendices

Appendix 1. Smellie J, 1999. Äspö Hard Rock Laboratory Test Plan: Sampling of matrix fluids from low conductive bedrock. SKB IPR-00-01, Svensk Kärnbränslehantering AB.

Appendix 2. Lindblom S, 2000. Matrix Fluid Chemistry Experiment: Mineralogy, textural relations, fluid inclusion occurrences and basic petrology. Äspö Hard Rock Laboratory. SKB ITD-00-09, Svensk Kärnbränslehantering AB.

Appendix 3. Andersson C and Säfvestad A, 2000. Groundwater chemistry data from the groundwater sampling of KF0051A01 within the matrix fluid chemistry experiment (April, 2000). Äspö Hard Rock Laboratory. SKB ITD-00-13, Svensk Kärnbränslehantering AB.

Appendix 4. Smellie J A T, 2000. Äspö HRL, Matrix Fluid Chemistry Experiment: Minutes of the workshop held at SKB Stockholm, September 25–26, 2000. Äspö Hard Rock Laboratory. SKB ITD-00-17, Svensk Kärnbränslehantering AB.

Appendix 5. Smellie J A T (ed), 2000. Matrix Fluid Chemistry Experiment: Status Report (June 1998 – June 2000). SKB Äspö Hard Rock Laboratory Int. SKB IPR-00-35, Svensk Kärnbränslehantering AB.

Appendix 6. Tullborg E-L, 2001. Matrix Fluid Chemistry Experiment: Porosity and density measurements on samples from drillcore KF0051A01, Äspö Hard Rock Laboratory. SKB ITD-01-03, Svensk Kärnbränslehantering AB.

Appendix 7. Gustafsson E, 2001. Matrix Fluid Chemistry Experiment: Hydraulic character of the rock matrix. Äspö Hard Rock Laboratory. SKB ITD-01-07, Svensk Kärnbränslehantering AB.

Appendix 8. Blyth A, 2001. Matrix Fluid Chemistry Experiment: Fluid inclusion investigation of quartz. Äspö Hard Rock Laboratory. SKB ITD-01-06, Svensk Kärnbränslehantering AB.

Appendix 9. Smellie J, 2001. Matrix Fluid Chemistry Experiment: Minutes of the Workshop held at SKB, Stockholm, October 17–18, 2001. Äspö Hard Rock Laboratory. SKB ITD-02-02, Svensk Kärnbränslehantering AB.

Appendix 10. Waber H N, 2001. Matrix Fluid Chemistry Experiment: Mineralogy and fluid inclusion studies. Äspö Hard Rock Laboratory. SKB ITD-02-03, Svensk Kärnbränslehantering AB.

Appendix 11. Tullborg E-L, 2002. Matrix Fluid Chemistry Experiment: Borehole KF0051A01:4 m – Results from chemical and SEM/EDS analyses and porosity/density measurements. ÄspöHard Rock Laboratory. SKB ITD-02-04, Svensk Kärnbränslehantering AB.

Appendix 12. Gehör S and Lindblom S, 2002. Matrix Fluid Chemistry Experiment: Texture, microthermometry and La-ICP-MS investigations of fluid inclusions in drillcore KF0051A01 (5.03–10.95 m). Djupförvarsteknik. SKB TD-02-13, Svensk Kärnbränslehantering AB.

Appendix 13. Waber H N and Frape S K, 2002. Matrix Fluid Chemistry Experiment: Drillcore pore water leaching studies and borehole water. Djupförvarsteknik. SKB TD-03-02, Svensk Kärnbränslehantering AB.

Appendix 14. Lindblom S, Blyth A, Gehör S, Waber N and Frape S, 2002. Matrix Fluid Chemistry Experiment: Quartz-fluid interaction – Fluid inclusions and the matrix fluid. Synthesis of an inter-laboratory study. Djupförvarsteknik. SKB TD-02-08, Svensk Kärnbränslehantering AB.

Appendix 15. Blyth A and Frape S, 2002. Matrix Fluid Chemistry Experiment: Evolution of the Äspö groundwaters with time – Additional information from tritium and $\delta^{37}Cl$. Djupförvarsteknik. SKB TD-02-18, Svensk Kärnbränslehantering AB.

Appendix 16. Waber H N and Smellie J A T, 2003. Analytical data of waters and gases from the MFE-borehole, and boreholes KF0066A01 and KF0069A01 (Sampling Phase 3, February 2003).

1 Background

(J Smellie, Conterra)

1.1 Matrix pore fluids and saline groundwaters

Much of the undisturbed groundwater sampled from the Äspö site, mostly to depths of 500–600 m, has been collected from water-conducting fracture zones with high transmissivities ($T > 10^{-9}$ m^2s^{-1}). Consequently, these groundwaters probably obtain their chemical character mostly through mixing along fairly rapid conductive flow paths, determined by hydrodynamically active conditions rather than by chemical water-rock interaction. In this upper part of the bedrock sampled groundwaters show salinities which range generally from fresh to brackish near the surface (< 2 g/L chloride) to moderately saline at 500 m (5–6 g/L chloride). At depths greater than 500 m, where hydrodynamic conditions are less active, the salinity progressively increases with depth to a maximum of 12.3 g/L chloride at around 1000 m /Smellie and Laaksoharju, 1992; Smellie et al, 1995; Laaksoharju et al, 1999a/. On the mainland at Laxemar, groundwaters from borehole KLX02 recorded concentrations of around 45 g/L chloride at 1700 m where near-stagnant groundwater flow conditions are encountered /Laaksoharju et al, 1995/.

In contrast, little is known about groundwater compositions from low transmissive parts ($T < 10^{-10}$ m^2s^{-1}) of the bedrock. Under such conditions interaction with circulating groundwater is limited or essentially does not occur at all. Long residence times therefore are characteristic and the composition of the groundwaters is more likely influenced to varying degrees by the rock matrix pore fluid chemistry. The term ‘matrix pore fluid’ as used here includes all fluid types: a) the water in the pore space of a rock that is only accessible by diffusion, b) the water residing in dead-end pores, and c) the fluid enclosed in mineral fluid inclusions. The Matrix Fluid Chemistry Experiment aimed at initially characterising these different types of fluids using various laboratory methods and approaches. The final goal of the investigations was to characterise the in-situ ‘matrix pore water’, i.e. the water in the connected pore space of the rock matrix that is accessible for interaction with groundwaters circulating in nearby fractures.

Under undisturbed conditions the matrix pore fluids/waters in crystalline rock environments are suspected to be highly saline in composition, and this has been borne out by studies in Canada and the USA /Gascoyne et al, 1996; Couture et al, 1983/. There are several potential sources to this salinity /e.g. Lampén, 1992/, for example allothtonous sources such as: a) ancient Proterozoic (older than ~ 570 Ma) seawater or basinal brines, b) Palaeozoic (older than ~ 250 Ma) basinal brines, c) seawater and evaporites, and d) young Holocene (10–0 ka) brackish waters, and authochtonous sources such as: a) residual metamorphic/igneous fluids, b) hydrolysis of silicate minerals, and c) dissolution/leaching of salts present interstitially in the rock matrix. Under disturbed conditions, emphasising crystalline rocks, an additional source may derive from the rupture and/or dissolution of fluid inclusions (which may be allochtonous or authochtonous in origin) located in and/or around some of the major rock-forming minerals (mostly quartz).

It is generally accepted that no one process or source can account for the observed salinities in basement Shield areas and most reported occurrences seem to represent mixtures of meteoric water with a highly concentrated brine.

1.2 Repository performance assessment implications

The Swedish disposal concept recognises that the long-term integrity of the near-field engineered barrier system, over time periods of thousands to hundreds of thousands of years, is closely related to the long-term hydrogeochemical stability of the repository host rock. To model near-field processes, therefore, requires specific knowledge of the near-field input groundwater compositions during the expected lifespan of the repository. Based on earlier considerations, knowledge of the composition and origin of the matrix pore fluid/water should help provide a realistic hydrochemical input to near-field performance and safety assessment calculations, since deposition of spent fuel will be restricted to rock volumes of low transmissivity.

During undisturbed hydrochemical conditions at repository depths prior to the construction phase, rock volumes of low permeability may be characterised by highly saline matrix fluid. In contrast, less saline groundwaters are expected to characterise the more permeable rock volumes. During the operational phase of the repository (tens of years) changes in groundwater chemistry will be expected in rock volumes of high permeability, less so in low permeable rock volumes where much of the matrix pore fluid in the bulk of the rock away from hydraulically active fractures may well retain its pre-construction chemistry. During the post-closure period hydrodynamic equilibrium should be re-established relatively rapidly (tens to hundreds of years) in the more highly permeable rock volumes, including saturation of the bentonite and bentonite/sand backfill materials. Since these backfill materials will be in contact with rock volumes largely of low permeability, the chemical differential between the groundwaters saturating the backfill materials and the surrounding more highly saline rock matrix pore fluids might well result in an increase in salinity towards the backfills such that, with time, may cause deterioration of their physical properties. This may impact on the long-term stability of the repository.

Even though it has been argued that the Swedish engineered barrier system may not be particularly sensitive to high salinity /Andersson and Säfvestad, 2000/, limits have been set (up to 100 g/L TDS) and the expected near-field salinities need therefore to be quantified.

1.3 Objectives, scope and reporting of the experiment

Based on the above considerations the main objectives of the Matrix Fluid Chemistry Experiment (MFE) were:

- to determine the origin and evolution of the matrix pore fluids/waters;

- to establish whether present or past in- or out-diffusion processes have influenced the composition of the matrix pore fluids/waters, either by dilution or increased concentration;
- to derive a range of matrix pore water compositions as suitable input for near-field model calculations; and
- to establish the influence of water-conducting microfractures (when present) on the pore fluid/water chemistry in the rock matrix and vice versa.

The main scope of the experiment was:

- to sample matrix pore waters and dissolved gases from a selected area of low conductive bedrock typical for Äspö;
- to characterise the matrix pore waters and dissolved gases hydrochemically and isotopically;
- to hydraulically characterise the sampled sections;
- to mineralogically and geochemically characterise the corresponding drillcore material from the borehole sections sampled;
- to sample matrix pore waters and dissolved gases from contrasting rock types (if present) to establish the degree of bedrock geochemical control on the pore water and gas compositions; and
- to sample groundwaters from fracture zone(s) of low hydraulic conductivity to establish their hydrochemical character.

To successfully achieve these objectives depended on identifying a rock mass of low hydraulic transmissivity; this was successfully accomplished. Locating suitable bedrock to drill the MFE-borehole, together with the designing and construction of specialised downhole equipment to accommodate long-term sampling of matrix pore waters, commenced late 1997 and continued into early 1998. The MFE-borehole was drilled and completed in June 1998.

To address the project objectives, several major areas of investigation were involved:

- drillcore studies (geochemistry, mineralogy, petrology, fluid inclusions, porosity measurements);
- drillcore crush/leach experiments;
- matrix pore water sampling, analysis and interpretation;
- hydraulic character of the rock matrix; and
- hydraulic and hydrogeochemical characterisation of near-vicinity fractures/fissures of low hydraulic transmissivity ($< 10^{-10}$ m^2s^{-1}).

Details of the objectives, scope, rationale and experimental set-up are presented in /Smellie, 1999; Appendix 1/, and the half-way progress of the experiment is detailed in /Smellie, 2000; Appendix 5/. An international team was involved in the experiment with groups representing Sweden, Switzerland, Finland, France and Canada all participating. The major part of the experiment was concluded on schedule at the end of December, 2002, but an additional sampling campaign was carried out in February 2003.

The responsible investigators were:

Alexander Blyth	(University of Waterloo, Canada)
Joél Casanova	(BRGM, France)
Shaun Frape	(University of Waterloo, Canada)
Seppo Gehör	(Kivitieto Oy, Finland)
Erik Gustafsson	(Geosigma AB, Sweden)
Douglas Hirst	(University of Waterloo, Canada)
Janette Carnström	(SKB, Sweden)
Marcus Laaksoharju	(GeoPoint AB, Sweden)
Sten Lindblom	(Stockholm University, Sweden)
Christina Mattsén	(SKB, Sweden)
Karsten Pedersen	(Göteborg University, Sweden)
Ann-Sofie Svensson	(SKB, Sweden)
Anna Säfvestad	(SKB, Sweden)
Eva-Lena Tullborg	(Terralogica AB, Sweden)
Niklaus Waber	(University of Bern, Switzerland)
Bill Wallin	(Geokema AB, Sweden)

Ingvar Rhén (VIAK VBB, Sweden) was involved in the initial planning, drilling and borehole completion activities of the programme. Technical support was provided by Patrik Hagman (SKB, Äspö) and Lars Andersson (SKB, Äspö).

Documentation of the project (including Workshop proceedings) produced 13 Technical Documents (ITD/TD); the original Test Plan and the half-way stage of the Project were reported as International Progress Reports (IPR). Documentation covered the following issues:

1. **Smellie J, 1999.** Äspö Hard Rock Laboratory Test Plan: Sampling of matrix fluids from low conductive bedrock. SKB IPR-00-01, Svensk Kärnbränslehantering AB.
2. **Lindblom S, 2000.** Matrix Fluid Chemistry Experiment. Mineralogy, textural relations, fluid inclusion occurrences and basic petrology. Äspö Hard Rock Laboratory. SKB ITD-00-09, Svensk Kärnbränslehantering AB.
3. **Andersson C, Säfvestad A, 2000.** Groundwater chemistry data from the groundwater sampling of KF0051A01 within the matrix fluid chemistry experiment (April, 2000). Äspö Hard Rock Laboratory. SKB ITD-00-13, Svensk Kärnbränslehantering AB.
4. **Smellie J A T, 2000.** Äspö HRL, Matrix Fluid Chemistry Experiment. Minutes of the workshop held at SKB Stockholm, September 25–26, 2000. Äspö Hard Rock Laboratory. SKB ITD-00-17, Svensk Kärnbränslehantering AB.
5. **Smellie J A T (ed), 2000.** Matrix Fluid Chemistry Experiment. Status Report (June 1998 – June 2000). SKB Äspö Hard Rock Laboratory. SKB IPR-00-35, Svensk Kärnbränslehantering AB.
6. **Tullborg E-L, 2001.** Matrix Fluid Chemistry Experiment. Porosity and density measurements on samples from drillcore KF0051A01, Äspö Hard Rock Laboratory. SKB ITD-01-03, Svensk Kärnbränslehantering AB.

7. **Gustafsson E, 2001.** Matrix Fluid Chemistry Experiment. Hydraulic character of the rock matrix. Äspö Hard Rock Laboratory. SKB ITD-01-07, Svensk Kärnbränslehantering AB.
8. **Blyth A, 2001.** Matrix Fluid Chemistry Experiment. Fluid inclusion investigation of quartz. Äspö Hard Rock Laboratory. SKB ITD-01-06, Svensk Kärnbränslehantering AB.
9. **Smellie J, 2001.** Matrix Fluid Chemistry Experiment. Minutes of the Workshop held at SKB, Stockholm, October 17–18, 2001. Äspö Hard Rock Laboratory. SKB ITD-02-02, Svensk Kärnbränslehantering AB.
10. **Waber N, 2001.** Matrix Fluid Chemistry Experiment. Mineralogy and fluid inclusion studies. Äspö Hard Rock Laboratory. SKB ITD-02-03, Svensk Kärnbränslehantering AB.
11. **Tullborg E-L, 2002.** Matrix Fluid Chemistry Experiment. Borehole KF0051A01:4 m – Results from chemical and SEM/EDS analyses and porosity/density measurements. Äspö Hard Rock Laboratory. SKB ITD-02-04, Svensk Kärnbränslehantering AB.
12. **Gehör S, Lindblom S, 2002.** Matrix Fluid Chemistry Experiment. Texture, microthermometry and La-ICP-MS investigations of fluid inclusions in drillcore KF0051A01 (5.03–10.95 m). Djupförvarsteknik. SKB TD-02-13, Svensk Kärnbränslehantering AB.
13. **Waber N, Frape S, 2002.** Matrix Fluid Chemistry Experiment. Drillcore pore water leaching studies and borehole water. Djupförvarsteknik. SKB TD-03-02, Svensk Kärnbränslehantering AB.
14. **Lindblom S, Blyth A, Gehör S, Waber N, Frape S, 2002.** Matrix Fluid Chemistry Experiment. Quartz-fluid interaction: Fluid inclusions and the matrix fluid. Synthesis of an inter-laboratory study. Djupförvarsteknik. SKB TD-03-08, Svensk Kärnbränslehantering AB.
15. **Blyth A, Frape S, 2002.** Matrix Fluid Chemistry Experiment. Evolution of the Äspö groundwaters with time – Additional information from tritium and $\delta^{37}Cl$. Djupförvarsteknik. SKB TD-02-18, Svensk Kärnbränslehantering AB.

Since the ITD/TD technical reports were for limited internal distribution only, this final report has included all reported data, not included in the main report chapters, as a series of 16 appendices.

2 MFE-borehole (KF0051A01)

(J Smellie, Conterra, A Säfvestad and C Mattesén, SKB, G Nilsson, JAA AB, Geosigma AB and I Rhén, VIAK VBB)

2.1 General

Initially it was considered to drill 4–5 boreholes at Äspö in bedrock of low to intermediate hydraulic transmissivity, at different depths and in different lithologies, allowing a comparison of potential matrix pore fluid/water chemistry with: a) increasing depth, b) differing lithology, and c) the presence or absence of nearby fractures/fissures. This programme was subsequently restricted to one borehole (Matrix Fluid Experimental (MFE) borehole) at one site in order to test both the robustness of the sampling equipment and also to determine if the sampling of matrix pore fluids/waters was altogether possible.

2.2 Location

On the basis of available data from geological, hydrological and tunnel construction activities from the Äspö HRL, and several reconnaissance trips, five potential locations were considered from tunnel sections characterised by:

- low fracture frequency; very few water-conducting fractures;
- homogeneous and similar rock-types (Äspö diorite and Småland Granite locally referred to as Ävrö granite);
- low transmissivity in probeholes;
- absence of grouting;
- possible access to tunnel niches to facilitate drilling; and
- additional information, for example in the vicinity of earlier (or on-going) studies (e.g. TRUE Experiment; Prototype Repository Experiment; Chemlab Experiment; Microbe Experiment; Pillar Stability Experiment) where groundwater sampling had been carried out and hydrogeochemical data existed.

The final selection of the borehole location was based on several criteria:

- that the experiment should be conducted at repository depths (~ 500 m);
- that the tunnel section chosen should be dry and free from water-conducting fractures;
- that the rock be macroscopically homogeneous, i.e. minimum potential influence from variations in composition;
- that there should be minimum future disturbance from tunnel activities; and
- that drilling could be carried out with minimum disturbance to tunnel activities.

Five locations were considered, and their respective priorities are summarised below; Priority (1) in Tunnel ‘F’ was selected (Table 2-1; Figure 2-1).

Table 2-1. Summary of the five locations selected for consideration.

Tunnel section (m)	Vertical depth (m)	Rock-type	Comments	Priority
2375	~ 320	Äspö diorite	Niche at 2375 m	3
2520	~ 345	Äspö diorite	Tunnel curve location	2
3010	~ 415	Ävrö granite	Near-vicinity of True Project	4
3375	~ 445	Ävrö granite	Vicinity of shaft lift	5
L = 51	~ 450	Äspö diorite	Tunnel 'F'	1

Priority (1) fulfilled most of the criteria listed above.

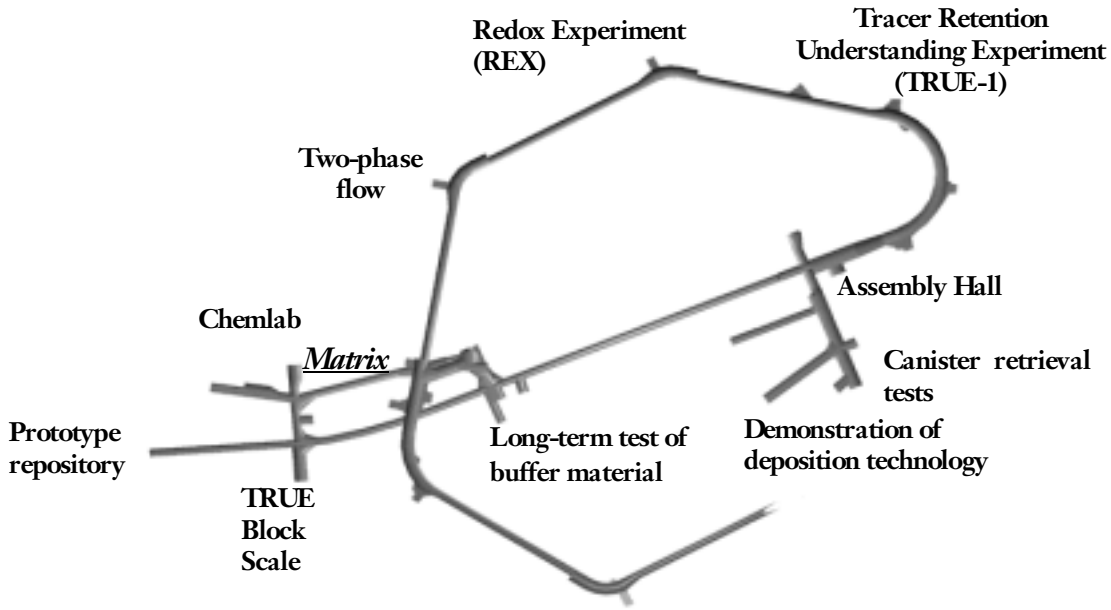

Figure 2-1. *Äspö HRL: Location of Matrix Fluid Borehole in Tunnel 'F' relative to the other experiments.*

2.3 Drilling

Drilling of the borehole was carried out on 26th May, 1998 according to the protocol detailed in /Smellie, 1999; Appendix 1/. To minimise potential groundwater contamination well characterised formation groundwater from borehole KA2598A (in the near-vicinity of Tunnel 'F') was used as flushing water; a total of 9.7 m^3 of water were used (Table 2-2). The flushing water is normally spiked with uranine so that subsequent water samples can be evaluated for contamination incurred during drilling. Furthermore, all borehole drilling activities were carried out under pressurised nitrogen gas to maintain reducing conditions in the borehole.

The first 2.10 m of the borehole were core drilled with a diameter of 131 mm to allow the installation of a special casing that could resist the high hydraulic head at this depth. In addition, this installation would effectively seal-off any potential influence from the Excavation Damage Zone (EDZ) bordering the tunnel. The casing was first glued and bolted in position and then a valve arrangement was mounted to secure the drilling rig; core drilling with a diameter of 76.2 mm then commenced through the valve. From start to finish the drilling operation took 24 hours and a total length of 11.70 m were drilled at an upwards inclination of ~ 30°; at all times an overpressure of nitrogen gas was applied. Following drilling the borehole was cleaned with flushing water, purged with nitrogen and then closed by bolting a metal cover over the casing opening; special inlet valves through the anchoring plate allowed pressurised nitrogen to circulate along the borehole.

The drillcore material was mapped as soon as possible to avoid undue evaporation of the matrix pore fluid prior to preservation. Long-term preservation was planned by first wrapping the drillcore in aluminium foil followed by a complete wax coating. This procedure, unfortunately, was not implemented by the field personnel, the core being first waxed and then wrapped in the aluminium foil.

Table 2-2. Chemistry of groundwater from borehole KA2598A used for drilling and cleaning the MFE-borehole.

Borehole KA2598A	
pH (lab)	7.50
	mg/L
Li	0.65
Na	1880
K	9.3
Ca	1215
Mg	82.5
Sr	17
Cl	5210
Br	27.6
SO_4	344
HCO_3 *	99
Si	5.6

* HCO_3 calculated from measured total alkalinity.

On May 28th the borehole was reopened, an overpressure of nitrogen applied and the TV-image logging (BIPS) carried out. The borehole was then closed apart from allowing nitrogen gas to circulate via the casing inlet valves. Results of the drillcore mapping (cf Appendix 5) and BIPS logging (cf Appendix 2) confirmed the chosen locality to be devoid of major open fractures and with no evidence of groundwater entering the borehole. Based on this information two borehole sections were chosen to sample matrix fluids. These were selected:

- to avoid any tunnel excavation damage zone (EDZ) that might have extended beyond the 2.1 m casing length – otherwise hydraulic short-circuiting may occur around the packer systems;
- to include a texturally homogeneous rock, and
- to avoid any kind of fractures, open or sealed.

The borehole sections chosen were 4.66–5.26 m and 8.85–9.55 m respectively. Fortuitously the former was located within the Äspö diorite and the latter within the Ävrö granite, thus providing the opportunity to establish if lithological differences influenced in any way the chemistry of the rock matrix pore fluids/waters.

2.4 Completion

The MFE-borehole completion was carried out on June 12th, 1998. Since the borehole activities two weeks earlier, an overpressure of circulating nitrogen gas had been maintained in the borehole to minimise oxidation effects.

The designed downhole packer equipment was constructed to exclude any contact between groundwater and metal which may have resulted in unwanted long-term reactions. All metal parts were therefore teflon coated and PEAK© tubing was used throughout; the packer material used was polyurethane to further minimise organic contamination. To reduce the dead volume space in the sampling sections, peak dummies were added (Figure 2-2). Finally, to ensure a 'microbe-free' environment, all internal parts of the packer equipment and peak tubing were cleaned in the laboratory with formaldehyde, purged with ultra-pure nitrogen and then sealed prior to transport to the tunnel. The presence of microbes may give rise to unwanted iron-oxidising and/or sulphate-reducing reactions which may alter the chemistry of sampled pore waters and may cause precipitation/clogging in the fine tubing preventing fluid flow.

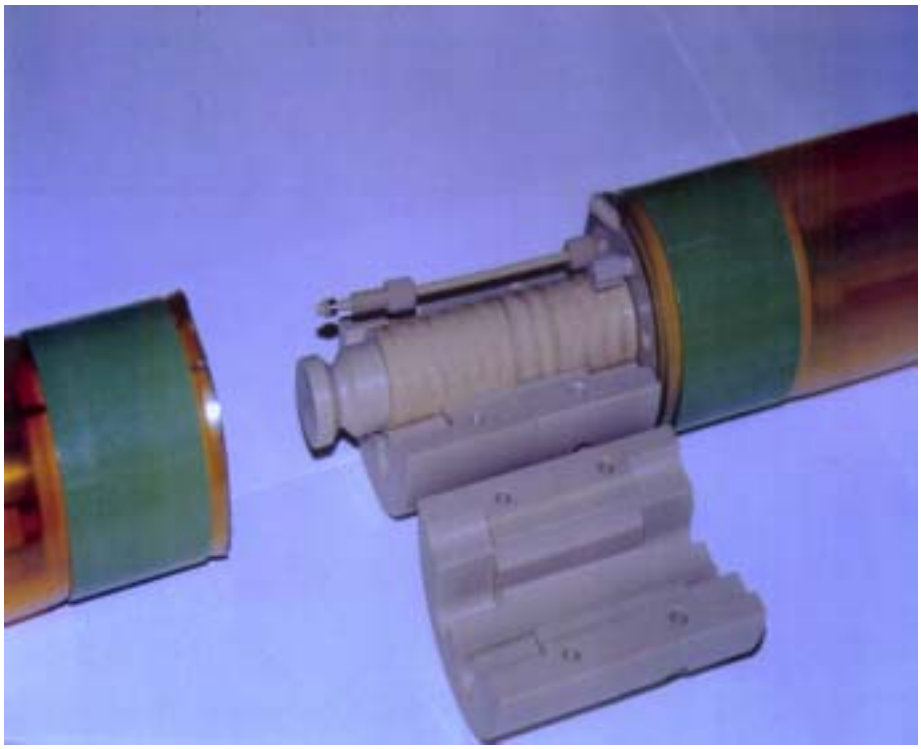

Figure 2-2. *Sampling Section 4 (length 0.6 m; see Figure 2-3) showing the design of the* PEAK© *dummy material to reduce the dead volume space. Packer material (brown colour) at either side is of polyurethane.*

Since the main emphasis during installation of the borehole equipment (Figure 2-3) was to ensure as much as possible a 'microbe-free' and 'oxygen-free' environment in the borehole, the following sequence was carried out:

- pressurised nitrogen gas was continuously circulated in the borehole during all activities;
- the borehole was first flushed with a high-pressure nitrogen spray containing 30% ethanol to destroy any existing microbes;
- the external parts of the packer/sampling system were cleaned with formaldehyde;
- the packer system was quickly inserted into the borehole and the packers inflated; and
- the PEAK© tubing ends were opened and quickly connected to the sampling and pressure monitoring cabinet fixed to the tunnel wall.

Table 2-3 lists the parameters of the isolated sections following borehole completion.

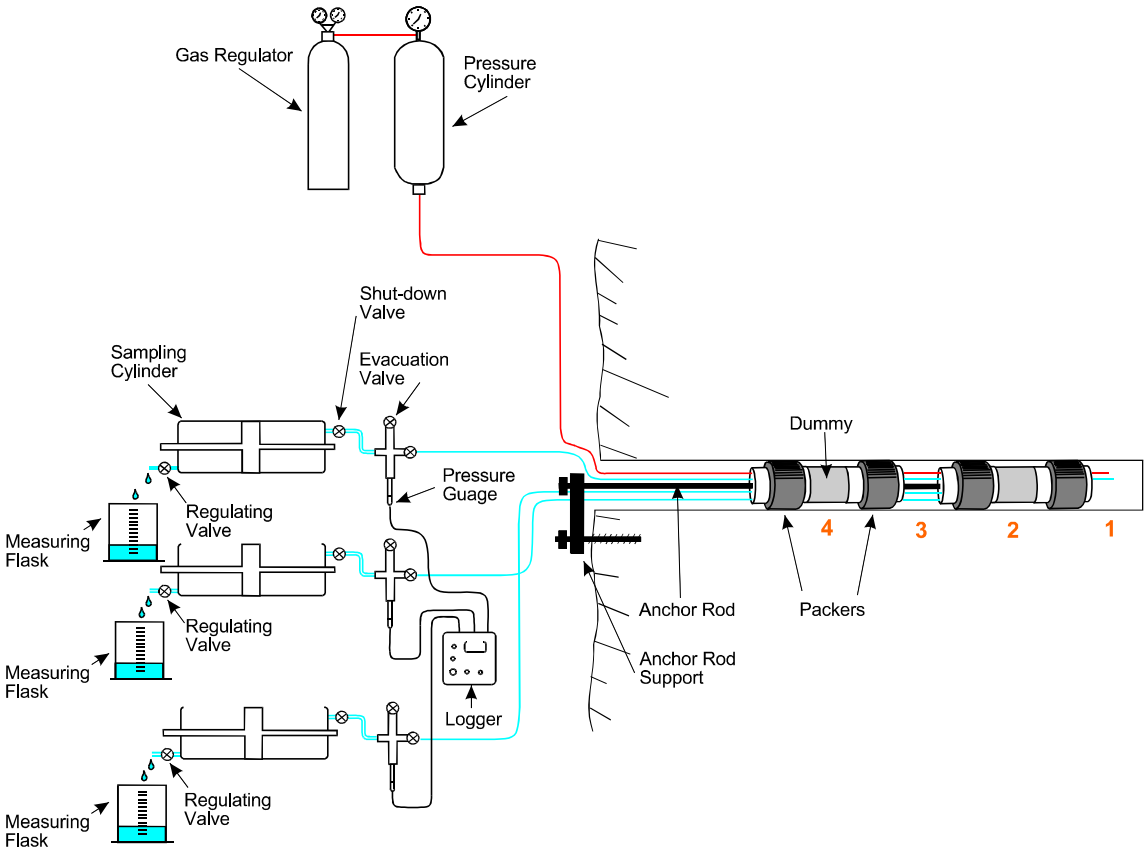

Figure 2-3. *Matrix Fluid Chemistry Experiment (MFE) set-up. MFE-borehole sections 2 and 4 were specifically selected to collect matrix pore water; sections 1–4 were continuously monitored for pressure. The contact between Äspö diorite and Ävrö granite occurs in section 3 at 8.5 m.*

Table 2-3. Borehole completion: Parameters of the isolated sections (P = pressure monitoring; S = sampling).

Borehole section	S/P	Length[+] (m)		Total volume (mL)	Residual* volume (mL)
1	S/P	10.55–11.80	(1.25)	5461	76
2	S/P	8.85–9.55	(0.70)	245	–
3	S/P	6.26–7.85	(1.59)	6237	7
4	S/P	4.66–5.26	(0.60)	210	20

[+] numbers in brackets refer to borehole section lengths.
* volume of collected water remaining in the borehole sections after sampling due to equipment design and borehole geometry.

2.5 Monitoring

With the outlet valves to the sampling cylinders closed, continuous monitoring of pressure in the four borehole sections using the HMS (Äspö Hydraulic Monitoring System) commenced directly after installation of the packer/sampling equipment and continued for the duration of the experiment (Figure 2-4). When the MFE-borehole was finally sealed the pressure in the isolated borehole sections was close to, but still less than the hydrostatic pressure. Any increase in pressure therefore should indicate a build-up of gas and/or matrix pore water diffusing into the isolated borehole sections from the host rock. Figure 2-4 shows the pressure curves from start to finish of the experiment (June 1998 to March 2003); the break in the curves in December 1999, October 2001 and February 2003 indicates the three sampling campaigns when sections 1 and 4 (first campaign), sections 1 to 4 (second campaign) and sections 1 to 4 (third sampling campaign) were opened for sampling.

As indicated above, pressure increases do not necessarily indicate that pore waters are accumulating. Several processes may be interacting, for example, two or three phase diffusion processes involving nitrogen (out-diffusion), and matrix gases and/or matrix pore fluids (in-diffusion). If these in- and out-diffusion processes balance out then little or no pressure increase would be expected in the isolated borehole sections. In any case, the out-diffusion of nitrogen, accompanied by a gradual pressure decrease, might be expected to characterise the initial stages of the experiment. This is suggested in Figure 2-4 by borehole sections 1 and 4; in contrast, Section 2 shows only a brief decrease followed by an increase and then a gradual decrease. A sharp increase in the early stages is shown by Section 3 before levelling off.

After March 1999, however, the system appears to have stabilised and, as might be expected from the section volumes, Section 4 (210 mL) showed a steady increase to a maximum in December 1999 before levelling off. At this stage borehole sections 4 and 1 were opened and sampled for fluids explaining the sharp drops in pressure; however only gas was released from Section 1. Section 2 (245 mL), also demarcated for sampling, in contrast showed a much more gradual increase which was allowed to continue to the second sampling campaign in October 2001 when all four borehole sections were opened. As might be expected from the large borehole volumes, Section 1 (5461 mL) and Section 3 (6237 mL) showed no marked response, although a small increase in Section 3 to October 2001 was suggested from the curves. Due to impending excavation activities close to the MFE-borehole which were expected to disturb the experiment, the third sampling campaign in February 2003 was carried out before total recovery of the borehole sections.

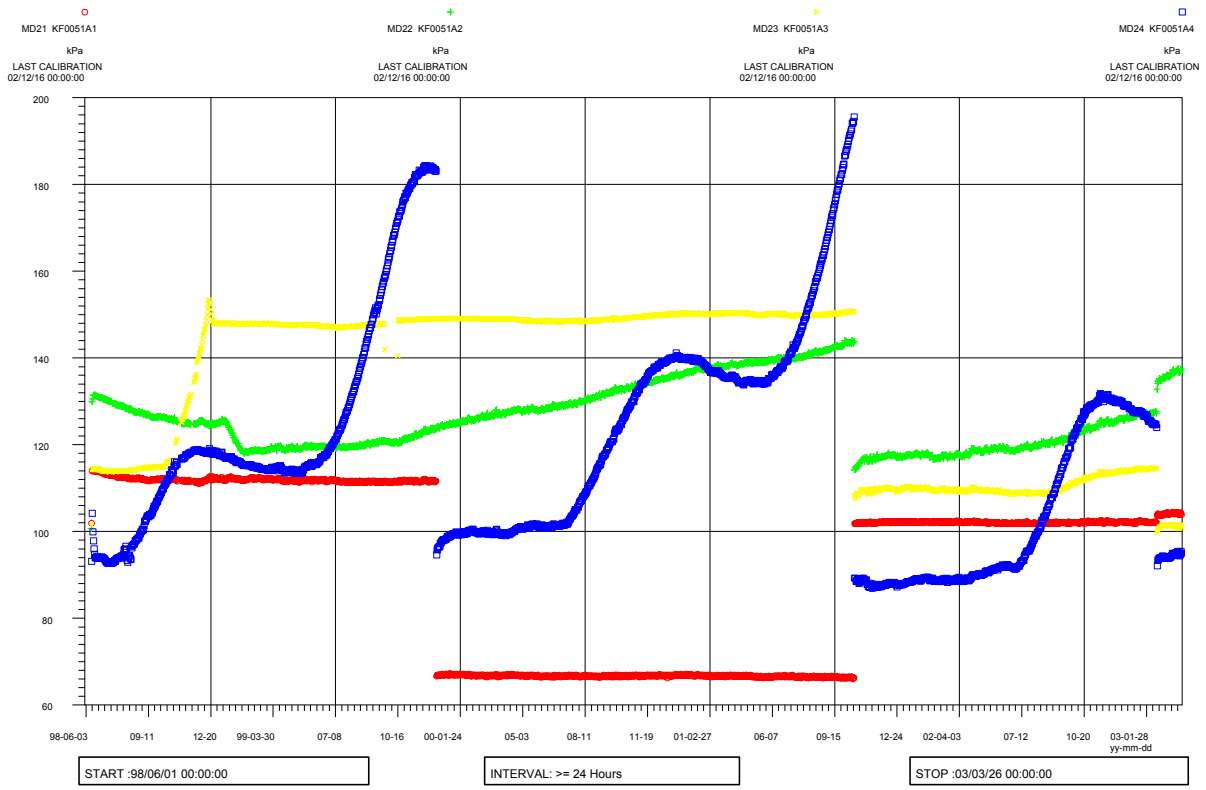

Figure 2-4. *Pressure monitoring curves for each of the four isolated MFE-borehole sections for the duration of the experiment (up to March 2003). Colours relate to borehole sections 1(red), 2 (green), 3 (yellow) and 4 (blue). Sections 2 and 4 were specifically demarcated for matrix fluid sampling. The break in the curves in December 1999, October 2001 and February 2003 indicates the three sampling campaigns when sections 1 and 4 (first), sections 1 to 4 (second) and sections 1 to 4 (third) were opened for sampling.*

An interesting observation is the shape of the Section 4 pressure curves. The small pressure decrease at the beginning of the experiment is not reflected in the following two sampling campaigns; as suggested above this may support some out-diffusion of nitrogen gas after the initial isolation of the borehole sections. However, it is the subsequent increase followed by a slight decrease and then a sharp increase that still has not been explained satisfactorily.

2.6 Sampling and analysis

Sampling of selected borehole sections for matrix pore water was carried out on three occasions; December 1999, October 2001 and February 2003. Details of the sampling campaigns, volumes of water collected and the analytical protocol are given in Table 2-4. The results, discussion and interpretation of the hydrochemical data are detailed in Chapters 6 and 7.

Table 2-4. Sampling and analytical protocols.

Borehole section (m)	Sampling date	Volume available (mg/L)	Volume collected (mg/L)	Analysis performed
1				
(10.55–11.80)	1999-12-07	5461	(only gas)	–
	2001-10-16	5461	(no gas/water)	–
	2003-02-13	5461	(no gas/water)	–
2				
(8.85–9.55)	1999-12-07	245	Not opened	–
	2001-10-16	245	35	pH, Alk, Na, K, Mg, Ca, Fe(tot), Si, F, Cl, Br, SO_4, Li, Sr, Mn, $\delta^{18}O$, δD, $\delta^{37}Cl$, $^{87}Sr/^{87}Sr$
	2003-02-13	245	17	pH, $\delta^{18}O$, δD, $\delta^{37}Cl$, $^{87}Sr/^{87}Sr$
3				
(6.26–7.85)	1999-12-07	6237	Not opened	–
	2001-10-16	6237	321	pH, Alk, Na, K, Mg, Ca, Fe (tot), Si, F, Cl, Br, SO_4, Li, Sc, Mn, $\delta^{18}O$, δD, $\delta^{37}Cl$, ^{14}C, $\delta^{13}C$, $^{87}Sr/^{87}Sr$
	2003-02-13	6237	117	pH, Alk, F, Cl, Br, SO_4,, $\delta^{18}O$, δD, $\delta^{37}Cl$, ^{14}C, $\delta^{13}C$, $^{87}Sr/^{87}Sr$
4				
(4.66–5.26)	1999-12-07	210	160	pH, Alk, Na, K, Mg, Ca, Fe (tot), Si, F, Cl, Br, SO_4, Li, Sc, Mn, Rb, Sr, Y, Cs, Ba, La, Ce, Nd, Th, U $\delta^{18}O$, δD, $\delta^{37}Cl$, $\delta^{10}B$, $^{87}Sr/^{87}Sr$
	2001-10-16	210	195	pH, Na, K, Mg, Ca, Fe(tot), Si, F, Cl, Br, SO_4, Li, Sr, Mn, $\delta^{18}O$, δD, $\delta^{37}Cl$, $^{87}Sr/^{87}Sr$
	2003-02-13	210	110	pH, F, Cl, Br, SO_4, $\delta^{18}O$, δD, $\delta^{37}Cl$, ^{14}C, $\delta^{13}C$, $^{87}Sr/^{87}Sr$

Alk = total alkalinity.

2.7 MFE-drillcore investigations

Not only is it important to sample and characterise the matrix pore waters, but also to understand their origin and how they move through the rock matrix. To address these issues a thorough understanding of the mineralogy, petrology, geochemistry and petrophysics of the rock mass is of paramount importance. To this end the MFE-drillcore, in particular those portions representing the borehole sections sampled, underwent a detailed characterisation to distinguish between accessible and inaccessible pore space fluids/waters. This rock material was supplemented by other drillcore sections selected, for comparative purposes, to represent variations in lithology (and therefore geochemistry) characteristic of the Äspö site as a whole. The coordinated approach employed is outlined in Figure 2-5.

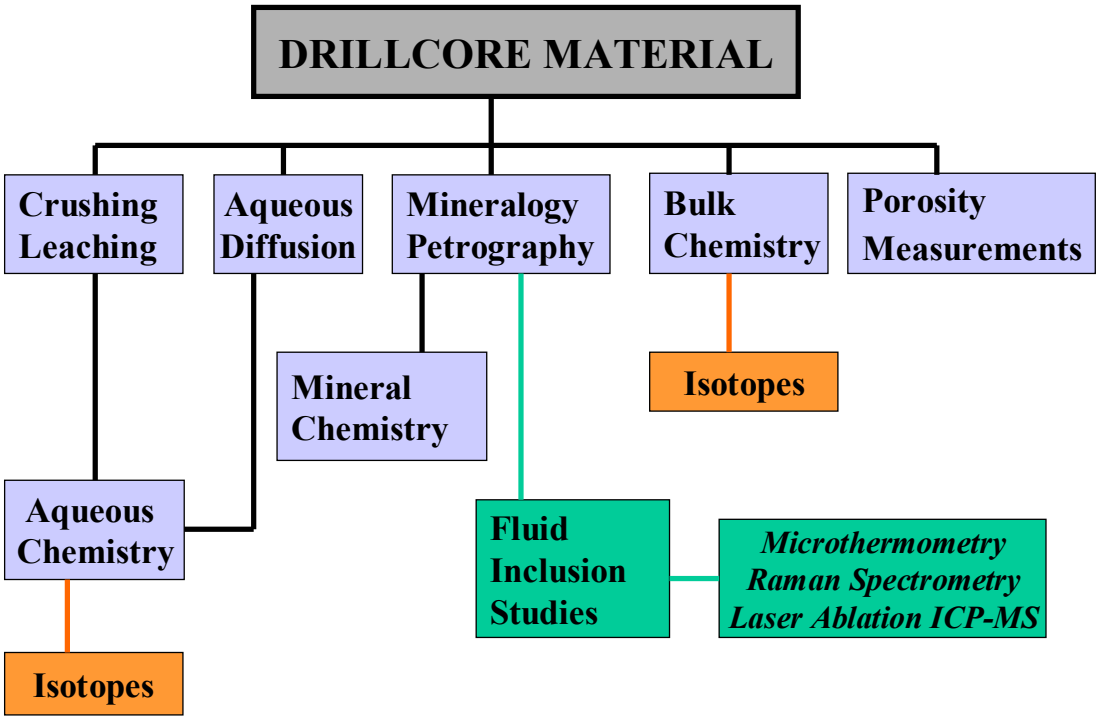

Figure 2-5. *MFE-drillcore: Investigative protocol.*

The following studies of the MFE-drillcore were structured to try and differentiate between accessible and inaccessible matrix pore fluids and determine their composition and origin:

- Mineralogy and fluid inclusion studies to initially identify where most of the inaccessible matrix fluids are located. Note however that fractured or decrepitated fluid inclusions may indicate past, present or on-going leakage of fluid into the matrix pore system.
- Crush/leach experiments on whole-rock samples were carried out in two stages: a) coarse crush and leach to obtain a general idea of the expected matrix pore fluid composition, and b) refined step-wise approach where successively finer size rock fractions (and also mineral separate fractions) were leached with the ultimate hope of determining the intergranular and interstitial fluid compositions (i.e. excluding fluid inclusions and crystalline mineral phases with matrix-bound salts).
- Laboratory permeability test to try and force out unbound accessible pore water from a rock matrix sample using deionised water. The main attraction of this experiment was to avoid many of the inherent uncertainties associated with mineralogical interpretation and the crush/leach experiments.
- Laboratory diffusion experiments on drillcore material to extract the accessible pore waters.
- Porosity measurements to provide an important basis for the understanding of pore fluid/water movement through the rock matrix.

3 MFE-borehole: Characterisation of drillcore rock material

3.1 Background

(S Lindblom, Stockholm University)

The Äspö diorite and Ävrö granite encountered in the MFE-borehole belong to the suite of postorogenic magmatic intrusions associated with the Småland-Värmland batholith and dated to within the range of 1760–1840 Ma /Jarl and Johansson, 1988/. These postorogenic granitoid intrusions followed the main culmination of an E-W trending orogenic zone, the Svecofennian, which was active some 1900 to 1600 Ma ago in the Bergslagen area. In the Oskarshamn region, later intrusive activity occurred between 1350–1400 Ma ago. The intrusion of dolerite dykes which occurred between 1000–900 Ma ago appears to be the latest magmatic event to influence the Äspö region. The time span of over 1500 Ma since the Svecofennian orogeny has not been characterised by any other major geotectonic event. However, considerable sedimentation (and subsequent erosion) of largely unknown proportions may have covered the area as indicated by remnants of Jotnian sandstone and Cambro-Silurian formations. During the late Pleistocene and the Holocene, the area was subjected to several glaciation cycles covering a span of around 750 ka /Imbrie and Imbrie, 1980/. The most recent major influence in the Äspö region is represented by the last glaciation, which culminated in a 3 km ice cap over Fennoscandia some 10 ka ago.

Structurally, regional lineament interpretation /Tirén et al, 1987/ in the Simpevarp region points to the intersection of four main lineament sets; an older one trending NW-SE and E-W and a younger one trending N-S and NE-SW. These sets form an orthogonal pattern and presumably reflect the dominant fracture zones in the area. Of the four lineament sets, the N-S and E-W sets dominate producing a suborthogonal first order system of lineaments. The other lineament sets, the NW-SE and NE-SW trending features, represent second order zones of a second almost orthogonal system. In general, the northern part of the region is characterised more by the NW-SE set and the southern part by the NE-SW set. Äspö island is located precisely at the intersection of the E-W and NW-SW lineament systems.

3.2 Mineralogy and petrology

(N Waber, University of Bern, and S Linblom, Stockholm University)

The MFE-drillcore represents two main rock-types; a porphyritic variation of Äspö diorite adjacent to the tunnel and an Ävrö (or Småland) granite type away from the tunnel. Downhole BIPS images (cf Appendix 2, Figure A2-10) and drillcore logging support the location of the transition zone between diorite and granite at around 8.40–8.50 m, i.e. within borehole Section 3 (cf Figure 2-3). Particular attention was paid to the two borehole sections earmarked for matrix pore fluid sampling, i.e. Section 2 between 8.85–9.55 m and Section 4 between 4.66–5.26 m. The selected drillcore samples were studied by Optical Microscopy and X-Ray Diffraction techniques (XRD).

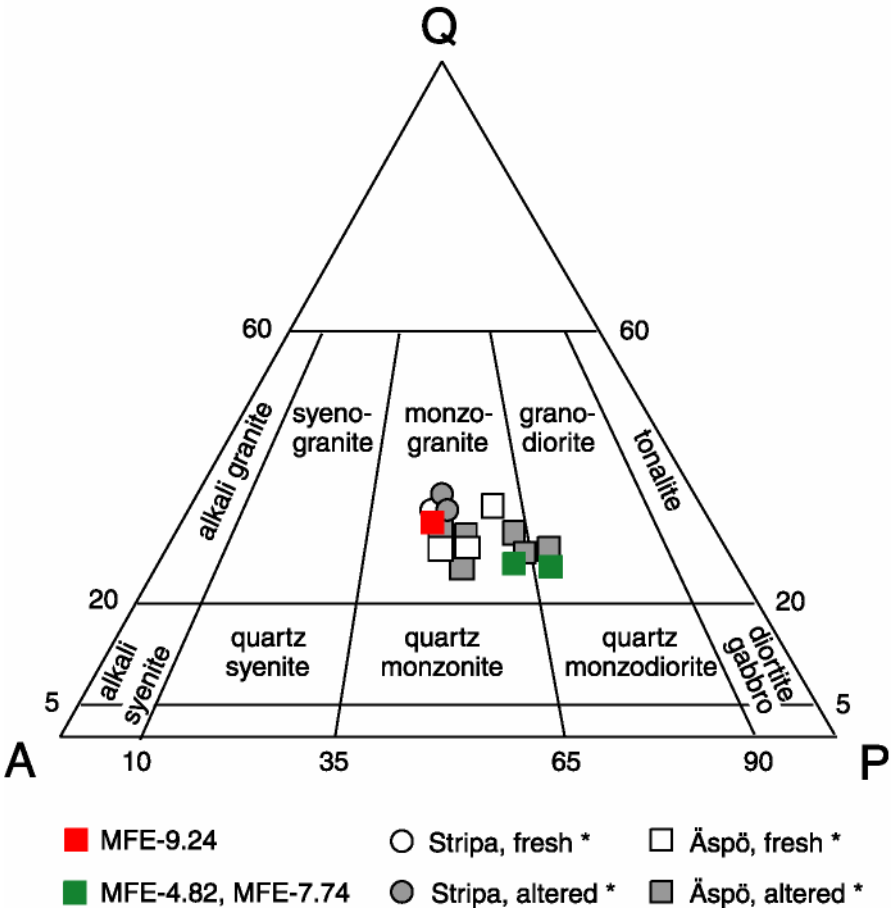

Figure 3-1. *Modal distribution of quartz, alkali feldspar and plagioclase (QAP) of Äspö diorite (green squares) and Ävrö granite (red square) from the matrix drillcore in comparison with fresh and altered crystalline rocks from the Äspö and Stripa sites /* data from Eliasson, 1993/.*

Results showed that, together with other studies at Äspö and also Stripa /e.g. Kornfält and Wikman, 1987; Eliasson, 1993/, the mineralogy conforms to a general monzogranite-type rock (Figure 3-1). Macroscopically, the Äspö diorite is greenish-grey to reddish-grey in colour and is medium- to coarse-grained with a porphyritic texture. The most noticeable features are the large K-feldspar phenocrysts which range up to 2 cm in diameter and are typically red in colour due to hydrothermal haematite staining. The Ävrö granite is more equigranular and lighter in colour reflecting its lower content in mafic minerals (cf Appendices 2 and 10).

In both rock types the main rock-forming mineral phases are in decreasing amounts, plagioclase, quartz, K-feldspar, biotite (often altered to chlorite), epidote, sphene and muscovite with accessory amounts of opaque phases (magnetite, pyrite), apatite and zircon (Table 3-1). A decrease in mafic content and plagioclase is countered by an increase in quartz and K-feldspar along the drillhole representing the transition of Äspö diorite to Ävrö granite. Veinlets containing calcite, prehnite and clay minerals are also sporadically present.

The feldspars consist of microcline and oligoclase; microcline, the dominant K-feldspar, is sometimes perthitic. Occasionally myrmeckite is observed at the grain boundaries of oligoclase, the primary plagioclase. Alteration is sometimes considerable within the feldspar grains giving them an almost opaque character under transmitted light. Alteration of microcline includes sericitisation and haematite staining, and alteration of primary plagioclase includes albitisation and strong saussuritic alteration with secondary epidote, calcite and sericite/muscovite. Along microfractures plagioclase displays a distinct argillaceous alteration similar to the otherwise better preserved K-feldspar.

Table 3-1. E-drillcore: Average modal values (wt%) of the major rock-forming minerals.

	Äspö diorite		Ävrö granite	
Sample	**MFE-4.82**	**MFE-6.43**	**MFE-9.11**	**MFE-10.90**
Plagioclase	40 ± 5	44 ± 5	38 ± 5	34 ± 5
Quartz	17 ± 3	17 ± 3	28 ± 3	26 ± 3
K-feldspar	7 ± 3	4 ± 3	18 ± 3	23 ± 3
Biotite	5–10	23	12	9
Epidote	5–10	x	x	2–3
Sphene	x[1)]	4	–	1–2
Muscovite	2–5	–	–	–
Apatite	x	–	–	–
Opaques	x	8	4	3–4

[1)] observed in trace amounts.

Quartz is mainly present in two grain-size fractions. The coarse-grained fraction consists of two generations and ranges in diameter from about > 300 μm to 1 mm. An older, magmatic generation shows internal deformation phenomena such as undulous extinction and microfracturing (cf Appendix 2, Figure A2-4; Appendix 12, Figure A12-1). These microfractures were subsequently healed at a later stage in the geological evolution. The second quartz generation, most probably of late magmatic origin, is less deformed. The edges of the large quartz crystals are recrystallised to smaller equidimensional grains (diameter of about 50–100 μm) which clearly show typical 120° triple points and an euhedral habit. A general feature is that quartz fills the pore space between microcline and plagioclase and it sometimes terminates in vuggy growth textures. Open vugs are still discernable and the feldspar crystals often have a perfect terminal shape towards the infilling quartz. All quartz types have abundant fluid inclusions within healed microfractures and along grain boundaries (Appendix 2, Figures A2-5 and A2-8; cf section 3.5)

Evidence of small-scale tectonic effects is common. For example, in many places the centres of quartz grains show healed microfractures now outlined with fluid inclusions. Even open delimited microfractures may be observed in the centre of quartz grains (cf Appendix 2, Figure A2-7). A special observation was noted at 5.45–5.55 m where a calcite-filled veinlet is lined with protruding euhedral quartz crystals. The quartz is stress-free, but the calcites show a slight deformation expressed as a network of rhombic cleavages.

Biotite is commonly altered to chlorite. Calcite, prehnite, epidote and clay minerals occur in the sporadically observed microfractures and as alteration products of the primary magmatic mineralogy. Despite the abundant very fine-grained haematite/limonite present, primary magnetite and (hydrothermal?) pyrite do not show oxidation phenomena.

The clay fraction of the microfracture-free rock matrix accounts for less than about 5% of the total rock volume and consists of illite/sericite (75–85%), illite/smectite mixed layers (5–15%) and chlorite (5–15%).

A decrease in mafic content and plagioclase is countered by an increase in quartz and K-feldspar along the MFE-borehole representing the transition of Äspö diorite to Ävrö granite. Importantly, the mineralogical composition of these two major rock types serves to constrain the matrix pore fluid composition. For example,

- the finely disseminated calcite will control the carbonate system of the pore fluid;
- to a certain degree cation exchange might also influence the pore fluid composition although the total clay content is rather small;
- the occurrence of reduced and oxidised Fe-oxides and Fe-hydroxides will have an impact on the redox potential of the pore fluid; and
- the present sulphide minerals also are very susceptible to changes in redox conditions.

3.3 Geochemistry

(N Waber, University of Bern, and S Linblom, Stockholm University)

In terms of whole-rock chemistry, typical major and trace element contents of the two rock-types encountered in the MFE-drillcore are given in Table 3-2 and Appendix 10. The major element compositions show the Äspö diorite to have higher CaO, Na_2O, Fe_{tot}, MgO, and TiO_2 than the Ävrö granite, but is lower in SiO_2, and K_2O. This is in accordance with the higher content of plagioclase, biotite, epidote, chlorite, sphene and opaque phases, and lower amounts of quartz and K-feldspar in the Äspö diorite.

Differences in the in trace element composition can also be associated with the different modal abundance of mineral phases. While Ba and Rb are mainly related to the occurrence of different feldspars and biotites, metallic elements such as Cr, Cu, Ni, and Pb have to be attributed to opaque phases such as magnetite and pyrite. In hydrogeochemical investigations Ba and Sr often represent important elements for the understanding of the sulphur and carbonate system. Since no single Ba or Sr mineral phases were detected and/or reported, it appears that these elements are associated mainly with feldspar, clay minerals and, for Sr, possibly calcite but more likely epidote.

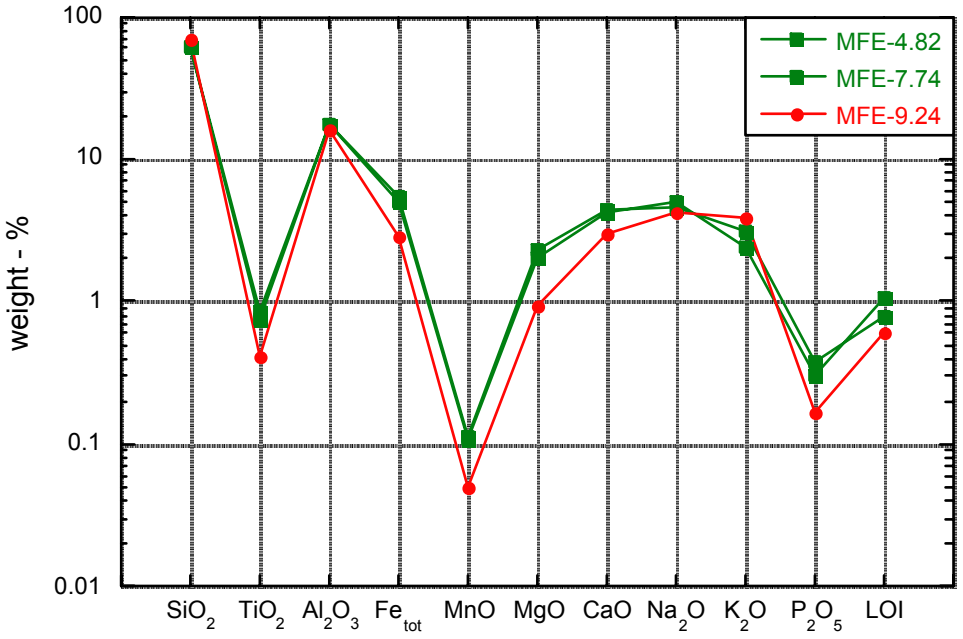

Figure 3-2. *Major element composition of the Äspö diorite (green) and the Ävrö granite (red) encountered in the MFE-drillcore. Differences in chemical composition are in accordance with the differences in modal mineral composition.*

Table 3-2. MFE-drillcore: Whole-rock chemistry.

Element		Äspö diorite		Ävrö granite
		MFE-4.82	**MFE-7.74**	**MFE-9.24**
Al_2O_3	wt%	17.46	17.8	16.0
CaO	wt%	4.15	4.51	3.04
Fe_{tot} as Fe_2O_3	wt%	5.13	5.45	2.91
K_2O	wt%	2.41	3.16	3.81
MgO	wt%	2.05	2.36	0.93
MnO_2	wt%	0.11	0.11	0.05
Na_2O	wt%	5.06	4.56	4.15
P_2O_5	wt%	0.31	0.38	0.16
SiO_2	wt%	60.17	60.9	68.9
TiO_2	wt%	0.75	0.87	0.42
LOI	wt%	1.09	0.8	0.6
Total	wt%	98.69	100.1	100.4
Trace Elements				
Ba	ppm	538	1030	1600
Be	ppm		1.93	1.73
Co	ppm		10.4	< 5.51
Cr	ppm	31	87.2	85.4
Cu	ppm	6	25.8	< 5.51
Ga	ppm		22.4	14.2
Hf	ppm		5.85	2.7
Mo	ppm		< 2.26	< 2.20
Nb	ppm	20	17.1	7.93
Ni	ppm	46	33.1	20.6
Rb	ppm	109	121	93.6
Sc	ppm		8.92	3.48
Sn	ppm		3	1.43
Sr	ppm	810	1180	1010
Ta	ppm		1.39	0.66
Th	ppm		5.83	3.68
U	ppm		2.58	2.11
V	ppm	74	77.7	31.4
W	ppm		0.79	0.65
Y	ppm	38	25.4	11.1
Zn	ppm	50	107	277
Zr	ppm	105	322	139
Ce	ppm		123	57.9
Dy	ppm		4.37	1.97
Er	ppm		2.17	0.95
Eu	ppm		1.48	0.87
Gd	ppm		5.92	2.86
Ho	ppm		1	0.40
La	ppm		44.8	22.7
Lu	ppm		0.45	0.19
Nd	ppm		58.2	24.8
Pr	ppm		16	7.11
Sm	ppm		8.25	3.23
Tb	ppm		0.93	0.38
Tm	ppm		0.54	0.20
Yb	ppm		2.08	1.03

3.4 Petrophysical measurements (density and porosity)

(E-L Tullborg, Terralogica, and N Waber, University of Bern)

3.4.1 General

Depending on the measurement technique applied different types of porosity are determined in a rock. For solute transport considerations it is important to understand what type of porosity contributes to what kind of transport. The following short summary about nomenclature and meaning of porosity in rocks of low-permeability is based on reviews by /Norton and Knapp, 1977; Freeze and Cherry, 1979; Domenico and Schwartz, 1990/ and /Pearson, 1999/.

The *physical* or *total porosity* of a crystalline rock is described by the ratio of (total) void volume to the total volume. Thus, the total porosity of a rock includes the volume not occupied by mineral grains such as pore spaces between mineral grains, microfractures, porous minerals (often secondary minerals) and fluid inclusions. The total porosity can be calculated from the bulk density of a dry sample and its grain density.

The *connected porosity* of a rock describes the volume of connected pores and is thus smaller than the total porosity. Values for connected porosity are often based on the measurements of the gravimetric water content, WC, of a sample (i.e. *water-content porosity*) or on sample impregnation techniques (e.g. *mercury-injection porosity*). Depending on rock mineralogy and texture, the values obtained by different methods might diverge due to, for example, the release of structured water during drying and the destruction of the original pore apertures by the required high impregnation pressures. Note also that localised variations in interconnected porosity may be influenced by stress-release mechanisms when deep cored samples are removed and transported to the laboratory.

For the description of fluid and solute transport through rock, the porosity accessible for transport is required. Transport of a substance can only take place through pores of which the minimum pore throat size is larger than the maximum size of the substance transported. Transport of a substance can take place either by advection or by diffusion. Groundwater hydrology is commonly interested in advective flow and transport, where the Darcy flux and the linear velocity of a tracer are related by the advective transport porosity. This *advective transport porosity* does not include isolated pores or dead-end pores and is thus smaller than the connected porosity.

In rocks of very low permeability, solute transport by diffusion might become important. The porosity accessible to diffusion, the *diffusion porosity*, is determined by various diffusion experiments (in-, out-, and through-diffusion). As for other porosity measurements, porosities derived from diffusion experiments might have different numerical values depending: a) on the rock texture (e.g. through-diffusion experiments performed parallel vs perpendicular to the foliation in a deformed crystalline rock or to the bedding in a sedimentary rock), and b) on the solute used in the experiments (e.g. ions with large hydration spheres vs ions with small hydration spheres). For diffusion of water molecules themselves the diffusion porosity becomes close to the water-content porosity, whereas for the diffusion of solutes the diffusion porosity is less than the water-content porosity, but higher than the advective transport porosity.

At Äspö, different porosity measurements were conducted at several localities as an integral part of other on-going experiments /Mazurek et al, 1997; Sundberg and Gabrielsson, 1999; Johansson et al, 1998/ and during the tunnel construction /e.g. Stanfors et al, 1993a,b/. Most commonly, the porosity was calculated from the gravimetric water content, which was determined by drying to stable weight conditions and/or water re-saturation of rock samples. Less frequently, He-pycnometric and Hg-injection techniques were also applied. The numerical values for porosities derived with different methods revealed rather small variations /Mazurek et al, 1997/. Yet, considering the overall small total porosity of the rocks at Äspö (generally < 1%) and taking the analytical accuracy of the methods into account, the observed differences still become significant when calculating, for example, the salinity of the pore fluid from aqueous leaching data and/or diffusion experiments. This underlines the necessity of utilising identical sampling and analytical protocols to allow a comparison of the data from different sample series. Furthermore, as emphasised above, comparison between different sampled series will also be influenced by the nature of the samples themselves, for example samples measured in the laboratory, in contrast to in-situ measurements, will have been subject to stress-release mechanisms whereby significantly higher interconnected porosities by a factor of two or more can be expected.

3.4.2 Parameters measured and methodologies employed

Petrophysical measurements were performed on MFE-drillcore material from the Äspö diorite and the Ävrö granite. In this respect it is important to recall that the Äspö diorite is richer in platy mafic minerals and that the foliation is more continuously developed compared to the Ävrö granite. This foliation is oriented between 45–60° to the drillcore axis.

At the Swedish National Testing and Research Institute, values for the total porosity were derived from measured bulk and grain density. Grain density measurements were carried out on ground rock samples (< 60 μm) by He-pycnometry. Total porosity, Φ_T, was then calculated according to

$$\Phi_T = [1-(\rho_{\beta/} \rho_\gamma] \quad (1)$$

where ρ_β is the bulk density and ρ_γ is the grain density.

The water content was determined by re-saturating the dried drillcore samples (cf Appendix 6, Figure A6-1). Samples of 5 cm in lengths were first dried at 110°C until a constant weight was reached (minimum for 24 hours), then stored at room temperature under controlled conditions for 24 hours before the dry weight was measured. The samples were then saturated with water until stable conditions were achieved after which the samples were weighed again. The gravimetric water content, WC, was as the difference between dry and water saturated (wet) weight:

In the Swedish studies the volume percent water content (Φ_{Tc}) was calculated by:

$$\Phi_{Tc} = (WC_{wet}/\rho_{water})/(DW/\rho_\beta)* 100 \quad (2a)$$

where:
Φ_{Tc} = Connected porosity based on water saturation.
DW = Dry Weight of the sample.

At Bern, the water-content porosity was calculated by:

$$\Phi_{WC} = \frac{WC_{wet} \cdot \rho_{grain}}{WC_{wet} \cdot \rho_{grain} + (1 - WC_{wet}) \cdot \rho_{water}} \qquad (2b)$$

For the Äspö diorite and the Ävrö granite it was assumed that the water-content porosity measured represented maximum values of the connected porosity in these rocks due to rock-stress influences incurred following removal and storage of the drillcores prior to examination.

As mentioned earlier, the MFE-drillcore was erroneously sealed with low-density beeswax immediately after the drilling to prevent evaporation. This unfortunate circumstance allowed, however, density and water re-saturation measurements to be performed before and after removal of the wax, therefore allowing the potential influence of the rock foliation on the measurements to be evaluated. This was achieved by initially carrying out measurements on a sequence of 5 cm long cylindrical core samples where the cylinder surfaces were still coated with wax except for the bottom and top planes, which were exposed to water. Subsequently, the outermost 3–6 mm of the core rim was removed by sawing and the samples were again analysed for density and water re-saturation. Following this, the samples were dried and weighed a second time.

A simple impregnation technique using ink was applied to two samples, one Äspö diorite and one Ävrö granite, to visually locate the connected porosity network in the rock matrix. Three different cuts were used (parallel to foliation, parallel to core axis, and perpendicular to foliation). Thin-sections were prepared from all three cuts and studied in transmissive light.

The water content was determined gravimetrically by drying rock chips of 3–6 cm^3 at 105°C for 24 hours (Phase 1), 24 and 48 hours (Phase 2), and 48 and 168 hours (Phase 3). The rock chips were obtained from the wax-coated drillcore by removing the outermost 5–10 mm of the core with a hammer and chisel. Thereby it was assumed that the central part of the core was still fully saturated. The water-content porosity was calculated according to equation (2b) and based on the wet weight of the samples.

The saturation state of drillcore samples was investigated on cores from borehole KF0093-A0 received for diffusion experiments (cf Chapter 5, section 5.5). Borehole KF0093-A0, drilled to carry out stress release measurements related to the Pillar Stability Experiment, is located some 30 m from the matrix borehole within the same structural block area in the 'F' Tunnel. To prevent evaporation, these drillcores were first wrapped in aluminium-foil and then sealed with a wax-coating immediately after core recovery. The drillcore investigated consisted of Äspö diorite cross-cut by an aplitic dyke of about 10 cm in thickness. There were no apparent differences in the mineralogy and texture of this rock material compared to the Äspö diorite and aplitic dyke (e.g. sample MFE-3.85) of the matrix borehole.

The *degree of saturation*, S, is the ratio of water-filled to total pore space accessible for water, (V_{wat}/V_{pores}) and the *volumetric moisture content*, θ, is the ratio of water-filled pore space to total volume (V_{wat}/V_{tot}). Degree of saturation and volumetric moisture content are thus related by:

$$\theta = S \bullet \Phi_{tot} \quad (3)$$

3.4.3 Bulk density, grain density and total porosity

The average bulk density determined on the samples with the wax removed was 2.748 g/cm^3 for the Äspö diorite and 2.678 g/cm^3 for the Ävrö granite (Table 3-3). A larger variation was observed for the diorite (2.731–2.766 g/cm^3) compared to the granite (2.675–2.679 g/cm^3), consistent with the greater textural heterogeneity of the diorite. Bulk densities obtained for the samples still coated with low-density wax were identical to these values, except for one sample (Table 3-3).

The average grain density determined by He-pycnometry was 2.767 g/cm^3 for the Äspö diorite and 2.699 g/cm^3 for the Ävrö granite. As for the bulk density, a larger variation was observed for the diorite (2.749–2.782 g/cm^3) compared to the granite (2.697–2.701 g/cm^3), here mainly due to the larger, but variable content of mafic minerals in the diorite. As expected and consistent with theory, grain densities were significantly higher than bulk densities in all the samples measured (Table 3-3).

Total porosity calculated according to equation (1) averaged at 0.66 ± 0.08 vol% for the Äspö diorite and 0.76 ± 0.04 vol% for the Ävrö granite.

3.4.4 Water-content porosity (connected porosity) and water saturation

Samples with retained wax-coating

Water-content measurements by resaturation, carried out on MFE-drillcore samples with freshly sawed planes perpendicular to the core axis, but wax-coated along the cylinder surface, showed large differences between the Äspö diorite and the Ävrö granite (Table 3-3). This translates into the water-content porosity, i.e. the connected porosity, calculated from the water-content and the grain density of these samples. While the difference between measurements performed on wax-coated samples and wax-free samples is relatively small and within one standard deviation for the Ävrö granite, it was much larger for the Äspö diorite (Figure 3-3).

Table 3-3. Density measurements and water-content porosity derived from water resaturation of samples from the MFE-drillcore.

		Äspö diorite					
Sample	**Units**	**MFE-4.87**	**MFE-5.70**	**MFE-6.08**	**MFE-7.66**	**MFE-7.73**	**MFE-8.38**
Core samples with surface covered with wax							
Sample weight	g	284	–	279	270	278	297
Bulk density	g/cm^3	2.732	–	2.755	2.771	2.754	2.766
Water content	wt%	0.03	–	0.03	0.03	0.03	0.02
Water content porosity	vol%	0.08	–	0.09	0.08	0.07	0.07
Core samples with waxed surface removed by sawing							
Sample weight	g	219	221	–	151	200	231
Bulk density	g/cm^3	2.731	2.740	–	2.744	2.752	2.766
Water content	wt%	0.12	0.13	–	0.13	0.12	0.09
Water content porosity	vol%	0.32	0.36	–	0.35	0.33	0.25
Ground core samples							
Grain density	g/cm^3	2.749	–	–	2.764	2.774	2.782
Total porosity	vol%	0.65	–	–	0.72	0.72	0.56

		Ävrö granite			
Sample		**MFE-9.24**	**MFE-9.78**	**MFE-9.83**	**MFE-10.65**
Core samples with surface covered with wax					
Sample weight	g	274	280	–	290
Bulk density	g/cm^3	2.677	2.681	–	2.680
Water content	wt%	0.13	0.09	–	0.13
Water content porosity	vol%	0.35	0.23	–	0.36
Core samples with waxed surface removed by sawing					
Sample weight	g	214	185	126	221
Bulk density	g/cm^3	2.675	2.679	2.679	2.679
Water content	wt%	0.14	0.12	0.15	0.11
Water content porosity	vol%	0.38	0.32	0.41	0.30
Ground core samples					
Grain density	g/cm^3	2.697	–	2.701	2.699
Total porosity	vol%	0.74	–	0.81	0.74

Ground core samples					
Grain density	g/cm^3	2.697	–	2.701	2.699
Total porosity	vol%	0.74	–	0.81	0.74

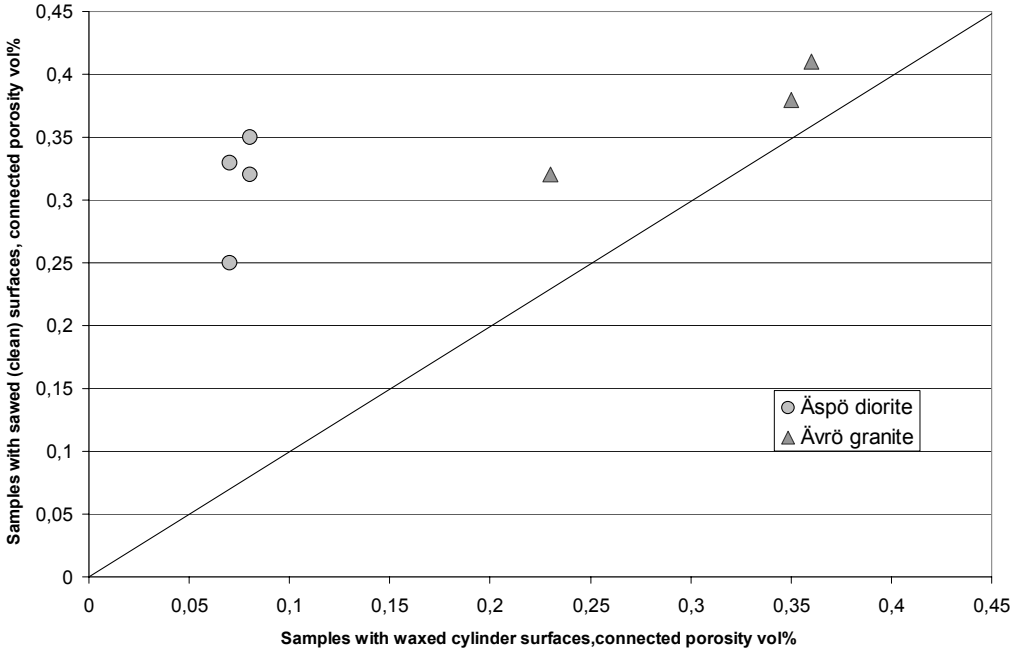

Figure 3-3. *Connected porosity (water-content porosity) measured on samples with wax-coated cylinder surfaces (x-axis) and all surfaces exposed to water (y-axis). The line represents a ratio of 1 to 1. Note large differences between the measurements for the Äspö diorite compared to the Ävrö granite samples.*

The reason for these differences is two-fold: During the initial drying of the samples at 110ºC, the wax-coating melted and penetrated some distance into the rock fabric thus effectively reducing the connected porosity to varying degrees. Measurements of samples where the wax-coated surface was removed to different thicknesses indicated that at least 2 mm had to be removed to achieve a porosity value that was comparable to known values. These pores, now blocked with low-density wax, could no longer be resaturated with water thus reducing the measured water content and consequently the water-content porosity. Because the volume affected by the wax penetration (a few millimetres) was small compared to the total sample volume, these effects were expected to be similar for the Äspö diorite and the Ävrö granite. The large discrepancy observed between the two rock types is therefore difficult to explain.

The larger impact, however, appears to be related to the rock texture, i.e. the differently developed foliation in the two rock types and the resaturation of the samples. In the wax-coated samples re-saturation can only occur via the freshly cut top and bottom planes of the cylindrical samples since the wax-coating on the cylinder surfaces acts as an impermeable layer. Because of the layered arrangement of platy mafic minerals in the Äspö diorite, water re-saturation will be significantly slower compared to the Ävrö granite although stable weight conditions were suggested already after one or two days. Such behaviour is in agreement with the differences in diffusion coefficients parallel and perpendicular to the foliation as, for example, suggested by /Byegård et al, 1998/ and /Johansson, 2000/. It is also in agreement with water contents measured as a function of drying time on samples uncoated by wax (see below).

Samples with wax-coating removed

Water-content porosity, i.e. connected porosity, determined by water re-saturation of the cylindrical Äspö diorite and Ävrö granite samples devoid of the wax-coating, averaged at 0.32 ± 0.04 vol% and 0.35 ± 0.05 vol%, respectively (Table 3-3). In comparison, the determination of the water content by drying rock chips from the centre of the core for 48 hours yielded water-content porosities of the Äspö diorite and Ävrö granite of 0.40 ± 0.04 vol% and 0.35 ± 0.04 vol%, respectively. Continued drying of the samples over 168 hours resulted in a further increase of the water loss changing the water-content porosity to 0.44 ± 0.07 vol% for the Äspö diorite and 0.40 ± 0.02 vol% for the Ävrö granite (Table 3-4). Water contents measured at 24 hours and 48 hours of drying were thus systematically lower by about 25% and 7–17%, respectively, than those measured after 168 hours of drying.

The differences of water contents derived by re-saturation of the 5 cm long drillcore samples, and those derived by drying of small sample chips, were thus significant and larger for the Äspö diorite compared to the Ävrö granite. This suggests that water re-saturation was not complete in these large scale samples although stable weight conditions were indicated. It further suggested that the textural differences between the two rock types have a significant impact onto the re-saturation as already observed by the wax-coated and wax-free samples.

Water-content porosities derived from water re-saturation were lower than the total porosity of the same samples by 45–60% (Figure 3-4). Even when taking the possibly of incomplete re-saturation into account, this relationship remained with the percentage of isolated pores being reduced to about 15–30%. This appears to be a high percentage of pores that are not accessible to diffusion of water. However, the difference between total porosity and connected porosity agreed well with the independently estimated fluid inclusion porosity (cf section 3.5), which is not accessible for water diffusion.

Table 3-4. Water content derived by drying and water-content porosity of samples from the MFE-drillcore.

Sample	Rock type	Water content [1] (wt% wet weight)			Water-content porosity n_{wc} [2] (vol%)		
		24h at 105°C	48h at 105°C	168h at 105°C	24h at 105°C	48h at 105°C	168h at 105°C
MFE-3.66	Äspö diorite	0.06	–	–	0.16	–	–
MFE-3.85	aplitic dyke	–	0.11	0.11	–	0.31	0.31
MFE-3.95	Äspö diorite	–	0.12	0.13	–	0.34	0.36
MFE-4.32	Äspö diorite	–	0.15	0.18	–	0.42	0.49
MFE-4.44	Äspö diorite	–	0.15	0.17	–	0.41	0.47
MFE-4.65	Äspö diorite	0.11	0.15	–	0.31	0.41	–
MFE-9.33	Ävrö granite	–	0.14	0.15	–	0.37	0.41
MFE-9.66	Ävrö granite	–	0.12	0.14	–	0.32	0.38

[1] average values of two or more subsamples.
[2] calculated according to equation (2a) using the average grain density values from Table 3-3 for the Äspö diorite and the Ävrö granite.

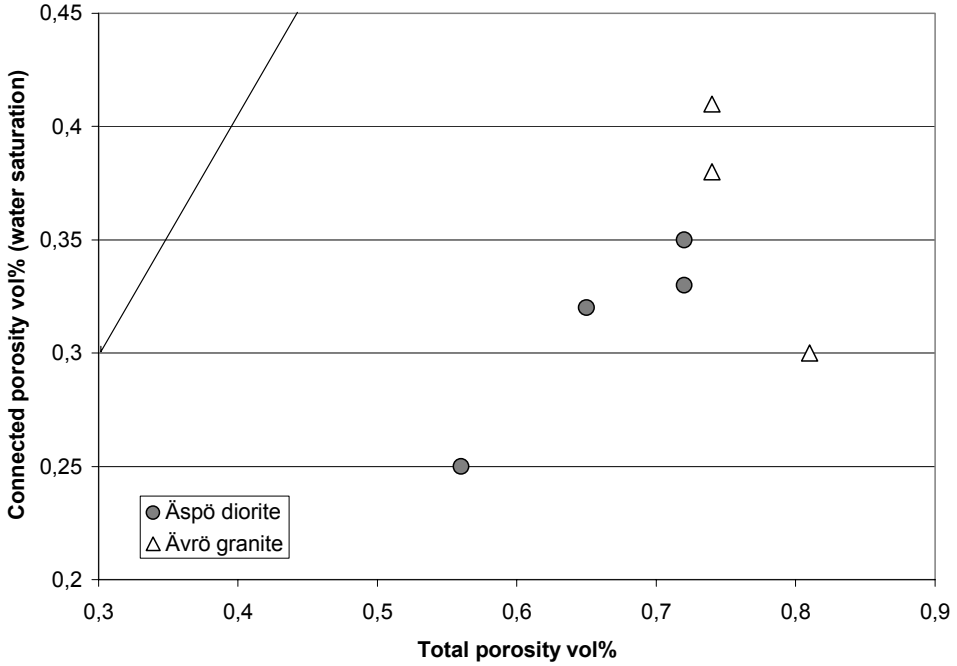

Figure 3-4. *Total porosity versus connected porosity derived by water re-saturation techniques. The line represents a ratio of 1 to 1.*

Uncoated samples from borehole KF0093-A0

Drillcore samples from borehole KF0093-A0 used for diffusion experiments (cf Chapter 5, section 5.5) were also investigated for their water content to derive the water-content porosity. On small aliquots (about 10–20 cm^3) from the core centre of the samples used for the experiments, the water content was determined by drying the samples at 105ºC for different time periods immediately after being received. Water-content porosity was calculated according to equation (2b) and using the average grain density of the MFE-borehole samples. The results obtained for the Äspö diorite (Table 3-5) overlapped with the range obtained with the same technique used on the MFE-drillcore samples (Table 3-4), while the aplite sample of the KF0093-A0 drillcore displayed a significantly higher water content.

Table 3-5. Water content derived by drying and water-content porosity of sample aliquots from borehole KF0093-A0.

Sample	Rock type	Water content (wt% wet weight)			Water-content porosity n_{wc} [1] (vol%)		
		48h at 105°C	72h at 105°C	168h at 105°C	48h at 105°C	72h at 105°C	168h at 105°C
KF93-1a	Äspö diorite	0.144	0.159	0.159	0.40	0.44	0.44
KF93-2a	Aplitic dyke	0.169	0.184	0.184	0.47	0.51	0.51
KF93-3a	Diorite/aplite	0.167	0.184	0.184	0.46	0.51	0.51

[1] calculated according to equation (2) using the average grain density values from Table 3-3 for the Äspö diorite.

The wet weight of the large-sized samples used for the experiments was determined immediately after receiving and storing the samples, and was again measured after completion of the experiments, i.e. after 60 and 150 days, respectively. The comparison of the two wet weights showed that the degree of saturation, S, was larger than 99.96% for all three samples (Table 3-6), i.e. the samples were essentially received in a saturated state.

Table 3-6. Water saturation and water content derived by drying and re-saturation, and water-content porosity of diffusion experiment samples from borehole KF0093-A0.

Sample	Rock type	Rock volume [1]	Wet weight [2]		Satu-ration (S)	Water content at saturation (168h at 105°C)		WC-porosity n_{wc} [3]
		(cm^3)	before (g)	after (g)	(%)	(g)	(vol%)	(vol%)
KF93-1	Äspö diorite	180.718	548.76	548.90	99.97	0.900	0.169	0.47
KF93-2	Aplitic dyke	137.310	417.13	417.30	99.96	0.730	0.175	0.48
KF93-3	Diorite/aplite	152.186	467.49	467.58	99.98	0.650	0.139	0.38

[1] approximate; assumes perfect cylindrical shape of the core.
[2] wet weight before and after diffusion experiment (KF93-3: 60 days, KF93-1 and KF93-2: 150 days).
[3] calculated according to equation (2) using the average grain density values from Table 3-3 for the Äspö diorite.

Water content and water-content porosity of the resaturated, large-sized samples used in the experiments differed by less than 10% from those determined for the sample aliquots except for mixed diorite-aplite sample KF93-3 (Tables 3-4 and 3-5). The reason for this difference is yet unknown.

3.4.5 Comparison with other porosity data

Previous investigations on water content and water-content porosity (connected porosity) revealed a distinct difference between the major rock-types found at the Äspö area. Characteristic average values for the connected porosity in the major unaltered rock types from several experimental sites at Äspö are given in Table 3-7. Altered Äspö diorite and Ävrö granite show higher porosity values than the corresponding fresh rock. Depending on type and intensity of alteration, the connected porosity in altered rocks varies between 0.15 to 1.5 vol% /Stanfors et al, 1993a,b; Eliasson, 1993/.

The petrographic studies showed that the rocks in the MFE-drillcore did not experience significant alteration. The connected porosity and density values obtained for these rocks compare with the average values from previous studies (Figure 3-5). While connected porosity values obtained by water-resaturation of large-sized samples for the Ävrö granite were close to the known average values, those for the Äspö diorite were generally lower and showed a larger variation. As discussed in the previous section, this appears to be due to incomplete re-saturation as shown by the comparison with values obtained by drying or long-term (i.e. months) saturation experiments. The incomplete re-saturation of the Äspö diorite is mainly related to the more heterogeneous mineralogical composition, larger variability in rock texture, and possibly the frequency of microfractures.

Although the discrepancies between connected porosity values obtained by different techniques might be small, they become important when calculating the concentrations of non-reactive solutes to the in-situ pore water concentration. As discussed in Chapter 5, already a 10% difference in the water content results in a significant change in the in-situ pore water salinity. It is thus of great importance that porosity measurements are conducted in parallel with detailed studies of the petrography and that the techniques for porosity measurements are adjusted to the rocks mineralogical and textural character.

Table 3-7. Average values of connected porosity for major rock types in the Äspö area /data from Stanfors et al, 1993a,b; Eliasson, 1993/.

Rock type	Connected porosity [1)]
Fine-grained granite	0.20 ± 0.1 vol%
Ävrö granite	0.35 ± 0.1 vol%
Äspö diorite	0.45 ± 0.1 vol%

[1)] based on 50 to 100 analyses.

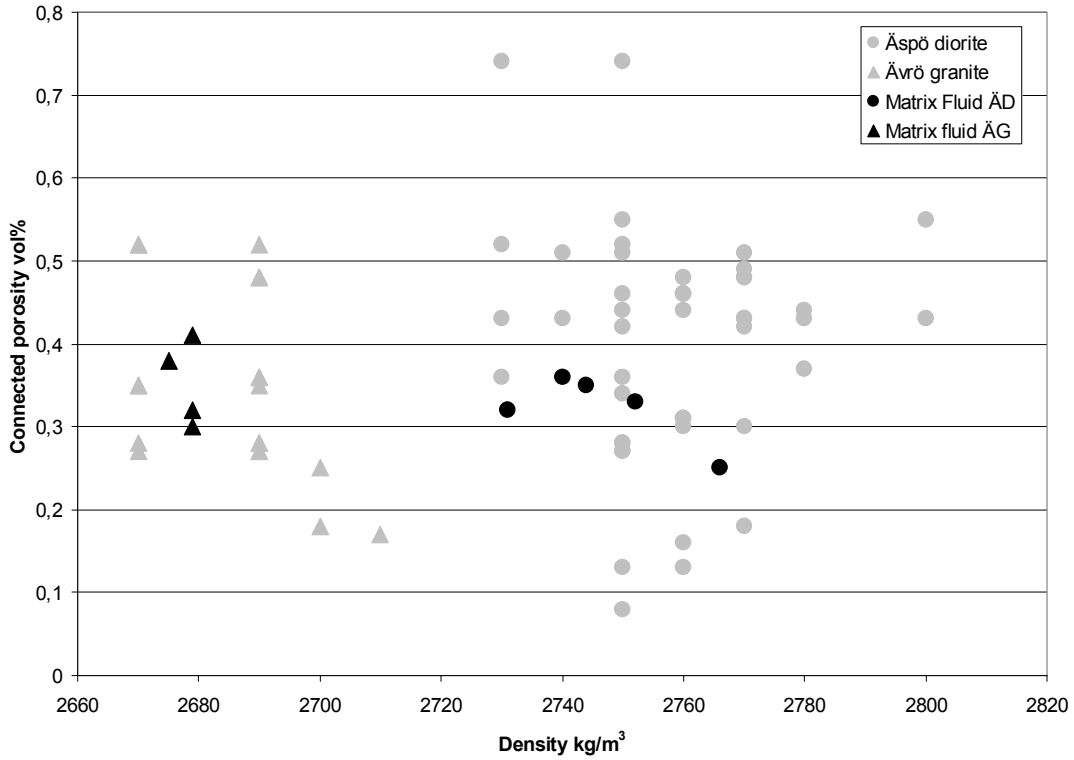

Figure 3-5. *Bulk density versus connected porosity derived using water re-saturation techniques for samples from the MFE-drillcore compared to various samples from the Äspö HRL tunnel /data from Stanfors et al, 1993a,b; Eliasson, 1993/.*

3.4.6 Porosity distribution: Results from impregnation studies

The frequency, orientation, and apertures of the connected pores in crystalline bed rock have been studied using different impregnation techniques in several previous studies carried out on samples from Äspö /e.g. Mazurek et al, 1997; Byegård et al, 1998; Byegård et al, 2001/. These studies show that the porosity distribution is heterogeneously distributed and, especially in foliated and tectonised samples, the orientation effects may be considerable.

On two samples (MFE-4.87: Äspö diorite; MFE-10.65: Ävrö granite) from the MFE-drillcore a simple impregnation using ink was carried out. The accessible (i.e. interconnected) pores partly follow grain boundaries, but there are also microfractures transecting mineral grains (Figure 3-6). The Äspö diorite has a greater biotite content and shows stronger orientation of the mafic minerals and pores/microfractures at the contacts between the mafic minerals and the quartz/feldspar-rich bands. In general the microfractures in the Äspö diorite samples show stronger orientation (parallel foliation) than those in the Ävrö granite where a more random microfracture distribution is observed (Figure 3-7) (cf Appendix 6, Figures A6-2 and A6-3).

Figure 3-6. *Äspö diorite sample dyed with blue ink. Note the parallel orientation of the bluish stained microfractures (Length of the photomicrograph = 0.5 mm).*

Figure 3-7. *Ävrö granite sample dyed with blue ink. Note the distribution pattern caused by a relatively large microfracture branching into very small fractures in all directions (Length of the photomicrograph = 2.5 mm).*

3.5 Fluid inclusions

(S Lindblom, Stockholm University, A Blyth, University of Waterloo, S Gehör, Kivitieto, N Waber, University of Bern, and S Frape, University of Waterloo)

3.5.1 General

One of the main objectives of the Matrix Fluid Chemistry Experiment was to study the origin and chemistry of the pore fluids in the rock matrix and how the accessible component of these interstitial pore fluids may have influenced the hydrochemistry in the surrounding bedrock environment. Based on published literature from other granitic domains /e.g. Nordstrom et al, 1989a; Savoye et al, 1998/, the matrix pore fluids were expected to be highly saline in character and one potential source of this salinity was the fluid inclusion populations associated dominantly with quartz. The objectives of the fluid inclusion studies were therefore to characterise the fluid inclusion populations, determine the nature (i.e. salinity) of the included fluids, to examine carefully for any evidence of leakage, and to establish the mechanisms of leakage if shown to have occurred.

The study of fluid inclusions focussed mainly on quartz, even though quartz represents only one third of the granite rock. Quartz is hard, brittle and not subject to alteration. Heterogeneities are restricted to open and healed fractures, isolated or clustered fluid inclusions and mineral inclusions. Grain boundaries within quartz aggregates also constitute heterogeneities. Feldspars, on the other hand, are altered to various degrees and contain twinning or cleavage that can have resulted from absorbing mechanical stress. Mica is softer and more elastic and its two-dimensional crystal habit may facilitate 'gliding/sliding' to absorb stress. Mica may occur as randomly oriented crystals in the granite, even though the granite may be slightly gneissic in character. In conclusion, mica will not fracture, it will bend and slide. Feldspar will fracture (becoming altered to kaolinite or mica along these fracture planes) but rarely form inclusion-filled, healed fracture planes. Therefore, quartz was the main focus for both fluid inclusion occurrence and later evidence of fracturing and subsequent healing of fractures.

The healing/sealing of microfractures and grain boundaries in quartz is an important process giving rise to the formation and trapping of fluid inclusions. There are numerous examples of fluid inclusion planes (FIPs) outlined by inclusion trails traversing different generations of quartz formation (Figure 3-11; Appendix 2, Figure A2-5). A key issue is at what times during the geological history of the Äspö region where these fractures formed and then sealed.

Four research groups (Stockholm, Bern, Waterloo and Oulu) participated in characterising the fluid inclusions; an additional objective was to derive a common methodology for the description, analysis and interpretation of fluid inclusion populations that could be transferred to a site characterisation protocol.

The methods used to characterise the morphology and chemistry of the fluid inclusions comprised Optical Microscopy, Cathodoluminescence, Microthermometry, Laser Raman Microspectroscopy and Laser Ablation ICP-MS.

3.5.2 Morphology and textures of the host quartz

Fluid inclusions were observed in quartz, feldspar and apatite, but the volumetric contribution of inclusions in feldspar and apatite to the total fluid inclusion volume in the rock matrix can be considered negligible. Inclusions in apatite, however, may have important implications for genetic/paragenetic relations. Three major quartz types were observed:

- Large primary grains (500 μm to 1 mm); xenomorphic in texture exhibiting abundant internal deformation such as cracks and undulous extinction; formed during emplacement of the granite.
- Medium to large secondary grains (300 μm to 1 mm), dual origin in type, exhibiting hypidiomorphic textures and showing weak undulous extinction; this type is volumetrically the most abundant quartz observed; represent two magma stages.
- Small, third generation recrystallised equigranular grains (50–100 μm) exhibiting triple junctions, formed along the edges of the larger primary and secondary quartz grains (up to 400 μm); exhibit strong optical anisotropy and are characterised by numerous trails of fluid inclusions.

The later, small equant quartz grains, appear to be recrystallised areas of earlier large grains and seem to occupy a greater volume in the Ävrö granite than in the Äspö diorite.

Regional evidence of tectonic activity is observed as distinct lineations, particularly in the Äspö diorite (from biotite orientation); these textural fabrics are thought to have resulted from metamorphic pressure linked to burial or consecutive granitic intrusions. The last major tectonic event was associated with the intrusion of Post-orogenic granites at ca. 1630 Ma ago. Other tectonic stresses following formation of the granite have been more localised and have resulted in the formation of open and healed microfractures. The main influence has been from stress release mechanisms which may have occurred early on from cooling of the granite magma, or may have occurred much later in the geological history of the bedrock, in particular during one or more of the several glaciations that have occurred in the last million years.

Optical evidence of stress and recrystallisation within the quartz grains include anisotropy and the presence of healed and open fractures, the open fractures having been interpreted as resulting from the restricted rotation of the quartz grains under applied tectonic pressure. Additional fracturing particularly along grain boundaries, but also cross-cutting the quartz mosaics, has also been documented. Orientations of the healed microfractures (usually outlined by fluid inclusions and termed Fluid Inclusion Planes; FIPs) were measured in thin sections and showed the main orientation to be E-W with variations to WNW and WSW with an inclination varying from 5°–60° to the north (Figure 3-8). The different orientations correlate closely with the regional lineament fabric of the Äspö region where four main lineament sets, NW-SE and E-W (older) and N-S and NE-SW (younger), form an orthogonal pattern and are presumed to reflect fracture zones in the area. Of the four lineament sets, the N-S and E-W sets dominate producing a suborthogonal first order system of lineaments. The other lineament sets, the NW-SE and NE-SW trending features, represent second order zones of another almost orthogonal system. In general, the northern part of the region is characterised more by the NW-SE set and the southern part by the NE-SW; Äspö is located precisely at the intersection of two lineament pairs (E-W and NW-SE).

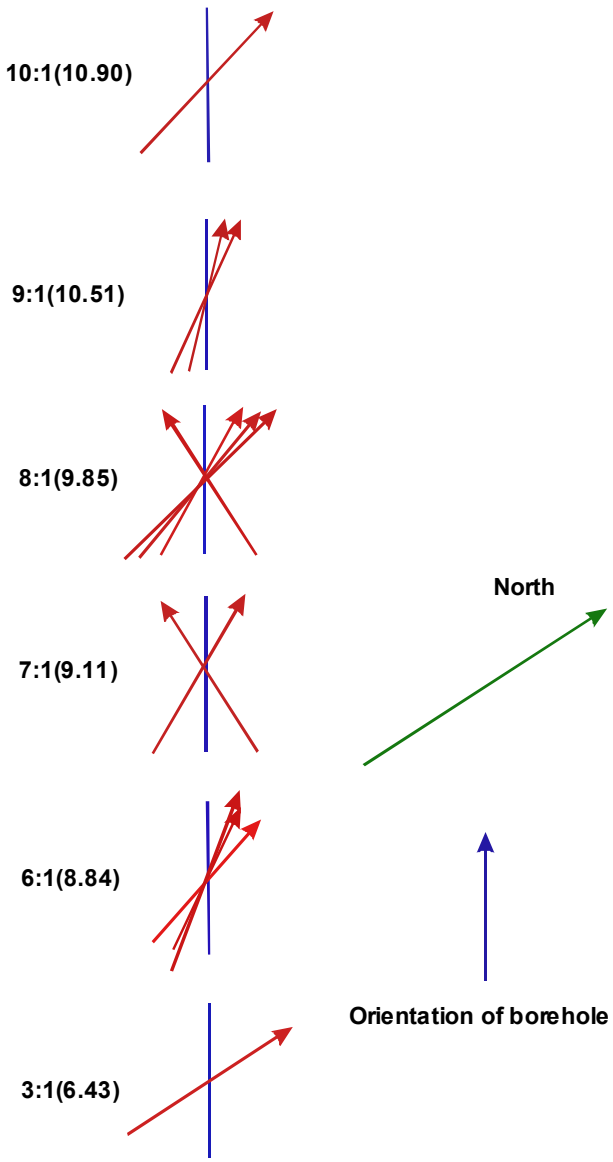

Figure 3-8. *Horizontal 'thick' sections illustrated from 6 samples; orientation of vertical FIPs or near vertical FIPs are shown as red arrows.*

3.5.3 Morphology and chemistry of the fluid inclusions

Morphology and abundance of fluid inclusions

Fluid inclusions are dominantly associated with quartz and occur as four main types schematically represented in Figure 3-9. These different types are described together with information on fluid compositions derived from microthermometry.

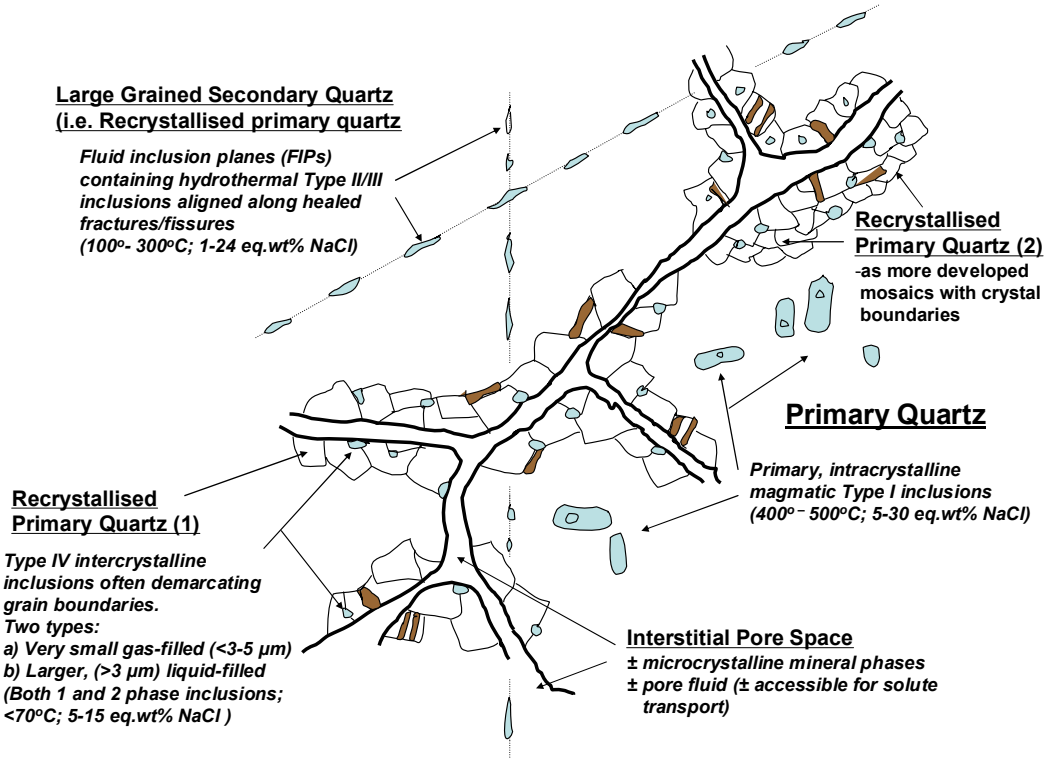

Figure 3-9. *Schematic representation of the major fluid inclusion types present in the Äspö diorite. Note that the Ävrö granite shows more examples of recrystallised quartz (but not necessarily more developed) than the Äspö diorite. Brown phases represent biotite laths.*

The four main fluid inclusion types identified were:

- **Type I:** Primary inclusions (generally larger than the other types; 5–45 µm in size) associated with the large primary quartz grains (Figure 3-10); occur as small isolated groups and sometimes cross-cut by younger inclusion trails; include both two (liquid/vapour) and three (plus solid; halite or calcite) phase types and salinities are in the order of 5–30 eq.wt% NaCl.
- **Type II:** Mainly present in primary quartz grains as trails along healed cracks (Figure 3-11);.majority are single phased liquid types and salinities are in the range of 1.7–10.5 eq.wt% NaCl.
- **Type III:** Inclusion trails adjacent to the edges of the medium to large secondary quartz grains (Figure 3-12); inclusions are irregularly-shaped; single phase liquid inclusions change to single phase vapour types via intermediate two phase types over a few micrometres; salinities are in the order of 3.4–26 eq.wt% NaCl.
- **Type IV:** Occurs as morphologically different forms along boundaries of the small, third generation recrystallised quartz grains (Figure 3-11); inclusions are small (< 2 µm), dark in colour and are characteristically single phase vapour in type; the non-fluorescent vapour phase is uncertain (CO_2 or CH_4?). Some are fluid inclusions with salinities of 5–15 eq.wt% NaCl.

Figure 3-10. *Primary, two-phase inclusion in magmatic quartz.*

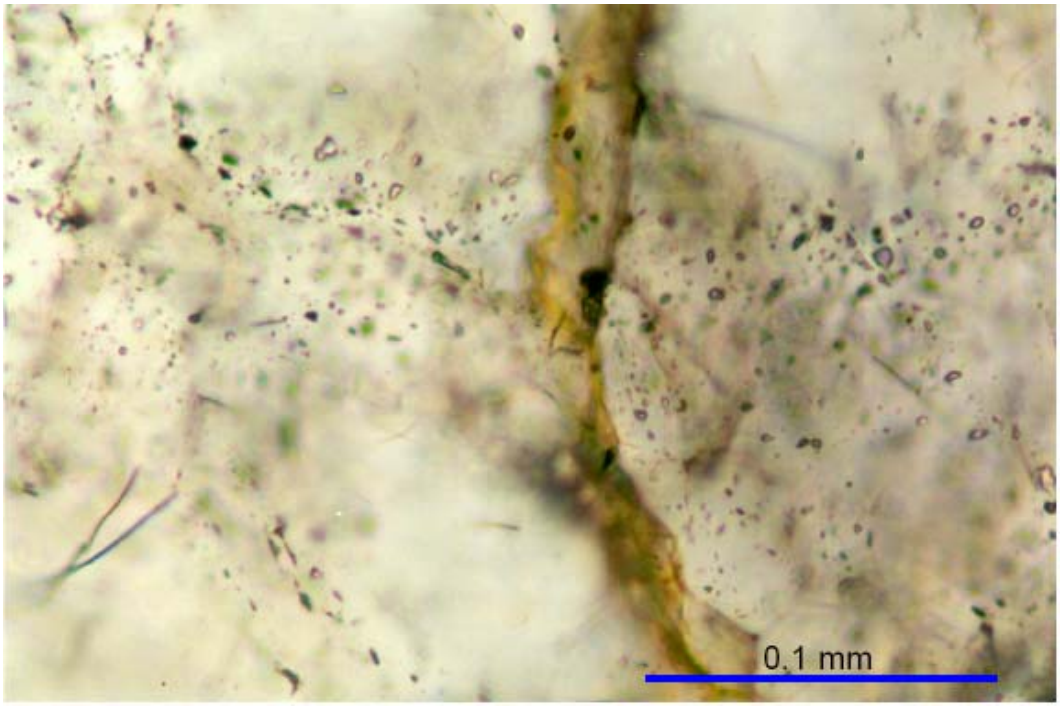

Figure 3-11. *Intracrystalline fluid inclusions in primary quartz. Includes individual fluid inclusions and clusters of inclusions as well as FIPs (fluid inclusion trails).*

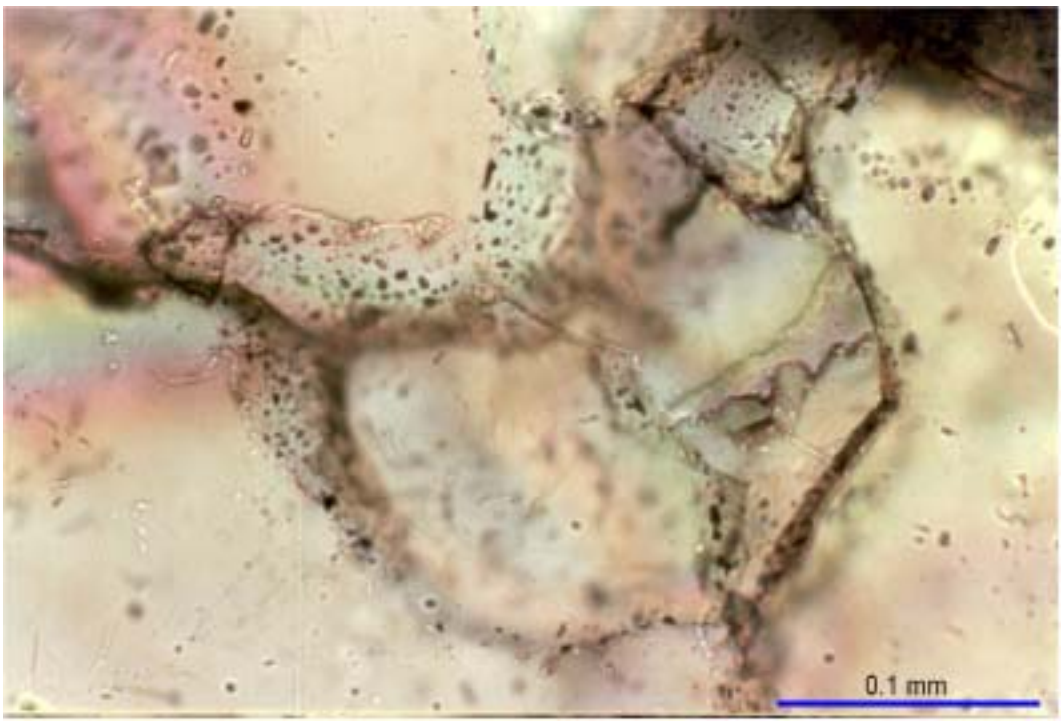

Figure 3-12. *Intercrystalline fluid inclusions located along grain boundaries.*

Some of the Type I inclusions contain a solid phase, although what is termed solid and liquid is a largely a matter of the temperature at which the observations are made. Normally phases are observed at room temperature for identification, but a NaCl-hydrate was identified by Raman spectrometry at low temperatures; no hydrates of $CaCl_2$ and $MgCl_2$ were found. Several inclusions contain a solid phase that has been confirmed as a carbonate. It is probably calcite, although there is a slight displacement of the principal line at 1086 cm-1. Another inactive phase, of cubic form, was also identified by Raman spectrometry in two-phase fluid inclusions and concluded to be probably halite.

The fluid inclusion types, and their relative abundance and fluid chemistry, are summarised in Table 3-8.

Table 3-8. Characteristics of the different fluid inclusion types.

Inclusion type	Phases	eq.wt% NaCl	Relative abundance
Type I	Aqueous liquid + solid + vapour	approx 30	± 5%
Type II	Aqueous liquid	1.7–10.5	± 20%
Type III	Aqueous liquid + vapour	3.4–26	± 10%
Type IV	Low-density vapour	–	± 65%
Type IV	Aqueous liquid	5–15	–

The younger cross-cutting fluid inclusion trails seen in the primary quartz grains have been subdivided further based on composition and orientation: a) pervasive E-W orientation of moderate to high salinity, b) WSW-ENE orientation comparable to (a), c) WNW-ESE orientation comparable to (a) but less pervasive, and d) randomly orientated intragranular inclusions of low to moderate salinity.

Volume of fluid associated with the inclusions

For the purpose of discussing the potential leakage of fluid inclusions into interstitial pore water, a key issue is the amount of fluid contained in the inclusions present in minerals and the rock (diorite or granite). Since quartz is the dominant host mineral, only fluid inclusions in quartz need be considered. At Äspö, for all practical purposes of assessing the volume of fluid, the fluid inclusions may be grouped into: (a) intracrystalline (fluid inclusions within quartz grains), and (b) intercrystalline (fluid inclusions in grain boundaries between quartz grains). This was the simplest distinction that could be made when estimating the number and volume of the inclusions; further divisions were too complicated. The amounts of fluid inclusions were estimated separately for each of these two types.

Using simple point counting methods it was possible to calculate an average fluid volume using the following assumptions and estimates:

- counting all inclusions > 2 μm in the field of view;
- using 5 μm as a mean diameter;
- assuming the fluid inclusion shape as approximating a sphere; and
- computing the highest, lowest and average numbers of fluid inclusion occurrences.

Taking 5 μm as a mean diameter, a reasonable estimate of fluid inclusion occurrences was obtained (see further discussion in /Nordstrom et al, 1989a/). The fluid present in the inclusions varies from 1 to 6 vol% in quartz over the length of the drillhole, depending on the intensity of fluid inclusion occurrence which may vary between grains. Together an average number of 2 vol% fluid inclusions was obtained in quartz comprising intracrystalline and grain boundary inclusions. In the whole rock this translates into a fluid inclusion volume of 0.3 vol% (0.17 x 2 vol%) for the Äspö diorite and 0.6 vol% (0.28 x 2 vol%) for the Ävrö granite.

Chemistry of fluid inclusions

Conventional microthermometric methods were used to determine qualitatively the salinity ranges of the fluid inclusions expressed in eq.wt% NaCl (Table 3-9).

The major problem is, however, to quantitatively characterise the fluid inclusion contents because of their small size which precludes the use of many analytical approaches and techniques. Some success has been gained from using Laser Raman Microspectroscopy which is the only analytical method that can analyse fluid inclusions without destroying the sample (Figure 3-13). However the technique does not provide data on ionic species, and small solid phases are often very difficult to identify because of weak signals and lack of sufficient reference spectral data. Consequently, most analytical data on fluid inclusions originate from bulk methods where a sample containing abundant fluid inclusions is crushed or heated to extract the inclusion liquid or gas.

Table 3-9. Summary of fluid inclusion data from the three laboratories relating to secondary inclusions in trails or grain boundaries. Decrepitated and isolated inclusions are excluded.

Borehole length (m)	Phases	Tmice °C	Salinity eq.wt%NaCl	Research group
4.60–4.89	L	–1 to –7	1.7 to 10.5	Bern
4.60–4.89	L+V	–2 to –20	3.4 to 26	Bern
5.03	L+V	–5.5 to –15.0	8.7 to 19.1	Stklm/Oulo
5.03	L+V	–2.1 to –16.4	3.5 to 19.9	Waterloo
5.18	L+V	–0.4 to –22.1	0.7 to 24.1	Waterloo
5.42	L+V	–4.0	6.6	Stklm/Oulo
7.81	L+V	–1.0 to –23	1.7 to 24.7	Stklm/Oulo
7.81	L+V	–0.2 to –12.9	0.4 to 16.9	Waterloo
8.84	L+V	–5.44 to –18	8.5 to 21.2	Stklm/Oulo
8.84	L+V	–2.6 to –13.8	4.3 to 17.7	Waterloo
9.11	L+V	–0.6 to –22.6	1.0 to 24.3	Waterloo
9.85	L+V	–4.5	7.3	Stklm/Oulo

L = Liquid; V = Vapour.

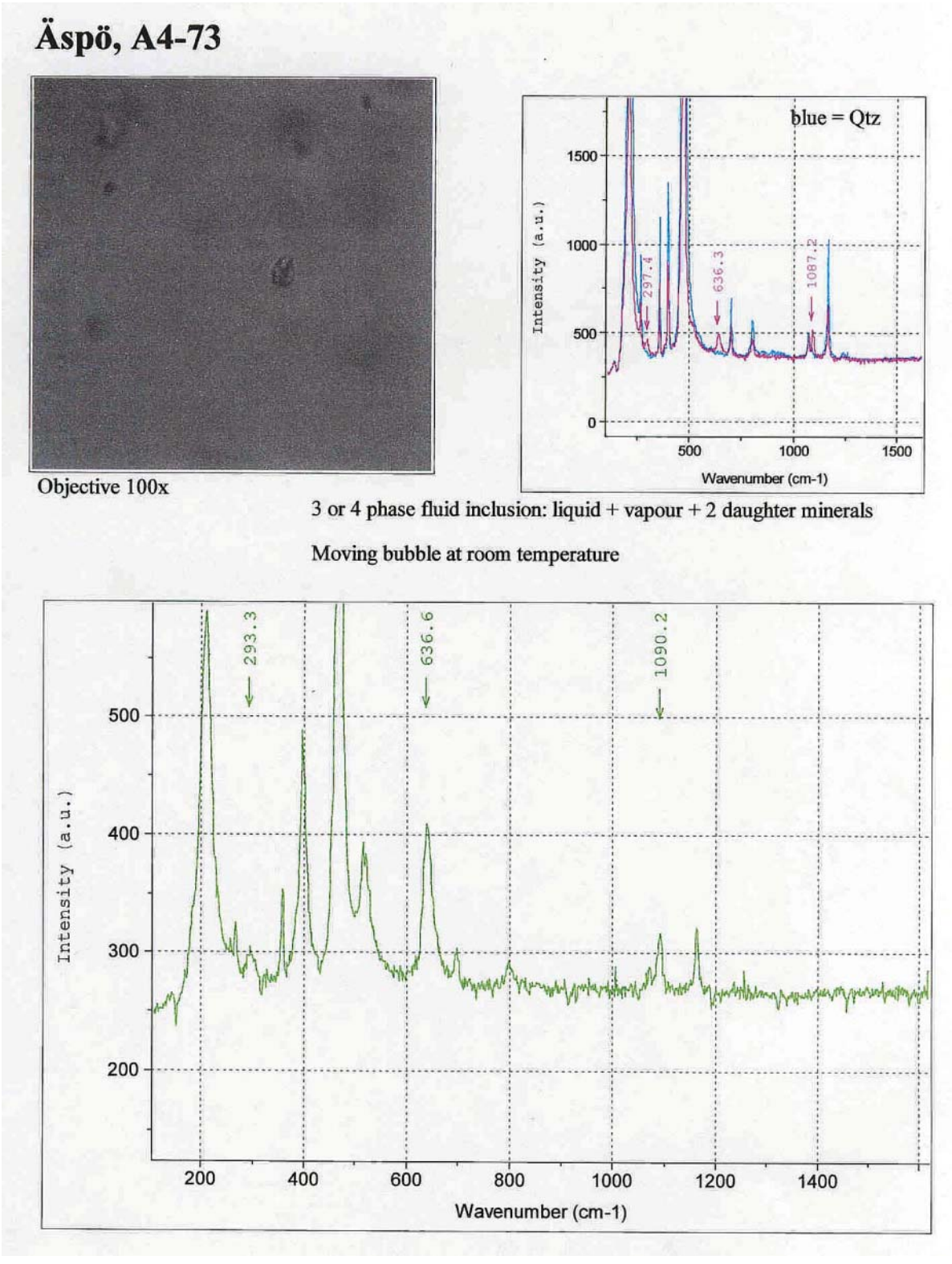

Figure 3-13. *Laser Raman microspectroscopy of a single multiphase fluid inclusion showing the NaCl-hydrate peaks.*

One promising avenue to quantitatively characterise fluid inclusions is the recently developed Laser Ablation ICP-MS method that has the capability of focussing an analytical beam almost to the size range of individual fluid inclusions. It has been used in this present study (cf Appendix 12) and the data obtained have: a) corroborated the microthermometry data, b) detected more dissolved components in single fluid inclusions (Figure 3-14a,b), and c) provided indications that the grain boundaries in quartz may have a much more complex composition than normally suspected (Figure 3-15a,b). However, as a cautionary note, because the analytical beam is usually greater than the size of the fluid inclusions under investigation, the 3-D area analysed both horizontally and vertically may give rise to contamination/interference from adjacent mineral phases.

Figure 3-14a. *Microphotograph of the laser ablated L1 line which cuts across a fluid inclusion cluster and extracts low salinity fluids.*

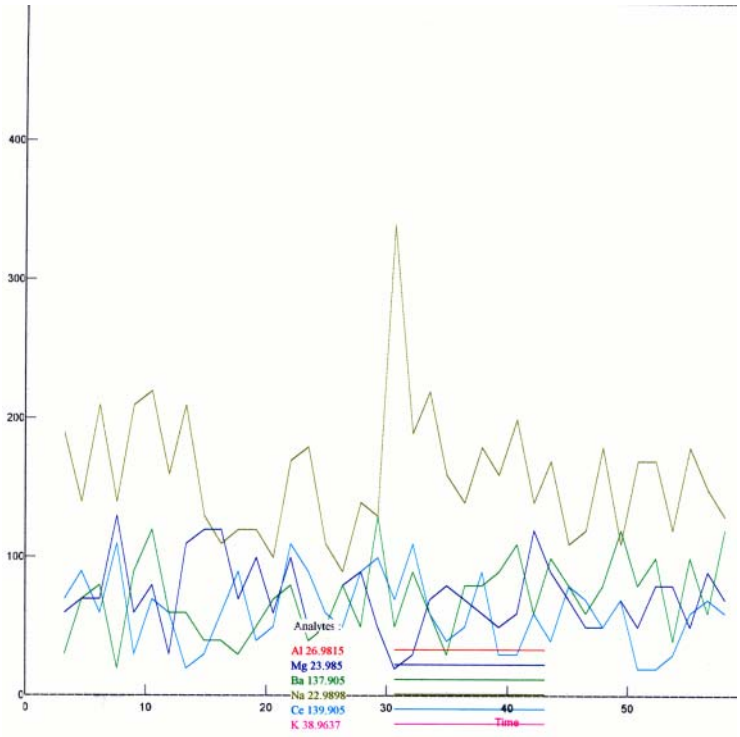

Figure 3-14b. *Laser Ablated ICP-MS spectra of the laser ablated L1 line (cf Figure 3-14a). The most prominent element in the analysed inclusions is sodium; a slight coincidence of Ba with Na can be detected.*

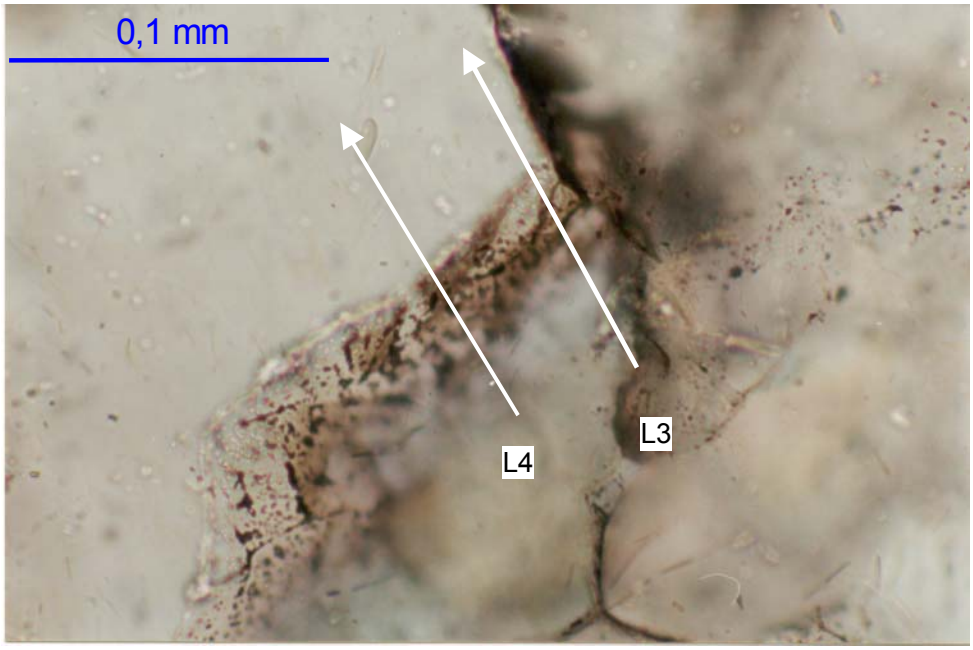

Figure 3-15a. *Microphotograph of grain boundary coatings showing the two profiles (L3 and L4) analysed by Laser Ablation ICP-MS. Analytical results are shown in Figure 3-15b.*

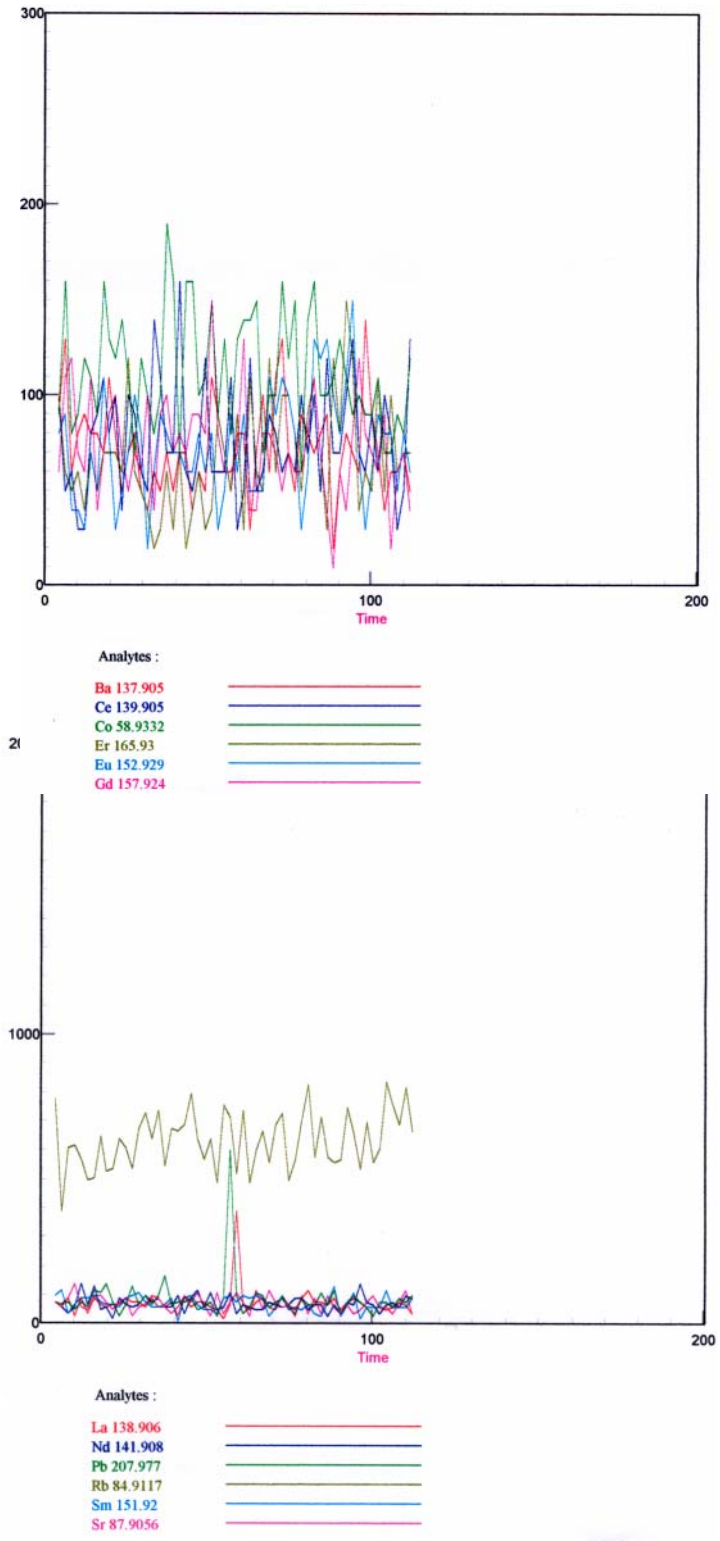

Figure 3-15b. *Laser Ablation-ICP-MS spectra of line L3 (upper) and line L4 (lower). The spectra indicate high fluctuations, especially for Co, Ce, Gd, Eu and Ba in L3. Traverse L4 illustrates the frequent occurrence of an unknown Pb-phase on the coating. At point 60 seconds the ablated material includes an unknown La-bearing phase.*

In summary, the following information can be drawn from the Laser Ablation ICP-MS studies:

- **Major elements:** Na, Ca, K and Mg. Sensitivity for K and Ca is low and high concentrations only are detected.
- **Minor and trace elements:** Ba and Sr, Ce and La. These occurrences are unusual and not generally reported elsewhere.
- **Proxies:** ^{88}Sr (for Ca), Si (for CO).
- **Interference:** Ar (for Ca), ^{85}Sr.

From petrography and microthermometry it was assumed that fluid inclusions at grain boundaries would give similar signatures to the fluid inclusions within quartz grains. However the grain boundary environment proved to be more complex since the acquired spectra from Laser Ablation ICP-MS reflected both mineral and fluid inclusion signatures and it was often not possible to separate them. There were, however, enough data to suggest the presence of fluid inclusions as well as more complex element combinations for minerals.

The grain boundary fluid inclusions gave both highly saline and less saline signatures where Na is dominant; Ca and Mg were indicated in the high salinity inclusions. These data are in agreement with the fluid inclusions within the quartz grains and therefore a strong Na signal was also taken to indicate high salinity. Unfortunately there are too few analytical data to be able to separate out any significant differences between the two types of fluid inclusion occurrences.

Attempts were made also to characterise the associated mineral phases at the quartz grain boundaries and the following major element combinations were suggested for the tentative interpretation of common rock-forming minerals which may be present along the grain boundaries:

Na+Al	(= albite)
K+Al	(= K-feldspar)
Na+Sr (for Ca) +Ca+Al	(= plagioclase)
Mg+Al	(= chlorite)
K+Mg+Al	(= biotite)
Na+Mg+Al	(= amphibole)
Al alone	(= kaolinite?)

As indicated earlier, however, because the analytical beam is usually much greater than the size of the grain boundary fluid inclusions and also the associated mineral phases, the 3-D area analysed may give rise to contamination, and therefore spectral interference, from adjacent mineral phases. Great care has to be exercised in interpretation.

3.5.4 Petrofabric studies

Microscopic evidence of deformation and stress is observed as healed and open fractures contained within individual quartz grains. Open fractures observed in the centre of quartz grains have the appearance of being tension fractures opened by externally directed rotating and oscillating pressure (cf Appendix 2, Figure A2-7). Stress is also observed as an anisotropic optical pattern in thin section within the quartz grains (strained quartz) (Figure 3-16) and is especially clear in the younger recrystallised quartz where the mosaic of small equant grains provide a collective view of the stress field. This anisotropy is also present in the larger, older quartz grains but is not so clearly seen because the quartz grain boundaries are often adjacent to more pliable, less competent mineral grains of biotite and chlorite.

Planar features are found as open and healed/sealed microfractures in quartz. The orientations of the healed microfractures usually outlined by inclusions were measured in thin sections which were cut both in a vertical and a horizontal plane along the direction of the drillcore.

The main orientation of the healed microfractures (i.e. Fluid Inclusion Planes; FIPs) is E-W with variations to WNW and WSW (cf Figures 3-8 and 3-11). The measured dip (inclination) is 5° to 60° towards the north. Several FIPs cut across several quartz grains indicating that these fluid inclusion planes were formed after the grain boundary inclusions. If the compositions of these two generations of inclusions are similar, it could indicate that the FIPs were formed coeval to the recrystallisation of the quartz. Unfortunately there were insufficient data to establish this relationship.

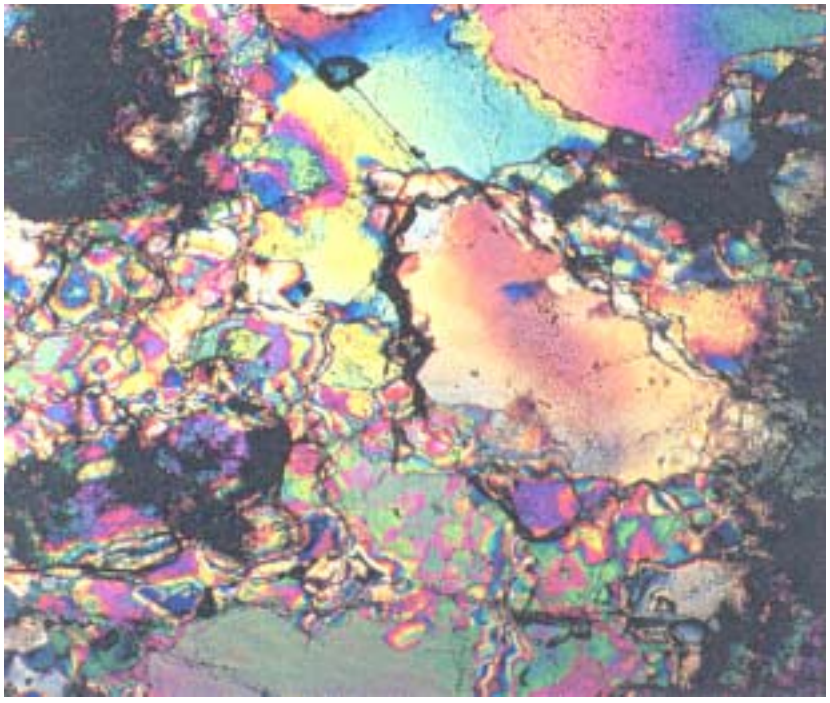

Figure 3-16. *Relationship between primary (large grains) and mosaics of recrystallised primary quartz and stress optical anisotropy.*

The different orientations of the younger, cross-cutting fluid inclusion trails probably reflect formation under varying regional tectonic stress directions at different geological time intervals.

3.5.5 Evidence and mechanisms for fluid inclusion leakage

Geological and textural evidence of major tectonic events

The geological history of the Äspö region provides three major tectonic scenarios that may be relevant in this context:

- Emplacement of the major rock types (dolerite and granite) and their subsequent evolution and alteration.
- Sedimentation and erosion.
- Cyclic glacial events.

During any one of these events the formation of new microfractures and the healing of old ones might be expected. Lineations in the Äspö diorite indicate metamorphic pressure from burial and/or consecutive magmatic intrusions. This has resulted in biotite alignment producing a distinct foliation fabric and the formation of open and healed microfractures within individual quartz grains. Measurement of the orientations of the healed microfractures, which often contain trapped fluid inclusions (i.e. FIPs), is E-W with variations to WNW and WSW. This generally corresponds to the large-scale regional structural features. The fact that several FIPs cut across quartz grains of different generations suggest that some of these planes were formed after the grain boundary inclusions. As noted in section 3.5.4 it was not possible to show whether the compositions of these two generations of inclusions were similar, which could have indicated that the FIPs were formed coeval to the recrystallisation of the quartz. Also noted above is the commonly observed optical anisotropy within quartz grains, especially clear in the younger recrystallised quartz.

In section 3.4 the occurrence of microfractures in both the Äspö diorite and Ävrö granite and the connected porosity (i.e. the network of microfractures and grain boundary pore space) were discussed. Staining techniques revealed that these microfractures preferentially form along grain boundaries in quartz, although some crosscut the primary and recrystallised quartz varieties. It is yet uncertain to what degree this fracturing represents in-situ conditions or a result of stress release and/or drilling disturbance.

Tectonic events and fluid inclusion leakage

At Äspö, open and sealed microfractures and their association with fluid inclusion populations may have formed shortly after emplacement of the granite in the same heating/cooling event, or they may have formed at any time since. It seems clear that the primary, intracrystalline magmatic Type I inclusions (Figure 3-9) are not related to any rock structural fabric and the host quartz has largely remained unchanged since its

formation apart from exhibiting a weak anisotropy. There is evidence, however, that later produced open fractures centrally located in some of these large quartz grains may have resulted in the limited fracturing of inclusions and the release of fluids into the interstitial pore space.

In contrast to Type I fluid inclusions, Type II/III inclusions (Figure 3-9) appear to have been trapped as the result of healing/sealing of microfractures in the recrystallised primary quartz grains and the orientation of these microfractures (i.e. FIPs) generally seem to correspond on a microscale to the Äspö regional suborthogonal first order system characterised by dominant E-W and NW-SW directions. In common with Type I inclusions, central fracturing of these large recrystallised quartz grains may also contribute to the leakage of Type II/III fluids into the system. Type IV fluid inclusions (Figure 3-9) may be more susceptible to fracturing and leakage during tectonic events since they are located close to the quartz grain boundaries where any stress-related movement, and therefore fracturing, might be most acute. The majority, however, are small and gas filled such that their contribution to fluid leakage appears to be limited. The aqueous types, however, may contribute significantly to the pore fluid salinity.

In summary, of the various textural relationships described, open fractures present in some central areas of large quartz grains and evidence of movement along quartz grain boundaries appear to be the most likely mechanisms for the fracturing of inclusions and the release of saline fluids into the interstitial pore spaces. The question is when were such mechanisms initiated and are they presently ongoing?

The open fractures observed in the centres of some large quartz grains have the appearance of being tension fractures opened by externally directed ‘rotational’ pressure, and one possible explanation is the isostatic instability from glacial loading/unloading during the last ice-age. Increased dynamic (vertical) pressure will be active during formation of the ice cap and a corresponding decrease in that pressure component will occur when the ice melts, accompanied by long-term isostatic recovery. Differential vertical movement during this process may explain the presence of open microfractures cross-cutting quartz aggregates and following quartz grain boundaries. Additionally, such an applied pressure on a quartz grain mosaic structure could have caused rotation of the equant grains, but because the quartz grains form a tightly interlocking angular mosaic, any rotation is counter-checked thus producing fractures in the central part of some of the large quartz grains. These features suggest that leakage from fluid inclusions, caused by fracturing, may be a real and ongoing process.

Since the Äspö region has been subject to several glacial events over the past million years, it is also likely that inclusion fluids have been systematically released by fracturing during this period. This leads to the question of whether fracture healing/sealing has also been occurring during these glacial and interglacial periods such that fractures opened by a previous glaciation have been subsequently sealed, thus trapping inclusions containing salinities representative of the pore fluid at that time. These salinities could be higher or lower compared to the situation today and may have contributed to the large variation in measured salinities recorded. There is, however, some doubt as to whether fracture healing/sealing could occur under such temperature/pressure conditions.

Presently observed microfractures thus represent formation after the maximum of the last glaciation, i.e. during the last 10 ka. The removal of the ice cap produced an uplift effect that is still seen in the isostatic recovery in the Äspö region. Depressing and uplifting such vast volumes of rock is bound to create intermittent rock translation leading to fracturing on different scales. Furthermore, the optical anisotropy of the quartz is very pronounced in the present case and maybe the result, at least in part, from the unloading of the ice mass.

3.5.6 Conclusions

Drillcore investigations from the low permeable MFE-borehole have involved a variety of analytical techniques and developed a convenient methodology that has yielded important data about the relation between mineralogy, porosity, tectonics and fluid inclusions.

Basically, four types of fluid inclusion populations have been identified:

- Primary, intracrystalline magmatic Type I fluid inclusions (400°–500°C; 5–30 eq.wt% NaCl).
- Fluid Inclusion Planes (FIPs) containing magmatic/hydrothermal Type II/III fluid inclusions aligned along healed fractures/fissures (100°–300°C; 1–20 eq.wt% NaCl).
- Type IV intracrystalline boundary grain inclusions (60°–70°C; mostly gas filled; some contain 5–15 eq.wt% NaCl).

The amount of fluid in the rock matrix contained in the fluid inclusions has been estimated to be around 0.5 vol%.

The general range of fluid inclusion salinity is between 0.2 and 30 eq.wt% NaCl. $CaCl_2$ sometimes dominates over NaCl. Most grain boundary inclusions are gas filled with only a few liquid varieties with salinities between 5 and 15 eq.wt% NaCl. Overall, the fluid inclusion populations are characterised by a moderately high salinity which may be accessible through deformation and leakage to the interstitial pore space in the rock matrix.

Grain boundaries constitute areas of structural weakness and represent ‘dark corners’ where hidden fluid and mineral inclusions may occur. In the case of dynamic deformation of the rock and rock/water interaction over a timescales relevant to radioactive waste storage, these grain boundaries may be a source of chemical components to the interstitial pore spaces.

The development of microscopic techniques such as computer scanning of thin sections and the use of Laser Ablation ICP-MS analysis of thick sections have been employed and may soon be used as routine tools for more precise assessment of volumetric properties, chemistry of fluid inclusions and further understanding grain boundary relationships.

The Laser Ablation ICP-MS technique is promising and analyses showed anomalies in element traces representing heterogeneities in quartz grains which may be interpreted as grain boundary phases, fluid inclusions or solid inclusions. Tentative proxies for fluid phases or minerals include Na (for NaCl inclusions), Na+Sr (for a Na-Ca-Cl-brine inclusion), Na+Al (for albite), Na+Al+Sr (for plagioclase), K+Al (for K-feldspar), K+Mg+Al (for biotite), Mg+Al (for chlorite), Mg (Ca-Mg-Cl inclusion) and Al (for kaolinite). Further development in this technique is recommended

The question of fluid inclusion leakage into the interstitial pore space and, ultimately influencing the matrix or interconnected pore space fluids/groundwaters, cannot be unequivocally resolved. However, there is evidence of an ongoing process of tectonic stress-release accompanying isostatic recovery following glacial ice melt which could provide a convenient mechanism for fracturing inclusions hosted by quartz and releasing fluids into the immediately accessible rock matrix.

3.6 Wall rock alteration: Evidence of in- and out-diffusion processes

(E-L Tullborg, Terralogica)

A Pilot Study was initiated to examine an identified microfracture (from BIPS images) located 56.5 cm from Section 4 and sealed by the packer sleeve (cf Appendix 11, Figure A11-1). There was a suspicion that this microfracture may have been a conduit for some of the waters collected in borehole Section 4. If this were the case, then 'water flow' along the microfracture might have been subject to in- or out-diffusion processes which, in turn may have left their signature in the adjacent host rock. The purpose, therefore, was to analyse a series of rock slices representing a profile across the microfracture in the Äspö diorite (Figure 3-17), with the objective to assess the nature of in- and out-diffusion processes around the microfracture using microscopic studies, porosity measurements, bulk rock chemistry and U-decay series isotopes (cf Appendix 11). Evidence of diffusion gradients may help to further understand the evolution of the pore space groundwater chemistry.

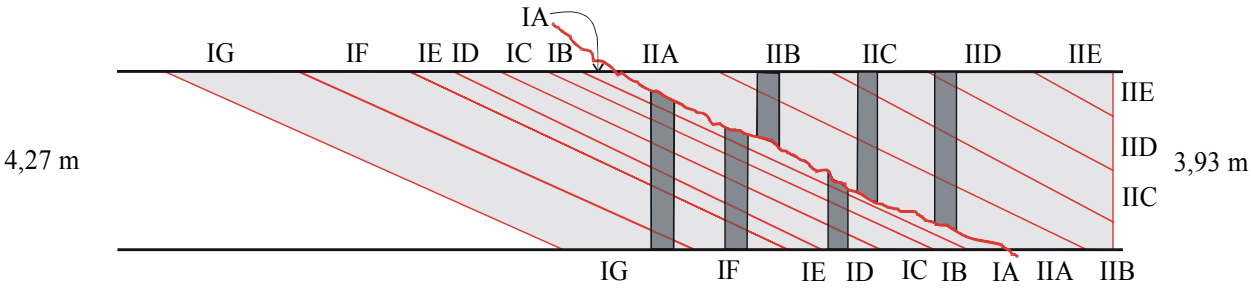

Figure 3-17. *Diagram showing sectioning of the MFE-drillcore across the microfracture (irregular thick red line). Dark grey areas represent missing core portions.*

Microscopically there was no obvious foliation parallel with the fracture but an increased frequency of fractures parallel/subparallel close to the surface was detected. Some 'continuous' microfractures perpendicular to the fracture surface also were recorded (Figure 3-18).

The main observations were:

- **Fracture Coating:** Irregular layer of chlorite, calcite and adularia (0–0.3 mm thick).
- **Wall Rock:** Biotite well preserved but thin rim (100–200 μm) of alteration to chlorite next to the fracture margin; some older hydrothermal alteration of plagioclase (saussuritisation) but no systematic changes towards the fracture; no red staining (i.e. no evidence of increased oxidation).
- **Porosity:** Increase in porosity in the outermost 1 cm sample (0.61 vol% compared with approx 0.4 vol% in the rock matrix); observed as an increased frequency of parallel microfractures.
- **Major and Trace Element Chemistry:** No clear trends; appears to reflect mineralogical heterogeneity; some Rb and Cs retained in the fracture coating.
- **Isotopes:** $^{234}U/^{238}U$ in secular equilibrium apart from the outermost sample closest to the fracture.

The results show no chemical evidence of low temperature alteration or chemical gradients and most chemical variation can be explained by mineralogical heterogeneity. In contrast there was an increase in porosity adjacent to the microfracture edge corresponding to $^{234}U/^{238}U$ disequilibrium. This isotopic disequilibrium suggests that within the last 1 Ma water/rock interaction has (and may be still) occurring marginal to the microfracture and this has been accompanied by an accumulation of uranium.

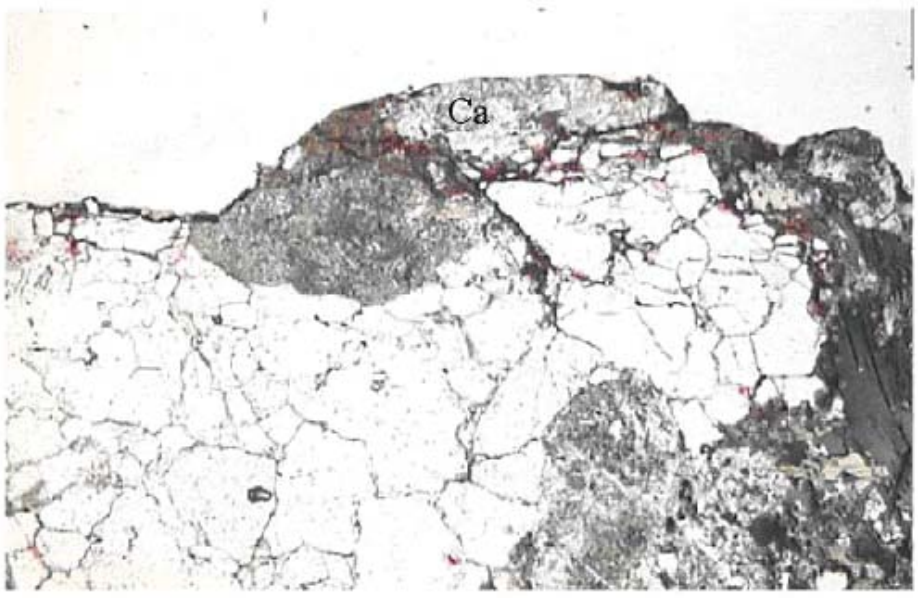

Figure 3-18. *Fracture coating and wall rock dyed with red ink (I KF0051A01:4.1 m). Note the increased microfracture frequency parallel with the fracture surface. The length of the photomicrograph corresponds to 1.25 mm.*

It has not been possible to determine whether the studied microfracture is a presently open, semi-open or mainly sealed in-situ fracture, but the uranium isotopic disequilibrium data suggest it has been open at some stage in the 'recent' geological past (< 1 Ma), and therefore it seems realistic to assume that it acts as a present-day 'more porous pathway' through the matrix bedrock and could be a likely source for some of the matrix waters sampled from MFE-borehole Section 4.

3.7 Summary and conclusions

Drillcore investigations from the low permeable MFE-borehole have involved a variety of analytical techniques and developed a convenient methodology that has yielded important data about the relation between mineralogy, porosity, tectonics and fluid inclusions.

3.7.1 Rock mineralogy

- Two major rock types are present in the matrix borehole; Äspö diorite and Ävrö granite.
- A decrease in mafic content and plagioclase is countered by an increase in quartz and K-feldspar along the drillhole representing the transition of Äspö diorite to Ävrö granite. The mineralogical composition of these two major rock types serves as an important constraint on the pore fluid composition. For example:
  - The finely disseminated calcite will control the carbonate system of the pore fluid.
  - To a certain degree cation exchange might also influence the pore fluid composition although the total clay content is rather small.
  - The occurrence of reduced and oxidised Fe-oxides and Fe-hydroxides will have an impact on the redox potential of the pore fluid.
  - Similarly, the present sulphide minerals are very susceptible to changes in redox conditions.

  - All these constraints are similar for diorite and granite.

3.7.2 Rock chemistry

- Differences between diorite and granite are in accordance with mineralogical differences.
- Chemical differences are too small to have a significant influence on the pore fluid; only exception might be certain metallic trace elements which are more abundant in the diorite in minerals susceptible to alteration.

3.7.3 Density and porosity

- Differences in grain density reflect differences in mineralogy (i.e. content of mafic minerals).
- Total porosity is greater for Ävrö granite (0.76 ± 0.04 vol%) than for Äspö diorite (0.66 ± 0.08 vol%).
- The connected porosity appears to be more variable in the Äspö diorite (0.44 ± 0.07 vol%) than in the Ävro granite (0.40 ± 0.02 vol%), but is the same for both rocks within the accuracy of the methodologies.
- The connected porosity determined by water resaturation is more difficult to achieve in the Äspö diorite than in the Ävrö granite, highlighting the textural differences between the rock types. Generally this supports the hydraulic measurements made in the borehole (cf Chapter 4).
- The difference in total to connected (i.e. water-content porosity) porosity is greater in the Ävrö granite than in the Äspö diorite.
- The difference in total to connected porosity corresponds closely to the independently calculated volume of fluid inclusions. This strongly indicates that the measured non-connected (i.e. not accessible for water diffusion) porosity constitutes almost entirely the amount of fluid inclusions present.
- These findings are in accordance with the greater abundance of quartz and fluid inclusions comprising the Ävrö granite compared to the Äspö diorite.

3.7.4 Fluid inclusions

- Basically, four types of fluid inclusion populations have been identified:
  - Primary, intracrystalline magmatic Type I fluid inclusions (400°–500°C; 5–30 eq.wt% NaCl).
  - Fluid Inclusion Planes (FIPs) containing magmatic/hydrothermal Type II/III fluid inclusions aligned along healed fractures/fissures (100°–300°C; 1–20 eq.wt% NaCl).
  - Type IV intracrystalline boundary grain inclusions (60°–70°C; mostly gas filled; some contain 5–15 eq.wt% NaCl).
- The amount of fluid in the rock matrix contained in the fluid inclusions has been estimated to be around 0.3 vol% for the Äspö diorite and 0.6 vol% for the Ävrö granite.
- The general range of fluid inclusion salinity is between 0.2 and 30 eq.wt% NaCl; $CaCl_2$ sometimes dominates over NaCl. Most grain boundary inclusions are gas filled with only a few liquid varieties with salinities between 5 and 15 eq.wt% NaCl. Overall, the fluid inclusion populations are characterised by a moderately high salinity which may be accessible through deformation and leakage to the interstitial pore space in the rock matrix.

- Grain boundaries constitute areas of structural weakness and represent 'dark corners' where hidden fluid and mineral inclusions may occur. In the case of dynamic deformation of the rock and rock/water interaction over a timescales relevant to radioactive waste storage, these grain boundaries may be a source of chemical components to the interstitial pore spaces.
- The development of microscopic techniques such as computer scanning of thin sections and the use of Laser Ablation ICP-MS analysis of thick sections have been employed and may soon be used as routine tools for more precise assessment of volumetric properties, chemistry of fluid inclusions and further understanding grain boundary relationships.
- The Laser Ablation ICP-MS technique is promising and analyses showed anomalies in element traces representing heterogeneities in quartz grains which may be interpreted as grain boundary phases, fluid inclusions or solid inclusions.
- The question of fluid inclusion leakage into the interstitial pore space and, ultimately influencing the matrix or interconnected pore space fluids/groundwaters, cannot be unequivocally resolved. However, there is evidence of an ongoing process of tectonic stress-release accompanying isostatic recovery following glacial ice melt which could provide a convenient mechanism for fracturing inclusions hosted by quartz and releasing fluids into the immediately accessible rock matrix.

3.7.5 Wall rock alteration

To assess in- and out-diffusion processes from a suspected water-bearing microfracture into the adjacent host rock, microscopic evaluation, porosity measurements and chemical and isotopic analysis were carried out on a perpendicular profile from the microfracture into the Äspö diorite.

- The results show no chemical evidence of low temperature alteration or chemical gradients and most chemical variation in the wall rock can be explained by mineralogical heterogeneity.
- In contrast there was an increase in porosity adjacent to the microfracture edge corresponding to $^{234}U/^{238}U$ disequilibrium. This isotopic disequilibrium suggests that within the last 1 Ma water/rock interaction has (and probably is) occurring marginal to the microfracture and this has been accompanied by an accumulation of uranium.
- It has not been possible to determine whether the studied microfracture is a presently open, semi-open or mainly sealed in-situ fracture, but the uranium isotopic disequilibrium data suggest it has been open at some stage in the 'recent' geological past (< 1 Ma), and therefore it seems realistic to assume that it acts as a present-day 'more porous pathway' through the matrix bedrock.

4 MFE-borehole: Hydraulic character of the rock matrix

(E Gustafsson, Geosigma)

4.1 General

From a general hydraulic viewpoint the MFE-borehole is 'dry' with no water inflow recorded during drilling and no evidence of water-bearing fractures (cf Chapter 2). Based on knowledge from other 'dry' locations at the Äspö HRL the hydraulic transmissivity of the rock surrounding the matrix borehole was expected to be in the range of 10^{-14}–10^{-11} m^2s^{-1}.

Available information useful in estimating the hydraulic properties of the rock matrix included:

- Changes in pressure recorded from each of the four isolated MFE-borehole sections of interest over a period of 3.5 years (cf Chapter 2, section 2.5; Figure 2-4).
- Following a period of 18 months borehole sections 1 and 4 were opened; Section 1 was dry but Section 4 gave 160 mL of water out of a total volume of 210 mL (cf Chapter 2, section 2.6).
- Following a further period of 1 year and 10 months all four sections were opened; Section 1 was again dry but sections 2, 3 and 4 produced respectively 34.14 mL (out of a total volume of 245 mL), 321.19 mL (out of a total volume of 6237 mL) and 195.02 mL (out of a total volume of 210 mL) (cf Chapter 2, section 2.6).
- Petrological and BIPS data located a fine fracture intersection with the borehole at 4.035 m were a packer is located (cf Appendix 11, Figure A11-1); this intersection is some 56.5 cm from Section 4 towards the tunnel.
- While the total porosity is slightly greater in the Ävrö granite compared to the Äspö diorite, the connected porosity is essentially the same in both rocks types (cf Chapter 3, section 3.4).
- Comparison with hydraulic data from other 'dry' locations at the Äspö HRL.

4.2 Predictions and calculated values

At an early stage in the experiment, estimated times to accumulate 250 mL matrix pore water (approximating to the respective volumes of sections 2 and 4 earmarked for sampling) were predicted based on a range of hydraulic conductivity values. Both 2-dimensional radial flow /Todd, 1980/ and 3-dimensional spherical Darcian flow /Moye, 1967/ were considered assuming differential pressures within 10–35 bar and a radius of influence of 5–10 m. The results of the predictions are shown in Figure 4-1. At a conductivity of $1{\cdot}10^{-13}$ ms^{-1} an accumulation of 250 mL matrix pore water would require 2–9 months, and at a conductivity of $1{\cdot}10^{-14}$ ms^{-1} it would need from 16 months to 7 years depending on the flow regime. Compared to the monitored boreholes

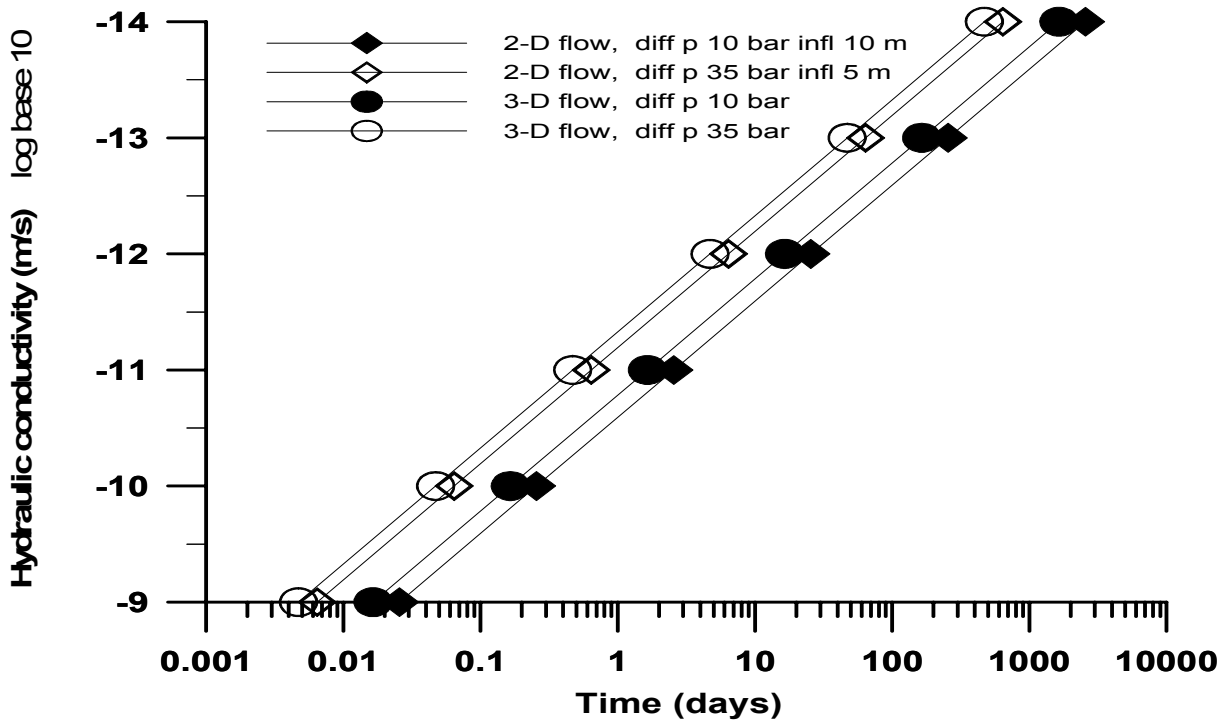

Figure 4-1. *Predicted times to accumulate 250 mL of matrix pore water, based on a range of hydraulic conductivities, considering both radial and spherical Darcian flow and assumed differential pressure within 10–35 bar and radius of influence 5–10 m.*

(cf Figure 2-4), after 15 months of the experiment still no pressure increase was measured in borehole Section 2. In Section 4 the pressure had increased, but not to a level corresponding to the accumulation of 250 mL of matrix water. This suggested that the hydraulic conductivity in the matrix rock block lies somewhere around 10^{-14}–10^{-13} ms^{-1}.

As described in Chapter 2, continuous monitoring of pressure in the four borehole sections, with the outlet valves to the sampling cylinders closed**,** commenced directly after installation of the packer/sampling equipment. Because of the reduced volumes in sections 2 and 4 due to the installation of dummies, it was expected that these two sections would record the most rapid pressure build-up. Increasing pressure should indicate a build-up of gas and/or matrix pore water seeping into the isolated borehole sections from the host rock. Figure 2-4 shows the pressure curves from June 1998 to March 2003; the break in the curves in December 1999, October 2001 and February 2003 indicates the three sampling campaigns when sections 1 and 4 (first campaign), sections 1 to 4 (second campaign) and sections 1 to 4 (third sampling campaign) were opened for sampling.

Pressure increases, however, do not necessarily indicate that pore water is accumulating. Several processes may be interacting, for example, multiple-phase diffusion processes involving nitrogen (out-diffusion) matrix gases and/or matrix pore waters (in-diffusion), and gas produced in the borehole sections (cf Chapter 6). If these processes occur under equilibrium conditions then little or no pressure increase would be expected in the isolated borehole sections until they are completely filled with matrix pore water. In any case, the out-diffusion of nitrogen, accompanied by a gradual pressure decrease, might

be expected to characterise the initial stages of the experiment. This was suggested by borehole sections 2 and 4 although, in contrast, Section 1 showed only a brief decrease followed by an increase and then a gradual decrease. A sharp increase in the early stages was shown by Section 3 before levelling off. After March 1999, however, the system appeared to have stabilised and, as might be expected from the section volumes, Section 4 (210 mL) showed a steady increase to a maximum in December 1999 before levelling off. The sampling carried out in December 1999, October 2001 and February 2003 confirmed that the pressure increases did largely correspond to accumulating waters and gases.

To test the earlier predictions of hydraulic conductivity in the matrix block, the hydraulic conductivity was calculated following the December 1999 sampling using as input the measured inflow rate, the actual pressure in the borehole section and an estimate of pressure in the surrounding rock The parameter values used included:

- measured inflow rate into the MFE-borehole: 180 mL during 18 months;
- measured pressure in the MFE-borehole section: 1–2 bar (0.1–0.2 MPa);
- estimate on pressure in the surrounding rock, creating differential pressures within 10–35 bar (1.0–3.5 MPa); and
- estimated radius of influence: 5–10 m (pressure).

The flow regimes considered were:

- Darcian flow;
- 2-D radial flow according to Thiems formula /e.g. Todd, 1980/; and
- 3-D spherical flow with spherical flow at a distance of half a section length /Moye, 1967/.

Hydraulic conductivity of the matrix rock block was calculated to $1 \cdot 10^{-14}$–$6 \cdot 10^{-14}$ ms^{-1}. Even though there are uncertainties in estimated pressure and the assumed flow regimes, the calculated conductivity is judged reasonable and in accordance with the predictions above, although in the lower region of the expected range.

4.3 Water movement in the rock matrix

The chemical analyses of the sampled pore waters from borehole sections 2, 3 and 4 (cf Chapters 6 and 7; Appendix 13) show a water composition more typical of low to intermediate conductive fractures in the near-vicinity of the matrix borehole (e.g. transmissivities of 10^{-10}–10^{-5} m^2s^{-1}) than what was expected from the rock matrix. Hence, the existence of preferential "flow paths" in the matrix rock, closely related to minor water-bearing fractures seems probable. To estimate the distance of such water-bearing fractures, feeding some tiny connected micro-scale fractures eventually entering or passing close by the sampled borehole sections, some calculations were carried out on MFE-borehole Section 4. Assuming that the hydraulic conductivity in Section 4 was due only to flow in microfractures, simple mass balance calculations were made based on the cubic law aperture /Snow, 1968; Tsang, 1992/. Based on the MFE-borehole and other detailed studies at the Äspö HRL, the

calculations assumed flow in 1–3 microfractures in Section 4 with transmissivities ranging from $1 \cdot 10^{-14} - 1 \cdot 10^{-13}$ $m^2 s^{-1}$, an accumulated volume of 180 mL, and radial and laminar flow characterising the borehole section. If most of the accumulated water in Section 4 originated from a microfracture(s), estimates showed that the sampled water in the borehole section was extracted from a distance not exceeding 3–7 m along the microfracture(s). Of interest in this respect, and as described in section 3.6, was a very fine, semi-permeable microfracture intersecting the borehole some 56.5 cm from Section 4 which from available data is assumed to be open (cf Chapter 3; section 3.6).

Alternatively, 180 mL of matrix pore water could be extracted from quite a small homogeneous block of porous rock. Therefore, if it is assumed that the matrix rock block consisted of a homogeneous porous media with connected pore space, a 41 litre volume of such a block would be sufficient to extract 180 mL water, considering a porosity of 0.44 vol% for the Äspö diorite (cf Chapter 3; section 3.4). This small rock volume could be contained easily within a sphere of 21 cm radius, or a cylinder with a radius of 15 cm, if the length is 60 cm, i.e. equivalent to the sampled Section 4.

The basis of the foregone discussion focussed on the Äspö diorite using the same average value of connected porosity as the Ävrö granite (0.44 and 0.40 vol% respectively). However, microscopic examination of the impregnated samples (cf Chapter 3; section.3.4) indicated that most of the porosity reflected a network of connected micro-scale fractures where the Äspö diorite, with more penetrative foliation than the Ävrö granite, showed stronger orientation of the fractures parallel to the foliation. This was also supported by the fact that MFE-borehole Section 4 (total section volume of 210 mL) in the diorite had already been sampled after 18 months (160 mL) and had recovered fully after a further 22 months (additional 195.02 mL), whilst Section 2 (total section volume of 245 mL) hosted by the Ävrö granite had only accumulated 34.74 mL over the full 38 month period.

4.4 Conclusions

Taking into consideration: a) petrology, b) porosity measurements, and c) long-term pressure monitoring and groundwater sampling of the isolated MFE-borehole sections, predictions of groundwater flow times to the borehole sections from the surrounding bedrock based on both 2-D radial and 3-D spherical flow (assuming differential pressures of 10–35 bar and a radius of influence of 5–10 m), where in accordance with the estimated rock matrix hydraulic conductivity (10^{-14}–10^{-13} ms^{-1}) and the measured porosity.

5 MFE-borehole: Rock pore water studies

(N Waber, University of Bern, S Frape, University of Waterloo, and D Hurst, University of Waterloo)

5.1 General

In crystalline rocks of very low permeability there exist two major origins of matrix fluids: a) fluids trapped in mineral fluid inclusions (cf Chapter 3.5), and b) fluid trapped in the pore space between minerals and along their grain boundaries. This latter pore fluid, further called 'pore water' is normally close to or at equilibrium with the rock mineralogy under present-day conditions. It interacts with flowing groundwater in water-conducting zones mainly via diffusion. The characterisation of this pore water has to be performed by applying indirect methods based on drillcore material and/or long-term in-situ sampling of pore water in isolated borehole intervals. While long-term in-situ sampling is only feasible in an underground laboratory, indirect methods based on the analysis of drillcore material from deep drillholes can be useful.

There exist several indirect methods for the chemical characterisation of in-situ pore waters in rocks of low-permeability including aqueous leaching of crushed drillcore material, diffusive equilibration techniques (in-situ or on drillcore material), high pressure squeezing of drillcores, and high pressure pore-water displacement in drillcores. All of these methods can only provide parts of the pore water chemistry and they have to be applied as a complement to, and in conjunction with, geochemical modelling in order to derive the complete chemical composition.

Furthermore, not all these methods are similarly applicable to different rock types. While aqueous leaching techniques combined with the appropriate mineralogy and porosity data and geochemical modelling are successfully applied in rocks with a high ratio of pore water to fluid trapped in fluid inclusions such as claystones /e.g. Beaucaire et al, 2000; Pearson et al, 2003/, these methods might not be applicable to rocks with a low ratio of pore water to fluid trapped in fluid inclusions. Similarly, high pressure squeezing and pore-water displacement techniques are successfully applied to rocks with high pore water contents /e.g. Bath et al, 1988; Fernández et al, 2001; Pearson et al, 2003/, but might not be applicable to rocks with low water contents.

In this present study the experimental approaches to characterise the pore water chemistry in the low-permeability rocks at Äspö HRL involved aqueous leaching, cation exchange, pore-water diffusion and pore-water displacement. In addition, long-term in-situ sampling of seepage water in isolated borehole sections was performed; these investigations are described and discussed in Chapters 6 and 7. It was hoped that the water accumulated in the intervals over several months is representative for the in-situ pore water and that its composition could act as a constraint for the identification of possible experimental artefacts in the indirect methods applied. The identification of such artefacts is important for the transferability of such indirect methods to sites where no long-term experiments can be performed in-situ.

5.2 Sample considerations

A drillcore length of Äspö diorite (3.25–3.60 m) was investigated by the University of Waterloo. The University of Bern studied rock portions selected from most of the rest of the drillcore (3.60–9.70 m) representing Äspö diorite, Avrö granite and also a minor aplitic vein/dyke. These samples were subjected to a series of experiments in an attempt to extract and characterise the accessible pore water. The samples investigated and the experiments performed are listed in Table 5-1.

As described earlier, to avoid evaporation of the pore water the MFE-drillcore was preserved following mapping. Unfortunately the procedural protocol was not adhered to and beeswax was applied directly on the drillcore instead of first wrapping the core in aluminium foil. There was some concern that this may contribute to some contamination during execution of the experiments. This was not the case for the University of Bern as the outer 5 mm core margin containing the wax was removed as an initial step. The University of Waterloo sample, however, was initially heated to remove the wax which may not have been complete. Furthermore, heating may have facilitated movement of the wax deeper into the drillcore via interconnected pores and/or microfractures etc. As a precaution the wax was analysed separately and the data indicated that any potential major contamination was minimal (cf Appendix 13, Table A13-3).

Table 5-1. Samples and experiments performed.

Sample	Drillcore length (m)	Rock type	Experiment [1)]	Laboratory
MFE-3.42	3.38–3.48	Diorite	High pressure displacement	Univ Waterloo
MFE-3.54	3.48–3.60	Diorite	Repeated aq leaching of same material	Univ Waterloo
MFE-3.66	3.62–3.70	Diorite	Aq leachate, CEC at different S:L, WC	Univ Bern
MFE-3.79	3.77–3.81	Diorite	Aq leachate at different grain sizes, WC	Univ Bern
MFE-3.85	3.81–3.89	Aplitic dyke	Aq leachate at different grain sizes, WC	Univ Bern
MFE-3.95	3.90–4.00	Diorite	Aq leachate at different grain sizes, WC	Univ Bern
MFE-4.32	4.27–4.37	Diorite	Aq leachate at different grain sizes, WC	Univ Bern
MFE-4.44	4.39–4.49	Diorite	Aq leachate at different grain sizes, WC	Univ Bern
MFE-4.65	4.59–4.71	Diorite	Aq leachate, CEC at different S:L, WC	Univ Bern
MFE-9.33	9.28–9.37	Granite	Aq leachate at different grain sizes, WC	Univ Bern
MFE-9.66	9.62–9.70	Granite	Aq leachate at different grain sizes, WC	Univ Bern
KF93-33.66	33.62–33.70	Diorite	Diffusion experiment (batch), WC	Univ Bern
KF93-33.75	33.70–33.79	Spilitic dyke	Diffusion experiment (batch), WC	Univ Bern
KF93-33.83	33.79–33.87	Diorite/ aplite	Diffusion experiment (batch), WC	Univ Bern

[1)] Aq leachate: aqueous leachate; WC: Water content.

5.3 Aqueous leaching experiments

5.3.1 General

Aqueous leaching is commonly performed on dried and ground (< 63 μm) rock material. During drying of the still intact core material, dissolved constituents in the pore water will precipitate as highly soluble salts following complex evaporation cycles. Crushing and grinding of the rock material will additionally liberate fluid trapped in mineral fluid inclusions. The mineralisation of a leachate solution is thus the sum of: a) the constituents originally dissolved in the pore water, b) the constituents present in inclusion fluid, and c) water-rock interaction during the leaching process.

Aqueous leaching provides useful data for pore water characterisation in claystones, where the volumetric ratio of pore water to fluid trapped in fluid inclusions is high and the salt contribution by inclusion fluid will be within the analytical error even if the fluid inclusions are of high salinity /e.g. Waber et al, 2003/. In contrast, the pore water content in crystalline rocks is much lower and fluid released from fluid inclusions during the grinding process may well have a significant impact on the leachate solution. Therefore, pore water leaching studies in crystalline rocks have to concentrate on the chemical behaviour of a dissolved constituent (reactive vs non-reactive) and the original residence of such a constituent (pore water vs fluid inclusion). While the first can be achieved by leaching rock material at different solid:liquid ratios, the latter is carried out by leaching different grain-size fractions of the rock under investigations.

5.3.2 Sample preparation and analysis

At the University of Waterloo the prepared core was coarse crushed in a jaw crusher and then pulped in a corundum shatter box. To the pulped sample (1.472 kg) one litre of ultrapure water was added and the mixture was shaken end-over-end for 24 hours under ambient conditions at room temperature. The mixture was coarse filtered (#4 filter paper) or centrifuged, followed by vacuum flask filtering through a 0.45 μ filter. The remaining rock mixture was dried and the above procedure repeated a second and a third time. Following each leach, the filtered supernatant solution was analysed for major and trace elements, $^{87}Sr/^{86}Sr$ isotopic ratios and the ^{37}Cl isotope composition (cf Appendix 13 for methods).

At the University of Bern aqueous leaching of sample splits was performed to investigate: 1) the leaching behaviour at different solid:liquid mass ratios, and 2) the leaching behaviour of different grain-size fractions. For the former, unpacking and all preparation steps were performed in a glove-box under a continuous N_2-gas stream with an oxygen content of < 0.1% to minimise oxidation and, for comparison, also under ambient laboratory conditions. First, the outer rim (approx 1 cm) of the core samples was removed by a chisel to ensure sample material that is neither influenced by the wax coating nor by the disturbed zone created by the drilling process. This was followed by determining gravimetrically the water content (cf section 3.4). The samples were crushed initially in the glove-box and then further ground by a carbide-tungsten mill to a grain size of < 63 μm. During these procedures exposure of the rock material to the atmosphere was kept to a minimum. Aqueous leaching with double deionised water was then performed in duplicate with up to four different solid:liquid mass ratios

(0.25, 0.5, 1.0, 1.5). Between 15–30 g of rock powder were used for each of the different solid:liquid ratios. The suspensions were shaken end-over-end in polypropylene tubes for 7 days and then allowed to sediment for one hour. When completed, pH and alkalinity measurements were initially made (in and outside the glove-box) and then the remaining solutions were centrifuged and then filtered with 0.2 μm millipore filters for cation, anion and isotopic analyses.

Aqueous leaching of the remaining samples was performed to investigate the leaching behaviour of different grain-size fractions. Preparation and leaching of these samples were carried out under ambient laboratory conditions. They were first coarse ground and then continuously ground to finer grain sizes. The various grain-size fractions were removed at each crushing/grinding step by sieving the material with different mesh sizes (< 3 mm, 2–3 mm, 1–2 mm, < 0.5 mm, < 63 μm). Aqueous leaching of the different grain-size fractions was performed with double deionised water at a solid:liquid mass ratio of 1:1 using 20–30 g of rock material. The leachates were treated and analysed as for the previously described leaching experiment, except that the suspensions were shaken only for two days.

5.3.3 Leachates at different solid:liquid ratios

Leaching of rock material at different solid:liquid ratios was performed to identify the mobile or free elements of the pore water. An element that has only readily soluble salt sources during leaching will result in a linear relationship between the element concentration in the aqueous leachate and the solid:liquid ratio used in the experiment. A similar linear relationship would be established from solutes originating from entirely dissolved, soluble rock minerals. Elements subjected to a mineral solubility control (e.g. calcite) should lead to (nearly) equal concentrations at all solid:liquid ratios.

Aqueous leaching tests at various solid:liquid ratios were carried out at the University of Bern on 15–30 g of ground Äspö diorite material (< 63 μm). In addition to the solutes dissolved from easily soluble pore water salts, it was expected that at this grain size most of the fluid contained in fluid inclusions would released also to the leachate.

In the leached solutions the total dissolved solids increased from 146 mg/L at a solid:liquid ratio of 0.25, to 246 mg/L at a solid:liquid-ratio of 1.5 (cf Appendix 13, Table A13-2). At all solid:liquid ratios the dominant anion in the leach solution was HCO_3 followed by Cl and SO_4, while Na and K were the dominant cations. All solutions had a charge imbalance of less than ± 4% indicating an acceptable accuracy.

The concentrations of Cl, SO_4 and Br in the leachates increased linearly with increasing solid:liquid ratios (Figure 5-1) indicating that none of these constituents were significantly influenced by rock dissolution reactions. In contrast, the less well-defined relationship observed for F^- was thought to be a result of rock mineral dissolution, such as, for example, accessory fluorite dissolution.

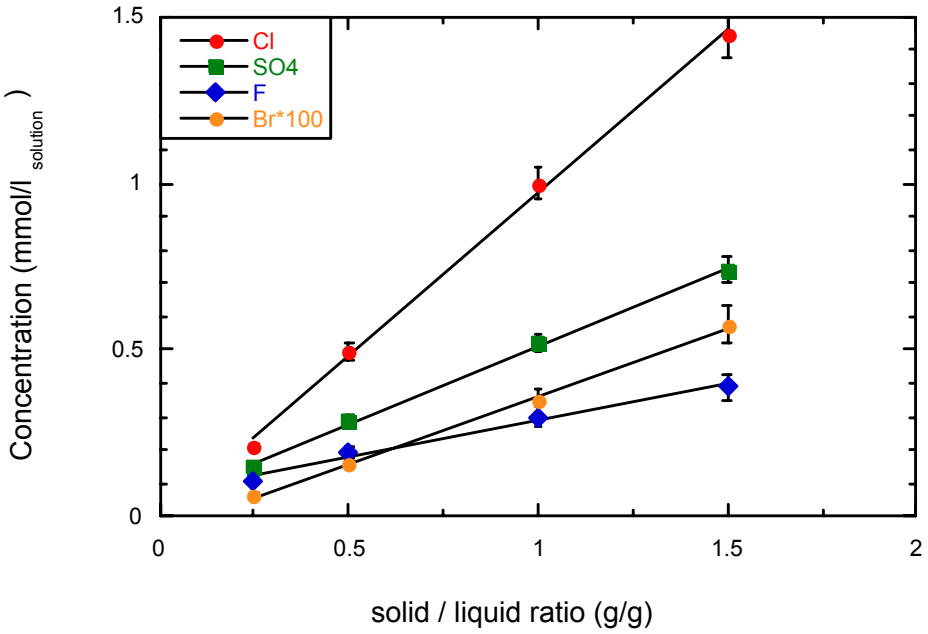

Figure 5-1. *Sample MFE-3.66: Anion concentrations in aqueous leachates as a function of different solid:liquid ratios (error bars indicate analytical error of 5% for Cl and SO_4 and 10% for Br and F).*

The concentrations of Na and K also increased with increasing solid:liquid ratio (Figure 5-2), but with a less well linear correlation than Cl. This indicated that Na and K were not only released into the leach solution from pore water salts (including fluid inclusion salts), but to a certain degree also from rock-water interactions. Possible sources included initial feldspar alteration promoted by the large surface areas in the ground material and cation exchange reactions. Of special interest to the pore water composition was the fact that the Na concentrations on a molar basis are significantly higher than those of Cl. The dominant salt in fluid inclusions was identified to be NaCl (cf Appendices 8, 10 and 12) and thus the molar Na/Cl from these sources should have been close to 1. This indicated that the pore water in the water accessible pore space of the rock must have a molar Na/Cl ratio greater than 1 because the leaching time was too short for introducing such a large amount of Na into the leach solution by Al-silicate mineral dissolution.

Within the analytical uncertainty, the low concentrations of Ca and Mg were similar at all solid:liquid ratios suggesting a mineral solubility control for these two constituents.

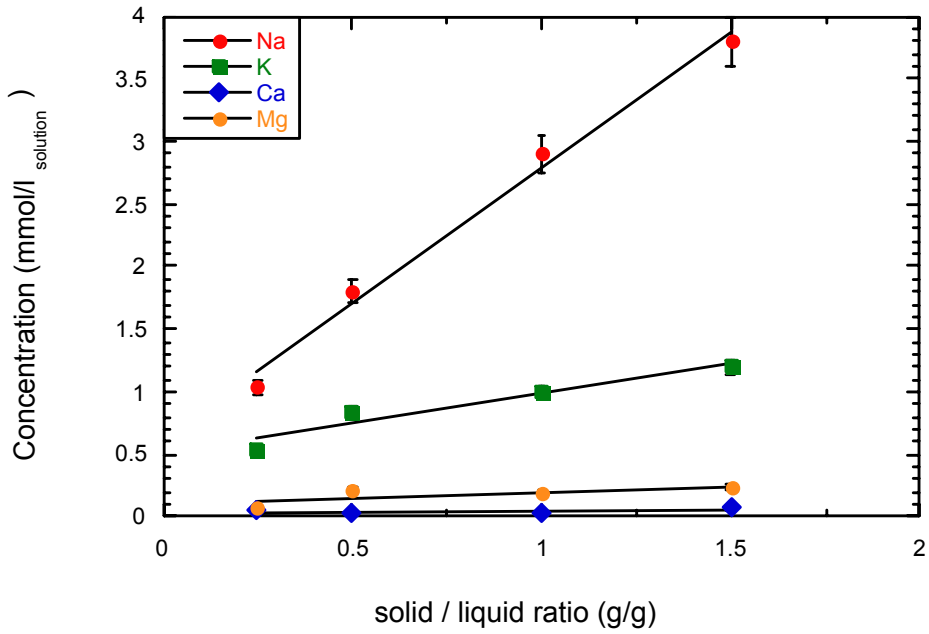

Figure 5-2. *Sample MFE-3.66: Cation concentrations in aqueous leachates as a function of different solid:liquid ratios (error bars indicate analytical error of 5% for Na and K, and 10% for Ca and Mg).*

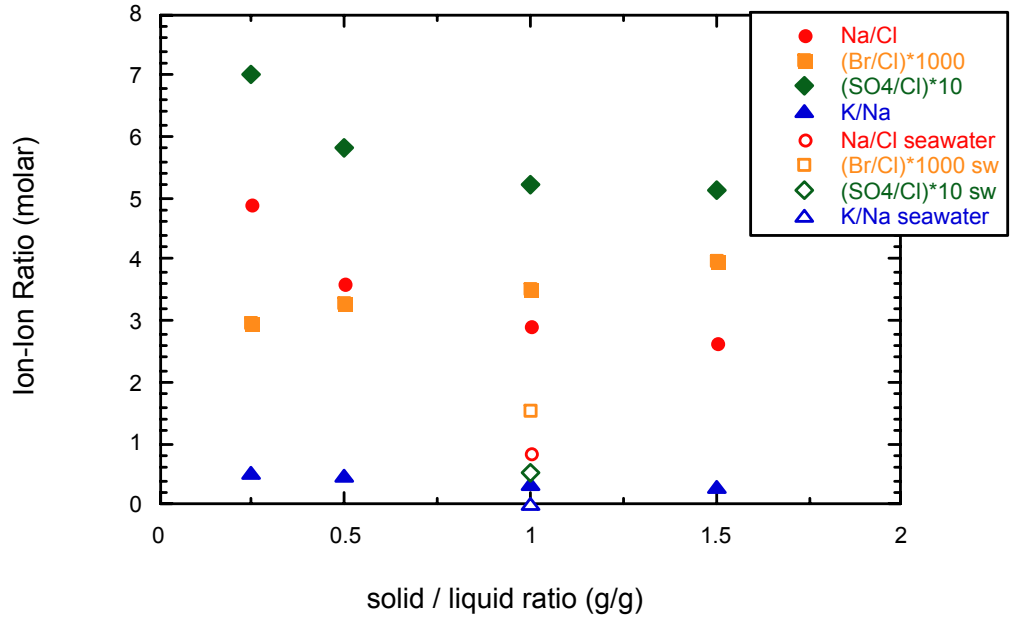

Figure 5-3. *Sample MFE-3.66: Ion-ion ratios in the leach solution as a function of solid:liquid ratio. Note the decrease of the Na/Cl, SO_4/Cl and K/Na ratios with increasing solid:liquid ratios while the Br/Cl ratio increases. For comparison the same ion-ion ratios of seawater are shown.*

The molar ratios of Na/Cl, SO_4/Cl, and K/Na decreased with increasing solid:liquid ratio, while the molar Br/Cl ratio increased (Figure 5-3). This indicated that in the leach solutions the contribution of a Cl-rich fluid with a high Br/Cl ratio increased with increasing solid:liquid ratio. The source of this fluid could only be fluids trapped in mineral fluid inclusions. All these ion-ion ratios were significantly higher compared to those of seawater at all solid:liquid ratios.

Saturation indices

Saturation index calculations indicated that the leachates were at equilibrium or oversaturated with respect to calcite (cf Appendix 13, Table A13-2). In an aqueous solution an oversaturation with respect to calcite is commonly due to analytical uncertainties (mainly pH and alkalinity) and/or artefacts during the experiment or the sampling procedure (in- or out-gassing of CO_2). Applying geochemical modelling it was shown that all leach solutions were at calcite equilibrium by allowing an analytical uncertainty of ± 10% for alkalinty and ± 0.1 log unit for pH. Such an uncertainty seemed reasonable considering the small sample volumes of a few millilitres.

This did neither explain, however, the very low concentrations of Ca nor their erratic behaviour with varying solid:liquid ratios. It appeared that the Ca concentrations were not only controlled by calcite solubility, but also by processes which could no longer be accounted for quantitatively. Such a process might be the sorption of Ca onto newly created and abundant quartz surfaces in the ground material. Similar processes might account for Mg.

Adopting the measured Ca concentrations as representative and adjusting the leach solution compositions to calcite equilibrium, the leach solutions were theoretically oversaturated with respect to dolomite and undersaturated with respect to fluorite, gypsum, strontianite and celestite. While fluorite might actually occur in the Äspö diorite and thus might potentially serve as a solubility control for dissolved fluoride, none of the other minerals was reported to occur in the Äspö diorite. For all leach solutions a partial pressure of CO_2 ($\log pCO_2 < -5.0$) far below that of the atmosphere ($\log pCO_2 = -3.5$) was calculated when using the measured values of pH and alkalinity.

Concentrations for dissolved Si and Al measured by ICP were also reported (cf Appendix 13, Table A13-2). With the pH (10.0) and the total alkalinity (1.7 meq/L) values measured for this solution, no convergence was reached in the Al speciation calculation. This indicated that the measured Al concentration was not representative for dissolved Al in the leach solution and that a large amount of Al in the leach solution was present in colloidal form. This was supported by the apparent oversaturation of the solution with respect to pure silica phases. It thus appeared that the concentrations of Al and Si were both too high and perturbed by colloids, which were most probably created during grinding of the rock sample.

5.3.4 Multiple leachates during grain-size reduction

A large-size Äspö diorite sample (1.472 kg) was used at the University of Waterloo to investigate the efficiency of the leaching and the existence of possible fluid sources that might not be accessible to the aqueous leach solution after only one grinding process (e.g. mineral fluid inclusions).

Experiments showed that the total mineralisation of the leach solutions decreased by almost a factor of four from the first leach to the third leach (cf Appendix 13, Table A13-3). The decrease was mainly related to decreasing concentrations in the major components Na, K, Cl and SO_4. A linear decrease with multiple leaching was observed for Na, Cl and SO_4, however, with a different slope (Figure 5-4). As already observed for the leachates at different solid:liquid ratios, the Na concentrations on a molar basis far exceeded those of Cl.

In contrast to the leachates at different solid:liquid ratios, the concentration of K no longer showed a similar behaviour to that of Na and the concentrations became equal in the second and third leach (Figure 5-5).

Most of the divalent cation concentrations (including also most heavy metals) showed a large decrease from the first to the second leach, followed by a slight increase from the second to the third leach (Figure 5-5). At present, the reason for this behaviour is unknown.

The concentrations of Al and Si in the first leach solution were very high and decreased by up to an order of magnitude in the second and third leach solution. As already mentioned with respect to leachates at different solid:liquid ratios, it appears that these high concentrations do not represent dissolved concentrations, but are due to colloidal perturbations.

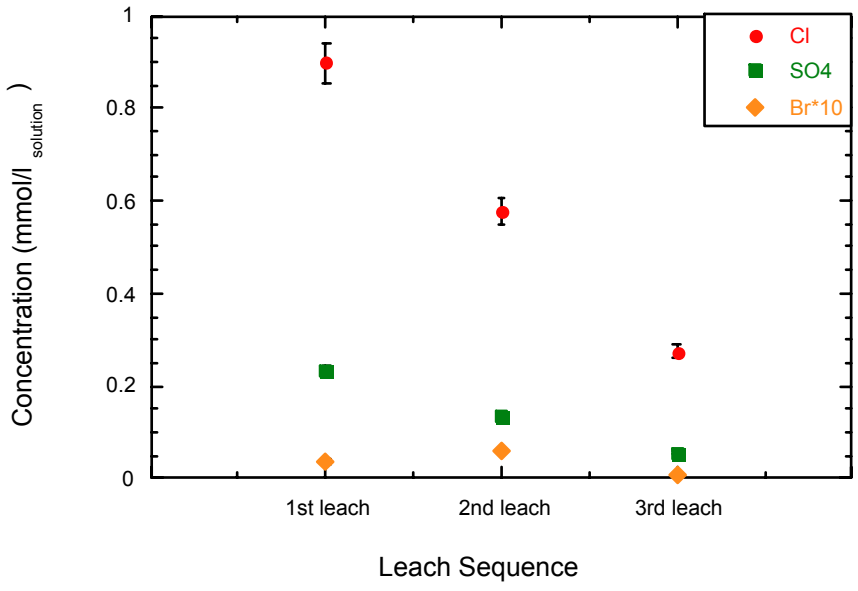

Figure 5-4. *Sample MFE-3.66: Anion concentrations in aqueous leach solutions of multiple ground and leached rock material (error bars indicate analytical error of 5% for Cl and SO_4 and 10% for Br).*

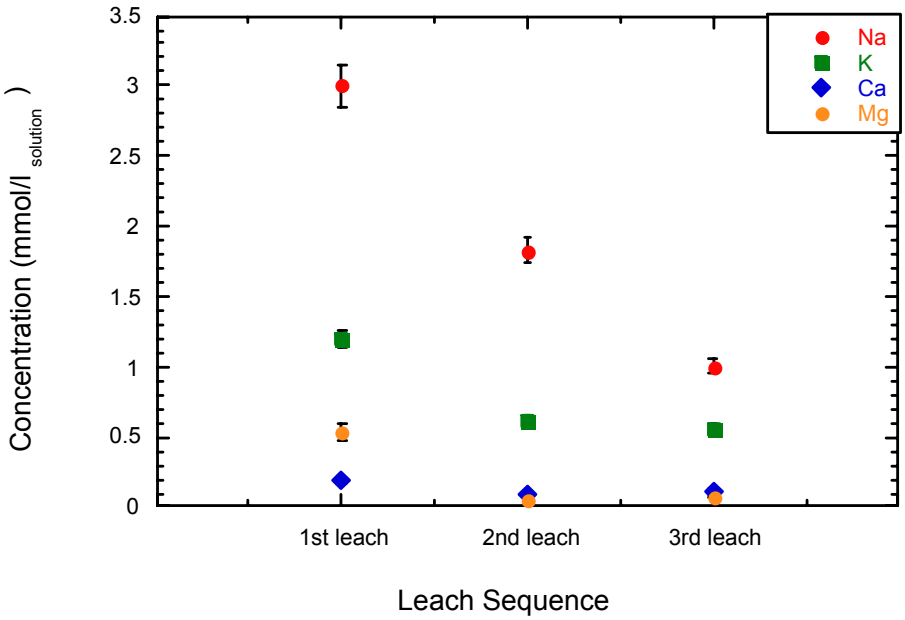

Figure 5-5. *Sample MFE-3.50: Cation concentrations in aqueous leach solutions of multiple ground and leached rock material (error bars indicate analytical error of 5% for Na and K and 10% for Ca and Mg).*

The molar ratios of Na/Cl, Br/Cl, SO_4/Cl and K/Na did not show any systematic trends (Figure 5-6) and appeared to be disturbed by analytical artefacts (e.g. Br concentration of second leach solution) and/or complex processes not presently resolved.

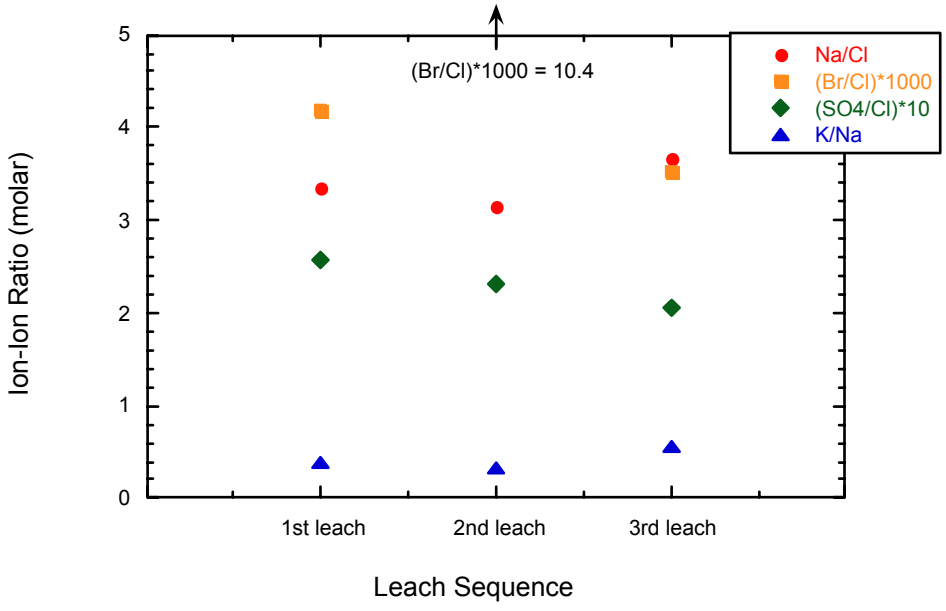

Figure 5-6. *Sample MFE-3.66: Ion-ion ratios in aqueous leach solutions of multiple ground and leached rock material. Note the irregular behaviour of the Na/Cl and Br/Cl ratios.*

5.3.5 Leachates of grain-size fractions

Leaching at different grain-size fractions was performed at the University of Bern to investigate the significance of fluid trapped in mineral fluid inclusions on the leach solutions. Depending on the impact of such fluid sources on the leach solution the calculation of free element concentrations per volume of pore water could be inhibited.

Leaching rock material (20–30 g) of different grain-size fractions at a solid:liquid ratio of 1:1 was carried out. Both the Äspö diorite and Ävrö granite were sampled, covering all three sections in the borehole where packer-systems were installed for long-term in-situ water sampling. Five different grain sizes were chosen to cover the range of mineral grain size in the undisturbed rocks. It was expected that in the finest grain size (< 63 μm) essentially all mineral grains would be completely destroyed thus liberating all fluid included in mineral inclusions. Since the coarsest grain-size fraction was more representative of a disintegrated rock with the individual mineral grains being left mainly intact, the fluid leached from this fraction was expected to be mainly the pore water from the in-situ interstitial pore space of the rock that was also accessible for solute transport.

In all leach solutions independent of the grain-size fraction leached, the major dissolved components were Na, K, HCO_3, Cl and SO_4 (cf Appendix 13, Table A13-4). The amounts of total dissolved solids in the leached solutions decreased with increasing grain size by a factor between 3 and 5 due to the decrease in major components (Figures 5-7 to 5-10).

Anion concentrations in all leach solutions decreased most pronounced between the grain sizes smaller than 0.5 mm and those larger than 1 mm (Figures 5-7 and 5-9) independent of rock type. From the most fine-grained to the most coarse-grained fraction the concentrations of Cl, Br and SO_4 decreased between a factor of 5 to 15 on a molar basis, while the decrease in F and alkalinity concentrations was only between a factor of 2 to 4. In absolute terms, the Äspö diorite leach solutions of grain sizes < 0.5 mm had generally higher concentrations of Cl, Br and SO_4 compared to the Ävrö granite and the aplitic dyke (Figures 5-7 and 5-9). In contrast, no additional differences were observed between the different rock types in the leach solutions of the most coarse-grained fraction.

The concentrations of Na and K also decreased most pronounced between the grain sizes smaller than 0.5 mm and those larger than 1 mm (Figures 5-8 and 5-10) independent of rock type. However, the decrease was generally only between a factor of 2 to 5 and thus significantly less than for most anions. For all grain-size fractions Na concentrations were significantly higher in the Äspö diorite compared to the Ävrö granite and the aplitic dyke (Figures 5-8 and 5-10), while K was present in similar concentrations in the leach solutions of all rock types.

The concentrations of Ca and Mg were close to or below the detection limit of the method applied in all leach solutions (cf Appendix 13, Table A13-4). This explained the somehow erratic behaviour of some individual samples although a general trend towards deceasing concentrations with increasing grain size was observed.

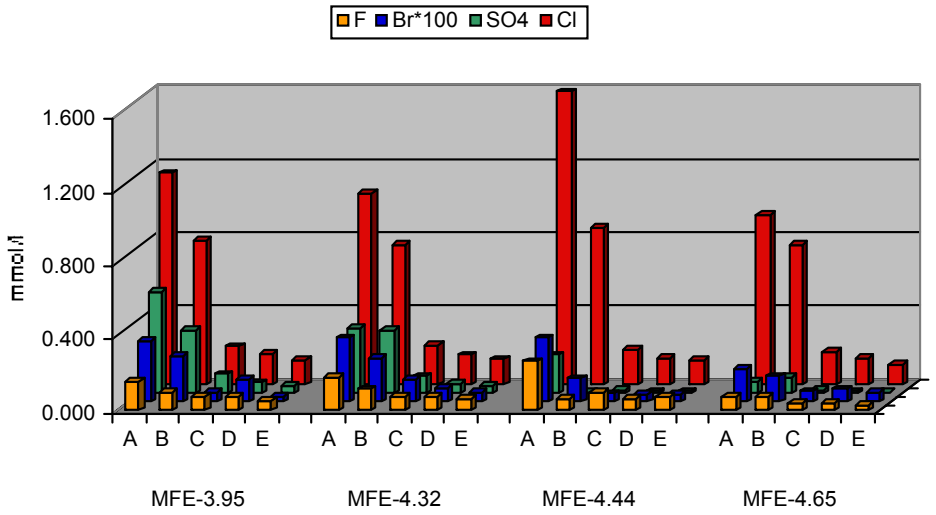

Figure 5-7. *Äspö diorite: Anion concentrations in leach solutions of different grain-size fractions (A=<63 µm, B=<0.5 mm, C=1–2 mm, D=2–3 mm, E=>3 mm).*

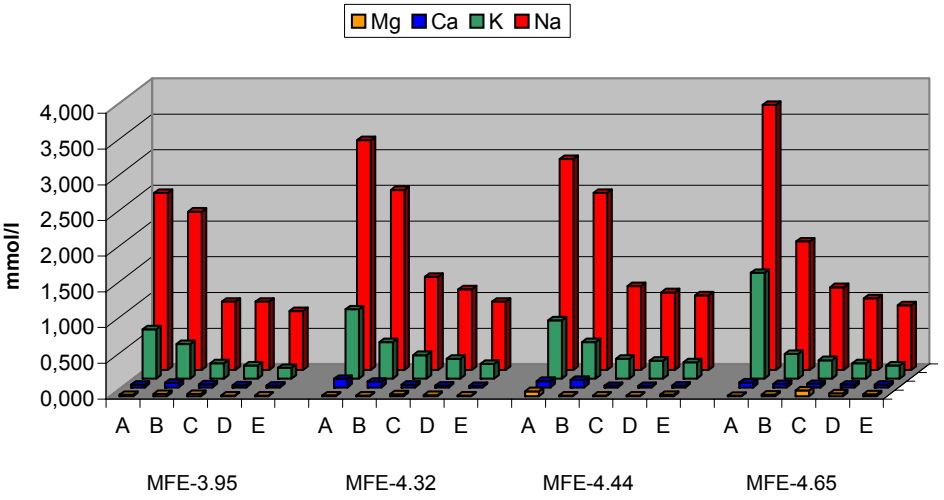

Figure 5-8. *Äspö diorite: Cation concentrations in leach solutions of different grain-size fractions (A=<63 µm, B=<0.5 mm, C=1–2 mm, D=2–3 mm, E=>3 mm).*

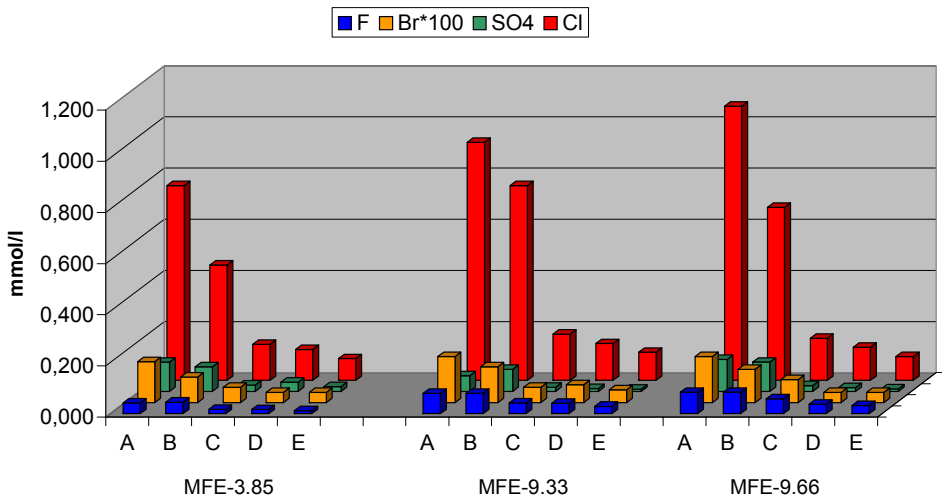

Figure 5-9. *Aplitic dyke (MFE-3.85) and Ävrö granite: Anion concentrations in aqueous leach solutions of different grain-size fractions (A=<63 µm, B=<0.5 mm, C=1–2 mm, D=2–3 mm, E=>3 mm).*

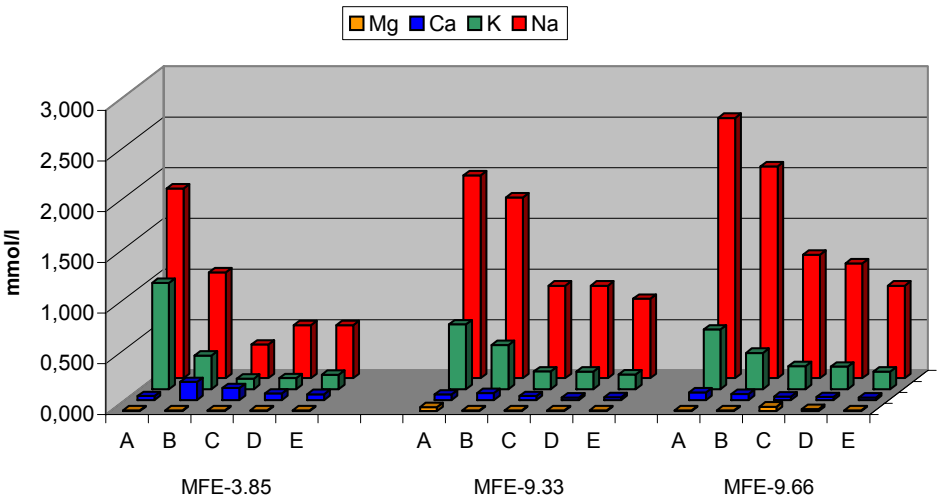

Figure 5-10. *Aplitic dyke (MFE-3.85) and Ävrö granite: Cation concentrations in aqueous leach solutions of different grain-size fractions (A=<63 µm, B=<0.5 mm, C=1–2 mm, D=2–3 mm, E=>3 mm).*

Molar Na/Cl ratios of the two most fine-grained and the coarser-grained fractions were similar in Äspö diorite and the Ävrö granite. In the fractions < 63 μm and < 0.5 mm they varied between 1.8 and 3, while they were mainly between 6 and 8 in the fractions 1–2 mm, 2–3 mm, and > 3 mm (Figures 5-11 and 5-12). Thus, the molar Na/Cl ratios were significantly higher than in seawater (0.858) in all leach solutions. In the aplitic dyke, the grain-size fractions < 63 μm, < 0.5 mm, and 1–2 mm had similar ratios as the Äspö diorite and the Ävrö granite and ratios between 4 and 6 in the two most coarse-grained fractions (Figure 5-12). This is consistent with more fine-grained texture of the aplitic dyke compared to the diorite and granite. The distinct difference in Na/Cl ratios as a function of grain size indicated that in the fine-grained fractions a significant proportion of a NaCl-rich fluid source contributed to the leach solution composition in addition to a Na-rich fluid leached from the coarser grain-size fractions. The sources of such a NaCl-rich fluid are fluid inclusions.

Molar Br/Cl ratios showed a general trend to increase from the most fine-grained fraction to fractions of 1–2 mm and 2–3 mm, and decrease again in the coarser-grained fractions (Figures 5-11 and 5-12). While the Br/Cl ratios in the most fine-grained fraction were similar or only slightly higher than that of seawater, the ratios deviated more with increasing grain-size.

Molar SO_4/Cl ratios in leach solutions of the Äspö diorite decreased regularly with increasing grain-size fraction. In the Ävrö granite and the aplitic dyke no such correlation was established (Figures 5-11 and 5-12). It appears that these differences are mainly related to differences in mineral composition, i.e. to differences in the trace amounts of sulphide minerals present in the rocks.

The molar K/Na ratios of all the leach solutions were higher by more than one order of magnitude compared to that of seawater (0.0218). The ratios decreased strongly from the fraction < 63 μm to that of < 5 mm, which had generally the lowest ratio of all fractions (Figures 5-11 and 5-12). The coarser fractions had all similar ratios with a slight tendency to decrease with increasing grain size. This underlines the complex behaviour of K during leaching already observed in the other leaching experiments (cf section 5.3.2).

Saturation indices

Saturation index calculations using the measured values indicated that the leachates of different grain-size fractions were all undersaturated with respect to calcite (Appendix 13, Table A13-4) The pH-values of the solutions covered a large range between 6.8 and 8.8 resulting in a similarly large range of associated partial pressures of CO_2. Most leach solutions had log pCO_2 values between –2 to –3 while those with pH values above about 8 had log pCO_2 values below –3.5, i.e. below atmospheric. Since it was expected that the solution would have equilibrated with calcite under atmospheric conditions, this erratic behaviour has to be attached to the sorption of Ca^{2+} (and possibly Mg^{2+}) onto the abundant new quartz surfaces as indicated by the very low concentrations of these elements.

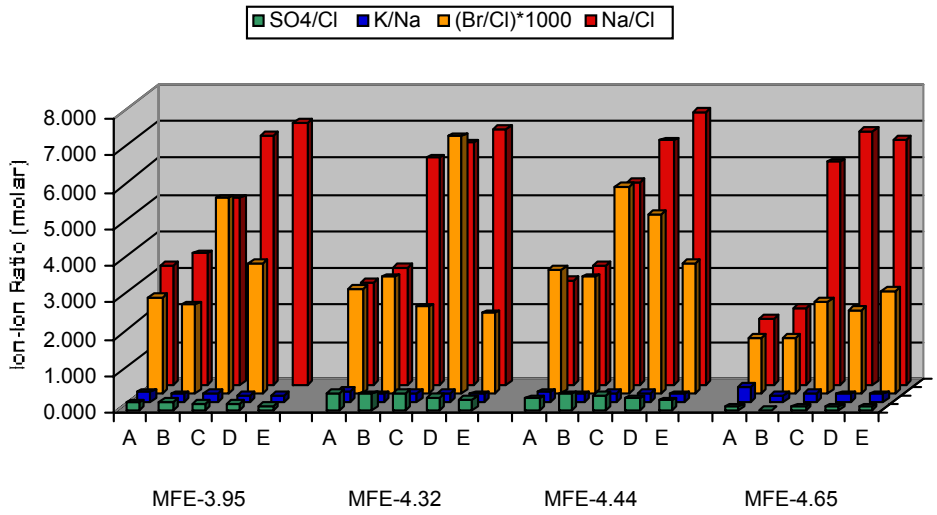

Figure 5-11. *Äspö diorite: Molar ion-ion ratios in leach solutions of different grain-size fractions (A=<63 µm, B=<0.5 mm, C=1–2 mm, D=2–3 mm, E=>3 mm).*

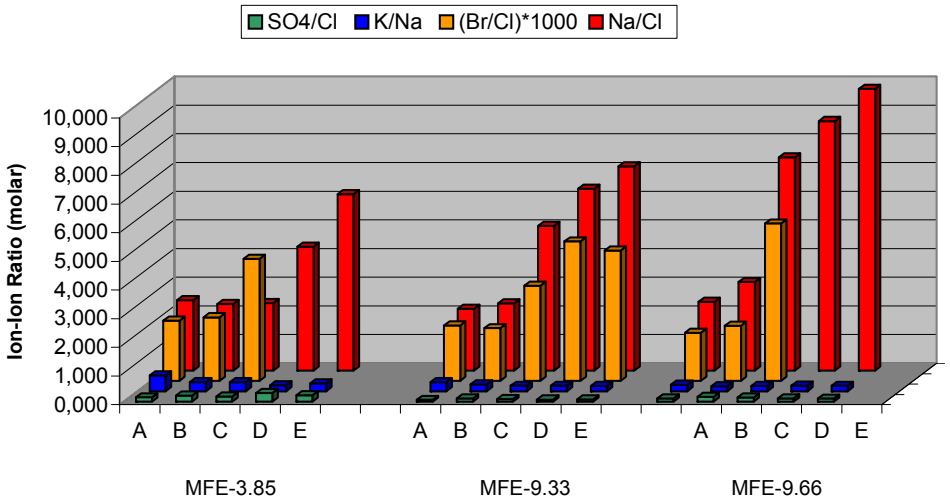

Figure 5-12. *Aplitic dyke (MFE-3.85) and Ävrö granite: Molar ion-ion ratios in leach solutions of different grain-size fractions (A=<63 µm, B=<0.5 mm, C=1–2 mm, D=2–3 mm, E=>3 mm).*

5.3.6 Sr-isotopes of aqueous leach solutions

The isotopic ratio of $^{87}Sr/^{86}Sr$ was measured at the University of Bern on leach solutions of the Äspö diorite from the MFE-borehole (sample MFE-3.66) and of three samples of different lithologies from other boreholes. These latter samples were prepared at the University of Waterloo for chloride isotope ratios measurements on the leach solutions (see below).

The $^{87}Sr/^{86}Sr$-ratios of leach solutions from Äspö diorite samples covered a wide range from 0.726 to 0.734 (Table 5-2). They appear to be controlled by the rock type, i.e. mainly by the content of plagioclase. The lowest ratio was observed for the "average" Äspö diorite (sample Core 1), followed by the more mafic variations of the Äspö diorite (samples MFE-3.66-d and Core 2). By far the highest $^{87}Sr/^{86}Sr$-ratio was obtained for the leach solution of the leucocratic aplite sample (Core 3). Considering all leach solutions the $^{87}Sr/^{86}Sr$-ratio was negatively correlated to the content of total Sr (Table 5-2).

In all leach solutions the $^{87}Sr/^{86}Sr$-ratios were significantly more radiogenic than those reported by /Peterman and Wallin, 1999/ for sampled surface waters (max 0.71849), deep waters below 300 m depth (max 0.71879) and Baltic Seawater (max 0.70947). The $^{87}Sr/^{86}Sr$-ratios of the leach solutions were also more radiogenic than those of the water sampled from the isolated sections in the MFE-borehole (cf Chapter 6).

Table 5-2. Sr-isotope composition of aqueous leach solutions.

Borehole	Matrix borehole	KA2865A01	KI0025F03	KJ0052F01
Borehole length	3.62–3.70 m	10.90–11.02 m	39.65–39.74 m	48.13–48.20 m
Sample	MFE-3.66-d	Core 1	Core 2	Core 3
Rock type	Äspö diorite	Äspö diorite	Äspö diorite, mafic	Aplitic dyke
Leaching	< 63 µm	< 63 µm	< 63 µm	< 63 µm
Laboratory	Bern	Waterloo	Waterloo	Waterloo
Conditions	Glovebox	Ambient	Ambient	Ambient
Solid/liquid	1.5:1	1:1	1:1	1:1
Sr (ppm)	0.055	0.200	0.082	0.024
2SE %	0.002	0.015	0.002	0.088
^{87}Sr / ^{86}Sr	0.734474	0.726695	0.732836	0.751077
2SE absolute	0.000080	0.000020	0.000024	0.000110

Fracture calcite from the Laxemar deep borehole KLX02 on the mainland close to the Äspö HRL has a maximum $^{87}Sr/^{86}Sr$-ratio of 0.71152 /Wallin and Peterman, 1999/, which is significantly lower than those observed for the leach solutions. In contrast, clay material from a fault gouge and cataclasite in the Äspö HRL, which yields K-Ar model ages between 350 Ma to 450 Ma, has $^{87}Sr/^{86}Sr$-ratios of 0.731965 and 0.752196 at corresponding total Sr contents of 401 ppm and 204 ppm, respectively /Maddock et al, 1993/. Because the matrix minerals and their fluid inclusions are much older than these fault gouge minerals, their $^{87}Sr/^{86}Sr$-ratio will be even higher. Thus, the $^{87}Sr/^{86}Sr$-ratio obtained for the leach solutions does not represent the ratio of the pore water, but is dominated by the (probably) variably radiogenic $^{87}Sr/^{86}Sr$-ratios of the rock minerals (such as feldspars, biotite etc) and/or possible fluid released from fluid inclusions of early quartz generations.

5.3.7 Cl-isotopes of aqueous leach solutions

Multiple leaching during grain size reduction showed an increase of the chloride isotope ratio, $\delta^{37}Cl$, as indicated by sample MFE-3.50 investigated at the University of Waterloo (Table 5-3). On the other hand, the $\delta^{37}Cl$-value of the leach solution from the 'average' Äspö diorite (sample Core 1) was significantly higher than that of the more mafic variations of the Äspö diorite (sample Core 2).

With respect to chloride, the two quantitatively important sources are the interstitial pore water and the fluid from fluid inclusions. In mafic minerals such as biotite and amphiboles, chloride may also occur in small amounts incorporated into the hydroxyl-site of the lattice. Although nothing is known about chloride isotope fractionation during incorporation of chloride into mafic minerals, the chloride in the solid phase was expected to be enriched on the heavier isotope and thus have a higher $\delta^{37}Cl$-value compared to a co-existing fluid. For the Äspö rocks such a chloride contribution from mafic minerals appears to be of no importance because the mafic variation of the Äspö diorite (sample Core 2) has the overall lowest $\delta^{37}Cl$-value. The increase of the $\delta^{37}Cl$-value in the leach solutions from multiple ground samples could therefore be attributed to a relative increase in the addition of fluid from fluid inclusions in quartz to the pore water present in the interstitial pore space. However, the chloride isotope signature of the two end members contributing solutions (i.e. the inclusion fluid and the pore water) cannot be determined based on these present data.

The $\delta^{37}Cl$-values of all leach solutions were significantly lower than those of the borehole waters sampled from the matrix borehole (cf Chapter 6) and more in the range of groundwaters sampled in the Prototyp and TRUE Block Scale sites in the Äspö HRL (cf Chapter 7).

Table 5-3. Cl-isotope composition of aqueous leach solutions.

Borehole	Matrix borehole	Matrix borehole	KA2865A01	KI0025F03
Borehole length	3.40–3.60 m	3.40–3.60 m	10.90–11.02 m	39.65–39.74 m
Sample	MFE-3.50	MFE-3.50	Core 1	Core 2
Rock Type	Äspö diorite	Äspö diorite	Äspö diorite	Äspö diorite, mafic
Leaching	1st leach	2nd leach	< 63 µm	< 63 µm
Laboratory	Waterloo	Waterloo	Waterloo	Waterloo
Conditions	Ambient	Ambient	Ambient	Ambient
Solid/Liquid	1.47228:1	1.443068:1	1:1	1:1
Solid weight (g)	1472	1443	1472	1443
Cl (ppm)	21.6	13.9	17	20
^{37}Cl / ^{35}Cl	0.26	0.35	0.38	0.14
1SE	0.12	0.12	0.12	0.12

5.3.8 Implications for pore-water composition

The aqueous leaching test performed on samples of Äspö diorite and Ävrö granite revealed that the impact of inclusion fluid on the leach solutions was significant. Therefore, the volumetric ratio of pore water in the connected porosity to fluid in mineral fluid inclusion in these rocks is low. This was based on the following arguments:

- The absolute concentrations of non-reactive solutes such as Cl and Br in the leach solutions of the same grain size varied significantly and non-systematically between adjacent samples in the drillcore and between different rock types (diorite, granite, aplite). In a system close to or at steady state conditions such large variations were not expected to occur in the pore water and its leachate from samples only a few metres apart.
- Ion-ion ratios of Br/Cl and Na/Cl showed considerable variations between leach solutions of different grain-size fractions, between different samples from the same rock type and between samples from different rock types. This can only be due to the addition of variable amounts of fluids with ion-ion ratios different from the pore water.
- Mineral fluid inclusions were the only fluid source available during leaching besides the pore water. By far most of the fluid inclusions occur in the various quartz generations where they have a large range of salinity. Leaching of the heterogeneously distributed fluid inclusion abundances, and the variable quartz content of the different rock types, has contributed significantly to the observed chemical variability of the leach solutions.
- The small ratio of pore water to leach solution and the large difference in ionic strength appeared to induce significant amounts of reactions which are difficult to quantify between the leach solutions and rocks, for example by the K/Na ratio which was constant in leach solutions despite originating from different grain sizes and rocks.

To conclude, the impact of fluid inclusion salts to the leach solution was so significant that it inhibited the derivation of pore water composition of the Äspö diorite and Ävrö granite based on aqueous leaching. Optical and microthermometric fluid inclusion investigations should be mandatory before any aqueous leaching experiments are performed in order to evaluate the feasibility of the latter for the derivations of the pore water composition of crystalline rocks.

5.4 Cation exchange experiments

Cation exchange equilibrium with the clay fraction of a rock is reached rapidly due to the fast reaction kinetics. The exchange equilibrium depends on the ionic strength and composition of the produced extract solution and the proportions of the different clay minerals in the sample.

In the Äspö crystalline rocks clay minerals are secondary products of hydrothermal or weathering alterations of the primary magmatic minerals. Although the clay fraction in these rocks comprises only about 5% of the total rock (cf Appendix 10), cation exchange might have some importance as a control on the pore water. This is because the clays mainly occur along grain boundaries and hair fissures. In such zones, which are accessible for pore water the relative abundance of clays is higher than in the whole rock. This is supported by geochemical modelling exercises where it was shown that the effect of cation exchange on major ion chemistry in groundwater from Äspö is significant in spite of the low content of clays /Viani and Burton, 1994/.

The cation exchange properties were determined for two samples (MFE-3.66 and MFE-4.65) using the Nickel-Ethylenediamine (Ni-(en)) Method /Baeyens and Bradbury, 1991, 1994/. This method has the advantage of high selectivity of the Ni-(en) complex which displaces all exchangeable cations from the clay and other mineral surfaces into solution. Optimum conditions are achieved when the added equivalents of Ni-(en) are approximately twice the exchange capacity. The resulting analytical data for the two rock samples are compiled in Appendix 13, Table A13-5.

In principle, cation inventories measured in the Ni-en extract solutions are the sum of cations displaced from minerals by the strongly sorbing Ni-ethylenediamine complex and cations present in readily soluble salts from pore water and fluid inclusions. In rocks with a large ratio of total exchangeable cations to pore water and fluid inclusion salts (e.g. claystones with moderately saline pore water and few fluid inclusions), the cation inventories obtained for the Ni-en extract solution expressed per mass of rock should therefore remain constant over different solid:liquid ratios. As can be seen from Table 5-4, this was only limited for the case for the Äspö diorite. All cation inventories in the Ni-en extract solutions tended to decrease with increasing solid:liquid ratio. The decrease was most pronounced for K, Mg and Ca. This indicated that at lower solid:liquid ratios mineral dissolution processes seem to play an important role, while mineral dissolution was increasingly suppressed at higher solid:liquid ratios by the common ion effect in the extract solutions. In the fine-grained (< 63 μm) rock material, partial dissolution of already altered biotite, K-feldspar and plagioclase could be responsible for the observed trends.

The derivation of the in-situ exchangeable cation population turns out to be complex because neither the contribution of the two salt sources (pore water, fluid inclusions) nor that of partial mineral dissolution could be quantified independently. This contribution is significant as can be seen from the sum of cations measured in the Ni-en extract solutions (Table 5-4) which was only twice as high as that measured in the corresponding aqueous extract solutions (cf Appendix 13, Table A13-4).

Table 5-4. Äspö diorite: Cation concentration in Ni-en extract solutions.

Sample	solid:liquid ratio	Na (meq/kg)	K (meq/kg)	Mg (meq/ kg)	Ca (meq/kg)	Sr (meq/ kg)	Sum (meq/ kg)
MFE-3.66-A-Ni	0.25:1.0	4.80	4.30	0.27	2.35	0.0018	11.72
MFE-3.66-B-Ni	0.5:1.0	4.60	4.05	0.17	1.85	0.0016	10.67
MFE-3.66-C-Ni	1.0:1.0	4.75	3.65	0.15	1.60	0.0018	10.15
MFE-3.66-D-Ni	1.5:1.0	4.30	3.15	0.15	1.70	0.0018	9.30
MFE-3.66		4.6	3.8	0.18	1.9	0.0018	10.5
Average ± StDev		± 0.2	± 0.5	± 0.1	± 0.3	± 0.0001	± 1.0
MFE-4.65-C-Ni	1.0:1.0	4.80	3.20	0.69	1.56	0.0073	10.3

In a first assumption it can be argued that the contribution from mineral dissolution was least at high solid:liquid ratios due to the common ion effect. Furthermore, cations present in readily soluble salts were associated with anions and were dissolved with them while those displaced from the clays were initially not associated with any anion. Thus, the inventories of Cl and SO_4 in the Ni-en extract solution were balanced by the most prominent cations, which were in this case Na and K. In contrast, the concentrations of Ca and Mg in the aqueous extract solutions were low and their influence on the inventories measured in the Ni-en solutions was also low and could be neglected.

Following this, two estimates were calculated and shown in Table 5-5. In the first case, (Case I), all Cl measured in the aqueous extract solutions was associated with Na and the concentration of Cl was subtracted from the Na inventory measured in the Ni-en extract solution. In the second case, (Case II), the Cl and SO_4 contents of the aqueous extract solutions were subtracted from the inventories of Na and K in the Ni-en extract solution according to the Na/K-ratio of the aqueous extract solution. Obviously the exchangeable populations of Na and K decrease and so does the sum of exchangeable cations, which is often used as a proxi for the cation exchange capacity. However, the fact that the in-situ population should be dominated by K instead of Na seems unreasonable because Na is generally preferred to K on the exchange sites under such conditions /Appelo and Postma, 1993/.

In conclusion, the Ni-en method has a limited applicability to crystalline rocks with a low cation exchange capacity. Representative cation exchange data for such types of rocks can only be derived by the (time consuming) experimental determination of exchange isotherms for the individual cations on the separated clay fraction of the rock.

Table 5-5. Äspö diorite: Calculated estimates of in-situ cation occupancy and sum of exchangeable cations.

Sample	Na (meq/kg)	K (meq/kg)	Mg (meq/kg)	Ca (meq/kg)	Sr (meq/kg)	Sum cations (meq/kg)
Case I: Na-Cl						
MFE-3.66-C-Ni	3.6	3.8	0.2	1.9	0.002	9.5
MFE-4.65-C-Ni	2.75	3.2	0.7	1.6	0.01	8.2
Case II: Na-K-Cl-SO_4						
MFE-3.66-C-Ni	3.1	3.3	0.2	1.9	0.002	8.4
MFE-4.65-C-Ni	3.0	2.5	0.7	1.6	0.01	7.8

5.5 Matrix pore water diffusion experiment

5.5.1 Background

At the University of Bern a feasibility study of simple out-diffusion experiments was performed on three core samples from borehole KF0093-A0 to explore the in-situ pore water composition. Borehole KF0093-A0 is located nearby the MFE borehole within the same matrix block area. Given appropriate time, diffusion of the components dissolved in the pore water of the rock matrix into the double deionised water was expected to reach steady-state. With knowledge of the water content of the rock samples the concentrations of non-reactive (free) solutes should be calculated to pore water concentrations. For reactive (controlled) solutes the concentration changes induced by rock-water interactions should be estimated utilising geochemical modelling strategies.

5.5.2 Sampling and experimental procedure

Immediately following recovery the core was wiped clean, wrapped in aluminium foil and subsequently coated with wax. Once in the laboratory it was placed in a glovebox under a continuous circulating stream of N_2-gas (oxygen content of < 0.1%) to minimise oxidation. Three fresh samples were selected consisting of Äspö diorite (sample KF93-1), aplitic dyke (sample KF93-2) and a mixture of Äspö diorite and aplitic dyke (sample KF93-3). There were no apparent differences in the mineralogy and texture of this rock material compared to the core from the MFE-borehole. The samples were weighed and placed inclined into polypropylene vessels which were filled to the top with double deionised water. By drying at 105°C to stable weight conditions (> 96 hours), the water content was determined on a rock aliquot taken from all samples. After 2 months of equilibration time one sample solution was analysed initially for pH and alkalinity and then removed from the glovebox for analyses of major ions and stable isotopes. For the two other samples, equilibration was allowed to continue. After intervals of 3, 4, and 5 months, a small amount of solution (about 7 mL) was removed from these samples for chloride analysis. After 5 months the samples were removed from the glove-box and the solutions analysed for pH, alkalinity, major ions and stable isotopes. All three core samples were weighed immediately after removal of the solution and dried until stable weight conditions (168 hours).

The out-diffusion experiments commenced on August 8th, 2001 and continued until October 10th, 2001 for sample KF93-3, and until January 16th, 2002 for samples KF93-1 and KF93-2.

5.5.3 Chemistry of the experimental solutions

Drillcore sample KF93-3 was removed from the reaction vessel after 60 days of equlibration time. Alkalinity, pH and Cl content were determined immediately after removal of the core, but outside the glovebox. From sample vessels KF93-1 and KF93-2 small amounts of solution (approx 7 mL) were sampled for chloride analysis after 90, 120 and 150 days of experimental time. On the final small-size sample (i.e. after 150 days), alkalinity and pH were also determined after exposure to the atmosphere for one night. After this last sampling the cores were removed from the reaction vessels and the total solution was sampled. The samples (including sample KF93-3) were then analysed for alkalinity, pH, major ion and stable isotope compositions after about three weeks of storage under atmospheric conditions.

The analysed solutions were Na-(Ca)-Cl-HCO_3 in type with a total dissolved solid content of between 68 mg/L and 125 mg/L. The complete analytical data are given in Appendix 13, Table A13-6. Unfortunately, close comparison of the chloride concentrations between the analysed samples suggested that the solutions were not homogenised in the reaction vessels and concentration gradients existed in the solution between the top and bottom of the vessels. Consequently, based on existing chloride data, it could not be concluded if steady-state conditions had been reached after 150 days of experimental time.

Saturation states

Geochemical modelling showed that all three solutions were undersaturated with respect to calcite when using the measured alkalinity and pH values. The calculated partial pressure of CO_2 for sample KF9-3 was below (log pCO_2 = –4.12) and equal to that of the atmosphere for samples KF93-1 and KF93-2 (cf Appendix 13, Table A13-6), which were stored overnight prior to analysis. Thus, under the unperturbed experimental conditions pCO_2 was below atmospheric, consistent with those pCO_2-values calculated from the leaching experiments performed in the glovebox (cf section 5.3).

Small amounts of calcite were present as alteration products in the investigated rocks. Considering the experiment time, it could therefore be assumed that the solutions had reached calcite equilibrium. By doing so, pH-values between 8.9 and 9.2 and log pCO_2 values between –4.3 to –5.0 were obtained for the three solutions. At calcite equilibrium the solutions were undersaturated with respect to all other mineral phases (cf Appendix 13, Table A13-6).

Isotopes

The solutions sampled from the reaction vessels after 60 and 150 days, respectively, showed $\delta^{18}O$ and $\delta^{2}H$ values that indicated a slight tendency towards less negative values compared to the deionised water used in the experiment (i.e. –11.19‰ $\delta^{18}O$

and –80.0‰ δ^2H V-SMOW for deionised water compared to –11.14 to –11.12‰ δ^{18}O and –79.4 to –79.1 δ^2H V-SMOW for the samples). This suggested that the stable isotope signature of the in-situ pore water was enriched in the heavy isotopes of water compared to the deionised water used in the experiments. However, the deviation for all samples lay within the analytical uncertainty so that the changes in isotopic composition between deionised water and experiment solutions are not significant.

The pore water fraction expected to mix during such experiments with the experimental solution would be very low (in the present case about 0.5–0.9%). In order to obtain a significant change in the final experiment solution the initial isotopic composition of the latter should be chosen to be strongly enriched in the light isotopes (i.e. very negative delta values).

5.5.4 Implications for pore water composition

Since steady-state conditions were most probably not attained in the out-diffusion experiments, no final conclusion could be drawn with respect to the pore water composition of the investigated rock samples. A comparison with the borehole waters sampled in the MFE-borehole was further inhibited by the fact that the core samples used came from a different borehole with partially different lithologies which may also lead to compositional differences in water sampled in-situ even if only a few metres apart. Therefore, no further geochemical modelling exercises were performed on the present data.

Nevertheless, certain statements can be made about the feasibility of such experiments for pore water characterisation of crystalline rocks of low-permeability. It appears that out-diffusion experiments are well suited to obtain valuable information about dissolved components in the pore water, at least about the non-reactive (free) ones. Thus, the impact of fluid contributed by mineral fluid inclusions is (almost) excluded and insignificant. A significant contribution would otherwise negate the value of all the different leaching techniques used to characterise the in-situ pore water. Success, however, depends on a proper design of the diffusion experiments where the rock sample size, the rock-water ratio, and experimental conditions (atmosphere) and time (steady-state) are optimised. The rock sample size should not be chosen too small such as to exclude: 1) any significant impact of inclusion fluid released in the excavation disturbed zone (EDZ) of the drillcore, 2) any significant contamination by drilling fluid entering the EDZ during drilling operations, and 3) minimisimg the analytical error in gravimetric measurements (water content). The water-rock ratio should be optimised for a most favourable ratio of the experiment solution to the pore-water content of the rock to exclude large uncertainties in the analysis of low concentrations, but to allow removal of small volumes to check for steady-state conditions. However, perturbations related to anion exclusion effects cannot be excluded in such out-diffusion experiments.

The effect of cumulated analytical uncertainties in the present experiments is illustrated in Table 5-6. Here the range of calculated chloride concentrations for a hypothetical pore water (because of non steady-state conditions) based on the concentrations measured in the experimental solutions and the water content determinations are given. The data show that an error of 10% in the water content determination and the standard analytical error of 5% in the chloride concentration resulted in a rather large range of

calculated pore-water chloride concentrations. In all further model calculations such a range will have substantial consequences on the final composition (e.g. due to electro-neutrality constraints).

Table 5-6. Effect of cumulated analytical uncertainty on calculated, hypothetical pore water compositions.

Sample [1]	Rock type	Solution volume (mL)	Chloride in solution (mg/L)	Chloride in pore water [2] (mg/L)		
				From measured values	Minimum	Maximum
KF93-1	Äspö diorite	106.83	32.6	3746	3235	4370
KF93-2	Aplitic dyke	155.37	16.5	3513	3034	4099
KF93-3	Diorite/aplite	133.73	15.0	3087	2666	3601

[1] Note that experimental time was 60 days for sample KF93-3 and 150 days for samples KF93-1 and KF93-2 and steady-state was most probably not attained.
[2] Minimum and maximum values are calculated for a cumulated error of 10% in the water content and 5% in the Cl analysis.

5.6 Pore water displacement experiment

In August 1999 a high pressure experiment was initiated at the University of Waterloo. In common with some of the other experiments the core length provided had been coated erroneously in wax; this was removed by gentle heating. Following this procedure the surface seemed to be free of wax but it was impossible to estimate how much wax was actually in the sample's external pores. It was decided that any residual wax should not pose a problem and if fluid flow was achieved through the sample any wax residue in the fluid could be easily explained. The sample was inspected for any fractures or visible cracks but none were found.

The sample, taken from 3.38–3.475 m of the MFE-drillcore, was cut on a rock saw and the ends were ground parallel to within 1 mm of each other. Table 5-7 summarises the sample dimensions along with the calculated volume.

Table 5-7. Summary of sample dimensions along with the calculated volume.

Sample Height (mm)	100
Sample Width (mm)	50
Sample Mass (grams)	565.81
Sample Volume (cc)	193.344

After the sample had been prepared it was inserted into a moisture proof membrane that was situated on the lower platen of the triaxial test cell (Figure 5-13). A layer of filter paper was placed on the platen beforehand and another layer of filter paper was placed

on the top edge of the platen. The upper platen was then placed on top of the sample and stainless steel hose clamps were tightened around the membrane so that they made contact with the o-rings on the platens thus ensuring a competent seal. The top and bottom end plates were fitted and the triaxial test cell was moved into position in the loading frame. The upper platen was fitted with a linear variable displacement transducer (LVDT) to record vertical displacement of the sample throughout the duration of the test. A pore pressure supply line was attached to the upper platen and a syringe with a clear plastic hose was attached to the bottom platen. The syringe was used so that the surrounding air would not contaminate any fluid expelled out of the cell. The pore pressure line was isolated from the test in the beginning to ensure the integrity of the cell before applying any pore water pressure. Once all the supply lines had been connected and the cell was properly situated a seating stress of 0.5 MPa was applied to the top platen. Then a corresponding stress of 0.5 MPa was applied in the confining port of the cell. This procedure was repeated until the pre-determined hydrostatic stress of 11.7 MPa (i.e. equivalent to the lithostatic stress at the MFE-borehole location in Tunnel 'F') had been reached. The sample was allowed to equilibrate for twenty-four hours to ensure that the sample was still intact. Since the pressures were stable and there was no axial displacement a small pore pressure was applied to the sample and again left to equilibrate for a period of time. Since the hydrostatic pressure was stable at 11.7 MPa the decision was made to apply a stress about half the hydrostatic stresses. The pore fluid used in the experiment was Ultrapure double distilled water from the water resources laboratory in the University of Waterloo. A pore pressure of 6 MPa was applied to the sample and the test cell was allowed to equilibrate. Once again the test cell was intact and no evidence of oil leaks or pore water leaks were observed.

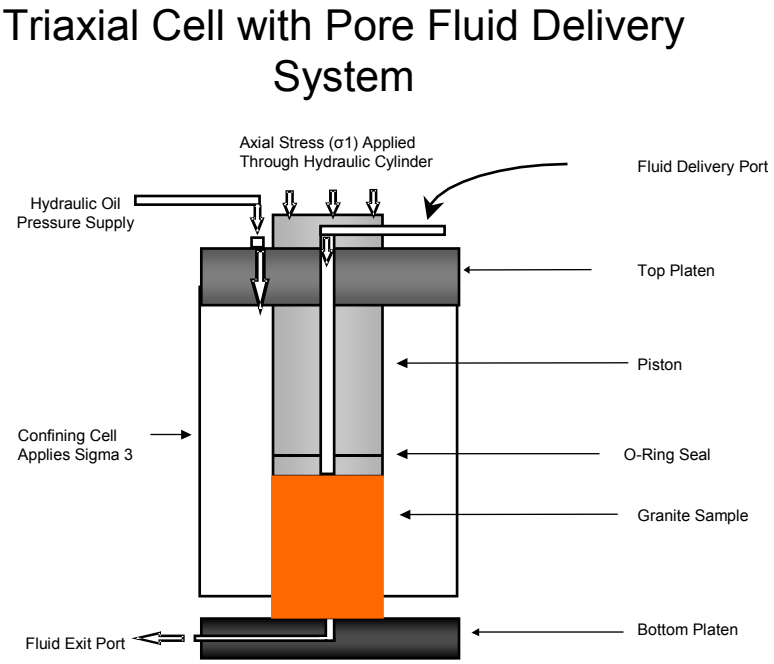

Figure 5-13. *Triaxial cell with pore fluid delivery system.*

Figure 5-14 shows the triaxial cell when loaded. This experiment essentially tried to force the double distilled (Ultrapure) water through the drillcore portion in order to extract unbound, intragranular pore water.

Up until October 1999 no movement was observed and the pore pressure was accordingly increased to 9.5 MPa. Some activity was observed in November 1999 which subsequently slowed down and stopped; since then no movement of matrix fluid through the core has been observed. However there have been indications of a loss of distilled water from above the core (some mLs) during the experiment. Since the water is not believed to be escaping from the highly pressurised sealed unit, this may suggest the filling of empty pore space in the rock or, alternatively, evaporation of fluid on the underside of the core. The possibility of carrying out a post-mortem on the drillcore length is being discussed.

Figure 5-14. *Experimental set-up for the pore water displacement experiment.*

5.7 Summary

- Aqueous leaching test performed on samples of Äspö diorite and Ävrö granite revealed that the impact of inclusion fluid onto the leach solutions was significant. Consequently the volumetric ratio of pore water in the connected porosity to fluid in mineral fluid inclusion in these rocks is low. This was in agreement with the measurements of total and connected porosity and the estimated fluid inclusion volume in the rocks.

- The strong impact of the inclusion fluids on the leached solutions inhibits the derivation of compositional aspects of the pore water residing in the connected porosity, not only for non-conservative but also for conservative compounds such as Cl and Br.

- Optical and microthermometric fluid inclusion investigations are mandatory before any aqueous leaching experiments are performed in order to evaluate the feasibility of the latter for the derivations of the pore water composition of crystalline rocks.

- Isotope ratios of strontium and chlorine of the leached solutions supported a mixing of fluids from different origins. The strontium isotopes further indicated a significant influence of Al-silicate alteration during leaching.

- Pore water diffusion experiments appear to be most promising to evaluate at least the conservative chemical and isotopic parameters of the pore water residing in the connected porosity of crystalline rocks. If steady-state conditions are reached, the non-conservative compounds can be estimated by geochemical modelling. The disadvantage of this method is the length of time required for completion.

- Pore water displacement experiments under high pressure appear to be of limited applicability for pore water characterisation of such crystalline rocks. The limiting factor here is the low water content of the rocks that requires a very large volume of rock in order to obtain a reasonable pore water volume displaced for analyses.

6 MFE-borehole: In-situ borehole water

(N Waber, University of Bern)

6.1 General

The term 'borehole water' as applied here describes the measured composition of the water that has seeped into the different packed-off sections in the MFE-borehole over time periods of several months. From similar long-term experiments it is well known that the composition of such borehole water can deviate substantially from the real in-situ pore water composition /e.g. Gascoyne et al, 1996; Pearson et al, 2003/. Reasons for perturbing the in-situ pore water composition include: a) possible processes during seepage into the borehole section (e.g. ion-exclusion), b) induced processes in the borehole section (e.g. microbial activity, redox reactions, corrosion), and c) modifications of the composition during sampling and storage of the water (e.g. in- or out-gassing). The combination of such processes might result in a rather unusual solution composition that can no longer be analysed with routine methods and which might lower the analytical accuracy due to interferences.

Water samples Included in this evaluation were obtained on December 7th, 1999, from Section 4 and on October, 16th, 2001 from sections 2, 3 and 4. The pressure build-up in Section 1 was constantly very low and no water could be sampled. Details about borehole installation, sampling and hydraulic measurements are given in Chapters 2 and 4, respectively. Hydrochemical data from the third sampling campaign in February 2003 (cf Table 7-4; Chapter 7) were not included in this present discussion as no cation data were available.

Between the three sampling campaigns gas with a strong H_2S smell accumulated in all four sampling sections. This suggested that sulphate reduction had occurred in the sections in spite of the attempt to sterilise the borehole and the equipment prior to installation (Chapter 2). The presence of large amounts of sulphate-reducing and iron-reducing bacteria in the borehole waters subsequently was confirmed /K Pedersen, written comm, 2000/.

The sampled borehole waters were examined for possible perturbation of the water composition during sampling and analyses. Processes that might have altered the compositions within the interval were then inspected by geochemical modelling combined with background knowledge of existing groundwater compositions at Äspo. This approach is described in the following sections.

Geochemical modelling calculations were performed with PHREEQC v 2.5 /Parkhurst and Appelo, 1999/ using the Nagra/PSI Chemical Thermodynamic Data Base 01/01 /Hummel et al, 2002/. The complete data set is given in Appendix 13 (Table A13-8) and, for comparison, chemical data of groundwaters from the vicinity of the matrix block are given in Chapter 7 (Table 7-3) and in Appendix 16 (Table A16-2). The results of geochemical modelling calculations are shown in Table 6-2.

6.2 Borehole water from Section 2 (MFE-S2-2)

A total of 35 mL of groundwater were sampled on October 16th, 2001, from Section 2 within the Ävrö granite. Sampling and on-site measurements for this section were completed within 5 minutes. Since the small volume did not allow an alkalinity titration, the dissolved carbon content of this sample had to be derived by charge balance calculations and/or geochemical modelling. The sampled groundwater was colourless initially, but became slightly brownish after long exposure to the atmosphere.

6.2.1 Chemical composition

The groundwater was in general Na-(Ca)-Cl in type with a total mineralisation of about 5500 mg/L and a Cl content of 2900 mg/L. On-site, an initial pH-value of 6.17 was measured immediately after water collection. In the small subsample used, the pH rose continuously under air exposure indicating degassing of CO_2 and H_2S. The groundwater was further characterised by high contents of F, Mg, K and Fe_{tot} and low SO_4 concentration (Figure 6-1). While the measured concentrations of Mg and K might represent in-borehole conditions, those of F, Fe_{tot} and SO_4 may have been modified by perturbations within the sampling section.

Based on charge balance considerations the water had a high content of total dissolved carbon (45.7 mmol/L) which converts at the measured pH to an alkalinity of about 20 meq/L. This value is one to two orders of magnitude higher than observed for flowing groundwater from similar depths in the Äspö HRL /Smellie et al, 1995; Laaksoharju et al, 1999a/. This indicated that the measured pH was not primarily controlled via the carbonate system alone and that the total alkalinity was far from being equal to the carbonate alkalinity. The reason for this could be seen in the very low SO_4 concentration (2.7 mg/L), which was one to two orders of magnitude lower than in-flowing groundwaters from similar depth. Sulphate reduction thus had an important impact on pH and the derivation of the alkalinity of this sample and introduced some ambiguity into calculations of the composition under in-borehole conditions.

The high fluoride concentration led to a molar F/Cl ratio that was about two orders of magnitude higher than for other groundwaters from the Äspö area. This suggested that at least part of the fluoride may have stemmed from contamination by borehole equipment (e.g. from teflonised metal parts).

6.2.2 Isotopic composition

Despite the small volume of borehole water, analysis of the stable isotopes of water and chloride, and the $^{87}Sr/^{86}Sr$-isotope ratio, was carried out successfully (cf Appendix 13, Table A13-8).

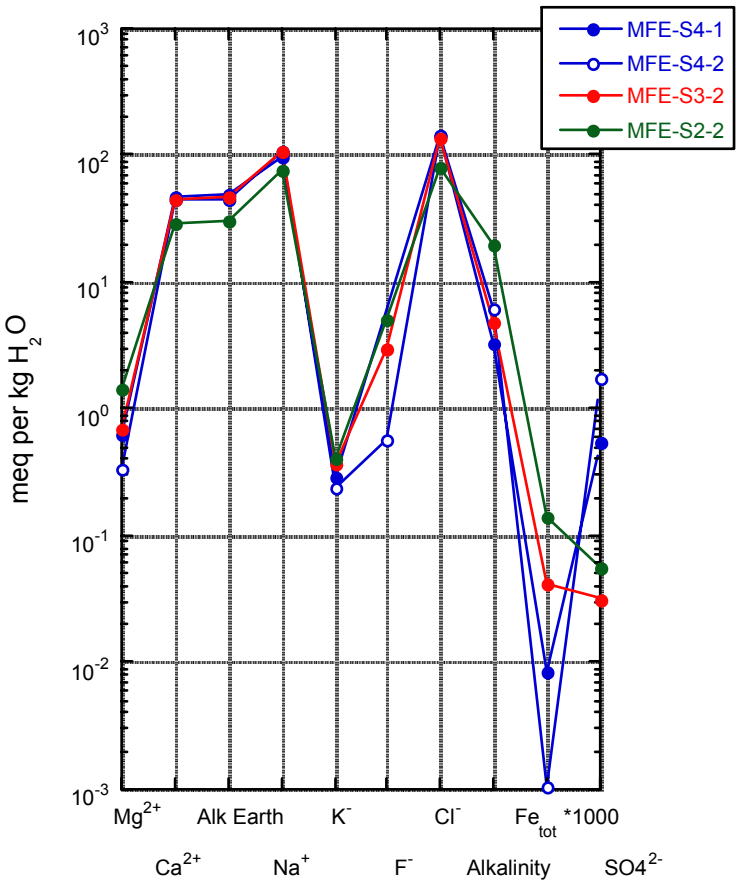

Figure 6-1. *Schoeller diagram of the borehole waters sampled from Sections 2, 3 and 4 in the matrix borehole (alkalinity = total alkalinity; Fe_{tot} is expressed as Fe^{2+}).*

Hydrogen and oxygen isotopes

The borehole groundwater was characterised by $\delta^{18}O$- and $\delta^{2}H$-values of –7.80‰ and –63.6‰ V-SMOW, respectively. The values plot to the right of the Global Meteoric Water Line (GMWL, Figure 6-2) on a line described by the meteoric and sea reference waters given by /Laaksoharju et al, 1999a/. The oxygen and hydrogen isotope composition was similar to that of groundwater from the Prototype locality in the tunnel and also close to the reference of altered sea water used by /Laaksoharju et al, 1999a/. Compared to the other matrix borehole waters it was significantly enriched in ^{18}O and ^{2}H.

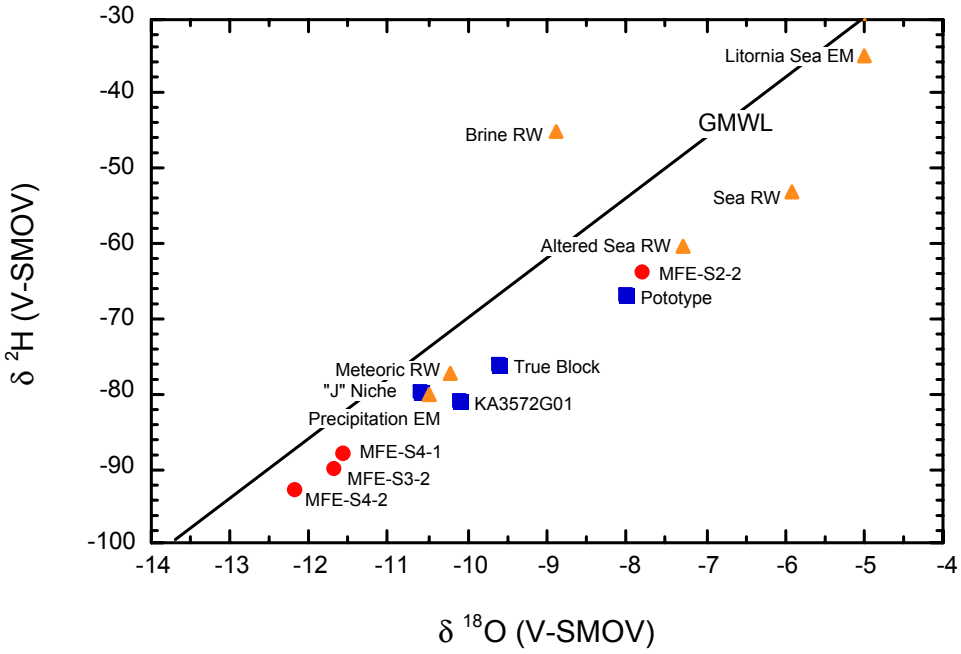

Figure 6-2. *$\delta^{18}O$ vs $\delta^{2}H$ of matrix borehole water (red). Also shown are groundwaters from locations in the vicinity of the matrix borehole (blue) compared with reference waters (RF) and end member waters (EM) proposed for the Äspö site /data from Laaksoharju et al, 1999a/.*

Chlorine isotopes

Chlorine isotope analysis yielded a reproducible value for $\delta^{37}Cl$ of 0.45 ± 0.01‰ SMOC. This value was identical to that of borehole water from Section 3, but lower than those of waters from Section 4.

Strontium isotopes

At a total Sr concentration about half of the other matrix borehole waters, the $^{87}Sr/^{86}Sr$ isotope ratio was the most radiogenic (0.715635; Figure 6-3). It was still, however, significantly less radiogenic than groundwaters from Äspö with similar low Sr concentrations (all > 0.716; cf /Peterman and Wallin, 1999/).

6.3 Borehole water from Section 3 (MFE-S3-2)

Within the Äspö diorite, a total of 321 mL of water were sampled on October 16th, 2001, from Section 3. Sampling and on-site measurements for this section were completed within 20 minutes. The relatively large amount of sampled water allowed the analyses of the total alkalinity (titration to the methyl-orange end-point in the Äspö HRL Laboratory) and the determination of the isotopic composition of dissolved carbon. Similarly to that observed for MFE-S2-2, the sampled groundwater turned slightly brownish after long atmospheric exposure.

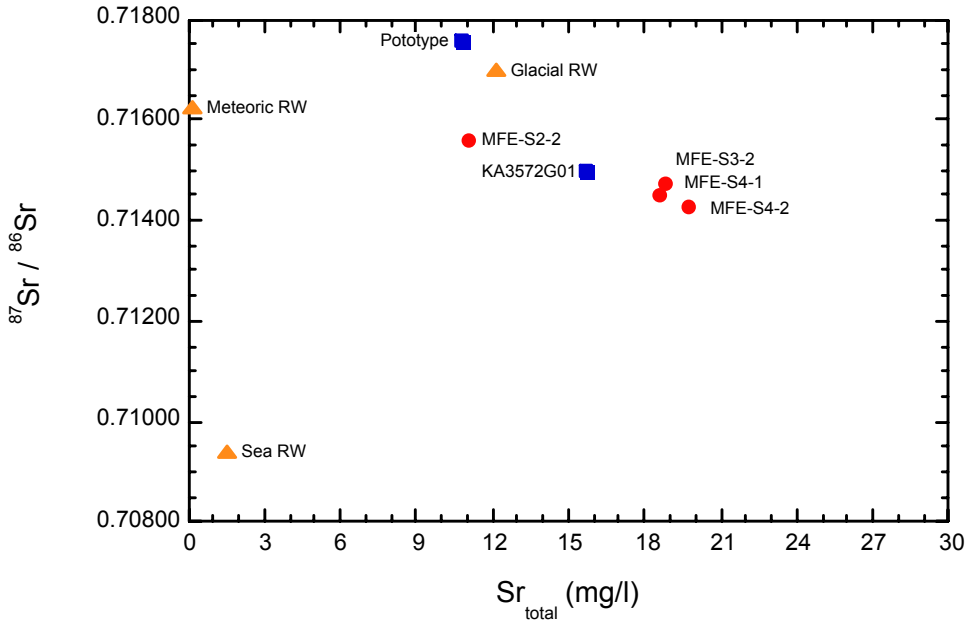

Figure 6-3. *Sr-isotope ratio vs 1/Sr of matrix borehole water. Also shown are some groundwaters from locations in the vicinity of the matrix borehole (cf Table 7-3) and reference waters (RW) proposed for the Äspö site /data from Peterman and Wallin, 1999/.*

6.3.1 Chemical composition

The sample MFE-S3-2 groundwater was in general Na-(Ca)-Cl in type with a total mineralisation of 8607 mg/L and a Cl content of 4780 mg/L. It was thus considerably more mineralised than the water from Section 2.

On-site, an initial pH-value of 6.08 was measured immediately after water collection and, as previously, the pH rose continuously under air exposure indicating degassing of CO_2 and H_2S. In the laboratory a pH of 7.4 was obtained after about 45 minutes following sampling. The titration of the total alkalinity proved difficult and the inflection point of the titration curve was not well defined. This was attributed to the initially high content of dissolved HS^- which contributed to the total alkalinity and the degassing of the dissolved sulphide as H_2S and/or its oxidation to sulphate. The measured values for total alkalinity and pH, therefore, did not represent the conditions of the water in the borehole and had to be interpreted with care.

The groundwater was further characterised by high contents of F, Sr and Fe_{tot} and low SO_4 concentration (Figure 6-1). The high Sr concentration coincided with the higher Ca concentration when compared to the borehole water of Section 2 and might thus represent in-borehole conditions. In contrast, the concentrations of F, Fe_{tot} and SO_4 may have been modified by perturbations within the sampling section.

The analysed total alkalinity was 4.9 meq/L; this converted to a total dissolved carbon content of 5.3 mmol/L at the pH measured in the laboratory. Such an alkalinity was still about five times higher than observed for flowing groundwater from similar depths in the Äspö HRL. In common with Section 2, the low SO_4 concentration (1.5 mg/L) indicated substantial sulphate reduction for this groundwater and thus indicated a perturbation of the pH and alkalinity measurements under in-borehole condition.

6.3.2 Isotopic composition

The rather large volume of borehole groundwater sampled allowed the analysis of the isotopic composition of total dissolved carbon ($\delta^{13}C$ and ^{14}C) in addition to the stable isotope signatures of water and chloride, and the $^{87}Sr/^{86}Sr$-isotope ratio (cf Appendix 13, Table A13-8).

Hydrogen and oxygen isotopes

$\delta^{18}O$- and $\delta^{2}H$-values of –11.70‰ and –89.70‰ V-SMOW, respectively, were obtained. Although plotting essentially on the same line as the MFE-S2-2 groundwater in the $\delta^{18}O$-$\delta^{2}H$-diagram, they were significantly more negative than MFE-S2-2, the sampled groundwater from near-by localities, and present-day precipitation (Figure 6-2). However, the $\delta^{18}O$- and $\delta^{2}H$-values of the MFE-S3-2 groundwater were not as negative as the glacial reference water ($\delta^{18}O$ = –15.8‰, $\delta^{2}H$ = –124.8‰ V-SMOW) given by /Laaksoharju et al, 1999a/.

Chlorine isotopes

Chlorine isotope analysis yielded a reproducible value for $\delta^{37}Cl$ of 0.46 ± 0.03‰ SMOC. This value is identical to that of borehole water from Section 2, but lower than that from Section 4 (see below).

Strontium isotopes

At a total Sr concentration of about 19 mg/L, the $^{87}Sr/^{86}Sr$ isotope ratio of borehole water was 0.714764. This value is considerably less radiogenic than groundwaters from Äspö with similar Sr concentrations (Figure 6-3). It plots approximately in the middle between Baltic Seawater and groundwaters from Äspö /cf Peterman and Wallin, 1999/.

Carbon isotopes

Total dissolved inorganic carbon (TIC) was depleted in ^{13}C ($\delta^{13}C$ = –21.9‰ V-PDB) and had a ^{14}C activity of 57.3 pmc. Calcite was present as fracture infills and in small amounts in the rock matrix . It could therefore be expected that the in-situ pore water was in chemical and isotopic equilibrium with such calcite. The bulk of fracture calcite from the near-by Laxemar boreholes had $\delta^{13}C$-values between 0‰ and –10‰ /Wallin and Peterman, 1999/. Under the prevailing pH-conditions a groundwater in equilibrium

with such calcite would have a substantially less negative $\delta^{13}C_{TIC}$ than measured. The measured $\delta^{13}C_{TIC}$ of sample MFE-S3-1 was therefore strongly influenced by organic carbon enriched in ^{12}C. Possible sources of such organic carbon included dissolved organic carbon ($\delta^{13}C_{DOC}$ around –25‰; /Pettersson, 1992/), dissolved methane ($\delta^{13}C_{CH4}$ between –32.7‰ and –50.8‰; /Wallin et al, 1995/) or contamination by borehole equipment (e.g. residual ethanol used for cleaning the borehole). All these organic compounds can be converted to inorganic carbon complexes during sulphate reduction reactions mediated by microbes.

The small accumulation rate of the water in the sampling section (cf Chapter 4) and the overall chemical composition suggests long residence times for all matrix borehole waters. In this context, the measured ^{14}C activity seemed unreasonably high. Contamination during sampling could be excluded because the water had a partial pressure of CO_2 that was higher than the atmosphere and therefore would tend to degass CO_2. This did not, however, exclude contamination during analyses. A modern soil-CO_2 component could also be excluded because the value of 57.3 pmc corresponded to about the dilution of the ^{14}C activity of infiltrating water by calcite dissolution until equilibrium. Since it seemed reasonable that calcite equilibrium was established in the MFE-S3-2 water (see also section 6.4), the water would thus have been of essentially modern origin. Although this conclusion appeared contradictory to the very low permeability of the rock matrix (10^{-14}–10^{-12} ms^{-1}) which hosts the matrix borehole, there is evidence (cf Chapter 7) that groundwater input from a nearby fracture(s) via an interconnected network of microfractures has contributed to the chemistry of some sampled borehole waters. On the other hand, the chemical data indicated that substantial amounts of dissolved CO_2 were derived from the oxidation of organic carbon, which could either be of modern age and/or old (i.e. ^{14}C-free) origin. Therefore, the measured ^{14}C-activity of borehole water MFE-S3-2 appeared to have various sources which could not be unambiguously quantified, thus inhibiting the derivation of a ^{14}C-residence time for this water.

6.4 Borehole water from Section 4 (MFE-S4-1 and MFE-S4-2)

From Section 4 within the Äspö diorite 160 mL of water were sampled on December 7th, 1999 and 195 mL on October 16th, 2001. During both sampling campaigns pH was measured on-site immediately after water recovery and again about one hour later in the Äspö laboratory during the titration of the total alkalinity. For sample MFE-S4-2 alkalinity and pH were also determined at the University of Bern after 3 days of storage in a high-density PE-bottle. The strong H_2S smell prevailed during these sampling campaigns. In contrast to the other samples, however, there was no obvious change of colour during exposure to air.

6.4.1 Chemical composition

Samples MFE-S4-1 and MFE-S4-2 were both of the general Na-(Ca)-Cl type with a total mineralisation of about 8640 mg/L and 8949 mg/L, and a Cl content of 5160 mg/L and 5020 mg/L, respectively.

On site, initial pH-values of 6.7 and 7.0 were measured for samples MFE-S4-1 and MFE-S4-2 immediately after water collection. Figure 6-4 shows the behaviour of pH for sample MFE-S4-2 during exposure to air and after 3 days of storage in high-density PE-bottles. This evolution of pH and alkalinity is consistent with initial degassing of CO_2 and H_2S under open system conditions and subsequent on-going sulphate reduction under closed system conditions in the sample bottle. Therefore, pH and alkalinity of water samples from Section 4 had also deviated from in-borehole conditions by processes related to de-gassing and microbial activity as observed for the other sections.

Major and trace element compositions remained within the analytical uncertainty for the samples from the two campaigns except for Br, SO_4, Fe_{tot} and total alkalinity (Figure 6-1). The differences in the latter three were related to the processes described above. The lower Br concentration recorded for MFE-S4-2, however, appeared to be an analytical artefact because the Br/Cl ratio of this sample deviated significantly from all other samples (cf Appendix 13, Table A13-8).

In common with the other sections, the high F concentration appeared to be modified by perturbations within the sampling section. In contrast to the other sections, the concentrations of Fe_{tot} were lower by more than one order of magnitude (Figure 6-1).

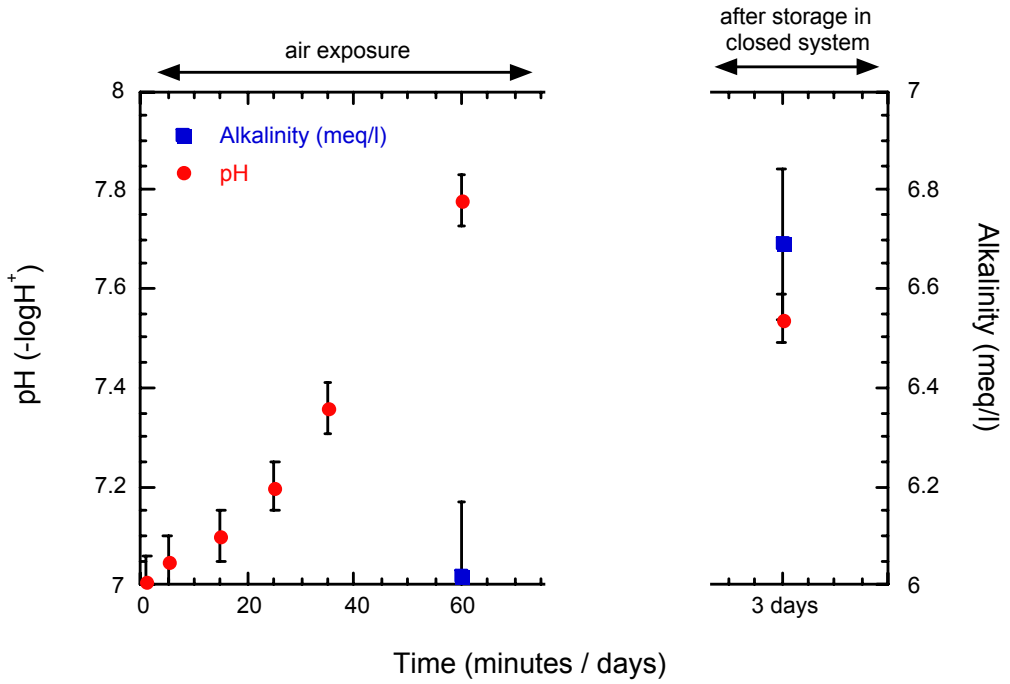

Figure 6-4. *Evolution of pH and alkalinity during sampling in the field (left) and after 3 days of storage in a tightly closed sample bottle (see text).*

6.4.2 Isotopic composition

Hydrogen and oxygen isotopes

The Section 4 groundwater isotope composition changed from $\delta^{18}O$ and $\delta^{2}H$ values similar to those of the Section 3 groundwater towards more negative values in the second sampling campaign (Figure 6-2). This was surprising since the two water samples had almost identical major element compositions, except for the components affected by perturbations (Figure 6-1). The reason for this shift was unknown. One possibility considered was contamination by flushing water from borehole KA2598A used to drill the MFE-borehole which had a similar chemical composition to the MFE-S4 waters (cf Appendix 13, Table A13-8); however no isotope data exist for this KA2598A water. Another possibility was an increasing contribution from near-vicinity hydraulic microfractures in the rock matrix (cf discussion in Chapter 7).

Chlorine isotopes

Chlorine isotope analysis of borehole waters from Section 4 yielded reproducible and identical values for $\delta^{37}Cl$ in both sampling campaigns (0.60 ± 0.01‰ SMOC). Borehole water from Section 4 thus appeared to be slightly enriched in ^{37}Cl compared to the borehole water from the other two sections.

Strontium isotopes

The Sr concentration and $^{87}Sr/^{86}Sr$ isotope ratio in the borehole water from Section 4 remained constant (Figure 6-3). As for Section 3 these values were considerably less radiogenic than groundwaters from Äspö with similar Sr concentrations which plotted approximately between Baltic Seawater and groundwaters from Äspö /cf Peterman and Wallin, 1999/. The Sr concentration of the water from borehole KA2598A used for drilling and cleaning was similar, but unfortunately no Sr-isotope data were available.

6.5 Geochemical modelling

6.5.1 Mineral saturation states and pCO_2

Based on the measured values for pH and alkalinity, the matrix borehole waters were strongly oversaturated with respect to calcite and had partial pressures of CO_2 ranging from about 10^{-3} to $10^{-2.1}$ bar (Table 6-1). This was geochemically unreasonable because the waters would have tended to equilibrate with the fast reacting calcite via calcite precipitation. The reason for this oversaturation was the coupled processes of sulphate reduction and production of CO_2 in the sampling sections, degassing of CO_2 and H_2S during sampling, and the fact that substantial amounts of HS^- contributed to the measured total alkalinity. In principle, adjustment of the solution alkalinity or the pH to calcite equilibrium can be done by geochemical modelling. In the case of the MFE-borehole waters this was, however, inappropriate because the titrated alkalinity

did not closely represent the carbonate alkalinity and therefore the calculated partial pressures of CO_2 became too high.

Bacterially mediated sulphate reduction via oxidation of organic carbon in the sampling sections was supported by the very negative $\delta^{13}C$-value of dissolved inorganic carbon in sample MFE-S3-1. The degassing of CO_2 and H_2S was indicated by the H_2S smell and the increase of the solution pH during air exposure (Figure 6-4) as was observed for all samples. While degassing of CO_2 did not alter the alkalinity, variable amounts of HS^- present in solution had a significant influence. Groundwaters from near-vicinity localities had SO_4 contents between about 3 to 6 mmol/L while 0.02 to 0.9 mmol/L characterised the matrix borehole waters. In aqueous leachates and diffusion experiments of matrix borehole core material sulphate is always present as a major anion despite treatment under controlled atmosphere (cf Chapter 3). Thus, there was no obvious reason why sulphate should be lower in the in-situ pore water than in such near-vicinity formational groundwaters. Therefore, sulphate reduction might have contributed as much as about 3 to 5 meq/L to the measured alkalinity that would have resulted in a carbonate alkalinity similar to that observed for contamination-free near-vicinity formational groundwaters.

To summarise, the pH and carbonate system of the MFE-borehole waters could not be adequately corrected for the perturbing effects and calculated to in-borehole conditions. As a consequence, the saturation states of all other carbonate phases also do not represent in-borehole conditions. This is unfortunate because some of them could potentially act as a solubility control for certain trace elements and thus help constrain the calculations for the in-situ pore water.

Fluorite was strongly oversaturated in all water sampled in the second campaign due to the very high fluoride concentrations measured in these samples (Table 6-1). In crystalline environments fluorite often acts as a solubility control for dissolved fluoride /e.g. Nordstrom et al, 1989b/. The oversaturation was thus due to contamination of fluoride from the teflon coating of the steel parts within the packer system. Under the aggressive chemical conditions prevailing in the sampling sections teflon is no longer chemically inert and will decompose.

Quartz was at equilibrium in all matrix borehole waters. This is geochemically reasonable and, because quartz solubility does not significantly vary in the observed pH-range (i.e. from about pH 6 to 7.5), its solubility might also control dissolved silicon in the in-situ pore water. It has to be noted that for quartz the new solubility data of /Rimstidt, 1997/ are used. These data are reviewed by /Gunnarsson and Arnósson, 2000/ and again by /Hummel et al, 2002/ and supersede earlier data given by /Nordstrom et al, 1989b/ and still used by most conventional thermodynamic databases.

Amorphous iron hydroxide and goethite were strongly supersaturated at the total iron concentration and pH measured in the laboratory. This is consistent with the change in colour of the water during air exposure and the strongly reducing in-borehole conditions. Under these conditions iron is mainly present as ferrous iron which will become oxidised when in contact with air and precipitate as ferric hydroxides. The presence of iron reducing bacteria in the sampled water further supports the presence of ferrous iron in the borehole sections.

Table 6-1. Modelled saturation indices from measured values of matrix borehole waters and conventionally sampled formation groundwaters in the near-vicinity of the matrix block area.

	MFE-S3-1	MFE-S4-1	MFE-S4-2	True Block	Prototype	"J" Niche	KA2598A
pH	7.40	8.1	7.78	8.0	7.3	7.4	7.75
Alk (meq/l)	4.923E-03	3.250E-03	6.026E-03	3.084E-04	2.521E-03	6.479E-04	1.637E-03
Carbonate system from analysed pH and alkalinity							
TIC (mmol/l)	5.315E-03	3.211E-03	6.186E-03	2.956E-04	2.734E-03	6.697E-04	1.647E-03
log pCO2	–2.12	–3.04	–2.43	–3.92	–2.27	–3.03	–2.98
Saturation indices							
Calcite	0.77	1.27	1.22	0.36	0.41	0.21	0.72
Dolomite_ord	–0.29	0.68	0.33	–0.48	0.20	–0.81	0.51
Magnesite	–1.64	–1.18	–1.47	–1.42	–0.80	–1.60	–0.80
Siderite_c	0.05	–0.17	–1.14	–3.02	–0.86	–1.11	
Rhodochr._c	0.02	0.62	0.20	–0.83	–0.28	–0.97	
Strontianite	–0.38	0.10	0.09	–0.99	–0.95	–1.06	–0.95
Fluoride	3.28		1.84	–0.08	–0.23		
Gypsum	–3.04	–1.77	–1.30	–0.65	–0.80	–0.43	–0.61
Barite	–1.11	–0.07		–0.05	–0.07	0.00	
Celestite	–3.01	–1.77	–1.24	–0.70	–0.93	–0.48	–1.11
Fe(OH)3 A	0.74	2.02	0.24	3.99	3.88	4.48	
Goethite	4.75	6.02	4.24	8.03	7.88	8.49	
SiO2 (am)	–1.02	–1.05	–1.00	–1.17	–1.10	–1.23	–1.19
Quarz	0.05	0.03	0.08	–0.12	–0.05	–0.18	–0.11

Note: Calculations are not performed for sample MFE-S2-1 due to missing data for alkalinity and/or TIC and a pH value modified by sulphate reduction and degassing (see text).

6.5.2 Redox

In the second sampling campaign dissolved total sulphur and sulphate were analysed by ICP-AES and IC, respectively. This allowed the amount of sulphur present as dissolved sulphide in the samples to be calculated. Based on this the redox potential can be obtained by the sulphide-sulphate couple (Table 6-2). As expected from the H_2S smell, all borehole water samples had a reducing redox potential. It should be noted, however, that the calculated redox potential represented minimum values due to the out-gassing of H_2S during sampling.

Table 6-2. Modelled redox potential based on the sulphide-sulphate couple of matrix borehole waters.

	MFE-S2-1	MFE-S3-1	MFE-S4-2
pH (-logH+)	6.17	7.40	7.78
Redox based on the HS^- / SO_4^{2-} couple			
Eh (mV)	–147	–225	–241
Pe	–2.60	–3.96	–4.24

6.6 Summary

Water was successfully sampled after several months of seepage into the isolated sections of the MFE-borehole. Extensive bacterially mediated sulphate- and iron-reduction processes, however, perturbed the water composition and altered in-situ conditions. With the available borehole water data these perturbations cannot be further quantified.

The sampled borehole waters are generally Na-(Ca)-Cl in type with Cl-concentrations around 5000 mg/L in the Äspö diorite and around 2900 mg/L in the Ävrö granite some 2 m away. The borehole waters sampled from the Äspö diorite and the Ävrö granite also differ significantly in their isotope composition of water and strontium. The chlorine isotope composition is identical for the waters sampled from the diorite and granite sampled within a distance of about 3 m in the borehole, but significantly enriched in the ^{37}Cl in the diorite water sampled further away.

7 MFE-borehole: The hydrogeology and hydrochemistry of the near-vicinity environment

(J Smellie, Conterra, A Blyth, University of Waterloo, S Frape, University of Waterloo, E Gustafsson, Geosigma, N Waber, University of Bern, M Laaksoharju, GeoPoint, E-L Tullborg, Terralogica, and K Pedersen, Göteborg University).

7.1 General

As noted earlier, matrix pore waters are here considered to constitute the waters in the rock matrix accessible for solute transport by diffusion and/or advection. It is thus important to try and relate the chemistry of these pore waters to that of groundwaters in nearby microfracture zone(s) of low hydraulic transmissivity ($T = 10^{-12}$–10^{-9} m^2s^{-1}). In turn, it is important to relate these microfracture groundwaters to larger scale fracture zone networks of even greater transmissivity ($T = 10^{-10}$–10^{-7} m^2s^{-1}), which is the range normally sampled in hydrogeochemical site characterisation programmes. Since the groundwaters that will come in contact eventually with the engineered barrier materials of a repository will gain access along such pathways through the low permeable host bedrock, the influence of the matrix pore water on the microfracture groundwaters (and vice versa) will be of importance as interaction may modify the chemistry of the near-field groundwater environment.

The larger-scale fracture zones, since they represent variations in transmissivity, orientation and also represent different geographical locations, may be characterised by different hydrochemical signatures. This hydrochemical heterogeneity may result from one or any combination of the following processes occurring within and close to the fracture zones:

- water/rock interaction during long residence times;
- mixing of palaeowaters from past marine stages;
- mixing of palaeowaters from past glacial periods; and
- mixing of modern groundwater components.

However, when these groundwater mixtures permeate to the low transmissive rock matrix, longer residence times and increased water/rock interaction plus the potential influence of diffusive exchange between the pore water(s) and the fracture groundwater(s) will all contribute to a greater homogenisation of the groundwaters representing the near-field hydrochemical environment. This is assuming that hydraulic conditions are suitably favourable.

To address these issues adequately, a reliable hydraulic and hydrochemical database on a site-scale was compiled. This involved available data related to hydraulic conductivity

and hydrochemistry at equivalent depths to the Matrix Fluid Chemistry Experiment. Four sources of data were used:

- data from fractures present in the near-vicinity of the MFE-borehole, i.e. from the 'J' Niche as part of the on-going CHEMLAB and Microbe experiments;
- data from the TRUE Block Scale Experiment programme;
- data from the deposition holes (and their surroundings) resulting from the Prototype Repository Experiment; and
- new $\delta^{37}Cl$ data from each of the above-mentioned sources in addition to the Äspö site as a whole.

It was hoped that the evaluation of these data might provide some link between hydraulic transmissivity and groundwater chemistry which hitherto has not been addressed quantitatively in the Äspö hydrochemical programme mainly because of the difficulty in measuring low transmissivities and also the time-consuming nature of sampling groundwater from such hydraulic features.

Chapters 3 to 6 have described in detail the matrix borehole in terms of: a) its geological, mineralogical and hydrogeological character, b) the characterisation of fluid inclusion populations and fluid chemistry: c) the chemistry of extracted matrix pore fluids through laboratory leaching and diffusion experiments, and d) the chemistry of the sampled borehole groundwaters. The objective of this present chapter is to discuss all available data, in particular the geology, hydrogeology and hydrochemistry, in the wider context of the host bedrock environment, and the potential influence this environment has had on the chemistry of the MFE-borehole water.

This section initially describes the site-scale hydrochemical conditions, followed by the sub site-scale hydrochemical conditions, and finally focuses in on the MFE-borehole (i.e. deposition hole scale) hydrochemical conditions.

7.2 Site-scale hydrochemical conditions

To interpret present-day hydrochemical data at the Äspö HRL consideration has to be given to the undisturbed conditions prior to tunnel excavation (i.e. Pre-investigation Phase from 1986–1990) and the disturbed conditions resulting from: a) tunnel excavation (Construction Phase from 1990–1995), and b) long-term drawdown effects on the surrounding hydrochemical environment from the tunnel and experimental galleries (Operation Phase from 1995–2050?). Hydrogeochemical interpretation and conclusions are documented in several reports and publications produced during the past 10–15 years /e.g. Smellie and Laaksoharju, 1992; Smellie et al, 1995; Laaksoharju et al, 1999a/. Additional regional information based on chlorine-37 isotopic studies at the University of Waterloo (cf Appendix 15) have been carried out as part of the Matrix Fluid Chemistry Experiment and provide support for the overall interpretation of the Äspö groundwater system.

7.2.1 Undisturbed, Pre-HRL conditions

In the Pre-investigation Phase, on a semi-regional scale, data were obtained from shallow, 100 m deep, percussion-drilled boreholes at Äspö, and from the nearby sites at Laxemar and Ävrö (Figure 7-1). At the site-scale, investigations included samples from sections isolated by packers in the deep core-drilled boreholes on Äspö island (~ 800–1000 m) and complemented by two deep boreholes on the nearby mainland at Laxemar (~ 1000–1700 m). Most of the sampling at Äspö was carried out in the first three cored boreholes (KAS01-KAS03) which penetrated the northern and southern parts of the island and intersected the Äspö EW-1 shear zone.

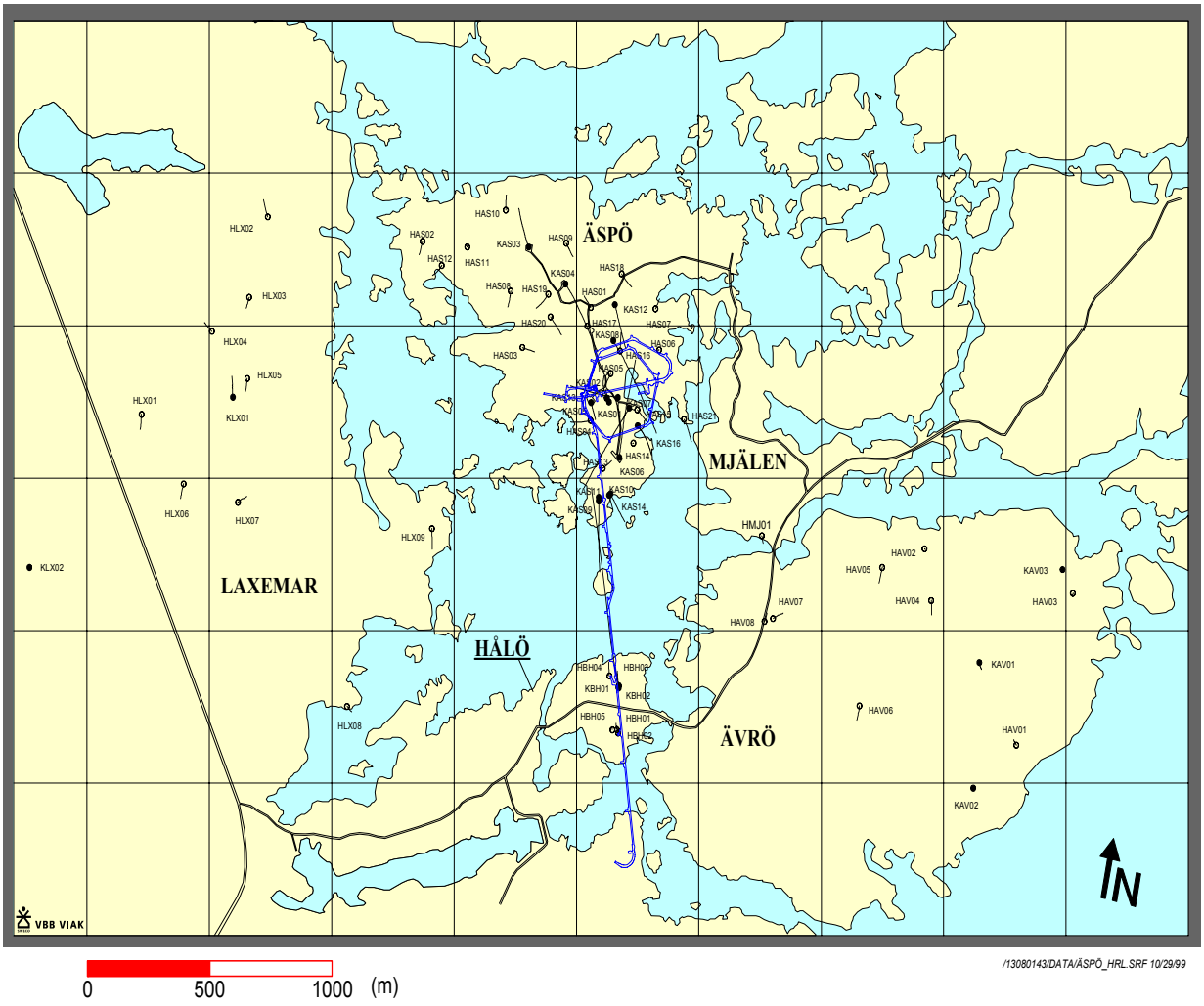

Figure 7-1. *The layout of the Äspö Hard Rock Laboratory and access tunnel (blue) in relation to boreholes drilled from the surface. (Prefix 'H' refers to percussion drilled boreholes; prefix 'K' refers to rotary cored boreholes).*

The major conclusion from the Pre-HRL groundwater investigations at Äspö (Figure 7-2) is that much of the water chemistry down to 800 m (represented by a range in salinity from 0.5–8 g/L chloride) can be related not only to known palaeo-events such as infiltration of glacial melt water (or cool climate recharge) periodically during the last 10–100 ka and different marine stages during the last 8 ka to recent, but also to infiltration of relatively young meteoric water (3 ka to recent). Below 800 m depth the chloride content increases markedly to 12.5 g/L Cl, probably approaching brine in composition at still greater depths as indicated at Laxemar, where ancient near-stagnant groundwater (45 g/L Cl) has suggested ages of at least 1.5 Ma /Louvat et al, 1999/. At these depths the groundwater is not affected by the different stages of the Baltic Sea evolution that have taken place since the last glaciation some 10 ka ago, and thus water/rock interactions and matrix pore fluids play an increasingly important role.

The sampled groundwaters were in general reducing at depths exceeding a few tens of metres. However, in exceptional cases, which are fracture-specific, oxidising conditions might have prevailed down to greater depths due to local hydraulic gradients. Oxygen-rich surface water rapidly becomes anoxic as it percolates into the rock due to microbial activity /e.g. Banwart et al, 1999/ and also due to the natural buffering capacity of fracture minerals rich in ferrous iron. Bacteria are important for developing a reducing redox potential in the groundwaters via the reduction of sulphate and dissolved Fe(III). This results in an increase of total dissolved inorganic carbon (TIC) and total dissolved Fe in the groundwaters, while sulphate concentrations decrease.

The use of tritium analyses in conjunction with $\delta^{37}Cl$ isotopic analyses further refined and confirmed the hydrogeochemical models of natural groundwater and seawater infiltration and mixing at the Äspö HRL site (cf Appendix 15). The earliest samples showed a lack of modern tritium-rich waters at depth and chlorine isotopic signatures (i.e. positive values) were consistent to heavier rock pore water chloride (Figure 7-3).

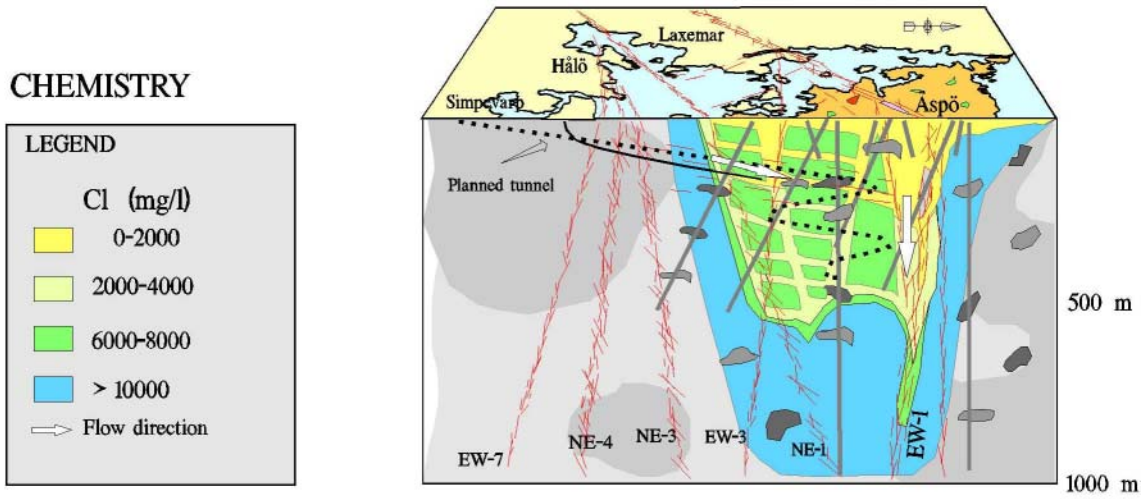

Figure 7-2. *Pre-investigation Phase: Schematic representation of the Äspö HRL during undisturbed groundwater conditions (after /Rhén and Wikberg, 2000/ and based on /Smellie and Laaksoharju, 1992/).*

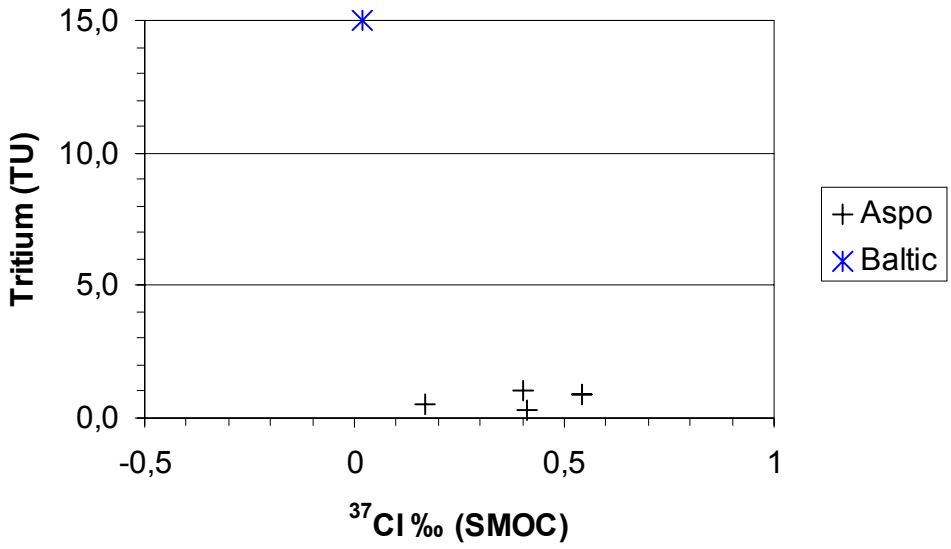

Figure 7-3. *Pre-investigation Phase (undisturbed, Pre-HRL conditions): Plot of $\delta^{37}Cl$ versus tritium indicating little or no modern water component and $\delta^{37}Cl$ values are consistent with the rock pore water chloride.*

In summary, the main bulk of groundwater at Äspö during Pre-investigation conditions is the result of mixing along flow paths of groundwaters of different origin, e.g. palaeowaters (saline, glacial) and modern meteoric waters. Chemically, the groundwater down to 500 m is altered mainly by rapid reactions (some microbially mediated) and less by long-term water/rock reactions due to the relatively short residence times and low temperatures. At greater depths (> 1000 m), due to longer residence times and temperature increase with depth, water/rock reactions play a more dominant role in modifying the groundwater composition. The position of the sampling points, in relation to depth (shallow/deep), geographical location, (under land/sea), fracture orientation (towards land/sea), reactions with fracture minerals, and present/palaeo groundwater systems, is generally determining, or at least influencing to varying degrees, the obtained groundwater compositions.

The hydraulic transmissivity determines the time the hydrochemical regime will require to adjust to the prevailing hydraulic conditions. A highly transmissive fracture will respond more rapidly to changes in hydraulic conditions than a low transmissive fracture, such that the groundwater composition will be mainly a product of mixing rather than water/rock interaction. Contrastingly, a low transmissive fracture will react slowly, and very low transmissive features may not react at all to such changes. This will result in a groundwater of long subsurface groundwater residence time which will have undergone significant water/rock interaction processes and may also contain a matrix pore water component through diffusion processes in response to chemical gradients.

7.2.2 Disturbed, Post-HRL conditions

Generally, excavation has resulted in a hydraulic drawdown causing younger, more surface-derived water to be circulated to greater depths; this has also led to an upconing of deeper, older, more saline water to shallower depths (Figure 7-4). Detailed evaluation of long-term monitoring along approximately the first 2900 m of the tunnel /Laaksoharju and Wallin, 1997/ indicated that during construction:

- the groundwater along the 500–1000 m tunnel section changed from meteoric to a marine signature due to the fact that the tunnel commenced under the landmass and continued under the sea towards Äspö island;
- the groundwater along the 1000–2000 m tunnel section showed an initial change from a marine to a meteoric/glacial/saline signature that later changed to a meteoric signature, reflecting that this tunnel section commenced under the sea, continued under Äspö island and then ended in the first spiral; and
- the groundwater along the 2000–2880 m section (which represents the distance from the end of the first spiral to the beginning of the second spiral) changed from meteoric to marine and then increased in saline content from the mixing of groundwaters originating at greater depths.

Furthermore, with increased disturbance from drilling, pump testing and tunnel construction, the amounts of fresh, tritiated shallow groundwaters with very distinctive depleted $\delta^{37}Cl$ signatures, and tritiated Baltic Sea 'type' waters, began to progressively increase in the deeper parts of the site. The infiltration rates seems to have been quite rapid and the flushing of resident fracture groundwater and matrix pore water appears to have continued in a very progressive manner (Figure 7-5).

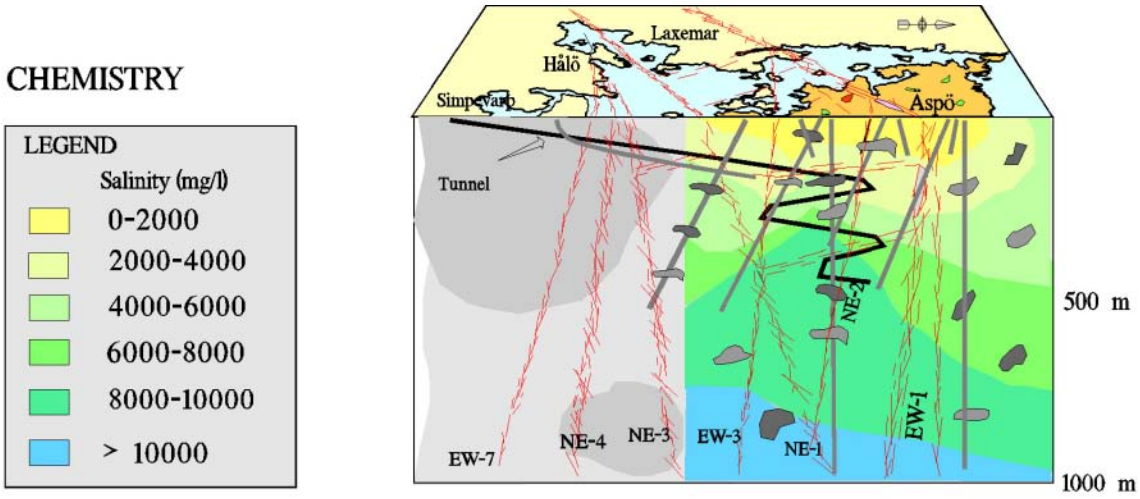

Figure 7-4. *Construction Phase: Schematic representation of the Äspö HRL during disturbed, Post-HRL groundwater conditions (after /Rhén and Wikberg, 2000/ and based on /Laaksoharju et al, 1999a/).*

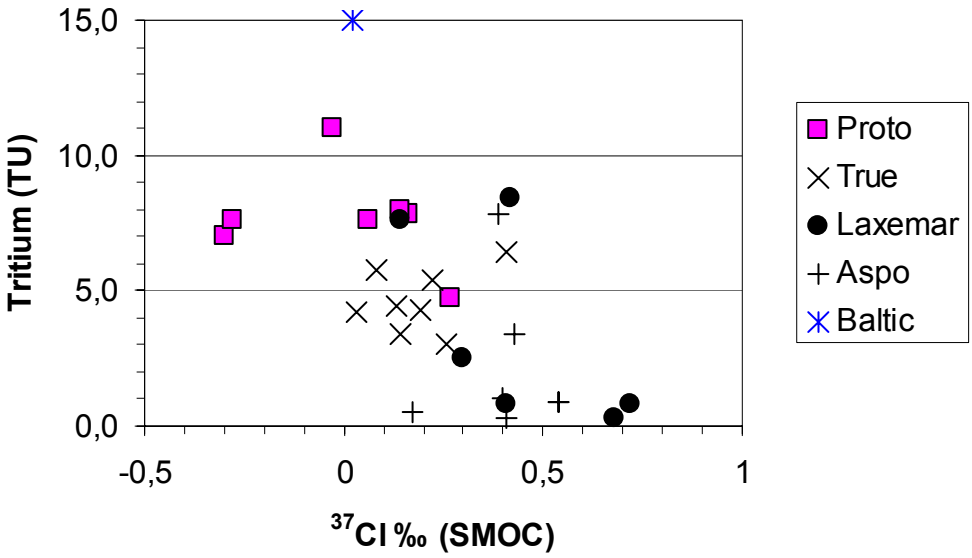

Figure 7-5. *Construction Phase (disturbed, Post-HRL conditions): Plot of $\delta^{37}Cl$ versus tritium indicating increasing mixing of a Baltic Sea-type water component. More depleted $\delta^{37}Cl$ values are observed from waters sampled from galleries at around 500 m depth (Prototype and TRUE samples); these samples have also elevated tritium indicating mixing with a younger shallow groundwater component.*

In conclusion, the major observed changes in the groundwater chemistry simply reflect the intersection of the tunnel during construction with a series of hydraulic fractures and fracture zones of varying geometry and geographic location such that groundwater mixing from different sources has occurred. However, chemical reactions during these changes have also contributed, for example, the observed carbonate increase (i.e. dissolved inorganic carbon (TIC)) under the landmass areas has been attributed to decomposition of organic matter and calcite dissolution, whilst under the sea the increase has resulted from sulphate reduction and associated oxidation of organic carbon. Decomposition of organic matter and sulphate reduction has been biologically mediated.

7.3 Sub site-scale hydrochemical conditions

7.3.1 General

'Sub site-scale' here relates to an area of approximately 100 x 100 m chosen to include the 'J' Niche (Microbe and CHEMLAB experiments), Prototype Repository Experiment, TRUE Block Scale Experiment and, more recently, the Pillar Stability Experiment (Figure 7-6).

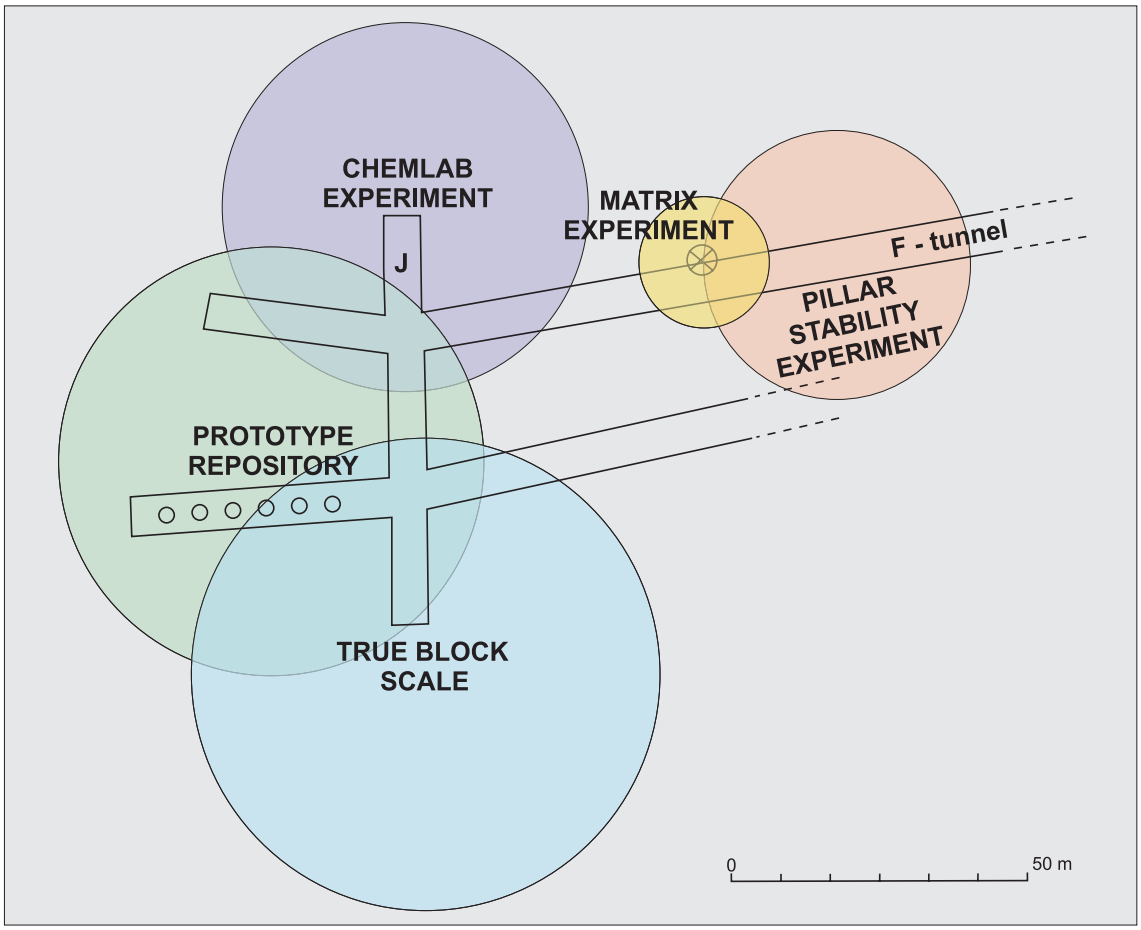

Figure 7-6. *Areas investigated at the Äspö HRL in the near-vicinity of the MFE-borehole and from which available hydraulic and hydrochemical data were compiled.*

7.3.2 Hydraulic parameters

The detail of available hydraulic data varied reflecting the main objectives of the respective experiments carried out. Quantitative data were available from the TRUE Block Scale and Prototype experiments, semi-quantitative data characterised the Pillar Stability experiment whilst data from the CHEMLAB and Microbe experiments located in the 'J' Niche were only qualitative at best.

Available data

The hydraulic data from the TRUE Block Scale experiment are well documented in /Olsson et al, 1994/ and /Hermanson and Doe, 2000/ where the measured hydraulic transmissivities of the sampled fractures range from 10^{-8}–10^{-5} m^2s^{-1} (Table 7-1).

Table 7-1. Hydraulic parameters of hydrochemically characterised fractures from the TRUE Block Scale Experiment.

Borehole	Section (m)	T'missivity[+] (m^2s^{-1})	T'missivity* (m^2s^{-1})	Structures[#]
KA2511A	52–54	4E-5	3E-5	?
	92–109	> 3E-5	2E-6	6 and 16
KA2563A	187–190	–	8.7E-7	20
K10023B	41.45–42.45	1.8E-5	4E-5	7
	70.95–71.95	8.1E-7	–	21
	84.75–86.20	5.8E-8	3.2E-7	13
K10025F	86–88	5.1E-7	8.5E-7	20
	164–168	1.1E-5	2.9E-5	19(21?)

From Figure 3-16 in /Olsson et al, 1994/:
[+] from flow and pressure build-up tests;
* from cross hole pump tests;
[#] designated fracture number

Hydraulic data from the Prototype Repository Experiment are documented in /Rhén and Forsmark, 1998a,b/. In close collaboration with this experiment several borehole sections were selected for quantitative hydrochemical characterisation (Class 5 protocol). The choice of boreholes, with emphasis on intersecting low-conductive fractures, was based on:

- geological homogeneity;
- structural simplicity;
- structural isolation from the excavated tunnel floor and walls
- low transmissive values;
- estimated low water flow rates; and
- measured low water flow rates.

The hydraulic characteristics of the chosen borehole sections are presented in Table 7-2.

No quantitative hydraulic data were available from the 'J' Niche Experiment but measured groundwater flow rates (0.6–4.0 L/min) from packed-off intervals in boreholes KJ0044FO1, KJ0050F01, KJ0052F01, KJ0052F02, KJ0052F03 suggested transmissivities in the range of 10^{-8}–10^{-7} m^2s^{-1} (Microbe Experiment: /Karsten Pedersen, written comm, 2001/). At a later stage in the investigations (May 2002) two sub-horizontal boreholes were drilled northwards into the rock matrix block from Tunnel 'F' as part of a feasibility study for the Äspö Pillar Stability Experiment (ASPE). Borehole KF0066A01 (16 m east from the MFE borehole) was drilled slightly upwards to a distance of 60.11 m from Tunnel 'F' and borehole KF0069A01 (19 m east from the MFE borehole) was angled slightly downwards to a distance of 70 09 m. Transmissivities ranged from $7.3\cdot10^{-9}$–$1.8\cdot10^{-7}$ m^2s^{-1} and $1.5\cdot10^{-10}$–$1.8\cdot10^{-7}$ m^2s^{-1} respectively; borehole KF0066A01 showed greater transmissivities close to the tunnel (7–8 m) and further into the rock matrix (56 m) and borehole KF0069A01 also further into the rock matrix (64–66 m) /Fransson, 2003/. These points were interpreted as intersections with sub-vertical fracture zones of high hydraulic conductivity which bound the matrix rock block.

Table 7-2. Hydraulic parameters of selected borehole sections from the Prototype Repository Experiment.

Borehole	Section (m)	T'missivity flow (m^2s^{-1})	Estimated flow (L/min)	Measured exchange[+] (L/min)	Time (days)
KA3566G01	12.3–19.8	1.00E-7	0.13	0.3	0.08
	20.8–30.0	1.00E-8	0.02	0.023	1.27 *
KA3566G02	1.3–6.8	5.00E-10	0.0015	0.003	5.85 *
	7.8–11.3	1.00E-9	0.006	0.0005	23.40 *
	12.3–18.3	1.00E-7	0.12	0.4	0.05 *
	19.3–30.0	5.00E-9	0.04	0.033	1.03 *
KA3572G01	1.3–5.3	1.0E-9	0.0015	0.001	13.31 *
KA3578G01			0.00005	0.0005	14.40
KA3590G02	8.3–16.3	1.00E-8	0.032	0.16	0.16
	17.3–22.3	5.00E-9	0.037	0.25	0.06 *
KA3593G	1.3–7.3	3.00E-8	0.2	0.074	0.27

* Samples subsequently chosen for Class 5 hydrochemical characterisation.
[+] Time to exchange the volume of water in one packed-off borehole section.
Estimated Flow – based on the measured transmissivity.
Measured Flow – based on direct outflow measurement from the isolated borehole sections.

7.3.3 Hydrochemistry

General

To facilitate comparison of the various data sets most of the hydrochemical data presented below for discussion are of Class 5 standard. Averaged analytical data from the TRUE Block Scale, Prototype and 'J' Niche experiments (together with boreholes KF00660A1 and KF0069A01) are presented in Table 7-3, and the borehole groundwaters are presented in Table 7-4. All available MFE-borehole water data, including the near-vicinity boreholes KF0066A01 and KF0069A01, are presented in Appendices 13 and 16.

Evaluation and discussion

Principal Component Analysis (M3)

Visually, the general distribution of the groundwaters from each of the sampled sites are shown against a background of all data from the Äspö and Laxemar areas in the M3 (**M**ultivariate **M**ixing and **M**ass balance) calculated PCA plot in Figure 7-7. The basis of this PCA plot including the derivation of the end-members used are detailed in several publications /e.g. Laaksoharju et al, 1999a,b; Svensson et al, 2002/.

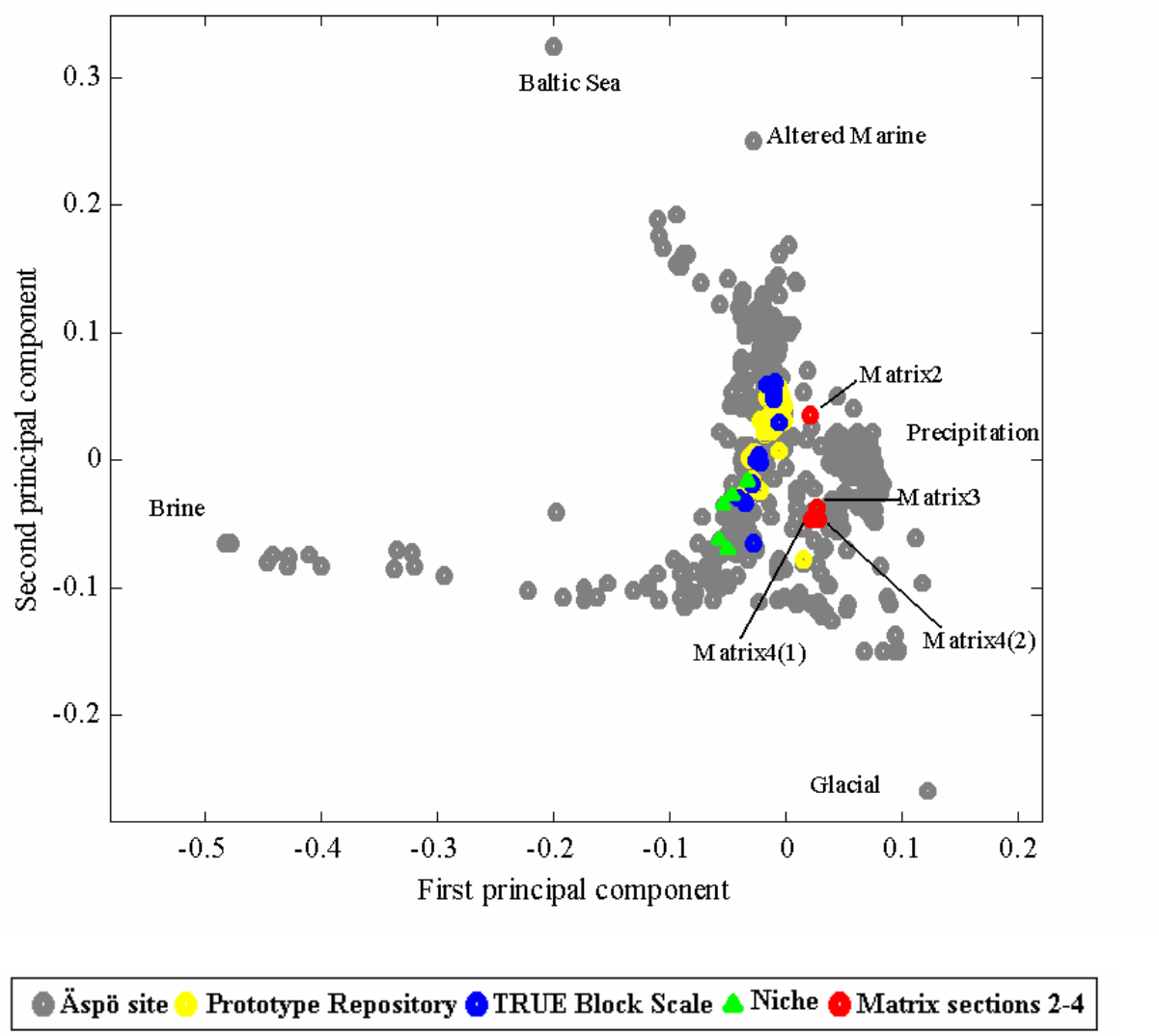

First Principal Componet = –0.49[Na] –0.03[K] –0.01[Ca] –0.03[Mg] +0.13[HCO_3] +0.24[Cl] +0.16[SO_4] –0.17[^2H] +0.75[^{18}O] +0.25[^3H]

Second Principal Component = –0.25[Na] +0.35[K] +0.04[Ca] +0.45[Mg] +0.31[HCO_3] –0.69[Cl] –0.18[SO_4] –0.09[^2H] +0.06[^{18}O] –0.003[^3H]

Variance: Comp 1 = 40%; Comp 1+2 = 70%

MFE-borehole data are given in Appendices 13 and 16.

Figure 7-7. *PCA plot showing the distribution of groundwaters from the TRUE Block Scale, Prototype Repository, 'J' Niche and Matrix Fluid experimental sites. For comparison these data are related to the overall Äspö database.*

The distribution of the PCA data is mainly controlled by the variation of the five representative reference or end-member waters, i.e. the Brine, Glacial, Precipitation, Altered Seawater and Baltic Sea components. Since the Äspö HRL construction has resulted in a significant drawdown of Baltic Sea water to the detriment of the Glacial component, and an upconing of deeper saline (Brine) groundwaters, the PCA plot tends to highlight these trends. For example, there is a separation of the 'J' Niche and Prototype Repository groundwaters (apart from one outlier: borehole KA3572G01) which may suggest that these latter groundwaters have been influenced by an increasing Baltic Sea component. The TRUE Block Scale groundwaters extend over the full range of the 'J' Niche and the Prototype Repository groundwaters suggesting in cases an increasing Baltic Sea component influencing some of the more accessible TRUE Block Scale fracture locations (e.g. as a consequence of orientation and/or geographic location).

Data from the MFE-borehole water samples (sections 2, 3 and 4; Figure 2-3) were included in the PCA plot at an early stage in the evaluation to establish whether there was any suggestion of influence from the surrounding present-day formation groundwaters. Subsequent evaluations documented in Chapter 6 (sampling phases 1 and 2) and this present chapter, however, have shown that MFE-borehole sections 3 and 4 have been unaffected by any recent influences and therefore their use in this PCA diagram is obsolete as they represent other palaeogroundwater systems constrained by different reference end-members. They have been retained only to emphasise that Section 2 has a different chemistry and it has been conjectured (see below) that this borehole section may have been influenced by recent groundwater not too dissimilar from the Prototype Repository type.

Borehole KA3572G01 plots distinctly separate from the rest of the Prototype Repository samples suggesting less influence from a modern Baltic Sea component and the probable retention of an older Glacial or cold climate recharge component.

Hydrochemistry

In the Prototype Repository groundwaters a modern Baltic Sea water component is supported by the moderate tritium values (av 8.4 TU) and high Mg (84.4 mg/L) which contrasts with lower Mg (54.1 mg/L) and tritium (av 2.9 TU) and more negative ^{18}O values and higher Cl content in the 'J' Niche groundwaters (Table 7-3). The TRUE Block Scale groundwaters show broadly similar hydrochemical trends to the 'J' Niche samples with an even lower Mg content (av 47.4 mg/L). These features would suggest that the 'J' Niche waters and the TRUE Block Scale waters are less influenced by drawdown of modern Baltic Sea waters due to tunnel construction than the Prototype Repository samples, even though the sampling locations for the Prototype Repository groundwaters represent a lower range of transmissivity. This may be explained partly by the fact that most of the Prototype Repository sampling points are close to the excavated tunnel (1–30 m; Table 7-2), whilst the TRUE Block Scale sample locations (40–190 m from the tunnel; Table 7-1) and to a lesser extent the 'J' Niche locations (9–44 m from the tunnel) are further into the surrounding bedrock where the tunnel drawdown effects may be less pronounced.

Table 7-3. Chemistry of fracture zone groundwaters sampled in the near-vicinity of the MFE-borehole. (TRUE Block Scale, Prototype Repository and 'J' Niche (Chemlab/Microbe) experiments; Prototype sample KA3572G01 is shown separately because of its anomalous chemistry; boreholes KF0066A01 and KF0068A01 represent groundwaters from intersected major fracture zones bounding the matrix block).

Element	TRUE [n = 8] (mg/L)	Prototype [n = 7] (mg/L)	KA3572G01 [n = 1] (mg/L)	'J'Niche [n = 5] (mg/L)	KA0066A01 [n = 1] (mg/L)	KA0069A01 [n = 1] (mg/L)
Na	1983	1887	2340	2286	3390	3130
K	–	–	–	–	14.7	15.8
Mg	42.4	86.4	24.8	54.1	33.1	33.1
Ca	1396	770	800	1996	4620	3980
Fe	0.09	0.34	–	0.90	0.08	0.01
Si	5.7	7.9	5.4	5.7	4.4	4.5
F	1.2	1.3	1.2	–	1.0	1.3
Cl	5675	4210	4810	6944	12883	12280
Br	30.7	19.9	27.2	39.3	97.1	86.6
SO_4	363	308	617	447	642	663
Alkalinity (as HCO_3)	19	155	–	40	13	5
pH (field)	–	–	–	–	7.8	8.1
pH (lab)	8.0	7.3	7.4	7.4	7.1	7.2
	µg/L	**µg/L**	**µg/L**	**µg/L**	**µg/L**	**µg/L**
Li	860	360	435	920	–	–
Sc	< 0.01	0.020	0.024	0.540	0.170	0.435
Mn	280	510	–	410	–	–
Rb	28	30	35	29	59	51
Sr	19900	10780	15700	33780	–	–
Y	0.145	0.130	0.118	0.331	0.551	0.427
Cs	2.37	2.29	1.43	3.63	4.87	4.21
Ba	60.3	52.3	59.3	69.4	103	97
La	0.13	0.05	0.15	0.17	1.51	0.44
Ce	0.29	0.14	0.07	0.19	1.28	0.16
Nd	0.03	0.02	0.02	0.06	0.26	< 0.05
Th	< 0.005	< 0.005	< 0.005	< 0.004	< 0.500	< 0.500
U	0.006	0.030	0.018	0.030	0.023	< 0.020
Isotope						
^3H	4.4	8.4	4.7	2.9	< 0.8	< 0.8
$\delta^{18}O$	–9.6	–8.0	–10.1	–10.6	–12.6	–12.4
δD	–75.9	–66.7	–80.9	–79.6	–86.1	–84.9
^{14}C	60	70	–	–	–	–
$\delta^{37}Cl$	+0.03	–0.28 to +0.16	+0.27	+0.34	–	–
$\delta^{11}B$	47.23	45.97	51.87	–	–	–
$\delta^{34}S$	25.3	25.6	–	–	12.9	13.8
$^{87}Sr/^{86}Sr$	–	0.717563	0.714990	–	0.719077	0.719144

^3H (TU); $\delta^{18}O$ (‰ SMOW); δD (‰ SMOW); ^{14}C (pmc); $\delta^{37}Cl$ (‰ SMOC); $\delta^{11}B$ (‰ NBS951); ^{34}S (‰ CD)
n = number of samples analysed/averaged.

In this context it is interesting to note that one of the Prototype Repository groundwaters (KA3572G01) appears to be less influenced by drawdown effects as suggested also in Figure 7-7. It is characterised by a greater glacial water or cold climate $\delta^{18}O$ signature (–10.1‰ SMOW compared to an average of –8.0‰ SMOW) and a lower marine (Baltic Sea?) component (less Mg; 24.8 mg/L) than the other Prototype Repository groundwaters. Comparison with the other locations (Table 7-3) shows this sample to be quite similar to the 'J' Niche and TRUE data with respect to δD [–80.9‰ (–79.6‰)], $\delta^{18}O$ [–10.1‰ (–10.6‰)] and SO_4 [617 mg/L (447 mg/L)] (average 'J' Niche values in brackets). Furthermore, it differs from the rest of the Prototype Repository samples by, for example, a more positive $\delta^{37}Cl$ value, lower $^{87}Sr/^{86}Sr$ ratio, higher Na, Sr, SO_4, Cl, Br and ^{11}B, and lower Mn.

Differentiation of the sample groups is also reflected by plotting $\delta^{37}Cl$ versus Br/Cl (Figure 7-8). For groundwater evaluation the ratio of bromine to chloride is commonly used an indicator of water origin, with elevated values showing waters that have undergone water/rock interaction /e.g. Nordstrom et al, 1989b/. This is characteristic of the Laxemar samples with a Br/Cl ratio consistent with the rock signature (i.e. non-marine signature). Most of the other samples show mixing with a modern Baltic Sea water component or a shallow $\delta^{37}Cl$ depleted water such as seen at Stripa /Sie and Frape, 2002/. Interesting is the increasing trend towards depleted $\delta^{37}Cl$ from the matrix borehole water samples through the 'J' Niche (i.e. CHEMLAB/microbe) samples to the TRUE Block Scale and Prototype Repository samples (see additional discussion in section 7.4). This once again reflects the degree of mixing during drawdown that has taken place and lends support to the other hydrochemical arguments.

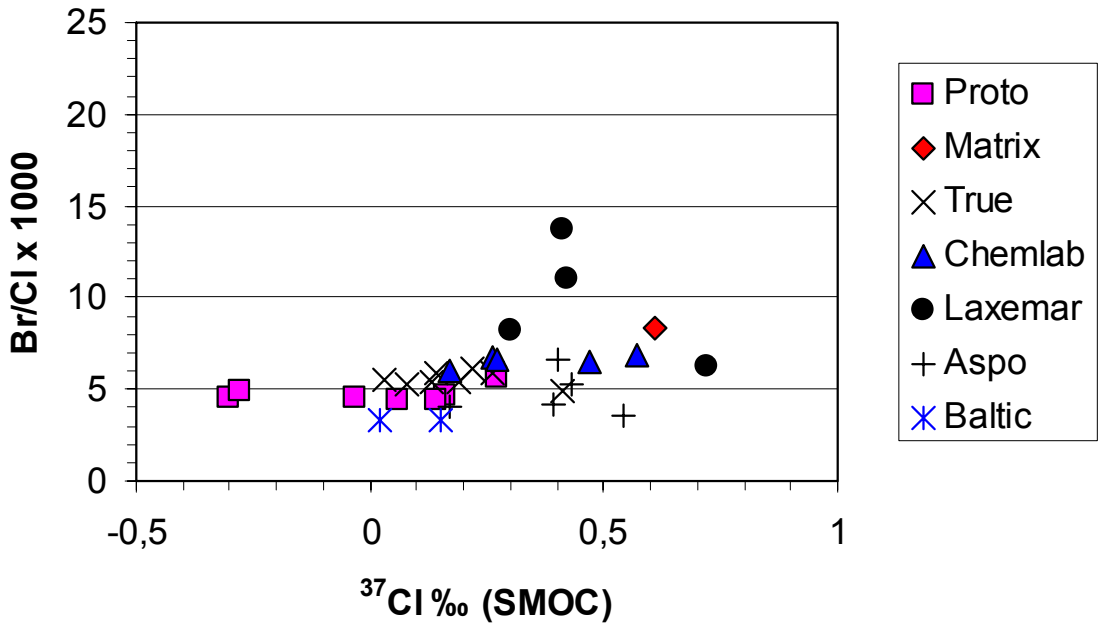

Figure 7-8. *Plot of Br/Cl versus $\delta^{37}Cl$ showing the separation of the sample groups based on water-rock interaction and variable mixing with Baltic Seawater during drawdown.*

Although not plotted in Figure 7-7, the borehole KF0066A01 and KF0069A01 groundwaters (Table 7-3) would plot towards the Brine end member since they are nearly identical in major ion and stable isotopic composition to the deepest saline groundwaters found at Äspö during the Pre-investigation stage studies /Smellie and Laksoharju, 1992; Smellie et al, 1995/. It is quite clear that upconing of deep, more saline groundwaters has occurred close to the MFE-borehole site in Tunnel 'F' via large-scale hydraulically active sub-vertical fracture zones, some of which have been transected by the tunnel. Generally, upconing at the Äspö HRL has been observed from long-term monitoring and also predicted from modelling calculations /Laaksoharju et al, 1999b; Svensson et al, 2002/.

7.4 MFE-borehole hydrochemical conditions

7.4.1 General

In a repository context the MFE-borehole may be considered to represent the scale of hydrochemical influence surrounding the deposition hole. The chemistry of the MFE-borehole water has been described and discussed in detail in Chapter 6. The main objective of this section is to relate the borehole waters to the surrounding environment to establish any evidence of influence from near-vicinity groundwaters via interconnected networks of fractures and microfractures. Figure 7-9 shows some of the major fracture systems and sampled borehole locations closest to the MFE-borehole.

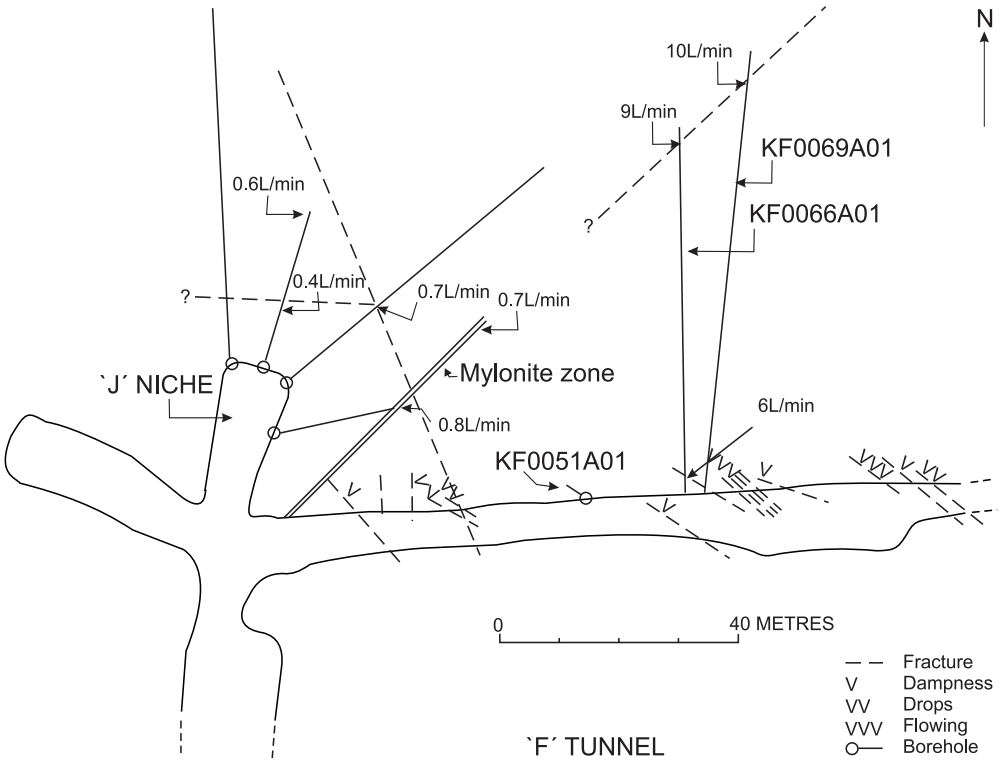

Figure 7-9. *Major fracture zones and borehole locations in the near-vicinity of the MFE-borehole (KF0051A01).*

In all probability the fracture zone intercepted by boreholes KF0066A01 and KF0069A01 represents a continuation of the Mylonite Zone. This is supported by a recent evaluation by /Hansen and Hermasson, 2002/ who refer to it as Zone 4, the most dominant structure in the 'F' Tunnel area.

7.4.2 Hydrochemistry

Chapter 6 emphasised the strong evidence of microbially mediated sulphate-reducing reactions in the isolated MFE-borehole sections. This is supported by microbe studies carried out in waters from borehole Section 4 (MFE-S4-1) which revealed 900 000 cells per mL of which 110 were sulphate-reducing bacteria and 35 were iron-reducing types /K Pedersen, written comm, 2000/. It is also important to note that sulphate reduction by microbial processes is not only characteristic of the MFE-borehole waters, but is also a common feature at the Äspö HRL in groundwaters at depth, particularly where recent sea sediments overlie the bedrock /Laaksoharju, 1995/. A further characteristic of the MFE-borehole waters was the high levels of dissolved fluoride which were attributed to corrosion of the Teflon coated sections of the downhole sampling equipment.

MFE-borehole waters and comparison with Äspö fracture groundwaters

With the exception of Section 2, the MFE-borehole water samples (Table 7-4) when compared with the surrounding fracture groundwater data in Table 7-3 are characterised by lower Mg, generally more negative stable isotope signatures, lower Sr-isotope ratios and generally higher ^{37}Cl. Although there are only trace element data from Section 4 (MFE-S4-1; Appendix 13, Table A13-8), lower trace element contents are generally indicated when compared with the remaining data with the exception of Li and Cs. In contrast, the Section 2 groundwater chemistry is quite different showing, with the exception of lower salinity and SO_4 (effectively reduced by microbial activity), similarities with the Prototype Repository-type groundwaters as noted in section 7.3.3.

Based on the chemistry of the sampled MFE-borehole waters (Table 7-4), specific trends and differences within and between each of the sampled sections were examined:

- time-series (39 months duration) exhibited by comparing Section 4 (MFE-S4-1 to MFE-S4-3);
- time-series (16 months duration) exhibited by comparing Section 2 (MFE-S2-2 and MFE-S2-3);
- time-series (16 months duration) exhibited by comparing Section 3 (MFE-S3-2 and MFE-S3-3);
- chemical variation between Section 2 (Ävrö granite) and Section 4 (Äspö diorite) due to differences in transmissivity and/or rock chemistry?; and
- the character of Section 3 located at the contact between the Ävrö granite and Äspö diorite.

Table 7-4. Chemistry of the MFE-borehole groundwaters. (The complete analytical data are given in Appendices 13 and 16).

Element	MFE-borehole						
	Section 2* MFE-S2-2 (mg/L)	**Section 2 MFE-S2-3 (mg/L)**	**Section 3* MFE-S3-2 (mg/L)**	**Section 3 MFE-S3-3 (mg/L)**	**Section 4 MFE-S4-1 (mg/L)**	**Section 4 MFE-S4-2 (mg/L)**	**Section 4 MFE-S4-3 (mg/L)**
Na	1760	–	2460	–	2200	2480	–
K	16.3	–	14.5	–	11.4	9.28	–
Mg	17.4	–	8.3	–	7.8	4.2	–
Ca	568	–	916	–	964	908	–
Fe	–	–	1.19	–	0.24	0.029	–
Si	–	–	8.2	–	7.6	8.7	–
Sr	–	–	–	–	18.6	–	–
F	98.8	–	57.8	18.4	–	11.1	0.92
Cl	2900	–	4780	4770	5160	5020	5020
Br	24.1	–	36.7	38	43.16	32	36
SO_4	2.7	–	1.5	158	26	84	159
Alkalinity (as HCO_3)	–	–	303	165	200	371	278
pH (field)	6.17	6.42	6.08	7.05	6.7	7.01	7.25
pH (lab)	–	6.18	7.04	7.50	8.1	7.78	7.93
	µg/L	**µg/L**	**µg/L**	**µg/L**	**µg/L**	**µg/L**	**µg/L**
Li	244	–	320	–	274	321	–
Isotope							
^3H	–	–	–	–	–	–	–
$\delta^{18}O$	–7.8	–8.7	–11.7	–12.3	–11.6	–12.2	–12.7
δD	–63.6	–66.6	–89.7	–89.5	–87.9	–92.4	–91.6
$\delta^{13}C$	–	–	–21.9	–3.7	–	–	–7.6
^{14}C	–	64.5 ± 0.4	57.3	39.0	–	–	54.2
$\delta^{37}Cl$	+0.46/+0.44	+0.31	+0.48/+0.43	+0.35	+0.61/+0.59	+0.58/+0.60	+0.32
$\delta^{11}B$	–	–	–	–	47.23	–	–
$\delta^{34}S$	–	–	–	–	–	–	–
$^{87}Sr/^{86}Sr$	0.715635	0.715213	0.714764	0.714531	0.714516	0.714300	0.714080

^3H (TU); $\delta^{18}O$ (‰ SMOW); δD (‰ SMOW); ^{14}C (pmc); $\delta^{13}C$ (PDB); $\delta^{37}Cl$ (‰ SMOC); $\delta^{11}B$ (‰ NBS591); $\delta^{14}S$ (‰ CD)

* Not sampled in the first sampling campaign in 1999-12-07 (no S2-1 or S3-1; cf Table 2-3)

With respect to Section 4 the passing of 39 months resulted in minimal differences in the major anion chemistry (Table 7-4). A more significant increase in SO_4 from 26 mg/L (first campaign) to 84 mg/L (second campaign) to 159 mg/L (third campaign) was observed, matched by an increasingly light $\delta^{18}O$ (–11.6 to –12.7‰ SMOW) and δD (–87.9 to –91.6‰ SMOW) signature, a decreasing $^{87}Sr/^{86}Sr$ ratio signature (0.714516 to 0.714080), a decreasing $\delta^{37}Cl$ signature (+0.60 to +0.32 SMOC), and a marked drop in fluoride content from 11.10 to 0.92 mg/L during the final 16 months.

Groundwater from Section 3 straddling the contact between the Äspö diorite and Ävrö granite showed close similarities to Section 4 (i.e. Äspö diorite). Moreover there was no real change in chemistry during the 16 months between the two sampling campaigns apart, once again, by a marked increase in SO_4 content (1.5 to 158 mg/L), which matched the maximum content recorded in Section 4(MFE-S4-3), an increase in the light isotope signature of $\delta^{18}O$ (–11.7 to –12.3‰ SMOW), a decrease in $\delta^{37}Cl$ signature (+0.45 to +0.35 SMOC), and a sharp drop in fluoride content from 57.8 mg/L (MFE-S3-2) to 18.4 mg/L (MFE-S3-3).

Section 2 showed major differences in chemistry to sections 3 and 4 which included significantly lower salinity (2900 mg/L Cl; 24.1 mg/L Br), slightly higher Mg (17.4 mg/L), much heavier $\delta^{18}O$ (– 8.7 to –7.8‰ SMOW) and δD (–66.6 to –63.6‰ SMOW), and the highest $^{87}Sr/^{86}Sr$ ratio recorded (0.715635). Furthermore the fluoride content was the highest recorded (98 mg/L). Differences in Section 2 during the 16 months between the two campaigns, where possible, showed a decrease in the $\delta^{37}Cl$ signature (+0.45 to +0.31 SMOC) and a decrease in the $^{87}Sr/^{86}Sr$ ratio signature (0.715635 to 0.715213).

Section 1 provided no water, only gas, which is not so surprising considering the large volume of this section compared to the others. During the third sampling phase (13th February, 2003) gas samples for analysis were collected from all MFE-borehole sections and the two near-vicinity boreholes KA0066A01 and KA0069A01 (cf Appendix 16, Table 7-5).

The gas content (MFE-S1-3) comprises mainly CO_2 with small amounts of H_2, CO, CH_4, C_2H_4 and C_2H_6; this composition shows similarities to Section 4 (MFE-S4-3) apart from somewhat higher CO and no C_2H_4 (Table 7-5). Sections 2 and 3 show similar gas proportions to sections 1 and 4 but CO_2, H_2 and CH_4 are an order of magnitude greater. The amounts of CH_4, higher hydrocarbons, and H_2 present indicates that the in-situ conditions in the rock are reducing and supports the proposed perturbation in water containing intervals by sulphate reduction (CH_4 consumption) and associated corrosion of installation material (H_2 as corrosion product).

Table 7-5 also includes analyses from the two major fracture zones in close proximity to the MFE-Borehole (cf Figure 7-9). These are more typical of deeper groundwater conditions and correspondingly show higher H_2 (only KA0066A01) and CH_4 contents, much lower CO_2 and traces of C_2H_6.

Table 7-5. MFE-borehole: Dissolved gas compositions for MFE-S1-3 to MFE-S4-3. (Also included are boreholes KA0066A01 and KA0069A01).

Sample	H_2 (ppm)	CO (ppm)	CH_4 (ppm)	CO_2 (ppm)	C_2H_4 (ppm)	C_2H_6 (ppm)
MFE-S1-3	3.0	9.8	4.9	961	0.9	0.8
MFE-S2-3	12.3	7.3	11.4	1959	b.d.	0.8
MFE-S3-3	10.8	13.9	9.8	2130	b.d.	1.4
MFE-S4-3	2.8	4.3	3.9	1473	b.d.	1.0
KA0066A01*	38.5	0.1	1001	395	b.d.	0.3
KA0069A01*	12.0	0.1	313	124	b.d.	0.1

* See Figure 7-9 for borehole locations.
b.d. = Below detection.

Discussion

Based on the data and reasoning presented in Chapter 6, microbially mediated reactions may be responsible for changes in time with respect to: a) the SO_4 content, b) behaviour of pH and total alkalinity (from field to laboratory and from sampling campaign to sampling campaign), c) decrease in $\delta^{13}C$ and ^{14}C, and d) the component ratios in the free gas above the water (especially comparing the 'dry' Section 1 with all other sections). Furthermore, corrosion may be responsible for the positive correlation between sulphate reduction and fluoride (from Teflon-coated components) with time. This makes it impossible to derive an absolute residence time for the MFE-borehole waters; only an estimate of minimum times can be derived which is in the order of several thousands of years.

The leading question is what effect, if any, have the surrounding fracture groundwaters had on the hydrochemical evolution of the MFE-borehole waters during the experimental period. There is little doubt that the main source of the waters sampled in the MFE-borehole is the surrounding near-vicinity rock matrix. Hydraulic considerations (cf Chapter 4) showed that extracted water required to fill Section 4, assuming advective flow in 1–3 connected microfractures with transmissivities ranging from $1 \cdot 10^{-14}$–$1 \cdot 10^{-13}$ m^2s^{-1}, would require a distance not exceeding 3–7 m. Assuming an absence of microfractures the calculated radius of matrix water extraction to Section 4 would only extend over a radius of 17 cm in a homogeneous block of porous rock. Based on mineralogy and porosity measurements (cf Chapter 3, section 3.4), there is much evidence to support that the rock matrix is characterised by networks of interconnected microfractures. Therefore, as discussed in detail below, the distance to extract the MFE-borehole waters during the experimental period may have exceeded the 3–7 m since greater volumes of water than calculated only for Section 4 have been extracted from around the MFE-borehole. Furthermore, in retrospect, transmissivities of the connected microfractures in or close to the MFE-borehole may be somewhat greater than used in the calculations above, more in the range of $1 \cdot 10^{-13}$–$1 \cdot 10^{-10}$ m^2s^{-1}, thus extending the radius of pore water/groundwater extraction

As discussed above, excavation during the construction and operation phases of the Äspö HRL has resulted in changes in groundwater chemistry, namely: a) a drawdown of modern Baltic Sea waters, b) the removal or mixing/dilution of older groundwaters containing a significant glacial component, and c) an upconing of old, deeper saline or brine groundwaters. Any recent influence from these changes during the experimental period of the MFE-borehole therefore should be evident from an increased component of one or more of these groundwater types. There is, however, no hard evidence from the MFE-borehole waters of such recent changes and, considering that the hydraulic predictions calculated in Chapter 4 seem to be realistic, more time would be expected in any case for hydrochemical changes to pervade through the rock matrix to the MFE-borehole location.

There is, however, one potential exception to this conclusion based on the possibility that there may be a short-circuiting of groundwater transport via nearby more highly transmissive fractures that cannot be observed, thus cutting down the time period for such changes to occur in the MFE-borehole. Comparing Section 2 matrix waters (Table 7-4) with the Prototype Repository groundwaters (Table 7-3) shows, bearing in mind the potential in-situ perturbations in the MFE-borehole, some close chemical and isotopic similarities which are difficult to ignore and may reflect the mixing of a recent component of Prototype Repository-type groundwater. Moreover, even though collecting a small volume of matrix pore water from Section 2 in Ävrö granite took much longer than the greater volumes extracted from sections 3 and 4 in Äspö diorite, the main transport mechanism between an assumed larger transmissive fracture and the MFE-borehole section (some decimetres apart?) was almost certainly diffusion-driven which would account for the length of time taken to accumulate matrix pore waters in Section 2.

In Chapter 6 it was concluded that the sampled MFE-borehole waters did not represent in-situ conditions and this is supported by the present discussion which suggests that part of the sampled matrix pore waters may have been extracted from a distance of at least 3–7 m from the MFE-borehole. Since the collected matrix pore waters (with the probable exception of Section 2) do not represent present-day hydrochemical conditions prevalent in the more transmissive parts of the surrounding bedrock, they probably represent palaeohydrochemical signatures of residual waters which once characterised the Äspö region at one or more evolutionary stages following the last glaciation. In the absence of reliable ^{14}C data due to in-situ perturbations in the MFE-borehole sections (cf Chapter 6), timescales within the last 10 ka, unfortunately, cannot be quantified.

Although there is no evidence to suggest whether highly saline fluids once occupied the rock matrix pore space and since then have been removed and replaced by less saline waters, the hydrochemical and hydraulic evidence indicates that the Äspö HRL at the depth investigated is hydraulically quite dynamic, not only in the more highly transmissive bedrock but also in the lowest transmissive parts of the rock matrix over timescales well within the intended lifespan of a repository.

In conclusion, MFE-borehole sections 3 and 4 contain brackish waters which represent a mixture of residual palaeowaters (derived from interconnected microfracture networks in the rock matrix) and rock matrix pore fluid (from diffusion dominated transport). Section 2 represents less brackish waters which appear to share similarities with the Prototype Repository-type groundwaters. These similarities maybe the result of a nearby (some decimetres?) transmissive fracture of unknown dimensions short-circuiting Prototype Repository-type groundwaters into the rock matrix block. The slow accumulation of pore water in the borehole suggests that diffusion was the main driving force between the fracture and the borehole section. If this were the case, then rock matrix pore fluids should also constitute an important component.

7.4.3 Conceptualisation

Figure 7-10 represents a schematic conceptualisation of the hydraulic conditions in the bedrock surrounding the MFE-borehole. The water-conducting fractures ranging in transmissivity from 10^{-10}–10^{-7} m^2s^{-1} represent most of the TRUE Block Scale, Prototype Repository and 'J' Niche experimental data which contrast with the rock matrix characterised by transmissivities of 10^{-14}–10^{-10} m^2s^{-1}. Microfractures within the rock matrix have been allocated a range of 10^{-12}–10^{-10} m^2s^{-1} and an example of such features is the ~ 1 mm microfracture documented some 56.5 cm from Section 4 towards the tunnel and assumed to be hydraulically active (cf Chapter 3; section 3.6).

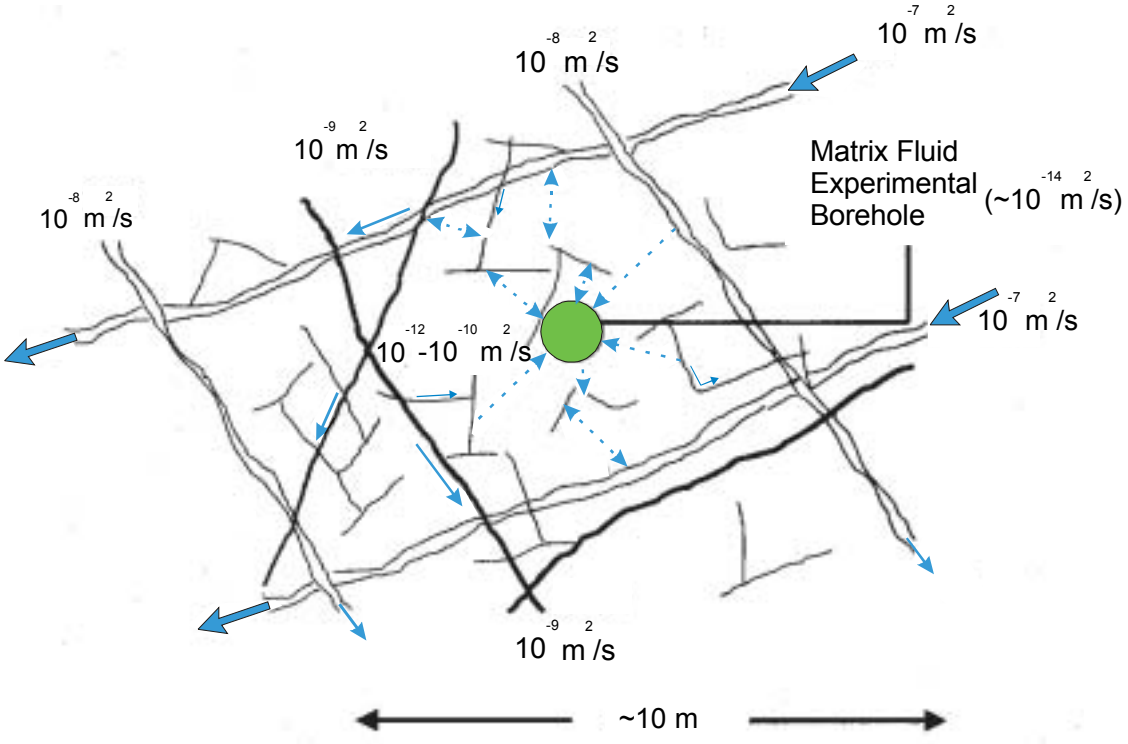

Figure 7-10. *Conceptual hydraulic model of the matrix rock block showing the location of the MFE-borehole.*

Large-scale groundwater movement through the bedrock occurs within the medium to high hydraulically conducting fractures. Access to the rock matrix is by flow through an interconnected network of fractures and microfractures characterised by ever decreasing dimensions and hydraulic conductivities. In the rock matrix itself transport is dominated by diffusion and will last as long as a chemical gradient between the matrix pore fluid/water and groundwaters in open microfractures is present. Thus, short-term movement of water (i.e. within the timescale of the experiment) will be mainly by small-scale advection via the connecting network of microfractures; some restricted contribution from diffusion may be expected also. Over repository timescales (i.e. thousands to hundreds to thousands of years) a greater contribution from diffusion of pore fluid/water from the rock matrix itself will be present since the microfracture groundwaters will have had more time to undergo exchange by in- or out-diffusion mechanisms depending on the nature of the chemical gradients existing between these groundwaters and the rock matrix pore fluids/waters. Evidence of matrix pore fluid in the MFE-borehole samples includes anomalous chlorine isotope and strontium isotope signatures and higher contents of most trace elements which may be characteristic.

Groundwater movement along these microfracture pathways has been greatly enhanced by the increased hydraulic gradients generated by the presence of the tunnel, and to a much lesser extent by the MFE-borehole itself. This enhanced water circulation results in chemical (and isotopic) changes of the groundwaters thus creating new chemical (and isotopic) gradients between the rock matrix pore fluid/water and groundwaters in the microfractures. These newly established chemical gradients are responsible for the reactivation of solute exchange between fracture groundwater and matrix pore fluid/water by diffusion.

Under undisturbed conditions the matrix pore fluids/waters in granitic rocks are suspected often to be saline in composition. This was shown by /Couture et al, 1983/ by carrying out high pressure displacement experiments on granite drillcore material from Illinois resulting in concentrations of ~ 80 mg/L Na-Ca-Cl. However, the presence or absence of saline pore water may be a function of depth and/or whether the locality sampled is in the near-vicinity of large-scale conducting fractures or fracture zones and thus influenced by the palaeohydrogeological evolution of the site. For example, at the 240 m level at the URL site in Canada pore waters entering an unfractured borehole 20 m from Fracture Zone 2 exhibited salinities only marginally greater than in the fracture zone /Gascoyne, written comm, 2000/. In this case it was suggested that the saline fluids had already been replaced in the rock matrix due to a combination of interconnected porosity and increased hydraulic gradient. This was borne out at greater depths in the URL site where salinities of ~ 90 g/L TDS were recorded from fluids sampled from the granite matrix at the 420 m level /Gascoyne et al, 1996/.

The present absence of highly saline rock matrix pore waters at Äspö suggests, in common with the URL situation at shallow depths, that the accessible matrix pore water has been replaced by brackish groundwaters which show some similarities to the surrounding low to intermediate water conducting fractures. This process has probably been in progress at least since the last glaciation but possibly also during earlier glaciations. Pore water replacement at Äspö appears to have been quite efficient. Large-scale fracturing of the upper 500 m of bedrock, associated with isostatic rebound following glacial melt, has greatly facilitated the long-term gradual replacement of old waters with newly infiltrating groundwaters in fractures at all scales of transmissivity.

Post-Äspö HRL conditions have only served to enhance this process by increasing the hydraulic gradients resulting in drawdown and upconing effects. At greater depths (> 1000 m) fracturing is less frequent and groundwater flow conditions will probably be near-stagnant as observed at nearby Laxemar /Laaksoharju et al, 1995/. Here, as at the URL in Canada, the matrix pore waters might be expected to be highly saline in character.

7.5 Conclusions

The general conclusions from this study are:

- Large-scale groundwater movement through the bedrock during disturbed conditions occurs within the medium to high hydraulically active fractures. Over the range of transmissivity represented by these sampled fractures ($T = 10^{-10}$–10^{-5} m^2s^{-1}), there is little obvious correlation between hydraulic properties and groundwater chemistry.
- Under disturbed conditions the hydrochemical and isotopic data indicate an influx of a modern groundwater component, such as Baltic Sea waters, associated with the hydraulic drawdown caused by tunnel construction, to the detriment of older saline and glacial melt water components which have been diluted or removed respectively.
- This drawdown has been particularly apparent with the Prototype Repository samples despite the generally low transmissive character of the sampling locations ($T = 10^{-10}$–10^{-7} m^2s^{-1}); this is probably due to their near-vicinity to the excavated tunnel opening.
- At least one of the lower transmissive Prototype Repository fractures (KA3572G01; 10^{-9} m^2s^{-1}) has been less influenced by the drawdown due to a longer response time, retaining a lower Mg content and more negative $\delta^{18}O$ and δD signatures, together with an overall higher TDS content. This may reflect a different fracture orientation than the other sampled fractures.
- Drawdown effects are less evident from the 'J' Niche and many of the TRUE Block Scale sites probably due to the sampling locations being further from the excavated tunnel opening. It would appear therefore that to achieve a more sensitive correlation between hydraulic properties and groundwater chemistry, smaller ranges of hydraulic transmissivity (e.g. 10^{-12}–10^{-10} m^2s^{-1}) need to be investigated at greater distances away from these open tunnel conditions.
- Groundwater compositions from boreholes KF0066A01 and KF0069A01, representing major water conducting sub-vertical fracture zones close to the experimental site, represent the result of upconing of highly saline groundwaters typical of the deepest (~ 1000 m) samples studied at Äspö.
- Access of groundwaters to the rock matrix is by flow through an interconnected network of fractures and microfractures characterised by ever decreasing dimensions and hydraulic conductivities. Within the rock matrix itself solute transport is dominated by diffusion processes.

- The MFE-borehole water samples reflect a generally similar major ion character to nearby fracture compositions with the exception of SO_4 (due to microbial activity in the MFE-borehole sections) and Mg. However the MFE-borehole waters exhibit anomalous chlorine isotop e and strontium isotope signatures and higher contents of most trace elements which may be more characteristic of a 'true' matrix pore fluid/water component.
- Borehole sections 3 and 4 represent older palaeogroundwaters preserved in the low hydraulically transmissive rock matrix. A component of matrix 'pore fluid' is also present.
- Borehole sections 3 and 4 represent older palaeogroundwaters preserved in the low hydraulically transmissive rock matrix. A component of matrix 'pore fluid' is also present.
- Section 2 in the MFE-borehole appears to be anomalous suggesting some similarity with the Prototype Repository samples which have been strongly influenced by a Baltic Sea drawdown. It is believed that access of this groundwater to the MFE-borehole is via the close proximity (decimetres?) of a transmissive fracture of unknown dimensions. Since diffusion was the main driving force between the fracture and the borehole section then rock pore fluids/waters also constitute an important component.
- Short-term solute transport (i.e. within the timescale of the experiment) through the rock matrix is mainly by small-scale advection via a connecting network of microfractures and by diffusion.
- Over repository timescales (i.e. thousands to hundreds to thousands of years) a greater contribution from diffusion of pore fluid/water from the rock matrix itself will be present since this will have had more time to undergo exchange by in- or out-diffusion mechanisms depending on the nature of the chemical gradients existing between the microfracture waters and the rock matrix pore fluids/waters.
- Groundwater movement within the bedrock as a whole has been greatly enhanced by the increased hydraulic gradients generated by the presence of the tunnel, and to a much lesser extent by the MFE-borehole itself.
- At Äspö, permeable bedrock at all scales has facilitated the continuous removal and replacement of the interconnected pore space waters over relatively short periods of geological time, probably hundreds to a few thousands of years.

8 Site characterisation implications

One of the objectives of the matrix experiment was to establish methodologies that could be transferred conveniently to site characterisation investigations. Obviously it would be impractical to conduct long-term sampling and analysis of matrix pore waters similar to that described in this report. Emphasis should therefore be on the rock matrix itself, focussing on suitable method(s) to rapidly extract and chemically characterise the accessible pore water. In this respect the rock pore water studies reported in Chapter 5 could form the basis to a methodology to accomplish this objective. Based on these studies the following site characterisation protocol is recommended:

- Sampling during drilling of rock matrix core sections (~ 40 cm lengths) macroscopically free of open fractures at approximately every 50 m (sampling distance will depend on the occurrence and distribution of water-conducting fractures and lithological variations).
- Immediate preservation of core sections in nitrogen flushed, evacuated and sealed heavy duty PVC bags to prevent evaporation of accessible pore water.
- Selection of more suitable samples following additional interpretative data such as downhole TV (BIPS)-imagery, drillcore mapping and flow meter logging etc.
- Final choice of samples to be based on mineralogical and textural examination.
- Scoping analysis of fluid inclusion populations in terms of volume percent and chemistry by mainly Microthermometry; some Laser Raman Microspectroscopy may also be used if necessary.
- One sample from each of the main lithological units to be studied using crush/leach experiments to estimate the chemistry of the accessible and inaccessible pore water fractions contained in the rock.
- Laboratory out-diffusion experiments on core splits using a well characterised low mineralised aqueous medium such that the extracted accessible pore waters can be detected readily and characterised chemically and isotopically.
- At an early stage of the diffusion experiment an initial pulse of high salinity pore water may be expected from rock matrix fluid inclusions close to the drillcore core surface which have been fractured/broken by drilling and removing the core. The aqueous medium should be replaced at this juncture and the experiment continued until chemical equilibrium is achieved between the core and the aqueous medium.
- More systematic core sampling (at ~ 0.5–1.0 m intervals) can be carried out perpendicular to water-conducting fracture zones. Diffusion experiments along such profiles using He, $\delta^{18}O$, $\delta^{2}H$, $\delta^{37}Cl$ and U-decay series measurements may reveal information on large-scale diffusion patterns from which diffusion rates may be calculated.

A complimentary approach, where URL facilities are available, is in-situ diffusion extraction using dilute water in predetermined borehole sections.

9 Overall conclusions

The main objective of the Matrix Fluid Chemistry Experiment at Äspö HRL was to drill a borehole in a very low permeable crystalline rock in order:

- to determine the origin and evolution of the rock matrix pore fluids;
- to establish whether present or past in- or out-diffusion processes have influenced the composition of the matrix pore fluids, either by dilution or increased concentration;
- to derive a range of groundwater compositions as suitable input for near-field model calculations; and
- to establish the influence of microfractures (when present) on the pore fluid chemistry in the rock matrix.

The following are the main conclusions of the study.

9.1 Rock mineralogy and chemistry

- Two major rock types are present in the matrix borehole; Äspö diorite and Ävrö granite.
- A decrease in mafic content and plagioclase is countered by an increase in quartz and K-feldspar along the drillhole representing the transition of Äspö diorite to Ävrö granite.
- The mineralogical composition of these two major rock types serves as an important constraint on the pore fluid composition.
- These constraints (e.g. presence of calcite, clay, Fe-oxyhydroxides, sulphides etc) are similar for diorite and granite.
- Differences between diorite and granite are in accordance with mineralogical differences.
- Chemical differences are too small to have a significant influence on the pore fluid; only exception might be certain metallic trace elements which are more abundant in the diorite in minerals susceptible to alteration.

9.2 Rock density and porosity

- Differences in grain density reflect differences in the content of mafic minerals.
- The total porosity is greater for Ävrö granite (0.76 ± 0.04 vol%) than for Äspö diorite (0.66 ± 0.08 vol%).

- The connected porosity appears to be more variable in the Äspö diorite (0.44 ± 0.07 vol%) than in the Ävro granite (0.40 ± 0.02 vol%), but is the same for both rocks within the accuracy of the methodologies.
- The connected porosity determined by water resaturation is more difficult to achieve in the Äspö diorite than in the Ävrö granite, highlighting the textural differences between the rock types. Generally this supports the hydraulic measurements made in the borehole.
- The difference in total to connected porosity (i.e. water-content porosity) is greater in the Ävrö granite than in the Äspö diorite.
- The difference in total to connected porosity corresponds closely to the independently calculated volume of fluid inclusions. This strongly indicates that the measured non-connected (i.e. not accessible for water diffusion) porosity constitutes almost entirely the amount of fluid inclusions present.
- These findings are in accordance with the greater abundance of quartz and fluid inclusions comprising the Ävrö granite compared to the Äspö diorite.

9.3 Fluid inclusions

- Basically, four types of fluid inclusion populations were identified:
  - Primary, intracrystalline magmatic Type I fluid inclusions (400°–500°C; 5–30 eq.wt% NaCl).
  - Fluid Inclusion Planes (FIPs) containing magmatic/hydrothermal Type II/III fluid inclusions aligned along healed fractures/fissures (100°–300°C; 1–20 eq.wt% NaCl).
  - Type IV intracrystalline boundary grain inclusions (60°–70°C; mostly gas filled; some contain 5–15 eq.wt% NaCl).
- The amount of fluid in the rock matrix contained in the fluid inclusions has been estimated to be around 0.3 vol% for the Äspö diorite and 0.6 vol% for the Ävrö granite.
- The general range of fluid inclusion salinity is between 0.2 and 30 eq.wt% NaCl; $CaCl_2$ sometimes dominates over NaCl. Most grain boundary inclusions are gas filled with only a few liquid varieties with salinities between 5 and 15 eq.wt% NaCl. Overall, the fluid inclusion populations are characterised by a moderately high salinity which may be accessible through deformation and leakage to the interstitial pore space in the rock matrix.
- Grain boundaries constitute areas of structural weakness and represent ‘dark corners’ where hidden fluid and mineral inclusions may occur. In the case of dynamic deformation of the rock and rock-water interaction over a timescales relevant to radioactive waste storage, these grain boundaries may be a source of chemical components to the interstitial pore spaces.

- The development of microscopic techniques such as computer scanning of thin sections and the use of Laser Ablation ICP-MS analysis of thick sections have been employed and may soon be used as routine tools for more precise assessment of volumetric properties, chemistry of fluid inclusions and further understanding grain boundary relationships.
- The Laser Ablation ICP-MS technique is promising and analyses showed anomalies in element traces representing heterogeneities in quartz grains which may be interpreted as grain boundary phases, fluid inclusions or solid inclusions.
- The question of fluid inclusion leakage into the interstitial pore space and, ultimately influencing the matrix or interconnected pore space fluids/groundwaters, cannot be unequivocally resolved. However, there is evidence of an ongoing process of tectonic stress-release accompanying isostatic recovery following glacial ice melt which could provide a convenient mechanism for fracturing inclusions hosted by quartz and releasing fluids into the immediately accessible rock matrix.

9.4 In- and out-diffusion processes

- Profiles analysed perpendicular to a suspected water-conducting microfracture showed no chemical evidence of low temperature alteration or chemical gradients and most chemical variation in the wall rock can be explained by mineralogical heterogeneity.
- In contrast there was an increase in porosity adjacent to the microfracture edge corresponding to $^{234}U/^{238}U$ disequilibrium. This isotopic disequilibrium suggests that within the last 1 Ma water/rock interaction has (and probably is) occurring marginal to the microfracture and this has been accompanied by an accumulation of uranium.
- It has not been possible to determine whether the studied microfracture is a presently open, semi-open or mainly sealed in-situ fracture, but the uranium isotopic disequilibrium data suggest it has been open at some stage in the 'recent' geological past (< 1 Ma), and therefore it seems realistic to assume that it acts as a present-day 'more porous pathway' through the matrix bedrock possibly contributing to some of the borehole waters sampled.

9.5 Hydraulic character of the rock matrix

- Taking into consideration: a) petrology, b) porosity measurements, and c) long-term pressure monitoring and groundwater sampling of the isolated MFE-borehole sections, predictions of groundwater flow times to the borehole sections from the surrounding bedrock based on both 2-D radial and 3-D spherical flow (assuming differential pressures of 10–35 bar and a radius of influence of 5–10 m), where in accordance with the estimated rock matrix hydraulic conductivity ($1 \cdot 10^{-14}$–$6 \cdot 10^{-14}$ ms^{-1}) and the measured connected porosities for the Äspö diorite and Ävrö granite (0.40 and 0.44 vol% respectively).

9.6 Character of the rock pore water

- Aqueous leaching test performed on samples of Äspö diorite and Ävrö granite revealed that the impact of inclusion fluid onto the leach solutions was significant. Consequently the volumetric ratio of pore water in the connected porosity to fluid in mineral fluid inclusion in these rocks is low. This was in agreement with the measurements of total and connected porosity and the estimated fluid inclusion volume in the rocks.
- The strong impact of the inclusion fluids on the leached solutions inhibits the derivation of compositional aspects of the pore water residing in the connected porosity, not only for non-conservative but also for conservative compounds such as Cl and Br.
- Optical and microthermometric fluid inclusion investigations should be mandatory before any aqueous leaching experiments are performed in order to evaluate the feasibility of the latter for the derivations of the pore water composition of crystalline rocks.
- Isotope ratios of strontium and chlorine of the leached solutions supported a mixing of fluids from different origins. The strontium isotopes further indicated a significant influence of Al-silicate alteration during leaching.
- Pore water diffusion experiments appear to be most promising to evaluate at least the conservative chemical and isotopic parameters of the pore water residing in the connected porosity of crystalline rocks. If steady-state conditions are reached, the non-conservative compounds can be estimated by geochemical modelling. The disadvantage of this method is the length of time required for completion.
- Pore water displacement experiments under high pressure appear to be of limited applicability for pore water characterisation of such crystalline rocks. The limiting factor here is the low water content of the rocks that requires a very large volume of rock in order to obtain a reasonable pore water volume displaced for analyses.

9.7 Character of the in-situ borehole water

- Water was successfully sampled after several months of seepage into the isolated sections of the MFE-borehole. Extensive bacterially mediated sulphate- and iron-reduction processes, however, perturbed the water composition and altered in-situ conditions. With the available borehole water data these perturbations cannot be further quantified.
- The sampled borehole waters are generally Na-(Ca)-Cl in type with Cl-concentrations around 5000 mg/L in the Äspö diorite and around 2900 mg/L in the Ävrö granite some 2 m away. The borehole waters sampled from the Äspö diorite and the Ävrö granite also differ significantly in their isotope composition of water and strontium. The chlorine isotope composition is identical for the waters sampled from the diorite and granite sampled within a distance of about 3 m in the borehole, but significantly enriched in the ^{37}Cl in the diorite water sampled further away.

9.8 Relationship of the in-situ borehole water with the surrounding groundwater environment

- Large-scale groundwater movement through the bedrock during disturbed conditions occurs within the medium to high hydraulically active fractures. Over the range of transmissivity represented by these sampled fractures ($T = 10^{-10}$–10^{-5} m^2s^{-1}), there is little obvious correlation between hydraulic properties and groundwater chemistry.
- The hydrochemical and isotopic data indicate an influx of a modern groundwater component, such as Baltic Sea waters, associated with the hydraulic drawdown caused by tunnel construction, to the detriment of older saline and glacial melt water components which have been diluted or removed respectively.
- This drawdown has been particularly apparent with the Prototype Repository samples despite the generally low transmissive character of the sampling locations ($T = 10^{-10}$–10^{-7} m^2s^{-1}); this is probably due to their near-vicinity to the excavated tunnel opening.
- At least one of the lower transmissive Prototype Repository fractures (KA3572G01; 10^{-9} m^2s^{-1}) has been less influenced by the drawdown due to a longer response time which may reflect a different fracture orientation than the other sampled fractures.
- Drawdown effects are less evident from the 'J' Niche and many of the TRUE Block Scale sites probably due to the sampling locations being further from the excavated tunnel opening.
- Groundwater compositions from boreholes KF0066A01 and KF0069A01 close to the experimental site, representing major water conducting sub-vertical fracture zones, represent the result of upconing of highly saline groundwaters typical of the deepest (~ 1000 m) samples studied at Äspö.
- Access of groundwaters to the rock matrix is by flow through an interconnected network of fractures and microfractures characterised by ever decreasing hydraulic conductivities. Within the rock matrix itself solute transport is dominated by diffusion processes.
- The MFE-borehole water samples reflect a generally similar major ion character to nearby fracture compositions with the exception of SO_4 (due to microbial activity in the MFE-borehole sections) and Mg. However the MFE-borehole waters exhibit anomalous chlorine isotope and strontium isotope signatures and higher contents of most trace elements which may be more characteristic of a 'true' matrix pore fluid component.
- Borehole sections 3 and 4 represent older palaeogroundwaters preserved in the low hydraulically transmissive rock matrix. A component of matrix 'pore fluid' is also present.
- Section 2 in the MFE-borehole appears to be anomalous suggesting some similarity with the Prototype Repository samples which have been strongly influenced by a Baltic Sea drawdown. Access of this groundwater to the MFE-borehole is probably via the close proximity (decimetres?) of a transmissive fracture of unknown dimensions.

- Short-term solute transport (i.e. within the timescale of the experiment) through the rock matrix is mainly by small-scale advection via a connecting network of microfractures and by diffusion.
- Over repository timescales (i.e. hundreds to thousands of years) a greater contribution from diffusion of pore fluid/water from the rock matrix itself will be present since this will have had more time to undergo exchange by in- or out-diffusion mechanisms depending on the nature of the chemical gradients existing between the microfracture groundwaters and the rock matrix pore fluids/waters.
- Groundwater movement within the bedrock as a whole has been greatly enhanced by the increased hydraulic gradients generated by the presence of the tunnel, and to a much lesser extent by the MFE-borehole itself.
- At Äspö, permeable bedrock at all scales has facilitated the continuous removal and replacement of the interconnected pore space waters over relatively short periods of geological time, probably hundreds to a few thousands of years.

9.9 Site characterisation implications

- One of the objectives of the matrix experiment was to establish methodologies that could be transferred conveniently to site characterisation investigations. With respect to understanding the chemistry of the matrix pore fluid the present study has shown it would be impractical to conduct long-term sampling and analysis of pore waters similar to that described in this report. Emphasis should therefore be on the rock matrix itself, focussing on suitable laboratory method(s) to rapidly extract and chemically characterise the accessible pore water. This has been one of the successful accomplishments of the study and a protocol has been formulated for potential use in site characterisation investigations studies of crystalline rocks.

10 References

Andersson C, Säfvestad A, 2000. Groundwater chemistry data from the groundwater sampling of KF0051A01 within the matrix fluid chemistry experiment. SKB ITD-00-13, Svensk Kärnbränslehantering AB.

Appelo C A J, Postma D, 1993. Geochemistry, groundwater and pollution. A A Balkema, Rotterdam, 536 pp.

Baeyens B, Bradbury M H, 1991. A physico-chemical characterisation technique for determining the pore-water chemistry in argillaceous rocks. Nagra Tech. Rep. (NTB 90-40), Nagra, Wettingen, Switzerland.

Baeyens B, Bradbury M H, 1994. Physico-Chemical Characterisation and Calculated In-situ Porewater Chemistries for a Low Permeability Palfris Marl Sample from Wellenberg. Nagra Tech. Rep. (NTB 94-22), Nagra, Wettingen, Switzerland.

Banwart S A, Gustafsson E, Laaksoharju M, 1999. Hydrological and reactive processes during rapid recharge to fracture zones. Appl. Geochem., 14, 873–905.

Bath A H, Entwisle D, Ross C A M, Cave M R, Falck W E, Fry M, Reeder S, Green K A, McEwen T J, Darling W G, 1988. Geochemistry of pore-waters in mudrock sequences: Evidence for groundwater and solute movements. In: Proc. Intl. Assoc. Hydrogeol. Symp. on Hydrogeology and Safety of Radioactive and Industrial Hazardous Waste Disposal (Documents de BRGM 160, p 87–97). BRGM, Orléans.

Beaucaire C, Pitsch H, Toulhoat P, Motellier S, Louvat D, 2000. Regional fluid characterisation and modelling of water-rock equilibria in the Boom clay Formation and in the Rupelian aquifer at Mol, Belgium. Appl. Geochem. 15, 667–686.

Byegård J, Johansson H, Skålberg M, Tullborg E-L, 1998. The interaction of sorbing and non-sorbing tracers with different Äspö rock types. SKB TR-98-18, Svensk Kärnbränslehantering AB. (ISSN 0284-3757).

Byegård J, Widestrand H, Skålberg M, Tullborg E-L, Siitari-Kauppi M, 2001. Complementary investigation of diffusivity, porosity and sorptivity of Feature A-site specific geological material. SKB ICR-01-04, Svensk Kärnbränslehantering AB.

Couture R A, Seitz M G, Steindler M J, 1983. Sampling of brine in cores of Precambrian granite from northern Illinois. J. Geophys. 88, B(9), 7331–7334.

Domenico P A, Schwartz F W, 1990. Physical and chemical hydrology. Wiley, New York.

Eliasson T, 1993. Mineralogy, geochemistry and petrpophysics of red coloured granite adjacent to fractures. SKB TR 93-06, Svensk Kärnbränslehantering AB, 68 p.

Fernández A M, Turrero M J, Rivas P, 2001. Analysis of squeezed pore water as a function of the applied pressure in Opalinus Clay material (Switzerland**).** In: R Cidu. (ed): Water-Rock Interaction: Proceedings of the 10th International Symposium on Water-Rock Interaction, Villasimius, Sardinia (Vol 2, p 1323–1326). A A Balkema, Rotterdam.

Fransson Å, 2003. Äspö Pillar Stability Experiment Core boreholes KF0066A01, KF0069A01, KA3386A01 and KA3376B01: Hydrogeological characterisation and pressure responses during drilling and testing. SKB IPR-03-06, Svensk Kärnbränslehantering AB.

Freeze R A, Cherry J A, 1979. Groundwater. Prentice–Hall, Englewood Cliffs, NJ.

Gascoyne M, Ross J D, Watson R L, 1996. Highly saline pore fluids in the rock matrix of a granitic batholith on the Canadian Shield. Abstract: 30th Int. Geol. Congr, Bejing, China (August, 1996).

Gascoyne, written comm, **2000.**

Gunnarsson I, Arnósson S, 2000. Amourphous silica solubility and the thermodynamic properties of $H_4SiO_4^0$ in the range of 0° to 350°C at P_{sat}. Geochim. Cosmochim. Acta, 64, 2295–2307.

Hansen L M, Hermansson J, 2002. Local model of geological structures close to the F-tunnel. Äspö HRL, SKB IPR-02-48, Svensk Kärnbränslehantering AB.

Hermanson J, Doe T, 2000. Structural and hydraulic model based on borehole data from K10025F03. Äspö HRL. SKB IPR-00-34, Svensk Kärnbränslehantering AB.

Hummel W H, Berner U, Curti E, Pearson F J, Thoenen T, 2002. Nagra/PSI Chemical Thermodynamic Data Base 01/01. Universal Publishers/uPUBLISH.com USA, available from: http://www.upublish.com/books/hummel.htm. Also issued as a Nagra Tech. Rep. (NTB 02-16), Nagra, Wettingen, Switzerland.

Imbrie J, Imbrie J, 1980. Modelling the climatic response to orbital variations. Science, 207, 943–953.

Jarl L-G, Johansson Å, 1988. U-Pb zircon ages of granitoids from the Småland-Värmland granite-porphyry belt, southern and central Sweden. GFF, 110, 21–28.

Johansson H, Siitari-Kauppi M, Skålberg M, Tullborg E-L, 1998. Diffusion pathways in crystalline rock-examples from Äspö-diorite and fine-grained granite. J. Contam. Hydrol. 35, 41–53.

Johansson H, 2000. Retardation of tracers in crystalline rocks. Ph D Thesis. Chalmers University of Technology, Ny serie 1582, ISSN0346-718x.

Kornfält K-A, Wikman H, 1987. Description of the map of solid rocks around Simpevarp. Äspö HRL. SKB PR 25-87-02, Svensk Kärnbränslehantering AB.

Laaksoharju M (ed), 1995. Sulphate reduction in the Äspö HRL tunnel. SKB TR-95-25, Svensk Kärnbränslehantering AB.

Laaksoharju M, Smellie J, Skårman C, 1995. Groundwater sampling and chemical characterisation of the Laxemar deep borehole KLX02. SKB TR-95-05, Svensk Kärnbränslehantering AB.

Laaksoharju M, Wallin B, (eds), 1997. Evolution of the groundwater chemistry at the Äspö Hard Rock Laboratory: Proceedings of the Äspö International Geochemistry Workshop, June 6–7, 1995. SKB ICR-97-04, Svensk Kärnbränslehantering AB.

Laaksoharju M, Tullborg E-L, Wikberg P, Wallin B, Smellie J, 1999a. Hydrogeochemical conditions and evolution of the Äspö HRL, Sweden. Appl. Geochem. 14, 819–834.

Laaksoharju M, Skårman C, Skårman E, 1999b. Multivariate mixing and mass balance (M3) calculations, a new tool for decoding hydrogeochemical information. Appl. Geochem. 14, 861–871.

Lampén P, 1992. Saline groundwater in crystalline bedrock – a literature study. Nucl. Waste Comm. Finnish Power Comp, Tech. Rep. (YJT-92-23), Helsinki, Finland.

Louvat D, Michelot J L, Aranyossy J-F, 1999. Origin and residence time of salinity in the Äspö groundwater system. Appl. Geochem. 14, 917–925.

Maddock R H, Hailwood E A, Rhodes E J, Muir Wood R, 1993. Direct fault dating trials at the Äspö Hard Rock Laboratory. SKB TR-93-24, Svensk Kärnbränslehantering AB.

Mazurek M, Bossart P, Eliasson T, 1997. Classification and characterization of water-conducting features at Äspö: Results of investigations on the outcrop scale. SKB ICR 97-01, Svensk Kärnbränslehantering AB. (ISSN 1104-3210).

Moye D G, 1967. Diamond drilling for foundation exploration. Civil Eng. Trans. Inst. Eng. Australia, 95–100.

Nordstrom K D, Lindblom S, Donahue R J, Barton C C, 1989a. Fluid inclusion leakage as a possible source of components in groundwater in crystalline rocks. Geocim. Cosmochim. Acta Vol 53, pp 1741–1755.

Nordstrom D K, Ball J W, Donahoe R J, Whittemore D, 1989b. Ground water chemistry and water-rock interactions at Stripa. Geochim. Cosmochim. Acta 53, 1727–1740.

Norton D, Knapp R, 1977. Transport phenomena in hydrothermal systems; the nature of porosity. Am. J. Sci. 277(8), 913–936.

Olsson O, Stanfors R, Ramqvist G, Rhén I, 1994. Localization of experimental sites and layout of turn 2 – Results of investigations. Äspö HRL. SKB PR 25-94-14, Svensk Kärnbränslehantering AB.

Parkhurst D L, Appelo C A J, 1999. User's Guide to PHREEQC (Version 2) – A Computer Program for Speciation, Batch-Reaction, One-Dimensional Transport, and Inverse Geochemical Calculations. U.S. Geolgical Survey, Water-Resources Investigations Report 99-4259, Denver, CO, 312 p.

Pearson F J, 1999. What is the porosity of a mudrock? In: Aplin A C, Fleet A J and Macquaker J H S (eds) Muds and Mudstones: Physical and Fluid flow properties, Geological Society London. Special Publications, 158, 9–21.

Pearson F J, Arcos D, Bath A, Boisson J-Y, Fernández A-Ma, Gäbler H-E, Gaucher E, Gautschi A, Griffault L, Hernán P, Waber H N, 2003. Geochemistry of Water in the Opalinus Clay Formation at the Mont Terri Rock Laboratory. Reports of the Federal Office for Water and Geology (FOWG), Geology Series, No. 5. Bern, Switzerland. (In press).

Pedersen K, written comm, **2000.**

Pedersen K , written comm, **2001.**

Peterman Z, Wallin B, 1999. Synopsis of strontium isotope variations in groundwater at Äspö, southern Sweden. Appl. Geochem. 14, 939–951.

Pettersson C, 1992. Properties of humic substances from groundwater and surface waters. Ph.D. Thesis, Linköping Studies of Arts and Sciences, University of Linköping.

Rhén I, Forsmark T, 1998a. Prototype repository. Hydrology – Drill campaign 1. Äspö HRL PR (HRL-98-12), Svensk Kärnbränslehantering AB.

Rhén I, Forsmark T, 1998b. Prototype repository. Hydrology – Drill campaign 2. Äspö HRL PR (HRL-98-22), Svensk Kärnbränslehantering AB.

Rhén I, Wikberg P, 2000. Hydrogeological and hydrochemical charaterisation of the Äspö Hard Rock Laboratory, Sweden (1986–1995). Extrait de Hydrogéologie, nr 2, 23–40.

Rimstidt J D, 1997. Quartz solubility at low temperatures. Geochim. Cosmochim. Acta 61, 2553–2558.

Savoye S, Aranyossy J F, Hunziker J C, Kirschner D, 1998. Fluid inclusions in granites and their relationships with present-day groundwater chemistry. Eur. J. Mineral. 10, 1215–1226.

Sie P, Frape S K, 2002. Evaluation of the groundwaters from the Stripa mine using stable chlorine isotopes. Chemical Geology, Vol 182, 565–582.

Smellie J A T, Laaksoharju M, 1992. Äspö Hard Rock Laboratory. Final evaluation of the hydrogeochemical pre-investigations in relation to existing geologic and hydraulic conditions. SKB TR-92-31, Svensk Kärnbränslehantering AB.

Smellie J A T, Laaksoharju M, Wikberg P, 1995. Äspö, S.E. Sweden: A natural groundwater flow model derived from hydrogeochemical observations. J. Hydrol. 172, 147–169.

Smellie J A T, 1999. Äspö Hard Rock Laboratory: Test Plan for: Sampling of Matrix fluids from low conductive bedrock. SKB IPR-00-01, Svensk Kärnbränslehantering AB.

Smellie J A T (ed), 2000. Matrix Fluid Experiment: Status Report (June 1998 – June 2000). Äspö HRL, SKB IPR-00-35, Svensk Kärnbränslehantering AB.

Snow D T, 1968. Rock fracture spacing, openings and porosities. J. Soil Mech. and Foundation Eng. ASCE 94, 1968. pp 73–91.

Stanfors R, Liedholm M, Munier R, Olsson P, Stille H, 1993a. Geological-structural and rock mechanical evaluation of data from tunnel section 700–1475 m. Äspö HRL. SKB PR 25-93-05, Svensk Kärnbränslehantering AB.

Stanfors R, Liedholm M, Munier R, Olsson P, Stille H, 1993b. Geological-structural and rock mechanical evaluation of data from tunnel section 1475–2265 m. Äspö HRL. SKB PR 25-93-10, Svensk Kärnbränslehantering AB.

Sundberg J, Gabrielsson A, 1999. Laboratory and field measurements of thermal properties of the rocks in the prototype repository at Äspö HRL. SKB IPR-99-17, Svensk Kärnbränslehantering AB.

Svensson U, Laaksoharju M, Gurban I, 2002. Impact of the tunnel construction on the groundwater system at Äspö, Task 5. In: Rhén I and Smellie J (eds), 2003. Task force on modelling of groundwater flow and transport of solutes. SKB TR-03-01, Svensk Kärnbränslehantering AB.

Todd D K, 1980. Groundwater Hydrology. Second edition. John Wiley & Sons, Inc. New York. ISBN 0-471-87616-X.

Tirén S, Beckholmen M, Isaksson H, 1987. Structural analysis of digital terrain models, Simpevarp area. Southeastern Sweden. Method study EBBA 11. SKB HRL PR 25-87-21, Svensk Kärnbränslehantering AB.

Tsang Y W, 1992. Usage of "Equivalent Apertures" for Rock Fractures as Derived From Hydraulic and Tracer Tests. Water Res. Research, Vol 28, No 5, 1451–1455.

Viani B E, Burton C J, 1994. Effect of cation exchange on major cation chemistry in the large scale redox experiment at Äspö. In: S Banwart (ed), Proceedings of the Äspö International Geocheimstry Workshop. SKB ICR 94-13, Svensk Kärnbränslehantering AB, p B78–B96.

Waber H N, Gaucher E C, Fernández A-M, Bath A, 2003. Aqueous Leachates and Cation Exchange Properties of Mont Terri Claystones. Annex 3 in Pearson et al (In press). Geochemistry of Water in the Opalinus Clay Formation at the Mont Terri Rock Laboratory. Reports of the Federal Office for Water and Geology (FOWG), Geology Series, No 5. Bern, Switzerland.

Wallin B, Tullborg E-L, Petterson C, 1995. Carbon cycling in the shallow water intrusion into a vertical fracture zone at the Äspö Hard Rock Laboratory. In: Banwart S (ed), The Redox experiment in block scale. SKB PR 25-05-06, Svensk Kärnbränslehantering AB.

Wallin B, Peterman Z, 1999. Calcite fracture fillings as indicators of paleohydrogeology at Laxemar at the Äspö Hard Rock Laboratory, southern Sweden. Appl. Geochem. 14, 953–962.

International
Progress Report

IPR-00-01

Äspö Hard Rock Laboratory

Test plan for

Sampling of matrix fluids from low conductive bedrock

John A T Smellie

Conterra AB

January 1999

Background

Much of the groundwater sampled from the Äspö site at depths greater than 500 m is saline in character, and salinity continues to increase with depth. These groundwaters have been collected from water-conducting fracture zones with hydraulic conductivities greater than $K= 10^{-9}$ ms^{-1}. The salinity of these groundwaters probably obtain their character mostly through mixing along fairly rapid conductive flow paths, being mainly determined by the hydraulic gradient, rather than by chemical water/rock interaction. In contrast, little is known about groundwater compositions from low conductive parts ($K< 10^{-10}$ ms^{-1}) of the bedrock (i.e. matrix fluids), which are determined mainly by the mineralogical composition of the rock and the result of water/rock reactions. As rock of low hydraulic activity constitutes the major volume of the bedrock mass in any granite body, matrix fluids are suspected to contribute significantly to the salinity of deep formation groundwaters. It is considered expedient therefore to sample and quantify such fluids and to understand their chemistry and origin.

Migration of matrix fluids will be facilitated by small-scale fractures and fissures. It is important therefore to relate the matrix fluid chemistry to the chemistry of groundwaters present in hydraulically-conducting minor fractures ($K= 10^{-10}$-$10^{-9}$$ms^{-1}$), since it will be these groundwaters that may initially saturate the bentonite buffer material.

Such knowledge of matrix fluids and groundwaters from rocks of low hydraulic conductivity will complement the hydrogeochemical studies already conducted at Äspö, and also provide a more realistic chemical input to near-field performance and safety assessment calculations, since deposition of spent fuel will be restricted to rock volumes of similar hydraulic character.

Objectives

The main objectives of the task are:

- to determine the origin and age of the matrix fluids;
- to establish whether present or past diffusion processes have influenced the composition of the matrix fluids, either by dilution or increased concentration;
- to derive a range of groundwater compositions as suitable input for near-field model calculations; and
- to establish the influence of fissures and small-scale fractures on fluid chemistry in the bedrock.

Rationale

Relevance to Repository Performance

Modelling near-field processes requires specific knowledge of the near-field input groundwater compositions. Hydrochemical data sets used in near-field calculations cover the range of compositions (fresh to saline) characteristic of the candidate site under investigation. So far groundwater sampling has been restricted to those water-bearing fracture zones of intermediate to high hydraulic conductivity. The groundwaters collected therefore tend to be more uniform in composition within these zones, probably obtaining their character mainly through rapid mixing and dilution rather than by chemical water/rock interaction.

The actual groundwater compositions likely to interact with the engineered barrier system of a repository will probably reflect more the matrix fluids characteristic of the low conductive bedrock volume selected to host the repository. Evidence to date indicates that such matrix fluids may be more saline than what is observed during the normal sampling campaign in a candidate site area. The engineered barrier system may not be particularly sensitive to high salinity, but there are limits set, and the expected near-field salinities need to be quantified.

International
Technical Document

ITD-00-09

Äspö Hard Rock Laboratory

Matrix Fluid Chemistry Experiment

Mineralogy, textural relations, fluid inclusion occurrences and basic petrology

Sten Lindblom

Stockholm University

June 2000

Summary

At the very low hydraulic conductivities (i.e. 10^{-14}–10^{-12} ms^{-1}) which characterise the matrix fluid experiment block, it is of special interest to study the fluid phases which least participate in the conductive flow in the rock. These fluids occur as fluid inclusions, i.e. trapped entities in minerals that have been shown to represent primary formation conditions of the minerals or subsequent alteration processes. As they often may have fairly high salinities as aqueous inclusions or contain gases like carbon dioxide, methane or nitrogen, their character may have a strong influence on the chemistry of any formation waters in the rock.

Fluid inclusions therefore form an important part of the Matrix Fluid Experiment.
This report is a summary of their distribution, morphology and chemistry, and their textural relationships with the matrix rock mass surrounding them. These data will form a base for the planned microthermometric and chemical studies. Furthermore, the study has led to the development of a new method of computer-interactive microscopy, briefly described, which may serve as a potential routine tool in some areas of mineralogy.

The investigations revealed that:

- Several textures indicate viable leakage of fluid inclusions during present and earlier stress regimes.
- Quartz varies between 14 and 29 vol.% in the drillhole, increasing as the Äspö diorite changes to Ävrö granite. There are three types of quartz: a) large irregular grains, b) small, equal-size grains in a heptagon mozaic, and c) vuggy quartz.
- Fluid inclusions in the quartz occur as: a) one-phase, b) two-phase vapor-liquid, c) two-phase gas-rich, and d) three-phase with a probable calcite daughter mineral.
- Several directions of fluid inclusion planes occur with distinct fluid inclusion populations.
- No oxygenated waters have influenced the rock mass studied.

Methods

The drillcore was corrected first, in relation to the borehole, for distance and alignment using the TV-imaging log (BIPS). Suitable samples were then selected and sawn for thin section preparation. Both double polished thick sections and ordinary thin polished sections were prepared. The former were investigated for mineralogy, textures and fluid inclusion content.

The double and single polished sections were studied using a Nikon Labophot microscope adapted for transparent and reflective microscopy. The double polished sections were scanned with a HP scanner using Photoshop 4 and TWAIN 32. Qualitative compositional analyses were made on a Phillips ESEM set up in a high vacuum mode. Finally, images have been treated with Corel Draw 6.

The double polished thick sections provide potentially useful information of minerals and textures that complement regular transparent light microscopy. However, during routine phase determinations it has always been a problem to view the complete section under the same configured microscope used for higher magnification studies. In this present study an attempt has been made to record images of the whole rock sections in different ways:

- The rock sections were photographed in daylight using a regular system camera and the colour prints subsequently scanned.
- The single polished thin sections were mounted in a special slide scanner and scanned. In contrast the double polished thick sections were mounted in an ordinary glass slide frame.
- The rock sections were scanned using a normal scanner for printed material in two ways: a) a special angled mirror, as used for scanning slides, was placed on top of the section and careful orientation assured an even spread of lighting over the section; scanning was carried out on the screened view of the double polished thick section only, and b) the sections were scanned without using the slide mirror; in this case it is important also to just screen off the double polished thick section.

The obtained scanned views were then printed using Photoshop 4. To facilitate comparison, the scanned section images from all sample locations have been positioned next to the BIPS image of the drillhole (see figures below). All double polished thick sections are between 32 and 37 mm in the images shown in this report.

Table A2-1: Modal mineralogical composition (volume %) of rock samples from MFE-drillcore KF0051A01 as derived by computer-based microscopy.

	Thick Sections					Thin Sections		
Sample	**MFE-5.03**	**MFE-6.43**	**MFE-8.84**	**MFE-9.11**	**MFE-9.85**	**MFE-5.03**	**MFE-9.11**	**MFE-10.90**
Lab-No.	1:2	3:1	6:1	7:1	8:1	5.03	9.11	10.90
Quartz	19	18	20	27	29	14	22	27
Microcline	4	4	17	18	22	7	25	24
Plagioclase	51	45	48	36	30	40	36	34
Biotite	16	21	6	10	7	18	7	8
Chlorite	+	+	+	+	+	4	1	1
Epidote	+	+	+	+	+	6	4	2
Sphene	5	3	2	-	5	5	2	1
Apatite	+	-	-	-	-	+	-	-
Opaques	2	4	2	2	4	3	2	2
Total	97	95	95	93	98	97	99	99

Notes:

1. It is easier to distinguish more types of dark phases in the ‘thin’ sections than in the ‘thick’ sections.
2. Quartz is probably hidden to some extent in the ‘thick’ sections.
3. Plagioclase and microcline are difficult to completely assess in the ‘thick’ sections. They often appear opaque from many solid inclusions.
4. The total sum in percent is somewhat low for the ‘thick’ sections due to difficulties to assign dark areas. Here one may have chlorite, biotite, epidote, plagioclase and microcline.

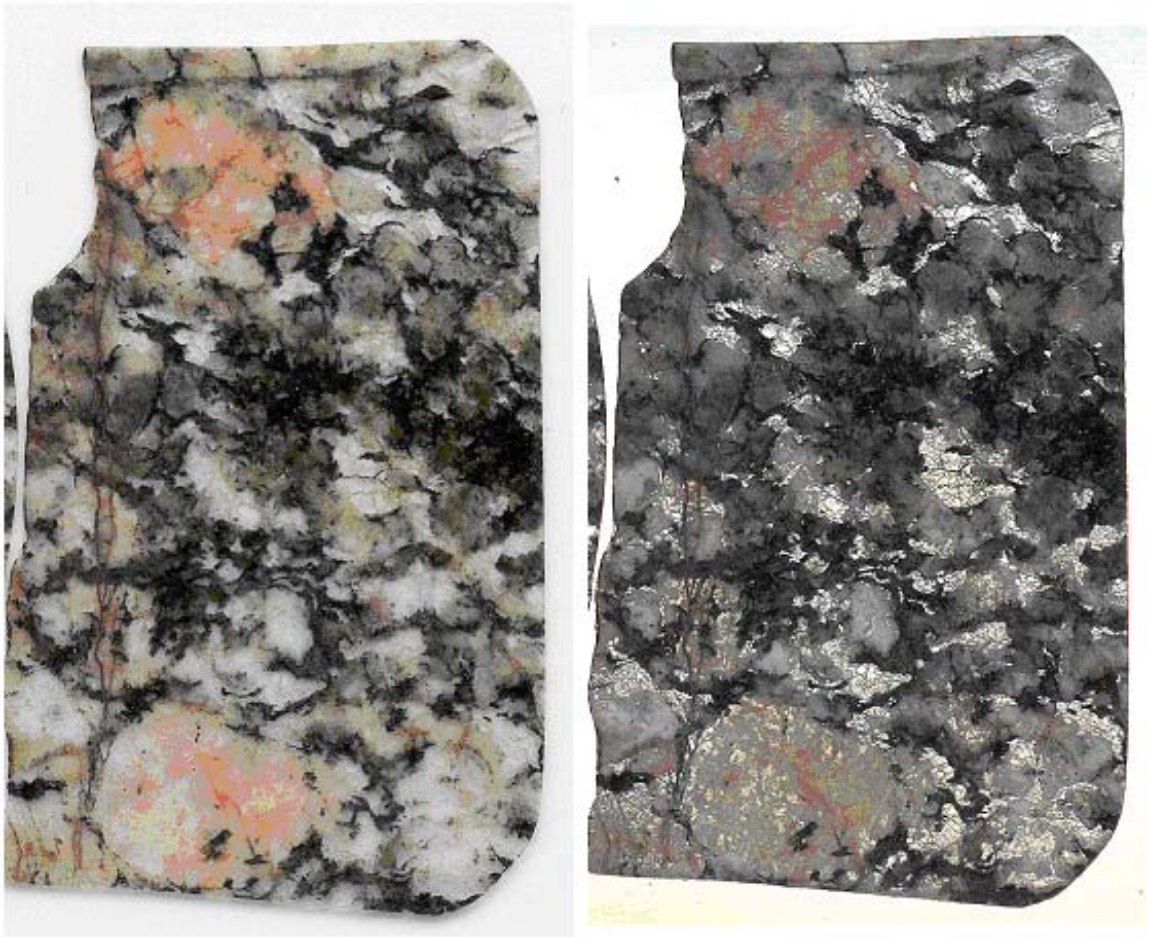

Figure A2-1: *Äspö diorite: Scanned thick section view from sample MFE-4.10. Scanning was performed without (right) and with (left) a slide mirror, the latter highlighting the quartz crystals (light grey colour; larger K-feldspars are orange-grey in colour).*

***Figure A2-2**: Ävrö granite: Scanned thick section views from sample MFE-10.90. Note the strong lineation visualised by biotite and chlorite streaks on the right side of the section. Quartz in the non-deformed part on the left occurs as equigranular grains with numerous fluid inclusions, while quartz in the strongly lineated part on the right is almost free of inclusions.*

Figure A2-3: *Äspö diorite: Comparison of scanned photo prints (above) and scanned thick sections (below). Right-hand sample: MFE-5.03; Left-hand sample: MFE-5.42.*

0.5 mm

Section 1:1

A. Euhedral quartz crystals protruding into calcite vein.

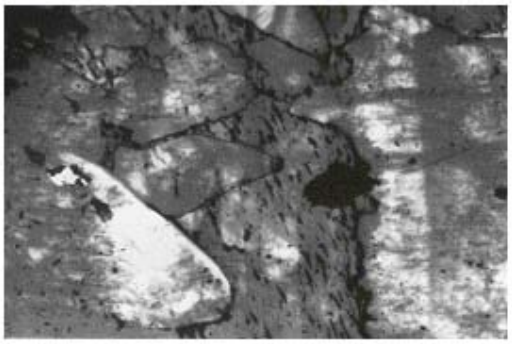

B. Slightly deformed calcite vein giving a rhombic twinning pattern.

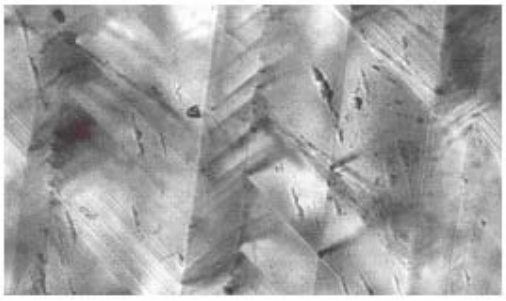

C. Twinned calcite surrounded by euhedral quartz.

D. Calcite in vein surrounded by feldspar crystals to the left and quartz crystals to the right.

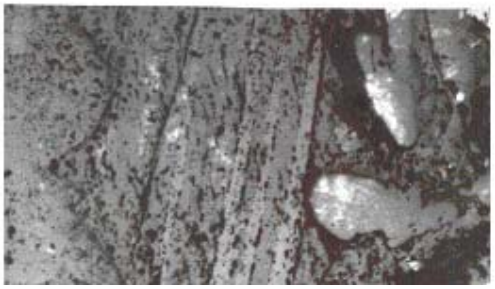

Figure A2-4: *Äspö diorite: Textural relationship between quartz and vein calcite. (Sample: MFE-5.42).*

A. Sketch of facetted feldspar crystals superseded by quartz. Dip of FIP is indicated by arrows.

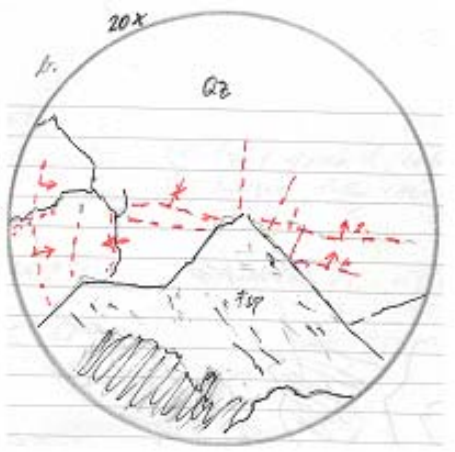

0.5 mm

B. Two parallel FIP:s are shown cut by a single FIP emanating from the plagioclase crystal face.

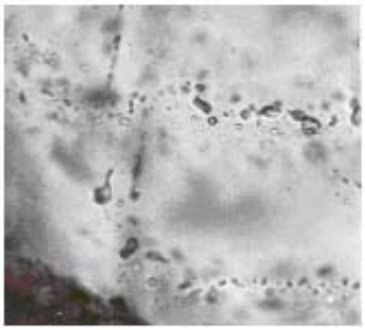

75 µm

C. Fluid inclusion occurrence in quartz. Enlargement shows mixture of one-phase and two-phase inclusions. The size of the large two-phase inclusion is 15µm long.

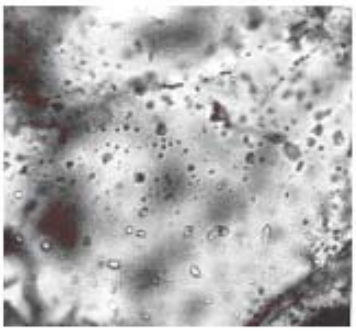

100 µm

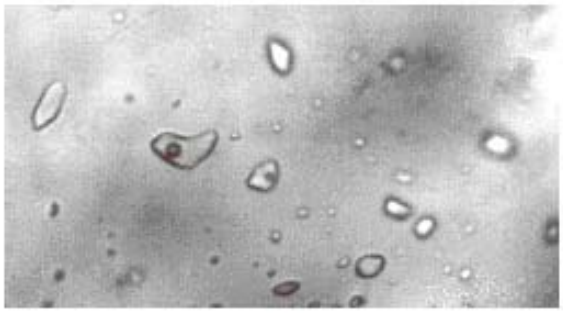

50 µm

Figure A2-5: *Äspö diorite: Fluid inclusion occurrences in quartz. (Sample MFE-5.03).*

Section 6:1

A. Euhedral plagioclase grain surrounded by later quartz. Sketch indicates FIP:s of different extension. Two stages of quartz may be discerned.

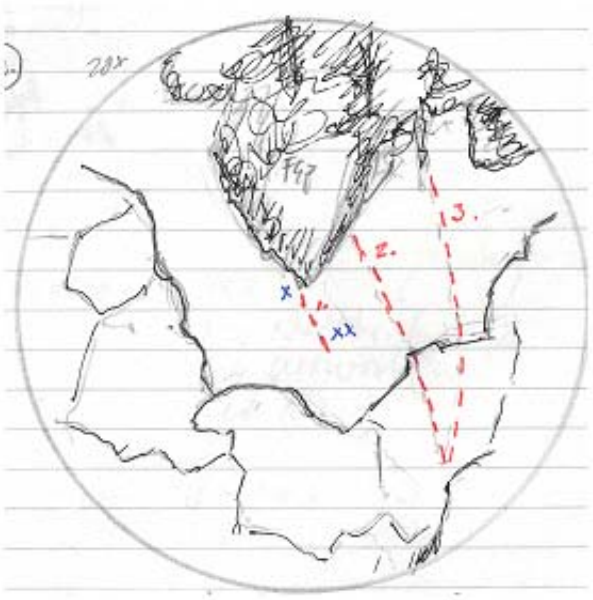

B. Parallel to zig-zag patterned fractures in the centre of quartz grain. A mixture of gas-rich and one-phase/two-phase inclusions occur.

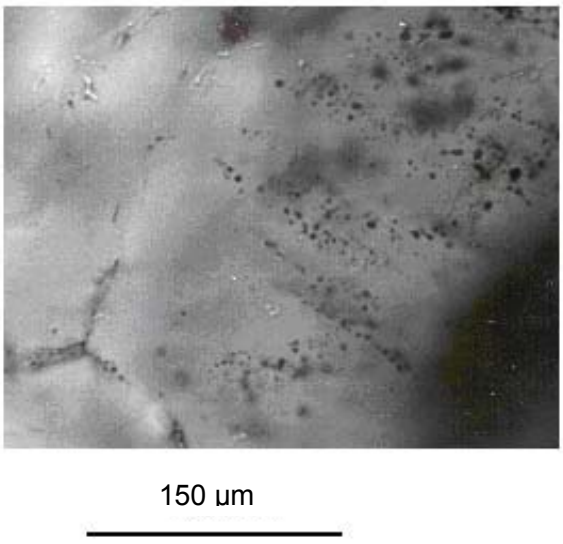

Figure A2-6: *Ävrö granite: Fluid inclusion occurrences in quartz. (Sample MFE-8.84).*

A. Star-shaped fluid inclusions indicating decrepitaion from overheating.
(Section 1:2, MFXSL-5.03)

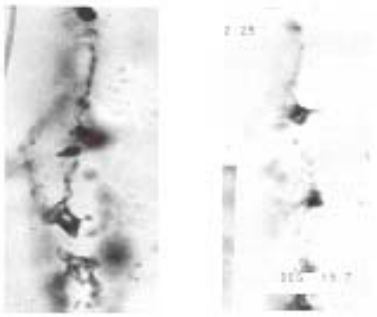

B. Open intragranular fracture, indicating minor shearing stress in quartz.
(Section 10:1, MFXSL-10.90)

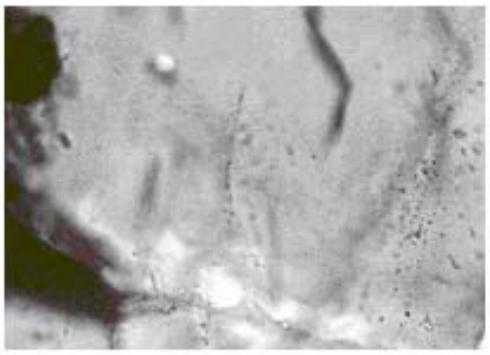

C. Open fractures in quartz induced by pressure between surrounding plagioclase grains.
(Section 10:2, MFXSL-10.90)

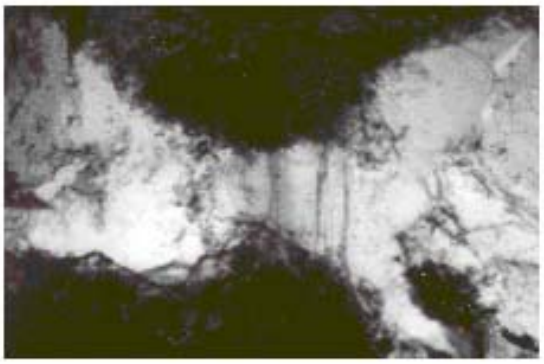

***Figure A2-7**: Microscopic evidence of small scale tectonic influences.*

A. Grain boundaries demarcating equant-shaped quartz crystals outlined by irregularly shaped fluid inclusions. (Section 2:1x, MFXSL-4.105)

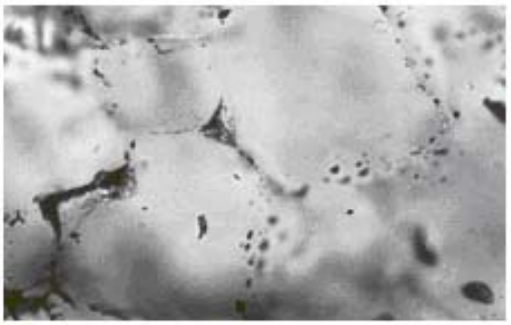

B. Grain boundaries in quartz shown on the polished surface where inclusions give 'etch'-like textures. (Section 4:1, MFXSL-7.81)

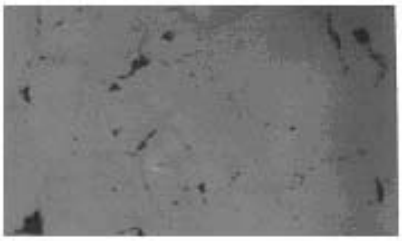

C. Same view but focused 20 µm below polished surface where fluid inclusions are seen to outline grain boundaries in quartz. (Section 4:1, MFXSL-7.81)

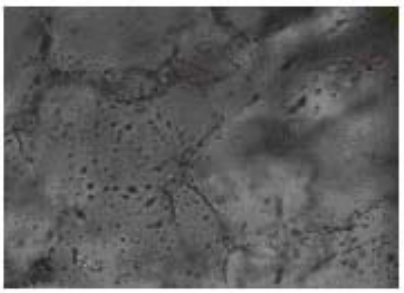

D. Flat-lying irregular fluid inclusions showing bottom of equant quartz grain. (Section 4:1 MFXSL-7.81)

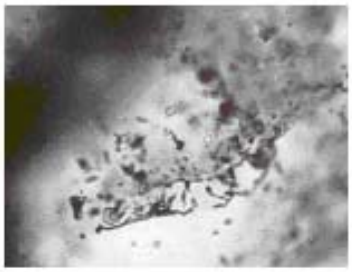

E. Similar 'bottom' inclusions. (Section 2:2, MFXSL-5.42)

Figure A2-8: *Grain boundary fluid inclusions.*

Section 1:2

A. Sketch of quartz containing gas-rich and 3-phase fluid inclusions in healed fracture planes.

500 µ

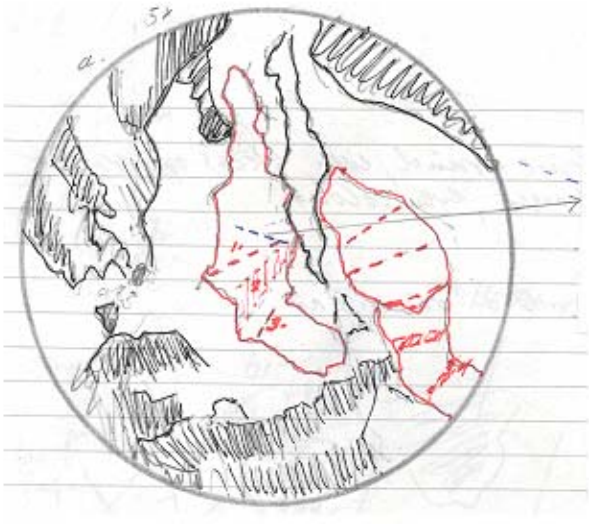

B. Gas-rich fluid inclusion

25 µm

C. 3-phase fluid inclusion containing an anisotropic daughter mineral. Several inclusions of the same type occur nearby with the same phase ratios.

25 µm

Figure A2-9: *Äspö diorite: 3-phase and gas-rich inclusions in quartz. (Sample MFE-5.03).*

Figure A2-10

BIPS image logs of the borehole walls. Scanned pictures with (lower scan) and without (upper scan) the slide mirror and representing thick, double polished sections, are indicated at the appropriate locations on the BIPS log. The red numbers represent corrected distances from the tunnel wall. Sample notations refer to the corrected values.

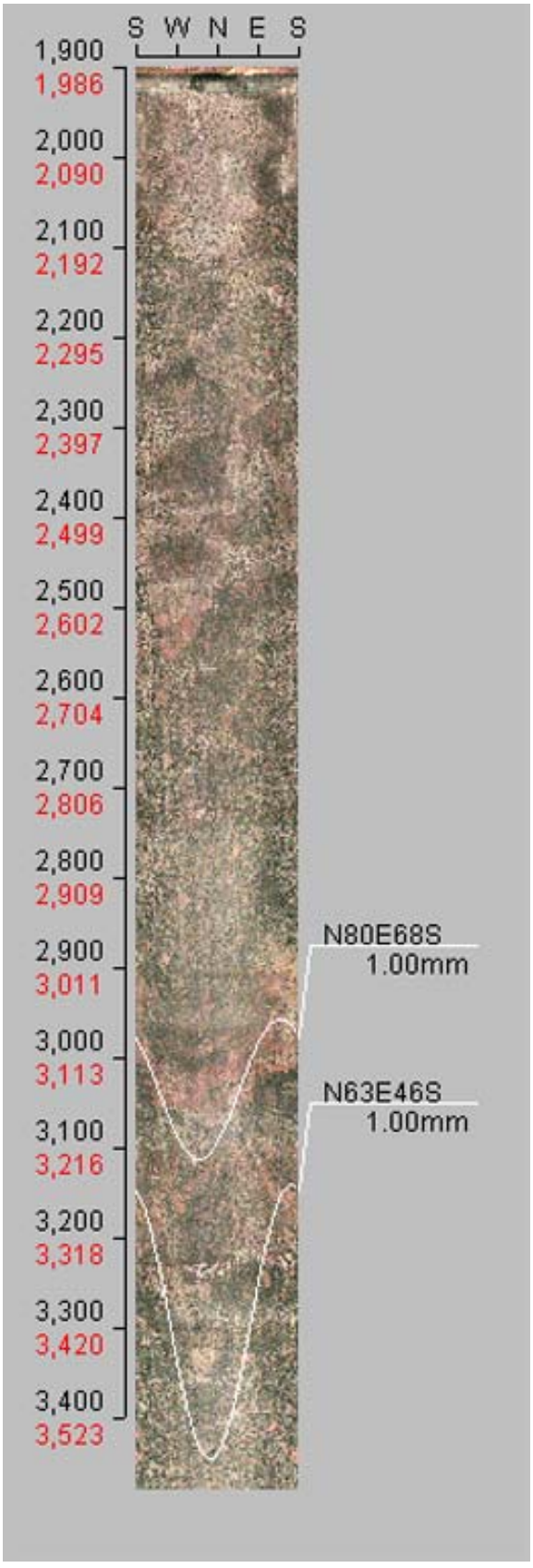
S W N E S
1,900
1,986
2,000
2,090
2,100
2,192
2,200
2,295
2,300
2,397
2,400
2,499
2,500
2,602
2,600
2,704
2,700
2,806
2,800
2,909
2,900
3,011
3,000
3,113
3,100
3,216
3,200
3,318
3,300
3,420
3,400
3,523
N80E68S
1.00mm
N63E46S
1.00mm

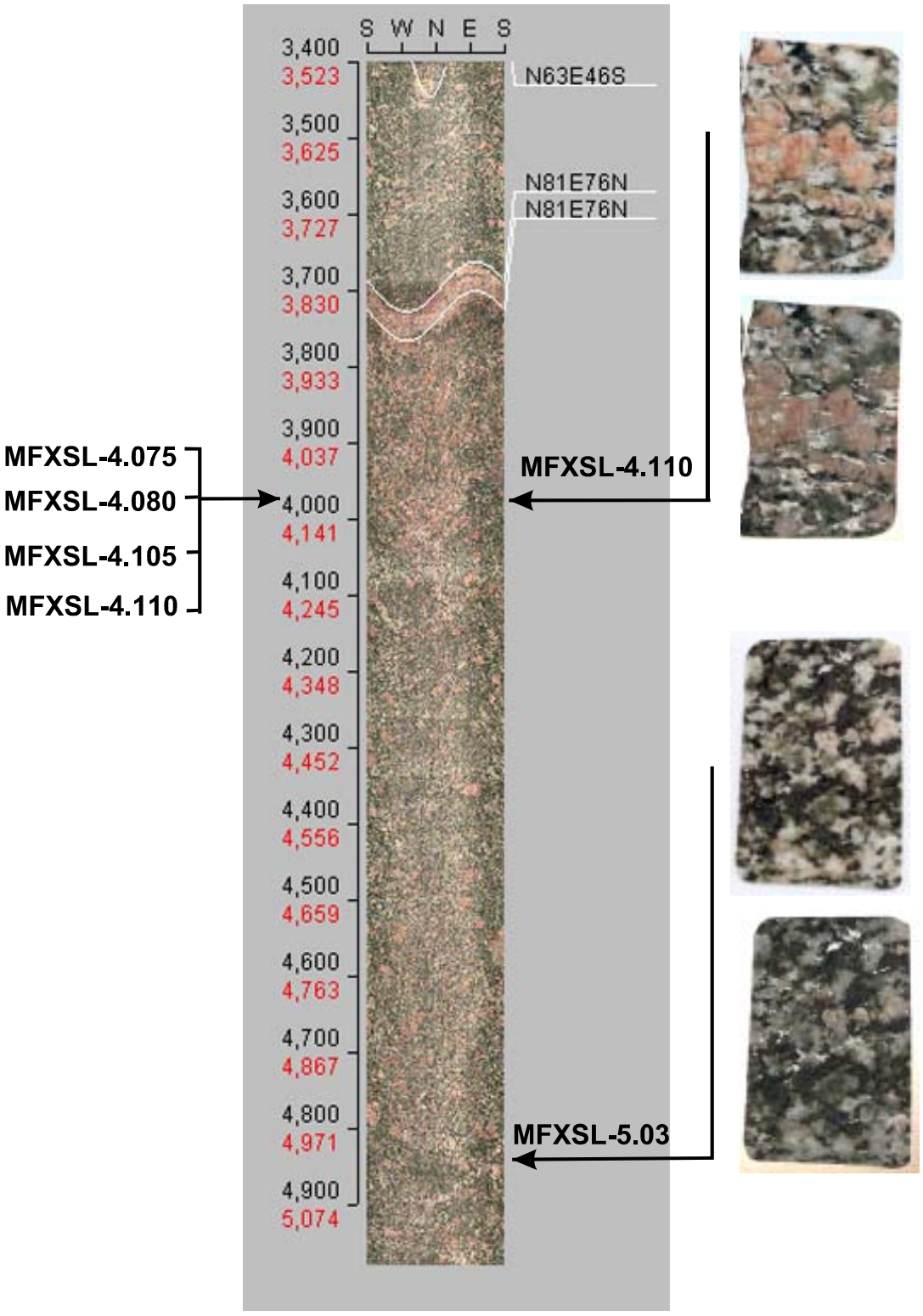
S W N E S
3,400
3,523
3,500
3,625
3,600
3,727
3,700
3,830
3,800
3,933
3,900
4,037
4,000
4,141
4,100
4,245
4,200
4,348
4,300
4,452
4,400
4,556
4,500
4,659
4,600
4,763
4,700
4,867
4,800
4,971
4,900
5,074
N63E46S
N81E76N
N81E76N
MFXSL-4.075
MFXSL-4.080
MFXSL-4.105
MFXSL-4.110
MFXSL-4.110
MFXSL-5.03

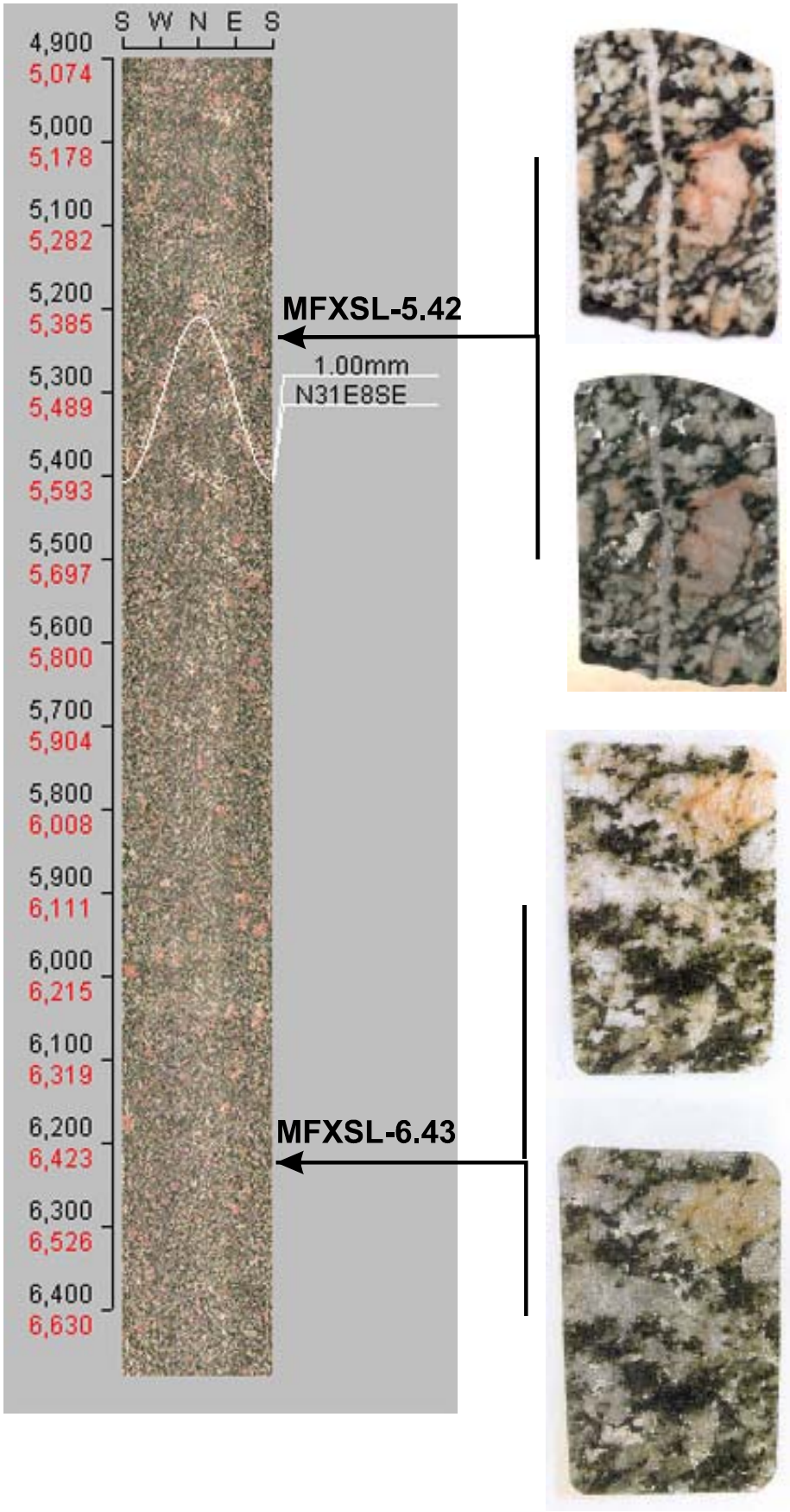
S W N E S
4,900
5,074
5,000
5,178
5,100
5,282
5,200
5,385
5,300
5,489
5,400
5,593
5,500
5,697
5,600
5,800
5,700
5,904
5,800
6,008
5,900
6,111
6,000
6,215
6,100
6,319
6,200
6,423
6,300
6,526
6,400
6,630
MFXSL-5.42
1.00mm
N31E8SE
MFXSL-6.43

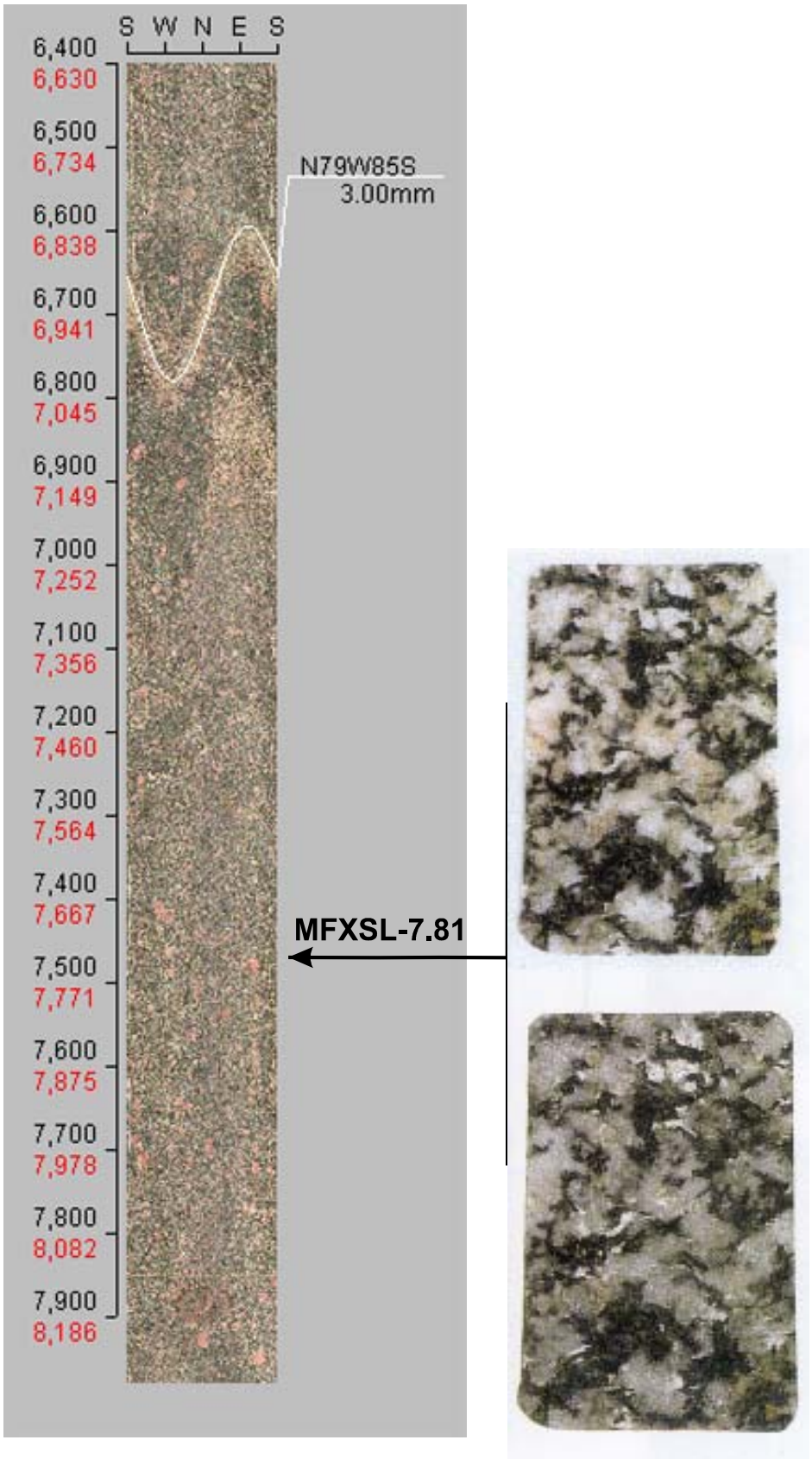
S W N E S
6,400
6,630
6,500
6,734
6,600
6,838
6,700
6,941
6,800
7,045
6,900
7,149
7,000
7,252
7,100
7,356
7,200
7,460
7,300
7,564
7,400
7,667
7,500
7,771
7,600
7,875
7,700
7,978
7,800
8,082
7,900
8,186
N79W85S
3.00mm
MFXSL-7.81

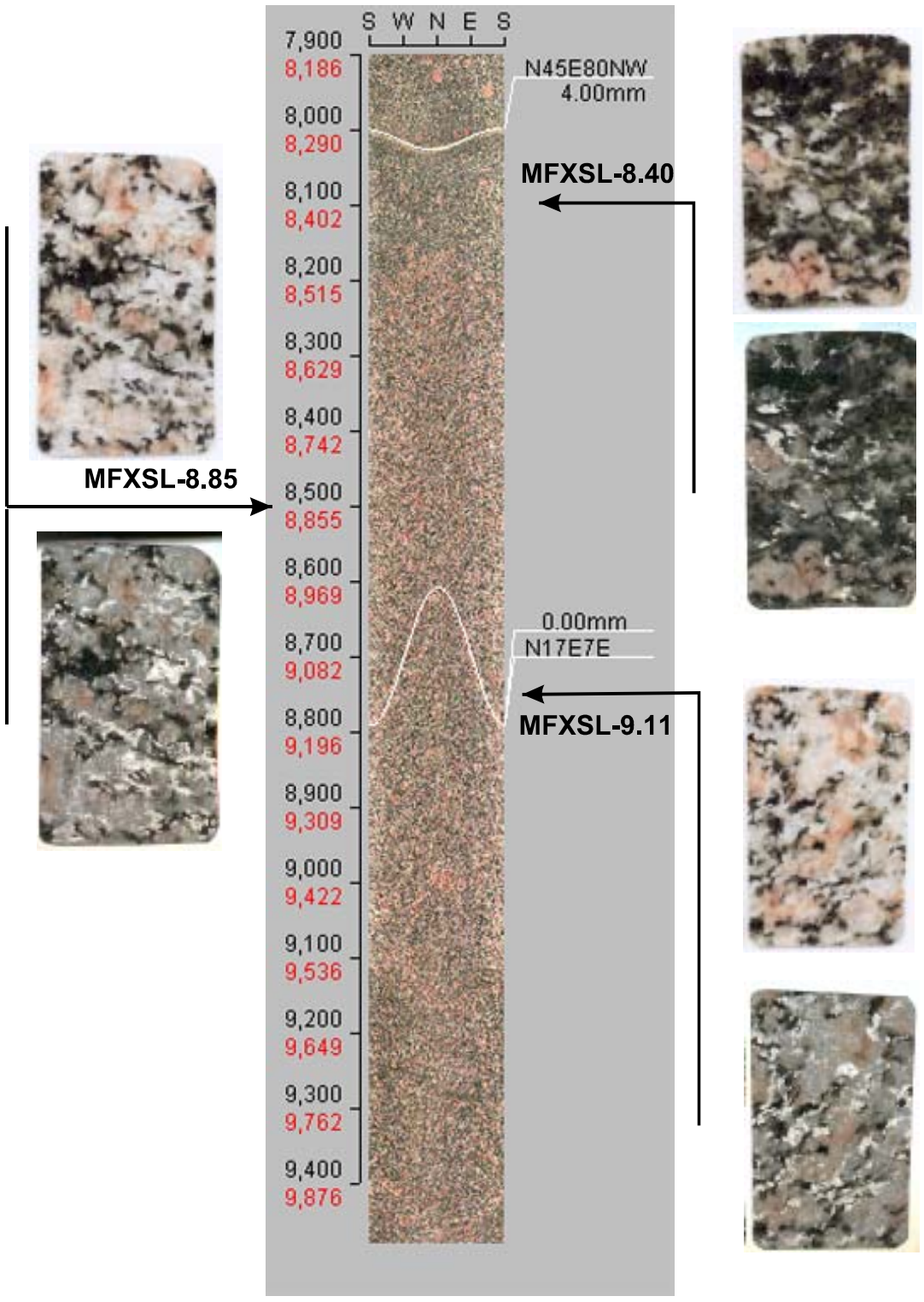
S W N E S
7,900
8,186
8,000
8,290
8,100
8,402
8,200
8,515
8,300
8,629
8,400
8,742
8,500
8,855
8,600
8,969
8,700
9,082
8,800
9,196
8,900
9,309
9,000
9,422
9,100
9,536
9,200
9,649
9,300
9,762
9,400
9,876
N45E80NW
4.00mm
MFXSL-8.40
MFXSL-8.85
0.00mm
N17E7E
MFXSL-9.11

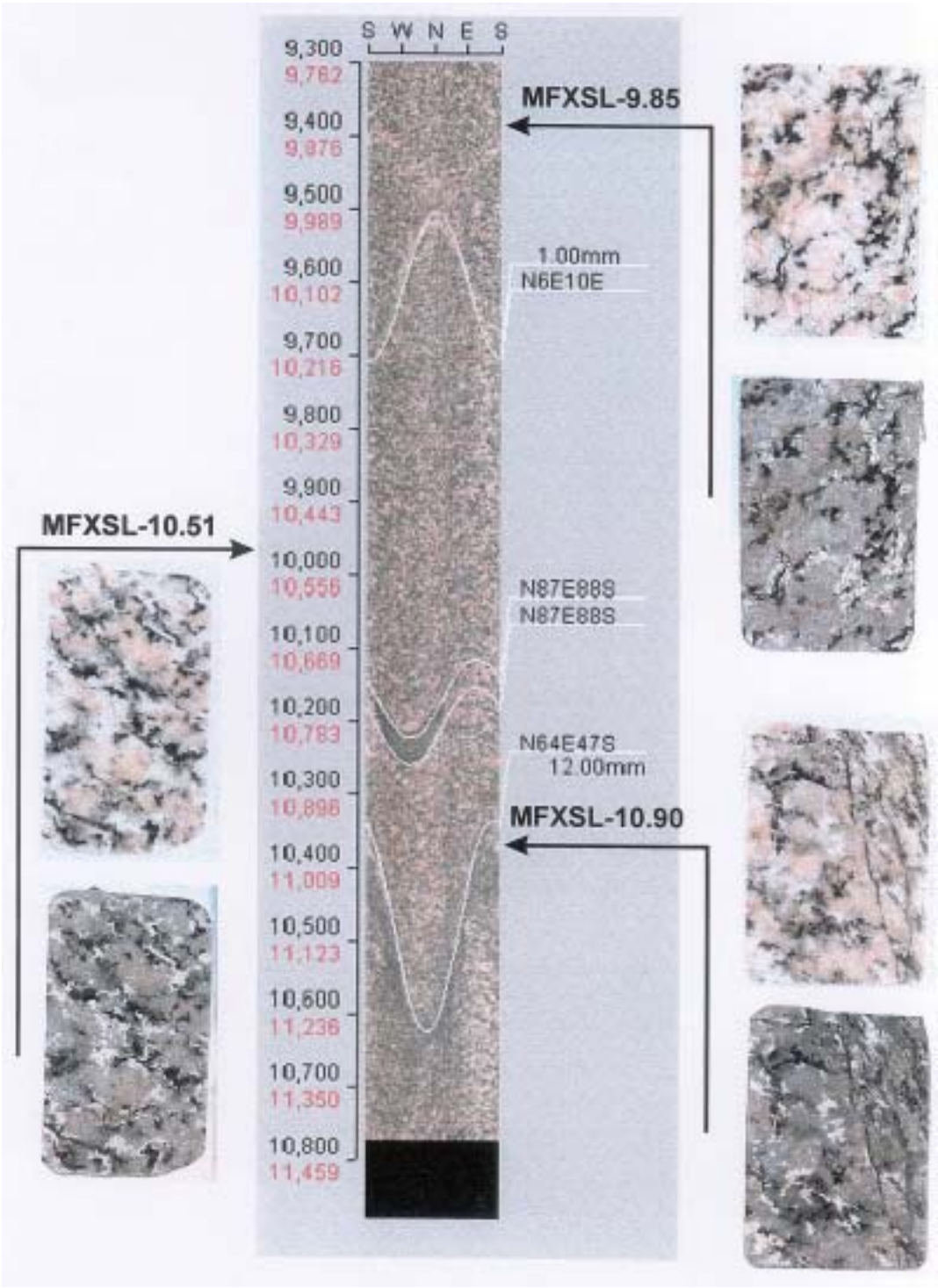
S W N E S
9,300
9,762
9,400
9,876
9,500
9,989
9,600
10,102
9,700
10,216
9,800
10,329
9,900
10,443
10,000
10,556
10,100
10,669
10,200
10,783
10,300
10,896
10,400
11,009
10,500
11,123
10,600
11,236
10,700
11,350
10,800
11,459
MFXSL-9.85
1.00mm
N6E10E
N87E88S
N87E88S
N64E47S
12.00mm
MFXSL-10.90
MFXSL-10.51

Technical Document

TD-00-13

Djupförvarsteknik

Groundwater chemistry data from the groundwater sampling of KF0051A01 within the Matrix Fluid Chemistry experiment

Christina Andersson
Anna Säfvestad

Svensk Kärnbränslehantering AB

April 2000

Summary

Groundwater sampled from the Äspö site has been collected from water-conducting fracture zones with hydraulic conductivities greater than K= 10^{-9} ms^{-1}. The chemistry of these groundwaters probably results from mixing along fairly rapid conductive flow paths, being mainly determined by the hydraulic gradient, rather than by chemical water-rock interaction. In contrast, little is known about groundwater compositions from low conductive parts (K< 10^{-10} ms^{-1}) of the bedrock (i.e. matrix fluids), which are determined mainly by the mineralogical composition of the rock and the result of water-rock reactions. As rock of low hydraulic activity constitutes the major volume of the bedrock mass in any granite body, matrix fluids are suspected to contribute significantly to the salinity of deep formation groundwaters. It is considered expedient therefore to sample and quantify such fluids and to understand their chemistry and origin.

From Section 4 of the MFE-borehole (borehole KF0051A01) 160 mL was collected for analysis on December 16th, 1999 (sample MFE-S4-1). The SICADA queries used when extracting data were:

ID Code: KF0051A01,
Start Date: 1999-12-16,
Project: Matrix Fluid Chemistry

Remarkable for the collected sample MFE-S4-1 is that the pH was low, only 6.7, and that the chloride content was lower than expected. The sample smelt of hydrogen sulphide and the bicarbonate content was high (about 170–200 mg/L). It was clear that sulphate reduction took place in the borehole section by the time sampling was carried out. This has resulted in a difference in sulphate concentration analysed with Ion Chromatography at Äspö compared to the SO_4-S expressed as S measured with ICP-AES at SGAB Analytica.

Methods

Water samples for Class 5 analysis (special arrangement) have been collected and analysed according to the 'Manual for Field Laboratory'. Only 160 mL of water were available for analysis so the analytical programme had to be revised. No tritium, ferrous iron or DOC could be analysed. There is no freeze stored back-up sample. Major ions, trace elements, $\delta^{37}Cl$, $\delta^{13}C/^{14}C$ and microbe analyses have been performed.

pH was measured directly after sampling with a portable pH-meter. The rest of the sample was collected under nitrogen atmosphere into an acid-washed (HNO_3) Erlenmeyer flask. Water for major components and trace element analysis was filtered through 0.45 um Millipore Filters at the Äspö HRL chemistry laboratory before the sample was exposed to oxygen. Water for microbe analysis was sent immediately to Gothenburg University.

Table A3-1 explains the different chemistry classes available for analysis and the analytical laboratories involved are given in Table A3-2. The chemical and isotopic data of the matrix water sample MFE-S4-1 are given in Table A3-3.

Table A3-1: SKB Analytical Chemistry Classes

Class no.	Description	Analyses	Optional
1	Simple sampling, basic control of water type	Electric conductivity pH Uranine*	
2	Simple sampling, control of water type	Electric conductivity pH, Cl, HCO_3, Uranine*	^{2}H, ^{3}H, ^{18}O Freeze stored back-up sample
3	Simple sampling, determination of non redox-sensitive major components	Electric conductivity, pH, Cl, HCO_3, SO_4, Br Uranine*, major cations** (except for Fe, Mn), SO_4 as Sulphur on ICP-AES	^{2}H, ^{3}H, ^{18}O Freeze stored back-up sample
4	Extensive sampling, complete chemical characterisation	Electric conductivity, pH Cl, HCO_3, SO_4, Br, Fe (total, ferrous), Uranine*, DOC, major cations** SO_4 as Sulphur on ICP-AES ^{2}H, ^{3}H, ^{18}O Freeze stored back-up sample, preserved and non-preserved	HS^-, NH_4
5	Extensive sampling, complete chemical characterisation including special analyses	Electric conductivity, pH Cl, HCO_3, SO_4, Br, Fe (total, ferrous), Uranine*, DOC, major cations** SO_4 as Sulphur on ICP-AES ^{2}H, ^{3}H, ^{18}O Freeze stored back-up sample, preserved and non-preserved	HS^-, NH_4 F, I NO_2, NO_3, PO_4 TOC ^{14}C-age, PMC, $\delta^{13}C$ per mill PDB U, Th (elements and/or isotopes) Other trace elements (INAA and/or ICP-MS) ^{226}Ra, ^{228}Ra, ^{222}Rn Or Your decision

* Only measured where uranine was used in the drilling procedure and as long as no extra uranine has been added to the borehole e.g. in tracer tests.
** Major cations are Na, K, Ca, Mg, Si, Fe, Mn, Li, Sr

Table A3-2: Laboratories used for analyses

Laboratory	Parameter (method)
Gothenburg University	Microbiology; Gases
Institutt for Energiteknikk (IFE), Norway	Oxygen-18, Deuterium
SGAB Analytica, Sweden	Major Cations (ICP-AES), trace elements (ICP-MS)
University of Waterloo, Canada	Cl-37
Ångströmslaboratoriet, Uppsala University, Sweden	C-isotopes
Äspö HRL, Sweden	pH, electric conductivity, Cl, HCO_3^-, SO_4^{2-}, Br-analyses, Uranine

Table A3-3: Chemical and isotopic data of water sample MFE-S4-1 from Section 4 of the MFE-borehole

MFE Borehole: Water Sample MFE-S4-1

Chemcial Composition

Temperature (°C)	
pH (field)	6.7
pH (lab)	8.1

	Analysis by IC
	mg / L
Na	2200
K	11.4
Mg	7.8
Ca	964
Fe_{tot}	0.24
Si	7.6
F	-
Cl	5160
Br	43.16
SO_4	26
Alkalinity as HCO_3	170-200

	Analysis by ICP-AES		
	µg / L		µg / L
Li	274	In	<0.02
B	1110	I	377
Al	27.7	Cs	0.685
P	<100	Ba	425
S	3240	La	1.29
Sc	0.099	Ce	0.89
V	1.08	Pr	0.067
Cr	7.27	Nd	0.38
Mn	890	Sm	<0.02
Co	0.207	Eu	<0.02
Ni	1.46	Gd	<0.02
Cu	<2.0	Tb	<0.02
Zn	<4.0	Dy	<0.02
As	2.75	Ho	<0.02
Rb	31	Er	<0.02
Sr	18600	Tm	<0.02
Y	0.198	Yb	<0.02
Mo	0.256	Tl	<0.02
Cd	<0.10	Th	<0.4
		U	0.103

Isotopes

^{3}H	(TU)	n.a.
$\delta^{18}O$	(‰ V-SMOW)	-11.6
$\delta^{2}H$	(‰ V-SMOW)	-87.9
^{14}C	(pmc)	n.a.
$\delta^{13}C$	(‰ PDB)	n.a.
$\delta^{37}Cl$	(‰ SMOC)	+0.61 / +0.59
$\delta^{11}Br$	(‰ EN-1)	n.a.
$\delta^{34}S_{SO4}$	(‰ CDT)	n.a.
$^{87}Sr / ^{86}Sr$		0.714561

International
Technical Document

ITD-00-17

Äspö Hard Rock Laboratory

Matrix Fluid Chemistry Experiment

Minutes of the Workshop held at SKB, Stockholm September 25-26, 2000

John Smellie

Conterra AB

October 2000

Agenda

Monday 25th.

Morning Session

10.00-10.10	Introduction *(P. Wikberg)*
10.10-11.00	Workshop: Purpose and objectives *(J. Smellie)*
11.00-11.20	General mineralogy of the drillcore *(J. Smellie)*
11.20-11.45	**Coffee**
11.45-12.45	Crush-leach experiments *(A. Blyth/S. Frape; N. Waber)*
12.45-13.00	Permeability experiment *(S. Frape)*
13.00-14.30	**Lunch**

Afternoon Session

14.30-16.00	Fluid inclusion studies *(S. Lindblom; S. Gehör)*
16.00-16.30	**Coffee**
16.30-17.30	Fluid inclusion studies *(N. Waber; A. Blyth)*

Tuesday 26th.

Morning Session

09.00-10.30	Rock porosity measurements *(E-L. Tullborg; N. Waber)*
10.30-11.00	**Coffee**
11.00-13.00	Hydrochemistry – matrix borehole and near-vicinity *(A. Säfvestad; M. Laaksoharju; N. Waber; S. Frape; B. Wallin; J. Casanova)*
13.00-14.00	**Lunch**

Afternoon Session

14.00-15.00	Hydraulic characterisation – matrix borehole and near-vicinity *(E. Gustafsson)*
15.00-16.00	Implications to radioactive waste disposal and repository performance assessment *(F. Karlsson; J. Smellie)*
16.00-16.30	Summing up and future plans *(J. Smellie)*

Purpose and Objectives

Rock Matrix

The matrix fluids are considered here to constitute the pore fluids in the rock matrix. However, the accessibility of these fluids, and their ability to move through the rock matrix, will depend on whether or not the pore spaces are interconnected.

Therefore, to interpret the origin of the matrix fluid, and how it moves through the rock, requires a thorough understanding of the rock mass.

This understanding requires detailed knowledge of:

- Mineralogy (e.g. fluid inclusions)
- Petrology (e.g. structural controls)
- Geochemistry (e.g. interstitial fluids)
- Petrophysics (e.g. porosity)
- Conductivity/transmissivity
- Present hydrogeochemistry
- Palaeohydrogeochemical events

Near-vicinity Environment

Assuming interconnected pore spaces, it is important to try and relate the matrix fluid (i.e. pore fluid) chemistry to the chemistry of the groundwaters present in nearby minor fracture zone(s) of low hydraulic transmissivity ($T= 10^{-12}$-10^{-9} m^2s^{-1}), since it will be these groundwaters that will come in contact eventually with the engineered barrier materials following repository closure.

These fracture zones, since they represent variations in transmissivity, may be characterised by different hydrochemical signatures. Is it possible to recognise a hydraulic 'cut-off' related to chemistry?

However, the hydrochemical signature may be influenced also by fracture orientation and geographical locations.

Consequently, the hydrochemical signatures may be the result of one or any combination of the following processes occurring within and close to the fracture zones:

- water/rock interaction during long residence times
- mixing of palaeowaters from past marine stages,
- mixing of palaeowaters from past glacial periods,
- mixing of modern groundwater components, and
- evolution of groundwater chemistry by out-diffusion of pore fluids from the rock matrix into fracture zones, or *vice versa*, in-diffusion of fracture waters to the matrix.

Hydrochemical/Hydraulic Database

To address these issues adequately, a reliable hydraulic and hydrochemical database is required. To build up such a database of fracture groundwater chemistry, related to hydraulic conductivity and at equivalent depths to the matrix fluid experiment, at least three sets of data are available:

- data from fractures present in the near-vicinity of the matrix fluid chemistry experiment borehole, i.e. from 'J' niche as part of the on-going CHEMLAB and Microbe experiments,
- data from the TRUE Block Scale Experiment programme, and
- data from the deposition holes (and their surroundings) resulting from the Prototype Repository Experiment.

Site-scale Context

The immediate groundwater environment of the Matrix Borehole needs to be put into the context of the Äspö site as a whole. Consequently the experimental site data are interpreted in the wider context of the Äspö site scale in terms of:

- Geology,
- Hydrogeology,
- Major and trace element chemistry,
- Mixing ratios, and
- Isotope geochemistry
  (e.g. ^{18}O, ^{2}H, ^{3}H, ^{37}Cl, ^{11}B, ^{86}Sr, ^{87}Sr etc.)

Synthesis

Monday 25th

Morning Session

The meeting was formally opened by ***Peter W.*** who briefly described the status of the various underground experiments being carried out at Äspö. This was followed by ***John S.*** who presented a detailed outline of the purpose and objectives of the Workshop (see Attachment 2).

Mineralogy and geochemistry of the drillcore

The general mineralogy and geochemistry of the matrix drillcore was described by ***John S.*** (see Attachment 3) and set in the context of the Äspö site as a whole. Of major interest is that within the drillcore length there is a transition (at approx. 8.4 - 8.5 m) between the Äspö diorite and the Ävrö granite. This allows the possibility of determining the influence of different physical and chemical rock properties on the matrix fluid chemistry.

Crush/leach experiments

Completed and on-going crush/leach experiments on the Äspö diorite drillcore material, being carried out at the Universities of Bern and Waterloo, were presented by ***Nick W.*** and ***Alec B.*** respectively (see Attachments 4 and 5). The studies largely confirm the high salinity of the rock fluids. Moreover there is the suggestion of a chemical gradient within the Äspö diorite towards the sampled borehole Section 4; this will be quantified. Further work will be carried out on the Ävrö core material since this is host to the presently accumulating matrix fluid in borehole Section 2.

In addition to the matrix drillcore experiments, three additional core sections representing respectively more and less mafic rock types were selected from other Äspö core material and studies have commenced at Waterloo. This is to further determine the influence of lithology on matrix fluid composition with specific emphasis on isotopic signatures. It is hoped that this may be helpful to interpret some of the matrix fluid isotopic data.

Permeability experiment

Shaun F. provided an up-date on the status of the permeability experiment (see Attachment 6). For some time no movement of matrix fluid through the core had been observed, however there has been a significant loss of distilled water from above the core. The water is not believed to be escaping from the highly pressurised sealed unit, but may suggest the filling of empty pore space in the rock; alternative reasons are being investigated. Since the Workshop a minute amount (drop) of fluid has emerged from the underside of the core and attempts are being made to collect this for analysis.

Afternoon Session

Fluid inclusions studies

Presentations were made from each of the four groups involved in the fluid inclusion studies – ***Sten L.*** (Univ. Stockholm), ***Seppo G.*** (Kivitieto), ***Nick W.*** (Univ. Bern) and ***Alec B.*** (Univ. Waterloo). Sten L's talk was based on his recent ITD Report (ITD-00-04) with some additional data on quartz grain sizes and fluid inclusion volume calculations (see Attachment 7). For the other presentations see Attachments 8, 9 and 10.

The fluid inclusions are mainly associated with the coarse-grained primary magmatic quartz and the later fine-grained recrystallised variety. They show a diverse distribution where grain boundary inclusions and fracture bound inclusions dominate. Multi-phase liquid, solid and gas fluid inclusion types are commonly associated with the primary quartz and mostly liquid and gas phase types with the recrystallised quartz. Preliminary microthermometric studies show that the fluid inclusions identified in both quartz types mostly represent highly saline populations. Salinity ranges from 8.2-20.9 wt% $NaCl_{eq}$ in the coarse types and from 4.3-10.8 wt% $NaCl_{eq}$ in the recrystallised types. In addition, several other fluid inclusion types containing non-fluorescent gas-rich inclusions (CO_2 or CH_4) have also been revealed; these may even dominate the grain boundary inclusion populations.

Tuesday 26th

Morning Session

Rock porosity measurements

Eva-Lena T. introduced this issue by trying to achieve a consensus of opinion relating to the definition, measurement and interpretation of total and interconnected porosity (see Attachment 11). These points were also touched on by ***Nick W.*** based on the Swiss experience of the Opalinus Clay Formation studied at Mont Terri. There was general agreement with the proposed nomenclature provided that the type of porosity being investigated was clearly defined beforehand, e.g. advective and/or diffusive porosity.

Examples of micro-fractures/fissures were shown from both the Äspö diorite and Ävrö granite rock types; whilst some showed a clear degree of interconnection, most were discontinuous.

Ivars N. presented the background and theory to determine rock matrix diffusion by *in situ* downhole electrical conductivity measurements (see Appendix 12). The potential usefulness of the Matrix fluid Chemistry Experiment to provide parameters to aid interpretation (e.g. rock porosity; matrix fluid chemistry etc.) was discussed.

Hydrochemistry – matrix borehole and vicinity

John S. provided the background objectives and scope of this study showing the potential hydrochemical relationship between very low (i.e. matrix), low and higher transmissive features, the latter data being derived from the TRUE Block Scale, Prototype Repository and Chemlab/Microbe ('J' Niche) experiments (see Attachment 12). He also emphasised the high quality and representativness of the sampling and analyses of the Prototype Repository groundwater samples used in the database (see Attachment 13).

Marcus L. discussed the composition of the matrix fluid in relation to the other experimental groundwater data and to the hydrochemical evolution of the Äspö site as a whole (see Attachment 14). The groundwater data were then correlated to the transmissivity of the fractures sampled To date the general conclusion from these studies is that over the range of hydraulic conductivity represented by the sampled fractures, most show little obvious correlation with groundwater chemistry. The data indicate an influx of a modern groundwater component, such as Baltic Sea and meteoric precipitation waters, associated with the hydraulic drawdown caused by tunnel construction, to the detriment of older saline and glacial melt water components which have been diluted or removed. This has been particularly apparent with the Prototype samples, despite the generally low transmissive character of the sampling locations, probably due to their near-vicinity to the excavated tunnel opening. Drawdown effects are less evident from the 'J' Niche and TRUE Block Scale sites most likely due to the sampling locations being further from the excavated tunnel walls.

The 'matrix' sample, whilst reflecting a generally similar major ion character to nearby fracture compositions (with the exception of SO_4 and Mg), exhibits anomalous chlorine isotope (***Shaun F***) and strontium isotope (***Bill W***.; see Attachment 15) signatures and higher contents of most trace elements which may be more characteristic of a 'true' matrix component. These isotopic signatures were also discussed in the broader context of the Äspö groundwater evolution as a whole.

Afternoon Session

Hydraulic characterisation

Erik G. provided an overview of the hydraulic characterisation of the matrix borehole and immediate surroundings (i.e. 'block scale'), and extending this to 'site scale' to include the data from the TRUE Block Scale, Prototype Repository and Chemlab/Microbe ('J' Niche) experiments (see Attachment 16).

The calculated hydraulic conductivity of $1 \cdot 10^{-14}$-$6 \cdot 10^{-14}$ ms^{-1} representing the matrix rock block is judged reasonable and in accordance with the earlier predictions. This was then related to the measured total and interconnected porosity measurements and to the presence of low transmissive microfractures/fissures to achieve an idea of the sphere of fluid movement through the rock which has contributed to the matrix groundwater sample

collected from borehole Section 4. The origin and movement of fluid in the matrix block was then extended in scale to include hydraulic (and hydrochemical) data from the other experimental sites. No obvious correlation between transmissivity and groundwater chemistry was indicated, but interestingly earth tidal effects have been measured from the Prototype Repository experiment which indicates a daily 'pumping' mechanism which probably contributes to groundwater mixing on a scale commensurate with the transmissivity of the fracture zones. As would be expected, no such effects have been measured from the matrix borehole.

The present status of the matrix borehole was also described. Matrix fluid pressure is continuing to increase in borehole Sections 2 and 4, demarcated for matrix fluid sampling. Section 4 is refilling after being sampled in December 1999 and Section 2 is still slowly filling for the first time. Both sections will be sampled when adequate water is judged to have accumulated.

Repository performance assessment implications

In the context of deep geological disposal of high-level radioactive wastes, to model near-field repository processes requires specific knowledge of the near-field input groundwater compositions expected during the lifespan of the repository. Therefore, knowledge of the composition and origin of the matrix fluid should provide a more realistic hydrochemical input to near-field performance and safety assessment calculations, since deposition of spent fuel will be restricted to rock volumes of low transmissivity. Evidence from other crystalline rock studies, for example in Canada, point to highly saline matrix fluid compositions which may be detrimental to the engineered barrier system.

John S. introduced this topic on a negative note quoting a recent SKB PA-related discussion on the influence of groundwater chemistry on the engineered barrier system which concluded that in terms of the human dose risk factor, groundwater flow rather than chemistry was the important parameter. Groundwater chemistry may influence to a degree canister corrosion, bentonite stability and radionuclide up-take and mobility etc., but these effects are less critical when compared to solute transport by flow. This statement was partly countered by ***Fred K.*** who pointed out that whilst the bentonite and the canister would probably remain stable in a highly saline groundwater environment, at least to a limit of 100 g/L TDS, the mixed bentonite/sand backfill material considered for the access tunnels etc. could very well deteriorate significantly and this is a issue of concern. The matrix fluid experiment could therefore provide important information that may influence the ultimate composition of this backfill material.

Miscellaneous presentations

Joël C. presented groundwater boron, strontium and oxygen isotopic data from several sites in the Fennoscandian Shield including those from Äspö to help constrain the various hypotheses on the nature of water/rock interaction and the end-members participating in mixing processes, i.e. to establish a possible origin to the highly saline waters and brines. He also pointed out the possibility of using ^{11}B as an indicator of permafrost conditions, as it appears to become isotopically enriched in the fluid phase during freeze-out conditions. The importance of the matrix fluid experiment would be to establish the extreme boron end-member which may facilitate interpretation of groundwater evolution at Äspö.

Andreas G. briefly described the Swiss experience from the Mont Terri Project which involves a study of a reconnaissance tunnel in the Opalinus Clay Formation in northern Switzerland. Despite the obvious difference in rock-type, he pointed out that the investigative methodology (e.g. pore water characterisation and diffusion processes) may be of importance since the transmissivity of the clay is similar to that of the Äspö matrix rock (~ 10^{-14} m^2/s). In particular, the use of the noble gases, especially helium, and chlorine-37, has shown these to be sensitive geochemical tracers for studying groundwater movement and residence times. He recommended that this approach could be focussed on a suitably drilled borehole at the Äspö site.

Discussion and Decisions

Following some discussion, the following decisions were taken:

- continuation of drillcore crush/leach experiments with specific emphasis on lithological variation and porosity profiles;
- continuation of the permeability test;
- continuation of fluid inclusion mineralogical/petrographical characterisation and chemistry;
- expand coverage of drillcore porosity measurements (some integrated with the crush/leach experiments) to achieve a better idea of large-scale heterogeneity or homogeneity in the matrix block, and also to further characterise the Ävrö granite rock type;
- detailed study of 1-2 micro-fractures/fissures with respect to in- or out-diffusion processes. This will include measurements of the U-decay series, ^{37}Cl, ^{11}B, ^{86}Sr and ^{87}Sr along rock profiles perpendicular to the fracture intersection with the drillcore;
- simple leaching of drillcore material using distilled water;
- scoping study to locate further examples of low transmissive features already characterised to increase the hydrogeological/hydrochemical database;
- eventual sampling of borehole Section 2 (and possibly a second sampling of Section 4) when indications show that enough water has accumulated; and
- coordinate with the future Äspö drilling programme to locate a suitable sampling site to measure in- and out-diffusion profiles on drillcore material using helium and chlorine-37.

Attachments

Attachment 1:	Agenda
Attachment 2:	Matrix Fluid Workshop: Main objectives and purpose (John Smellie, Conterra AB).
Attachment 3:	Matrix drillcore: General mineralogy and geochemistry (John Smellie, Conterra AB).
Attachment 4:	Status of crush/leach experiments (Nick Waber, Univ. Bern).
Attachment 5:	Status of crush/leach experiments (Alec Blyth, Univ. Waterloo).
Attachment 6:	Status of permeability test (Shaun Frape, Univ. Waterloo).
Attachment 7:	Fluid inclusion studies (Sten Lindblom, Univ. Stockholm)
Attachment 8:	Fluid inclusion studies (Seppo Gehör, Kivitieto, Oulu).
Attachment 9:	Fluid inclusion studies (Nick Waber, Univ. Bern)
Attachment 10:	Fluid inclusion studies (Alec Blyth, Univ. Waterloo).
Attachment 11:	Porosity measurements (Eva-Lena Tullborg, Terralogica AB).
Attachment 12:	Background to hydrochemical and hydrogeological database studies (John Smellie, Conterra AB).
Attachment 13:	Prototype Repository Experiment groundwaters: Quality assurance (Anna Säfvestad, SKB).
Attachment 14:	Hydrochemistry – Regional setting and PCA evaluation (Marcus Laaksoharju, GeoPoint AB).
Attachment 15:	Hydrochemistry – Strontium isotope systematics (Bill Wallin, Geokema AB).
Attachment 16:	Hydraulic characterisation (Erik Gustafsson, Geosigma AB).

International Progress Report

IPR-00-35

Äspö Hard Rock Laboratory

Status Report of the Matrix Fluid Experiment June 1998 - June 2000

Compiled and edited by:
John Smellie

Conterra AB

December 2000

Report Contents

Summary

Much of the undisturbed groundwaters sampled from the Äspö site, mostly to depths of 500-600 m, have been collected from water-conducting fracture zones with high transmissivities ($T > 10^{-9}$ m^2s^{-1}) and probably attain their chemical character mostly by mixing waters of different origin. These groundwater compositions have been compiled, evaluated and interpreted to explain the hydrochemical character of the site. In contrast, little is known about groundwater compositions from low transmissive parts ($T < 10^{-10}$ m^2s^{-1}) of the bedrock. Under such conditions long residence times are characteristic and the composition of the formation waters is more dependent on water-rock reactions than mixing, and also more likely influenced to varying degrees by the rock matrix fluid chemistry. Matrix fluids are considered here to constitute the pore fluids in the rock matrix. However the accessibility of these fluids, and their ability to move through the rock matrix, will depend on whether or not the pore spaces are connected. Assuming a rock fabric of interconnected pores and fine fissures, and bearing in mind that rocks of low transmissivity constitute the major volume of the bedrock mass in any granite body, matrix fluids are suspected to contribute significantly to the chemistry of deep formation groundwaters.

In the context of deep geological disposal of high-level radioactive wastes, to model near-field repository processes requires specific knowledge of the near-field input groundwater compositions expected during the lifespan of the repository. Therefore, knowledge of the composition and origin of the matrix fluid should provide a more realistic hydrochemical input to near-field performance and safety assessment calculations, since deposition of spent fuel will be restricted to rock volumes of low transmissivity.

To address these issues, the main objectives of the Matrix Fluid Experiment are:

- to determine the origin and age of the matrix fluids;
- to establish whether present or past in- or out-diffusion processes have influenced the composition of the matrix fluids, either by dilution or increased concentration;
- to derive a range of groundwater compositions as suitable input for near-field model calculations; and
- to establish the influence of fissures and small-scale fractures (when present) on fluid chemistry in the bedrock.

This report describes and interprets the results so far available, and represents the halfway stage of the Matrix Fluid Experiment scheduled to continue to the end of 2001.

Future Activities

The following activities planned for the immediate future will include:

- continuation of drillcore crush/leach experiments with specific emphasis on lithological variation and porosity profiles;
- continuation of the permeability test;
- continuation of fluid inclusion mineralogical/petrographical charaterisation and chemistry;
- expand coverage of drillcore porosity measurements (some integrated with the crush/leach experiments) to achieve a better idea of large-scale heterogeneity or homogeneity in the matrix block, and also to further characterise the Ävrö granite rock type;
- detailed study of 1-2 micro-fractures/fissures with respect to in- or out-diffusion processes. This will include whole-rock measurements of the U-decay series, ^{37}Cl, ^{11}B, ^{86}Sr and ^{87}Sr along profiles perpendicular to the fracture intersection with the drillcore,
- simple leaching of drillcore material using distilled water;
- scoping study to locate further examples of low transmissive features already characterised to increase the hydrogeological/hydrochemical database; and
- eventual sampling of borehole Section 2 (and possibly a second sampling of Section 4) when indications show that enough water has accumulated.

Figure A5-1: *MFE-borehole KF0051A01: Extracted drillcore showing sections (taped) removed for investigation.*

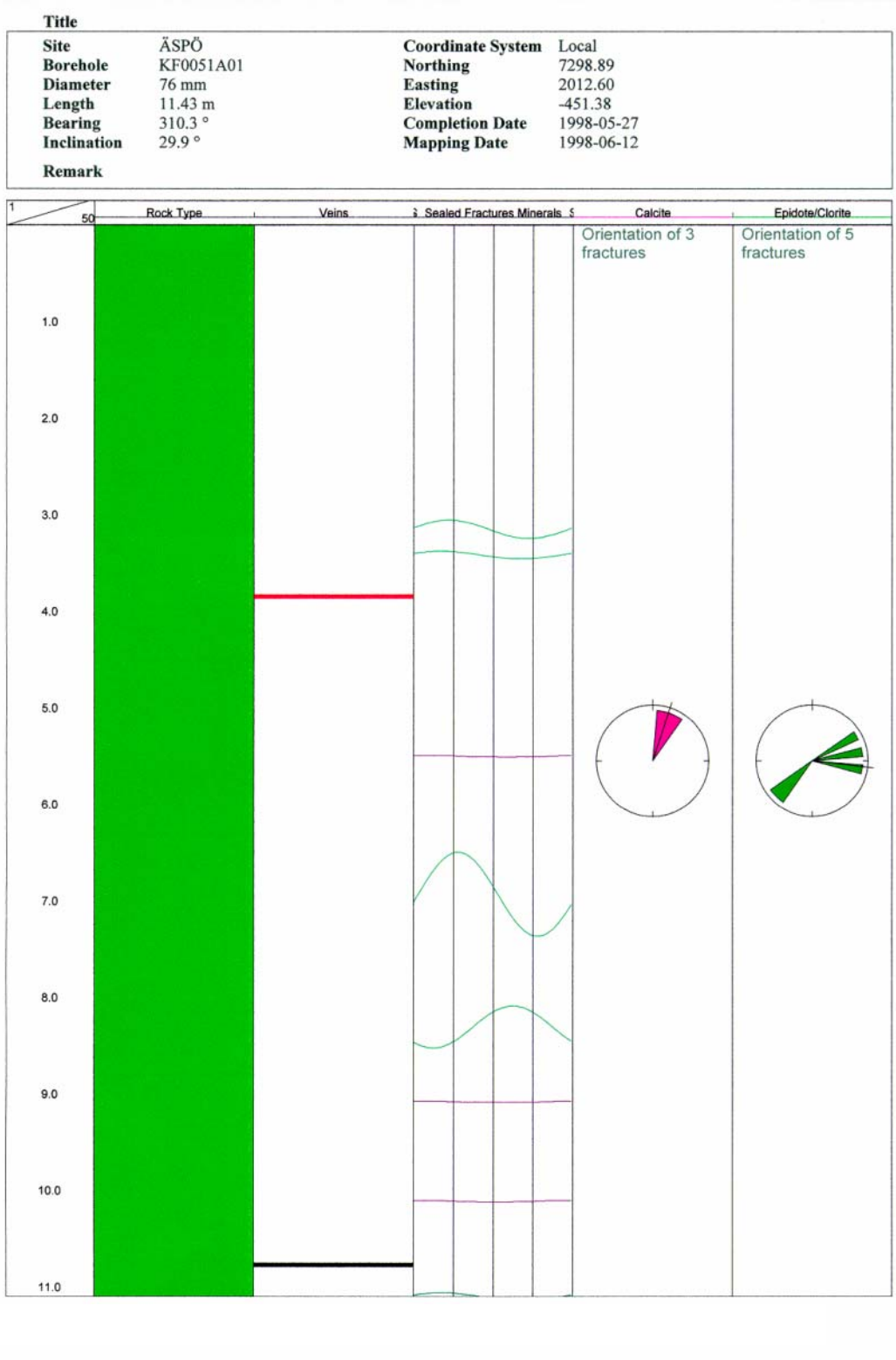

Figure A5-2: *MFE-borehole KF0051A01: Geological log.*

International
Technical Document

ITD-01-03

Äspö Hard Rock Laboratory

Matrix Fluid Chemistry Experiment

Porosity and density measurements on samples from drillcore KF0051A01

Eva-Lena Tullborg

Terralogica AB

May 2001

Summary

The Matrix Fluid Chemistry Experiment (MFE) at the Äspö Hard Rock Laboratory (HRL) was carried out within a rock block with very low hydraulic permeability and low fracture frequency and aimed at studying the chemistry of matrix fluids hosted in such an environment. For this reason the connected pore system was focussed.

The total pore space in a crystalline rock is the sum of microfractures, intragranular pores and fluid inclusions. The total porosity can be divided into connected and non-connected porosity and the separation between these two is not only due different measuring methods, but also reflects the sample size and shape. Within the MFE-project water saturation measured on 5 cm long core pieces to calculate the total porosity has been carried out by first determining the connected porosity and then the bulk and compact density on the same samples. Previous studies using different impregnation techniques had indicated that the connected porosity (e.g. effective porosity for diffusion) is heterogeneously distributed. As a complement, therefore, ink has been used for impregnation purposes to recognise pores and microfractures.

The MFE-drillcore (KF0051A01) consists of Äspö diorite from 0-8.5m and Ävrö granite from 8.5 m to the end of the borehole at 11.8 m. Connected porosity (water saturation) measurements were carried out on 9 samples showing values in the range 0.25-0.36 vol.% for Äspö diorite and 0.3 to 0.41 vol.% for Ävrö granite. Total porosity calculated from bulk and compact density measurements showed values in the range of 0.56-0.72 vol.% and 0.74-0.81 vol.% for Äspö diorite and Ävrö granite respectively. Microscopy of the impregnated samples indicated that most of the porosity (and especially the connected porosity) comprises microfractures. The Äspö diorite, with more penetrative foliation than the Ävrö granite, showed even stronger orientation of the microfractures parallel to the foliation.

Methods

Although the drillcore had been sealed and preserved erroneously with beeswax immediately after the drilling, it has allowed nevertheless the possibility to study connected porosity in different directions. Porosity measurements were carried out in a sequence (Fig. A6-1-1), comprising water saturation measurements of 5 cm long core pieces with cylinder surfaces still covered with beeswax and only the perpendicular saw cuts exposed to the water. Subsequently, the outermost 3-6 mm was cut clean (sawed) and water saturation (and density) measurements were carried out a second time. Finally, seven of the samples were ground down to very fine powders and the compact density (grain density) of the powders was measured.

Measurements of connected physical porosity presently were carried out at the Swedish National Testing and Research Institute, Stockholm. The samples (5 cm pieces of drillcore) were first dried at 110 ^{o}C until a constant weight was reached (minimum 24 h), then they were stored at room temperature under controlled conditions for 24 hours and a dry weight was measured. The sample was then water saturated until stable conditions were achieved after which the sample was reweighed. Following this, the samples were dried a second time and a new dry weight determined.

Compact density (grain density) measurements were carried out on fine ground rock samples and the sample volume measured by use of He-pycnometry. Together with the sample weight this gives the compact density.

Two samples, one Äspö diorite and one Ävrö granite sample were used for a test of simple impregnation using ink. Three different cuts were used (parallel with foliation, parallel with core axis, and orthogonal to foliation); thin-sections were prepared from all three cuts and studied under transmissive light.

Table A6-1: Samples from the MFE-drillcore (KF0051A01) used for porosity and density measurements.

Sample	Depth	Water Saturation, Bulk Density		Compact Density (Grain Density)
		Cylindric core (Surface covered with wax)	**Sawed surfaces** (Wax-free)	**Ground samples**
Äspö diorite				
*MFE-4.87**	4.84 - 4.89	X	X	X
MFE-5.70	5.66 - 5.73		X	
MFE-6.08	6.05 - 6.10	X	(X, ground)	
MFE-7.66	7.63 - 7.68	X	X	X
MFE-7.73	7.71 - 7.76	X	X	X
MFE-8.38	8.35 - 8.40	X	X	X
Ävrö granite				
MFE-9.24	9.21 - 9.26	X	X	X
MFE-9.78	9.75 - 9.80	X	X	
MFE-9.83	9.80 - 9.85		X	X
*MFE-10.65**	10.62 -10.67	X	X	X

* samples used for impregnation studies

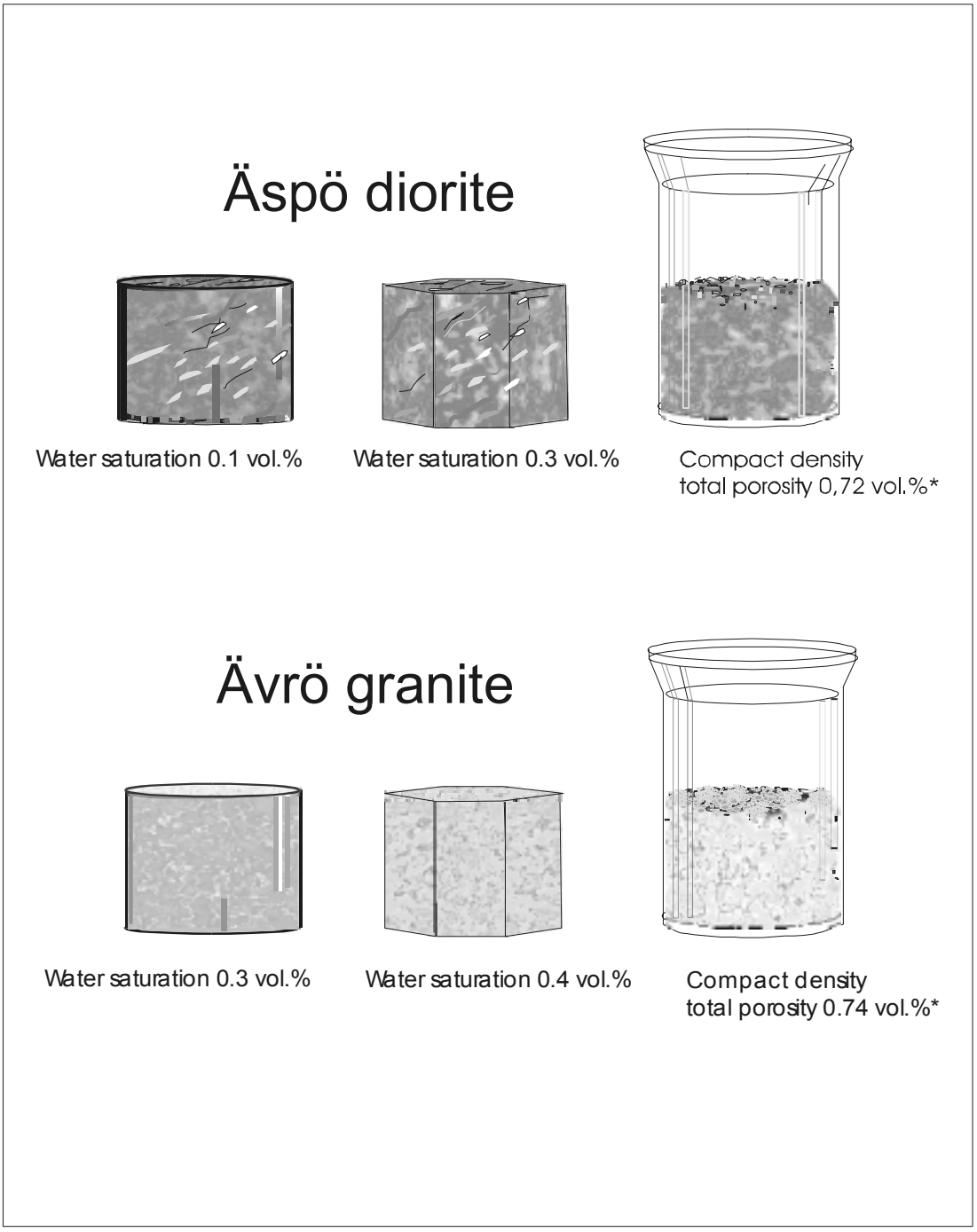

Figure A6-1: *Illustration showing sequence of measurements applied on most of the drillcore samples.*

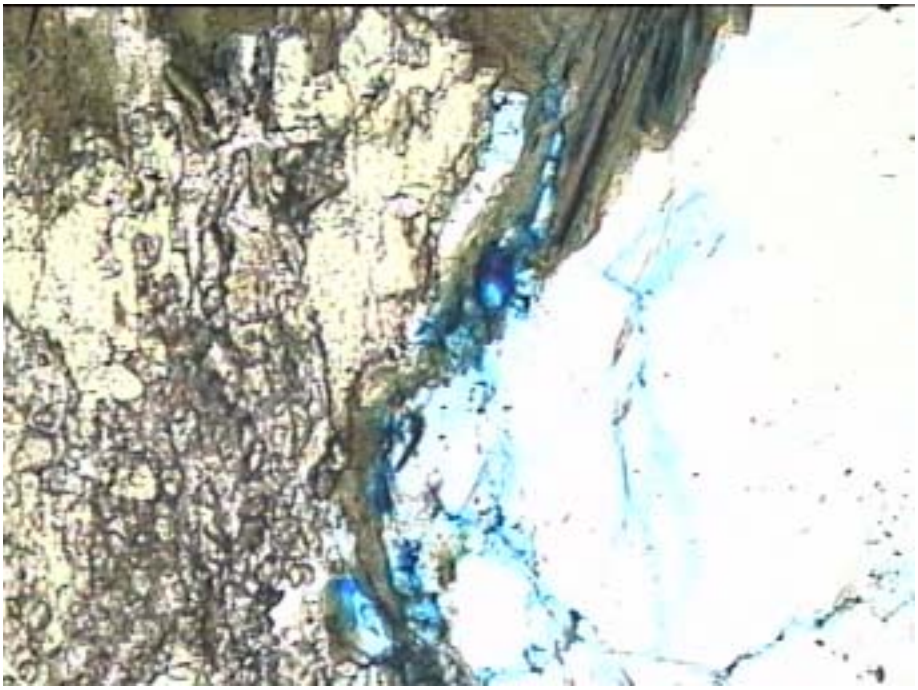

Figure A6-2: *Äspö diorite sample dyed with blue ink showing increased porosity along the foliation planes (bands of biotite/epidote parallel with bands of quartz and feldspar). The length of the photomicrograph corresponds to 1.25mm.*

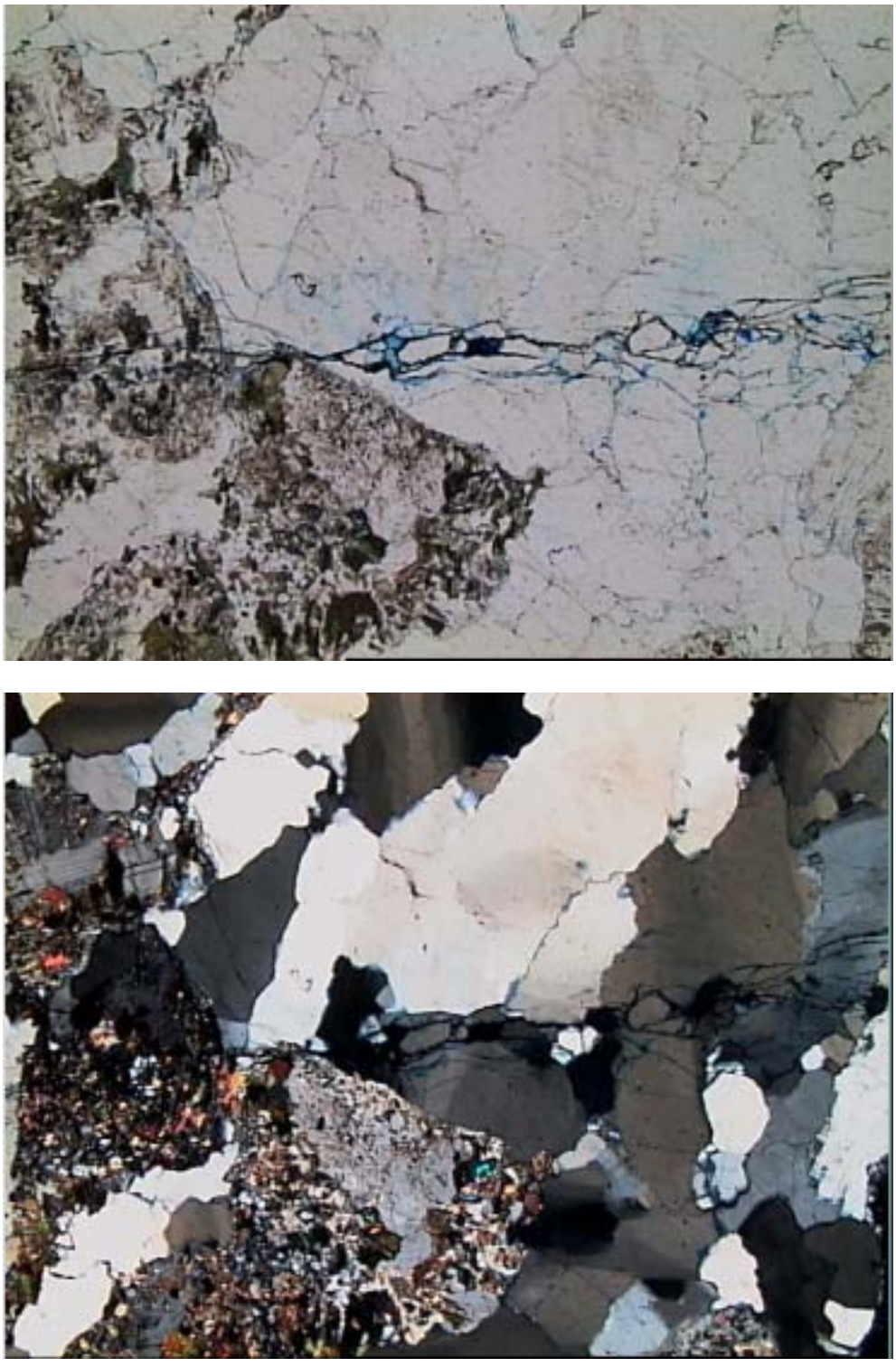

Figure A6-3: *Ävrö Granite sample dyed with blue ink showing increased porosity along microfractures transecting grains of quartz and feldspar.*
(Upper image with parallel nicols; Lower image with crossed nicols; Length of photomicrograph corresponds to 2.5mm).

International
Technical Document

ITD-01-07

Äspö Hard Rock Laboratory

Matrix fluid chemistry experiment

Hydraulic character of the rock matrix

Erik Gustafsson

Geosigma AB

September 2001

Summary

The Matrix Fluid Chemistry Experiment (MFE) at the Äspö Hard Rock Laboratory (HRL) was carried out within a rock block of very low hydraulic conductivity and low fracture frequency, at depth of a future repository i.e. ~500m, and aimed at studying the chemistry of matrix fluids hosted in such an environment.

Groundwater sampled from the Äspö site has hitherto been collected from water-conducting fracture zones with hydraulic conductivity greater than $1 \cdot 10^{-9}$ ms^{-1}. The chemistry of these groundwaters probably results from mixing along fairly rapid conducting flow path, being mainly determined by the hydraulic gradient, rather than by chemical water/rock interaction. In contrast, little is known about groundwater compositions and hydraulic character of such low conductive parts ($K < 10^{-10}$ ms^{-1}) of the bedrock as the MFE was focussed on. For that reason determination of the hydraulic character of the matrix rock surrounding the experimental set-up at the MFE-borehole (borehole KF0051A01) and the near-vicinity fractures/fissures of low hydraulic conductivity is of importance.

Sampling and monitoring equipment was installed in the MFE-borehole, providing pressure monitoring and sampling of matrix fluid in four isolated sections. Following the opening of two borehole sections in December 1999 the hydraulic conductivity of the matrix block surrounding the MFE-borehole was calculated, based on inflow rates, the actual pressure in the borehole section and an estimate of pressure in the surrounding rock. The hydraulic conductivity was calculated to be $1 \cdot 10^{-14}$ ms^{-1} to $6 \cdot 10^{-14}$ ms^{-1}. Inflow rates and the chemistry of the sampled water in borehole sections 2 and 4 indicated possible fluid movement in connected pores and small-scaled fractures.

A conceptual hydraulic model of the matrix block was suggested, based on available hydraulic and hydrochemical data. Hydraulic conductivity of the matrix rock was estimated to be in the range of $1 \cdot 10^{-14}$ ms^{-1} to $1 \cdot 10^{-13}$ ms^{-1}, with fluid movement mainly confined to the connected porosity, i.e. a network of microfractures and grain boundary pores. In a metre scale, this matrix rock is intersected by preferential “flow paths” (small-scaled fractures), in turn connected to water-conducting fractures with hydraulic transmissivities in the range of 10^{-11} ms^{-1} to 10^{-8} ms^{-1}. Spacing between these water-conducting fractures is within a few metres.

Even though the hydraulic conductivity of the rock matrix surrounding the MFE-borehole has been calculated from the obtained experimental data, complementary studies are proposed aiming at enhancing knowledge and understanding of the hydraulic system of the low-conductive host rock matrix.

International
Technical Document

ITD-01-06

Äspö Hard Rock Laboratory

Matrix fluid chemistry experiment

Fluid inclusion investigation of quartz

Alexander Blyth
University of Waterloo

October 2001

Summary

The study of quartz at the Äspö site provided an opportunity to study the thermal and fluid history of the rock formation. It also gave an indication of fluids that may become mobilised in the future, an important consideration for the disposal of radioactive waste in crystalline rock, especially in Sweden were the bedrock is still undergoing stress-release following deglaciation. Fluid inclusion investigations are used to determine the temperature and chemical nature of the fluids that were recorded by the quartz. The quartz from the matrix borehole recorded several generations of fluids, each with a specific salinity and recrystallisation temperature range.

The first group of fluid inclusions formed at temperatures between 418 and 510°C from a 4.6 to 15 wt. % NaCl dominated fluid. These inclusions were trapped at the critical point and are likely primary inclusions trapped during the crystallisation of the quartz.

Another group of inclusions formed at temperatures between 102.5 and 377.0°C from a 0.2 to 20 wt. % NaCl dominated fluid. These inclusions are secondary and formed as a result of healed micro-fractures in the quartz grains and along grain boundaries.

Another group of inclusions formed at temperatures between 80.9 to 233.8°C from a 12 to 21 wt. % $CaCl_2$ dominated fluid. These inclusions are also secondary and formed as a result of healed micro-fractures in the quartz grains and along grain boundaries.

Another group of secondary inclusions contained only a liquid phase. They occurred as planes of inclusions within a grain or were along grain boundaries. These inclusions showed no change upon heating or cooling so very little can be said about them. They are most likely low salinity (H_2O) inclusions.

The final group of inclusions found in the quartz was also secondary and contained only a gas phase. They occurred primarily along grain boundaries. These inclusions also showed no change upon heating or cooling so very little can be said about them. They are most likely low density vapour (H_2O) inclusions.

Methods

Sample selection and identification

Six samples from the MFE-borehole (KF0051A01) were supplied by Sten Lindblom, University of Stockholm (Table A8-1). These were sub-samples of the material used for parallel studies at the University of Stockholm and by Seppo Gehör at Kivitieto Oy, Oulu. Borehole log identified the first three samples (MFE-5.03, MFE-5.18 and MFE-7.81) as Äspö Diorite and the last three samples (MFE-8.84, MFE-9.11 and MFE-10.90) as Ävrö Granite.

Fluid inclusion section preparation

Double polished thin sections were made from these samples, with special care to avoid heating the samples during preparation. Samples of the core were cut with a small diamond rock saw using water as a coolant. The samples were then set in epoxy glue that cures at room temperature. Samples were then ground flat by hand on a grinding wheel then polished with diamond powder and mineral oil on a Duren ore polisher equipped with a water cooling system. Samples were then attached to a frosted glass slide using Loctite 411 instant adhesive (Crazy Glue). Excess sample was removed using a diamond wafering blade and by hand grinding. Finally, the second side of the slide was polished on a Duren ore polisher with diamond powder and mineral oil.

Fluid inclusion analysis

Fluid inclusion analysis was carried out at the University of Waterloo using a USGS type heating/freezing stage built by Fluid Inc. and methods described by Roedder (1984, Chapter 7). Small chips from sections were supercooled until the inclusions were completely frozen. They were then gradually warmed at a rate of 5 to 10°C/min until the first melting (T_{1st}) occurred. The samples were further warmed at a rate of about 5°C/min until the last ice (Tm) present in the inclusion melted. During melting, an attempt was made to observe salt hydrate phases such as hydrohalite and antarcticite. The presence of these phases was not observed. Several cooling runs were performed on each inclusion until consistent melting temperatures were obtained to ensure metastable melting temperatures were not recorded. The samples were then heated at a rate of 1 to 5°C/min until the gas phase homogenised with the liquid phase and the temperature (Th) recorded. A cycling technique (Roedder, 1984, p. 201) was used when phase changes were difficult to observe. Once a Th value was determined for an inclusion, the chip was discarded from further thermometric use to eliminate the potential of stretching lower Th inclusions. The precision for temperatures measurements was ±0.5°C for Tm, ±5°C for T_{1st} (due to difficulties observing small amounts of the first melt) and ±0.5°C for Th.

Two additional experiments were done on the fluid inclusions. First, the sections were exposed to UV light to see if any minerals would fluoresce (thus showing most hydrocarbons if present); no fluorescence was found. Second, several samples from the three groups of inclusions were immersed in oil and cracked to observe for non-compressible gasses (methane or CO_2) escaping; no gasses were observed, indicating a CO_2 concentration of < 0.1 mole % (Bodnar et al., 1985).

Cathodoluminescence

Cathodoluminescence is an additional microscopic technique to observe the quartz by bombarding it with an electron beam. The quartz responds by emitting light of various wavelengths. The wavelength and intensity of the light is characteristic of the mineral and certain impurities within it. The technique provides information on multi-generations of quartz deposition not available through normal microscopic observations (Marshall, 1988). Analyses were done at the University of Waterloo using a model 8200 Mk II Technosyn cold cathode luminescence machine.

The calibration of the fluid inclusion stage was checked with several standards at the start, during and end of the analyses. Standards used to calibrate the stage included a set of four synthetic fluid inclusions produced for calibration purposes. The precision for calibration was ±0.1°C for freezing temperatures and ±1°C for the critical point of water (374.1°C).

References

Bodnar, R.J., Reynolds, T.J. and Kuehn, C.A., 1985. Fluid inclusion systematics in epithermal systems. In: B.R. Berger and P.M. Bethke, (Eds.), Reviews in Economic Geology, Geology and Geochemistry of Epithermal Systems. Soc. Econ. Geol., 2 (Chap. 5), 73-96.

Marshall, D.J., 1988. Cathodoluminescence of geological material. Unwin Hyman Ltd. Oakes, C.S., Bodnar, R.J. and Simonson J.M., 1990. The system NaCl-$CaCl_2$-H_2O: I. The ice liquidus at 1 atm. total pressure. Geochim. Cosmochim. Acta, 54, 603-610.

Roedder, E., 1984. Reviews in Mineralogy, Fluid Inclusions. Min. Soc. Amer., 12, 644p.

Table A8-1: List of Äspö samples provided for the fluid inclusion studies

MFE-Borehole (KF0051A01)		
Sample	**Section (m)**	**Rock Type**
MFE-5.03	5.03-5.08	Diorite
MFE-5.18	5.18-5.23	Diorite
MFE-7.81	7.81-7.85	Diorite
MFE-8.84	8.84-8.89	Granite
MFE-9.11	9.11-9.17	Granite
MFE-10.90	10.90-10.95	Granite

Table A8-2: Fluid inclusion data from the Äspö samples. Final melting temperatures Tm have been converted to a salinity (Roedder, 1984).

Sample	Chip	P/S/S'	Size	Vapour	Tfreeze	T1st	Tm	Salinity	Th	Comments
			µm	%	(°C)	(°C)	(°C)	Wt.% NaCl	(°C)	
MFE-5.03	1	S	13	4	-50		-8.1	11.8	318.5	isolated inclusion
	1	S	8	3	-56.6	-48.0	-9.2	13.1	233.8	inclusion train
	2	S	5	2	-43	-9.8	-2.3	3.9	189.8	inclusion train
	2	S	3	3	-60		-0.2	0.4		inclusion train, decrepitated
	3	P?	8	10	-58	-16.0	-11.0	15.0	510.0	trapped at critical?
	3	S	5	5		-17.0	-10.8	14.8	354.5	inclusion train
	3	P?	5	10			-10.8	14.8	510.0	trapped at critical?
	3	S	5	4	-49.4	-16.1			118.0	grain boundary inclusion
	3	S	4	4	-46	-19.0	-16.4	19.9	213.5	inclusion train
	4	S	7.5	4	-58.2	-19.9	-10.8	14.8	142.5	grain boundary inclusion
	4	S	6	4	-58.0	-16.4	-9.4	13.3	128.5	grain boundary inclusion
	4	S	5	4	-58	-17.5	-8.8	12.6	102.5	grain boundary inclusion
	4	S	2.5	4	-58.0	-16.5	-9.5	13.4	120.5	grain boundary inclusion
	4	S	5	3	-58.0	-17.0	-9.4	13.3	120.5	grain boundary inclusion
	5	S	6.5	2	-61.6	-38.1	-8.1	11.8	80.9	
	5	S	5	15	-40	-17.2	-1.7	2.9	336.3	
	5	S	7.5	10	-41	-15.7	-2.1	3.5	242.2	
	6	S	7.5	75	-54	-19.5	-0.3	0.5	377.0	V to L homogenization
MFE-5.18	1	S	5	4	-43	-16.9	-0.1	0.2	157.5	
	2	S	5	3	-61	-17.5	-15.3	19.0	114.8	inclusion train
	2	S	8	3	-43	-19.2	-13.1	17.1	133.2	inclusion train
	3	S	8	3	-55.5	-18.2	-0.5	0.9	172.3	inclusion train
	4	S	15	4	-51.8	-18.1	-5.3	8.3		gb inclusion, decrepitated
	6	S	10	4	-62	-17.7	-12.8	16.8	257.3	inclusion train
	6	S	18	4	-53.7	-26.7	-22.1	24.1	181.4	isolated inclusion
	7	S	7	4	-50	-16.5	-2.2	3.7	284.3	inclusion train
	8	S	10	4		-12.0	-0.7	1.2	145.2	inclusion train
	8	S	10	4	-40.9		-0.4	0.7		inclusion train
MFE-7.81	1	S	5	3	-56	-16.0	-5.8	8.9		inclusion train, decrepitated
	3	S	6	3	-43.2	-15.4	-0.9	1.6	139.6	
	4	P?	6	50		-18.2	-6.6	10.0	455.0	trapped at critical?
	4	S	6	5	-52.2	-19.9	-6.6	10.0	194.0	inclusion train
	5	S	5	5	-43.5	-20.0	-2.5	4.2	235.3	
	6	S	7.5	4	-42.2	-15.7	-0.2	0.4	114.6	inclusion train
	7	S	12	3	-61.8	-42.8	-12.9	16.9	144.8	inclusion train
	8	S	7	10		-20.0	-1.6	2.7	321.6	inclusion train
MFE-8.84	1	S	12	20	-45	-19.4	-2.6	4.3	285.7	
	2	S	10	4	-47	-18.9	-7.1	10.6	232.8	inclusion train
	3	S	7.5	3	-53	-42.0	-12.9	16.9	141.4	inclusion train
	3	S	7	3	-58	-38.0	-13.3	17.3	142.3	inclusion train
	3	S	7	3	-58	-40.0	-13.8	17.7	149.8	inclusion train
	3	S	7	3	-58.3	-38.0	-13.3	17.3	139.9	inclusion train
	3	S	7.5	3	-59.9	-39.0	-13.8	17.7	139.5	inclusion train
	4	S	10	4	-57.4	-18.4	-12.7	16.7	251.8	inclusion train
	4	S	4	4	-69.9	-15.0	-8.5	12.3	171.8	inclusion train
	5	S	10	5	-44.8	-19.2	-2.9	4.8	244.5	inclusion train

Table A8-2: Continued

Sample	Chip	P/S/S'	Size	Vapour	Tfreeze	T1st	Tm	Salinity	Th	Comments
			µm	%	(°C)	(°C)	(°C)	wt % NaCl	(°C)	
MFE-8.84	6	S	12	4	-38.7	-15.6	-8.3	12.1	218.3	inclusion train
	7	S	4	3	-52.5	-15.0	-7.3	10.9	134.3	inclusion train
	8	S	4	4	-40.0	-18.7	-7.2	10.7	221.7	inclusion train
MFE-9.11	1	S	4	3	-42.1	-18.8	-1.6	2.7	246.8	inclusion train
	2	S	4	3	-80.0	-42.8	-22.6	24.4	124.8	inclusion train
	3	S	7.5	5	-42.0	-18.6	-0.6	1.0	229.3	inclusion train
	4	S	7.5	4	-39.1	-14.8	-0.9	1.6	162.3	inclusion train
	5	P?	7.5	50	-42.0	-14.8	-2.8	4.6	418.0	trapped at critical?
	6	S	11	3		-18.3	-5.5	8.5		inclusion train

Table A8-3: Summary of statistical data for the Äspö fluid inclusions.

Fluid Inclusion T_{1st} (°C)

Inclusion Type	*n*	*Min*	*Max*	*Mean*	*Median*	*Std*
$CaCl_2$	10	-48.00	-26.70	-39.54	-39.50	5.49
NaCl	38	-20.00	-9.80	-17.25	-17.50	2.19
Critical	3	-18.20	-14.80	-16.33	-16.00	1.72

Fluid Inclusion Tm (°C)

Inclusion Type	*n*	*Min*	*Max*	*Mean*	*Median*	*Std*
$CaCl_2$	10	-22.60	-8.10	-14.20	-13.30	4.72
NaCl	40	-16.40	-0.10	-5.58	-5.40	4.75
Critical	4	-11.00	-2.80	-7.80	-8.70	3.90

Fluid Inclusion Th (°C)

Inclusion Type	*n*	*Min*	*Max*	*Mean*	*Median*	*Std*
$CaCl_2$	10	80.9	233.8	147.86	141.9	39.08
NaCl	36	102.5	377.0	206.48	203.8	76.31
Critical	4	418.0	510.0	473.25	482.5	45.04

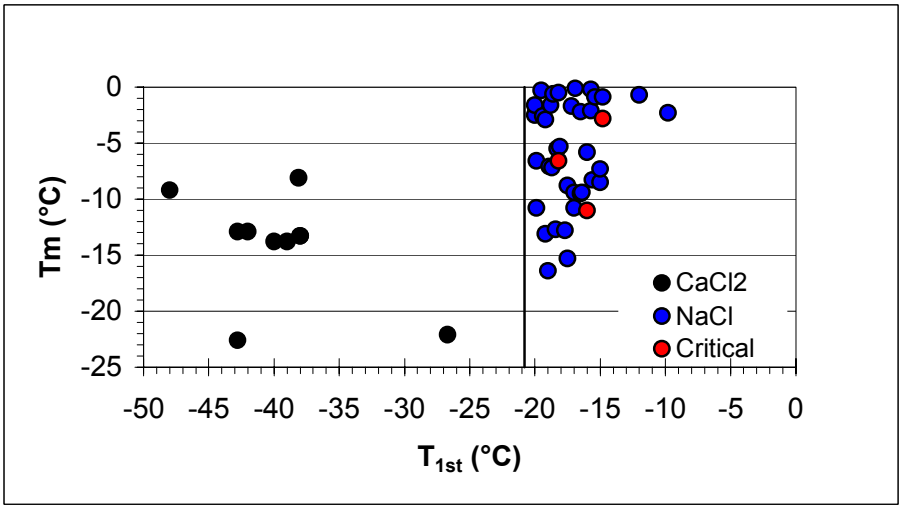

Figure A8-1: *Final melting temperature (Tm) versus first melting temperature (T_{1st}) for fluid inclusions from Äspö. Samples are coded for fluid type.*

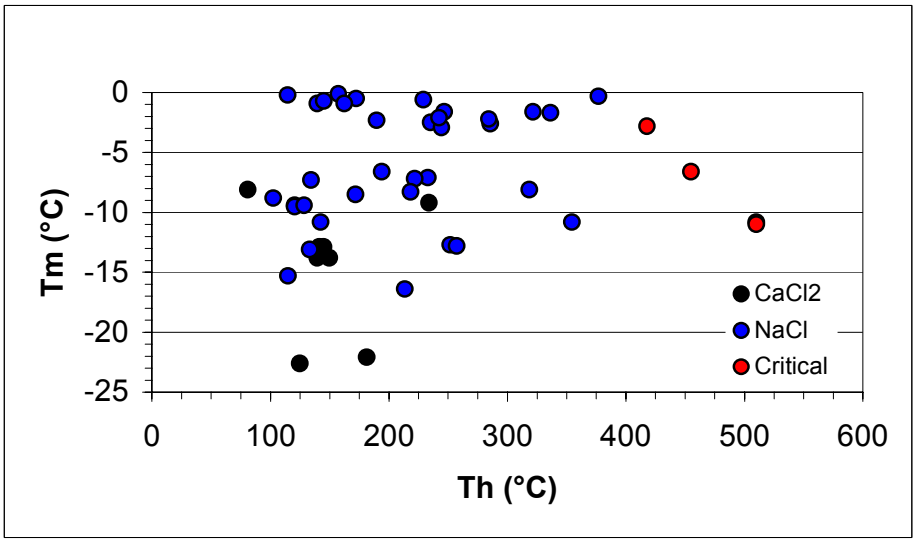

Figure A8-2*: Final melting temperature (Tm) versus homogenisation temperature (Th) for fluid inclusions from Äspö. Samples are coded for fluid type*

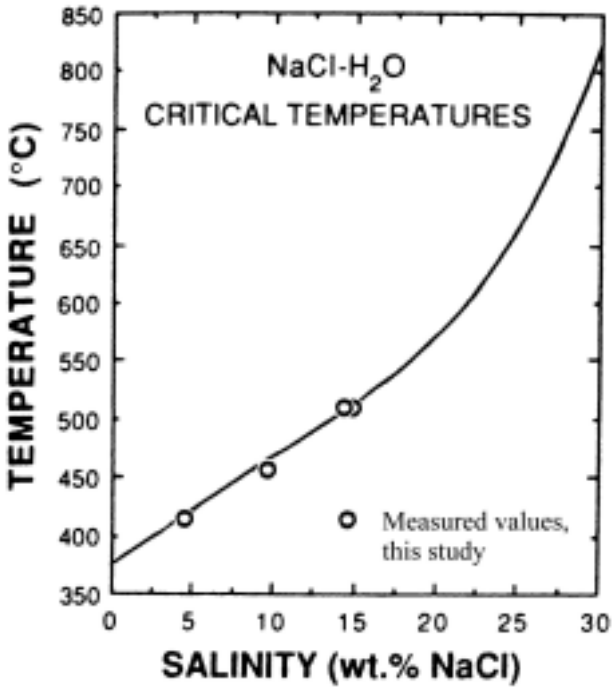

Figure A8-3: *Critical temperatures for the NaCl-H_2O system. The curve is the theoretical critical point for a given salinity. The circles are fluid inclusion measured in this study (modified from Knight and Bodnar, 1989).*

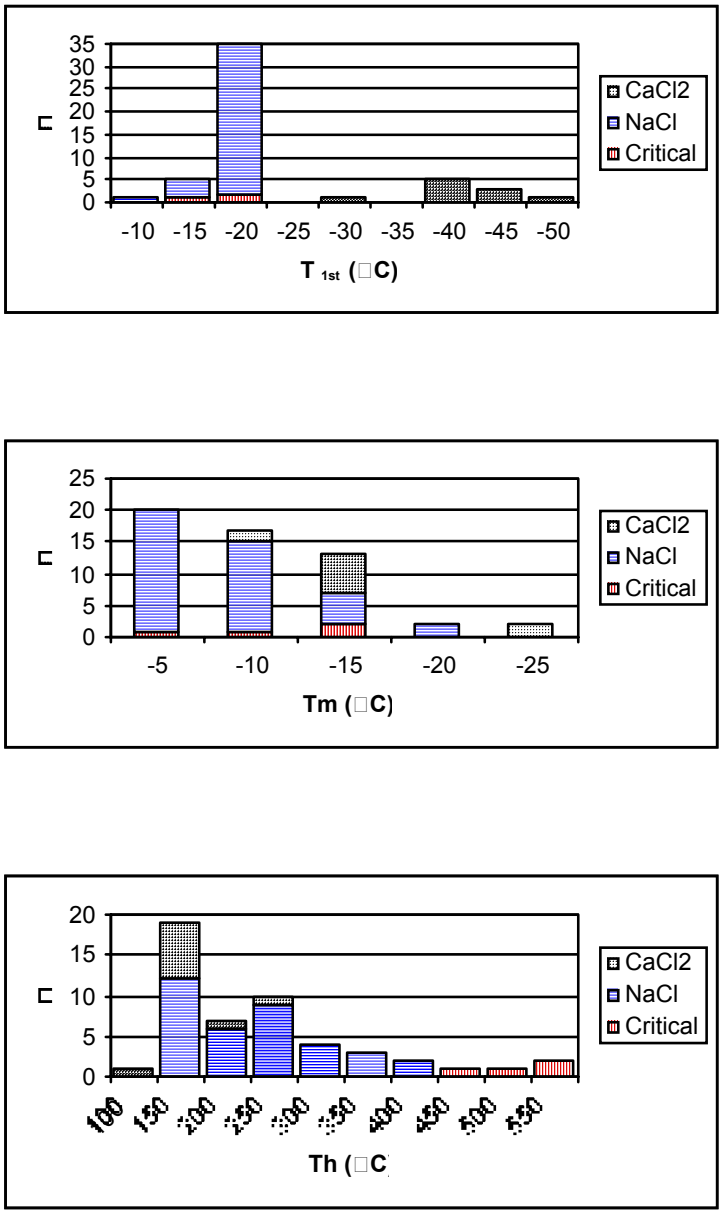

Figure A8-4: *Histograms of the fluid inclusion data from Äspö. Samples are coded for fluid type.*

Figure A8-5: *Primary, critical point inclusion*

Figure A8-6: *Secondary, single phase (liquid) inclusions*

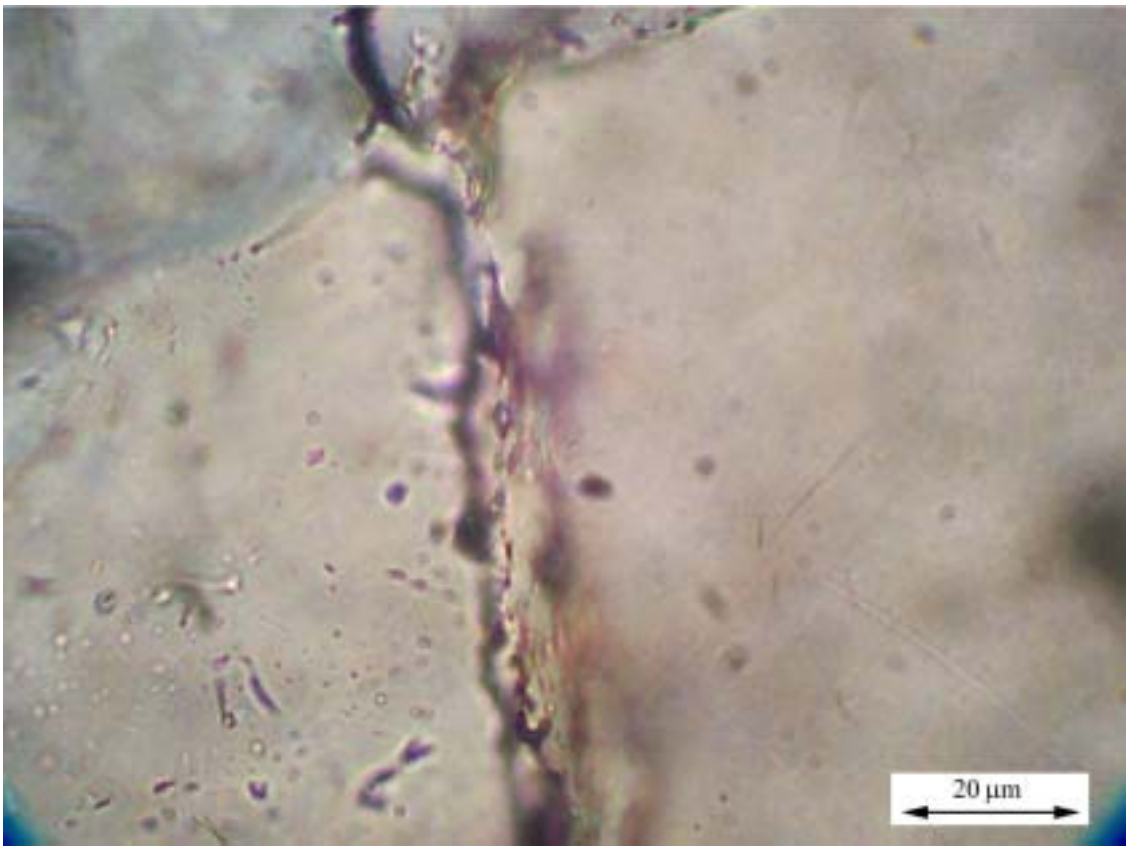

Figure A8-7: *Secondary, single phase (gas) inclusion*

Figure A8-8: *Secondary, two phase (liquid-gas) NaCl dominated inclusion*

International
Technical Document

ITD-02-02

Äspö Hard Rock Laboratory

Matrix Fluid Chemistry Experiment

Minutes of the Workshop held at SKB Stockholm, October 17-18, 2001

John Smellie

Conterra AB

November 2001

Agenda

Wednesday 17th.

Morning Session

10.00-10.10	Introduction *(P. Wikberg)*
10.10-11.00	Experimental status, reporting and present conceptual ideas *(J. Smellie)*
11.00-11.20	Purpose and objectives of the workshop *(J. Smellie)*
11.20-11.45	**Coffee**
11.45-12.05	Crush/leach experiments *(A. Blyth/S. Frape)*
12.05-12.30	Synthesis of crush/leach experiments *(N. Waber)*
12.30-12.45	Laboratory-controlled leaching experiment *(N. Waber)*
12.45-13.00	Permeability experiment *(S. Frape)*
13.00-14.30	**Lunch**

Afternoon Session

14.30-15.00	Fluid inclusion studies *(A. Blyth)*
15.00-15.45	Fluid inclusion studies *(S. Lindblom/S. Gehör)*
15.45-16-15	**Coffee**
16.15-16.45	Fluid inclusion studies *(N. Waber)*
16.45-17.30	Synthesis of fluid inclusion studies *(S. Lindblom)* Discussion

Thursday 18th.

Morning Session

09.00-09.30	Rock matrix: Porosity measurements *(E-L. Tullborg)*
09.30–10.00	Rock matrix: Evidence of large-scale chemical gradients *(N. Waber)*
10.00-10.30	Äspö diorite fissure/fracture: Evidence of in- and out-diffusion *(E-L. Tullborg)*
10.30-11.00	**Coffee**
11.00-11.30	Bedrock formation factors: In-situ logging by resistivity methods *(M. Löfgren)*
11.30-12.15	Hydraulic characterisation – matrix borehole and near-vicinity *(E. Gustafsson)*
12.15-13.00	Evolution and chemistry of the Äspö groundwaters *(J. Cassanova)*
13.00-14.00	**Lunch**

Afternoon Session

14.00-14.30	Evolution and chemistry of the Äspö groundwaters *(S. Frape)*
14.30-15.30	1) Characterisation of porewaters – available techniques and their applications *(N. Waber/A. Gautschi)* Discussion: Interest for Äspö? 2) Future use of the matrix borehole to increase hydraulic understanding *(E. Gustafsson)* Discussion
15.30-16.00	Summing up and future plans *(J. Smellie)*

Purpose and Objectives

- On-going studies – present status.
- Winding up and final reporting.
- Future activities?
- What have we learnt?
- If we had to do it again, what lessons have been learnt and what improvements would be made?
- How successful have we been to establish working methodologies that can be conveniently transferred to site-specific investigations?
- Is the matrix block studied representative of the Äspö site as a whole?
- Is Äspö unique? Or, does it demonstrate that Swedish crystalline rocks are ’open’ to significant matrix groundwater movement over repository timescales?

Synthesis

Wednesday 17th

Morning Session

The meeting was formally opened by ***Peter W.*** who briefly described the status of the various underground experiments being carried out at Äspö. This was followed by ***John S.*** who presented an outline of the experimental status/on-going activities and reporting, and a review of present conceptual ideas based on completed work.

Opportunity was taken during this opening phase of the Workshop to present an up-date on the matrix groundwaters sampled the previous day (October 16th). The pressure monitoring curves for borehole sections 1-4 prior to sampling, shown in Figure A9-1, indicate that Section 4 (blue) in the Äspö diorite (previously sampled 2 years ago in December 1999) appears to have recovered, and Section 2 (green) in the Ävrö granite (unopened since the commencement of the experiment 3.5 years ago) continues to show a steady, although small, increase with time. Section 1 (red) also opened in December 1999 shows no change as might be expected because of the large borehole section volume involved, and Section 3 (yellow), located between the packed-off sections 2 and 4, shows a very slight increase over the 3.5 year period.

Adequate water was collected from Sections 3 and 4; Section 2 produced a small but important volume which took several attempts to remove using evacuated glass vials. Surprisingly Section 1 was underpressurised and nothing was collected.
Of the three water samples, only Section 2 had to be prioritised as to what species to be analysed; this involved major cations and anions, stable isotopes (^{18}O, ^{2}H), strontium isotopes (^{86}Sr, ^{87}Sr) and ^{37}Cl. Samples collected from sections 3 and 4 additionally will include: pH (field and laboratory), alkalinity, ^{13}C and ^{14}C, and ^{10}B. Other analyses will include gas samples (normal suite: N_2, O_2, CO_2, H_2, CH_3, CH_4 etc.) from sections 3 and 4, and Section 3 also will be checked for microbe activity.

Initial impressions from the *in-situ* and laboratory measurements of pH and alkalinity is that the samples may not differ too much from the Section 4 water sampled in December 1999 (see IPR-00-35).

This sampling up-date was followed by outlining the purpose and objectives of the Workshop and presenting a list of future activities for discussion.

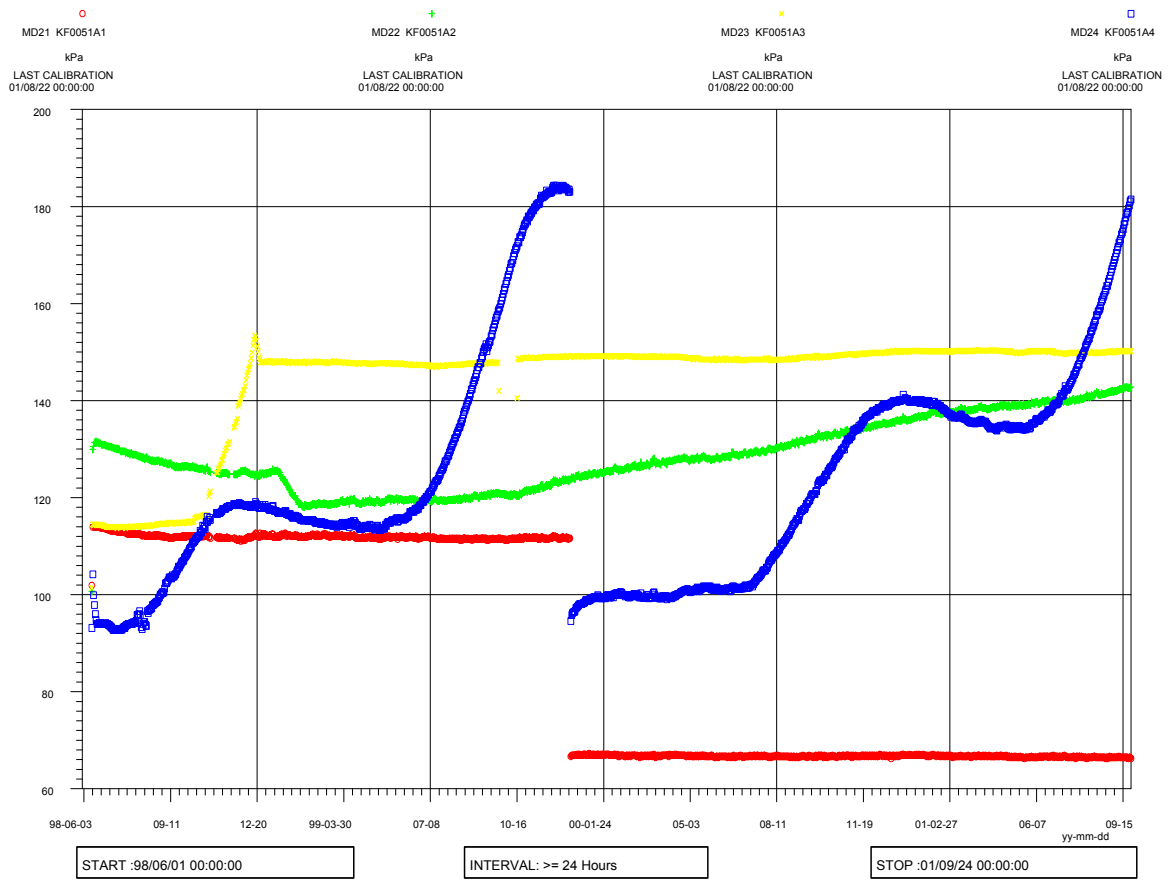

Figure A9-1: *Pressure monitoring curves for each of the four isolated borehole sections:1 (red), 2 (green), 3 (yellow) and 4 (blue). Sections 2 and 4 are specially equipped for matrix fluid sampling.*

Sampling resulted in the following:

Section 1: No water or gas; under pressure in section!
(Previous sampling in Dec. 1999 gave only gas)
Section 2: Some gas and small water volume (34.74 mL); only water sampled
Section 3: Gas and water (321.19 mL); both gas and water sampled
Section 4: Gas and water (195.02 mL); both gas and water sampled
(Previous sampling in Dec. 1999 gave 160 mL)

(Note: H_2S was detected from all sections apart from Section 1)

Crush/leach experiments on drillcore material

These experiments have mainly concentrated on drillcore material (both the Äspö diorite and Ävrö granite varieties) from the matrix fluid borehole. For comparison and also to provide more background data on which to base some of the isotopic data (i.e. ^{37}Cl, ^{11}B, $^{87/86}Sr$), additional drillcore material, representing respectively more and less mafic rock types, were selected from other Äspö core material and studied at the University of Waterloo. Preliminary results show them to represent a wide range of salinity and ^{37}Cl signatures; Sr isotope analysis are presently underway at the University of Bern. This study is to further determine the influence of lithology on matrix fluid composition with specific emphasis on isotopic signatures. It is hoped that this may be helpful to interpret some of the matrix groundwater/fluid isotopic data.

Since the matrix borehole studies carried out at the University of Waterloo were presented at the last Workshop (see Minutes: ITD-00-17) a preliminary synthesis of the crush/leach work carried out by the University of Bern, supplemented by initial data from the laboratory-controlled leaching experiment, was presented by ***Nick W.***. The main conclusions reached are:

- The overall assumption is that given enough time a chemically homogeneous pore water can be expected in an undisturbed matrix block due to diffusive equilibration.
- Aqueous leachate data cannot unequivocally support the existence of such a homogeneous pore water composition.
- Aqueous leachate data of fine-grained rock fractions are disturbed by a strongly variable contribution of salts from mineral fluid inclusions independent of rock-type.
- Aqueous leachate data of coarse-grained rock fractions suggest a more homogeneous Cl-distribution. The recalculation to pore water Cl contents is, however, seriously interfered with by the exact determination of the Cl accessible porosity.
- The overall Cl inventory of the rock is high and the impact of possible fluid inclusion leakage on the pore water is large.
- The best estimate of the pore water salinity is derived from leachates of the coarse-grained fractions.
- This, however, results in a salinity that is lower than the one observed in the water sampled from borehole Section 4.

- Molar Br/Cl and Na/Cl ratios clearly indicate: 1) the contribution of fluid inclusions to the fine-grained leachate solutions, and 2) that the pore water must be relatively low in Cl with a Na/Cl ratio much higher than sea water.
- First results of a laboratory controlled diffusion experiment confirm a moderate Cl content for the pore water, lower than the one in the sampled water, but this has to be confirmed by continued sampling.

The systematic crush/leach studies of the matrix drillcore by University of Bern revealed the possibility of a large-scale (decimetres) chemical gradient within the Äspö diorite towards the sampled borehole Section 4. This was discussed at the last Workshop (see Minutes: ITD-00-17). However, subsequent work over the last year suggests that the rock matrix interconnected porosity appears to be too heterogeneous for reliable interpretation of chemical gradients.

Permeability experiment

Shaun F. provided an up-date on the status of the permeability experiment (see instrumental details in last year's Minutes: ITD-00-17). Still no movement of matrix fluid through the core has been observed; however there still are indications of a loss of distilled water from above the core. Since the water is not believed to be escaping from the highly pressurised sealed unit, this may suggest the filling of empty pore space in the rock or, alternatively, evaporation of fluid on the underside of the core. The experiment may progress in two directions:

- Continue the experiment as presently set-up
- Dismantle the experiment and carry out a post-mortem on the drillcore

The outcome will be discussed in the near-future

Afternoon Session

Fluid inclusions studies

Presentations were made from each of the four groups involved in the fluid inclusion studies – ***Alec B.*** (Univ. Waterloo) ***Sten L.*** (Univ. Stockholm), ***Seppo G.*** (Kivitieto) and ***Nick W.*** (Univ. Bern). The presentations of Waterloo and Bern were based on their respective ITD reports presently being published and largely reflect the work presented in the last Workshop (see Minutes: ITD- 00-17). New work by Stockholm and Kivitieto was presented by Sten L. In addition to the mineralogy, distribution and textural relationships of the fluid inclusion populations, some chemistry of the included fluids based on Microthermometry, Laser Ablation and Raman Spectrometry techniques was presented. The chemistry was further detailed in the presentation of ***Seppo G.*** who provided a synthesis of the results from Microthermometry and Laser Ablation. These data show that the dominant fluid inclusion population (mainly associated with the coarse-grained primary magmatic quartz and the later fine-grained recrystallised variety) belongs to the H_2O-NaCl-$CaCl_2$-CO_2 system. Carbon oxide compounds comprise a prominent fraction of the constituents in younger fluid inclusion trails which have been formed late within the host

quartz. These populations are characterised by the H_2O-CO_2-NaCl system. Finally the concentrations of Al and REEs were found to be greater in inclusions within the intercrystalline spaces and trails in comparison to the intracrystalline fluid inclusion clusters.

The afternoon session was rounded off by a synthesis presentation of the fluid inclusion studies presented by ***Sten L.*** This represents a first draft and has still to be commented on by the other involved groups, scheduled for the next 4-6 weeks.

Thursday 18th

Morning Session

Rock porosity measurements

Since the last Workshop, additional work to address the nature of the rock porosity along the matrix borehole and compared to the Äspö site as a whole has been presented and discussed in ITD-01-03. Since then, rock porosity studies have centred round a Pilot Study to evaluate the evidence of in- or out-diffusion processes.

At this juncture the opportunity was given to ***Anders W.*** to present the findings of the TRUE studies relating to porosity measurements since the same method approach has been used on similar rock types. In addition, he outlined the on-going long-term diffusion experiment (LTDE) and the shared interests between the Matrix Fluid Experiment and the LTDE. Where applicable, these TRUE and LTDE data will be integrated in the final reporting of the matrix experiment.

Evidence of in- and out-diffusion processes

A Pilot Study was initiated in September 2001 to study an identified micro-fracture/fissure some 56.5 cm from Section 4, already sampled for matrix groundwaters in December 1999. The purpose was to analyse a series of rock slices representing a profile across the micro-fracture/fissure in the Äspö diorite, with the objective to assess the nature of in- and out-diffusion processes around the fracture/fissure using U-decay series, ^{11}B, ^{37}Cl and strontium isotopes. The results were presented and discussed by ***Eva-Lena T.*** The main observations are as follows:

- ***Fracture Coating:*** Irregular layer of calcite and chlorite (0-0.3 mm thick)
- ***Wall Rock****:* Biotite preserved; no increase in alteration of plagioclase; no red staining (i.e. no evidence of increased oxidation)
- ***Porosity:*** Increase in porosity in the outermost 1 cm sample (0.61 vol% compared with approx. 0.4 vol %)
- ***Major and Trace Element Chemistry:*** No clear trends; appears to reflect mineralogical heterogeneity
- ***Isotopes:*** $^{234}U/^{238}U$ in secular equilibrium apart from the outermost sample closest to the fracture

More data are expected and will be presented as an ITD report in February 2002.

Bedrock formation factors: In-situ logging by resistivity methods

Martin L. presented the background and theory to obtaining bedrock formation factors (essential to determine rock matrix diffusion) by *in situ* downhole electrical conductivity measurements and their comparison with laboratory measurements. The method is based on electro-migration instead of diffusion as in traditional liquid phase through-diffusion experiments. The main conclusions were:

- Good correlation between *in-situ* and laboratory measurements
- The *in-situ* method seems to work
- Alternating current can be used
- Results indicate connectivity over large distances in the crystalline rock
- The *in-situ* method is very fast, inexpensive, and large samples are used under *in-situ* conditions
- Surface conductivity needs to be investigated

Hydraulic characterisation

Erik G. provided a brief overview of the hydraulic characterisation of the matrix borehole and immediate surroundings (i.e. 'block scale'), extending this to 'site scale' to include the data from the TRUE Block Scale, Prototype Repository and Chemlab/Microbe ('J' Niche) experiments. Based on these data, he discussed the present status of the conceptual model for the matrix rock block. The following features were noted:

- Hydraulic conductivity of 10^{-14}-10^{-13} ms^{-1} in the matrix rock.
- Fluid movement mainly in connected porosity (i.e. network of micro-fractures/fissures and grain boundary pores).
- In the metre scale, preferential 'flow paths' occur associated with small-scale fractures (T= 10^{-11}-10^{-8} m^2s^{-1}).
- The spacing between the water-conducting fractures are within a few metres.

Evolution and chemistry of the Äspö groundwaters

Joël C. presented groundwater boron, strontium and oxygen isotopic data from several sites in the Fennoscandian Shield including those from Äspö to help constrain the various hypotheses on the nature of water/rock interaction and the end-members participating in mixing processes, i.e. to establish a possible origin to the highly saline waters and brines. Boron (^{11}B) was used as an indicator of permafrost conditions as it appears to become isotopically enriched in the fluid phase during freeze-out conditions. The importance of the matrix fluid experiment would be to establish the extreme boron end-member which may facilitate interpretation of groundwater evolution at Äspö.

Afternoon Session

Evolution and chemistry of the Äspö groundwaters (contd.)

Shaun F. introduced and discussed the additional information derived from tritium and ^{37}Cl collected from 1987 to the present day that could be used to explain further the evolution of the Äspö groundwater system; in particular, the evolution of the groundwaters with time. The data generally supported the conceptual groundwater models development from 1987 to 1990, representing the undisturbed conditions prior to tunnel excavation, and also the post-1990 groundwater mixing incurred during excavation due to drawdown effects. He indicated that by using a wide variety of geochemical and isotopic tools it would be possible to work out groundwater mixing proportions similar to the M3 approach.

Characterisation of porewaters – available techniques and their applications

Nick W. briefly described the Swiss experience from the Mont Terri Project which involves a study of a reconnaissance tunnel in the Opalinus Clay Formation in northern Switzerland. Despite the obvious difference in rock-type, he pointed out that the investigative methodology (e.g. pore water characterisation and diffusion processes) may be of importance since the transmissivity of the clay is similar to that of the Äspö matrix rock (~ 10^{-14} m^2/s). In particular, the use of the noble gases, especially helium, and chlorine-37, has shown these to be sensitive geochemical tracers for studying groundwater movement and residence times. He recommended that this approach could be focussed on a suitably drilled borehole at the Äspö site where there is a clear intersection of a water-conducting feature with a substantial thickness of matrix rock. This would allow measurements from a profile which has not been influenced by other nearby fractures.

Future use of the matrix borehole to increase hydraulic understanding

Erik G. presented and discussed complementary studies in the matrix borehole following the final groundwater sampling. There was a general consensus that such studies are warranted to finally confirm some of the earlier assumptions and calculations made during conceptualisation. Two main areas were identified:

- Determination of hydraulic conductivity and chemical composition of waters in the smallest hydraulic conductors (i.e. T= 10^{-11}-10^{-8} m^2s^{-1}).
- Determination of hydraulic conductivity and *in-situ* leaching of matrix rock in Sections 2 and 4 (i.e. those sections demarcated for sampling).

Summing up and future plans

John S. provided a brief summary of what had been presented and discussed. The various studies were generally on schedule and there were high hopes that the matrix groundwater sampling just carried out would follow predictions. With respect to future activities, this would depend very much on the outcome of the project as a whole and whether funding would be available. The decision to continue or complement areas of interest would be made after June 2002, when the final synthesis report will be completed. At this juncture additional funding partners may include Ontario Power Generation and may also include some 'in kind' support from Nagra/University of Bern.

Areas of potential interest where identified on the basis of the list earlier presented and the consensus reached for each of the topics is indicated below in italics:

Äspö Diorite fracture: Small-scale in- and out-diffusion studies

University of Bern, University of Waterloo, Terralogica: Depending on the outcome of the Pilot Study, plus available resources, a complete profile suite of samples could be analysed and interpreted.

- mostly a methodology test
- matrix mineralogy would probably dominate

There was some skepticism as to whether it was worth continuing with this task since major ion and trace element data showed no systematic trends towards the fissure – the trends were too mineral-specific. However, more recent results show an increase in porosity over some mm's towards the fissure edge; this is accompanied by $^{234}U/^{238}U$ disequilibrium. The suggestion is, therefore, that this fissure is probably active and may reveal some additional information from ^{11}B and ^{37}Cl analysis along the profile.
Funding required

Matrix block: Large-scale in- and out-diffusion profile using helium

For some time Nagra has shown interest in carrying out He in- and out-diffusion studies on a crystalline rock profile – along similar lines to the Mont Terri clay experiment which was very successful (^{37} Cl, ^{11}B and U-decay series measurements should also be carried out).

University of Bern/Nagra are prepared to support sampling, analysis and interpretation
Part funding required

Fluid inclusions

Universities of Bern, Waterloo and Stockholm; Kivitieto: Potential to further use laser ablation techniques to characterise selected fluid inclusions of importance

- since theoretical diagrams are commonly used to estimate salinity, usually expressed as molar equivalent NaCl, it would be particularly interesting to know the exact composition of the important fluid inclusion phases

Task was supported – funding required

Permeability test

University of Waterloo: How long should the experiment continue? Should a post-mortem be carried out on the core?

Post-mortem was supported – funding required

Linking of databases

Universities of Bern and Waterloo: Need to link/integrate more closely the available leaching data

This will form part of the presently funded synthesis report on the crush/leach experiments and is the responsibility of the University of Bern.

Future use of the borehole

Geosigma: Proposal to increase the hydraulic understanding of the matrix borehole

Universites of Bern and Waterloo: Leaching experiment to be compared with laboratory leaching studies

Considered important to successfully conclude the project; funding required.

Conducting similar studies at other locations at Äspö

Based on controlled crush/leach experiments, coupled to connected porosity determinations and fluid inclusion characterisation, other rock matrix locations at Äspö should be studied to confirm or otherwise the results from the Matrix Fluid Experiment.

Have the objectives of the Workshop been met?

Several important questions were posed at the beginning of the Workshop. These were discussed at the final stages of the meeting and the following observations were drawn:

What lessons have been learnt and what improvements could be made?

From an experimental viewpoint the designed equipment functioned very well, although the sampling arrangements are better suited to collecting slightly larger volumes of groundwater from low hydraulically conducting microfractures/fissures (i.e. T= 10^{-11}-10^{-8} m^2s^{-1}) rather than fluids/groundwaters from the matrix over a period of years. A much simpler arrangement probably would have sufficed although this would have to be carefully designed to facilitate the sampling of small and uncontaminated water and gas volumes.

Complete sterilisation of the borehole was not successful as evidenced by the microbial activity observed in the sampling sections. This requires a much more rigorous approach.

How successful have working methodologies been established that can be conveniently transferred to site-specific investigations?

One of the highlights of the experiment has been the crush/leaching studies (coupled to connected porosity measurements and fluid inclusion characterisation) to predict the composition of the matrix fluid/groundwater. The crush/leach determines the total salinity of the matrix fluids/groundwaters in the rock matrix; the fluid inclusion studies determine the contribution of inclusions to the total salinity. By removing the fluid inclusion contribution (i.e. those generations considered to represent closed systems) and using the porosity data, an idea of the accessible fluids/groundwaters and their composition in the rock matrix can be estimated. This circumvents waiting several years to sample from the rock matrix and the measurements can be carried out conveniently, fairly quickly and economically on drillcore material from site characterisation investigations.

Is the matrix block studied representative of the Äspö site as a whole?

Without investigating other locations at varying depths, it is not possible to say.

Is Äspö unique?

Given other locations which are similarly ‘open’ to significant matrix groundwater movement (i.e. due to a generally high fracture density), Äspö is probably not unique.

Attachments

Attachment 1:	Agenda
Attachment 2:	Matrix Fluid Workshop: On-going studies and status (John Smellie, Conterra AB).
Attachment 3:	Matrix Fluid Workshop: Purpose and objectives (John Smellie, Conterra AB).
Attachment 4:	Matrix Fluid Workshop: Future activities? (John Smellie, Conterra AB).
Attachment 5:	Synthesis of crush/leach experiments carried out at the University of Bern (Nick Waber, University of Bern).
Attachment 6:	Fluid inclusion studies (Alec Blyth, University of Waterloo).
Attachment 7:	Fluid inclusion studies (Sten Lindblom, University of Stockholm).
Attachment 8:	Fluid inclusion studies (Seppo Gehör, Kivitieto, Oulu and Sten Lindblom, University of Stockholm).
Attachment 9:	Synthesis of the fluid inclusion studies (Sten Lindblom, University of Stockholm).
Attachment 10:	Porosity measurements (Eva-Lena Tullborg, Terralogica AB).
Attachment 11:	Formation factor logging by in-situ electrical conductivity measurements. Comparison of in-situ and laboratory measurements (Martin Löfgren, KTH).
Attachment 12:	Hydraulic conductors and 'matrix rock' (Erik Gusrafsson, Geosigma, AB).
Attachment 13:	Connecting deep brines from the Fennoscandian Shield with the Baltic Sea through strontium isotopes (Philippe Négrel/Joël Casanova (BRGM) and Runar Blomqvist (GTK)).
Attachment 14:	Evolution of the Äspö groundwaters with time (Shaun Frape, University of Waterloo).
Attachment 15:	Proposed complementary studies in KF0051A (Erik Gustafsson, Geosigma AB).

International Technical Document

ITD-02-03

Äspö Hard Rock Laboratory

Matrix Fluid Chemistry Experiment

Mineralogy and Fluid Inclusion Studies

Nick Waber

GGWW
University of Bern

December 2001

Summary

The Matrix Fluid Chemistry Experiment (MFE) at the Äspö Hardrock Laboratory (HRL) has the main objectives to determine the origin and residence time of matrix fluids, and to establish the influence of small-scale fractures on the fluid chemistry in the bedrock. In crystalline rocks of very low permeability there exist two major origins of matrix fluid: a) the fluid trapped in interstices and along grain boundaries, and b) the fluids trapped in mineral fluid inclusions. The characterisation of these fluids requires a sound knowledge of the rock mineralogy and indirect, often complementary techniques, have to be applied because conventional groundwater sampling methods are no longer applicable in zones of very low hydraulic conductivity. The mineralogical and chemical composition of the rocks samples investigated are given in this report together with a first characterisation of the fluids trapped in fluid inclusions.

From the MFE-borehole (KF0051A01) two drillcore sections (3.25-3.85 m and 4.57-5.06 m) were investigated. Based on the mineralogical composition the rock was classified as a monzogranite (locally termed "Äspö diorite"). Major characteristics of the rock are its porphyritic texture, the hydrothermal alterations of the feldspars including haematite staining and saussuritisation, and the partial recrystallisation of quartz. The mineralogy and chemistry of the samples compare well with previously investigated samples of the same rock type. The water content ranges from 0.05% to 0.06% yielding a water-content porosity of 0.1% to 0.2%.

Quartz is by far the major host mineral for fluid inclusions and the volumetric contribution of fluid inclusions in feldspars and apatite is negligible. In the different quartz populations four main types of fluid inclusions can be distinguished. In all cases NaCl dominates the salt content as confirmed by Raman micro-spectroscopy. Type A inclusions contain a highly saline fluid of about 30 eq.wt.% NaCl as indicated by the presence of halite crystals. Type B inclusions are single phased (all-liquid) with salinities ranging from 1.7 to 10.5 eq.wt.% NaCl. Type C inclusion fluids range from all-liquid to all-vapour with intermediate phase ratios within this range. Their salinity varies from 3.6 to 26 eq.wt.% NaCl. Type A, B, and C inclusions occur exclusively in the abundant magmatic quartz generations. The relative abundance of the three types comprises about 5%, 20%, and 10%, respectively. Type D inclusions only occur in recrystallised, small-grained quartz and are single-phased all-vapour inclusions. Although these inclusions have the greatest relative abundance, their volumetric contribution to the total of fluid inclusion is small due to their very small size.

Methods

Two drillcore sections (3.25-3.85 m and 4.57-5.06 m) from the MFE-borehole (KF0051A01) were investigated mineralogically and geochemically. Mineralogical characterisation and fluid inclusion investigations were carried out on the 4.57-5.06 m section, whereas various leaching experiments and water loss determinations were conducted on the 3.25-3.85 m section.

Note that the drillcore section when removed during drilling was erroneously waxed and wrapped in aluminium foil; the drillcore should have been first wrapped in foil and then the wax coating applied.. To safeguard against wax impregnation/contamination into the core samples, the wax and the outermost 5mm of core material were first removed. Thin and thick rock sections were prepared for conventional microscopic and fluid inclusion investigations, respectively. The remaining central part of the core was crushed and milled to a grain size of <63µ and homogenised. The material was then split into three aliquots and used for the quantification of bulk and clay mineralogy by X-ray diffractometry and for bulk chemical analyses by X-ray fluorescence. For the identification of the clay mineralogy the <2µ grain size fraction was separated by sedimentation. Water loss was determined gravimetrically on bulk samples of about 4-5cm^3 by drying at 105°C for 24h and 48h immediately after core unpacking.

Fluid inclusion petrography and microthermometry were conducted using a Linkham™ THMSG-600 heating-cooling stage equipped with a 100x objective lens at the University of Bern and Leoben. At the University of Leoben laser Raman micro-spectroscopy was performed using a Dilor LABRAM confocal-laser Raman microprobe equipped with a frequency-doubled Nd-YAG laser and a 100x objective lens. The relative abundance of fluid inclusion populations was assessed by simple point-counting methods.

Table A10-1: Samples and methods used.

Sample	Drillcore Length (m)	Purpose	Method	Laboratory
MFE-4.58	4.57-4.59	Petrography	Microscopy	Univ. Bern
MFE-4.71	4.70-4.72	Petrography	Microscopy	Univ. Bern
MFE-4.84	4.83-4.85	Petrography	Microscopy	Univ. Bern
MFE-4.82	4.58-5.05	Rock mineralogy	XRD	Univ. Bern
MFE-4.82	4.58-5.05	Rock chemistry	XRF	Univ. Bern
MFE-3.64	3.63-6.65	Water loss at 105°C	Gravimetry	Univ. Bern
MFE-3.82	3.81-3.83	Water loss at 105°C	Gravimetry	Univ. Bern
MFE-4.60	4.59-4.61	Fluid inclusions	Microthermometry, Raman spec.	Univ. Leoben
MFE-4.73	4.72-4.74	Fluid inclusions	Microthermometry	Univ. Bern
MFE-4.73	4.72-4.74	Fluid inclusions	Microthermometry, Raman spec.	Univ. Leoben
MFE-4.89	4.88-4.90	Fluid inclusions	Microthermometry, Raman spec.	Univ. Leoben

Table A10-2: Mineralogical composition of the investigated Äspö diorite (monzogranite).

Mineral	Content (wt.%)	Method
Quartz	17 ± 3	XRD
Plagioclase	40 ± 5	XRD
K-feldspar	7 ± 3	XRD
Epidote	5-10	Thin section
Biotite	5-10	Thin section
Muscovite	2-5	Thin section
Prehnite	1-4	Thin section
Calcite	1 ± 1	XRD
Accessories: sphene, zircon, apatite, opaque phases		Thin section
Clay Mineralogy (fraction	**Content (%)**	**Method**
Illite	75-85	XRD
Illite/Smectite Mixed Layers	5-15	XRD
Chlorite	5-15	XRD

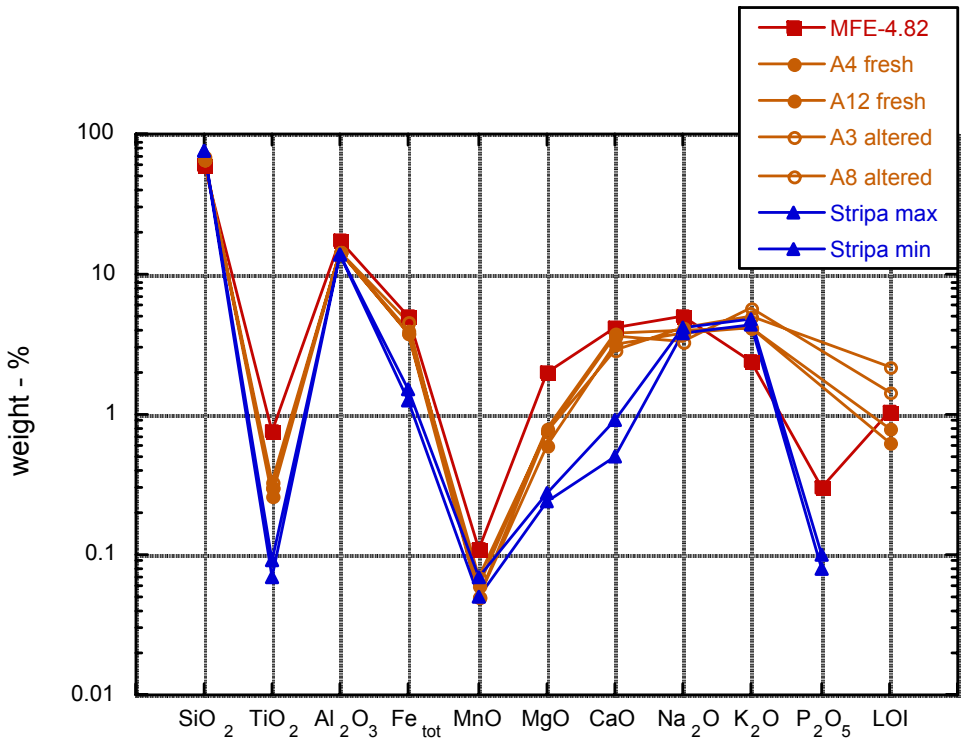

Figure A10-1: *Major element composition of sample MFE-4.82 in comparison to the compositions from other Äspö monzogranites and from the Stripa granite (Data: Äspö sample Ax from Eliasson, 1993; Stripa samples from Nordstrom et al., 1989).*

Table A10-3: Summary of fluid inclusion investigations performed on samples MFE-4.60, MFE-4.73, and MFE-4.89.

Host Mineral	Type	Phases	Solid	Hy-drate	Tn ice °C	Tm ice °C	Salinity eq.wt.% NaCl	Lab
Quartz	A	L+S+V	halite and carbonate?	NaCl			ca. 30	UniLeo
Quartz	A	L+S+V	halite + ?	NaCl			ca. 30	UniBe
Quartz	B	All-liquid		None	-55 to -65	-1 to -7	1.7 to 10.5	UniLeo
Quartz	B	All-liquid		None	-52 to -55	-5.3 to -5.8	8.2 to 8.9	UniBe
Quartz	C	L+V			-49 to -54	-2 to -20	3.4 to 26	UniLeo
Quartz	C	L+V			-37 to -58	-2.6 to -17.9	4.3 to 20.9	UniBe
Quartz	D	All-vapour						UniLeo
Quartz	D	All-vapour						UniBe

Abbr.: L = liquid, S = solid, V = vapour, Tn ice = nucleation temperauter of ice, Tm ice = final ice melting temperature; UniLeo: University of Leoben, UniBe: University of Bern

Table A10-4: Point counting estimate of the relative abundance of the inclusion types in sample MFE-4.60.

Inclusion	Phases	eq.wt% NaCl	Relative abundance
Type D	Low-density vapour		± 65%
Type B	Aqueous liquid	1.7 – 10.5	± 20%
Type C	Aqueous liquid + aqueous vapour	3.4 – 26	± 10%
Type A	Aqueous liquid + solid + vapour	approx. 30	± 5%

Figure A10-2

Äspö diorite, sample MFE-4.73: Photographs and Raman spectra of fluid inclusion Type A.

Äspö, A4-73

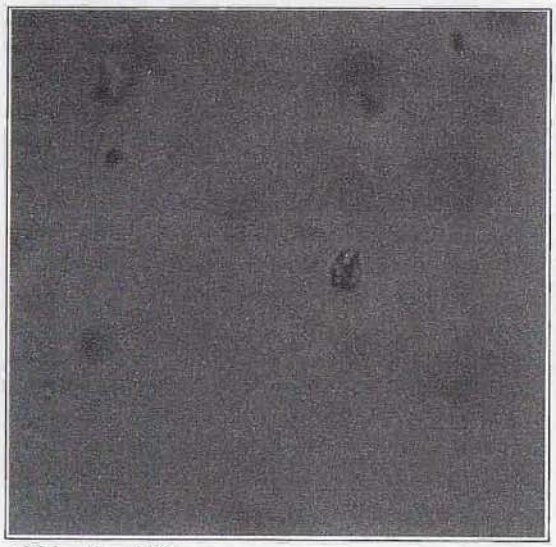

Objective 100x

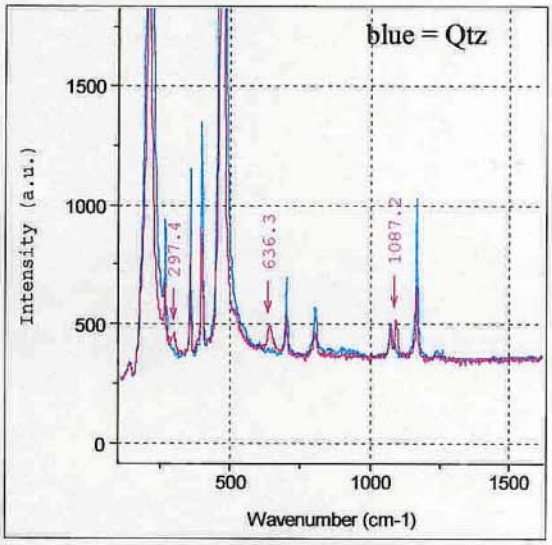

3 or 4 phase fluid inclusion: liquid + vapour + 2 daughter minerals

Moving bubble at room temperature

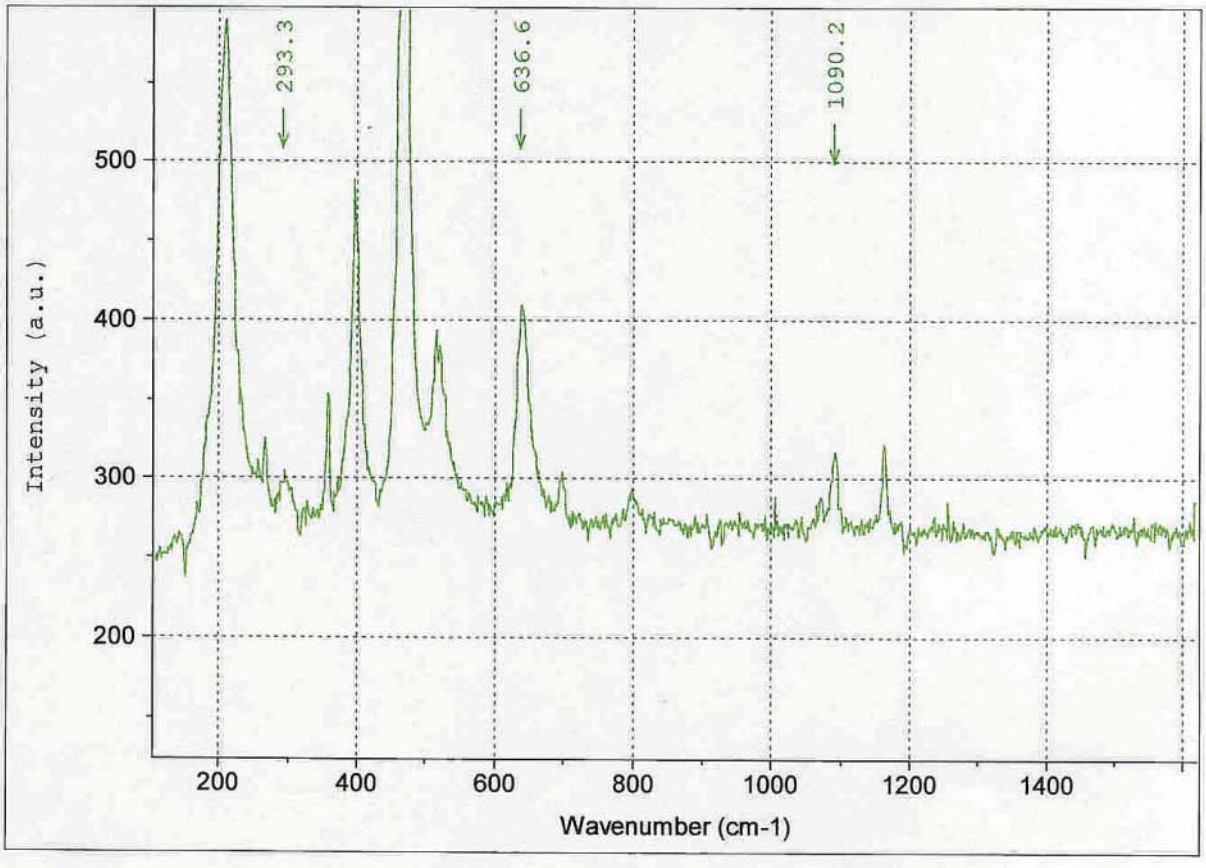

Äspö, A4-73

objective 100x

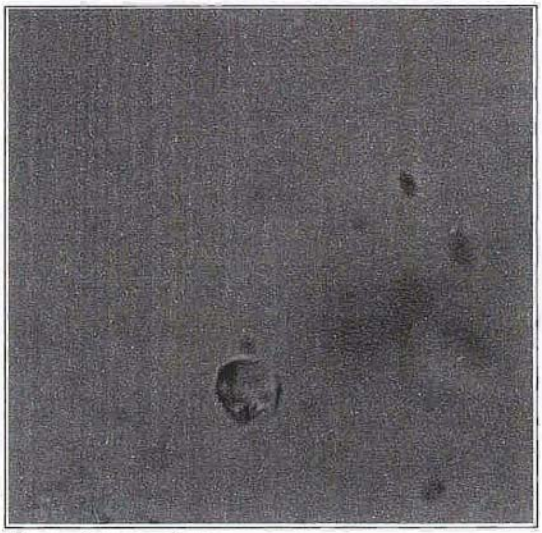

Room temperature

-40 °C

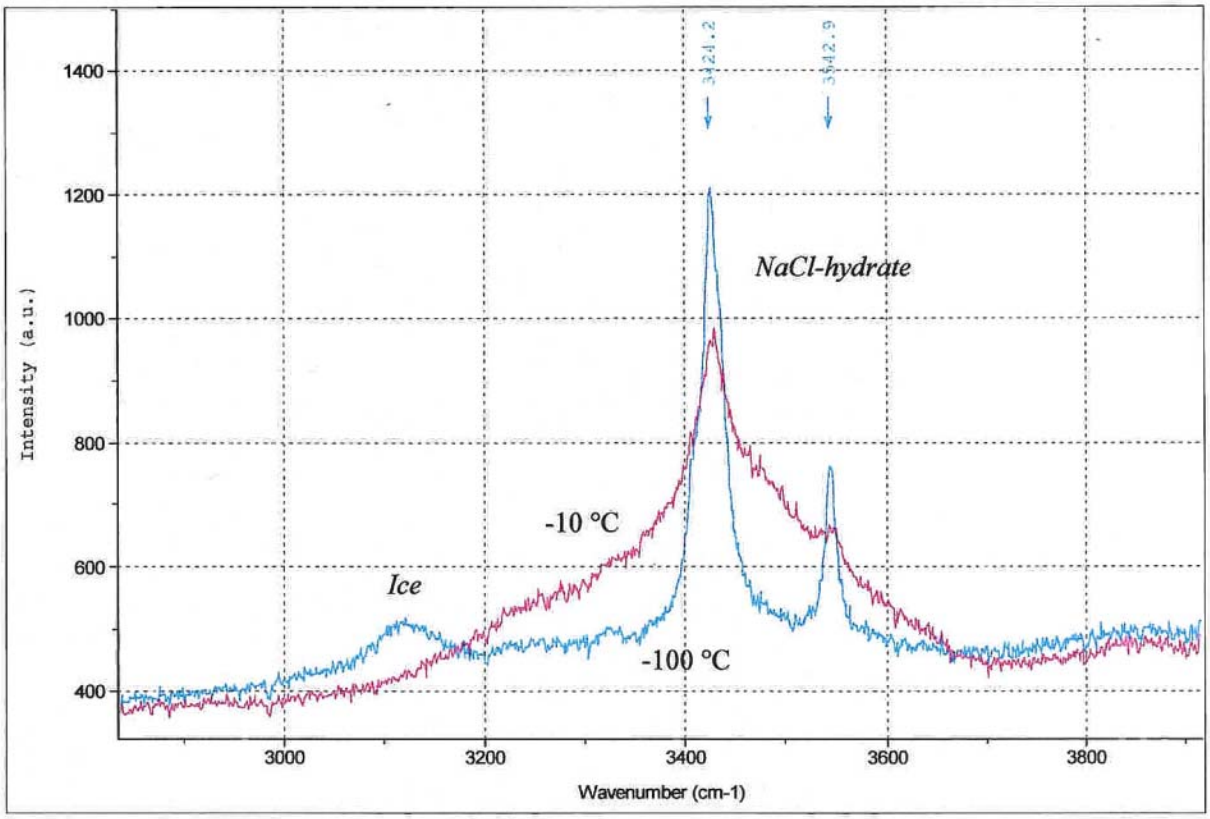

Figure A10-3

Äspö diorite, samples MFE-4.60a, b: Photograph and Raman spectra of fluid inclusion Type B.

Äspö, A4-60a

All liquid inclusion at room temperature

Tn - 61 °C

during heating: at -44 °C first melting phenomena

Tm(ice) -5.1 °C

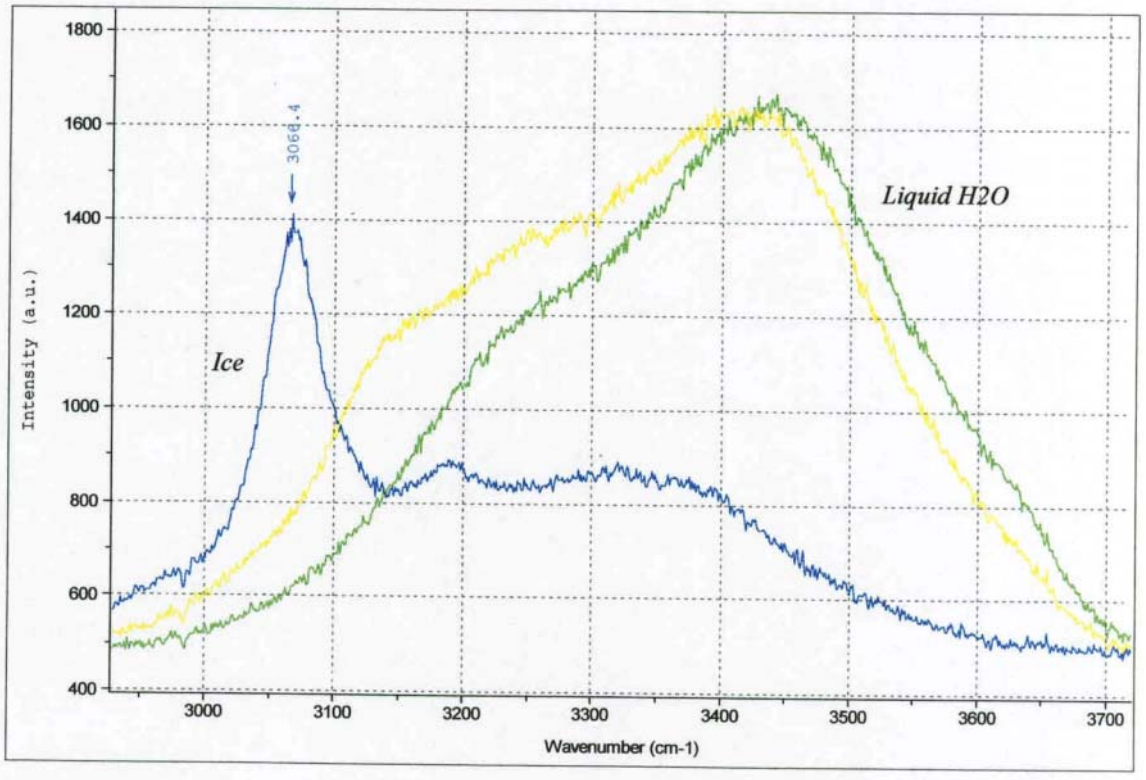

Äspö, A4-60b

Moving bubble at room temperature

Tn -47 °C (vapour remains)

Only a Raman Ice-peak

At -30°C a liquid rim appears

Tm(ice) 0.0 °C

Pure H2O?

Objective 100x

-117 °C

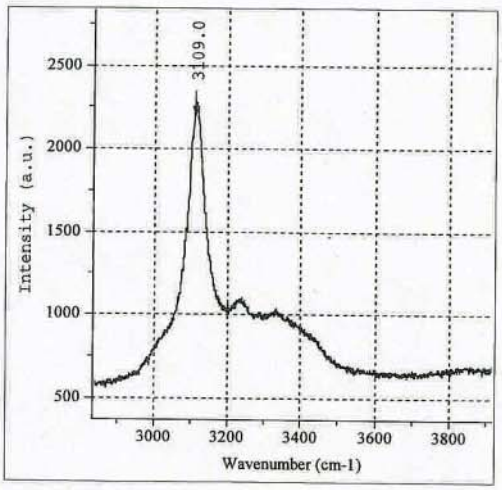

-100 °C

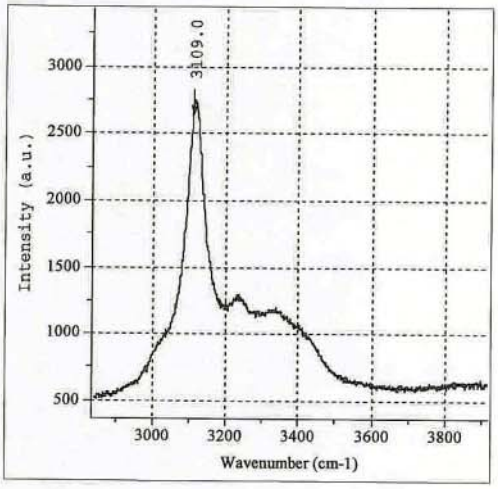

-30 °C

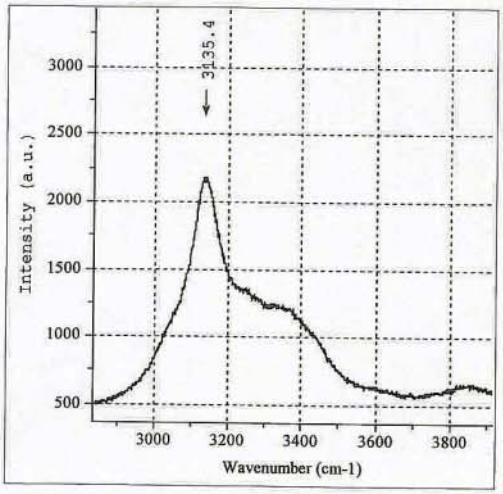

-7 °C

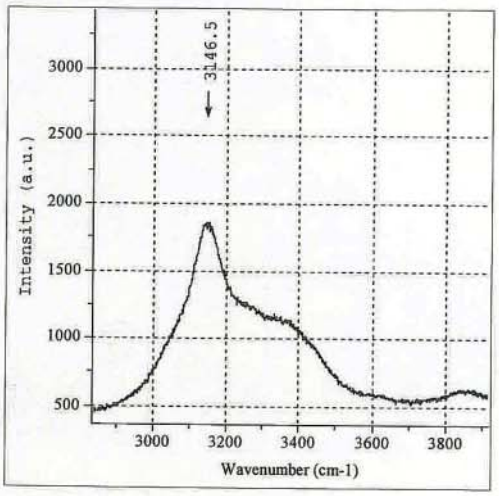

Figure A10-4

Äspö diorite, samples MFE-4.60a, b: Photograph and Raman spectra of fluid inclusion Type C.

Äspö, A4-60a

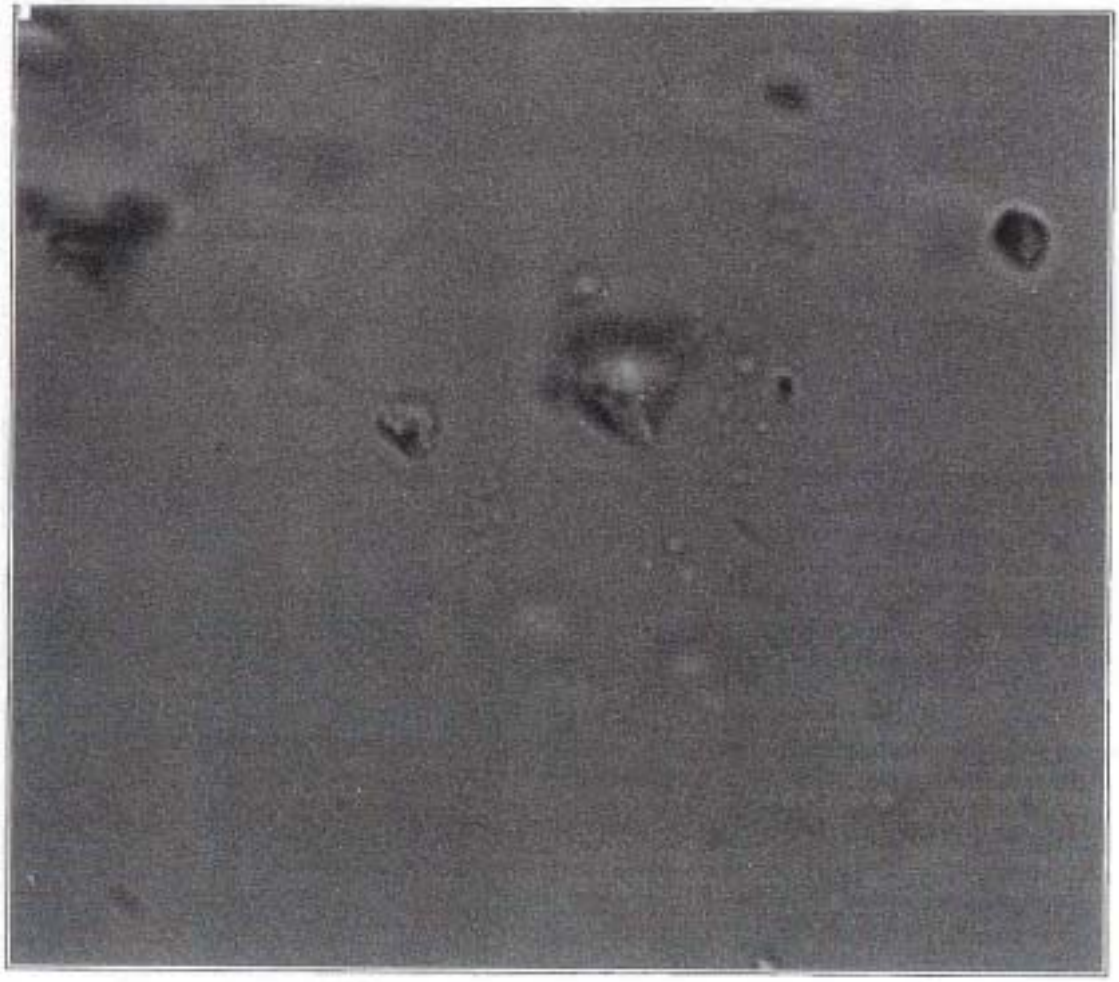

Moving bubble at room temperature objective 100x

NaCl-hydrate Raman peaks detected at lower T

Äspö, A4-60a

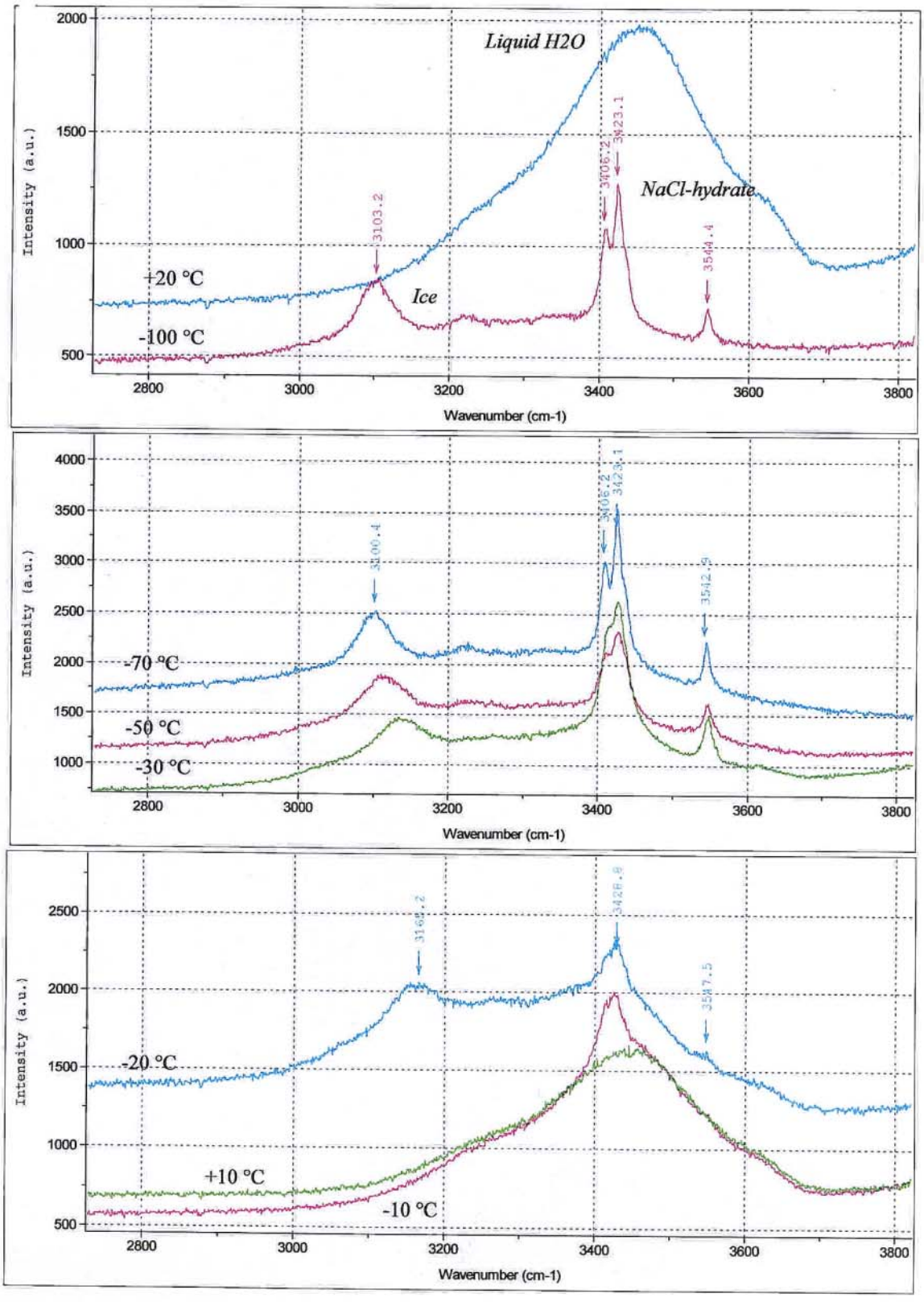
Liquid H2O
NaCl-hydrate
Ice
+20 °C
-100 °C
3103.2
3406.2
3423.1
3544.4
Intensity (a.u.)
Wavenumber (cm-1)
-70 °C
-50 °C
-30 °C
3100.4
3542.9
-20 °C
+10 °C
-10 °C
3168.2
3426.8
3547.5

Äspö, A4-60b

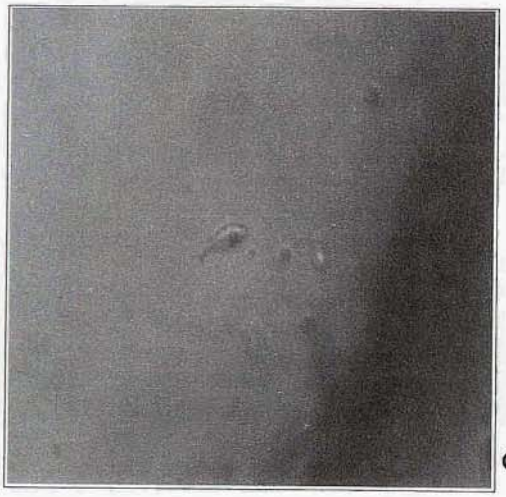

Objective 100x

Moving bubble at room temperature

Tn -45 °C
Te -23 °C
Tm(ice) -8.9 °C (in the presence of liq + vap)

Raman peak of ice at stable position (3114 cm-1) as long as liquid is not present

-100 °C

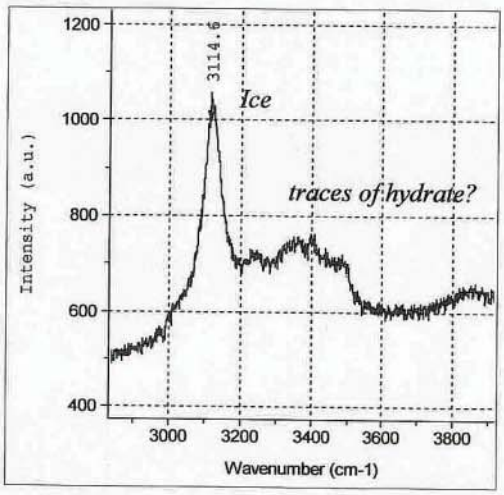

-60 °C

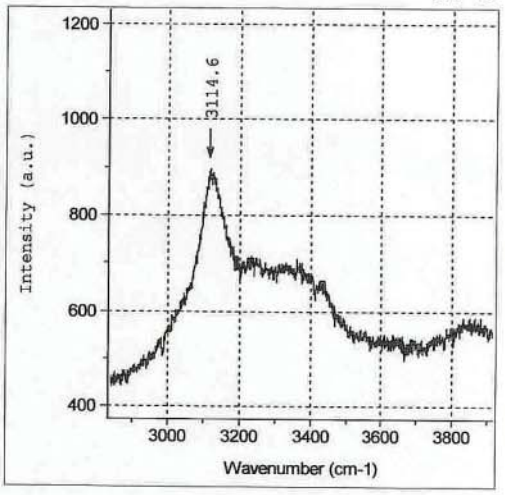

-20 °C

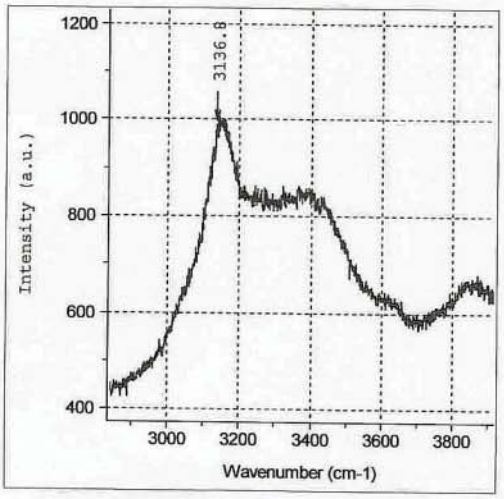

-8 °C

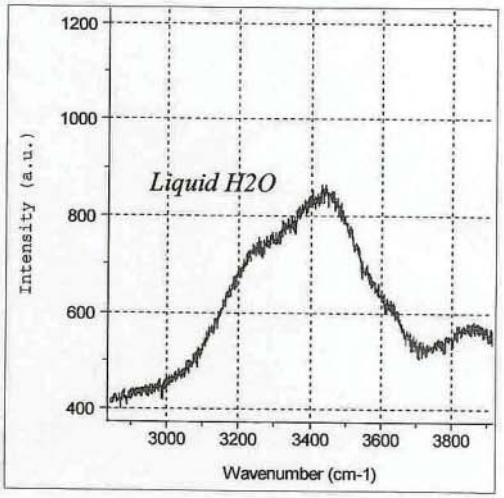

Äspö, A4-60b

Objective 100x

Moving bubble at room temperature

Bubble disappears on ice nucleation (Tn -49 °C)

Salt hydrate peaks appear on heating

At about -30 °C a liquid rim appears

Hydrate peaks are disappeared at -20 °C

Tm(ice) -10.1 °C (in the presence of liq)

Th(total) 131.1 °C
(again nucleation problems for bubble on cooling)

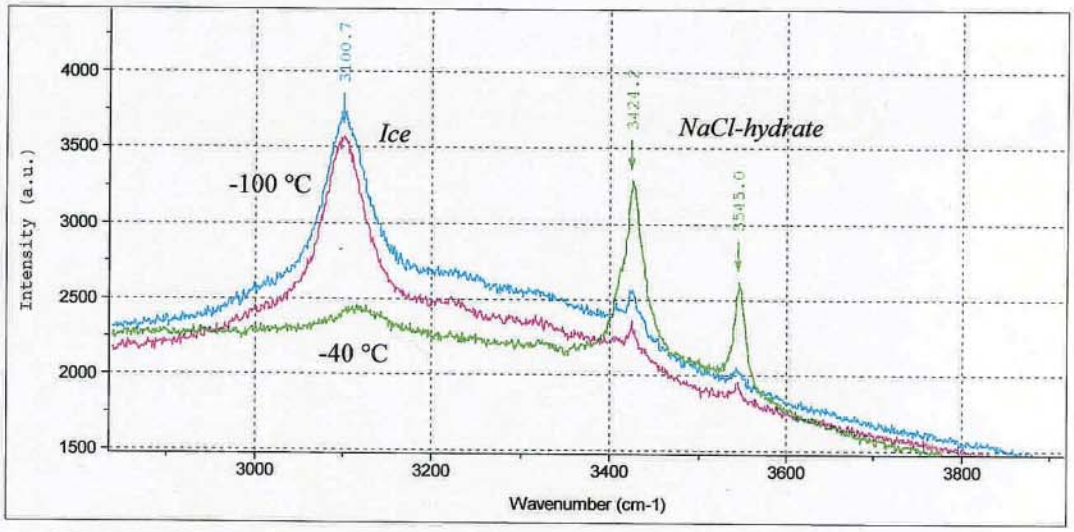

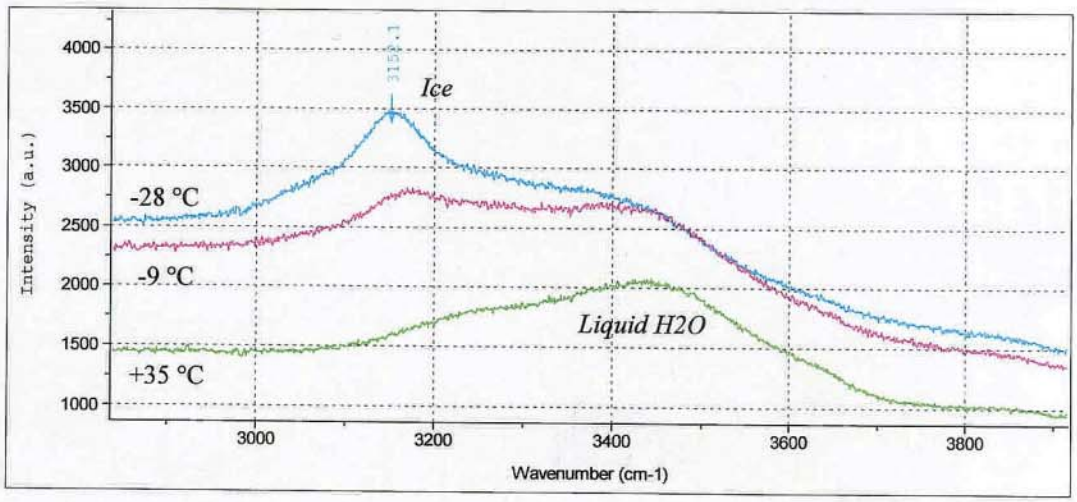

Äspö, A4-60b

first cooling cycle

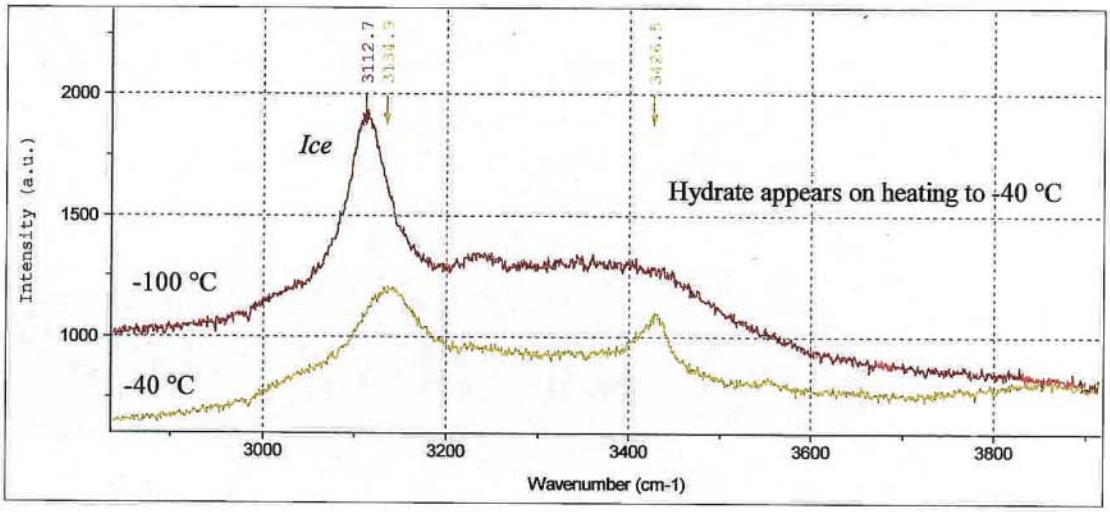

second cooling cycle

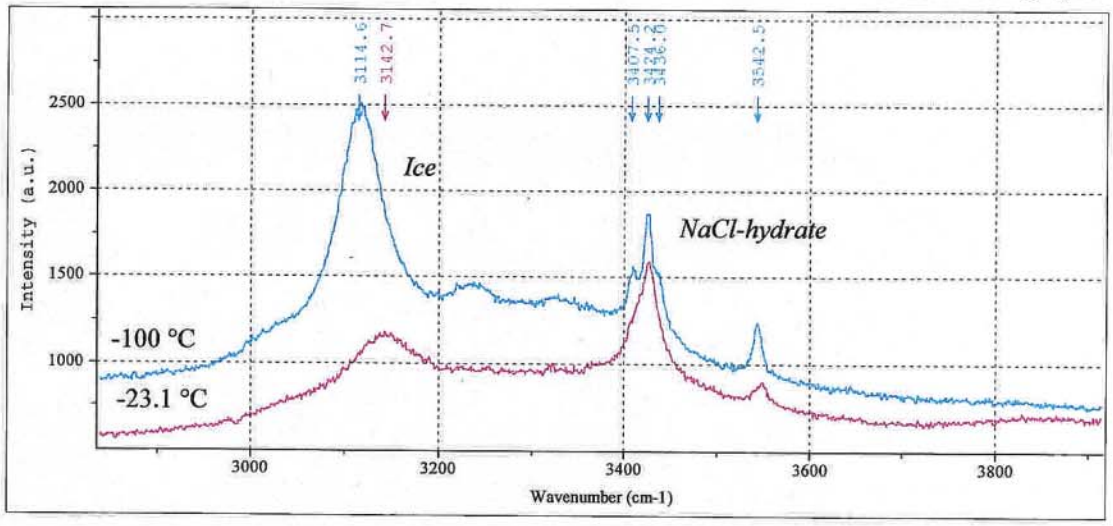

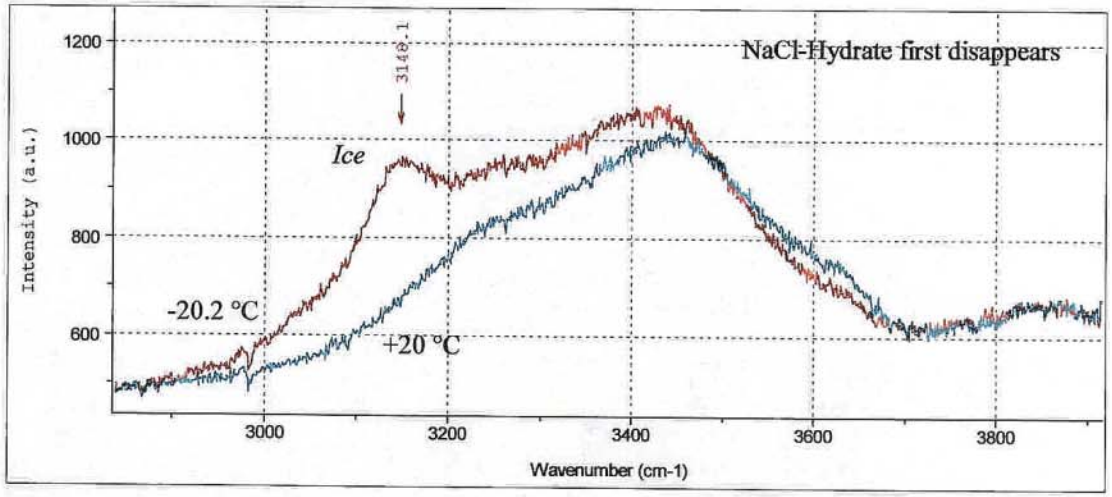

Figure A10-5

Äspö diorite, sample MFE-4.60a: Photograph of fluid inclusion Type D.

Äspö, A4-60a

One phase inclusion at room temperature (all-vapour) objective 100x

Nothing detected with Raman and Microthermometry

International Technical Document

ITD-02-04

Äspö Hard Rock Laboratory

Matrix Fluid Chemistry Experiment

Borehole KF0051A01:4 – Results from chemical and SEM/EDS analyses and porosity/density measurements

Eva-Lena Tullborg

Terralogica AB

January 2002

Summary

The Matrix Chemistry Fluid Experiment (MFE) at the Äspö Hard Rock Laboratory (HRL) is carried out within the MFE-borehole (KF 0051 A01) drilled in a very low conductive rock block at around 450 metres depth. A packer system installed in the borehole made it possible to sample "matrix fluids" from four different sections. Samples from Section 4 (and possibly Section 2) indicated possible influence from small scale fractures and for this reason a potentially open fracture identified at a core length of approx. 4 m, in the MFE-borehole, i.e. relatively close to Section 4, was investigated.

The study includes: a) determination of porosity/density of the fracture coating and wall rock, b) analyses of the chemical (and U-decay series) composition in a profile from the fracture edge and into the bedrock, and c) additional thin-section studies and SEM/EDS analyses.

The fracture coating consists of an inhomogeneous and non-continuous layer of chlorite and calcite with a maximum thickness of some hundred micrometres. The only hydrothermal alteration observed penetrating the wall rock is a somewhat increased alteration (saussuritisation) of plagioclase in the rock adjacent to the fracture edge and extending about 20 mm. Increased porosity in the fracture coating and in the bordering wall rock to a depth of some millimetres (observed as an increased frequency of parallel micro fractures) was detected. This, together with indicated recent accumulation of U ($^{234}U/^{238}U$ ratios >1) in the fracture coating sample make the fracture a probable pathway for groundwater.

Methods

Based on the BIPS-imaging log (Fig. A11-1) the drillcore was cut in slices parallel with the fracture coating so that on one side (I) of the fracture, five 3 mm thick slices and two 10 mm thick slices were prepared. On the opposite side of the fracture (II), five 10 cm thick slices were cut (cf. Fig. A11-2). Two polished thin sections, one from each side (I and II) were also made and stained with ink in order to facilitate studies of micro fractures. Material from the 3 mm and 10 mm thick slices (side I) were crushed and milled in an agate mortar for chemical analyses.

Water saturation measurements (connected porosities) and bulk density determinations have been carried out at the Swedish Research and Testing Institute in Borås. The same methods were used as for the previously measured whole-rock samples of fresh Äspö diorite and Ävrö granite from the MFE-borehole (Tullborg, 2001). For comparison both 1 cm slices from side II and 3 mm slices from side I were measured (Table A11-1).

Two thin sections were studied by transmissive light microscopy and SEM-EDS (Scanning electron microscopy with an energy dispersive system).

Major and trace element analyses and determination of $^{234}U/^{238}U$ ratios have been carried out at SGAB Analytica, Luleå using ICP- MS and ICP-AES.

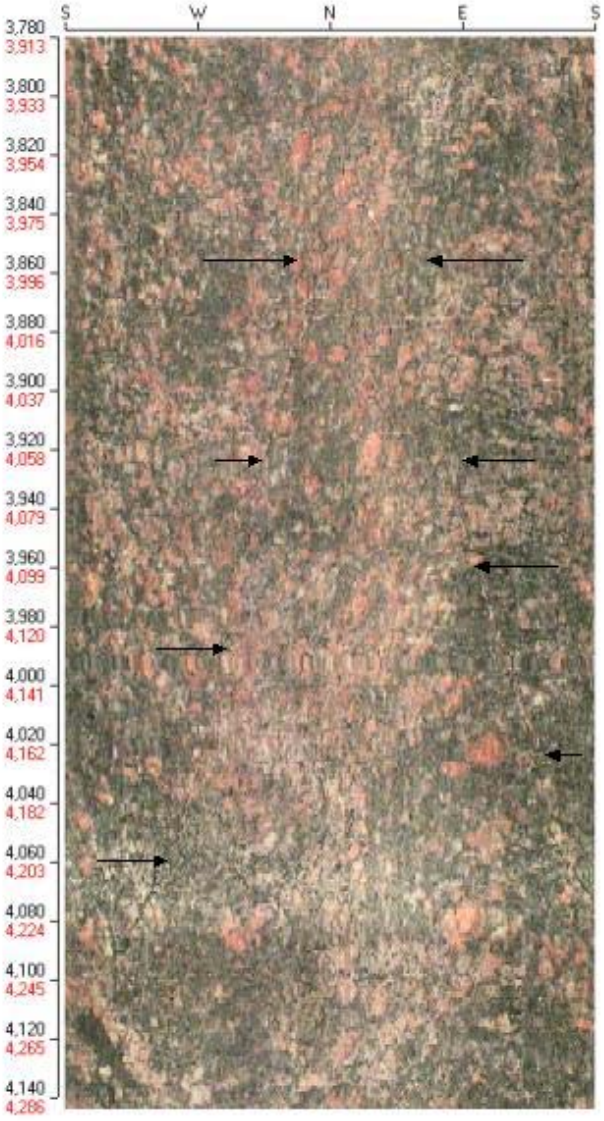

Figure A11-1: *BIPS (Borehole Image Processing System) image log covering the interval 3.9 m to 4.3 in the MFE-borehole. Arrows indicate the fracture intercept with the borehole. Note the heterogeneous character of the wall rock.*

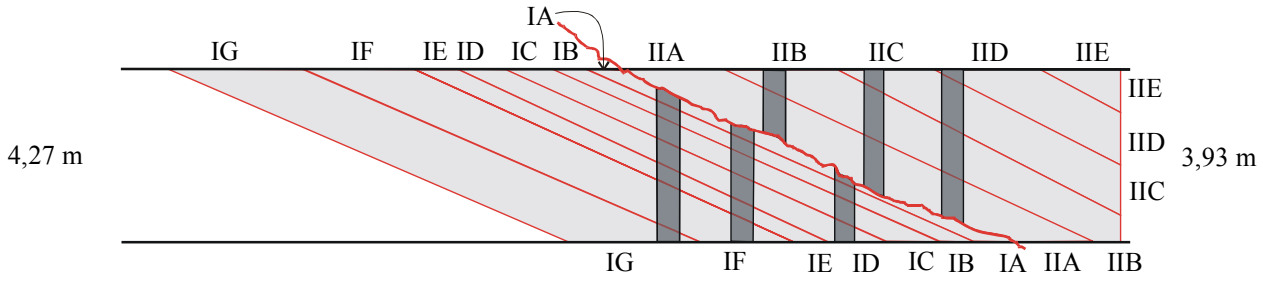

Figure A11-2: *Diagram showing sectioning of the core and the labelling of the different slices studied. (Grey areas = missing parts).*

Table A11-1: Porosity (water saturation) and bulk density of wall rock samples adjacent to the fracture at 4 m in the MFE-borehole (sample numbers corresonpd to those given in Figure A11-2).

Sample	Weight (g)	Distance to fracture edge (cm)	Density (kg/m^3)	Connected porosity vol.% (water saturation)
IIA 10 mm	35.29	0.5	2698	0.61
IIB 10 mm	42.78	1.5	2663	0.44
IIC 10 mm	53.77	2.5	2674	0.35
IID 10 mm	45.77	3.5	2682	0.35
IIE 10 mm	25.06	4.5	2685	0.43
IA 3 mm	14.46	0.15	2664	0.92
IB 3 mm	14.89	0.65	2675	0.54
IC 3 mm	7.42	1.15	2647	0.36
IDa 3 mm	15.19	1.65	2784	0.55
IDb 3 mm	6.93	1.65	2683	0.39
IE 3 mm	6.71	2.25	2681	0.8

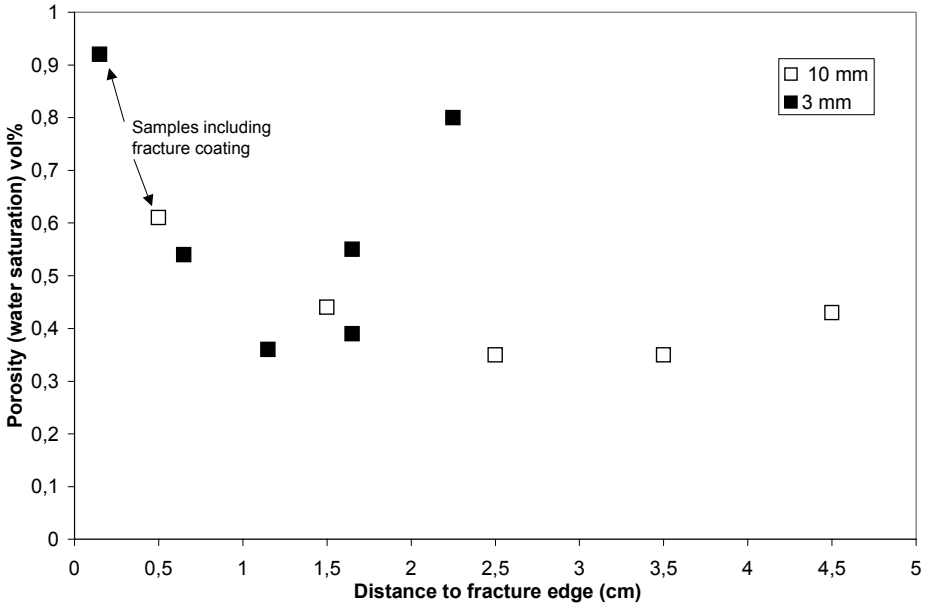

Figure A11-3: *Connected porosity (water saturation) in volume % plotted versus distance from fracture edge (MFE-borehole: 4 m).*

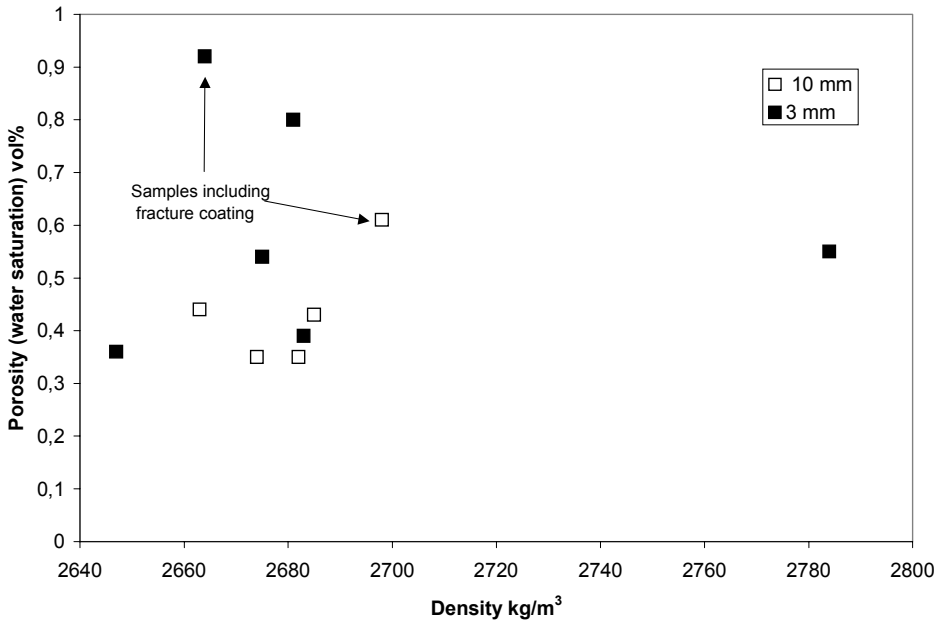

Figure A11-4: *Density versus porosity for wall rock samples (MFE-borehole: 4m). Note the larger variation in density as well as in porosity values for the thin (3 mm) samples.*

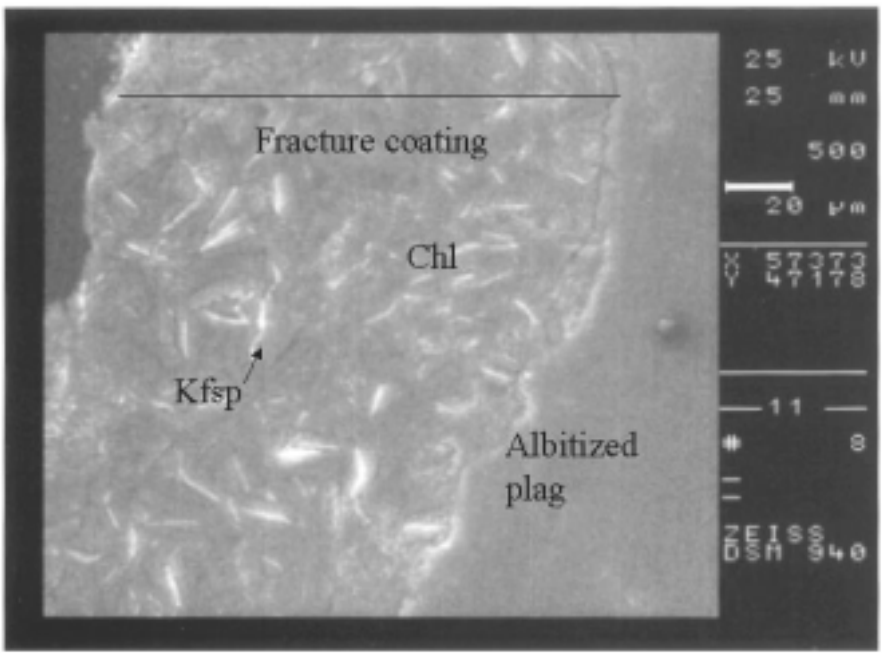

II KF0051 A01:4,3 m SEM/EDS photo

Figure A11-5: *SEM photo showing part of the fracture coating adjacent wall rock; MFE-borehole: 4 m. Scale bar to the right.*

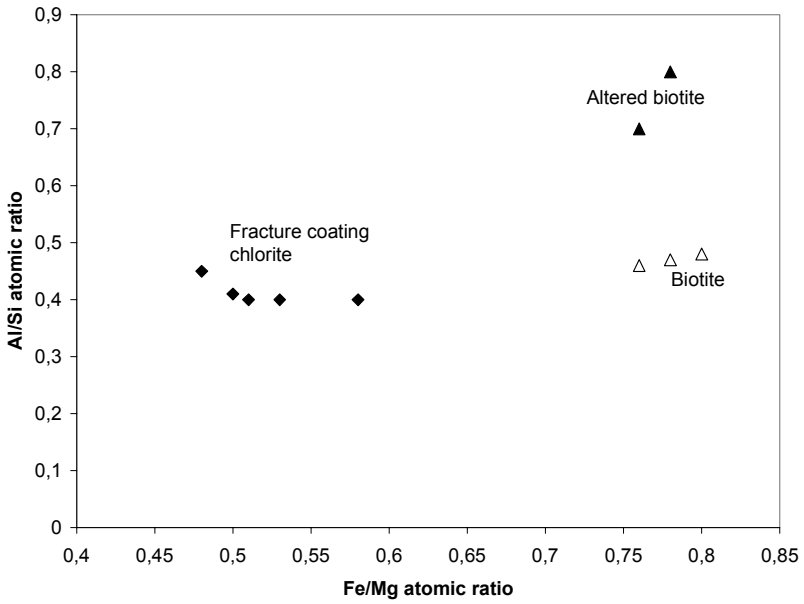

Figure A11-6: *Al/Si atomic ratio versus Fe/Mg atomic ratio for fracture coating chlorite, wall rock biotite and fresh biotite from other sites at Äspö (open triangles) and altered biotite (chloritisation; closed triangles) along the fracture. (Analyses carried out using SEM/EDS; MFE-borehole: 4 m).*

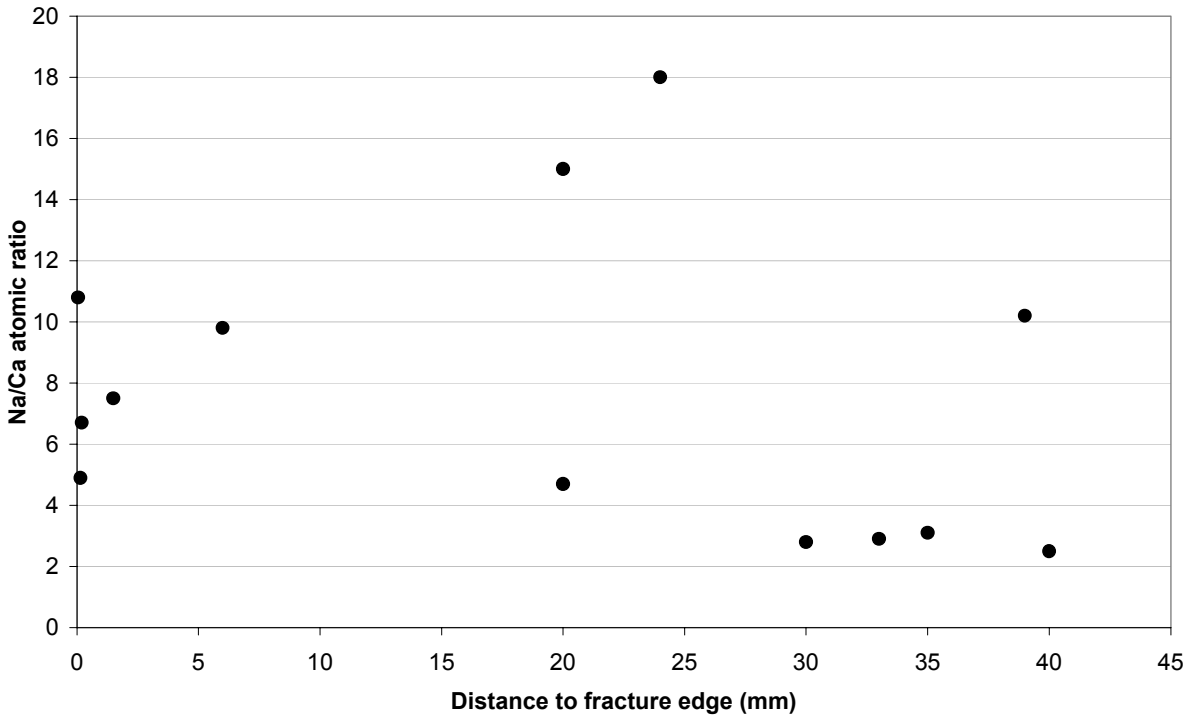

Figure A11-7: *Na/Ca atomic ratio in plagioclase versus distance to fracture edge. Fresh Äspö diorite/Ävrö granite usually show values between 2.5 to 3.0 Na/Ca atomic ratio (oligoclase).*

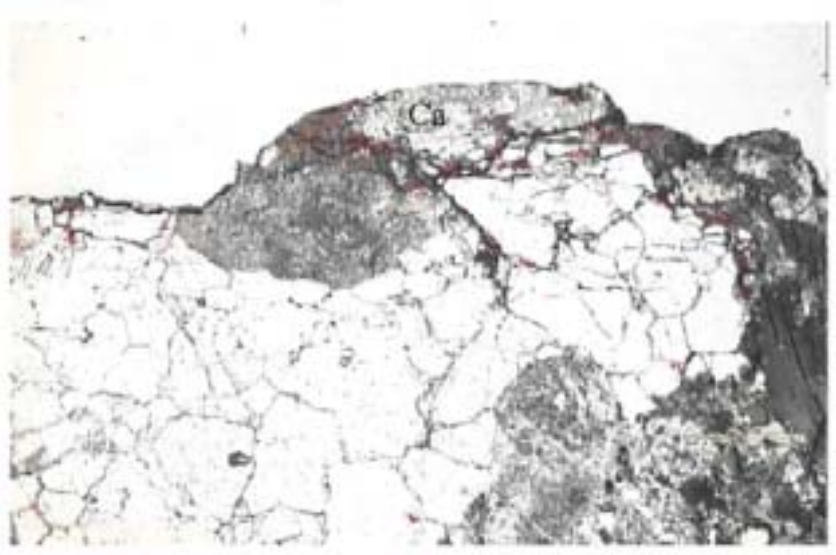

Figure A11-8: *Fracture coating and wall rock dyed with red ink (I KF0051A01:4.1 m). Note the increased microfracture frequency parallel with the fracture surface. The length of the photomicrograph corresponds to 1.25 mm.*

Figure A11-9: *Fracture coating and wall rock dyed with red ink (KF0051 A01:4.03 m). Note the connected microfractures perpendicular to the fracture surface. The length of the photomicrograph corresponds to 5.0 mm.*

Table A11-2: Chemical analyses of fracture coating and wall rock at 4m in the MFE-borehole (sample numbers correspond to those in Fig. A11-2).

Major Elements		4m I	IA	IB	IC	ID	IE	IF	IG
		Coating	Wall rock	Wall rock	Wall rock	Wall rock	Wall rock	Wall rock	Wall rock
SiO_2	% TS	39,3	65,4	68,4	68,7	69	68,9	66,2	66,3
Al_2O_3	% TS	9,7	16,1	16	16,1	15,3	15,4	15,1	15
CaO	% TS	8,79	2,97	2,73	2,75	2,65	2,46	3,26	3,1
Fe_2O_3	% TS	13,5	3,42	2,99	2,91	3	2,76	3,8	3,89
K_2O	% TS	2,84	4,16	3,68	3,82	3,76	4,16	3,36	3,31
MgO	% TS	10,4	1,45	1,16	1,11	1,05	0,99	1,5	1,66
MnO_2	% TS	0,222	0,0872	0,0771	0,0746	0,0728	0,0677	0,1	0,103
Na_2O	% TS	0,713	4,61	4,68	4,69	4,52	4,49	4,59	4,23
P_2O_5	% TS	0,0965	0,202	0,203	0,182	0,206	0,188	0,27	0,27
TiO_2	% TS	0,131	0,455	0,409	0,496	0,409	0,468	0,645	0,598
LOI	% TS		1,3	0,9	0,9	0,8	0,8	0,9	1
Tot	% TS	85,7	98,9	100,3	100,8	100	99,9	98,8	98,5
Trace Elements									
Ba	ppm	563	1420	1250	1110	1070	1210	864	789
Be	ppm	0,677	2,62	2,89	3,05	2,89	2,74	2,86	3,31
Co	ppm	19	8,85	<5	6,63	<5	<6	8,13	6,4
Cr	ppm	705	30,6	15,8	17,2	14,3	13,1	46,2	13,2
Cs	ppm	3,57	1,56	1,58	1,56	1,25	1,27	1,54	2,22
Cu	ppm	<7	<5	9,1	<6	84,2	104	13,4	13,1
Ga	ppm	15,7	20,6	18,4	23,2	16,8	22	17,7	18,7
Hf	ppm	1,8	3,29	4	3,52	3,8	4,56	4,79	4,85
Mo	ppm	<3	<2	3,49	3,16	2,24	<2	3,85	<2
Nb	ppm	2,83	8,61	7,3	11,1	8,07	11,4	13,3	11,9
Ni	ppm	33,2	<10	11,1	<10	12	<10	28,7	17,8
Rb	ppm	243	88,7	80	83,4	79,9	86,2	80,7	100
Sc	ppm	2,46	5,48	4,45	4,11	3,59	3,67	7,28	5,8
Sn	ppm	2,4	1,4	2,44	3,24	3,04	3,71	2,82	31,7
Sr	ppm	162	710	771	766	720	680	820	794
Ta	ppm	0,146	0,829	0,696	1,04	0,838	1,17	1,79	1,29
Th	ppm	10,8	16,9	12,9	23,3	14,8	12,9	6,01	25,5
U	ppm	1,81	4,67	2,91	5,68	5,57	4,4	2,39	3,87
V	ppm	22,1	43,5	38,8	40,5	39,7	36,9	52,8	48,5
W	ppm	<0,4	<0,3	0,4	0,81	0,547	0,504	0,766	1,22
Y	ppm	3,84	16,8	14,9	19,4	16	18,5	27,4	29,6
Zn	ppm	131	57,1	56,5	58,3	52,8	56,4	74,9	82,9
Zr	ppm	61,4	178	191	172	181	207	271	219

Table A11-2: ***continued***

Rare Earth Elements		4m I	IA	IB	IC	ID	IE	IF	IG
		Coating	Wall rock	Wall rock	Wall rock	Wall rock	Wall rock	Wall rock	Wall rock
La	ppm	253	48,9	34,9	31,9	33,7	33,2	25,8	114
Ce	ppm	315	81,4	59,6	59,3	56	76,7	51,7	159
Pr	ppm	24,7	9,24	6,74	8,25	6,89	10,2	8,13	15,6
Nd	ppm	77,8	34,6	25,4	32,5	26,3	41,7	29,9	51,5
Sm	ppm	4,59	4,14	3,72	5,65	4,2	6,71	4,83	6,91
Eu	ppm	0,297	1,01	1,03	0,228	0,928	0,38	1,27	0,559
Gd	ppm	2,22	2,73	2,39	3,66	2,9	4,41	3,76	5,18
Tb	ppm	0,177	0,36	0,343	0,442	0,38	0,693	0,497	0,859
Dy	ppm	0,651	2,19	2,15	2,83	1,99	3,81	2,79	3,42
Ho	ppm	<0,08	0,477	0,389	0,608	0,488	0,751	0,643	0,919
Er	ppm	0,31	0,884	0,716	1,53	1,25	1,65	1,61	1,95
Tm	ppm	<0,1	0,263	0,267	0,293	0,303	0,396	0,311	0,519
Yb	ppm	0,315	1,76	1,63	1,78	1,7	2,2	1,77	2,21
Lu	ppm	0,0416	0,228	0,193	0,276	0,233	0,338	0,315	0,388

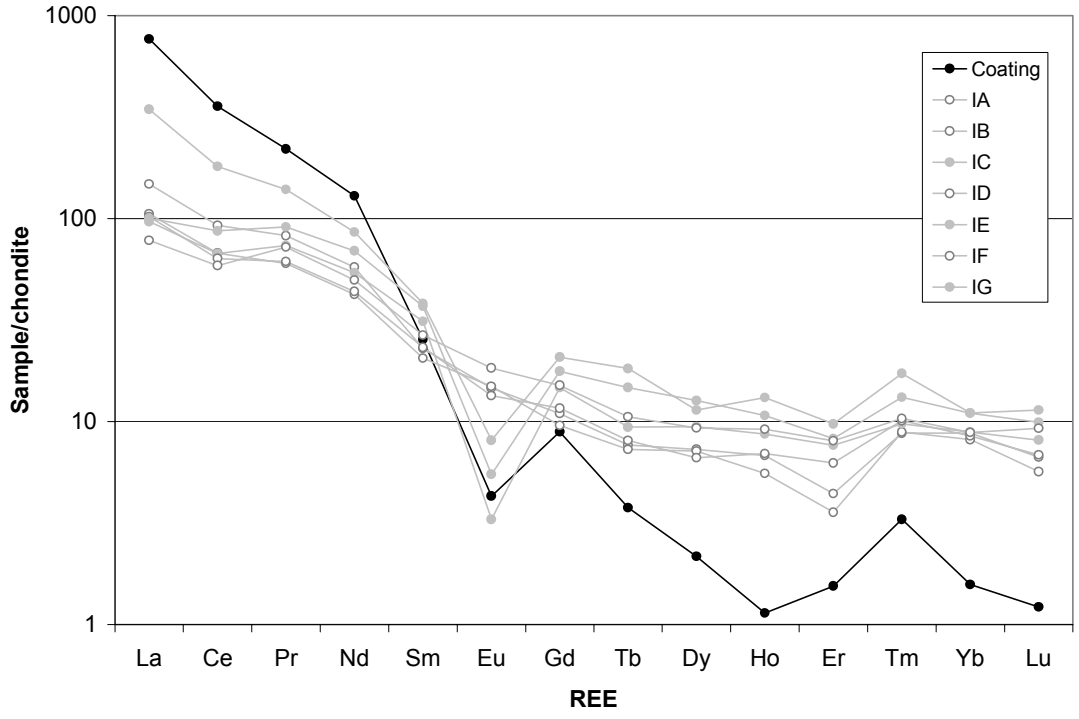

Figure A11-10: *Chondrite-normalised patterns of REEs in fracture coating and adjacent wall rock samples (MFE-borehole: 4m)*

Table A11-3: Uranium isotope ratios measured using ICP mass spectrometer and activity ratios calculated using λ values given below.

Sample	$^{238}U/^{234}U$ atomic ratio	$^{238}U/^{234}U$ activity ratio	$^{234}U/^{238}U$ activity ratio
MFE-borehole :4m	15387	0,843	1,19
MFE-borehole :4m IA	18440	1,001	0,990
MFE-borehole :4m IB	19150	1,049	0,953
MFE-borehole :4m IC	18250	0,999	1,000
MFE-borehole :4m ID	18250	0,999	1,000
MFE-borehole :4m IE	17900	0,980	1,020
MFE-borehole :4m IF	18410	1,008	0,998
MFE-borehole :4m IG	18625	1,021	0,980

λ ^{234}U = 2.8057E-06; λ ^{238}U = 1,537E-10; Decay constant ratio $^{238}U/^{234}U$ = 5.4768 E-05

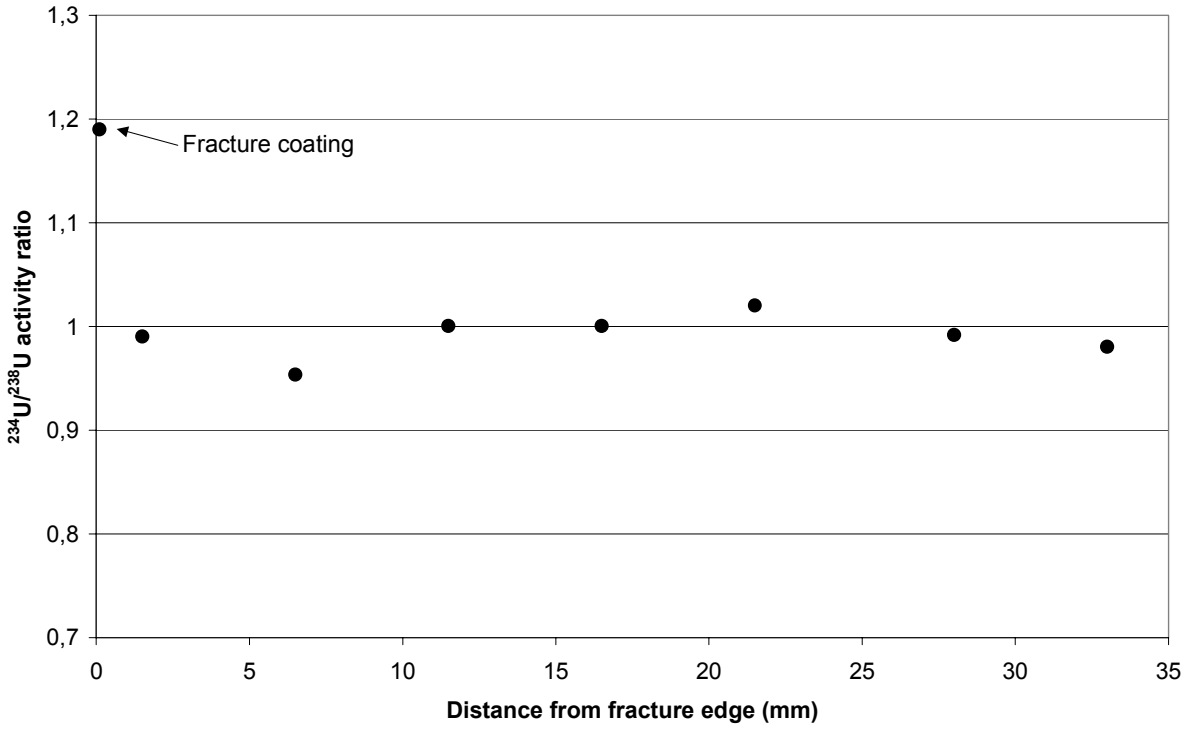

Figure A11-11: *$^{234}U/^{238}U$ activity ratio calculated from atomic ratios measured with mass spectrometry for samples from the fracture coating and adjacent wall rock to the fracture at approx. 4 m core length in the MFE-borehole.*

Technical Document

TD-02-13

Djupförvarsteknik

Matrix Fluid Chemistry Experiment

Textural, microthermometry and Lacer Ablation ICP-MS investigations of fluid inclusions in drillcore KF0051A01 (5.03–10.95 m)

Seppo Gehör
Kivitieto Oy

Sten Lindblom
Stockholm University

March 2002

Summary

This study on the chemical and textural characteristics of fluid inclusions in the Äspö diorite and Ävrö granite forms part of the Matrix Fluid Chemical Experiment (MFE) carried out at the Äspö Hard Rock Laboratory (HRL).

Ten samples were selected from the MFE-borehole (KF0051A01) from 5.05-10.95 m along the drillcore. The investigative methods used included analysis of the textural relationships of the fluid inclusion patterns and the chemical composition of the fluid inclusions. The analytical work has been carried out by microthermometry, Laser ablation ICP-MS and Raman spectrometry.

Textural evidence shows a major set of microfractures propagated in an approximately east-west direction indicating pressure from the north to northwest. A large percentage of the fluid inclusions are very small (< 2 µm) and many of these contain only gas. The average size of the fluid inclusions is estimated to be 5 µm in diameter, suggesting that 1 vol. % fluid is present in the quartz. Considering the modal proportion of quartz to be 30 %, the content of fluid is estimated to be about 0.3 vol. % in the rock as a whole.

The fluid inclusions are divided into five groups: *Group I* is composed of inclusions which follow trails in primary quartz; their salinity ranges from 19 to 24 eq. wt.% NaCl. *Group II* is defined by the grain boundary inclusions in recrystallised quartz. The size of these inclusions varies from 3 to 25 µm and the range of salinity is from14 to 23 eq. wt.% NaCl. *Group III* types, size 5 to 45 µm, comprise three-phase fluid inclusions containing calcite or halite. *Group IV* fluid inclusions occur in grain boundaries and their size is less than 2 µm; they are either empty or contain CO_2. *Group V* fluid inclusions are secondary and occur in crosscutting trails. According to their orientation these are subdivided into: a) pervasive, E-W-oriented fluid inclusions; these represent the majority of high salinity inclusions. b) randomly orientated, intragranular fluid inclusions with a salinity of 3.3 to 14 eq. wt.% NaCl, c) WSW–ENE-orientated fluid inclusions, comparable to (a), and d) WNW-ESE orientated fluid inclusions, comparable to (a) but less pervasive.

The Laser Ablation ICP-MS study demonstrates that the dominant fluid inclusion population belongs to the H_2O-NaCl-$CaCl_2$-CO_2 system; the data suggest also a probable incidence of $MgCl_2$ in solution. Na is usually the overwhelming component in solution but the others are frequent. Na has been detected in both high and low salinity inclusions whereas Ca has been found only in very high salinity inclusions. The concentrations of aluminium, alkaline and alkaline rare-earth elements are found to be higher in inclusions within the intercrystalline spaces and trails in comparison to intracrystalline fluid inclusion clusters. The analytical data imply the occurrence of ^{88}Sr and ^{138}Ba in significant amounts in inclusion trails as well as within intercrystalline spaces and coatings. The rather pronounced fluctuation of ^{29}Si suggests that Si could act as a proxy for possibly CO, thus reflecting occurrences of CO_2 gas inclusions. An analysis of a fluid inclusion from the intercrystalline space suggests the presence of Pb and La in measurable concentrations.

Methods

Polished sections (approximately 0.2 mm in thickness) were prepared for microthermometry and laser-ablation studies. The microthermometric analyses were performed using a Fluid Inc. Gas-flow Heating-freezing Stage at Oulu University. The laser-ablation (LA) ICP-MS work was carried out at Åbo Akademi, Turku, using a LSX-200, CETAC Technologies Inc. instrument, and the ICP-MS analyses used for chemical analysis was an Elan 6000, Perkin Elmer Sciex. The diameter of the ablation crater burned by the laser beam was adjusted to 20 μm. The observed pulse intensities of the selected elements give a qualitative relationship of the respective abundance of the elements and their isotopes, but attempts to achieve quantitative analysis were not performed.

Volume of fluid inclusions

The volume of average sized fluid inclusions was estimated by counting and measuring the inclusions in the samples and by performing a set of basic calculations. First the volume of fluid inclusions with different diameters (assuming a sphere-shape) was estimated. Then the volume of the minerals hosting the inclusions was taken as the field of view area multiplied by the average diameter of the inclusions. From this a number was derived for the counted inclusions in order to calculate the volumes and relative volumes.

Counting inclusions in several hundred fields of view, going step-wise down through the thin section, was time consuming but yielded a statistical spread of inclusion occurrence.

Laser ablation ICP-MS-techniques (LA-ICP-MS)

The LA-ICP-MS technique used in this study is the conventional quadruple-mass spectrometry. The method is based on the principle that material (solid or solution) is ablated for analysis using a laser beam, which can be adjusted from microns to tens of microns in diameter. The analysis is carried out under argon gas in a mass spectrometer. The laser beam is capable of extracting a sample at any depth from the polished section and, furthermore, it is possible to control the beam in horizontal and vertical directions. The initial target can be located using an optical microscope or video camera and the course of extraction/analysis is possible to follow on a video monitor.

Not only does this method provide high sensitivity and low detection limits for single fluid inclusion studies, but it is effective also in determining the compositional variation of selected areas by scanning, thus creating a contour map of the chemical composition of the demarcated area. However, such techniques are still the subject of rapid development and that used in this study involves analytical restrictions that concern some of the elements and isotopes of present interest. For example, the method itself does not provide absolute element abundance; instead the output is received as a pulse count from which the abundance in the fluid inclusions is possible to estimate over a relative scale when the volume of the ablated material is known. To conduct quantitative analyses was not within the scope of this study.

For fluid inclusion analysis the detection limit ranges from 10 to 1000 ppm in a 20 µm diameter inclusion. The limit of detection is dependent on the size of the fluid inclusion, the concentration of elements and on the physico-chemical characters of the element in question. According to the microthermometric analyses the samples of the present study have moderate to low salinity which, combined with the small size of the inclusions, results in moderate to weak signals. Under these circumstances the method lacks sensitivity for analysing, in particular, light anions, which are known to constitute an important fraction of the salinity contained in the inclusions.

Similarly, the elements like sulphur and carbon, constituting the molecular groups in the fluid inclusions, are in several cases not possible to analyse due to their small quantities in the fluid inclusions. On the other hand, detection of some of the essential cations in fluid inclusions, such as potassium, may be masked by high background noise, as their concentration seems to remain substantially low in the fluid inclusions studied.

Furthermore, the carrier gas, argon, in the laser-ablation configuration easily reacts in certain circumstances, depending on the elements extracted from the sample. These and several other polyatomic derivatives produced in the course of laser-ablation are capable of creating interference effects due to the isotonic overlapping for certain compounds.

The area analysed by the laser-ablation is in practice controlled by means of a signal passing through the video camera. However, despite the rapid improvement of these assemblies, the resolution was not always good enough to detect the tiniest fluid inclusions. In the course of study the resolution of the equipment used was improved by up-grading the software for laser-ablation and the camera, and by modification of the illumination.

Due to technical reasons a 20 µm ablation crater diameter was used for laser ablation. This size exceeds, in most of the cases, the size of fluid inclusions and has resulted in a significant fraction of host mineral being ablated with the fluid. When the host material (i.e. calcite, albite, clay minerals, iron oxides, sulphides etc.) is composed of many tiny mineral inclusions, the ablated material is a blend of all these sources.

Table A12-1: List of samples from the MFE-borehole selected for microthermometry and ICP-MS investigations. The direction of double polished thin sections is given in column "d.p.s.", where the number after the colon gives the direction: 1 = horizontal plane, 2 = vertical plane, and 3 = plane perpendicular to longitudinal axis of drillcore.

No	Sample	Section	d.p.s	Host Rock
1	***MFE-5.03***	5.03-5.08	1:1, 1:2	Äspö diorite
2	***MFE-5.42***	5.42-5.42	2:1, 2:2	Äspö diorite
3	***MFE-6.43***	6.43-6.48	3:1	Äspö diorite
4	***MFE-7.81***	7.81-7.85	4:1, 4:2	Äspö diorite
5	***MFE-8.40***	8.40-8.44	5:1	Ävrö granite
6	***MFE-8.84***	8.84-8.89	6:1, 6:2, 6:3	Ävrö granite
7	***MFE-9.11***	9.11-9.17	7:1, 7:2	Ävrö granite
8	***MFE-9.85***	9.85-9.90	8:1	Ävrö granite
9	***MFE-10.51***	10.51-10.57	9:1, 9:2, 9:3	Ävrö granite
10	***MFE-10.90***	10.90-10.95	10:1, 10:2	Ävrö granite

General textural and microstructural setting of the fluid inclusions

Table A12-2: Grain size of recrystallised quartz.

Sample	Sample Section	Size Range µm	Mean Size µm
MFE-4.11	2:1x	50-350	170
MFE-7.81	4:+	50-300	150
MFE-8.84	6:1	80-260	180
MFE-10.51	9:1	75-200	110

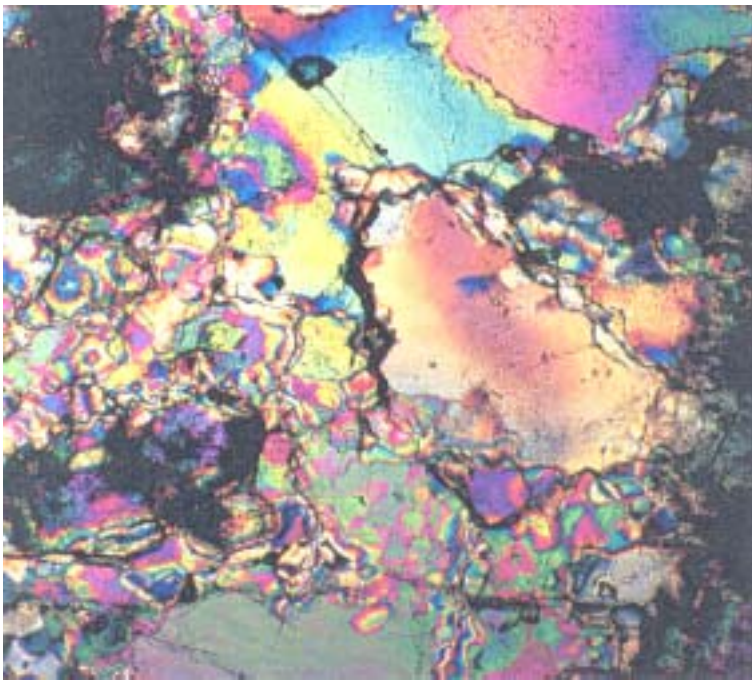

6:3

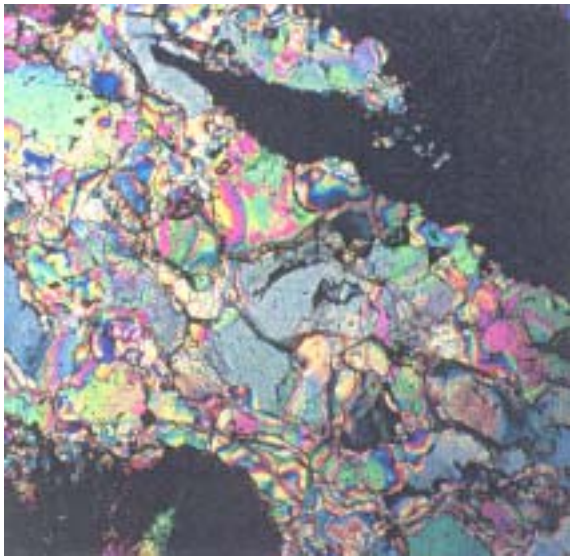

6:1

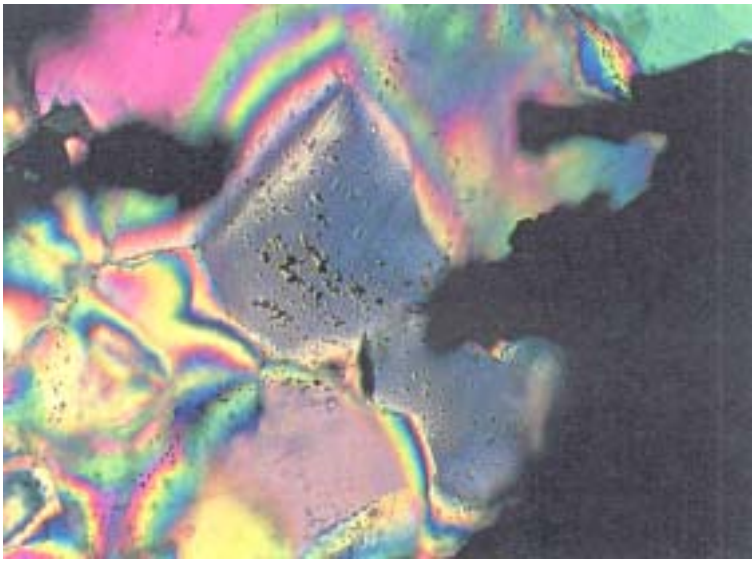

6:3

A12-1: *Relation between primary and recrystallised quartz and stress optical anisotropy (numbers indicate sample sections).*

Vertical sections (horizontal or near-horizontal Fluid Inclusion Planes (FIP:s)

- Vertical to 5° inclination; striking along borehole.
- Around 70° inclination; striking W20° from borehole direction.
- Around 31° inclination; striking W60° from borehole direction
- Around 45° inclination; striking W45° from borehole direction

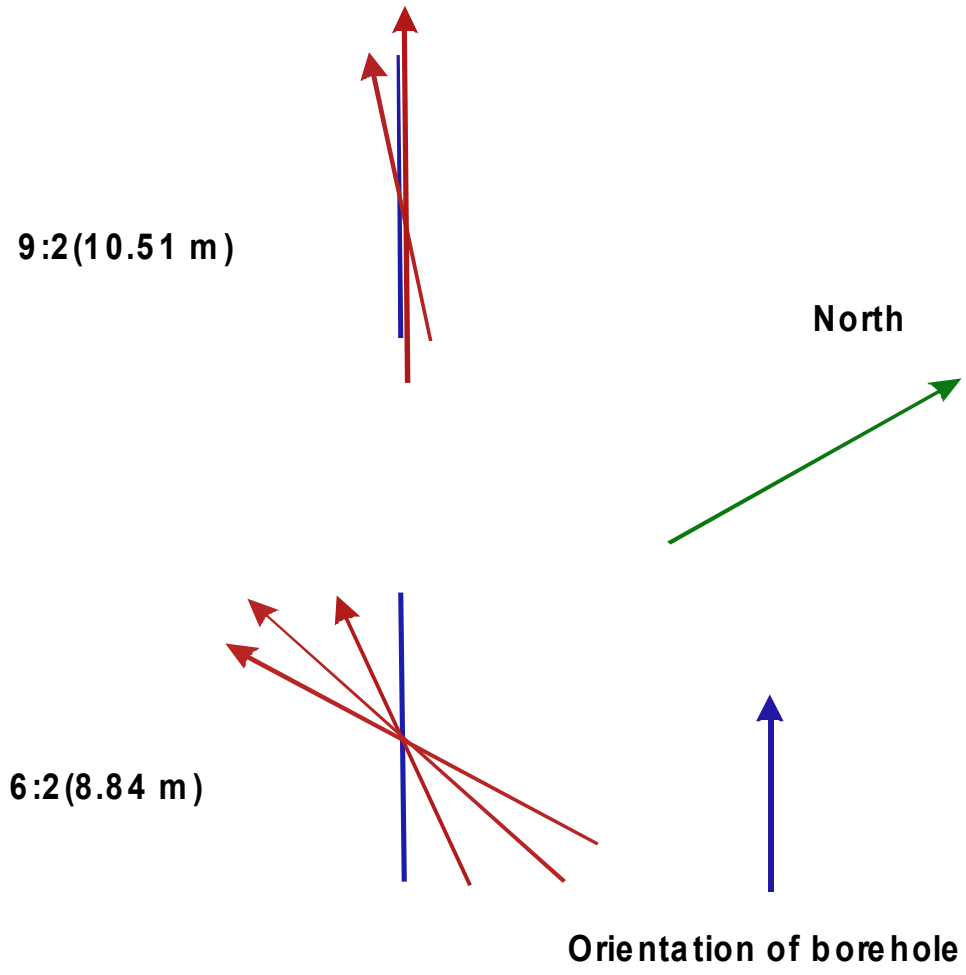

Figure A12-2: *Orientation of fractures in vertical thick sections where dip coincides with the strike in horizontal sections. (Numbers indicate sample sections and borehole length, respectively.)*

8:1 (9.85 m)

9:1 (10.51 m)

10:1 (10.90 m)

Figure A12-3: *Vertical thick sections; orientation of horizontal or near-horizontal FIP:s are recorded (numbers indicate sample sections and depth in borehole, respectively).*

Horizontal sections (vertical or near-vertical Fluid Inclusion Planes (FIP:s)

- Around horizontal to 3^{o} inclination; no obvious strike.
- Around 63^{o} inclination; striking E30^{o} from borehole direction

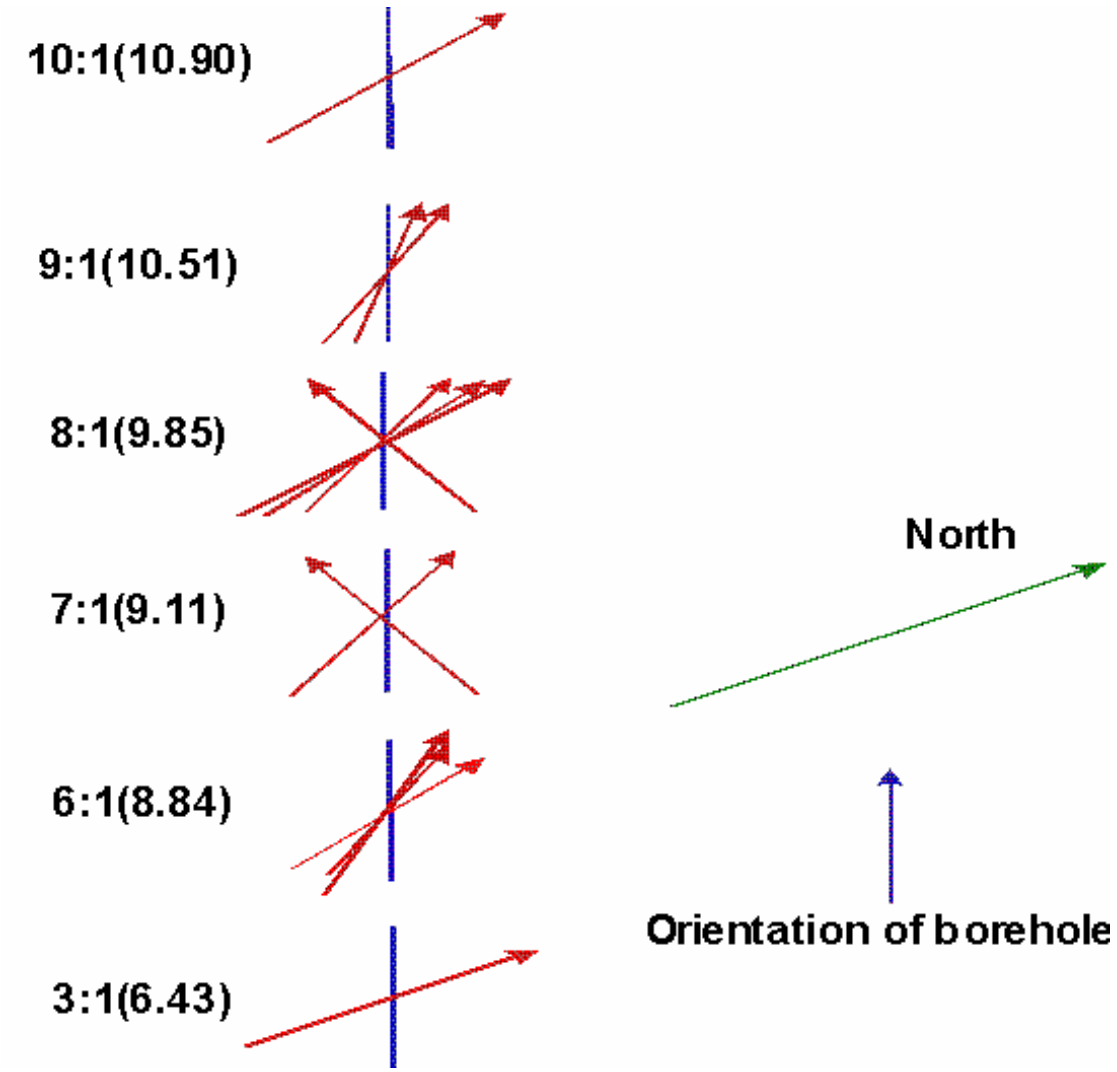

Figure A12-4: *Horizontal thick sections illustrated for six samples; orientation of vertical FIP:s or near-vertical FIP:s are shown as red arrows (numbers indicate sample sections and depth in borehole, respectively).*

1:2 (5.03 m)

2:2 (5.42 m)

4:2 (7.81 m)

6:2 (8.84 m)

7:2 (9.11 m)

Figure A12-5: *Horizontal thick sections; orientation of vertical or near-vertical FIP:s are recorded (number indicate sample sections and depth in borehole, respectively).*

Volume of fluid inclusions

Table A12-3: Calculation of the volume of inclusion fluids, using different size inclusions and average number of inclusions in a slice of "thick" section.

Φ, mm = diameter of fluid inclusion. V(F.I.) = volume of fluid inclusion. Vslice = volume of slice of thin section (= area of field of view x thickness of thin section). N = number of fluid inclusions counted in the field of view (average of 10 to 15 places in thin section).

Φ, mm	V(F.I.), m^3	Vslice, m^3
5	0.0654×10^{-15}	0.7772×10^{-12}
10	0.5233×10^{-15}	1.554×10^{-12}
20	4.1867×10^{-15}	3.109×10^{-12}
50	65.416×10^{-15}	7.772×10^{-12}

Low density of occurrence

Φ, mm	N	V(F.I.)/slice, m^3/m^3	V(F.I.)/m^3, m^3/m^3	vol-%
5	49	3.2046×10^{-15}	4.123×10^{-3}	0.4
10	49	25.64×10^{-15}	16.499×10^{-3}	1.6
20	49	205.15×10^{-15}	65.986×10^{-3}	6.6
50	49	3205×10^{-15}	412.10×10^{-3}	41

High density of occurrence

Φ, mm	N	V(F.I.)/slice, m3/m3	V(F.I.)/m^3, m^3/m^3	vol-%
5	147	9.614×10^{-15}	12.37×10^{-3}	1.2
10	147	76.925×10^{-15}	49.5×10^{-3}	4.9
20	147	615.44×10^{-15}	198.0×10^{-3}	19.8
50	147	9616×10^{-15}	1237×10^{-3}	"124"

Table A12-4: Calculation of the volume of inclusion fluids for intracrystalline fluid inclusions. Calculated values refer to the relative volume of fluid inclusions in quartz as microscopically recorded. ("low density" refers to volume calculations using the lowest density of fluid inclusions occurrences, "high density" to those with the highest density of fluid inclusions occurrences; symbols as in Tab. A12-2).

4.11 m, low density

Φ, µm	$V_{F.I.}$ %
3	0.2
5	0.5
8	1.2
10	1.9

4.11 m, high density

Φ, µm	$V_{F.I.}$ %
3	0.6
5	1.8
8	4.6
10	7.2

8.84 m, low density

Φ, µm	$V_{F.I.}$ %
3	0.2
5	0.5
8	1.4
10	2.2

8.84 m, high density

Φ, µm	$V_{F.I.}$ %
3	0.6
5	1.8
8	4.6
10	7.2

10.51 m, low density

Φ, µm	$V_{F.I.}$ %
3	0.2
5	0.5
8	1.2
10	1.9

10.51 m, high density

Φ, µm	$V_{F.I.}$ %
3	0.6
5	1.8
8	4.6
10	7.2

Fluid inclusion populations

- **Type I:** Primary magmatic inclusions, homogenisation temperatures between 400°-500°C, associated with large primary quartz grains, generally larger than the other types (4-45 μm in size), salinities between 5 - 30 eq.wt.% NaCl, include two-phase (liquid/vapour) and three-phase (plus solid: halite, calcite) inclusions
- **Type II:** Hydrothermal inclusions, homogenisation temperatures between 100°-300°C, mainly present in primary quartz grains as trails along healed cracks, salinities between 1-24 eq.wt.% NaCl, the majority is single phase liquid inclusions.
- **Type III:** Hydrothermal inclusions, homogenisation temperatures between 100°-300°C, trails adjacent to the edges of the medium to large secondary quartz grains; inclusions are irregularly-shaped, salinities between 5-15 eq.wt.% NaCl, single phase liquid inclusions change to single phase vapour types via intermediate tow phase inclusions over a few micrometers.
- **Type IV:** Low temperature inclusions, homogenisation temperatures <70°C, occurring as morphologically different forms along boundaries of the small, third generation recrystallised quartz grains, the inclusions are small (< 2μm), dark in colour and characteristically single phase vapour-type, the composition of the non-fluorescent vapour phase is uncertain (CO_2 or CH_4), some inclusions are two phase with salinities between 5-15 eq.wt.% NaCl.

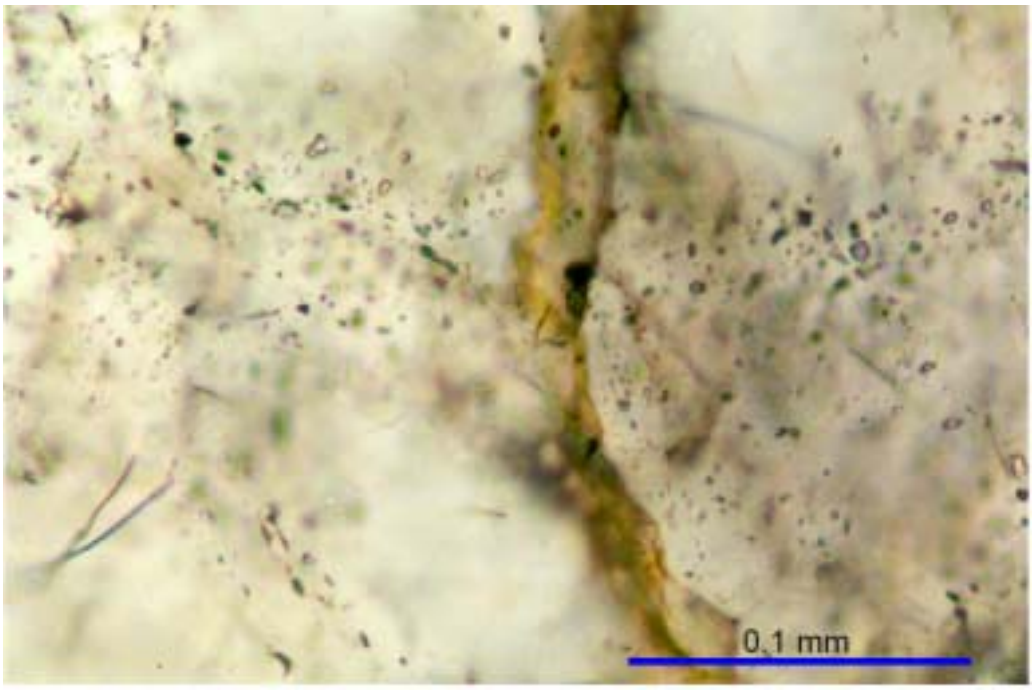

Figure A12-6: *Intracrystalline fluid inclusions. Includes individual fluid inclusions and clusters of inclusions as well as FIP:s.*

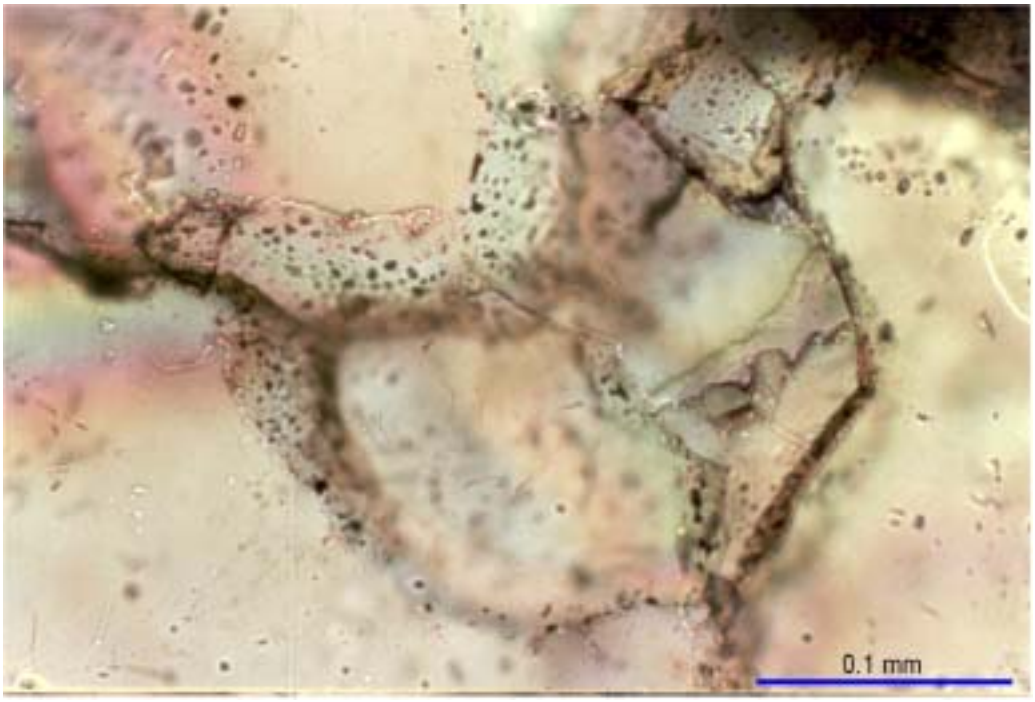

Figure A12-7: *Intracrystalline fluid inclusions concentrated at grain boundaries.*

Component analysis

Microthermometry

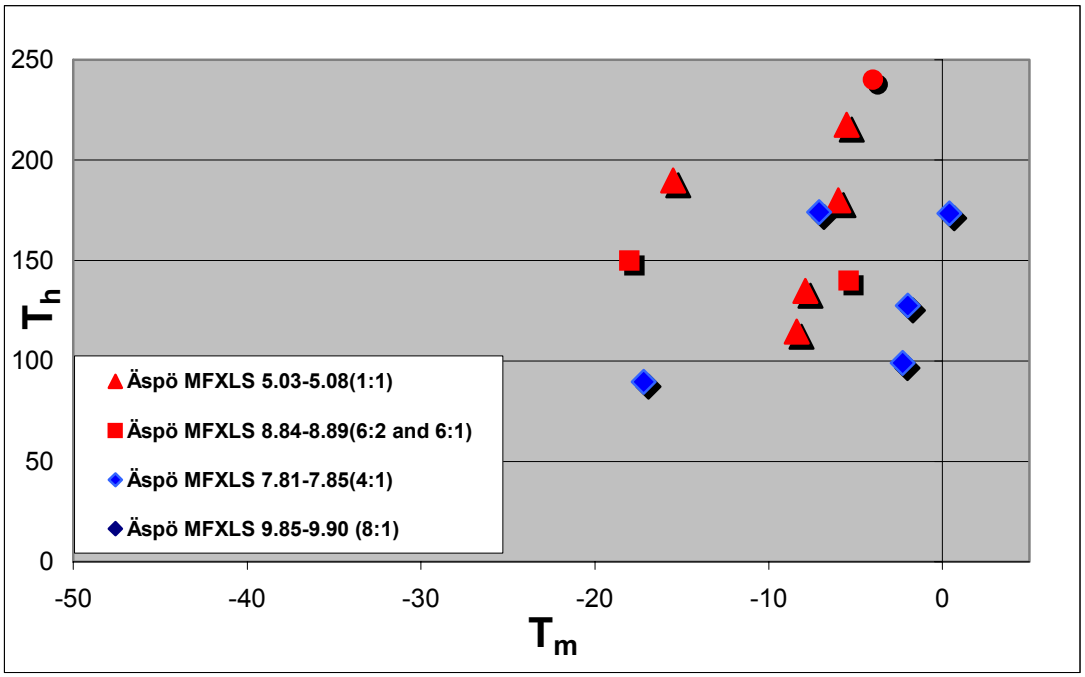

Figure A12-8: *Microthermometry results for quartz-hosted fluid inclusions in Äspö diorite samples 5.03-5.08 m, 5.42 m and 8.84-8.89 m within the MFE-drillcore. Microthermometric analyses were performed on samples: 1:1, 2:1, 4:1 and 6:2. The melting temperatures (Tm) determined, range in general from –4°C to –18°C which suggests 5-22 eq.wt.% NaCl. The homogenisation temperatures (Th) range from 89.6-190°C in most of the determinations with a few values up to 271.2°C.*

Table A12-5: Averaged data of final melting (Tm) and homogenisation (Th) temperatures of quartz in the MFE-drillcore.

Sample	Tm (°C)	Th (°C)	Sample	Tm (°C)	Th (°C)
5.03-5.08(1:1)	-5.50	217.8	***7.81-7.85(4:1)***	-2.3	99.0
	-7.90	134.9		-2.5	
	-15.50	190.0		-23.2	271.2
	-6.00	180.0		-7.1	174.1
	-8.40	114.6		-2.0	127.7
5.42 (2:1 CC-HOST)	-4.00	240.0	***8.84-8.89 (6:2, 6:1)***	-5.40	140.1
7.81-7.85(4:1)	0.40	173.50		-18.0	150.0
	-17.2	89.6	***9.85-9.90 (8:1)***	-4.5	150.0

Laser ablation ICP-MS-techniques (LA-ICP-MS)

Table A12-6: Element combinations in LA-ICP-MS analysis and interpreted to represent fluid inclusions and mineral phases.

Element combinations obtained	What they represent	Chemical formula
Na alone	Fluid inclusion	NaCl solution
Na+K+Mg+Ca	Fluid inclusion	salt solution
Na+Sr	Fluid inclusion	Na-Ca-Cl-brine
Na+Al	Albite	$NaAlSi_3O_8$
K+Al	K-feldspar	$KAlSi_3O_8$
Na+Al+Sr	Plagioclase	$(Na,Ca)AlSi_3O_8$
Mg alone	Serpentine	$(Mg,Fe)_3Si_2O_5(OH)_4$
Mg+Al	Chlorite	$(Mg,Fe^{2+})_5Al(Si,Al)_4O_{10}(OH)_8$
K+Mg+Al	Biotite	$K(Mg,Fe)_3(Al,Fe)Si_3O_{10}(OH,F)_2$
Al alone	Kaolinite	$Al_2Si_2O_5(OH)_4$
Na+Ca+K+Al	Feldspar	$(Na,Ca)AlSi_3O_8$
Na+Mg+Al	Amphibole (hornblende)	$(Ca,Na)_{2-3}(Mg,Fe,Al)_5(Al,Si)_8O_{22}(OH)_2$

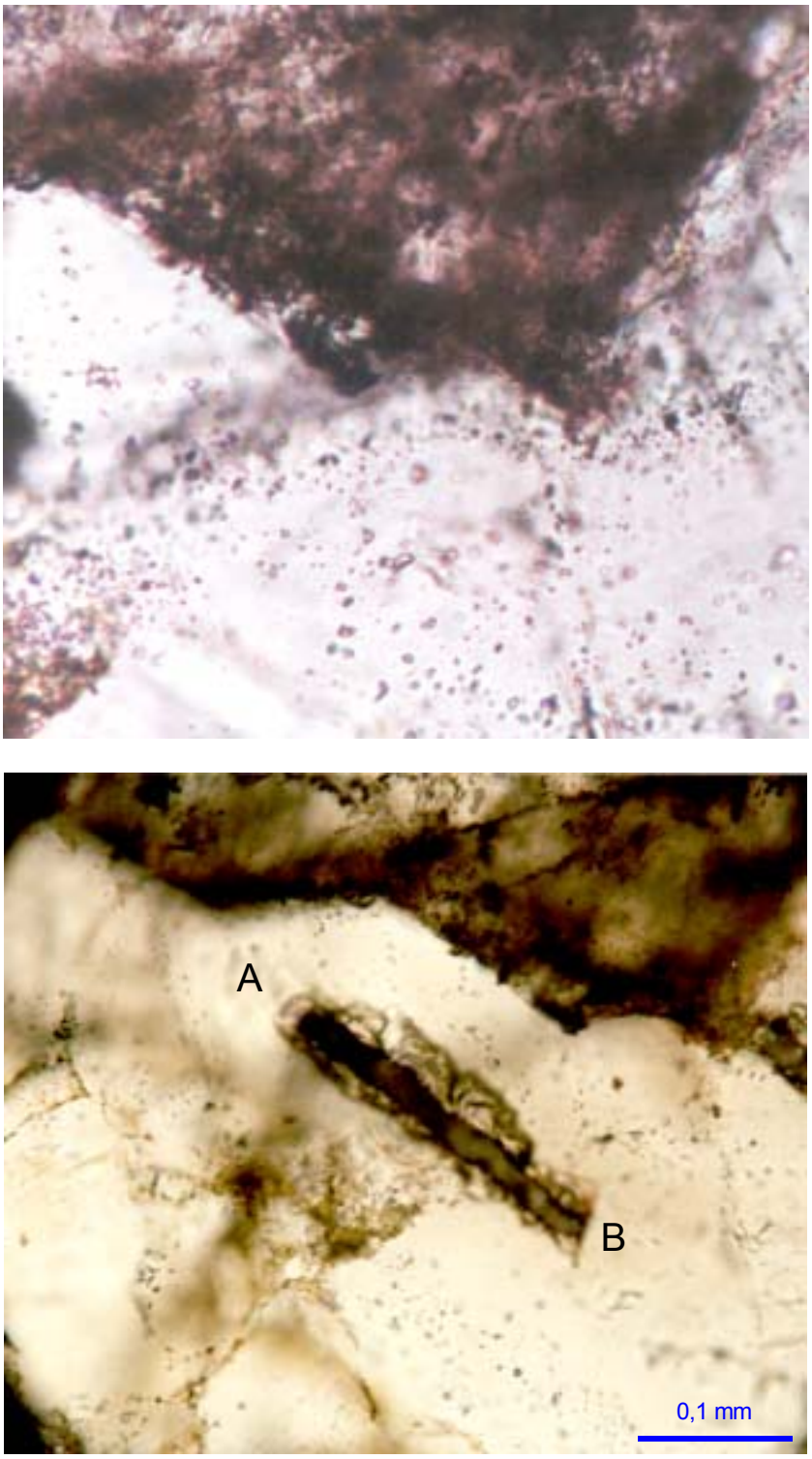

Figure A12-9a: *A cluster of fluid inclusions characterising an intracrystalline site. The photomicrograph shows the target area before (upper picture) and after (lower picture) laser ablation. Laser ablation commenced at point A and terminated at point B.*

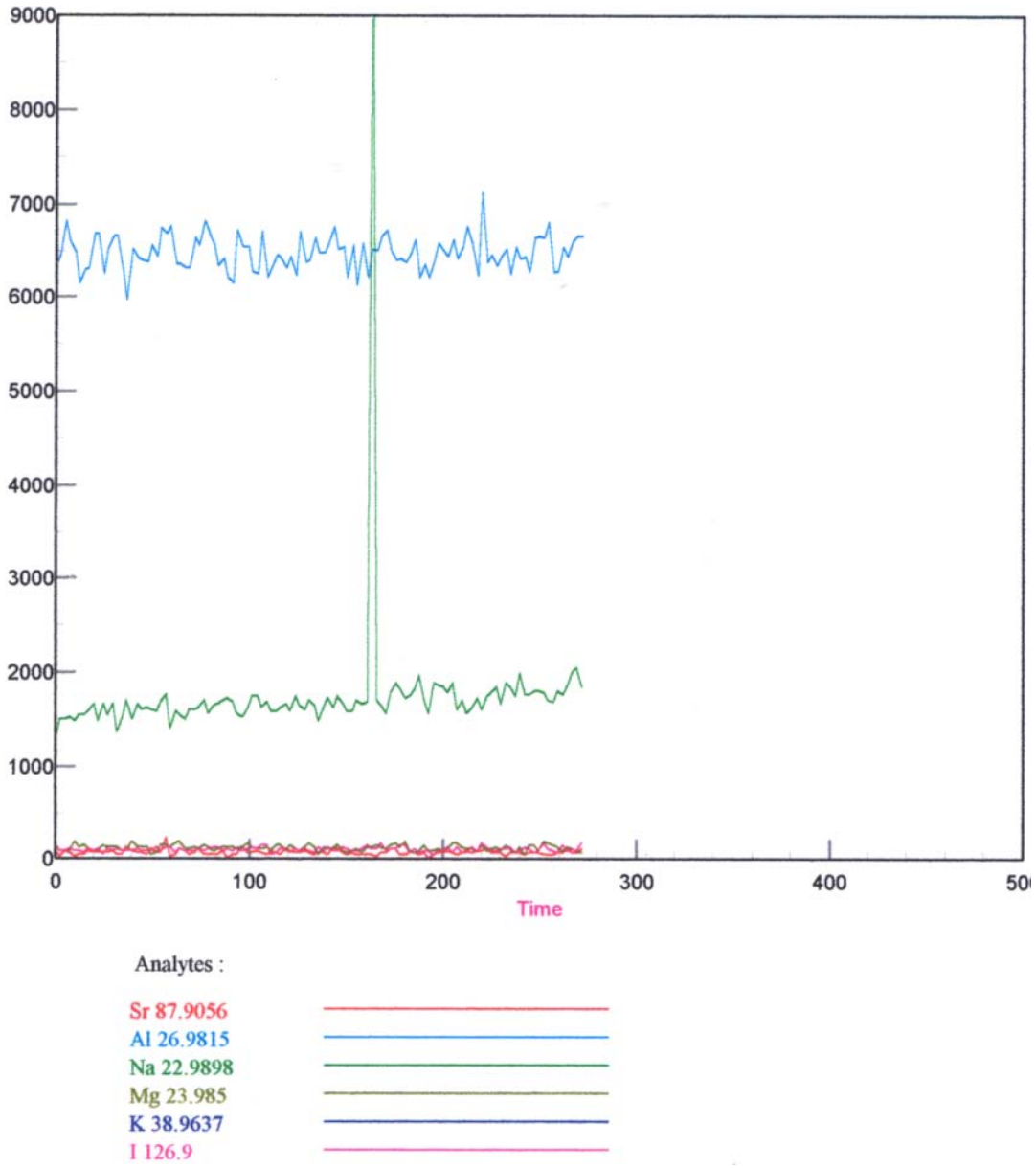

Figure A12-9b: *The LA-ICP-MS analysis demonstrates a high salinity fluid inclusion intersected at point 160 seconds after the start of ablation. The only element indicated in the analysis is* ^{23}Na.

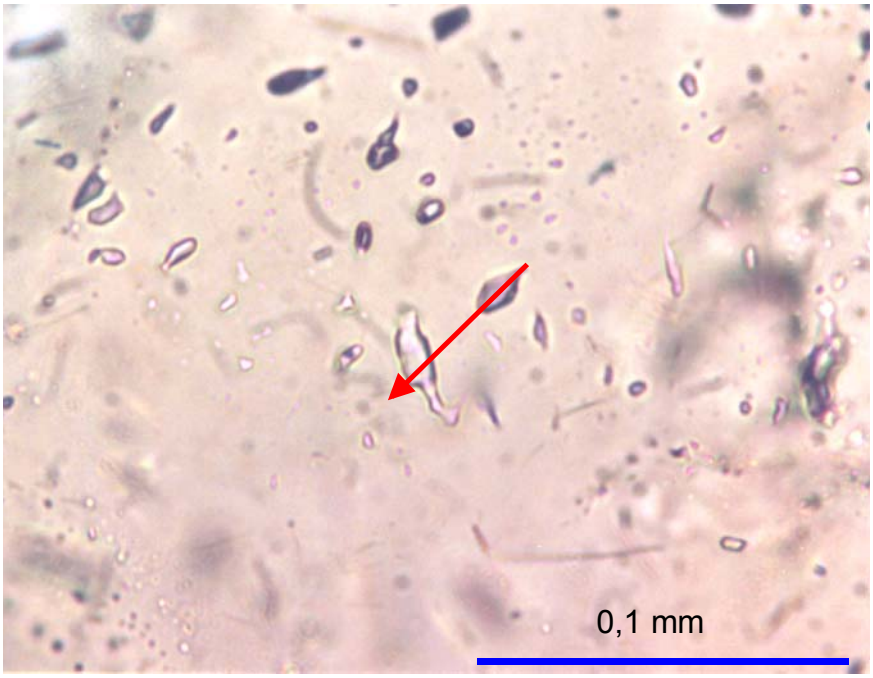

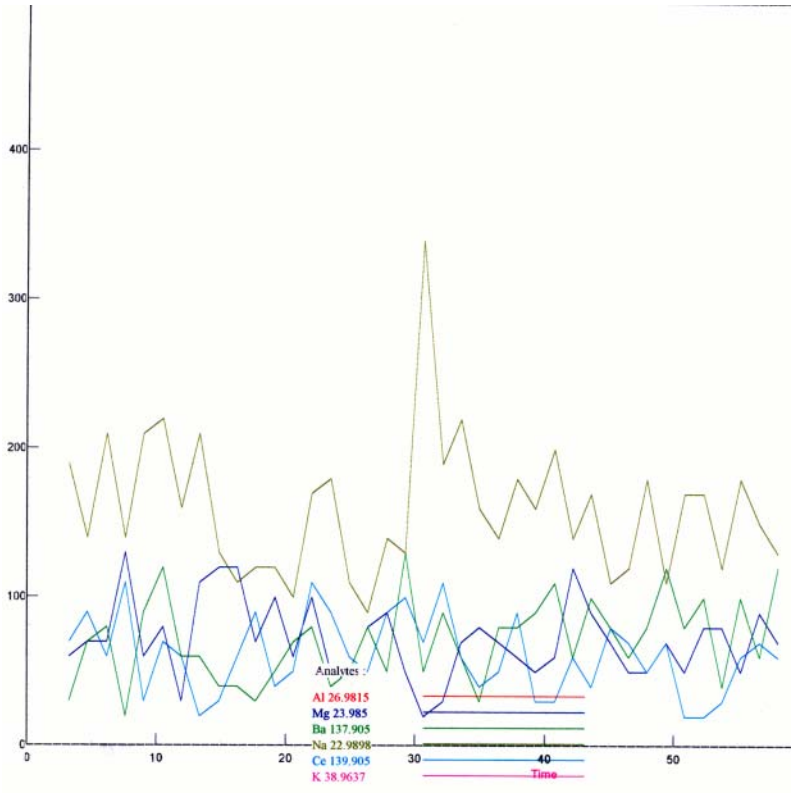

Figure A12-10: *Microphotograph of the ablated L1 line in sample 4. The line traverses a fluid inclusion cluster and extracts of low salinity fluids. The most prominent element in these inclusions is Na; a slight coincidence of Ba with Na can be detected.*

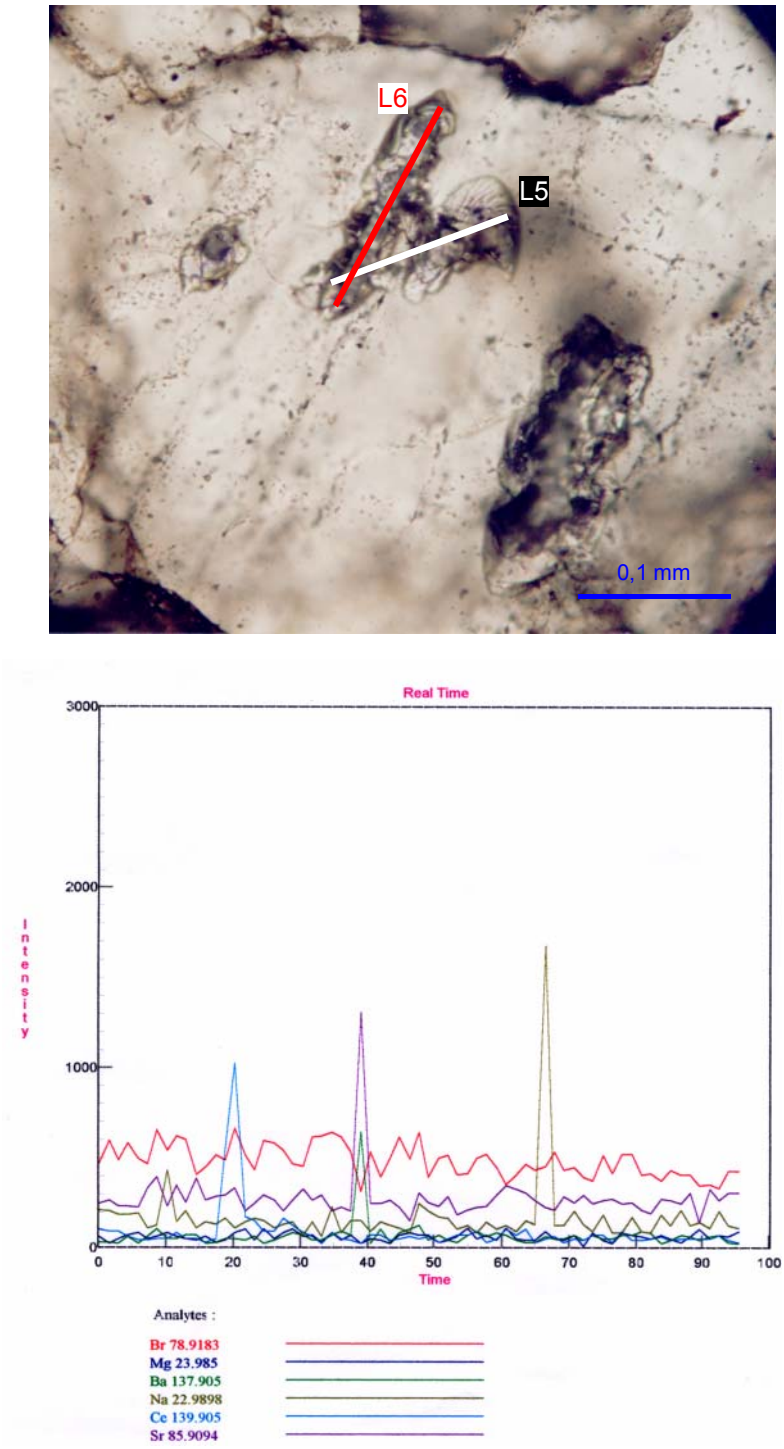

Figure A12-11: *Laser ablation traverse over a fluid inclusion cluster in sample 4. A fluid inclusion with moderate Na concentration is intersected at point 67 seconds from the beginning of the ablation. The other ablated inclusions were intersected at point 20 seconds (^{140}Ce) and point 38 seconds (^{86}Sr and ^{138}Ba).*

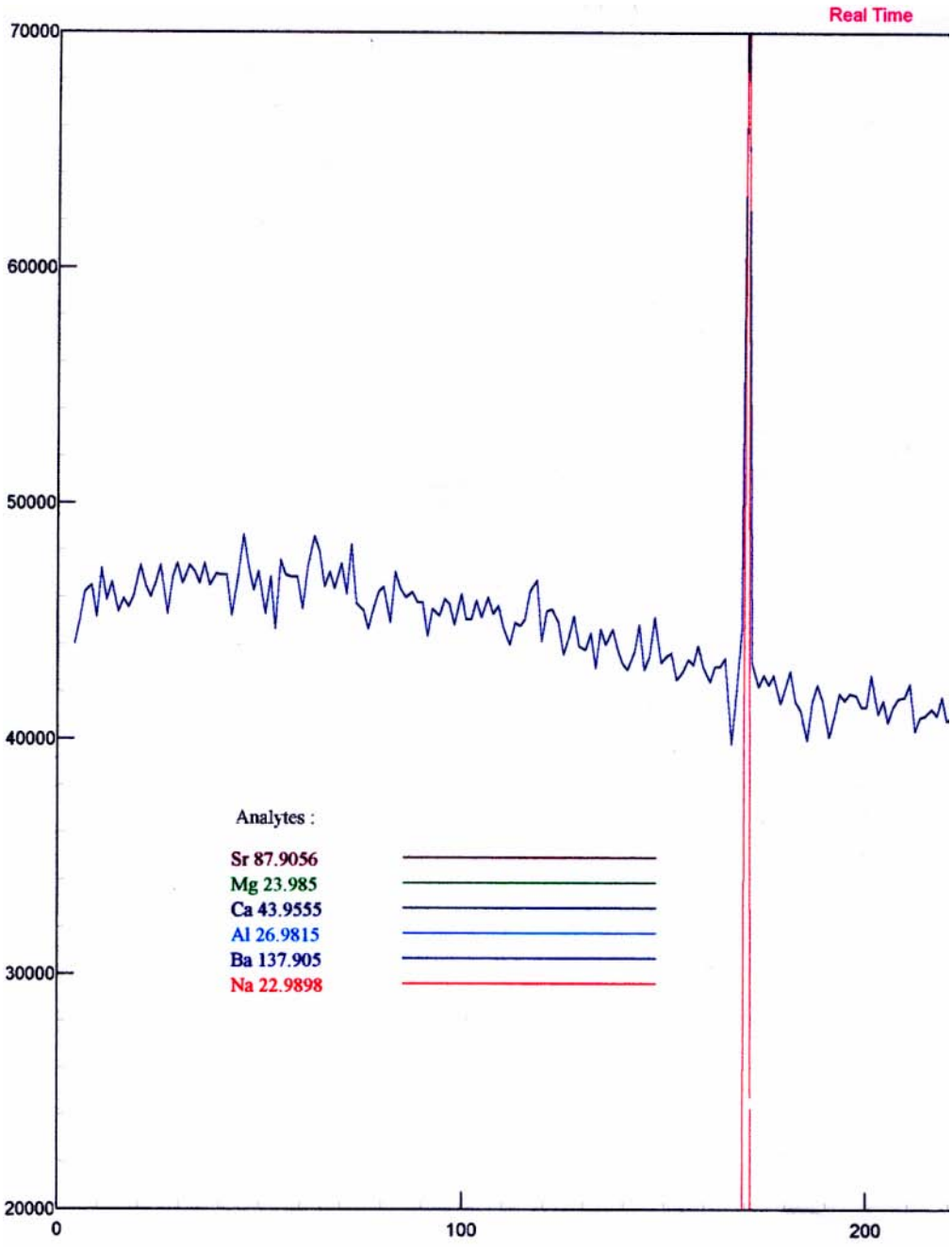

Figure A12-12: *A traverse through a single intracrystalline fluid inclusion in sample 7. The LA-ICP-MS spectrum indicates that the fluid inclusion at point 170 seconds from the beginning of the ablation belongs to a H_2O-NaCl-$CaCl_2$-CO_2 system.*

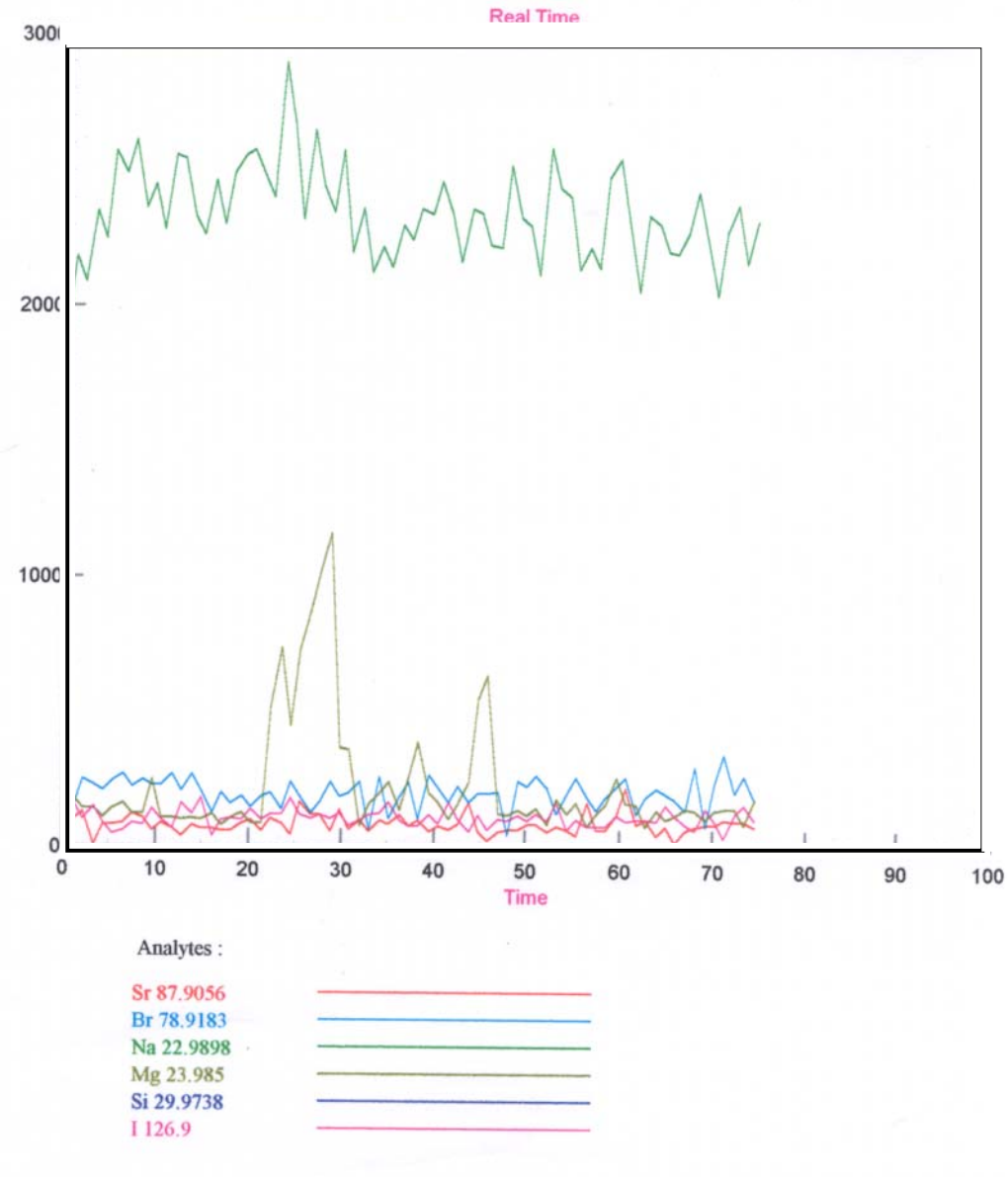

Figure A12-13: *Sample 1, line 3 through an intracrystalline fluid inclusion cluster. The LA-ICP-MS spectrum for Sr, Br, Na, Mg, and I indicates three Na-free, Mg-rich inclusions along the profile.*

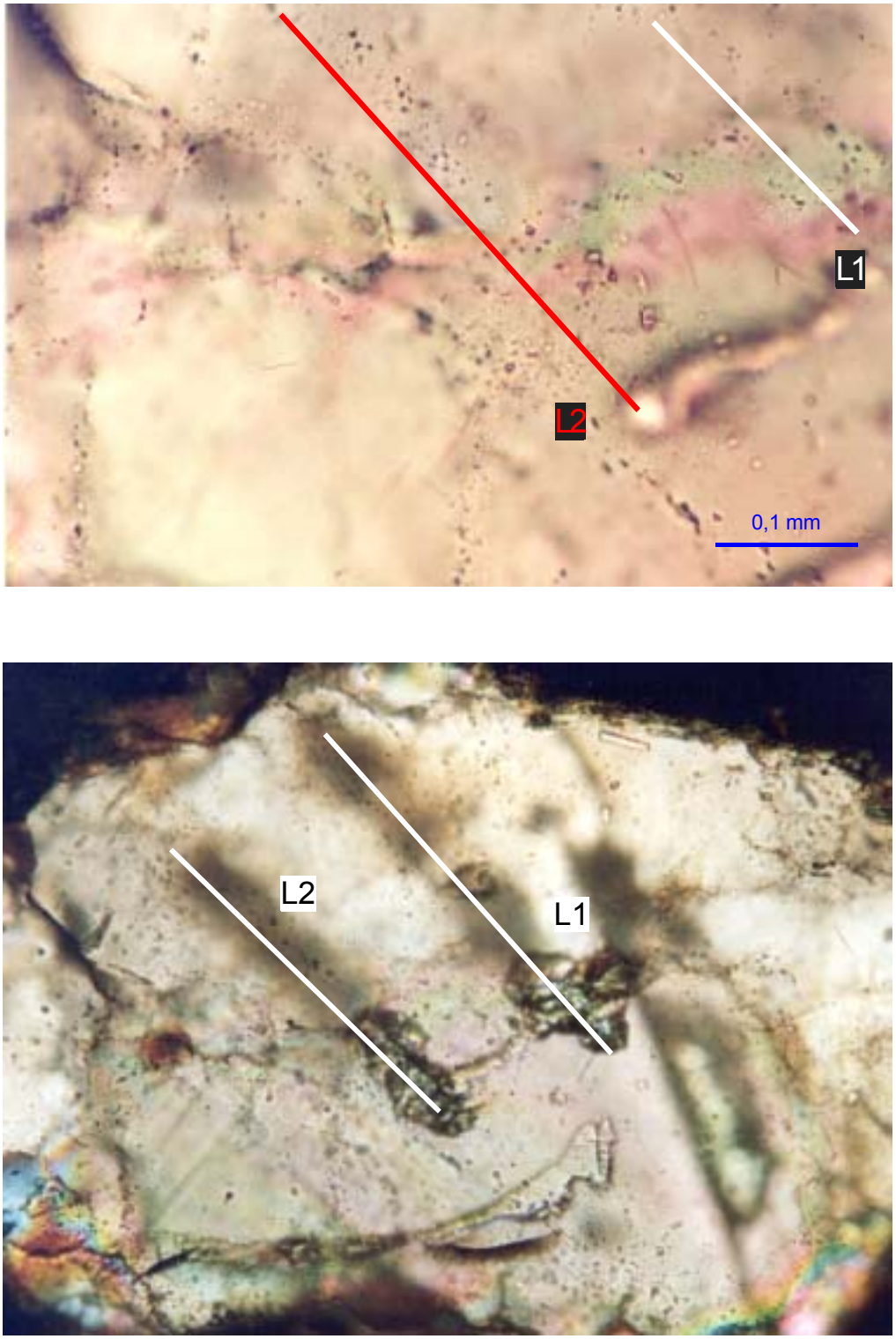

Figure A12-14: *Microphotographs of intercrystalline fluid inclusion trails before (upper picture) and after (lower picture) LA-ICP-MS analysis; sample 7.*

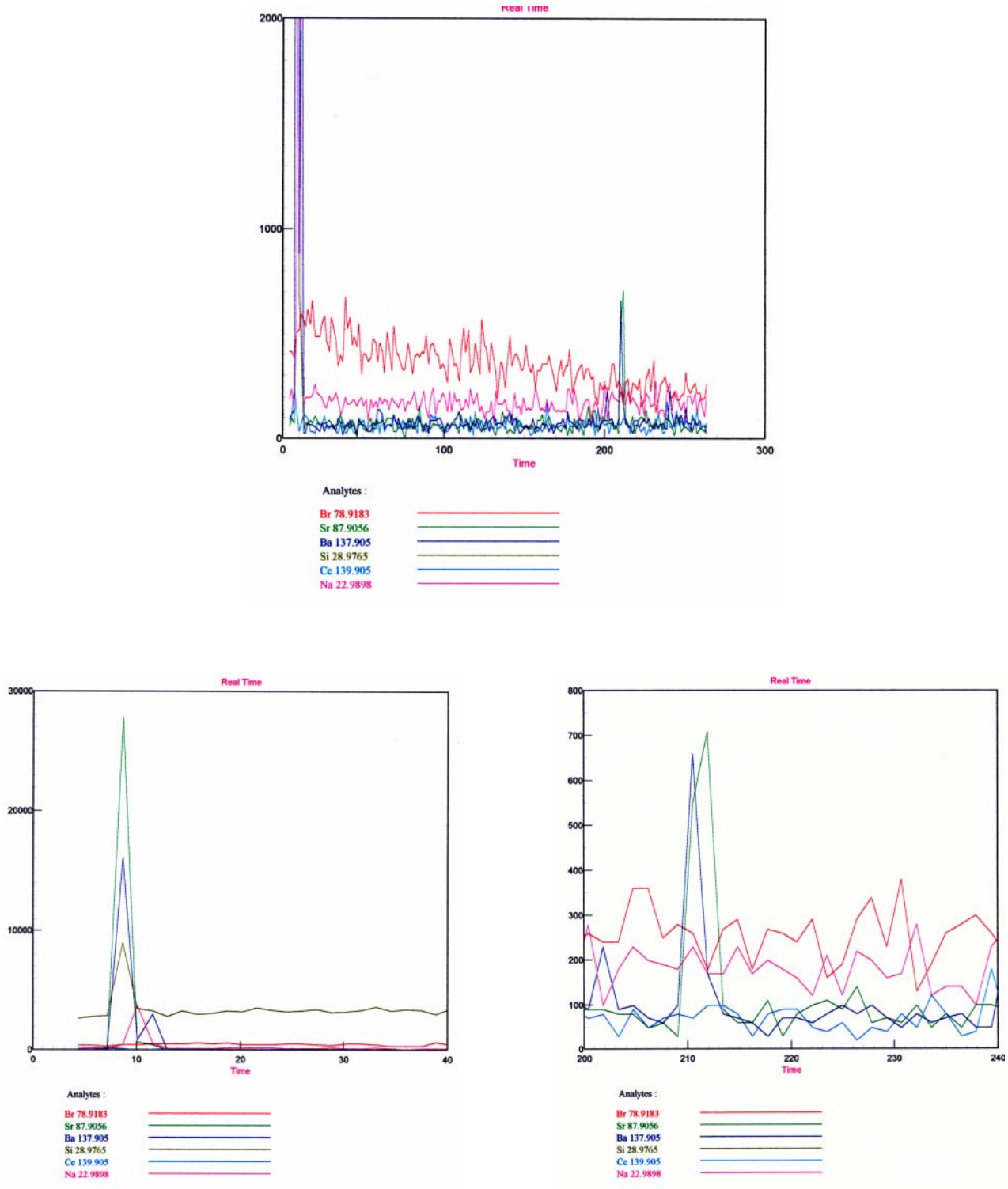

Figure A12-15: *LA-ICP-MS spectrum from sample No. 7, line 1 (cf. Fig. A12-14). The traverse intercepts fluid inclusions at points 8 seconds and 210 seconds from the start of ablation (upper picture). Details of the peaks at 8 seconds (lower right picture) and 210 seconds (lower left picture).*

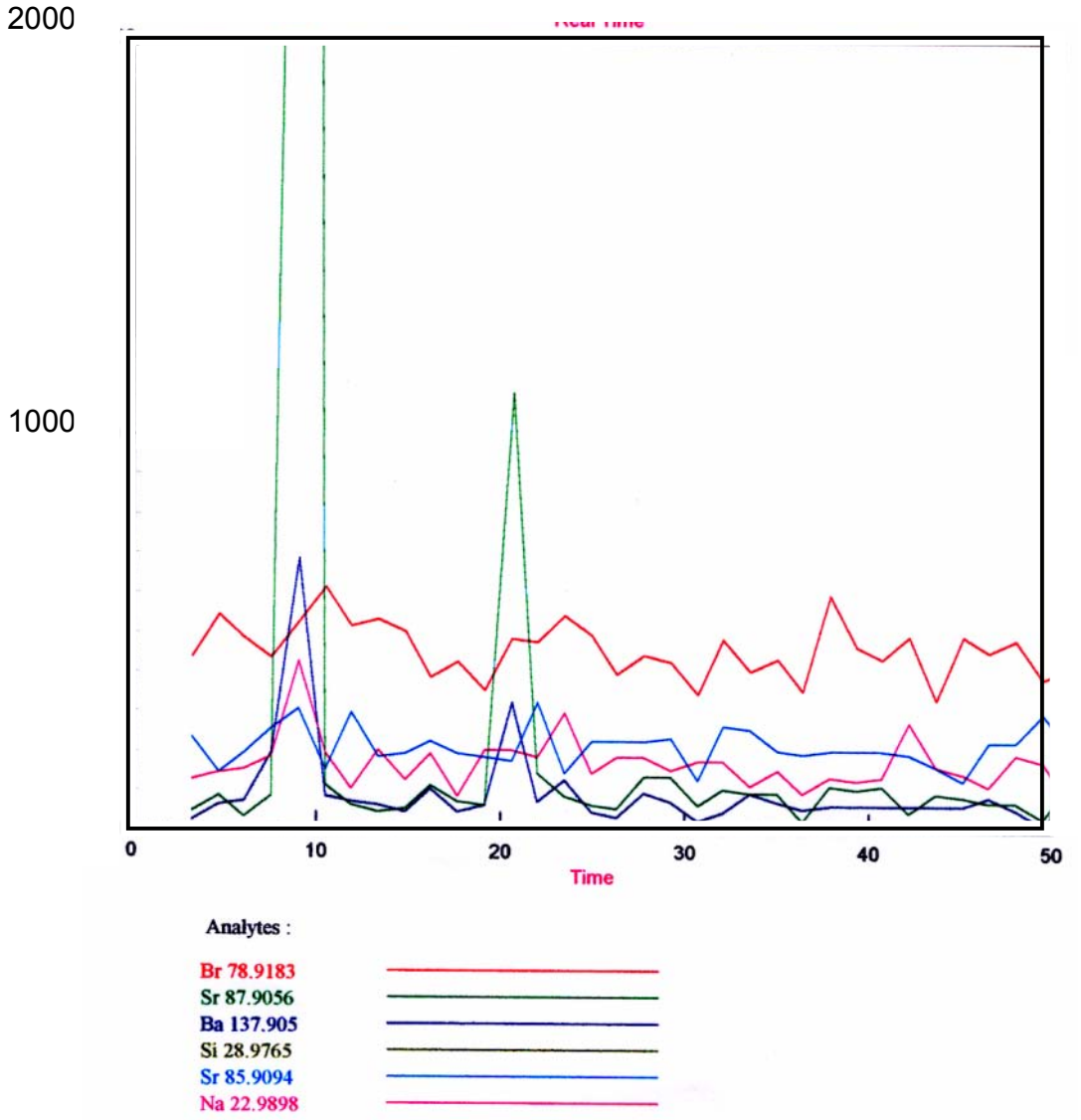

Figure A12-16: *LA-ICP-MS spectrum of sample 7, line 2 (cf. Fig. A12-14). The inclusion at point 9 seconds from the start of ablation is a low-salinity NaCl type. The peaks of Ba and two Sr isotopes coincide with Na. For ^{29}Si (cf. Fig. A12-17).*

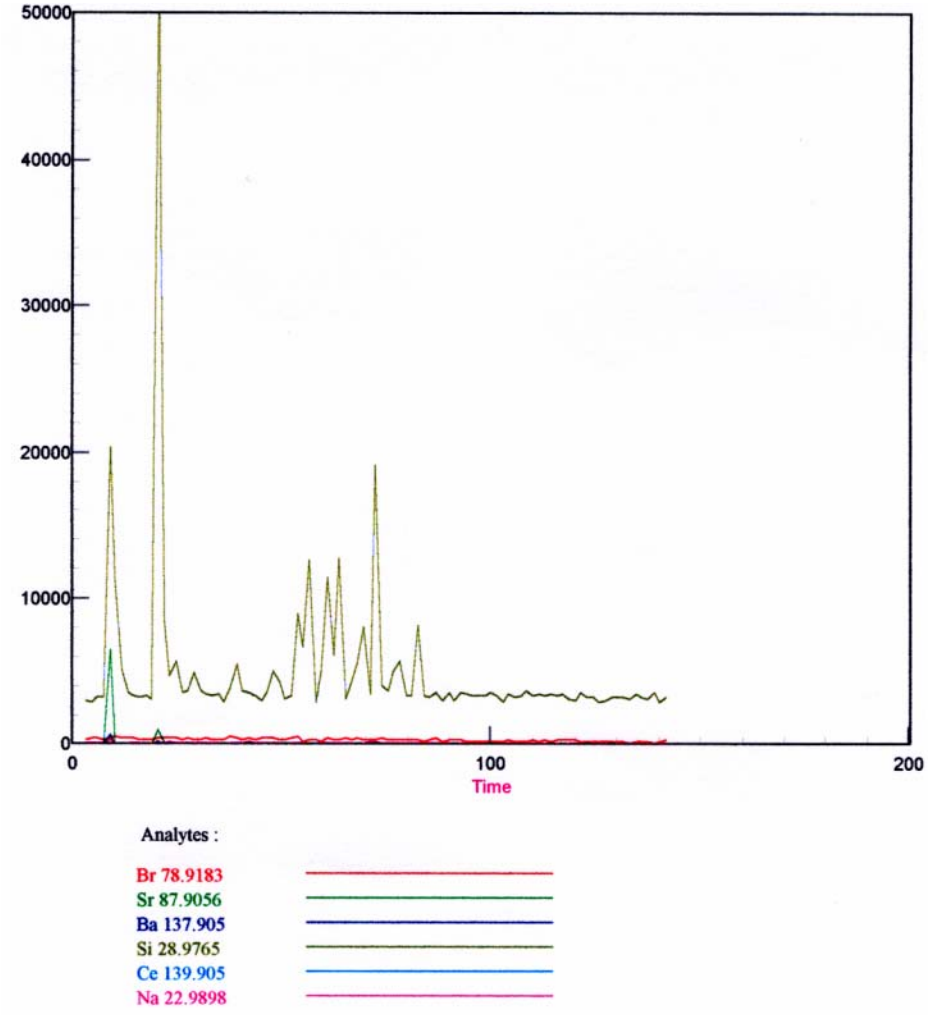

Figure A12-17: *LA-ICP-MS spectrum crossing a fluid inclusion trail in sample 7, line 2 (cf. Fig. A12-14). The analysis indicates a significant fluctuation for ^{29}Si. The host is quartz and the fluctuation is an interference phenomenon, apparently due to the CO-gas inclusions. At points 10 seconds and 20 seconds the Si-peak coincides with ^{88}Sr and Ba. A detailed spectrum of the former peak is given in Figure A12-16.*

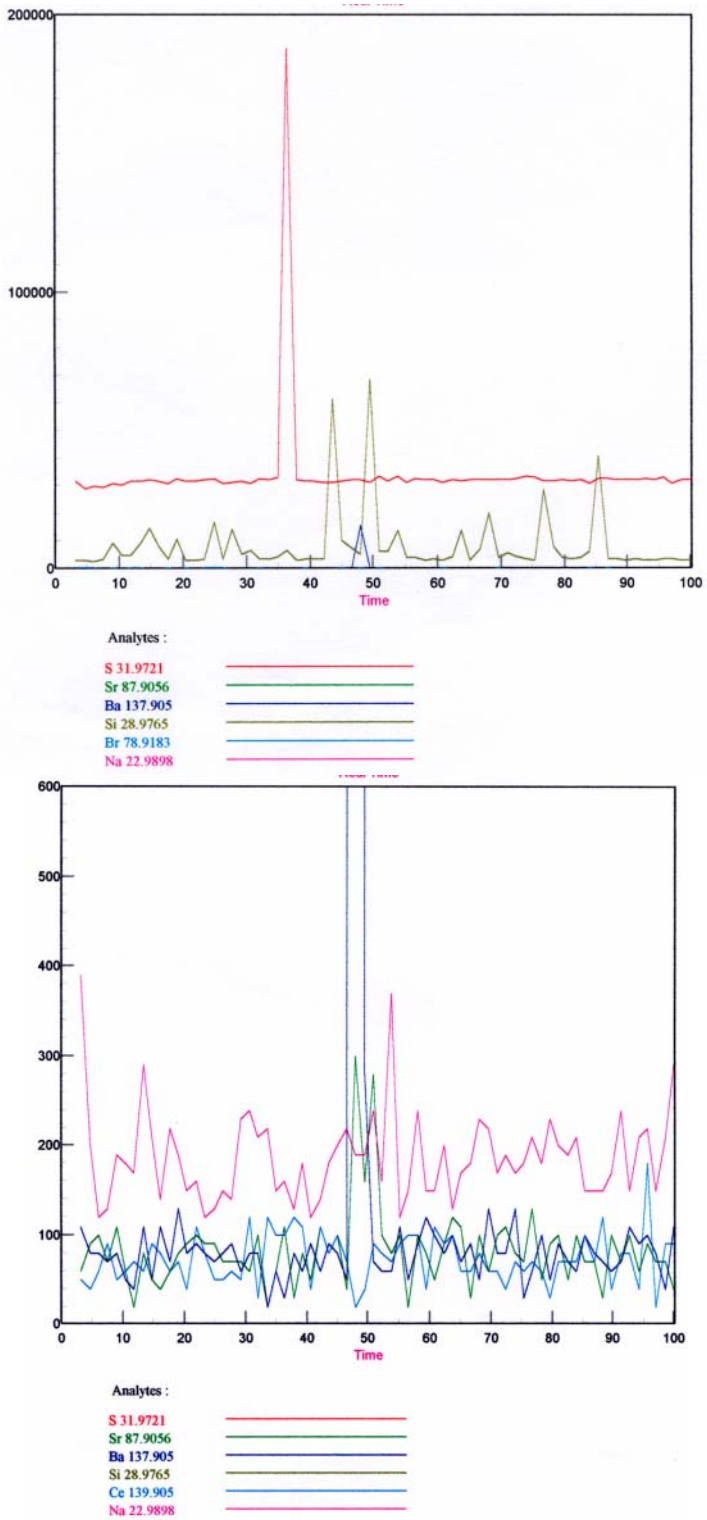

Figure A12-18: *LA-ICP-MS spectrum from sample 2, line 8. In the upper figure the traverse crosses a tiny iron sulphide grain (which gives high intensity for sulphur) on a grain boundary. The ^{29}Si is assumed to imply the extraction of CO_2-gas inclusions. The lower figure from the same traverse locates fluid inclusions with low Na (10, 30 and 53 secs.). At a point 48 seconds the traverse extracts an inclusion with high Ba and ^{88}Sr. This peak is located between two Si-peaks (upper figure).*

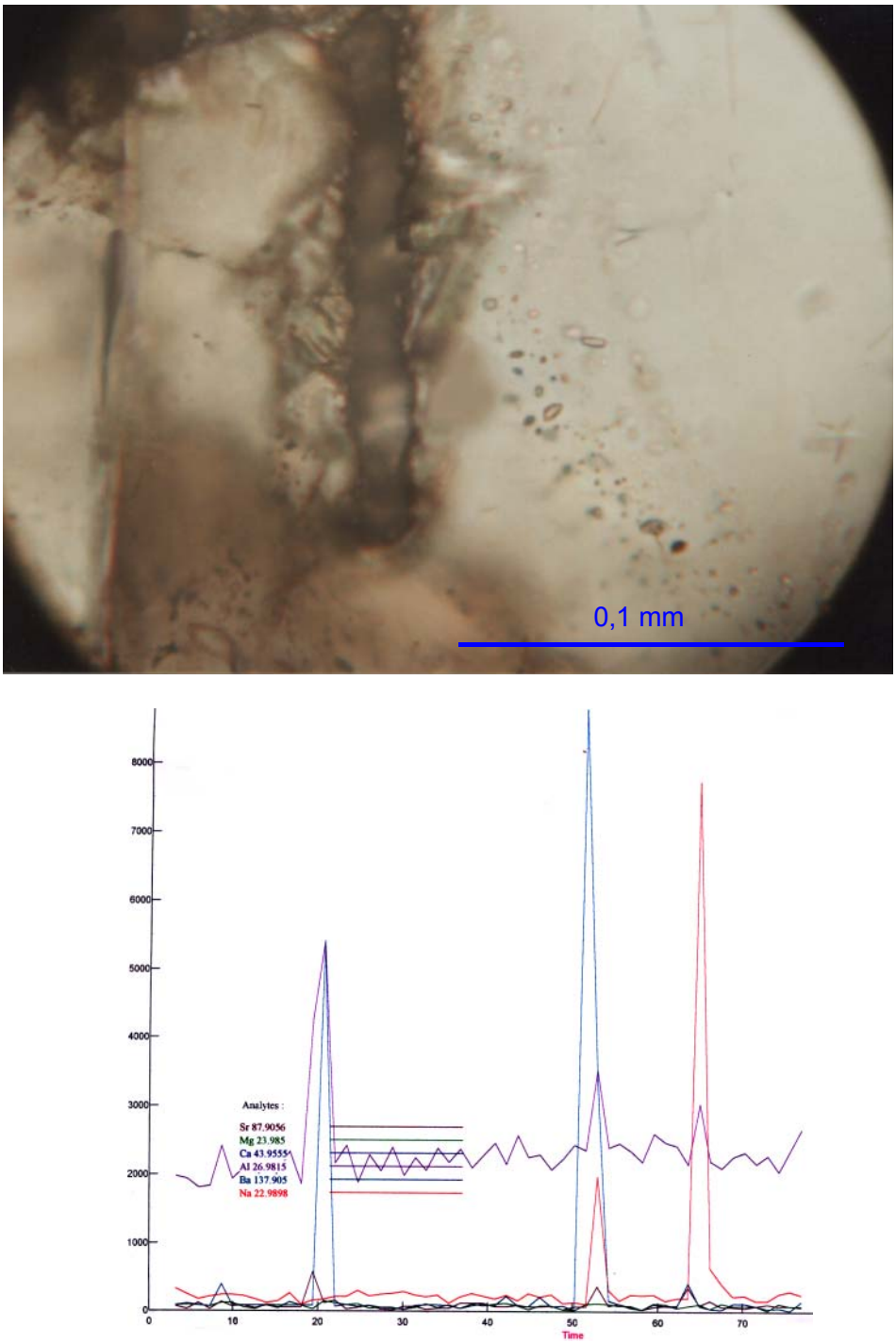

Figure A12-19: *Microphotograph of fluid inclusion trail traversed by laser line L4. The LA-ICP-MS spectrum indicates a few aluminium-bearing inclusions, which also have indications of Ba and Sr. The high Na-peak extracted at point 68 seconds is interpreted to indicate a fluid inclusion rather than a solid mineral phase; the intensity of Na is much too high, in comparison to Al, for explaining it to be an aluminosilicate (i.e. albite).*

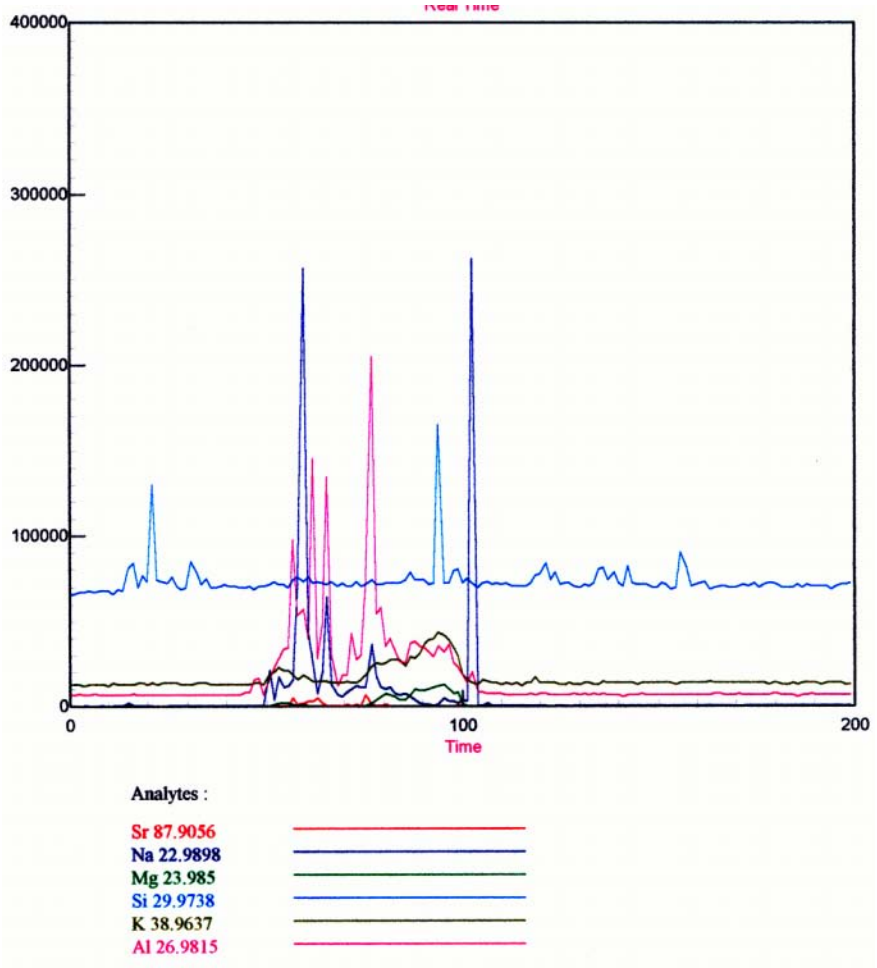

Figure A12-20: *LA-ICP-MS spectrum from sample 6, line (cf. Fig. A12-19). The traverse crosses a grain boundary in which the majority of the inclusions are Al-rich. The high Na-peak at point 110 seconds indicates a traversed fluid inclusion with moderate salinity.*

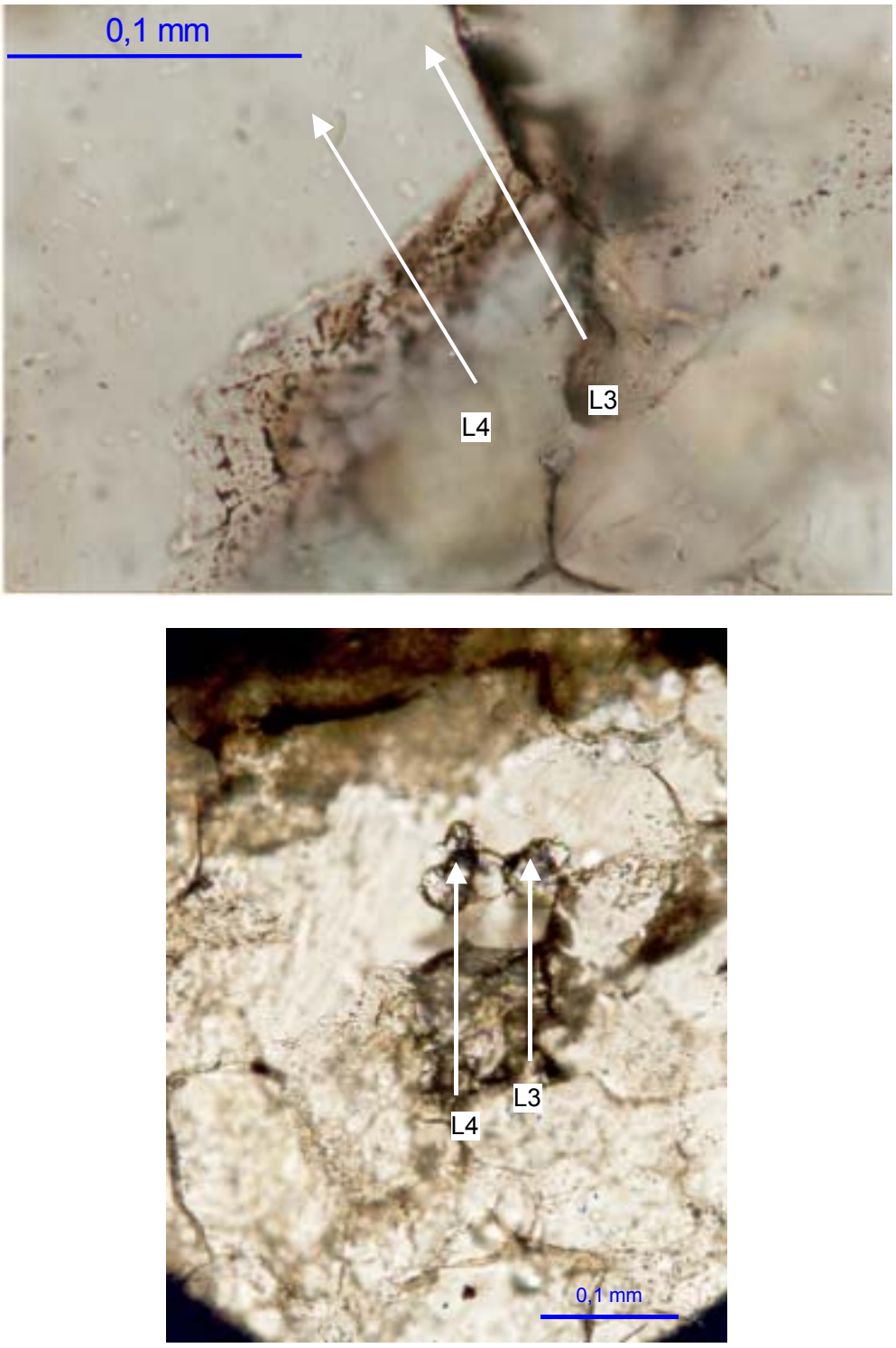

Figure A12-21: *Microphotographs of grain boundary coatings in sample 7. The upper photograph was taken before and the lower photograph (sample rotated clockwise) after the laser ablation. The corresponding LA-ICP-MS spectra are given in Figure A12-22.*

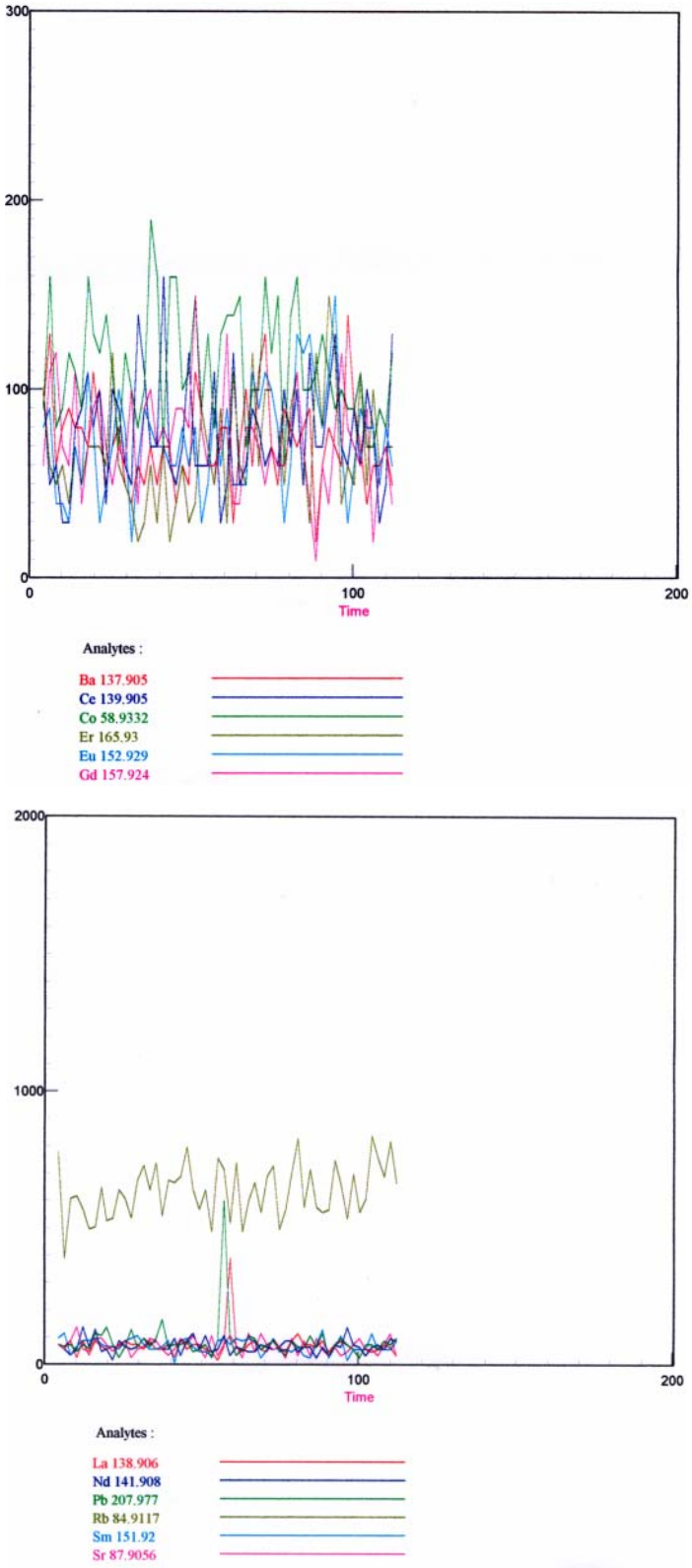

Figure A12-22: *LA-ICP-MS spectra of line 3 (upper figure) and line 4 (lower figure). The spectrum indicates high fluctuations, especially for Co, Ce, Gd, Eu and Ba in line 3. Traverse L4 illustrates the frequent occurrence of an unknown ^{208}Pb-phase on the coating. At point 60 seconds the ablated material includes an unknown La-bearing phase.*

Technical Document

TD-03-02

Djupförvarsteknik

Matrix Fluid Chemistry Experiment

Synthesis Report: Drillcore pore water leaching studies and borehole water

H.N. Waber
University of Bern

S.K. Frape
University of Waterloo

November 2002

Summary

In crystalline rocks of very low permeability the chemical characterisation of pore water has to be performed by applying indirect methods based on drillcore material and/or long-term *in-situ* sampling of pore water in packed-off borehole intervals. While long-term *in-situ* sampling is only feasible in an underground laboratory, indirect methods based on drillcore material can also be applied to deep boreholes.

Long-term sampling of water from the Matrix Fluid Chemistry Experiment (MFE) borehole yielded large enough volumes of water for chemical and isotopic analyses; initially after 14 months and subsequently after a further15 months. Waters sampled only a few metres apart within the Äspö diorite and the Ävrö granite are of the Na-(Ca)-Cl-type, but differ in their salinity with Cl-contents of about 5000 mg/L and 2900 mg/L, respectively, and in their isotopic composition of hydrogen, oxygen, chloride and strontium. The sampled water and gas were strongly perturbed by microbial activity in the sampling sections in spite of all precautions taken during borehole installation. The large amount of bacterially mediated sulphate reduction in the sampling intervals results in a strong deviation of the carbonate system and related parameters because dissolved sulphide contributes significantly to the measured total alkalinity. This further implies that non-conservative compounds (and their isotopic composition) of the sampled water cannot be further judged for their representativeness under *in-situ* conditions.

In their general chemical and isotopic characteristics, the MFE-borehole waters show some similarities with known compositions of groundwaters flowing in the complex fracture system at the Äspö HRL. While the borehole water from the Äspö diorite shares an affinity to the glacial water components known from the Äspö HRL, that from the Ävrö granite resembles isotopically, but not chemically, a composition more in line with groundwaters sampled from the Prototype locality in the HRL.

In an unperturbed system where diffusion might be considered the dominant solute transport mechanism, compositional differences over a few metres would be expected to be homogenised within some thousands of years. In the MFE-borehole this is obviously not the case. It appears that the pore water varies from place to place as a function of the distance from nearby conducting fractures and the degree of active groundwater circulation in these fractures. Therefore, the sampled borehole waters do not represent an *in-situ* pore water end-member *sensu-stricto*, but rather a series of pore water compositions reflecting the transient nature of the groundwater flow system and the microstructural heterogeneity of the bedrock where both advection and diffusion transport mechanisms play a part.

Various indirect methods for pore water characterisation were carefully investigated bearing in mind potential alteration processes that may occur during sampling, storage, sample preparation, and during the performed experiment itself. Leaching ground rock material at various solid:liquid ratios under different atmospheric conditions resulted in the definition of truly non-reactive pore water solutes and the identification of processes modifying the pore water from the drilling to the experimental stage. Leaching of different grain-size fractions and leaching of multiple ground rock material allowed the identification

of the contribution of fluid from fluid inclusions to the interstitial pore water. These experiments further show that the salinity contribution to the pore water from inclusion fluid becomes already significant at a low percentage (< about 5%) of the total fluid inclusions leaked. Differences in the impact of fluid inclusion leakage to the leach solutions as a function of rock type are only related to the abundance of quartz, i.e. the abundance of fluid inclusions, but not to chemical differences in fluid inclusions from different rock types.

Diffusive equilibration techniques proved to be more feasible for *in-situ* pore water characterisation. For non-reactive solutes batch experiments appear to yield directly *in-situ* pore water conditions while reactive solutes can be estimated by geochemical modelling. However, no final confirmation can be made because the drillcores used for these experiments come from a different location with possibly different pore water compositions than those sampled in the MFE-borehole.

Pore water displacement under high pressure did not yield any pore water after three years of experiment, most probably due to the very low permeability and low water content of the Äspö diorite from the MFE-borehole.

The investigations clearly showed that the characterisation of *in-situ* pore water in crystalline rocks of very low permeability is susceptible for perturbation during sampling and storage (e.g. evaporation, oxidation) and the impact of fluid inclusion salts if destructive methods are applied. Recommendations to minimise such effects are discussed.

Materials

Various pore water extraction studies have been performed on different sections from the Matrix Fluid Experiment (MFE) borehole (drillcore KF0051 A01) at the Universities of Bern and Waterloo (Table A13-1). Unfortunately following drilling and mapping of the drillcore the sample preparation protocol to prevent evaporation of pore water was not strictly adhered to. Instead of first wrapping the core in aluminium foil followed by a beeswax coating, the wax coating was first applied to the core followed by wrapping in the foil. In this condition the individual core samples were shipped to the different laboratories for further investigations. In the event that the faulty preservation of the drillcore material may have contributed to some contamination of the experiments described below, the beeswax was analysed as a precaution. The results show that any potential contamination should be minimal (Table A13-2). Any potential contamination was further minimised by specific sample conditioning before the experiments or using samples from a nearby drillcore where the sampling protocol was adhered to.

In June 2001, the University of Bern received additional freshly drilled core material from borehole KF0093 A01 for simple batch diffusion experiments. This time the correct preservation procedure was carried out. The borehole, drilled to carry out *in-situ* stress measurements within another experiment, is located in the same structural rock matrix block some 30 metres from the MFE borehole along the 'F' Tunnel.

From the MFE-borehole groundwater was successfully sampled in December 1999 from Section 4 and in October 2000 from sections 2, 3, and 4. Sections 1 to 4 describe the packed-off intervals in which water was allowed to seep over several months.

A third sampling campaign was conducted in February 2003. The results of this campaign are given in Appendix 16.

Table A13-1: Samples and experiments performed.

Sample	Drillcore Length (m)	Rock Type	Experiment [1)]	Laboratory
MFE-3.32	3.27-3.37	diorite	high pressure displacement	Uni Waterloo
MFE-3.50	3.40-3.60	diorite	repeated aq. leaching of same material	Uni Waterloo
MFE-3.66	3.62-3.70	diorite	aq leachate, CEC at different S:L, WC	Uni Bern
MFE-3.79	3.77-3.81	diorite	aq. leachate at different grain sizes, WC	Uni Bern
MFE-3.85	3.81-3.89	aplitic dyke	aq. leachate at different grain sizes, WC	Uni Bern
MFE-3.95	3.90-4.00	diorite	aq. leachate at different grain sizes, WC	Uni Bern
MFE-4.32	4.27-4.37	diorite	aq. leachate at different grain sizes, WC	Uni Bern
MFE-4.44	4.39-4.49	diorite	aq. leachate at different grain sizes, WC	Uni Bern
MFE-4.65	4.59-4.71	diorite	aq leachate, CEC at different S:L, WC	Uni Bern
MFE-9.33	9.28-9.37	granite	aq. leachate at different grain sizes, WC	Uni Bern
MFE-9.66	9.62-9.70	granite	aq. leachate at different grain sizes, WC	Uni Bern
KF93-33.66	33.62-33.70	diorite	diffusion experiment (batch), WC	Uni Bern
KF93-33.75	33.70-33.79	aplitic dyke	diffusion experiment (batch), WC	Uni Bern
KF93-33-83	33.79-33.87	diorite/aplite	diffusion experiment (batch), WC	Uni Bern

[1)] aq. Leachate: aqueous leachate; WC: water content

Methods

Aqueous leaching experiments

At the University of Waterloo the wax coating on the MFE-drillcore samples was first largely removed by scraping and heating with a heat gun. The core sample MFE-3.50 was then coarsely crushed in a jaw crusher and then pulped in a corundum shatter box. To the pulped sample (1.472 kg) one litre of ultrapure water was added and the mixture was shaken end-over-end for 24 hours under ambient conditions at room temperature. The mixture was coarse filtered (#4 filter paper) or centrifuged, followed by vacuum flask filtering through a 0.45µ filter. The remaining rock mixture was dried and the above procedure repeated a second and a third time. Following each leach, the filtered supernatant solution was analysed by ion chromatography (IC) for its major ion composition at the University of Waterloo and the SKB Äspö Laboratory, and for major and trace element compositions by ICP-AES and HR-ICP-MS at SGAB Analytica (Luleå, Sweden).

At the University of Waterloo the $^{37}C1/^{35}C1$ isotope ratio in different leachate solutions was measured according to the methodology described below (section "Borehole water").

At the University of Bern unpacking and all preparation steps were performed in a glove-box under a continuous N_2-gas stream (oxygen content of <0.1%) to minimise oxidation and under ambient laboratory conditions. All treatment of the rock material for samples MFE-3.66 and MFE-4.65 were performed wearing chloride-free gloves. First, the rim (approx. 1cm) of the core samples was removed by a chisel to ensure sample material that was neither influenced by the wax coating nor by the disturbed zone created by the drilling process. This was followed by weighing two aliquots of about 4-5cm^3 of each sample for water content measurements immediately after receiving the drillcores. The water content was determined gravimetrically by drying these aliquots at 105°C for 24, 48, and 168 hours respectively.

Aqueous leaching of samples MFE-3.66 and MFE-4.65 was performed to investigate the leaching behaviour at different solid:liquid mass ratios. The samples were crushed in the glove-box and put into N_2-filled plastic containers which were then placed in a desiccator containing phosphorous-pentoxide (P_2O_5) and transported to a carbide-tungsten mill where the crushed material was ground under N_2-gas to a grain size of <63µm (approx. 10 minutes). The ground material was then returned to the glove-box in the same way. The crushed and ground material were each exposed to air for about 2 minutes; storage in the N_2-filled plastic container outside the glove-box varied between 5-15 minutes. Aqueous leaching with double deionised water was then performed in duplicate with up to four different solid:liquid mass ratios (0.25, 0.5, 1.0, 1.5). For the different solid:liquid ratios between 15-30g of rock powder were used. The suspensions were shaken end-over-end in polypropylene tubes for 7 days and then allowed to sediment for one hour. Alkalinity and pH and measurements were carried out on small solution aliquots in the glove-box. The remaining solutions were brought outside the glove-box, centrifuged and filtered with 0.2µm millipore filters for cation and anion analyses.

Aqueous leaching of the remaining samples was performed to investigate the leaching behaviour of different grain-size fractions. Preparation and leaching of these samples were carried out under ambient laboratory conditions. They were first coarsely crushed in a jaw crusher and then continuously ground to finer grain sizes in a carbide-tungsten mill. The various grain-size fractions were removed in the interval between each crushing/grinding step by sieving the material with different mesh sizes (<3mm, 2-3mm, 1-2mm, <0.5mm, <63μm). Aqueous leaching of the different grain-size fractions was performed with double deionised water at a solid:liquid mass ratio of 1:1 using 20-30g of rock material. The suspensions were shaken end-over-end in polypropylene tubes for 2 days and then allowed to sediment for one hour. Alkalinity and pH measurements on small solution aliquots were carried out under ambient conditions. The remaining solutions were centrifuged and filtered with 0.2μm millipore filters for cation and anion analyses.

An Orion 720A pH meter with a Ross glass electrode was used for pH measurements and alkalinity was determined by titration to the methyl-orange endpoint. Cations were analysed by atomic adsorption spectroscopy (AAS) at the University of Bern and anions were analysed by ion chromatography (IC) at Hydroisotop GmbH and at the University of Neuchâtel.

The $^{87}Sr/^{86}Sr$ isotope ratio was measured at the University of Bern using a modified VG Sector® thermal ionisation mass spectrometer (TIMS) in simple collector mode, using oxidised Ta filaments. The analytical uncertainty is given with 2σ of multiple measurements of the same sample. Total Sr concentrations are given in ppm.

The removed rock material from the borehole rim was used for quantitative determination of the whole-rock and clay mineralogy, whole-rock chemical analysis, and thin section and fluid inclusion investigations. The results of these investigations are given in Appendix 10.

Cation exchange experiments

The cation exchange properties were determined for samples MFE-3.66 and MFE-4.65 using the Nickel-Ethylenediamine (Ni-(en)) Method (Baeyens and Bradbury, 1991, 1994). This method takes advantage of the high selectivity of the Ni-(en) complex which displaces all exchangeable cations from the clay and other mineral surfaces into solution. Optimum conditions are achieved when the added equivalents of Ni-(en) are approximately twice the exchange capacity. The pH of the Ni-(en) solution is buffered to 8.0-8.2 by adding HNO_3 Titrisol™ solution. Extractions were performed at different solid:liquid mass ratios and the amount of powdered rock material used was between 15g and 25g. The samples were shaken in the glove-box end-over-end for 7 days in polypropylene tubes. After phase separation by centrifuging, the supernatant leachate was removed using a syringe, filtered to 0.2μm and analysed for pH, major cations and nickel.

Cation concentrations in the Ni-en extract solutions were analysed by atomic adsorption spectroscopy (AAS) and an Orion 720A pH meter with a Ross glass electrode was used for pH-measurements.

Pore water diffusion experiment

At the University of Bern simple batch diffusion experiments have been performed on three fresh drillcore samples from borehole KF0093 A01. In this case, immediately after recovery, the core was packed correctly first into aluminium foil and subsequently coated with wax. Once received in the laboratory it was placed in a glove-box with a continuous N_2-gas stream (oxygen content of <0.1%) to minimise oxidation. All sample preparation was performed manually. Three fresh samples were weighed and placed into polypropylene vessels, which were then filled to the top with double deionised water. The water content was determined on an aliquot of all samples by drying at 105°C to stable weight conditions (>96 hours). After 2 months of equilibration time, one sample solution was analysed for pH and alkalinity and then removed from the glove-box for analyses of major ions and stable isotopes of water. For the two other samples, equilibration was allowed to continue. After 3, 4 and 5 months, a small amount of solution (about 7 mL) was removed from these samples for Cl analysis. After 5 months, the samples were removed from the glove-box and the solutions analysed for pH, alkalinity, major ions and stable isotopes of water. All three core samples were weighed immediately after removal of the solution and dried until stable weight conditions (168 hours).

An Orion 720A pH meter with a Ross glass electrode was used for pH-measurements and alkalinity was determined at the University of Bern by titration to the methyl-orange endpoint directly after recovery of the solution. Chloride was analysed by $AgNO_3$ titration. After about 21 days of storage, alkalinity and pH were determined a second time by titration to the methyl-orange endpoint and with a WTW SenTix41 electrode, respectively, in the Hydroisotop GmbH laboratory. Major cations and anions were analysed at Hydroisotop GmbH by IC, except for barium and strontium which were analysed by ICP-OES and fluoride which was analysed using an ion selective electrode.

Isotope measurements at Hydroisotop GmbH were performed using conventional mass spectrometer techniques for $\delta^{18}O$ (± 0.5‰) and $\delta^{2}H$ (± 1.5‰).

Pore water displacement experiment

At the beginning of the project it was decided to attempt a pore water displacement test in a modified triaxial test cell (section 5.6). Ten centimetres of core from the matrix block site was to be used (sample MFE-3.32). In retrospect the core length chosen was probably too long to obtain meaningful results during the lifetime of the project.

The core was first cleaned to remove any extraneous residue on its outer surface. Both ends were polished absolutely flat and a sintered metal plate was attached to each end. The core was then mounted into a special latex sheath that shrinks onto the core surface to prevent any passage of fluid along the outside of the core.

The assembled core was then mounted into the triaxial cells. A specially designed ram, with the capability of injecting fluid (i.e. double distilled water) into the specimen at high pressure, provided vertical pressure along the length of the core. The pressure in the horizontal direction (confining pressure) was maintained on the latex sleeve by hydraulic oil.

Borehole water

Immediately after recovery, the borehole waters were analysed on-site for pH using an Orion 720A pH meter with a Ross glass electrode. The pH was monitored over several tenths of minutes to investigate the solutions behaviour during exposure to the atmosphere.

At the Äspö HRL laboratory the sampled borehole waters were measured for pH and analysed for alkalinity using an Autotitrator TIM 900 (Radiometer, Copenhagen) within two hours of sampling. In the same laboratory Cl, SO_4 and Br were subsequently analysed using conventional ion chromatograpy (IC, Radiometer, Copenhagen).

The stable isotopes of water were analysed at the Institutt för Energiteknikk (IFE), Norway, using conventional mass spectrometry and expressed as per mille relative to the IAEA mean ocean water standard V-SMOW. The isotopic composition of dissolved inorganic carbon ($\delta^{13}C$, ^{14}C) was analysed at the Ångströmlaboratoriet, Uppsala University, Sweden, using a Tandem-Accelerator Mass Spectrometer. The isotope ratio of $\delta^{13}C$ is reported in per mille relative to the V-PDB standard and ^{14}C is expressed as percent modern carbon (pmc). The isotope ratio of B ($\delta^{11}B$) was analysed at BRGM, Orléan, France, on a Finnigan MAT 261 solid source mass spectrometer and is expressed as per mille relative to the NBS951 boric acid standard.

The chloride isotope ratio of the borehole waters was measured at University of Waterloo. The method used to analyse the borehole water samples for their $^{37}C1/^{35}C1$ isotopic ratios is an adaptation of that developed by Kaufmann (1984), Flatt and Heemskerk (1993) and Long et al. (1993). Briefly, AgC1 is precipitated from the aqueous chloride by the addition of $AgNO_3$. The dry AgC1 is then reacted with CH_3I to produce CH_3C1 and AgI. CH_3C1 gas, excess CHI and AgI are then cryogenically separated using a vacuum line and a gas chromatograph. In the last step, the CH_3C1 gas is measured for its $^{37}C1/^{35}C1$ ratio against a standard known as standard mean ocean chloride (SMOC). This is done at the University of Waterloo Environmental Isotope Lab (EIL) using a VG SIRA 9 Mass Spectrometer. Results are reported as the difference between the isotope ratio of the sample and that of SMOC and are expressed in per mil units according to:

$$\delta^{37}C1 = [(^{37}C1/^{35}C1)_{sample}/(^{37}C1/^{35}C1)_{SMOC} - 1] \times 1000$$

Measurements were made with a precision of ±0.12% (1σ) based on repeat analyses of SMOC, although it should be noted that others have reported deviations as low or lower than ±0.09% (Long et al., 1993; Eggenkamp, 1994; Kaufmann, 1984).

At the University of Bern, an Orion 720A pH-meter with a Ross glass electrode was used for pH-measurements, alkalinity was determined by titration to the methyl-orange endpoint, and chloride was analysed by $AgNO_3$ titration on sample MFE-S4-2.

The $^{87}Sr/^{86}Sr$ isotope ratios were measured on all samples at the University of Bern using a modified VG Sector® thermal ionisation mass spectrometer (TIMS) in simple collector mode, using oxidised Ta filaments. The analytical uncertainty is given with 2σ of multiple measurements of the same sample.

Pore water leaching studies

Table A13-2: Aqueous leachate test data for samples MFE-3.66 and MF4.65 at different solid:liquid (S:L) ratios (page 1 of 4).

SAMPLE DESCRIPTION					
Borehole		**KF0051 A01**	**KF0051 A01**	**KF0051 A01**	**KF0051 A01**
Type of Sample		Aq. Extract	Aq. Extract	Aq. Extract	Aq. Extract
Sample		MFE-3.66-a	MFE-3.66-b	MFE-3.66-c	MFE-3.66-d
Interval		3.62-3.70	3.62-3.70	3.62-3.70	3.62-3.70
Laboratory Analytics		UniBe / HI	UniBe / HI	UniBe / HI	UniBe / HI
Laboratory Extract		UniBe	UniBe	UniBe	UniBe
Extraction Date		Aug. 99	Aug. 99	Aug. 99	Aug. 99
Conditions Extraction		glovebox	glovebox	glovebox	glovebox
Extraction Time		7 days	7 days	7 days	7 days
S:L ratio		0.25	0.5	1.0	1.5
MISCELLANEOUS PROPERTIES					
pH (lab)	-log(H+)	9.9	10	10	9.9
Pt Elec Potential vs. SHE	mV				
Sample Temperature	ºC	20	20	20	20
Density (calc.)	kg / l				
DISSOLVED CONSTITUENTS					
CATIONS					
Lithium (Li^{+})	mg/l				
Sodium (Na^{+})	mg/l	23.9	41.4	66.7	87.4
Potassium (K^{+})	mg/l	21.1	32.8	39.1	46.9
Rubidium (Rb^{+})	mg/l				
Magnesium (Mg^{+2})	mg/l	2	5.3	4.9	5.8
Calcium (Ca^{+2})	mg/l	1.9	1	1.4	2.8
Strontium (Sr^{+2})	mg/l	0.05	0.08	0.09	0.11
Barium (Ba^{+2})	mg/l				
Manganese (Mn^{+2})	mg/l				
Iron (Fe^{+2})	mg/l				
Aluminium (Al)	mg/l				
Uranium (U)	mg/l				
ANIONS					
Fluoride (F^{-})	mg/l	2.1	3.6	5.7	7.4
Chloride (Cl^{-})	mg/l	7.5	17.6	35.4	51.2
Bromide (Br^{-})	mg/l	0.05	0.13	0.28	0.46
Iodide (I^{-})	mg/l				
Sulfate (SO_4^{-2})	mg/l	14.3	27.8	50.1	71.2
Phosphate (P)	mg/l				
Nitrite (NO_2^{-})	mg/l				
Nitrate (NO_3^{-})	mg/l				
Total Alkalinity	meq/l	1.2	1.7	1.7	2.5
NEUTRAL SPECIES					
Tot. Sulpfide (H_2S,HS^{-},S^{-2})	mg/l				
Silica (Si)	mg/l				
Boron (B)	mg/l				
Total Iron (Fe total)	mg/l				
Total Organic C (TOC)	mg/l				
Total Inorganic C (TIC)	mg/l				

Table A13-2: (page 2 of 4)

SAMPLE DESCRIPTION					
Borehole		**KF0051 A01**	**KF0051 A01**	**KF0051 A01**	**KF0051 A01**
Type of Sample		Aq. Extract	Aq. Extract	Aq. Extract	Aq. Extract
Sample		MFE-3.66-a	MFE-3.66-b	MFE-3.66-c	MFE-3.66-d
Interval		3.62-3.70	3.62-3.70	3.62-3.70	3.62-3.70
S:L ratio		0.25	0.5	1.0	1.5
PARAMETERS CALCULATED FROM ANALYTICAL DATA					
Sum of Analysed Constituents	mg/l	146	233	307	426
Charge Balance:					
Difference/Total	%	0.49	2.67	3.85	-1.77
ION-ION RATIOS					
Br/Cl molal	mol/mol	2.96E-03	3.28E-03	3.51E-03	3.99E-03
Na/Cl molal	mol/mol	4.92E+00	3.63E+00	2.90E+00	2.63E+00
K/Na molal	mol/mol	5.19E-01	4.66E-01	3.45E-01	3.16E-01
SO_4/Cl molal	mol/mol	7.04E-01	5.83E-01	5.22E-01	5.13E-01
CARBONATE SYSTEM					
CALCULATED USING MEASURED VALUES					
TIC from alkalinity	mol/kg	8.798E-04	1.190E-03	1.213E-03	1.840E-03
Calcite saturation index		0.22	0.05	0.16	0.54
log $P(CO_2)$		-5.34	-5.36	-5.29	-5.05
CALCULATED AT CALCITE SATURATION					
pH		9.88	10.00	9.94	9.89
log $P(CO_2)$		-5.33	-5.36	-5.29	-5.02
TIC adjusted to calcite sat.	mol/kg	8.619E-04	1.187E-03	1.203E-03	1.791E-03
SATURATION INDICES					
CALCITE (adjusted)		0.00	0.00	0.00	0.00
DOLOMITE_ORD		0.55	1.11	1.03	1.17
FLUORITE		-2.03	-1.78	-1.35	-1.24
GYPSUM		-4.07	-4.01	-3.73	-3.71
STRONTIUM		-0.84	-0.48	-0.48	-0.32
CELESITE		-3.68	-3.26	-2.99	-2.80
BARITE					
CHALCEDONY					
QUARTZ					
$Al(OH)_3$ amorph.					
KAOLINITE					

Table A13-2: (page 3 of 4)

SAMPLE DESCRIPTION				
Borehole		**KF0051 A01**	**KF0051 A01**	**KF0051 A01**
Type of Sample		Aq. Extract	Aq. Extract	Aq. Extract
Sample		MFE-3.66-c1	MFE-4.65-a	MFE-4.65-b
Interval		3.62-3.70	4.59-4.71	4.59-4.71
Laboratory Analytics		SGAB	UniBe / HI	UniBe / HI
Laboratory Extract		UniBe	UniBe	UniBe
Extraction Date		Aug. 99	Jun. 00	Jun. 00
Conditions Extraction		glovebox	glovebox	glovebox
Extraction Time		7 days	7 days	7 days
S:L ratio		1.0	0.5	1.0
MISCELLANEOUS PROPERTIES				
pH (lab)	-log(H+)		10.0	10.1
Pt Elec Potential vs. SHE	mV			
Sample Temperature	ºC	20	20	20
Density (calc.)	kg / l			
DISSOLVED CONSTITUENTS				
CATIONS				
Lithium (Li^{+})	mg/l	0.031		
Sodium (Na^{+})	mg/l	66.0	49.4	84.4
Potassium (K^{+})	mg/l	42.0	38.3	59
Rubidium (Rb^{+})	mg/l	0.088		
Magnesium (Mg^{+2})	mg/l	7.5	0.8	0.6
Calcium (Ca^{+2})	mg/l	3.8	1.5	2.6
Strontium (Sr^{+2})	mg/l	0.081	0.05	0.04
Barium (Ba^{+2})	mg/l	0.12		
Manganese (Mn^{+2})	mg/l	0.35		
Iron (Fe^{+2})	mg/l			
Aluminium (Al)	mg/l	11.0		
Uranium (U)	mg/l	0.0015		
ANIONS				
Fluoride (F^{-})	mg/l		2.9	5.1
Chloride (Cl^{-})	mg/l		33.8	72.6
Bromide (Br^{-})	mg/l	0.36	0.12	0.25
Iodide (I^{-})	mg/l	0.0014		
Sulfate (SO_4^{-2})	mg/l	47.9	8.3	20.3
Phosphate (P)	mg/l	0.28		
Nitrite (NO_2^{-})	mg/l			
Nitrate (NO_3^{-})	mg/l			
Total Alkalinity	meq/l		1.9	2.4
NEUTRAL SPECIES				
Tot. Sulfide (H_2S,HS^{-},S^{-2})	mg/l			
Silica (Si)	mg/l	24.0		
Boron (B)	mg/l	0.12		
Total Iron (Fe total)	mg/l	15.0		
Total Organic C (TOC)	mg/l			
Total Inorganic C (TIC)	mg/l			

Table A13-2: (page 4 of 4)

SAMPLE DESCRIPTION				
Borehole		**KF0051 A01**	**KF0051 A01**	**KF0051 A01**
Type of Sample		Aq. Extract	Aq. Extract	Aq. Extract
Sample		MFE-3.66-c1	MFE-4.65-a	MFE-4.65-b
Interval		3.62-3.70	4.59-4.71	4.59-4.71
S:L ratio		1.0	0.5	1.0
PARAMETERS CALCULATED FROM ANALYTICAL DATA				
Sum of Analysed Constituents	mg/l		245	391
Charge Balance:				
Difference/Total	%		3.03	2.12
ION-ION RATIOS				
Br/Cl molal	mol/mol	4.51E-03	1.59E-03	1.52E-03
Na/Cl molal	mol/mol	2.88E+00	2.26E+00	1.79E+00
K/Na molal	mol/mol	3.74E-01	4.56E-01	4.11E-01
SO_4/Cl molal	mol/mol	4.99E-01	9.06E-02	1.03E-01
CARBONATE SYSTEM				
CALCULATED USING MEASURED VALUES				
TIC from alkalinity	mol/kg	-	1.279E-03	1.624E-03
Calcite saturation index		-	0.28	0.60
log $P(CO_2)$		-	-5.32	-5.37
CALCULATED AT CALCITE SATURATION				
pH		9.98*	9.99	10.08
log $P(CO_2)$		-5.86*	-5.31	-5.36
TIC adjusted to calcite sat.	mol/kg	3.692E-04*	1.261E-03	1.576E-03
SATURATION INDICES				
CALCITE (adjusted)		0.00	0.00	0.00
DOLOMITE_ORD		0.76	0.33	0.29
FLUORITE			-1.99	-1.65
GYPSUM		-3.26	-4.56	-4.34
STRONTIANITE		-0.99	-0.64	-0.65
CELESTITE		-3.02	-3.98	-3.76
BARITE		0.35		
CHALCEDONY		0.19		
QUARTZ		0.63		
$Al(OH)_3$ amorph.		-2.72		
KAOLINITE		2.10		

*sample MFE3-66-c1 is an aliquot of sample MFE-3.66-c and was calculated using pH and alkalinity from this sample and Al adjusted to gibbsite saturation

Table A13-3: Aqueous leachate test data for multiply leached sample MFE-3.66 (page 1 of 2).

SAMPLE DESCRIPTION					
Borehole		**KF0051 A01**	**KF0051 A01**	**KF0051 A01**	**KF0051 A01**
Type of Sample		Aq. Extract	Aq. Extract	Aq. Extract	Beeswax
Sample		MFE-3.50-I	MFE-3.50-II	MFE-3.50-III	
Interval		3.40-3.60	3.40-3.60	3.40-3.60	
Laboratory Analytics		SGAB	SGAB	SGAB	SGAB
Laboratory Extract		UniWaterloo	UniWaterloo	UniWaterloo	
Extraction Date					
Conditions Extraction		ambient	ambient	ambient	
Extraction Time					
S:L ratio		1.47228 : 1	1.443068 : 1	1.41603 : 1	
Comments		1st leach	2nd leach	3rd leach	used for core sample preservation
MISCELLANEOUS PROPERTIES					
pH (lab)	-log(H+)				
Pt Elec Potential vs. SHE	mV				
Sample Temperature	ºC				
Density (calc.)	kg / l				
DISSOLVED CONSTITUENTS					
CATIONS					
Lithium (Li^{+})	mg/l	0.042	0.021	0.017	0.0002
Sodium (Na^{+})	mg/l	69	42	23	0.022
Potassium (K^{+})	mg/l	47	24	22	0.025
Rubidium (Rb^{+})	mg/l	0.11	0.027	0.024	
Magnesium (Mg^{+2})	mg/l	13	1.2	1.84	0.0014
Calcium (Ca^{+2})	mg/l	7.3	3.4	4.7	0.01
Strontium (Sr^{+2})	mg/l	0.13	0.045	0.048	0.00006
Barium (Ba^{+2})	mg/l	0.21	0.078	0.038	0.0001
Nickel (Ni^{+2})	mg/l	0.041	0.0021	0.0028	
Cobalt (Co^{+2})	mg/l	0.01	0.00048	0.00069	
Copper (Cu^{+2})	mg/l	0.015	0.012	0.0025	0.0001
Chromium (Cr tot)	mg/l	0.021	0.0012	0.0016	0.0001
Zinc (Zn^{+2})	mg/l	0.11	0.014	0.012	0.0003
Lead (Pb^{+2})	mg/l	0.013	0.0009	0.002	0.00002
Cadmium (Cd^{+2})	mg/l	0.00011	0.00005	0.00004	
Manganese (Mn^{+2})	mg/l	0.63	0.028	0.042	0.00005
Iron (Fe^{+2})	mg/l				
Arsenic (As tot)	mg/l	0.0026	0.0045	0.00087	
Selenium (Se tot)	mg/l	0.0006	0.007	0.00041	
Titanium (Ti tot)	mg/l	1.1	0.054	0.061	
Aluminium (Al)	mg/l	18	1	2.1	0.0088
Uranium (U)	mg/l	0.0043	0.0078	0.0051	
ANIONS					
Fluoride (F^{-})	mg/l				
Chloride (Cl^{-})	mg/l	31.8	20.5	9.7	
Bromide (Br^{-})	mg/l	0.3	0.48	0.077	0.008
Iodide (I^{-})	mg/l	0.0032	0.03	0.0069	
Sulfate (SO_4^{-2})	mg/l	22.2	12.9	5.4	0.007
Phosphate (P)	mg/l	0.42	0.44	0.044	0.001
Nitrite (NO_2^{-})	mg/l				
Nitrate (NO_3^{-})	mg/l				
Total Alkalinity	meq/l				

Table A13-3: (page 2 of 2)

SAMPLE DESCRIPTION					
Borehole		**KF0051 A01**	**KF0051 A01**	**KF0051 A01**	**KF0051 A01**
Type of Sample		Aq. Extract	Aq. Extract	Aq. Extract	Beeswax
Sample		MFE-3.50-I	MFE-3.50-II	MFE-3.50-III	
Interval		3.40-3.60	3.40-3.60	3.40-3.60	
S:L ratio		1.47228 : 1	1.443068 : 1	1.41603 : 1	
Comments		1st leach	2nd leach	3rd leach	used for core sample preservation
NEUTRAL SPECIES					
Tot. Sulfide (H_2S,HS^-,S^{-2})	mg/l				
Silica (Si)	mg/l	27	5.6	7.5	0.008
Boron (B)	mg/l	0.1	0.058	0.033	0.004
Total Iron (Fe total)	mg/l	24	0.92	1.6	0.0015
Total Organic C (TOC)	mg/l				
Total Inorganic C (TIC)	mg/l				
PARAMETERS CALCULATED FROM ANALYTICAL DATA					
Sum of Analysed Constituents	mg/l	263	113	78	0.10
Charge Balance: Difference/Total	%				
ION-ION RATIOS					
Br/Cl molal	mol/mol	4.19E-03	1.04E-02	3.52E-03	
Na/Cl molal	mol/mol	3.35E+00	3.16E+00	3.66E+00	
K/Na molal	mol/mol	4.01E-01	3.36E-01	5.62E-01	
SO_4/Cl molal	mol/mol	2.58E-01	2.32E-01	2.05E-01	

Table A13-4: Aqueous leachate test data for MFE-samples at different grain-size fractions (page 1 of 16).

SAMPLE DESCRIPTION			
Borehole		**KF0051 A01**	**KF0051 A01**
Type of Sample		Aq. Extract	Aq. Extract
Sample		MFE-3.66-A	MFE-3.79-A
Interval		3.62-3.70	3.77-3.81
Rock Type		Äspö Diorite	Äspö Diorite
Laboratory Analytics		UnibBe/HI	Hydroisotop
Laboratory Extract		UniBe	UniBe
Extraction Date		Jan. 00	Jan. 00
Conditions Extraction		glovebox	ambient
Extraction Time		7 days	2 days
S:L ratio		1.0	1.0
Grain Size		<63µm	<63µm
MISCELLANEOUS PROPERTIES			
pH (lab)	-log(H+)	10.0	7.4
Pt Elec Potent. vs. SHE	mV		
Sample Temperature	ºC		
Density (calc.)	kg / l		
DISSOLVED CONSTITUENTS			
CATIONS			
Lithium (Li^{+})	mg/l		
Sodium (Na^{+})	mg/l	66.7	57
Potassium (K^{+})	mg/l	39.1	35
Rubidium (Rb^{+})	mg/l		
Magnesium (Mg^{+2})	mg/l	4.9	0.94
Calcium (Ca^{+2})	mg/l	1.4	2.2
Strontium (Sr^{+2})	mg/l	0.09	0.049
Barium (Ba^{+2})	mg/l		
Manganese (Mn^{+2})	mg/l		
ANIONS			
Fluoride (F^{-})	mg/l	5.7	2.1
Chloride (Cl^{-})	mg/l	35.4	31
Bromide (Br^{-})	mg/l	0.28	0.16
Iodide (I^{-})	mg/l		
Sulfate (SO_4^{-2})	mg/l	50.1	55
Phosphate (P)	mg/l		
Nitrite (NO_2^{-})	mg/l		
Nitrate (NO_3^{-})	mg/l		
Total Alkalinity	meq/l	1.7	1.5
NEUTRAL SPECIES			
Tot. Sulfide	mg/l		
Silica (Si)	mg/l		
Boron (B)	mg/l		
Total Iron (Fe total)	mg/l		
Total Organic C (TOC)	mg/l		
Total Inorganic C (TIC)	mg/l		

Table A13-4: (page 2 of 16)

SAMPLE DESCRIPTION

Borehole		**KF0051 A01**	**KF0051 A01**
Type of Sample		Aq. Extract	Aq. Extract
Sample		MFE-3.66-A	MFE-3.79-A
Interval		3.62-3.70	3.77-3.81
S:L ratio		1.0	1.0
Grain Size		<63µm	<63µm
PARAMETERS CALCULATED FROM ANALYTICAL DATA			
Sum of Anal. Constit.	mg/l	307	275
Charge Balance:			
Difference/Total	%	3.85	-0.97
ION-ION RATIOS			
Br/Cl molal	mol/mol	3.51E-03	2.29E-03
Na/Cl molal	mol/mol	2.91E+00	2.84E+00
K/Na molal	mol/mol	3.45E-01	3.61E-01
SO_4/Cl molal	mol/mol	5.22E-01	6.55E-01
CARBONATE SYSTEM			
CALCULATED USING MEASURED VALUES			
TIC from alkalinity	mol/kg	1.180E-03	1.630E-03
Calcite saturation index		0.17	-1.79
log P(CO_2)		-5.37	-2.47

Table A13-4: (page 3 of 16)

SAMPLE DESCRIPTION						
Borehole		**KF0051 A01**	**KF0051 A01**	**KF0051 A01**	**KF0051 A01**	**KF0051 A01**
Type of Sample		Aq. Extract	Aq. Extract	Aq. Extract	Aq. Extract	Aq. Extract
Sample		MFE-3.85-A	MFE-3.85-B	MFE-3.85-C	MFE-3.85D	MFE-3.85-E
Interval		3.83-3.87	3.83-3.87	3.83-3.87	3.83-3.87	3.83-3.87
Rock Type		Aplitic Dyke	Aplitic Dyke	Aplitic Dyke	Aplitic Dyke	Aplitic Dyke
Laboratory Analytics		Hydroisotop	Hydroisotop	Hydroisotop	Hydroisotop	Hydroisotop
Laboratory Extract		UniBe	UniBe	UniBe	UniBe	UniBe
Extraction Date		Jan. 00	Jan. 00	Jan. 00	Jan. 00	Jan. 00
Conditions Extraction		ambient	ambient	ambient	ambient	ambient
Extraction Time		2 days	2 days	2 days	2 days	2 days
S:L ratio		1.0	1.0	1.0	1.0	1.0
Grain Size		<63µm	<0.5mm	1-2mm	2-3mm	>3mm
MISCELLANEOUS PROPERTIES						
pH (lab)	-log(H+)	8.9	n.a.	n.a.	n.a.	6.8
Pt Elec Potent. vs. SHE	mV					
Sample Temperature	ºC					
Density (calc.)	kg / l					
DISSOLVED CONSTITUENTS						
CATIONS						
Lithium (Li^{+})	mg/l					
Sodium (Na^{+})	mg/l	43	24	7.6	12	12
Potassium (K^{+})	mg/l	41	13	4.1	4.3	5.6
Rubidium (Rb^{+})	mg/l					
Magnesium (Mg^{+2})	mg/l	< 0.2	< 0.2	< 0.2	< 0.2	< 0.2
Calcium (Ca^{+2})	mg/l	1.7	7.2	4.8	2.7	2.4
Strontium (Sr^{+2})	mg/l	0.055	0.099	0.052	0.041	0.036
Barium (Ba^{+2})	mg/l					
Manganese (Mn^{+2})	mg/l					
ANIONS						
Fluoride (F^{-})	mg/l	0.8	0.85	0.33	0.31	0.23
Chloride (Cl^{-})	mg/l	27	16	5	4.3	3
Bromide (Br^{-})	mg/l	0.13	0.081	0.05	< 0.03	< 0.03
Iodide (I^{-})	mg/l					
Sulfate (SO_4^{-2})	mg/l	11	9.3	2.4	3.6	1.8
Phosphate (P)	mg/l					
Nitrite (NO_2^{-})	mg/l					
Nitrate (NO_3^{-})	mg/l					
Total Alkalinity	meq/l	1.9	n.a.	n.a.	n.a.	0.7
NEUTRAL SPECIES						
Tot. Sulfide	mg/l					
Silica (Si)	mg/l					
Boron (B)	mg/l					
Total Iron (Fe total)	mg/l					
Total Organic C (TOC)	mg/l					
Total Inorganic C (TIC)	mg/l					

Table A13-4: (page 4 of 16)

SAMPLE DESCRIPTION						
Borehole		**KF0051 A01**	**KF0051 A01**	**KF0051 A01**	**KF0051 A01**	**KF0051 A01**
Type of Sample		Aq. Extract	Aq. Extract	Aq. Extract	Aq. Extract	Aq. Extract
Sample		MFE-3.85-A	MFE-3.85-B	MFE-3.85-C	MFE-3.85D	MFE-3.85-E
Interval		3.83-3.87	3.83-3.87	3.83-3.87	3.83-3.87	3.83-3.87
S:L ratio		1.0	1.0	1.0	1.0	1.0
Grain Size		<63µm	<0.5mm	1-2mm	2-3mm	>3mm
PARAMETERS CALCULATED FROM ANALYTICAL DATA						
Sum of Anal. Constit.	mg/l	241	-	-	-	68
Charge Balance: Difference/Total	%	1.15	-	-	-	-3.04
ION-ION RATIOS						
Br/Cl molal	mol/mol	2.14E-03	2.25E-03	4.44E-03	-	-
Na/Cl molal	mol/mol	2.46E+00	2.31E+00	2.34E+00	4.30E+00	6.17E+00
K/Na molal	mol/mol	5.61E-01	3.18E-01	3.17E-01	2.11E-01	2.74E-01
SO_4/Cl molal	mol/mol	1.50E-01	2.15E-01	1.77E-01	3.09E-01	2.21E-01
CARBONATE SYSTEM						
CALCULATED USING MEASURED VALUES						
TIC from alkalinity	mol/kg	1.830E-03	-	-	-	9.580E-04
Calcite saturation index		-0.32	-	-	-	-2.58
log $P(CO_2)$		-3.90	-	-	-	-2.18

Table A13-4: (page 5 of 16)

SAMPLE DESCRIPTION						
Borehole		**KF0051 A01**	**KF0051 A01**	**KF0051 A01**	**KF0051 A01**	**KF0051 A01**
Type of Sample		Aq. Extract	Aq. Extract	Aq. Extract	Aq. Extract	Aq. Extract
Sample		A3.95-A	A3.95-B	A3.95-C	A3.95-D	A3.95-E
Interval		3.90-4.00	3.90-4.00	3.90-4.00	3.90-4.00	3.90-4.00
Rock Type		Äspö Diorite	Äspö Diorite	Äspö Diorite	Äspö Diorite	Äspö Diorite
Laboratory Analytics		Hydroisotop	Hydroisotop	Hydroisotop	Hydroisotop	Hydroisotop
Laboratory Extract		UniBe	UniBe	UniBe	UniBe	UniBe
Extraction Date		Jan. 00	Jan. 00	Jan. 00	Jan. 00	Jan. 00
Conditions Extraction		ambient	ambient	ambient	ambient	ambient
Extraction Time		2 days	2 days	2 days	2 days	2 days
S:L ratio		1.0	1.0	1.0	1.0	1.0
Grain Size		<63µm	<0.5mm	1-2mm	2-3mm	>3mm
MISCELLANEOUS PROPERTIES						
pH (lab)	-log(H+)	7.3	7.3	7.5	7.4	7.4
Pt Elec Potent. vs. SHE	mV					
Sample Temperature	ºC					
Density (calc.)	kg / l					
DISSOLVED CONSTITUENTS						
CATIONS						
Lithium (Li^{+})	mg/l					
Sodium (Na^{+})	mg/l	57	51	22	22	19
Potassium (K^{+})	mg/l	27	19	8.4	7.3	6
Rubidium (Rb^{+})	mg/l					
Magnesium (Mg^{+2})	mg/l	0.51	0.78	0.76	< 0.2	< 0.2
Calcium (Ca^{+2})	mg/l	1.6	2.6	1.8	1.2	1.1
Strontium (Sr^{+2})	mg/l	0.039	0.048	0.026	0.013	0.013
Barium (Ba^{+2})	mg/l					
Manganese (Mn^{+2})	mg/l					
ANIONS						
Fluoride (F^{-})	mg/l	1.9	1.9	1.1	0.92	0.8
Chloride (Cl^{-})	mg/l	27	22	6.7	5	4.1
Bromide (Br^{-})	mg/l	0.16	0.12	0.077	0.041	< 0.03
Iodide (I^{-})	mg/l					
Sulfate (SO_4^{-2})	mg/l	15	14	3.3	2.3	1.5
Phosphate (P)	mg/l					
Nitrite (NO_2^{-})	mg/l					
Nitrate (NO_3^{-})	mg/l					
Total Alkalinity	meq/l	2.1	1.8	1.1	1.0	0.9
NEUTRAL SPECIES						
Tot. Sulfide	mg/l					
Silica (Si)	mg/l					
Boron (B)	mg/l					
Total Iron (Fe total)	mg/l					
Total Organic C (TOC)	mg/l					
Total Inorganic C (TIC)	mg/l					

Table A13-4: (page 6 of 16)

SAMPLE DESCRIPTION						
Borehole		**KF0051 A01**	**KF0051 A01**	**KF0051 A01**	**KF0051 A01**	**KF0051 A01**
Type of Sample		Aq. Extract	Aq. Extract	Aq. Extract	Aq. Extract	Aq. Extract
Sample		A3.95-A	A3.95-B	A3.95-C	A3.95-D	A3.95-E
Interval		3.90-4.00	3.90-4.00	3.90-4.00	3.90-4.00	3.90-4.00
S:L ratio		1.0	1.0	1.0	1.0	1.0
Grain Size		<63µm	<0.5mm	1-2mm	2-3mm	>3mm
PARAMETERS CALCULATED FROM ANALYTICAL DATA						
Sum of Anal. Constit.	mg/l	258	221	111	100	87
Charge Balance: Difference/Total	%	0.26	1.48	-3.34	-1.36	-2.68
ION-ION RATIOS						
Br/Cl molal	mol/mol	2.63E-03	2.42E-03	5.10E-03	3.64E-03	-
Na/Cl molal	mol/mol	3.26E+00	3.57E+00	5.06E+00	6.79E+00	7.15E+00
K/Na molal	mol/mol	2.79E-01	2.19E-01	2.25E-01	1.95E-01	1.86E-01
SO_4/Cl molal	mol/mol	2.05E-01	2.35E-01	1.82E-01	1.70E-01	1.35E-01
CARBONATE SYSTEM						
CALCULATED USING MEASURED VALUES						
TIC from alkalinity	mol/kg	2.340E-03	2.000E-03	1.180E-03	1.090E-03	9.820E-04
Calcite saturation index		-1.85	-1.70	-1.83	-2.14	-2.22
log P(CO_2)		-2.22	-2.28	-2.69	-2.63	-2.67

Table A13-4: (page 7 of 16)

SAMPLE DESCRIPTION						
Borehole		**KF0051 A01**	**KF0051 A01**	**KF0051 A01**	**KF0051 A01**	**KF0051 A01**
Type of Sample		Aq. Extract	Aq. Extract	Aq. Extract	Aq. Extract	Aq. Extract
Sample		A4.32-A	A4.32-B	A4.32-C	A4.32-D	A4.32-E
Interval		4.27-4.37	4.27-4.37	4.27-4.37	4.27-4.37	4.27-4.37
Rock Type		Äspö Diorite	Äspö Diorite	Äspö Diorite	Äspö Diorite	Äspö Diorite
Laboratory Analytics		Hydroisotop	Hydroisotop	Hydroisotop	Hydroisotop	Hydroisotop
Laboratory Extract		UniBe	UniBe	UniBe	UniBe	UniBe
Extraction Date		Jan. 00	Jan. 00	Jan. 00	Jan. 00	Jan. 00
Conditions Extraction		ambient	ambient	ambient	ambient	ambient
Extraction Time		2 days	2 days	2 days	2 days	2 days
S:L ratio		1.0	1.0	1.0	1.0	1.0
Grain Size		<63µm	<0.5mm	1-2mm	2-3mm	>3mm
MISCELLANEOUS PROPERTIES						
pH (lab)	-log(H+)	7.7	7.3	7.3	8.8	7.2
Pt Elec Potent. vs. SHE	mV					
Sample Temperature	ºC					
Density (calc.)	kg / l					
DISSOLVED CONSTITUENTS						
CATIONS						
Lithium (Li^{+})	mg/l					
Sodium (Na^{+})	mg/l	74	58	30	26	22
Potassium (K^{+})	mg/l	38	20	13	11	8.2
Rubidium (Rb^{+})	mg/l					
Magnesium (Mg^{+2})	mg/l	0.26	0.23	0.63	0.41	< 0.2
Calcium (Ca^{+2})	mg/l	4.9	3.3	1.6	1.1	0.91
Strontium (Sr^{+2})	mg/l	0.094	0.06	0.023	0.015	0.01
Barium (Ba^{+2})	mg/l					
Manganese (Mn^{+2})	mg/l					
ANIONS						
Fluoride (F^{-})	mg/l	3	1.9	1.5	1.4	1
Chloride (Cl^{-})	mg/l	41	28	7.5	6.1	4.9
Bromide (Br^{-})	mg/l	0.26	0.2	0.038	0.092	0.02
Iodide (I^{-})	mg/l					
Sulfate (SO_4^{-2})	mg/l	53	33	10	5.9	3.9
Phosphate (P)	mg/l					
Nitrite (NO_2^{-})	mg/l					
Nitrate (NO_3^{-})	mg/l					
Total Alkalinity	meq/l	1.9	1.6	1.2	1.1	1.0
NEUTRAL SPECIES						
Tot. Sulfide	mg/l					
Silica (Si)	mg/l					
Boron (B)	mg/l					
Total Iron (Fe total)	mg/l					
Total Organic C (TOC)	mg/l					
Total Inorganic C (TIC)	mg/l					

Table A13-4: (page 8 of 16)

SAMPLE DESCRIPTION						
Borehole		**KF0051 A01**	**KF0051 A01**	**KF0051 A01**	**KF0051 A01**	**KF0051 A01**
Type of Sample		Aq. Extract	Aq. Extract	Aq. Extract	Aq. Extract	Aq. Extract
Sample		A4.32-A	A4.32-B	A4.32-C	A4.32-D	A4.32-E
Interval		4.27-4.37	4.27-4.37	4.27-4.37	4.27-4.37	4.27-4.37
S:L ratio		1.0	1.0	1.0	1.0	1.0
Grain Size		<63µm	<0.5mm	1-2mm	2-3mm	>3mm
PARAMETERS CALCULATED FROM ANALYTICAL DATA						
Sum of Anal. Constit.	mg/l	330	242	138	119	102
Charge Balance: Difference/Total	%	1.57	0.57	2.02	1.05	-2.42
ION-ION RATIOS						
Br/Cl molal	mol/mol	2.81E-03	3.17E-03	2.25E-03	6.69E-03	1.81E-03
Na/Cl molal	mol/mol	2.78E+00	3.19E+00	6.17E+00	6.57E+00	6.92E+00
K/Na molal	mol/mol	3.02E-01	2.03E-01	2.55E-01	2.49E-01	2.19E-01
SO_4/Cl molal	mol/mol	4.77E-01	4.35E-01	4.92E-01	3.57E-01	2.94E-01
CARBONATE SYSTEM						
CALCULATED USING MEASURED VALUES						
TIC from alkalinity	mol/kg	1.979E-03	1.779E-03	1.337E-03	1.067E-03	1.145E-03
Calcite saturation index		-1.05	-1.66	-2.06	-0.79	-2.46
log P(CO_2)		-2.67	-2.34	-2.45	-4.02	-2.43

Table A13-4: (page 9 of 16)

SAMPLE DESCRIPTION

Borehole		**KF0051 A01**	**KF0051 A01**	**KF0051 A01**	**KF0051 A01**	**KF0051 A01**
Type of Sample		Aq. Extract	Aq. Extract	Aq. Extract	Aq. Extract	Aq. Extract
Sample		A4.44-A	A4.44-B	A4.44-C	A4.44-D	A4.44-E
Interval		4.39-3.49	4.39-3.49	4.39-3.49	4.39-3.49	4.39-3.49
Rock Type		Äspö Diorite	Äspö Diorite	Äspö Diorite	Äspö Diorite	Äspö Diorite
Laboratory Analytics		Hydroisotop	Hydroisotop	Hydroisotop	Hydroisotop	Hydroisotop
Laboratory Extract		UniBe	UniBe	UniBe	UniBe	UniBe
Extraction Date		Jan. 00	Jan. 00	Jan. 00	Jan. 00	Jan. 00
Conditions Extraction		ambient	ambient	ambient	ambient	ambient
Extraction Time		2 days	2 days	2 days	2 days	2 days
S:L ratio		1.0	1.0	1.0	1.0	1.0
Grain Size		<63µm	<0.5mm	1-2mm	2-3mm	>3mm
MISCELLANEOUS PROPERTIES						
pH (lab)	-log(H+)	7.2	7.2	7.5	7.2	7.6
Pt Elec Potent. vs. SHE	mV					
Sample Temperature	ºC					
Density (calc.)	kg / l					
DISSOLVED CONSTITUENTS						
CATIONS						
Lithium (Li^{+})	mg/l					
Sodium (Na^{+})	mg/l	68	57	27	25	24
Potassium (K^{+})	mg/l	32	20	11	9.8	9
Rubidium (Rb^{+})	mg/l					
Magnesium (Mg^{+2})	mg/l	1.7	< 0.2	< 0.2	< 0.2	0.51
Calcium (Ca^{+2})	mg/l	3.7	4.2	1	0.93	1.1
Strontium (Sr^{+2})	mg/l	0.068	0.062	0.013	0.01	0.015
Barium (Ba^{+2})	mg/l					
Manganese (Mn^{+2})	mg/l					
ANIONS						
Fluoride (F^{-})	mg/l	3.4	2.2	1.5	1.4	1.2
Chloride (Cl^{-})	mg/l	37	27	7.6	5.8	5
Bromide (Br^{-})	mg/l	0.28	0.19	0.094	0.061	0.039
Iodide (I^{-})	mg/l					
Sulfate (SO_4^{-2})	mg/l	34	33	8.8	5.3	3.7
Phosphate (P)	mg/l					
Nitrite (NO_2^{-})	mg/l					
Nitrate (NO_3^{-})	mg/l					
Total Alkalinity	meq/l	2.1	1.6	1.1	1.1	1.1
NEUTRAL SPECIES						
Tot. Sulfide	mg/l					
Silica (Si)	mg/l					
Boron (B)	mg/l					
Total Iron (Fe total)	mg/l					
Total Organic C (TOC)	mg/l					
Total Inorganic C (TIC)	mg/l					

Table A13-4: (page 10 of 16)

SAMPLE DESCRIPTION						
Borehole		**KF0051 A01**	**KF0051 A01**	**KF0051 A01**	**KF0051 A01**	**KF0051 A01**
Type of Sample		Aq. Extract	Aq. Extract	Aq. Extract	Aq. Extract	Aq. Extract
Sample		A4.44-A	A4.44-B	A4.44-C	A4.44-D	A4.44-E
Interval		4.39-3.49	4.39-3.49	4.39-3.49	4.39-3.49	4.39-3.49
S:L ratio		1.0	1.0	1.0	1.0	1.0
Grain Size		<63µm	<0.5mm	1-2mm	2-3mm	>3mm
PARAMETERS CALCULATED FROM ANALYTICAL DATA						
Sum of Anal. Constit.	mg/l	308	241	124	115	112
Charge Balance: Difference/Total	%	0.82	0.53	-2.37	-2.28	-0.44
ION-ION RATIOS						
Br/Cl molal	mol/mol	3.36E-03	3.12E-03	5.49E-03	4.67E-03	3.46E-03
Na/Cl molal	mol/mol	2.83E+00	3.26E+00	5.48E+00	6.65E+00	7.40E+00
K/Na molal	mol/mol	2.77E-01	2.06E-01	2.40E-01	2.30E-01	2.20E-01
SO_4/Cl molal	mol/mol	3.39E-01	4.51E-01	4.27E-01	3.37E-01	2.73E-01
CARBONATE SYSTEM						
CALCULATED USING MEASURED VALUES						
TIC from alkalinity	mol/kg	2.390E-03	1.830E-03	1.180E-03	1.260E-03	1.160E-03
Calcite saturation index		-1.61	-1.66	-2.09	-2.42	-1.94
log P(CO_2)		-2.12	-2.24	-2.69	-2.39	-2.79

Table A13-4: (page 11 of 16)

SAMPLE DESCRIPTION						
Borehole		**KF0051 A01**	**KF0051 A01**	**KF0051 A01**	**KF0051 A01**	**KF0051 A01**
Type of Sample		Aq. Extract	Aq. Extract	Aq. Extract	Aq. Extract	Aq. Extract
Sample		MFE-4.65-A	MFE-4.65-B	MFE-4.65-C	MFE-4.65-D	MFE-4.65-E
Interval		4.59-4.71	4.59-4.71	4.59-4.71	4.59-4.71	4.59-4.71
Rock Type		Äspö Diorite	Äspö Diorite	Äspö Diorite	Äspö Diorite	Äspö Diorite
Laboratory Analytics		UniBe/ UniNe	UniBe/ UniNe	UniBe/ UniNe	UniBe/ UniNe	UniBe/ UniNe
Laboratory Extract		UniBe	UniBe	UniBe	UniBe	UniBe
Extraction Date		Jan. 00	Jan. 00	Jan. 00	Jan. 00	Jan. 00
Conditions Extraction		glovebox	ambient	ambient	ambient	ambient
Extraction Time		7 days	2 days	2 days	2 days	2 days
S:L ratio		1.0	1.0	1.0	1.0	1.0
Grain Size		<63µm	<0.5mm	1-2mm	2-3mm	>3mm
MISCELLANEOUS PROPERTIES						
pH (lab)	-log(H+)	10.1	n.a.	8.4	8.6	8.6
Pt Elec Potent. vs. SHE	mV					
Sample Temperature	ºC					
Density (calc.)	kg / l					
DISSOLVED CONSTITUENTS						
CATIONS						
Lithium (Li^{+})	mg/l					
Sodium (Na^{+})	mg/l	84.4	41.4	26.6	23.2	20.8
Potassium (K^{+})	mg/l	59	13.5	10.2	8.4	7.4
Rubidium (Rb^{+})	mg/l					
Magnesium (Mg^{+2})	mg/l	0.60	0.56	1.94	0.98	0.64
Calcium (Ca^{+2})	mg/l	2.60	1.92	2.00	1.68	1.54
Strontium (Sr^{+2})	mg/l	0.038	0.027	0.050	0.028	0.024
Barium (Ba^{+2})	mg/l					
Manganese (Mn^{+2})	mg/l					
ANIONS						
Fluoride (F^{-})	mg/l	5.1	1.3	1.9	1.3	1.4
Chloride (Cl^{-})	mg/l	72.6	30.5	6.8	5.2	4.8
Bromide (Br^{-})	mg/l	0.248	0.100	0.038	0.026	0.030
Iodide (I^{-})	mg/l					
Sulfate (SO_4^{-2})	mg/l	20.3	0.8	1.8	1.3	1.2
Phosphate (P)	mg/l					
Nitrite (NO_2^{-})	mg/l					
Nitrate (NO_3^{-})	mg/l					
Total Alkalinity	meq/l	2.4	n.a.	1.4	1.2	1.0
NEUTRAL SPECIES						
Tot. Sulfide	mg/l					
Silica (Si)	mg/l					
Boron (B)	mg/l					
Total Iron (Fe total)	mg/l					
Total Organic C (TOC)	mg/l					
Total Inorganic C (TIC)	mg/l					

Table A13-4: (page 12 of 16)

SAMPLE DESCRIPTION						
Borehole		**KF0051 A01**	**KF0051 A01**	**KF0051 A01**	**KF0051 A01**	**KF0051 A01**
Type of Sample		Aq. Extract	Aq. Extract	Aq. Extract	Aq. Extract	Aq. Extract
Sample		MFE-4.65-A	MFE-4.65-B	MFE-4.65-C	MFE-4.65-D	MFE-4.65-E
Interval		4.59-4.71	4.59-4.71	4.59-4.71	4.59-4.71	4.59-4.71
S:L ratio		1.0	1.0	1.0	1.0	1.0
Grain Size		<63µm	<0.5mm	1-2mm	2-3mm	>3mm
PARAMETERS CALCULATED FROM ANALYTICAL DATA						
Sum of Anal. Constit.	mg/l	391	-	137	115	99
Charge Balance: Difference/Total	%	2.13	-	-1.39	-2.03	-0.49
ION-ION RATIOS						
Br/Cl molal	mol/mol	1.52E-03	1.46E-03	2.48E-03	2.22E-03	2.77E-03
Na/Cl molal	mol/mol	1.79E+00	2.10E+00	6.03E+00	6.88E+00	6.68E+00
K/Na molal	mol/mol	4.11E-01	1.92E-01	2.25E-01	2.13E-01	2.09E-01
SO_4/Cl molal	mol/mol	1.03E-01	9.09E-03	9.77E-02	9.23E-02	9.23E-02
CARBONATE SYSTEM						
CALCULATED USING MEASURED VALUES						
TIC from alkalinity	mol/kg	1.630E-03	-	1.390E-03	1.180E-03	9.830E-04
Calcite saturation index		0.63	-	-0.81	-0.75	-0.86
log P(CO_2)		-5.37	-	-3.50	-3.77	-3.85

Table A13-4: (page 13 of 16)

SAMPLE DESCRIPTION						
Borehole		**KF0051 A01**	**KF0051 A01**	**KF0051 A01**	**KF0051 A01**	**KF0051 A01**
Type of Sample		Aq. Extract	Aq. Extract	Aq. Extract	Aq. Extract	Aq. Extract
Sample		A9.33-A	A9.33-B	A9.33-C	A9.33-D	A9.33-E
Interval		9.28-9.37	9.28-9.37	9.28-9.37	9.28-9.37	9.28-9.37
Rock Type		Ävrö Granite	Ävrö Granite	Ävrö Granite	Ävrö Granite	Ävrö Granite
Laboratory Analytics		Hydroisotop	Hydroisotop	Hydroisotop	Hydroisotop	Hydroisotop
Laboratory Extract		UniBe	UniBe	UniBe	UniBe	UniBe
Extraction Date		Jan. 00	Jan. 00	Jan. 00	Jan. 00	Jan. 00
Conditions Extraction		ambient	ambient	ambient	ambient	ambient
Extraction Time		2 days	2 days	2 days	2 days	2 days
S:L ratio		1.0	1.0	1.0	1.0	1.0
Grain Size		<63µm	<0.5mm	1-2mm	2-3mm	>3mm
MISCELLANEOUS PROPERTIES						
pH (lab)	-log(H+)	7.3	7.2	8.8	7.3	8.6
Pt Elec Potent. vs. SHE	mV					
Sample Temperature	ºC					
Density (calc.)	kg / l					
DISSOLVED CONSTITUENTS						
CATIONS						
Lithium (Li^{+})	mg/l					
Sodium (Na^{+})	mg/l	46	41	21	21	18
Potassium (K^{+})	mg/l	25	17	6.9	6.8	5.7
Rubidium (Rb^{+})	mg/l					
Magnesium (Mg^{+2})	mg/l	1	< 0.2	0.21	< 0.2	< 0.2
Calcium (Ca^{+2})	mg/l	2.3	2.9	1.7	1.1	1.2
Strontium (Sr^{+2})	mg/l	0.052	0.047	0.022	0.012	0.017
Barium (Ba^{+2})	mg/l					
Manganese (Mn^{+2})	mg/l					
ANIONS						
Fluoride (F^{-})	mg/l	1.5	1.5	0.8	0.77	0.55
Chloride (Cl^{-})	mg/l	33	27	6.4	5.1	3.9
Bromide (Br^{-})	mg/l	0.14	0.11	0.051	0.054	0.037
Iodide (I^{-})	mg/l					
Sulfate (SO_4^{-2})	mg/l	6	8.4	1.5	1.1	0.85
Phosphate (P)	mg/l					
Nitrite (NO_2^{-})	mg/l					
Nitrate (NO_3^{-})	mg/l					
Total Alkalinity	meq/l	1.6	1.3	1.0	1.0	0.9
NEUTRAL SPECIES						
Tot. Sulfide	mg/l					
Silica (Si)	mg/l					
Boron (B)	mg/l					
Total Iron (Fe total)	mg/l					
Total Organic C (TOC)	mg/l					
Total Inorganic C (TIC)	mg/l					

Table A13-4: (page 14 of 16)

SAMPLE DESCRIPTION						
Borehole		**KF0051 A01**	**KF0051 A01**	**KF0051 A01**	**KF0051 A01**	**KF0051 A01**
Type of Sample		Aq. Extract	Aq. Extract	Aq. Extract	Aq. Extract	Aq. Extract
Sample		A9.33-A	A9.33-B	A9.33-C	A9.33-D	A9.33-E
Interval		9.28-9.37	9.28-9.37	9.28-9.37	9.28-9.37	9.28-9.37
S:L ratio		1.0	1.0	1.0	1.0	1.0
Grain Size		<63µm	<0.5mm	1-2mm	2-3mm	>3mm
PARAMETERS CALCULATED FROM ANALYTICAL DATA						
Sum of Anal. Constit.	mg/l	213	177	100	97	85
Charge Balance: Difference/Total	%	1.82	1	-2.62	-2.83	-3.33
ION-ION RATIOS						
Br/Cl molal	mol/mol	1.88E-03	1.81E-03	3.54E-03	4.70E-03	4.21E-03
Na/Cl molal	mol/mol	2.15E+00	2.34E+00	5.06E+00	6.35E+00	7.12E+00
K/Na molal	mol/mol	3.20E-01	2.44E-01	1.93E-01	1.90E-01	1.86E-01
SO_4/Cl molal	mol/mol	6.71E-02	1.15E-01	8.65E-02	7.96E-02	8.04E-02
CARBONATE SYSTEM						
CALCULATED USING MEASURED VALUES						
TIC from alkalinity	mol/kg	1.780E-03	1.490E-03	9.690E-04	1.110E-03	8.850E-04
Calcite saturation index		-1.80	-1.88	-0.63	-2.27	-1.00
log P(CO_2)		-2.33	-2.32	-4.06	-2.53	-3.89

Table A13-4: (page 15 of 16)

SAMPLE DESCRIPTION						
Borehole		**KF0051 A01**	**KF0051 A01**	**KF0051 A01**	**KF0051 A01**	**KF0051 A01**
Type of Sample		Aq. Extract	Aq. Extract	Aq. Extract	Aq. Extract	Aq. Extract
Sample		A9.66-A	A9.66-B	A9.66-C	A9.66-D	A9.66-E
Interval		9.62-9.70	9.62-9.70	9.62-9.70	9.62-9.70	9.62-9.70
Rock Type		Ävrö Granite	Ävrö Granite	Ävrö Granite	Ävrö Granite	Ävrö Granite
Laboratory Analytics		Hydroisotop	Hydroisotop	Hydroisotop	Hydroisotop	Hydroisotop
Laboratory Extract		UniBe	UniBe	UniBe	UniBe	UniBe
Extraction Date		Jan. 00	Jan. 00	Jan. 00	Jan. 00	Jan. 00
Conditions Extraction		ambient	ambient	ambient	ambient	ambient
Extraction Time		2 days	2 days	2 days	2 days	2 days
S:L ratio		1.0	1.0	1.0	1.0	1.0
Grain Size		<63µm	<0.5mm	1-2mm	2-3mm	>3mm
MISCELLANEOUS PROPERTIES						
pH (lab)	-log(H+)	7.4	7.3	8.8	7.5	7.4
Pt Elec Potent. vs. SHE	mV					
Sample Temperature	ºC					
Density (calc.)	kg / l					
DISSOLVED CONSTITUENTS						
CATIONS						
Lithium (Li^{+})	mg/l					
Sodium (Na^{+})	mg/l	59	48	28	26	21
Potassium (K^{+})	mg/l	23	14	8.9	8.7	6.8
Rubidium (Rb^{+})	mg/l					
Magnesium (Mg^{+2})	mg/l	< 0.2	< 0.2	1.1	0.53	<0.2
Calcium (Ca^{+2})	mg/l	3.1	2.5	1.5	1.3	1.1
Strontium (Sr^{+2})	mg/l	0.07	0.042	0.028	0.023	0.012
Barium (Ba^{+2})	mg/l					
Manganese (Mn^{+2})	mg/l					
ANIONS						
Fluoride (F^{-})	mg/l	1.6	1.6	1.1	0.71	0.6
Chloride (Cl^{-})	mg/l	38	24	5.8	4.6	3.3
Bromide (Br^{-})	mg/l	0.14	0.1	0.075	< 0.03	<0.03
Iodide (I^{-})	mg/l					
Sulfate (SO_4^{-2})	mg/l	12	11	2.2	1.4	0.95
Phosphate (P)	mg/l					
Nitrite (NO_2^{-})	mg/l					
Nitrate (NO_3^{-})	mg/l					
Total Alkalinity	meq/l	1.7	1.6	1.4	1.3	1.0
NEUTRAL SPECIES						
Tot. Sulfide	mg/l					
Silica (Si)	mg/l					
Boron (B)	mg/l					
Total Iron (Fe total)	mg/l					
Total Organic C (TOC)	mg/l					
Total Inorganic C (TIC)	mg/l					

Table A13-4: (page 16 of 16)

SAMPLE DESCRIPTION						
Borehole		**KF0051 A01**	**KF0051 A01**	**KF0051 A01**	**KF0051 A01**	**KF0051 A01**
Type of Sample		Aq. Extract	Aq. Extract	Aq. Extract	Aq. Extract	Aq. Extract
Sample		A9.66-A	A9.66-B	A9.66-C	A9.66-D	A9.66-E
Interval		9.62-9.70	9.62-9.70	9.62-9.70	9.62-9.70	9.62-9.70
S:L ratio		1.0	1.0	1.0	1.0	1.0
Grain Size		<63µm	<0.5mm	1-2mm	2-3mm	>3mm
PARAMETERS CALCULATED FROM ANALYTICAL DATA						
Sum of Anal. Constit.	mg/l	241	199	134	123	95
Charge Balance: Difference/Total	%	3.14	-0.41	-1.78	-1.16	-0.17
ION-ION RATIOS						
Br/Cl molal	mol/mol	1.63E-03	1.85E-03	5.74E-03		
Na/Cl molal	mol/mol	2.39E+00	3.08E+00	7.44E+00	8.72E+00	9.81E+00
K/Na molal	mol/mol	2.29E-01	1.71E-01	1.87E-01	1.97E-01	1.90E-01
SO_4/Cl molal	mol/mol	1.17E-01	1.69E-01	1.40E-01	1.12E-01	1.06E-01
CARBONATE SYSTEM						
CALCULATED USING MEASURED VALUES						
TIC from alkalinity	mol/kg	1.850E-03	1.780E-03	1.360E-03	1.390E-03	1.090E-03
Calcite saturation index		-1.55	-1.76	-0.56	-1.90	-2.17
log P(CO_2)		-2.41	-2.33	-3.91	-2.62	-2.63

Cation exchange data

Table A13-5: Äspö diorite: Cation concentrations in Ni-en extract solutions and corresponding aqueous leachate test data at different solid:liquid (S:L) ratios (page 1 of 2).

SAMPLE DESCRIPTION					
Borehole		**KF0051 A01**	**KF0051 A01**	**KF0051 A01**	**KF0051 A01**
Type of Sample		Ni-en Extract	Ni-en Extract	Ni-en Extract	Ni-en Extract
Sample		MFE-3.66-aNi	MFE-3.66-bNi	MFE-3.66-cNi	MFE-3.66-dNi
Interval		3.62-3.70	3.62-3.70	3.62-3.70	3.62-3.70
Laboratory Analytics		UniBe	UniBe	UniBe	UniBe
Laboratory Extract		UniBe	UniBe	UniBe	UniBe
Extraction Date		Aug. 99	Aug. 99	Aug. 99	Aug. 99
Conditions Extraction		glovebox	glovebox	glovebox	glovebox
Extraction Time		7 days	7 days	7 days	7 days
S:L ratio		0.25	0.5	1.0	1.5
N-i-en EXTRACTION TEST DATA :					
pH (lab)	-log(H+)	9.9	9.9	9.7	9.6
Sample Temperature	ºC	20	20	20	20
EXCHANGED CATIONS					
Sodium (Na^{+})	meq/kg rock	4.8	4.6	4.75	4.3
Potassium (K^{+})	meq/kg rock	4.3	4.1	3.7	3.2
Magnesium (Mg^{+2})	meq/kg rock	0.27	0.17	0.15	0.15
Calcium (Ca^{+2})	meq/kg rock	2.35	1.85	1.6	1.7
Strontium (Sr^{+2})	meq/kg rock	0.0019	0.0016	0.0018	0.0018
Sum exchanged cations	meq/kg rock	11.7	10.7	10.2	9.3
AQUEOUS EXTRACTION TEST DATA :					
Type of Sample		Aq. Extract	Aq. Extract	Aq. Extract	Aq. Extract
Laboratory Analytics		UniBe / HI	UniBe / HI	UniBe / HI	UniBe / HI
Laboratory Extract		UniBe	UniBe	UniBe	UniBe
pH (lab)	-log(H+)	9.9	10	10	9.9
Sample Temperature	ºC	20	20	20	20
DISSOLVED CONSITIUENTS					
CATIONS					
Sodium (Na^{+})	mg/l	23.9	41.4	66.7	87.4
Potassium (K^{+})	mg/l	21.1	32.8	39.1	46.9
Magnesium (Mg^{+2})	mg/l	2	5.3	4.9	5.8
Calcium (Ca^{+2})	mg/l	1.9	1	1.4	2.8
Strontium (Sr^{+2})	mg/l	0.05	0.08	0.09	0.11
ANIONS					
Fluoride (F^{-})	mg/l	2.1	3.6	5.7	7.4
Chloride (Cl^{-})	mg/l	7.5	17.6	35.4	51.2
Bromide (Br^{-})	mg/l	0.05	0.13	0.28	0.46
Sulfate (SO_4^{-2})	mg/l	14.3	27.8	50.1	71.2
Total Alkalinity	meq/l	1.2	1.7	1.7	2.5

Table A13-5: (page 2 of 2).

SAMPLE DESCRIPTION

Borehole		**KF0051 A01**	**KF0051 A01**
Type of Sample		Ni-en Extract	Ni-en Extract
Sample		MFE-4.65-a	MFE-4.65-bNi
Interval		4.59-4.71	4.59-4.71
Laboratory Analytics		UniBe	UniBe
Laboratory Extract		UniBe	UniBe
Extraction Date		Jun. 00	Jun. 00
Conditions Extraction		glovebox	glovebox
Extraction Time		7 days	7 days
S:L ratio		0.5	1.0
N-i-en EXTRACTION TEST DATA :			
pH (lab)	-log(H+)		9.7
Sample Temperature	ºC		20
EXCHANGED CATIONS			
Sodium (Na^{+})	meq/kg rock		4.8
Potassium (K^{+})	meq/kg rock		3.2
Magnesium (Mg^{+2})	meq/kg rock		0.69
Calcium (Ca^{+2})	meq/kg rock		1.56
Strontium (Sr^{+2})	meq/kg rock		0.0073
Sum exchanged cations	meq/kg rock		10.25
AQUEOUS EXTRACTION TEST DATA :			
Type of Sample		Aq. Extract	Aq. Extract
Laboratory Analytics		UniBe / HI	UniBe / HI
Laboratory Extract		UniBe	UniBe
pH (lab)	-log(H+)	10.0	10.1
Sample Temperature	ºC	20	20
DISSOLVED CONSITIUENTS			
CATIONS			
Sodium (Na^{+})	mg/l	49.4	84.4
Potassium (K^{+})	mg/l	38.3	59
Magnesium (Mg^{+2})	mg/l	0.8	0.6
Calcium (Ca^{+2})	mg/l	1.5	2.6
Strontium (Sr^{+2})	mg/l	0.05	0.04
ANIONS			
Fluoride (F^{-})	mg/l	2.9	5.1
Chloride (Cl^{-})	mg/l	33.8	72.6
Bromide (Br^{-})	mg/l	0.12	0.25
Sulfate (SO_4^{-2})	mg/l	8.3	20.3
Total Alkalinity	meq/l	1.9	2.4

Pore water diffusion experiment

Table A13-6: Chemical data of solutions from diffusion experiments (page 1 of 6).

SAMPLE DESCRIPTION					
Borehole		**KF0093-A0**	**KF0093-A0**	**KF0093-A0**	**KF0093-A0**
Type of Sample		Diff.-Ex.	Diff.-Ex.	Diff.-Ex.	Diff.-Ex.
Sample		KF93-1	KF93-1	KF93-1	KF93-1
Interval		33.62-33.70	33.62-33.70	33.62-33.70	33.62-33.70
Rock Type		diorite	diorite	diorite	diorite
Laboratory Analytics		UniBe	UniBe	UniBe	Hydroisotop
Experiment Conditions		glovebox	glovebox	glovebox	glovebox
Date Sampling		12-Nov-01	10-Dec-01	16-Jan-02	16-Jan-02
Date Analysis		12-Nov-01	10-Dec-01	17-Jan-02	Feb. 02
Sample Volume		approx. 7ml	approx. 7ml	total Vol.	total Vol.
WATER TYPE					Na-(Ca)-Cl-HCO_3
MISCELLANEOUS PROPERTIES					
pH (lab)	-log(H+)			8.05	7.9
Pt Elec Potential vs. SHE	mV				
Sample Temperature	ºC				20
Density (calc.)	kg / l				
DISSOLVED CONSTITUENTS					
CATIONS					
Lithium (Li^{+})	mg/l				
Sodium (Na^{+})	mg/l				31.7
Potassium (K^{+})	mg/l				1.1
Rubidium (Rb^{+})	mg/l				
Magnesium (Mg^{+2})	mg/l				<0.5
Calcium (Ca^{+2})	mg/l				7.9
Strontium (Sr^{+2})	mg/l				0.088
Barium (Ba^{+2})	mg/l				
Manganese (Mn^{+2})	mg/l				
Iron (Fe^{+2})	mg/l				
ANIONS					
Fluoride (F^{-})	mg/l				3.8
Chloride (Cl^{-})	mg/l	55.1	53.7	48.6	32.6
Bromide (Br^{-})	mg/l				<0.05
Iodide (I^{-})	mg/l				
Sulfate (SO_4^{-2})	mg/l				5.5
Phosphate (P)	mg/l				
Nitrite (NO_2^{-})	mg/l				
Nitrate (NO_3^{-})	mg/l				
Total Alkalinity	meq/l			0.52	0.7
NEUTRAL SPECIES					
Tot. Sulfide (H_2S,HS^{-},S^{-2})	mg/l				
Silica (Si)	mg/l				
Boron (B)	mg/l				
Total Iron (Fe total)	mg/l				
Total Organic C (TOC)	mg/l				
Total Inorganic C (TIC)	mg/l				

Table A13-6: (page 2 of 6).

SAMPLE DESCRIPTION					
Borehole		**KF0093-A0**	**KF0093-A0**	**KF0093-A0**	**KF0093-A0**
Type of Sample		Diff.-Ex.	Diff.-Ex.	Diff.-Ex.	Diff.-Ex.
Sample		KF93-1	KF93-1	KF93-1	KF93-1
Interval		33.62-33.70	33.62-33.70	33.62-33.70	33.62-33.70
Date Sampling		12-Nov-01	10-Dec-01	16-Jan-02	16-Jan-02
PARAMETERS CALCULATED FROM ANALYTICAL DATA					
Sum of Analysed Constituents	mg/l				125
Charge Balance:					
Difference/Total	%				-2.52
ION-ION RATIOS					
Br/Cl molal	mol/mol				<6.81E-04
Na/Cl molal	mol/mol				1.50E+00
K/Na molal	mol/mol				2.04E-02
SO_4/Cl molal	mol/mol				6.23E-02
CARBONATE SYSTEM					
CALCULATED USING MEASURED VALUES					
TIC from alkalinity	mol/kg				7.087E-04
Calcite saturation index					-0.86
log $P(CO_2)$					-3.45
CALCULATED AT CALCITE SATURATION					
pH					8.96
log $P(CO_2)$					-4.40
TIC adjusted to calcite sat.	mol/kg				6.611E-04
SATURATION INDICES					
CALCITE (adjusted)					0.00
DOLOMITE_ORD					-0.91
FLUORITE					-0.60
GYPSUM					-3.57
STRONTIANITE					-1.47
CELESTITE					-3.82

* calculated using pH-values of UniBe and alkalinity of Hydroisotop

Table A13-6: (page 3 of 6).

SAMPLE DESCRIPTION					
Borehole		**KF0093-A0**	**KF0093-A0**	**KF0093-A0**	**KF0093-A0**
Type of Sample		Diff.-Ex.	Diff.-Ex.	Diff.-Ex.	Diff.-Ex.
Sample		KF93-2	KF93-2	KF93-2	KF93-2
Interval		33.70-33.79	33.70-33.79	33.70-33.79	33.70-33.79
Rock Type		aplite	aplite	aplite	aplite
Laboratory Analytics		UniBe	UniBe	UniBe	Hydroisotop
Experiment Conditions		glovebox	glovebox	glovebox	glovebox
Date Sampling		12-Nov-01	10-Dec-01	16-Jan-02	16-Jan-02
Date Analysis		12-Nov-01	10-Dec-01	17-Jan-02	Feb. 02
Sample Volume		approx. 7ml	approx. 7ml	total Vol.	total Vol.
WATER TYPE					Na-(Ca)-Cl-HCO_3
MISCELLANEOUS PROPERTIES					
pH (lab)	-log(H+)			8.2	7.8
Pt Elec Potential vs. SHE	mV				
Sample Temperature	ºC				20
Density (calc.)	kg / l				
DISSOLVED CONSTITUENTS					
CATIONS					
Lithium (Li^{+})	mg/l				
Sodium (Na^{+})	mg/l				20.9
Potassium (K^{+})	mg/l				0.7
Rubidium (Rb^{+})	mg/l				
Magnesium (Mg^{+2})	mg/l				<0.5
Calcium (Ca^{+2})	mg/l				7.3
Strontium (Sr^{+2})	mg/l				0.073
Barium (Ba^{+2})	mg/l				
Manganese (Mn^{+2})	mg/l				
Iron (Fe^{+2})	mg/l				
ANIONS					
Fluoride (F^{-})	mg/l				3.2
Chloride (Cl^{-})	mg/l	21.5	21.6	20.7	16.5
Bromide (Br^{-})	mg/l				<0.05
Iodide (I^{-})	mg/l				
Sulfate (SO_4^{-2})	mg/l				2.6
Phosphate (P)	mg/l				
Nitrite (NO_2^{-})	mg/l				
Nitrate (NO_3^{-})	mg/l				
Total Alkalinity	meq/l			0.66	0.8
NEUTRAL SPECIES					
Tot. Sulfide (H_2S,HS^{-},S^{-2})	mg/l				
Silica (Si)	mg/l				
Boron (B)	mg/l				
Total Iron (Fe total)	mg/l				
Total Organic C (TOC)	mg/l				
Total Inorganic C (TIC)	mg/l				

Table A13-6: (page 4 of 6)

SAMPLE DESCRIPTION					
Borehole		**KF0093-A0**	**KF0093-A0**	**KF0093-A0**	**KF0093-A0**
Type of Sample		Diff.-Ex.	Diff.-Ex.	Diff.-Ex.	Diff.-Ex.
Sample		KF93-2	KF93-2	KF93-2	KF93-2
Interval		33.70-33.79	33.70-33.79	33.70-33.79	33.70-33.79
Date Sampling		12-Nov-01	10-Dec-01	16-Jan-02	16-Jan-02
PARAMETERS CALCULATED FROM ANALYTICAL DATA					
Sum of Analysed Constituents	mg/l				100
Charge Balance:					
Difference/Total	%				-0.52
ION-ION RATIOS					
Br/Cl molal	mol/mol				<1.34E-03
Na/Cl molal	mol/mol				1.95E+00
K/Na molal	mol/mol				1.97E-02
SO_4/Cl molal	mol/mol				5.82E-02
CARBONATE SYSTEM					
CALCULATED USING MEASURED VALUES					
TIC from alkalinity	mol/kg				8.022E-04
Calcite saturation index					-0.65
log $P(CO_2)$					-3.56
CALCULATED AT CALCITE SATURATION					
pH					8.92
log $P(CO_2)$					-4.29
TIC adjusted to calcite sat.	mol/kg				7.614E-04
SATURATION INDICES					
CALCITE (adjusted)					0.00
DOLOMITE_ORD					-0.88
FLUORITE					-0.76
GYPSUM					-3.91
STRONTIANITE					-1.52
CELESTITE					-4.20

* calculated using pH-values of UniBe and alkalinity of Hydroisotop

Table A13-6: (page 5 of 6).

SAMPLE DESCRIPTION			
Borehole		**KF0093-A0**	**KF0093-A0**
Type of Sample		Diff.-Ex.	Diff.-Ex.
Sample		KF93-3	KF93-3
Interval		33.79-33.87	33.79-33.87
Rock Type		aplite+diorite	aplite+diorite
Laboratory Analytics		UniBe	Hydroisotop
Experiment Conditions		glovebox	glovebox
Date Sampling		10-Oct-01	10-Oct-01
Date Analysis		10-Oct-01	Feb. 02
Sample Volume		total Vol.	total Vol.
WATER TYPE			$Na-(Ca)-Cl-HCO_3$
MISCELLANEOUS PROPERTIES			
pH (lab)	-log(H+)	8.5	7.3
Pt Elec Potential vs. SHE	mV		
Sample Temperature	ºC		
Density (calc.)	kg / l		
DISSOLVED CONSTITUENTS			
CATIONS			
Lithium (Li^+)	mg/l		
Sodium (Na^+)	mg/l		14
Potassium (K^+)	mg/l		0.8
Rubidium (Rb^+)	mg/l		
Magnesium (Mg^{+2})	mg/l		<0.5
Calcium (Ca^{+2})	mg/l		6.1
Strontium (Sr^{+2})	mg/l		0.055
Barium (Ba^{+2})	mg/l		
Manganese (Mn^{+2})	mg/l		
Iron (Fe^{+2})	mg/l		
ANIONS			
Fluoride (F^-)	mg/l		1.8
Chloride (Cl^-)	mg/l	16.4	15.0
Bromide (Br^-)	mg/l		<0.05
Iodide (I^-)	mg/l		
Sulfate (SO_4^{-2})	mg/l		2.5
Phosphate (P)	mg/l		
Nitrite (NO_2^-)	mg/l		
Nitrate (NO_3^-)	mg/l		
Total Alkalinity	meq/l	0.45	0.45
NEUTRAL SPECIES			
Tot. Sulfide (H_2S,HS^-,S^{-2})	mg/l		
Silica (Si)	mg/l		
Boron (B)	mg/l		
Total Iron (Fe total)	mg/l		
Total Organic C (TOC)	mg/l		
Total Inorganic C (TIC)	mg/l		

Table A13-6: (page 6 of 6).

SAMPLE DESCRIPTION

Borehole	**KF0093-A0**	**KF0093-A0**
Type of Sample	Diff.-Ex.	Diff.-Ex.
Sample	KF93-3	KF93-3
Interval	33.79-33.87	33.79-33.87
Date Sampling	10-Oct-01	10-Oct-01

PARAMETERS CALCULATED FROM ANALYTICAL DATA

Sum of Analysed Constituents	mg/l	68
Charge Balance:		
Difference/Total	%	-2.20
ION-ION RATIOS		
Br/Cl molal	mol/mol	<1.48E-03
Na/Cl molal	mol/mol	1.44E+00
K/Na molal	mol/mol	3.36E-02
SO_4/Cl molal	mol/mol	6.15E-02

CARBONATE SYSTEM

CALCULATED USING MEASURED VALUES *		
TIC from alkalinity	mol/kg	4.424E-04
Calcite saturation index		-0.67
log P(CO_2)		-4.12
CALCULATED AT CALCITE SATURATION		
pH		9.21
log P(CO_2)		-4.96
TIC adjusted to calcite sat.	mol/kg	3.977E-04

SATURATION INDICES

CALCITE (adjusted)	0.00
DOLOMITE_ORD	-0.80
FLUORITE	-1.33
GYPSUM	-3.91
STRONTIANITE	-1.52
CELESTITE	-4.32

* calculated using pH-values of UniBe and alkalinity of Hydroisotop

Table A13-7: $\delta^{18}O$ and $\delta^{2}H$ of deionised water and experimental solutions.

Sample	Rock Type	Deionised Water Volume [1] (ml)	Fraction Pore Water [2]	$\delta^{18}O$ (‰ V-SMOW)	$\delta^{2}H$ (‰ V-SMOW
Deionised Water			0	-11.19± 0.15	-80.0 ± 1.5
KF93-1	Äspö diorite	106.97	0.0087	-11.12 ± 0.15	-79.4 ± 1.5
KF93-2	aplitic dyke	155.51	0.0047	-11.12 ± 0.15	-79.4 ± 1.5
KF93-3	diorite/aplite	133.83	0.0049	-11.14 ± 0.15	-79.1 ± 1.5

[1] includes volume used for re-saturation; [2] based on water content at saturation (Table 4-2)

MFE-borehole water: Sampling Phases 1 and 2

Table A13-8: Borehole Water chemical and isotopic data (page 1 of 4).

SAMPLE DESCRIPTION					
Borehole		KF0051 A01		KF0051 A01	
Rock Type		Äspö Diorite		Äspö Diorite	
Type of Sample		Borehole Water		Borehole Water	
Sample		**MFE-S4-1**		**MFE-S4-2**	
Interval		4.66-5.26		4.66-5.26	
Source of Water		Section 4		Section 4	
Sample Volume		160 ml		195 ml	
Date Collected		4-Dec-1999		16-Oct-2001	
Comments		H_2S smell		H_2S smell	
GROUNDWATER TYPE		Na-(Ca)-Cl		Na-(Ca)-Cl	
MISCELLANEOUS PROPERTIES					
pH (field)	-log(H+)	6.7		7.01	
pH (lab)	-log(H+)	8.1		7.78	
Electrical Conductivity	µS/cm				
Pt Elec Potential vs. SHE	mV				
Sample Temperature	ºC	12		13	
Density (calc.)	kg / l	1.008640		1.008949	
DISSOLVED CONSTITUENTS					
		mg / l	mmol / kgH_2O	mg / l	mmol / kgH_2O
CATIONS					
Lithium (Li^+)		0.247	3.528E-05	0.321	4.584E-05
Sodium (Na^+)		2200	9.487E-02	2480	1.069E-01
Potassium (K^+)		11.4	2.891E-04	9.28	2.352E-04
Ammonium (NH_4^+)					
Magnesium (Mg^{+2})		7.8	3.182E-04	4.2	1.713E-04
Calcium (Ca^{+2})		964	2.385E-02	908	2.245E-02
Strontium (Sr^{+2})		18.6	2.105E-04	19.7	2.228E-04
Barium (Ba^{+2})		0.425	3.068E-06		
Manganese (Mn^{+2})		0.89	1.606E-05		
Iron (Fe^{+2})					
Uranium (U)		1.03E-04	4.290E-10		
ANIONS					
Fluoride (F^-)				11.1	5.791E-04
Chloride (Cl^-)		5160	1.443E-01	5020	1.403E-01
Bromide (Br^-)		43.16	5.355E-04	32.1	3.982E-04
Iodide (I^-)					
Sulfate (SO_4^{-2})		26	2.684E-04	84.1	8.677E-04
Phosphate (P)					
Nitrate (NO_3^-)					
Total Alkalinity	meq / l	200	3.250E-03	371	6.026E-03
NEUTRAL SPECIES					
Tot. Sulfide (H_2S,HS^-,S^{-2})					
Silica (Si)		7.6	2.683E-04	8.7	3.070E-04
Boron (B)					
Total Iron (Fe total)		0.24	4.261E-06	0.029	5.147E-07
Total Organic C (TOC)					
Total Inorganic C (TIC)					

Table A13-8: (page 2 of 4)

SAMPLE DESCRIPTION			
Borehole		KF0051 A01	KF0051 A01
Type of Sample		Borehole Water	Borehole Water
Sample		**MFE-S4-1**	**MFE-S4-2**
Interval		4.66-5.26	4.66-5.26
Source of Water		Section 4	Section 4
Sample Volume		160 ml	195 ml
Date Collected		4-Dec-1999	16-Oct-2001
PARAMETERS CALCULATED FROM ANALYTICAL DATA			
Sum of Analysed Constituents	mg/l	8640	8949
Charge Balance: Difference/Total	%	-1.58	1.26
ION-ION RATIOS			
Br/Cl molal	mol/mol	3.711E-03	2.837E-03
Na/Cl molal	mol/mol	6.575E-01	7.619E-01
K/Na molal	mol/mol	3.047E-03	2.200E-03
SO_4/Cl molal	mol/mol	1.860E-03	6.183E-03
CALCULATED FROM STOICHIOMETRIC VALUES			
Ionic Strength	mol/kg H_2O	1.727E-01	1.754E-01
ISOTOPIC COMPOSITION OF WATER AND SOLUTES			
WATER			
$\delta^{18}O$	‰ SMOW	-11.60	-12.20
$\delta\ ^{2}H$	‰ SMOW	-87.90	-92.40
Tritium	TU		
DISSOLVED INORGANIC CARBON			
$\delta^{13}C$	‰ PDB		
^{14}C	pmc		
DISSOLVED SULPHATE			
$\delta^{34}S$ (SO_4)	‰ CD		
$\delta^{18}O$ (SO_4)	‰ SMOW		
DISSOLVED STRONTIUM			
^{87}Sr / ^{86}Sr		0.714516	0.714300
DISSOLVED CHLORINE (duplicate analysis)			
$\delta^{37}Cl$	‰ SMOC	0.61 / 0.59	0.58 / 0.60
DISSOLVED BORON			
$\delta^{11}B$	‰ NBS951	47.23	

Table A13-8: (page 3 of 4).

SAMPLE DESCRIPTION					
Borehole		KF0051 A01		KF0051 A01	
Rock Type		Äspö Diorite		Avrö Granite	
Type of Sample		Borehole Water		Borehole Water	
Sample		**MFE-S3-2**		**MFE-S2-2**	
Interval		6.26-7.85		8.85-9.55	
Source of Water		Section 3		Section 2	
Sample Volume		321 ml		35 ml	
Date Collected		16-Oct-2001		16-Oct-2001	
Comments		H_2S smell		H_2S smell	
GROUNDWATER TYPE		Na-(Ca)-Cl		Na-(Ca)-Cl	
MISCELLANEOUS PROPERTIES					
pH (field)	-log(H+)		6.08		6.17
pH (lab)	-log(H+)		7.4		
Electrical Conductivity	µS/cm				
Pt Elec Potential vs. SHE	mV				
Sample Temperature	ºC		13		
Density (calc.)	kg / l		1.008607		1.005412
DISSOLVED CONSTITUENTS					
		mg / l	mmol / kgH_2O	mg / l	mmol / kgH_2O
CATIONS					
Lithium (Li^+)		0.32	4.571E-05	0.244	3.496E-05
Sodium (Na^+)		2460	1.061E-01	1760	7.614E-02
Potassium (K^+)		14.5	3.677E-04	16.3	4.147E-04
Ammonium (NH_4^+)					
Magnesium (Mg^{+2})		8.3	3.386E-04	17.4	7.120E-04
Calcium (Ca^{+2})		916	2.266E-02	568	1.410E-02
Strontium (Sr^{+2})		18.8	2.127E-04	11	1.249E-04
Barium (Ba^{+2})		0.695	5.018E-09		
Manganese (Mn^{+2})					
Iron (Fe^{+2})					
Uranium (U)		8.80E-06	3.665E-11		
ANIONS					
Fluoride (F^-)		57.8	3.016E-03	98.8	5.172E-03
Chloride (Cl^-)		4780	1.337E-01	2900	8.136E-02
Bromide (Br^-)		36.7	4.554E-04	24.1	3.000E-04
Iodide (I^-)					
Sulfate (SO_4^{-2})		1.5	1.548E-05	2.7	2.796E-05
Phosphate (P)					
Nitrate (NO_3^-)					
Total Alkalinity	meq / l	303	4.923E-03	n.a.	n.a.
NEUTRAL SPECIES					
Tot. Sulfide (H_2S,HS^-,S^{-2})					
Silica (Si)		8.2	2.895E-04	9.2	3.258E-04
Boron (B)					
Total Iron (Fe total)		1.19	2.113E-05	3.95	7.035E-05
Total Organic C (TOC)					
Total Inorganic C (TIC)					

Table A13-8: (page 4 of 4)

SAMPLE DESCRIPTION			
Borehole		KF0051 A01	KF0051 A01
Type of Sample		Borehole Water	Borehole Water
Sample		**MFE-S3-2**	**MFE-S2-2**
Interval		6.26-7.85	8.85-9.55
Source of Water		Section 3	Section 2
Sample Volume		321 ml	35 ml
Date Collected		16-Oct-2001	16-Oct-2001
PARAMETERS CALCULATED FROM ANALYTICAL DATA			
Sum of Anal. Constituents	mg/l	8607	5412
Charge Balance: Difference/Total	%	3.67	10.12
ION-ION RATIOS			
Br/Cl molal	mol/mol	3.407E-03	3.687E-03
Na/Cl molal	mol/mol	7.937E-01	9.359E-01
K/Na molal	mol/mol	3.466E-03	5.446E-03
SO_4/Cl molal	mol/mol	1.158E-04	3.436E-04
CALCULATED FROM STOICHIOMETRIC VALUES			
Ionic Strength	mol/kg H_2O	1.724E-01	1.119E-01
ISOTOPIC COMPOSITION OF WATER AND SOLUTES			
WATER			
$\delta^{18}O$	‰ SMOW	-11.70	-7.80
$\delta\ ^{2}H$	‰ SMOW	-89.70	-63.60
Tritium	TU		
DISSOLVED INORGANIC CARBON			
$\delta^{13}C$	‰ PDB	-21.9	
^{14}C	pmc	57.3	
DISSOLVED SULPHATE			
$\delta^{34}S$ (SO_4)	‰ CD		
$\delta^{18}O$ (SO_4)	‰ SMOW		
DISSOLVED STRONTIUM			
^{87}Sr / ^{86}Sr		0.714764	0.715635
DISSOLVED CHLORINE (duplicate analysis)			
$\delta^{37}Cl$	‰ SMOC	0.48 / 0.43	0.46 / 0.44
DISSOLVED BORON			
$\delta^{11}B$	‰ NBS951		

Comparison of indirect methods for pore-water characterisation and *in-situ* sampling

Table A13-9: Chloride inventory of fluid inclusions per mass of rock and per volume of pore water if all inclusions would leak to the pore water.

		Äspö Diorite		Ävrö Granite	
	units	minimum	maximum	minimum	maximum
Density [1)]	g/cm3	2.767	2.767	2.693	2.693
Quartz content [2)]	wt.-%	17	17	28	28
FI abundance [2)]	vol.-%	0.3	0.3	0.6	0.6
FI salinity [2)]	eq.-wt% NaCl	1	20	1	20
Cl inventory per kg rock	wt.-%	0.0019	0.038	0.0039	0.077
Case A (mimum porosity)					
Water-content porosity [3)]	vol.-%	0.30	0.30	0.32	0.32
Cl inventory per L pore water	g/l	17.5	350	32.8	666
Case B (maximum porosity)					
Water-content porosity [3)]	vol.-%	0.40	0.40	0.37	0.37
Cl inventory per L pore water	g/l	13.1	263	28.4	576
Chloride in MFE-borehole water					
Cl	g/l	4.78 - 5.16		2.9	

[1)] from Tullborg (Appendix 6), [2)] from Lindblom et al. (Appendix 14) [3)] minimum and maximum water-content porosity from samples used for aqueous leaching experiements

Table A13-10: Molar ion-ion ratios of aqueous leach solutions, solutions from the diffusion experiments, and the *in-situ* sampled borehole water.

	Äspö Diorite				Ävrö Granite			
	(Br / Cl) * 1000	**Na /Cl**	**K / Na**	**Ca / Mg**	**(Br / Cl) * 1000**	**Na /Cl**	**K / Na**	**Ca / Mg**
Aqueous Leachates [1]								
<63µ	1.7-3.5	1.8-3.2	0.3-0.6	0.2-11.1	1.7-1.9	2.1-2.4	0.2-0.3	1.4
<5 mm	1.5-3.2	2.1-3.6	0.2 [3]	0.2-9.1	1.8-1.9	2.3-3.1	0.1-0.2	- [2]
1-2 mm	2.4-5.6	5.0-6.2	0.2-0.3	0.2-1.6	3.3-5.5	5.0-7.4	0.2 [3]	0.8-4.7
2-3 mm	2.7-6.9	6.6-6.9	0.2-0.3	1.1-1.6	4.9 [3]	6.3-8.7	0.2 [3]	1.4
>3 mm	2.1-3.5	6.6-7.4	0.2 [3]	1.3-1.5	4.5 [3]	7.8-9.8	0.2 [3]	- [2]
Diffusion Experiment								
KF93	- [2]	1.4-1.9	0.02-0.03	-[2]				
Borehole Water								
S2-2					3.7	0.9	0.005	20
S3-2	3.4	0.8	0.003	67				
S4-1&2	2.8-3.7	0.7-0.8	0.002-0.003	75-131				

[1] diorite n=6, granite n=2; [2] one concentration below detection limit; [3] all ratios equal for different samples

Technical Document

TD-03-08

Djupförvarsteknik

Matrix Fluid Chemistry Experiment

Quartz-fluid interaction: Fluid inclusions and matrix fluid– Synthesis of an inter-laboratory study

Sten Lindblom
Stockholm University

Alec Blyth
Shaun Frape
University of Waterloo

Seppo Gehör
Kivitieto Oy

Nick Waber
University of Bern

October 2002

Summary

The Matrix Fluid Experiment (MFE) borehole (11.9 m length) was designed to collect matrix or interconnected pore space water in the least transmissive rock so far encountered at Äspö, ranging from 10^{-12}-10^{-14} ms^{-1}. The water sampled from isolated borehole sections has been slowly moving through the bedrock and its final composition when sampled is the product of influence from: (a) matrix fluid, (b) groundwaters in open microfractures (K = 10^{-8}-10^{-11} ms^{-1}), and (c) groundwaters in large hydraulically conductive fractures (K < 10^{-8} ms^{-1}).

In crystalline rocks of low permeability there exist two major origins of matrix fluid: a) the fluid present in interstices and along grain boundaries, and b) the fluid trapped in mineral fluid inclusions. Fluid (a) is normally in equilibrium with the rock mineralogy under present-day conditions and interacts with flowing groundwater in nearby water-conducting zones/fractures via diffusion. Fluid (b) is in equilibrium with the host mineral and may be of magmatic, metamorphic or hydrothermal origin, depending on the geological history of the rock; these fluids may be accessible if fracturing or dissolution of the host mineral occurs.

The MFE-drillcore has been studied in four laboratories (Stockholm, Oulo, Waterloo and Bern) and the results are combined in order to obtain a methodology to characterise the fluid inclusions present in the rock, and their potential contribution to the rock matrix fluid chemistry in bedrock environments intended for radioactive waste storage. The MFE-borehole was located in an area with no visible evidence of water seepage. The drillcore indicated very few crosscutting veins or fractures most of which were sealed; careful scrutiny of the borehole BIPS images showed some additional open microfractures.

Microthermometry, Raman Spectroscopy, Computer Scanning Microscopy, Laser Ablation ICP-MS and micro tectonic systematics have been used to characterise the fluid inclusion populations.

Textures. A new method of directly scanning thin (about 200 μm thick) sections of rock samples could separate out quartz clearly from other minerals, especially feldspar, in the scanned image. This tool is very useful for both quartz identification and overall orientation in the 'thick' section. Quartz consists of primary grains and recrystallised, smaller, equant grains. A slight tectonic stress is evident from anisotropic variability under crossed polars. This method also shows open fractures resulting from shearing/rotation in the centre of quartz grains, and compression on small grains, cutting parallel through these.

The drillcore was oriented and fractures were measured as to regional orientation. Healed fractures outlined by fluid inclusions indicate mainly E-W directions with variations to WNW and WSW with a measured dip of 5 to 60 ^{o} towards the north.

Fluid inclusions. Rare primary or early inclusions were formed around 500°C with a salinity of 5-15 eq. wt.% NaCl. Secondary inclusions in trails and grain boundaries are mainly one phase, but abundant two-phase inclusions range within homogenisation temperatures from 100° to 300°C with salinities mainly between 4-26 eq. wt.% NaCl. Some fluid inclusions contain a solid phase of calcite or halite. There is no discernable difference in fluid inclusion characteristics between the Äspö diorite and Ävrö granite. Grain boundaries are a special case since they constitute a weakness feature susceptible to rupture by tectonic influence. Fluid inclusions along grain boundaries are abundant in recrystallised quartz that is often marked by triple junctions. These inclusions are commonly small and contain a CO_2-rich fluid, but larger saline fluid inclusions also occur frequently. They are prone to tectonic stress, breakage and leakage.

The volume of fluid inclusions was calculated to be about 0.4 vol.% for the Äspö diorite and 0.5 vol.% for the Ävrö granite.

Chemistry. The chemistry of the fluid inclusions was found by microthermometry to be NaCl or $CaCl_2$ dominated with 2 to >30 eq. wt.% NaCl total salt with CO_2 also present. Laser Ablation ICP-MS also corroborates the presence of Na and Ca salts; Mg and K were found also. Barium is a prominent signature from fluid inclusions and La and Ce are also indicated. These Laser Ablation ICP-MS data, however, should be treated with some caution since the laser beam areas analysed are much greater than the diameter of the fluid inclusion of interest thus impinging on underlying and adjacent mineral grains. Nevertheless as a qualitative tool it is very useful and laser trails crosscutting grain boundaries in quartz could identify possible fluid inclusions as well as mineral inclusions and coatings: Mg+Al for chlorite, Na+Al for albite, Na+Mg+Al for amphibole etc. Chlorine is not sensitive to ICP-MS analysis, but the detection of Na, Ca and Mg on their own (correlation plus textural image before and after laser ablation) might indicate the presence of fluid inclusions.

Overall conclusions. Ongoing stress-strain relations in quartz give evidence of possible fracturing thus providing a leakage mechanism for fluid inclusions in quartz. Grain boundaries are features of weakness in quartz and may further contribute by chemical reactions with exposed minor mineral phases and fluids which characterise some of these boundary environments. The cause of deformation is most likely due to isostatic rebound resulting from previous glaciations.

Based on these fluid inclusion studies, a common methodology to identify, characterise and interpret fluid inclusions has been produced for use in site characterisation investigations.

Petrography

Quartz Grain variability

(a) **(b)**

Figure A14-1: *Comparison of scanned visual image and transparent light microscopy on doubly polished 'thick' sections of Äspö diorite (sample 10:1; 10.90 m length along core) in modes: a) without angled mirror (left), and b) with angled mirror (right) showing quartz (moderately grey colours), K-feldspar (rose/brown colour) and plagioclase feldspar (white colour).*

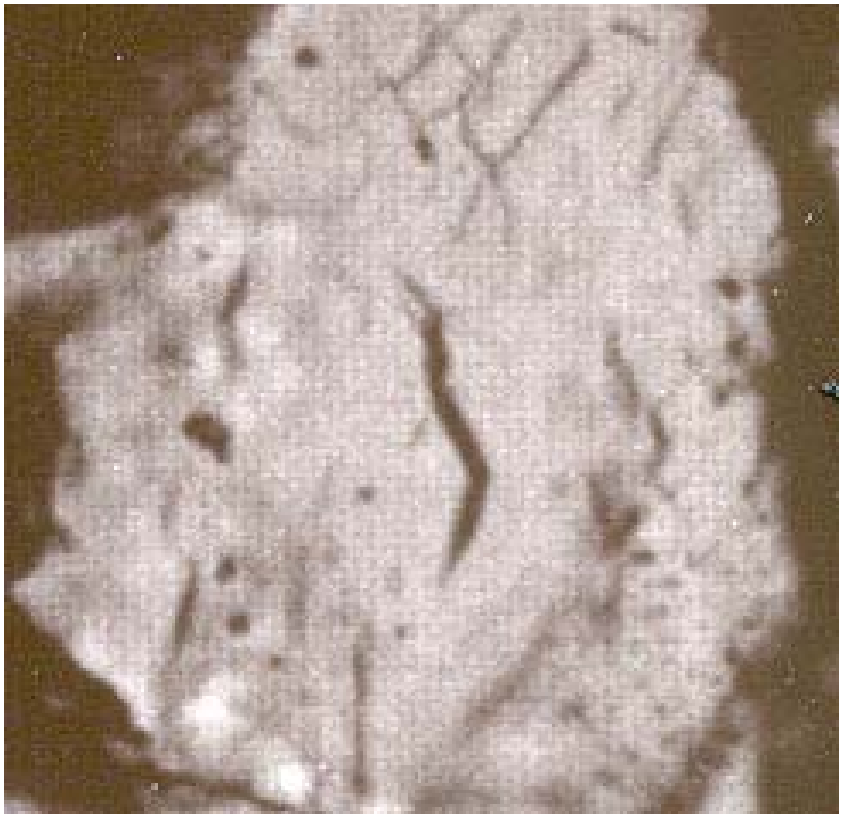

Figure A14-2: *Open fracture in the centre of a primary quartz grain.*

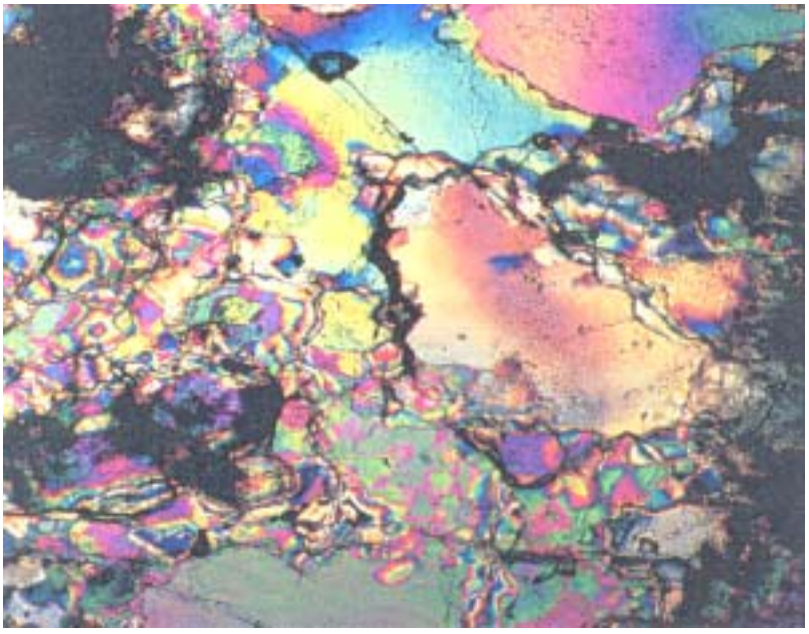

Figure A14-3: *Relation between primary (large grains) and mosaics of recrystallised primary quartz and stress optical anisotropy.*

Fluid inclusion studies

Table A14-1: Summary of fluid inclusion data from the three laboratories. (Secondary inclusions in trails or grain boundaries are included; decrepitated and isolated inclusions are excluded).

Sample	Phases	Tm (ice) ^{o}C	Salinity Eq. wt% NaCl	Research group
4.60-4.89 m	L	-1 to -7	1.7 to 10.5	Bern
4.60-4.89 m	L+V	-2 to -20	3.4 to 26	Bern
5.03 m	L+V	-5.5 to -15.0	8.7 to 19.1	Stockholm/Oulo
5.03 m	L+V	-2.1 to -16,4	3.5 to 19.9	Waterloo
5.18 m	L+V	-0.4 to -22.1	0.7 to 24.1	Waterloo
5.42 m	L+V	-4.0	6.6	Stockholm/Oulo
7.81 m	L+V	-1.0 to -23	1.7 to 24.7	Stockholm/Oulo
7.81 m	L+V	-0.2 to -12.9	0.4 to 16.9	Waterloo
8.84 m	L+V	- 5.4 to -18	8.5 to 21.2	Stockholm/Oulo
8.84 m	L+V	-2.6 to -13.8	4.3 to 17.7	Waterloo
9.11 m	L+V	-0.6 to -22.6	1.0 to 12.4	Waterloo
9.85 m	L+V	-4.5	7.3	Stockholm/Oulo

L= Liquid; V = Vapour.

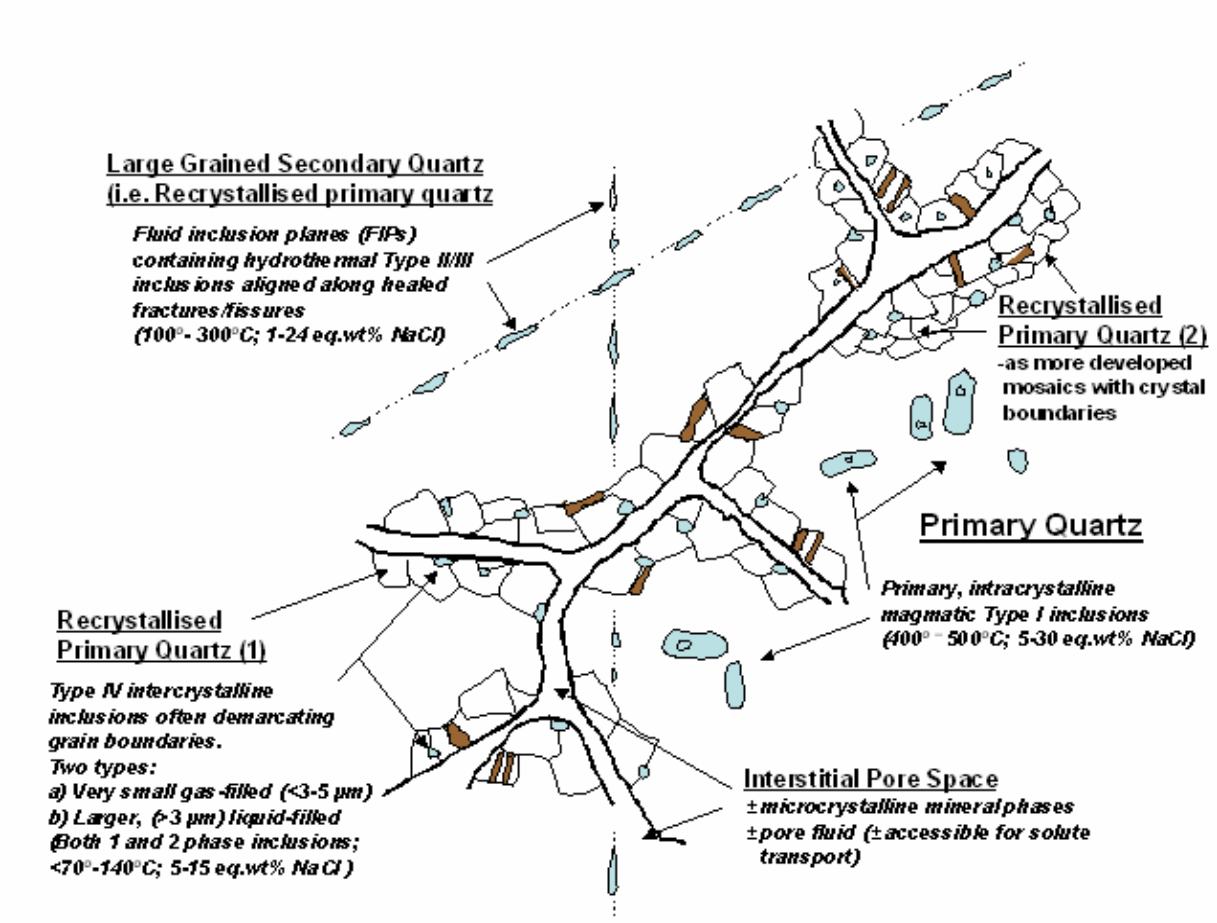

Figure A14-4: *Schematic representation of the major fluid inclusion types present in the Äspö diorite (Note: The Ävro granite shows less development of the recrystallised quartz along the primary grain boundaries).*

Technical Document

TD-02-18

Djupförvarsteknik

Matrix Fluid Chemistry Experiment

Evolution of Äspö groundwaters with time: Additional information from tritium and $\delta^{37}Cl$

Alexander Blyth
Shaun Frape

University of Waterloo, Ontario

September 2002

Summary

Groundwater investigations at the Äspö site by previous researchers indicate that the groundwaters are a mixture of several end members. Additional investigation of the tritium and stable chlorine isotopes confirm this previous finding and showed that mixing with surface waters has increased with drilling and hydraulic testing during site characterisation studies. Early drilling at the site found waters that were indicative of non-modern, rock equilibrated waters. Extensive drilling and hydraulic testing at Laxemar may be responsible for the mixed water signature present in samples, and a similar explanation may also account for later water samples from Äspö. The construction of the access tunnel and underground facility at Äspö has led to groundwater mixing with a Baltic type water and a low salinity, $\delta^{37}Cl$ depleted water, such as that seen regionally in Sweden and at the Stripa mine site. The bromine to chlorine ratio of the groundwater also indicates a mixture between a deep saline brine, a rock equilibrated water and the $\delta^{37}Cl$ depleted water. The $\delta^{18}O$ and $\delta^{2}H$ signatures of groundwaters from the Äspö site show the deep Laxemar samples are typical of a shield brine while the rest of the samples have a meteoric or evaporated meteoric signature.

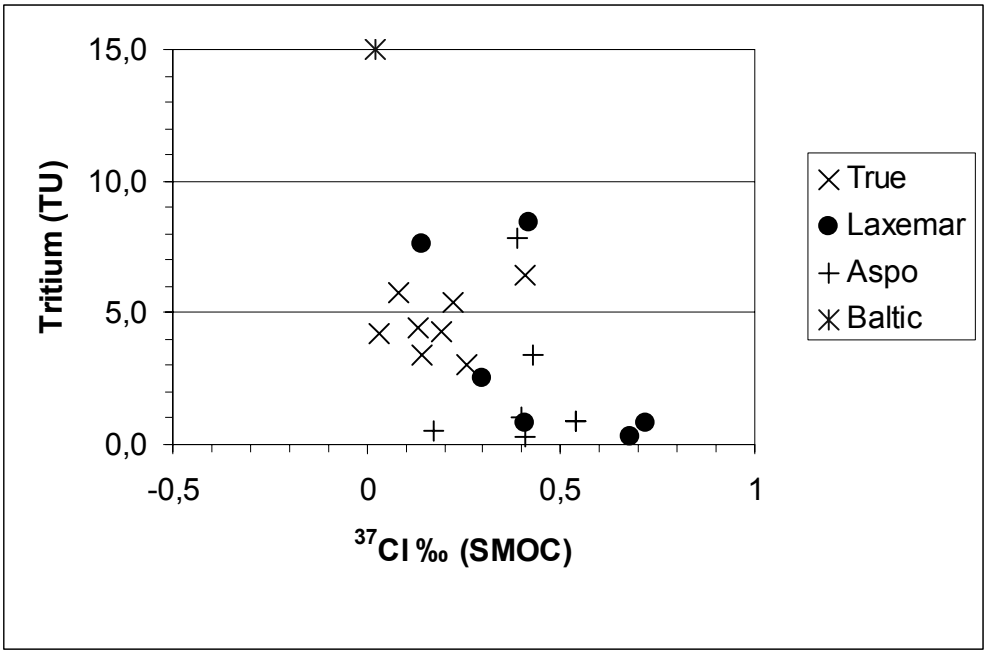

***Figure A15-1**: $\delta^{37}Cl$ versus Tritium for sampling up to 1995 (TRUE experiment).*

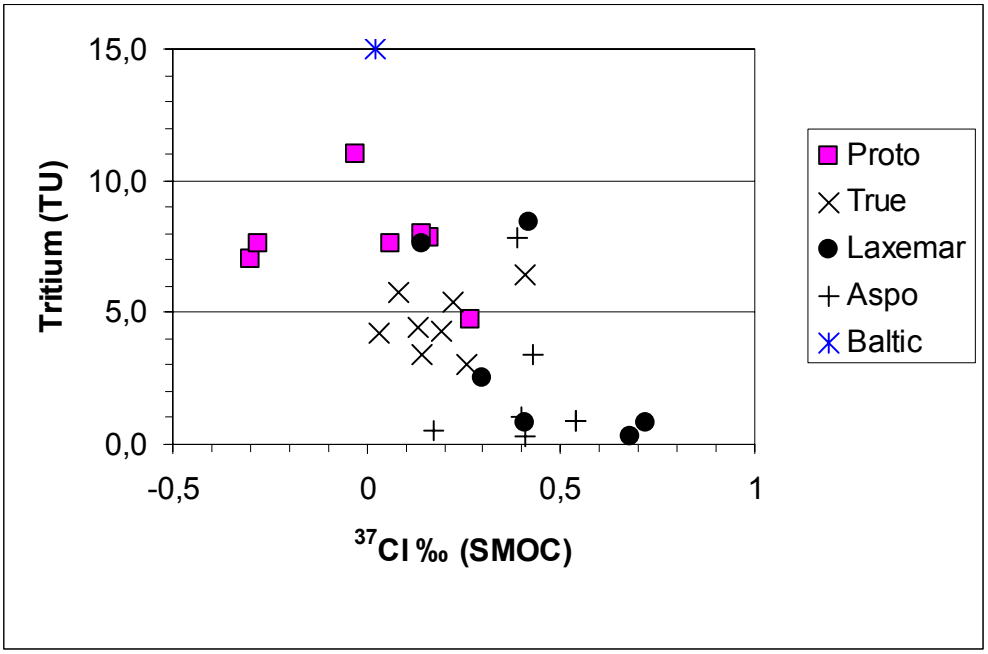

Figure A15-2: *δ^{37}Cl versus Tritium for sampling up to 1995 (PROTOTYPE experiment).*

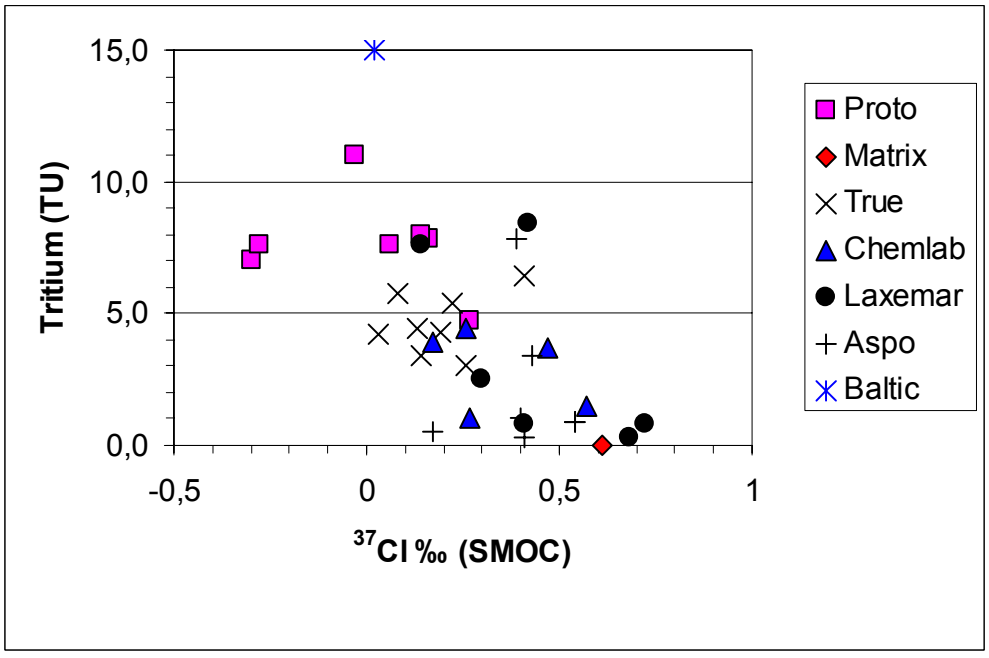

Figure A15-3: *δ^{37}Cl versus Tritium for sampling up to 1995 (CHEMLAB experiment).*

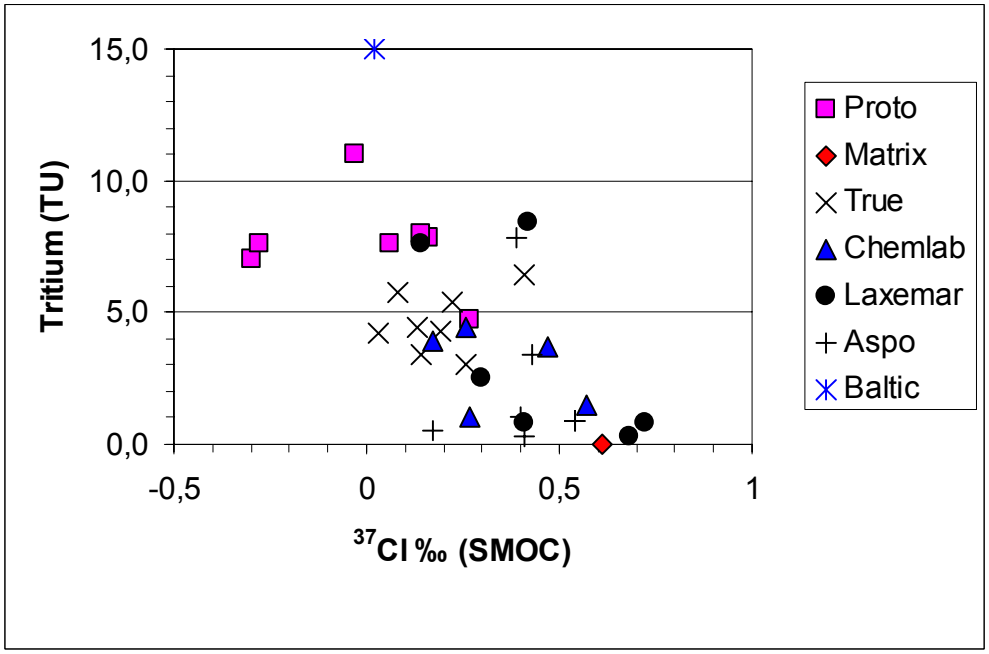

Figure A15-4: *$\delta^{37}Cl$ versus Chlorine for Äspö and other sites. The curved line represents a mixing trend between deep Laxemar brines and shallow groundwater.*

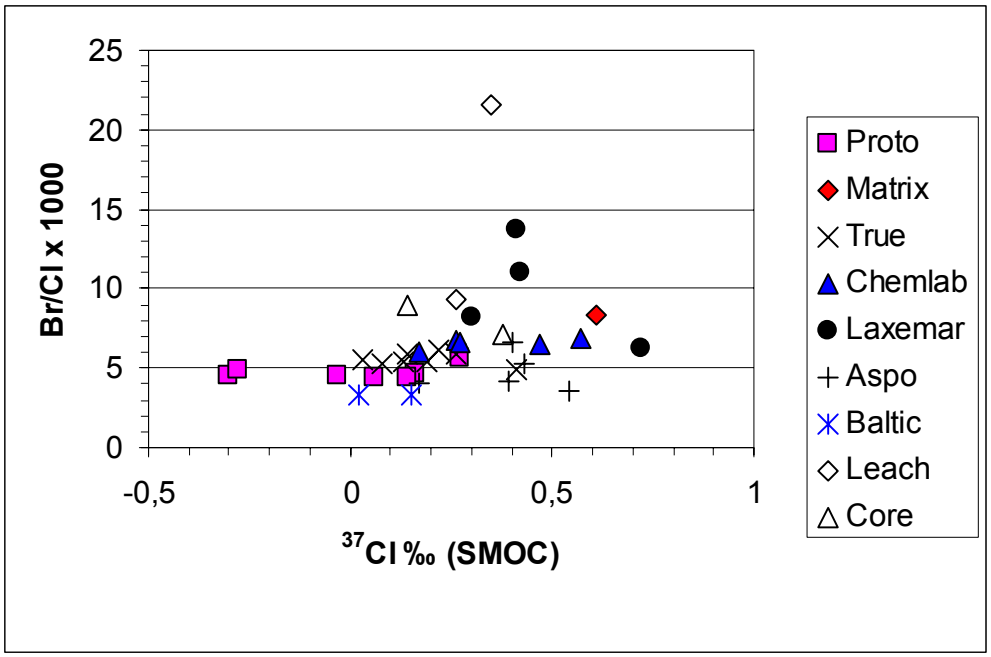

Figure A15-5: *$\delta^{37}Cl$ versus Cl/Br for Äspö and other sites..*

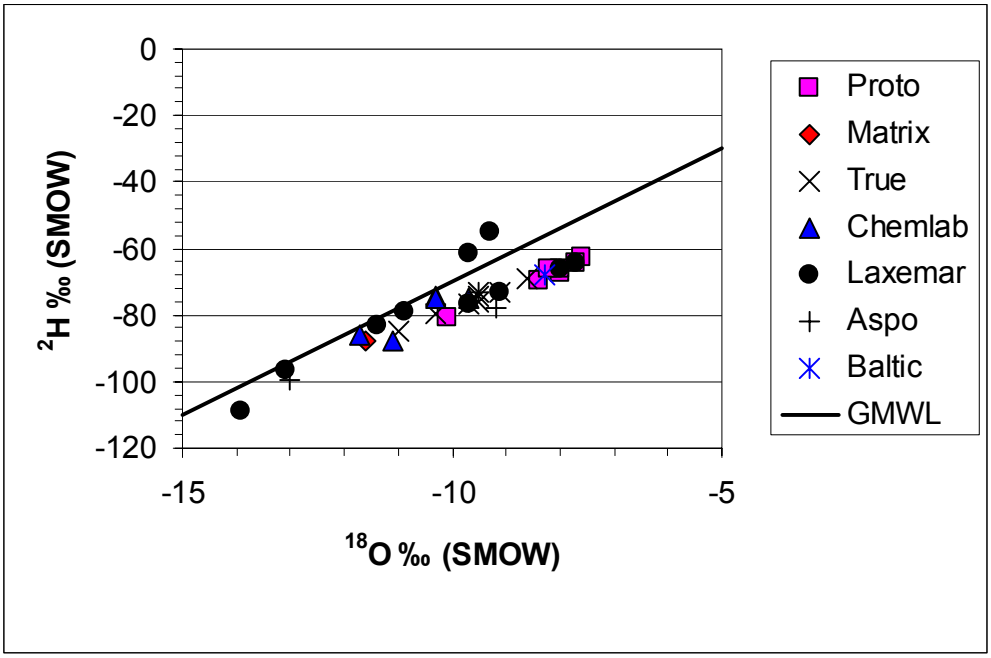

Figure A15-6: *$\delta^{18}O$ versus $\delta^{2}H$ for Äspö groundwaters.*

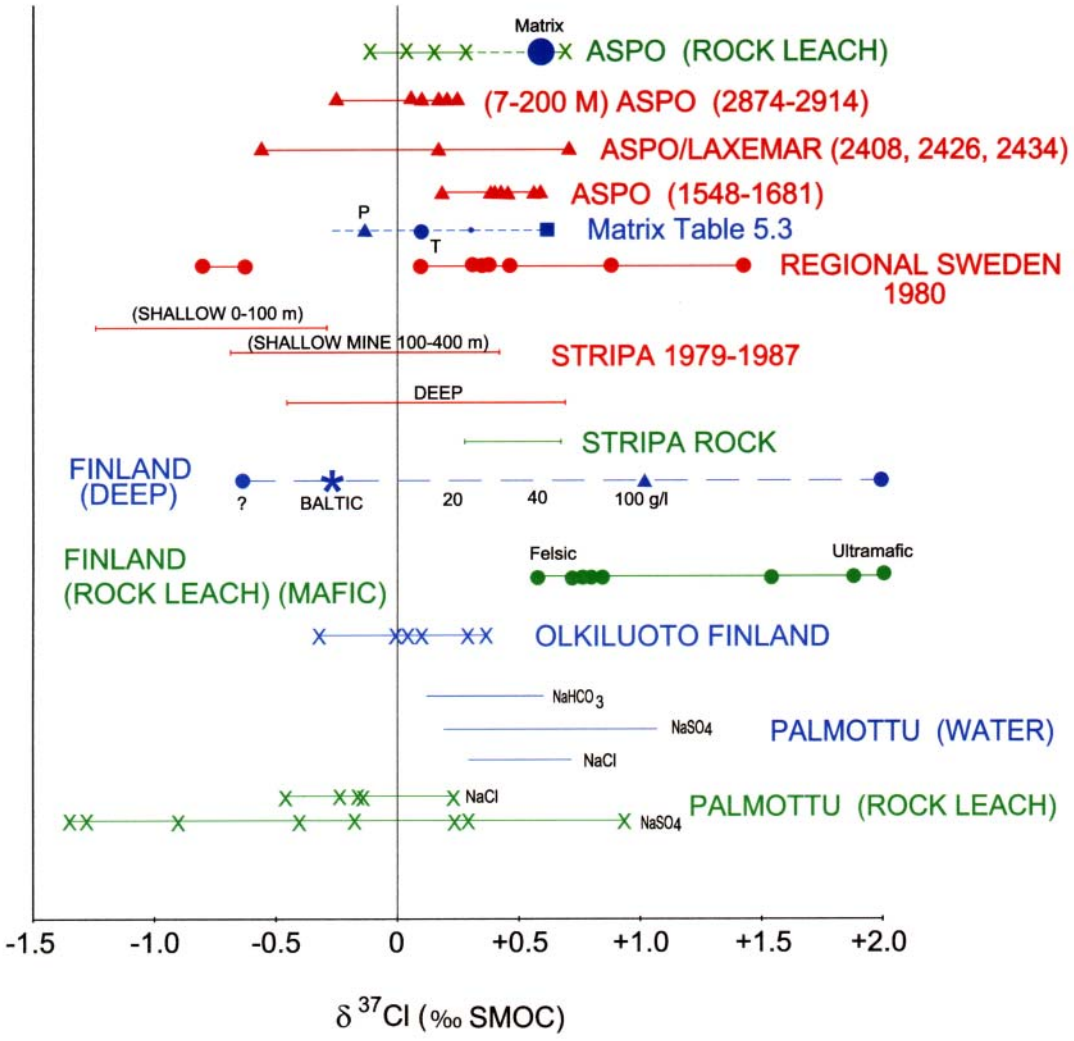

Figure A15-7: *$\delta^{37}Cl$ isotopic range of groundwater and rock leach samples from Äspö and Stripa in Sweden and from several sites in Finland.*

Table A15-1: Selected water analyses from the Äspö Hard Rock Laboratory and other sites (page 1 of 2).

Experiment	IDCode	Depth	Sample	Sampling Date	Cl	Br	δ^2H	$\delta^{18}O$	d^3H	$\delta^{37}Cl$
		m			mg/L	mg/L	‰ SMOW	‰ SMOW	TU	‰ SMOC
PROTO	***KA3566G01***	20.8-30.01	2910	990416	4070	18.5	-67.4	-8	11	-0.03
	KA3566G02	12.3-18.3	2880	990408	4110	18.5	-62.9	-7.6	7	-0.3
	KA3566G02	19.3-30.01	2907	990415	4210	20.4	-66.4	-8	7.6	-0.28
	KA3566G02	7.8-11.3	2914	990503	4240	19.7	-69.7	-8.4	7.8	0.16
	KA3566G02	1.3-6.8	2921	990517	3940	17.6	-66.1	-8.2	8	0.14
	KA3572G01	1.3-5.3	2928	990517	4810	27.2	-80.9	-10.1	4.7	0.27
	KA3590G02	17.3-22.3	2892	990413	4220	18.8	-64.5	-7.7	7.6	0.06
MATRIX	***KF0051A01***	4.66-5.26	3039	991216	5160	43.2	-87.9	-11.6	0	0.61
TRUE	***KI0025F02***	73.3-77.25	2879	990408	5540	32.9	-73.4	-9.5	3.4	0.14
	KI0025F02	73.3-77.25	2968	990928	5570	29.6	-76.2	-9.5	5.8	0.08
	KI0025F02	64-72.3	2973	990928	5560	29.7	-74.5	-9.5	4.4	0.13
	KI0025F02	93.35-99.25	2972	990928	6110	35.7	-79.9	-10.3	3	0.26
	KA2563A	187-190	2874	990408	5350	29.4	-72.9	-9.1	4.2	0.03
	KA2563A	206-208	2875	990408	5010	27.2	-76.5	-9.7	4.3	0.19
	KA2563A	187-190	2971	990928	4480	21.8	-69.3	-8.6	6.4	0.41
	KA2563A	206-208	2970	990928	5730	35	-84.7	-11	5.4	0.22
CHEMLAB	***KJ0044F01***	16-17.25	3154	000223	7030	45.9	-74.6	-10.3	3.7	0.47
	KJ0050F01	12.64-12.84	3153	000223	6580	44.4	-75.1	-10.3	4.4	0.26
	KJ0052F01	43.7-43.9	3155	000223	7230	47.6	-86.2	-11.7	1	0.27
	KJ0052F02	1521.42	3157	000223	8130	55.4	-87.6	-11.1	1.5	0.57
	KJ0052F02	9.23-9.43	3156	000223	5750	34.2	-74.7	-9.7	3.9	0.17
LAXEMAR	***KLX02***	1345-1355	2931	990719	31230	196	-61.7	-9.7	0.8	0.72
	KLX02	1155-1165	2934	990901	15130	125	-83.2	-11.4	2.5	0.3
	KLX02	1090-1097	3035	990927	4730	52.3	-79.1	-10.9	8.4	0.42
	KLX02	1385-1392	3038	991206	36970	509	-54.9	-9.3	0.8	0.41
	KLX02	50-100	2408	970925			-72.9	-9.1	4.2	-0.61
	KLX02	100-150	2413	970925	119.6	0.55	-76.5	-9.7	4.3	
	KLX02	650-700	2426	970925			-66.4	-8	7.6	0.14
	KLX02	700-750	2427	970925	35.4	0.19	-64.5	-7.7	7.8	
	KLX02	1350-1400	2434	970925			-108.9	-13.9	0.3	0.68
	KLX02	1400-1450	2407	970925	34341	229.6	-96.8	-13.1	0.2	
ÄSPÖ	***KAS02***	202-214.5	1548	890111	3820	13.4			0.9	0.54
	KAS02	860-924.04	1560	890131	11100	74			1	0.4
	KAS02	800-854	1676	900606	10000				0.9	0.54
	KAS03	129-134	1566	890215	1240	4.94	-99.6	-13	0.5	0.17
	KAS03	533-626	1681	900613	5130		-77.8	-9.2	0.3	0.41
	KAS04	334343	1603	890427	3030	15.9	-73.4	-9.5	3.4	0.43
	KAS06	304-377	1610	890607	5680	24			7.8	0.39

Table A15-1: (page 2 of 2)

Experiment	IDCode	Depth	Sample	Sampling Date	Cl	Br	δ^2H	$\delta^{18}O$	d^3H	$\delta^{37}Cl$
		m			mg/L	mg/L	‰ SMOW	‰ SMOW	TU	‰ SMOC
BALTIC					3550 6180	11.6 20.6	-68	-8.3	15	0.02 0.15
Leach	leach1				21.6	0.2				0.26
	leach2				13.9	0.3				0.35
	core1				17	0.12				0.38
	core2				20	0.18				0.14
Stripa	V2-1				560	4.6				0.65
	V2-4				670	6				0.23
	SBH-3				3.7					-1.22
Others	Kaga				1400	14.3				0.69
	Osmo				10					-0.81
	Smed + ofta				1100	3.33				-0.71

Waber, H.N. and Smellie, J.A.T., 2003. Analytical data of waters and gases from the MFE-borehole, and boreholes KF0066A01 and KF0069A01 (Sampling Phase 3, February 2003).

Summary

In February 2003, a total water volume of 17 ml, 117 ml, and 110 ml could be successfully sampled from the MFE-borehole Sections 2, 3, and 4 during the 3rd sampling campaign. As during the earlier campaigns only gas could be sampled from Section 1. In addition to the MFE-borehole, water was sampled under artesian conditions from the two boreholes KF0066A01 and KF0069A01 located some 16 m and 19 m away from the MFE-borehole and penetrating highly conducting fractures.

In the borehole waters the concentrations of Cl and Br remained constant over a time period of 50 months (Section 4) and 16 months (Section 3). In contrast, the water from Section 2 shows an increase in Cl concentration. Borehole water from Sections 3 and 4 have a higher field pH-value, a lower total alkalinity, up to a hundred-fold increase in SO_4 concentrations, and up to ten-fold decrease in F concentrations compared to earlier samples from the same sections. These changes are in accordance with a ceasing microbial activity that resulted in an intense sulphate reduction as already suggested after the Phase 2 sampling campaign (*cf.* Chapter 6). In Section 2 bacterially mediated sulphate reduction and related corrosion of installation material is still prominent as indicated by the low field pH-value, the very low SO_4 concentration and the very high F concentration.

Similar as the conservative anions, the $\delta^{18}O$ and $\delta^{2}H$ values of borehole water from sections 3 and 4 remained constant, while the isotopic compositions of carbon, sulphur, strontium changed significantly. These changes are consistent with the perturbation effects of sulphate reduction in the intervals. Interestingly also $\delta^{37}Cl$ shows a significant decrease in spite of the constant total Cl concentrations. For the water from Section 3 the $\delta^{13}C_{TIC}$ value (-3.7 ‰ V-PDB) is much less negative and ^{14}C activity (39 pmc) much lower than in the Phase 2 water with the $\delta^{13}C_{TIC}$ value being compatible with isotopic equilibrium between total dissolved inorganic carbon fracture calcite. Although a certain contamination might still be present, the minimum residence time of this water is thus in the order of several thousands of years.

Water from Section 2 shows similar trends for the isotopic compositions of carbon, sulphur, strontium as observed in those of Sections 3 and 4. However, the $\delta^{18}O$ and $\delta^{2}H$ values of Section 2 water have become significantly more negative since the last sampling campaign. Together with the changes in the Cl concentration these suggest the addition of small amounts of a different water type over the past 16 months.

In all intervals the composition of free gas accumulated in the interval is dominated by CO_2. However, large amounts of CH_4, higher hydrocarbons, and H_2 are also present. Section 1, where only gas could be sampled, has the highest CH_4/CO_2 ratio and the lowest H_2/CO_2 ratio. This indicates that the *in-situ* conditions in the rock are reducing and supports the proposed perturbation in water containing intervals by sulphate reduction (CH_4 consumption) and associated corrosion of installation material (H_2 as corrosion product).

In boreholes KF0066A01 and KF0069A01 water occurs under high hydraulic pressure. The boreholes are not equipped with a pressure-resistant sampling device and sampling of these waters occurred under partially open system conditions. The waters from both boreholes are similar in composition being of a saline Ca-Na-Cl type water with a total mineralisation of 21 781 mg/L and 20 271 mg/L. Chloride concentrations are 12 883 mg/L and 12 280 mg/L while SO4 is present only with about 650 mg/L. Calcium dominates over Na and the waters have low Mg concentrations of about 33 mg/L. The groundwaters have a very low total alkalinity at pH-values of around 8. They are in equilibrium with calcite with an associated partial pressure of CO_2 below that of the atmosphere.

The water from boreholes KF0066 A01 and KF0069 A01 are ^{3}H-free. Together with the low pCO_2 this indicates that measured high ^{14}C activities are due to contamination with air-CO_2. Their $^{87}Sr/^{86}Sr$ ratio is higher than any ratio previously recorded for waters from the Äspö area including those of the deep saline waters from the Äspö HRL and the Laxemar boreholes. They are further characterised by low $\delta^{18}O$ and $\delta^{2}H$ values that plot to the left of the GMWL, low $\delta^{13}C$ values, low $\delta^{11}B$ values, and $\delta^{37}Cl$ values within the range of the Phase 3 MFE-borehole waters. The chemical and isotopic composition are characteristic for a deep brine origin of these waters.

Methods

Immediately after recovery, the borehole waters were analysed on-site for T and pH using an Orion 720A pH-meter with a Ross glass electrode. The pH was monitored over several tenths of minutes to investigate the solutions behaviour during exposure to the atmosphere.

At the Äspö HRL laboratory the sampled borehole waters were measured for pH and analysed for alkalinity using an Autotitrator TIM 900 (Radiometer, Copenhagen) within two hours of sampling. In the same laboratory Cl, SO_4 and Br were subsequently analysed using conventional ion chromatograpy (IC, Radiometer, Copenhagen).

The stable isotopes of water were analysed at the Institutt för Energiteknikk (IFE), Norway, using conventional mass spectrometry and expressed as per mille relative to the IAEA Mean Ocean Water Standard V-SMOW.

Samples for the analyses of the isotopic composition of dissolved inorganic carbon ($\delta^{13}C$, ^{14}C) were collected under closed system conditions into pre-evacuated glass tubes. A small amount of HgCl was added to the glass tubes used for the analysis of $\delta^{13}C$ to inhibit microbial activity in the water-filled tubes during storage and shipping. The stable isotopic composition of dissolved inorganic carbon ($\delta^{13}C$) was analysed at Hydroisotop GmbH, Schweitenkirchen, with a Finnigan MAT 250 mass spectrometer and is reported in per mille relative to the V-PDB standard. The analytical error for $\delta^{13}C$ is reported to be 0.3‰. Analysis of radiogenic ^{14}C was performed at Lawrence Livermore National Laboratory, California, by Tandem-Accelerator Mass Spectrometry and is expressed as

percent modern carbon (pmc). Sample preparation backgrounds ranged between 0.14 and 0.19 pmc, based on repeated measurements of ^{14}C-free calcite samples, and have been subtracted from the water values. The analytical error is 2σ of multiple measurements of the same sample.

The chlorine isotope ratio ($\delta^{37}Cl$) of the borehole waters was measured at University of Waterloo. The method used is described in detail in Appendix 13. Measurements were made with a precision of ±0.12% (1σ) based on repeat analyses of SMOC.

The isotope ratio of B ($\delta^{11}B$) was analysed at BRGM, Orléan, France, on a Finnigan MAT 261 solid source mass spectrometer and is expressed as per mille relative to the NBS951 boric acid standard.

The $^{87}Sr/^{86}Sr$ isotope ratios were measured at the University of Bern using a modified VG Sector® thermal ionisation mass spectrometer (TIMS) in simple collector mode, using oxidised Ta filaments. The analytical uncertainty is given with 2σ of multiple measurements of the same sample.

MFE-Borehole water: Sampling Phase 3

Table A16-1: Borehole water chemical, isotopic and gas data (page 1 of 6).

SAMPLE DESCRIPTION			
Borehole		KF0051 A01	KF0051 A01
Rock Type		Äspö Diorite	Äspö Diorite
Type of Sample		Borehole Water	Borehole Water
Sample		**MFE-S4-3**	**MFE-S3-3**
Interval		4.66-5.26	6.26-7.85
Source of Water		Section 4	Section 3
Sample Volume		110 ml	117 ml
Date Collected		13-Feb-2003	13-Feb-2003
Comments		H_2S smell	H_2S smell
GROUNDWATER TYPE		Na-(Ca)-Cl	Na-(Ca)-Cl
MISCELLANEOUS PROPERTIES			
pH (field)	-log(H+)	7.25	7.05
pH (lab)	-log(H+)	7.93	7.50
Electrical Conductivity	µS/cm	-	-
Pt Elec Potential vs. SHE	mV	-	-
Sample Temperature	ºC	8.1	8.1
Density (calc.)	kg / l	-	-
DISSOLVED CONSTITUENTS			
		mg / l	mmol / kgH_2O	mg / l	mmol / kgH_2O
CATIONS					
Lithium (Li^+)		-	-	-	-
Sodium (Na^+)		-	-	-	-
Potassium (K^+)		-	-	-	-
Ammonium (NH_4^+)		-	-	-	-
Magnesium (Mg^{+2})		-	-	-	-
Calcium (Ca^{+2})		-	-	-	-
Strontium (Sr^{+2})		-	-	-	-
Barium (Ba^{+2})		-	-	-	-
Manganese (Mn^{+2})		-	-	-	-
Iron (Fe^{+2})		-	-	-	-
Uranium (U)		-	-	-	-
ANIONS					
Fluoride (F^-)		0.92	4.843E-05	18.4	9.685E-04
Chloride (Cl^-)		5020	1.416E-01	4770	1.345E-01
Bromide (Br^-)		36	4.505E-04	38	4.756E-04
Iodide (I^-)		-	-	-	-
Sulfate (SO_4^{-2})		159	1.655E-03	158	1.645E-03
Phosphate (P)		-	-	-	-
Nitrate (NO_3^-)		-	-	-	-
Total Alkalinity	meq / l	278	4.556E-03	165	2.704E-03
NEUTRAL SPECIES					
Tot. Sulfide (H_2S,HS^-,S^{-2})		-	-	-	-
Silica (Si)		-	-	-	-
Boron (B)		-	-	-	-
Total Iron (Fe total)		-	-	-	-
Total Organic C (TOC)		-	-	-	-
Total Inorganic C (TIC)		-	-	-	-

Table A16-1: (page 2 of 6)

SAMPLE DESCRIPTION					
Borehole		KF0051 A01		KF0051 A01	
Type of Sample		Borehole Water		Borehole Water	
Sample		**MFE-S4-3**		**MFE-S3-3**	
Interval		4.66-5.26		6.26-7.85	
Source of Water		Section 4		Section 3	
Sample Volume		110 ml		117 ml	
Date Collected		13-Feb-2003		13-Feb-2003	
PARAMETERS CALCULATED FROM ANALYTICAL DATA					
Sum of Analysed Constituents	mg/l				
Charge Balance:		-	-	-	-
Difference/Total	%	-	-	-	-
ION-ION RATIOS					
Br/Cl molal	mol/mol	-	3.182E-03	-	3.535E-03
Na/Cl molal	mol/mol	-	-	-	-
K/Na molal	mol/mol	-	-	-	-
SO_4/Cl molal	mol/mol	-	1.169E-02	-	1.223E-02
CALCULATED FROM STOICHIOMETRIC VALUES					
Ionic Strength	mol/kg H_2O	-	-	-	-
ISOTOPIC COMPOSITION OF WATER AND SOLUTES					
WATER					
$\delta^{18}O$	‰ SMOW	-12.7	-	-12.3	-
$\delta\ ^{2}H$	‰ SMOW	-91.6	-	-89.5	-
^{3}H	TU	-	-		-
DISSOLVED INORGANIC CARBON					
$\delta^{13}C$	‰ PDB	-7.6 ± 0.3	-	-3.7 ± 0.3	-
^{14}C	pmc	54.2 ± 0.2	-	39.0 ± 0.2	-
DISSOLVED SULPHATE					
$\delta^{34}S$ (SO_4)	‰ CD	-	-	-	-
$\delta^{18}O$ (SO_4)	‰ SMOW	-	-	-	-
DISSOLVED STRONTIUM					
^{87}Sr / ^{86}Sr		0.714080 ± 0.000015		0.714531 ± 0.000042	
DISSOLVED CHLORINE (duplicate analysis)					
$\delta^{37}Cl$	‰ SMOC	0.32	-	0.35	-
DISSOLVED BORON					
$\delta^{11}B$	‰ NBS951	-	-	-	-

Table A16-1: (page 3 of 6)

SAMPLE DESCRIPTION					
Borehole		KF0051 A01		KF0051 A01	
Type of Sample		Borehole Water		Borehole Water	
Sample		**MFE-S4-3**		**MFE-S3-3**	
Interval		4.66-5.26		6.26-7.85	
Source of Water		Section 4		Section 3	
Sample Volume		110 ml		117 ml	
Date Collected		13-Feb-2003		13-Feb-2003	
FREE GAS IN THE SAMPLING INTERVAL					
H_2	ppm	2.84	-	10.77	-
CO_2	ppm	1473.3	-	2129.9	-
CO	ppm	4.26	-	13.83	-
CH_4	ppm	3.93	-	9.77	-
C_2H_4	ppm	present *	-	present *	-
C_2H_6	ppm	1.04	-	1.36	-

* C_2H_4 probably present, but hidden in CO_2 tail

Table A16-1: (page 4 of 6).

SAMPLE DESCRIPTION					
Borehole		KF0051 A01		KF0051 A01	
Rock Type		Äspö Diorite		Äspö Diorite	
Type of Sample		Borehole Water		Borehole Gas	
Sample		**MFE-S2-3**		**MFE-S1-3**	
Interval		8.85-9.55		10.55-11.80	
Source of Water		Section 2		Section 1	
Date Collected		13-Feb-2003		13-Feb-2003	
Sample Volume		17 ml		no water	
Comments		H_2S smell		H_2S smell	
GROUNDWATER TYPE		Na-(Ca)-Cl			
MISCELLANEOUS PROPERTIES					
pH (field)	-log(H+)	-	6.42	-	-
pH (lab)	-log(H+)	-	6.18	-	-
Electrical Conductivity	µS/cm	-	-	-	-
Pt Elec Potential vs. SHE	mV	-	-	-	-
Sample Temperature	ºC	-	8.1	-	-
Density (calc.)	kg / l	-	-	-	-
DISSOLVED CONSTITUENTS					
		mg / l	mmol / kgH_2O	mg / l	mmol / kgH_2O
CATIONS		-	-	-	-
Lithium (Li^+)		-	-	-	-
Sodium (Na^+)		-	-	-	-
Potassium (K^+)		-	-	-	-
Ammonium (NH_4^+)		-	-	-	-
Magnesium (Mg^{+2})		-	-	-	-
Calcium (Ca^{+2})		-	-	-	-
Strontium (Sr^{+2})		-	-	-	-
Barium (Ba^{+2})		-	-	-	-
Manganese (Mn^{+2})		-	-	-	-
Iron (Fe^{+2})		-	-	-	-
Uranium (U)		-	-	-	-
ANIONS					
Fluoride (F^-)		120	6.316E-03	-	-
Chloride (Cl^-)		3154	8.896E-02	-	-
Bromide (Br^-)		25	3.129E-04	-	-
Iodide (I^-)		-	-	-	-
Sulfate (SO_4^{-2})		6.1	6.350E-05	-	-
Phosphate (P)		-	-	-	-
Nitrate (NO_3^-)		-	-	-	-
Total Alkalinity	meq / l	-	-		
NEUTRAL SPECIES					
Tot. Sulfide (H_2S,HS^-,S^{-2})		-	-	-	-
Silica (Si)		-	-	-	-
Boron (B)		-	-	-	-
Total Iron (Fe total)		-	-	-	-
Total Organic C (TOC)		-	-	-	-
Total Inorganic C (TIC)		-	-	-	-

Table A16-1: (page 5 of 6)

SAMPLE DESCRIPTION					
Borehole		KF0051 A01		KF0051 A01	
Type of Sample		Borehole Water		Borehole Gas	
Sample		**MFE-S2-3**		**MFE-S1-3**	
Interval		8.85-9.55		10.55-11.80	
Source of Water		Section 2		Section 1	
Sample Volume		17 ml		no water	
Date Collected		13-Feb-2003		13-Feb-2003	
PARAMETERS CALCULATED FROM ANALYTICAL DATA					
Sum of Anal. Constituents	mg/l	-	-	-	-
Charge Balance:		-	-	-	-
Difference/Total	%	-	-	-	-
ION-ION RATIOS					
Br/Cl molal	mol/mol	-	3.517E-03	-	-
Na/Cl molal	mol/mol	-	-	-	-
K/Na molal	mol/mol	-	-	-	-
SO_4/Cl molal	mol/mol	-	7.138E-04	-	-
CALCULATED FROM STOICHIOMETRIC VALUES					
Ionic Strength	mol/kg H_2O	-	-	-	-
ISOTOPIC COMPOSITION OF WATER AND SOLUTES					
WATER					
$\delta^{18}O$	‰ SMOW	-8.7	-	-	-
$\delta\ ^{2}H$	‰ SMOW	-66.6	-	-	-
^{3}H	TU	-	-	-	-
DISSOLVED INORGANIC CARBON					
$\delta^{13}C$	‰ PDB	-	-	-	-
^{14}C	pmc	64.5 ± 0.4	-	-	-
DISSOLVED SULPHATE					
$\delta^{34}S$ (SO_4)	‰ CD	-	-	-	-
$\delta^{18}O$ (SO_4)	‰ SMOW	-	-	-	-
DISSOLVED STRONTIUM					
^{87}Sr / ^{86}Sr		0.715213 ± 0.000032			
DISSOLVED CHLORINE (DUPLICATE ANALYSIS)					
$\delta^{37}Cl$	‰ SMOC	0.31	-	-	-
DISSOLVED BORON					
$\delta^{11}B$	‰ NBS951	-	-	-	-

TABLE A16-1: (PAGE 6 OF 6)

SAMPLE DESCRIPTION					
Borehole		KF0051 A01		KF0051 A01	
Type of Sample		Borehole Water		Borehole Gas	
Sample		**MFE-S2-3**		**MFE-S1-3**	
Interval		8.85-9.55		10.55-11.80	
Source of Water		Section 2		Section 1	
Sample Volume		17 ml		no water	
Date Collected		13-Feb-2003		13-Feb-2003	
FREE GAS IN THE SAMPLING INTERVAL					
H_2	ppm	12.33	-	2.97	-
CO_2	ppm	1958.6	-	960.9	-
CO	ppm	7.27	-	9.75	-
CH_4	ppm	11.40	-	4.93	-
C_2H_4	ppm	present *	-	0.89	-
C_2H_6	ppm	0.75	-	0.83	-

* C_2H_4 probably present, but hidden in CO_2 tail

Groundwater from boreholes KF0066A01 & KF0069A01

Table A16-2: Groundwater chemical, isotopic and gas data (page 1 of 3).

SAMPLE DESCRIPTION					
Borehole			KF0066 A01		KF0069 A01
Rock Type			Äspö diorite		Äspö diorite
Type of Sample			Groundwater		Groundwater
Sample			KF66-1		KF69-1
Interval			0-60.11m		0-70.09m
Source of Water			Artesian outflow (7-8m; 56m)		Artesian outflow (64-66m)
Date Collected			13-Feb-2003		13-Feb-2003
Comments			Sampling at well head		Sampling at well head
GROUNDWATER TYPE			Ca-Na-Cl (SO_4)		Ca-Na-Cl (SO_4)
MISCELLANEOUS PROPERTIES					
pH (field)	-log(H+)	-	7.81	-	8.09
pH (lab)	-log(H+)	-	7.05	-	7.17
Electrical Conductivity	mS/cm	-	-	-	-
Pt Elec Potential vs. SHE	mV	-	-	-	-
Sample Temperature	ºC	-	8.1	-	8.1
Density (calc.)	kg / l	-	1.021699	-	1.020199
DISSOLVED CONSTITUENTS					
		mg / l	mmol / kgH_2O	mg / l	mmol / kgH_2O
CATIONS					
Lithium (Li^+)		-	-	-	-
Sodium (Na^+)		3390	1.475E-01	3130	1.361E-01
Potassium (K^+)		14.7	3.760E-04	15.8	4.041E-04
Ammonium (NH_4^+)		0.077	4.269E-06	0.030	1.663E-06
Rubidium (Rb^+)		0.059	6.903E-07	0.051	5.967E-07
Cesium (Cs^+)		0.00487	3.664E-08	0.00421	3.168E-08
Magnesium (Mg^{+2})		33.1	1.362E-03	33.1	1.362E-03
Calcium (Ca^{+2})		4620	1.153E-01	3980	9.930E-02
Strontium (Sr^{+2})		78.6	8.971E-04	67.7	7.727E-04
Barium (Ba^{+2})		0.103	7.500E-07	0.097	7.063E-07
Iron (Fe^{+2})		0.022	3.939E-07	< 0.002	< 3.581E-08
Uranium (U)		0.000023	9.663E-11	< 0.000020	< 8.402E-11
ANIONS					
Fluoride (F^-)		1	5.264E-05	1.3	6.843E-05
Chloride (Cl^-)		12883	3.634E-01	12280	3.464E-01
Bromide (Br^-)		97.1	1.215E-03	86.6	1.084E-03
Iodide (I^-)		-	-	-	-
Sulphate (SO_4^{-2})		642	6.683E-03	663	6.902E-03
Nitrate (NO_3^-)		-	-	-	-
Total Alkalinity	meq / l	13.5	2.212E-04	5.5	9.014E-05
NEUTRAL SPECIES					
Tot. Sulfide (H_2S,HS^-,S^{-2})		0.06	1.761E-06	0.07	12.054E-06
Silica (Si)		4.4	1.567E-04	4.5	1.602E-04
Boron (B)		-	-	-	-
Total Iron (Fe total)		0.082	1.432E-06	0.011	1.791E-06
Total Organic C (TOC)		< 0.1	< 8.326E-06	< 0.1	< 8.326E-06
Total Inorganic C (TIC)		-	-	-	-

Table A16-2: (page 2 of 3)

SAMPLE DESCRIPTION					
Borehole		KF0066 A01		KF0069 A01	
Rock Type		Äspö diorite		Äspö diorite	
Type of Sample		Groundwater		Groundwater	
Sample		KF66-1		KF69-1	
Interval		0-60.11m		0-70.09m	
Source of Water		Artesian outflow (7-8m; 56m)		Artesian outflow (64-66m)	
Date Collected		13-Feb-2003		13-Feb-2003	
Comments		Sampling at well head		Sampling at well head	
PARAMETERS CALCULATED FROM ANALYTICAL DATA					
Sum of Anal. Constituents	mg/l	21781	-	20271	-
Charge Balance:		-	-	-	-
Difference/Total	%	-	0.67	-	-3.08
ION-ION RATIOS					
Br/Cl molal	mol/mol	-	3.344E-03	-	3.129E-03
Na/Cl molal	mol/mol	-	4.058E-01	-	3.931E-01
K/Na molal	mol/mol	-	2.550E-03	-	2.968E-03
SO_4/Cl molal	mol/mol	-	1.839E-02	-	1.993E-02
CALCULATED FROM STOICHIOMETRIC VALUES					
Ionic Strength	mol/kg H_2O	-	5.021E-01	-	4.547E-01
ISOTOPIC COMPOSITION OF WATER AND SOLUTES					
WATER					
$\delta^{18}O$	‰ SMOW	-12.6	-	-12.4	-
$\delta\ ^{2}H$	‰ SMOW	-86.1	-	-84.9	-
^{3}H	TU	< 0.8	-	< 0.8	-
DISSOLVED INORGANIC CARBON					
$\delta^{13}C$	‰ PDB	-11.5 ± 0.3	-	-15.0 ± 0.3	-
^{14}C	pmc	90.5 ± 0.3	-	71.5 ± 0.3	-
DISSOLVED SULPHATE					
$\delta^{34}S$ (SO_4)	‰ CD	12.9	-	13.8	-
$\delta^{18}O$ (SO_4)	‰ SMOW	-	-	-	-
DISSOLVED STRONTIUM					
^{87}Sr / ^{86}Sr		0.719077 ± 0.000062		0.719144 ± 0.000053	
DISSOLVED CHLORINE (duplicate analysis)					
$\delta^{37}Cl$	‰ SMOC	0.31	-	0.46	-
DISSOLVED BORON					
$\delta^{11}B$	‰ NBS951	0.24	-	0.24	-

Table A16-2: (page 3 of 3)

SAMPLE DESCRIPTION					
Borehole		KF0066 A01		KF0069 A01	
Rock Type		Äspö diorite		Äspö diorite	
Type of Sample		Groundwater		Groundwater	
Sample		KF66-1		KF69-1	
Interval		0-60.11m		0-70.09m	
Source of Water		Artesian outflow (7-8m; 56m)		Artesian outflow (64-66m)	
Date Collected		13-Feb-2003		13-Feb-2003	
Comments		Sampling at well head		Sampling at well head	
CARBONATE SYSTEM					
CALCULATED USING MEASURED VALUES					
TIC from alkalinity	mol/kg	-	2.157E-04	-	8.249E-05
Calcite saturation index		-	0.26	-	0.07
log $P(CO_2)$		-	-4.04	-	-4.73
CALCULATED AT CALCITE SATURATION					
pH		-	7.81	-	8.09
log $P(CO_2)$		-	-4.31	-	-4.81
TIC adjusted to calcite sat.	mol/kg	-	1.178E-04	-	6.993E-05
SATURATION INDICES					
CALCITE (adjusted)		-	0.00	-	0.00
DOLOMITE_ORD		-	-1.87	-	-1.81
FLUORITE		-	0.18	-	0.37
GYPSUM		-	-0.13	-	-0.14
STRONTIANITE		-	-1.23	-	-1.18
CELESTITE		-	-0.17	-	-0.13
BARITE		-	0.22	-	0.25
SiO_2 amorph		-	-1.25	-	-1.25
QUARTZ		-	-0.17	-	-0.17

SAMPLE DESCRIPTION					
Borehole		KF0066 A01		KF0069 A01	
Type of Sample		Äspö diorite		Äspö diorite	
Sample		Groundwater		Groundwater	
Interval		KF66-1		KF69-1	
Source of Water		0-60.11m		0-70.09m	
Sample Volume		Artesian outflow (7-8m; 56m)		Artesian outflow (64-66m)	
Date Collected		13-Feb-2003		13-Feb-2003	
FREE GAS IN THE SAMPLING INTERVAL					
H_2	ppm	38.49	-	12.03	-
CO_2	ppm	395.2	-	123.5	-
CO	ppm	0.14	-	0.05	-
CH_4	ppm	1001.3	-	312.9	-
C_2H_4	ppm	present *	-	present *	-
C_2H_6	ppm	0.26	-	0.08	-

* C_2H_4 probably present, but hidden in CO_2 tail

ISSN 1404-0344

CM Digitaltryck AB, Bromma, 2003